Beiträge zur Chemie Schiff'scher Basen mit Aminosäuren und deren Metallkomplexe

Kumulative Dissertation

Zur Erlangung des akademischen Grades eines Doktors der Naturwissenschaften
(Dr. rer. nat.)

dem Fachbereich Chemie der Philipps-Universität Marburg
vorgelegt von

Diplom-Chemiker Simon G. M. Muche

aus Räckelwitz

Erstgutachterin: PD Dr. Małgorzata Hołyńska
Zweigutachterin: Prof. Dr. Stefanie Dehnen

Termin der Einreichung: 27.10.2017
Termin der mündlichen Prüfung: 19.12.2017

Marburg (Lahn) 2017
Hochschulkennziffer 1180

Erklärung

Ich erkläre, dass eine Promotion noch an keiner anderen Hochschule als der Philipps-Universität Marburg, Fachbereich Chemie, versucht wurde.

Ich versichere, dass ich die vorgelegte Dissertation mit dem Titel „Beiträge zur Chemie Schiff'scher Basen mit Aminosäuren und deren Metallkomplexe" selbst und ohne fremde Hilfe verfasst, nicht andere als die in ihr angegebenen Quellen oder Hilfsmittel benutzt und alle vollständig oder sinngemäß übernommenen Zitate als solche gekennzeichnet habe.
Diese Dissertation wurde in der vorliegenden oder einer ähnlichen Form noch bei keiner anderen in- oder ausländischen Hochschule anlässlich eines Promotionsgesuches oder zu anderen Prüfungszwecken eingereicht.

Marburg, den _____

Simon Muche

Die vorliegende Arbeit entstand in der Zeit von März 2014 bis Oktober 2017 unter der Betreuung von PD Dr. Małgorzata Hołyńska am Fachbereich Chemie der Philipps-Universität Marburg.

¡Es mejor morir de pie que vivir toda una vida de rodillas!

Besser aufrecht sterben, als auf den Knien leben!

(Emiliano Zapata Salazar, 1879-1919)

Danksagung

Das erfolgreiche Verfassen dieser Arbeit wäre ohne die Unterstützung anderer nicht möglich gewesen. Darum an dieser Stelle ein paar Worte des Dankes:

Ich danke PD Dr. Małgorzata Hołyńska für die Möglichkeit, in ihrer Arbeitsgruppe an diesem Thema zu arbeiten zu können.

Prof Dr. Stefanie Dehnen danke ich für Übernahme des Koreferats. Weiterhin danke ich dir, Steffi, für dein stets offenes Ohr, deine Ratschläge und deine Unterstützung bei allen kleineren und größeren Problemen, sowie deine Bereitschaft, bei finanziellen Engpässen auszuhelfen.

Prof. Dr. Udo Bakowsky und Prof. Dr. Ulrich Tallarek danke ich, dass sie sich bereit erklärt haben, in der Prüfungskommission mitzuwirken.

Ein besonderer Dank gilt den Mitarbeitern der Service-Abteilungen des Fachbereichs Chemie, ohne die ein Großteil der hier präsentierten Ergebnisse nicht zustande gekommen wäre. Insbesondere möchte ich an dieser Stelle Dr. Klaus Harms aus der Abteilung für Kristallstrukturanalyse, Jan Bamberger aus der Abteilung für Massenspektrometrie, Heike Mallinger und Martina Gerlach aus der Abteilung für Elementanalytik, sowie Cornelia Mischke aus der NMR-Abteilung für deren Hilfestellungen bei sämtlichen Fragen und für die Erfüllung von allerlei Sonderwünschen danken.

Ebenfalls großen Anteil an den präsentierten Ergebnissen haben natürlich auch die vielfältigen Kooperationspartner, sowie Vertiefer und Praktikanten, denen ich für die gute Zusammenarbeit danken möchte.

Das Arbeitsklima einer Arbeitsgruppe hängt nicht nur vom Arbeitsgruppenleiter, sondern auch von den entsprechenden Gruppenmitgliedern ab. Mit dem AK Dehnen und den dazugehörigen Nachwuchsgruppen und deren Leitern kann man es an dieser Uni dahingehend eigentlich nicht besser treffen. Euch allen noch Anwesenden, weiterhin Anwesenden und Ehemaligen vielen Dank für eure Unterstützung und eine unglaublich tolle Zeit! Besonderer Dank ergeht an die gute Fee des Arbeitskreises, Ursula Siepe, die sehr viel für mich ermöglicht und vermittelt hat.

Auch außerhalb der Uni habe ich in den zurückliegenden Jahren meiner Doktorarbeit viel Unterstützung und Zuspruch durch das freundliche Thekenpersonal in den verschiedensten Marburger Kneipen und ganz besonders durch meine Freunde erfahren. Speziell danken möchte ich Dipl.-Psych. Farina Bludau und Marco Velten für die vielen unvergesslichen Spieleabende, Parties, Kneipengänge, etc. Danke, dass ihr da ward wenn‘s gut lief, aber insbesondere wenn ich Frust geschoben oder gejammert habe.

Last but not least, danke ich meiner Familie für die vielfältige und fortwährende Unterstützung in den vergangenen Jahren, ohne die diese Arbeit nicht zustande gekommen wäre.

Inhaltsverzeichnis

1. Einleitung

Abbildung 1: Pressemeldungen zum Thema Antibiotikaresistenz bei Bakterien (abgerufen bei Spiegel Online).

Meldungen wie diese sind in den vergangenen Jahren zunehmend häufiger in den Medien zu lesen gewesen. Durch die zunehmende und teils auch überflüssige Verschreibung von Antibiotika, sowie den verstärkten Einsatz von Antibiotika in der Tiermast, bilden Bakterienstämme immer öfter Resistenzen gegen Antibiotika aus. Nicht selten mit tödlichen Folgen. Daher ist nicht nur die Weiterentwicklung bereits vorhandener Antibiotika ein äußerst wichtiges Forschungsfeld, sondern auch die Entwicklung neuer, antimikrobiell wirksamer Verbindungen. Schiff'sche Basen und ihre Metallkomplexe, deren antimikrobielles Potenzial bereits in einer Vielzahl von Publikationen beschrieben wurde, sind dafür interessante Kandidaten.

Auch im Bereich der Krebstherapie sind insbesondere Metallkomplexe von Schiff'schen Basen Gegenstand der Forschung. *Cis*-Platin, eines der wirksamsten Chemotherapeutika überhaupt, ist der wahrscheinlich bekannteste Vertreter von metallbasierten, zytostatisch wirksamen Arzneistoffen. Allerdings ist für diese Verbindung ebenfalls eine Resistenzentwicklung zu beobachten. Außerdem schädigt *Cis*-Platin auch gesunde Zellen. Bei der Entwicklung neuer zytostatisch wirksamer Substanzen spielt also nicht nur die allgemeine Wirksamkeit der neuen Verbindungen eine Rolle, sondern ebenfalls die Vermeidung bzw. Überwindung von Zytostatikaresistenzen und die Selektivität.

1.1 Schiff‘sche Basen

Schiff’sche Basen, benannt nach dem deutschen Chemiker Hugo Schiff (1843-1915), welcher sie im Jahr 1864 erstmals beschrieb[(1)], können durch die Kondensation von Aldehyden bzw. Ketonen mit primären Aminen hergestellt werden. Schiff’sche Basen gehören zu den sekundären Aldiminen bzw. Ketiminen und bilden damit eine Untergruppe der Imine. Abbildung 2 zeigt den Bildungsmechanismus im neutralen Milieu sowie die generelle Struktur von Schiff’schen Basen. Damit ein Imin als Schiff’sche Base klassifiziert werden kann, ist es zwingend erforderlich, dass der Rest R^1 am Stickstoffatom organischer Natur, z.B. eine Alkyl- oder Arylgruppe, ist. Die Reste R^2 und R^3 können sowohl organischer Natur, als auch Wasserstoffatome sein.

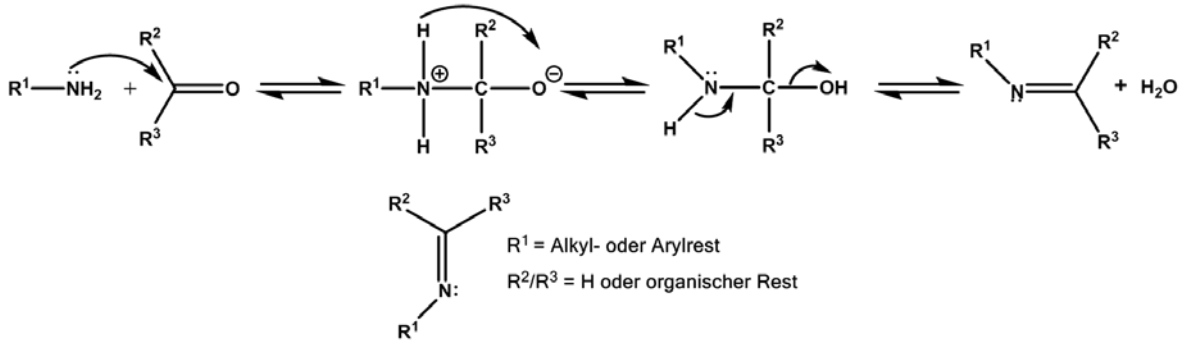

Abbildung 2**:** Bildungsmechanismus in neutralen Milieu und allgemeine Struktur von Schiff’schen Basen.

Im ersten Schritt der Bildung von Schiff’schen Basen erfolgt ein nukleophiler Angriff des freien Elektronenpaares des Aminostickstoffs am Carbonylkohlenstoff. An dem dabei entstehenden Zwitterion findet eine Protonenübertragung auf das negativ geladene Sauerstoffatom statt und es bildet sich ein instabiles Aminol Im letzten Schritt wird ein weiteres Proton vom Stickstoffatom auf die Hydroxylgruppe übertragen und unter Eliminierung eines Wassermoleküls die Kohlenstoff-Stickstoff-Doppelbindung ausgebildet. Da alle Schritte der Iminbildung reversibel sind, sind Imine äußerst hydrolyseempfindlich und damit instabil. Phenylsubstituenten am Kohlenstoff- und/oder Stickstoffatom der Doppelbindung stabilisieren sie jedoch hinreichend, sodass auch in wässrigem Medium das Gleichgewicht auf der Produktseite liegt. Die Bildung von Iminen in neutralem Milieu ist möglich, läuft aber nur langsam ab. Durch Zugabe von Säure wird die Reaktion katalysiert. Der ideale pH-Bereich für die Iminbildung liegt zwischen 4 und 6[(2)].

Wichtigstes strukturelles Merkmal von Schiff’schen Basen ist die Kohlenstoff-Stickstoff-Doppelbindung. Sowohl das Kohlenstoff- als auch das Stickstoffatom sind sp^2 hybridisiert. Je

ein sp^2-Hybridorbital wird für die σ-Bindung zwischen den Atomen verwendet. Die beiden *p*-Orbitale bilden die π-Bindung aus. Die verbleibenden sp^2-Hybridorbitale des Kohlenstoffes werden für die σ-Bindungen zu den Substituenten heran gezogen. Von den verbleibenden sp^2-Hybridorbitalen des Stickstoffs wird eines für die σ-Bindung zum Substituenten genutzt. Im zweiten Orbital befindet sich das freie Elektronenpaar[3]. Sie sind damit planare Verbindungen. Durch den hohen *p*-Anteil des Orbitals wird das freie Elektronenpaar attraktiv für die Ausbildung von koordinativen Bindungen zu Metallen. Eine Überlappung mit den entsprechenden *p*-Orbitalen sowie dem d_Z^2-Orbital von Übergangsmetallen machen die Bildung von Metallkomplexen möglich.

In vielen biologischen Prozessen spielt die Ausbildung von Schiff'schen Basen eine wichtige Rolle. Beim Abbau von Aminosäuren etwa, bindet eine ε-Aminogruppe eines spezifischen Lysinrest am aktiven Zentrum der Aminotransferase an das Coenzym Pyridoxalphosphat. Es wird ein Imin ausgebildet, welches den Merkmalen einer Schiff'schen Base entspricht. Im nächsten Schritt verdrängt die α-Aminogruppe einer Aminosäure die ε-Aminogruppe des Lysinrestes und bildet mit dem Pyridoxalphosphat ein protoniertes Imin, welches ebenfalls einer Schiff'sche Base entspricht. Dieses Gebilde bleibt durch nichtkovalente Wechselwirkungen an das Enzym gebunden (Abb. 3 A).

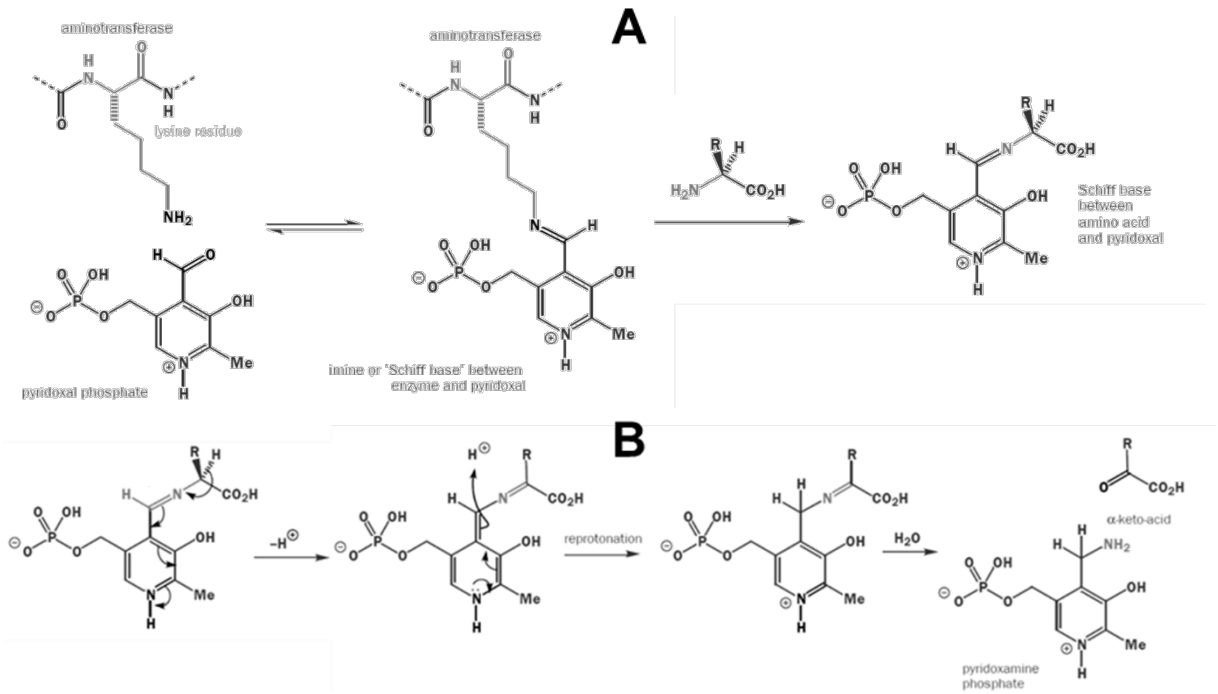

Abbildung 3: Mechanismus des Aminosäureabbaus[2].

Anschließend wird ein Proton der α-Aminogruppe der gebundenen Aminosäure abgespalten. Das erhaltene chinoide Zwischenprodukt wird wiederum protoniert. Durch anschließende Hydrolyse des erhaltenen Ketimins werden die entsprechende α-Ketosäure und

Pyridoxaminphosphat erhalten[2, 4]. In der Folge wird die auf das Pyridoxalphospat übertragene Amingruppe von einer weiteren α-Ketosäure aufgenommen, wodurch nicht essentielle Aminosäuren vom Organismus selbst hergestellt werden können (Abb. 3B). Alternativ wird die Amingruppe von α-Ketoglutarat aufgenommen. Das gebildete Glutamat kann dann durch die Glutamatdehydrogenase mittels oxidativer Desaminierung in α-Ketoglutarat und Ammonium gespalten werden, welches anschließend zur weiteren Dissimilation in den Harnstoffzyklus geleitet wird.

Weitere Beispiele für das Vorkommen von Schiff'schen Basen in biochemischen Prozessen sind der Transaldolasemechanismus[5] oder die β-Untereinheit der Tryptophan-Synthase in *E. coli*, welche die Kondensation von Serin und Indol zu Tryptophan katalysiert[4].

1.2 Eigenschaften von Schiff'schen Basen und deren Metallkomplexen

Für die biologischen Eigenschaften von Schiff'schen Basen spielt nicht nur die planare Kohlenstoff-Stickstoff-Doppelbindung eine Rolle, sondern ebenfalls die Substituenten. Durch die nahezu unbegrenzte Auswahl an Substituenten ergibt sich auch eine hohe Mannigfaltigkeit an Eigenschaften von Schiff'schen Basen. Dementsprechend hoch ist auch die Zahl an Publikationen zu diesem Thema.

Eine hohe antifungale Aktivität (MIC_{50} = 1.2 µM) gegen den Hefepilz *C. albicans* konnte für eine Schiff'sche Base, erhalten aus der Reaktion von 7-Amino-4-methyl-coumarin mit 3,5-Diiodo-2-hydroxybenzaldehyd (Abb. 4), beobachtet werden. Der daraus synthetisierte mononukleare Cu(II)-Komplex zeigte mit einer MIC_{50} = 0.7 µM eine noch höhere Aktivität, welche gleich der Aktivität des kommerziellen Antimykotikums Amphotericin B ist[6].

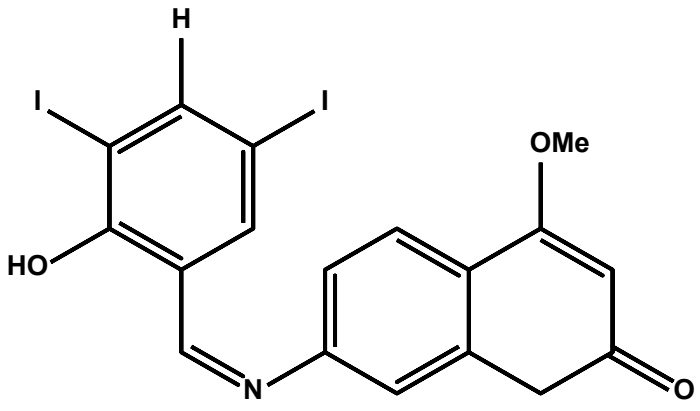

Abbildung 4: Schiff'sche Base aus 7-Amino-4-methyl-coumarin mit 3,5-Diiodo-2-hydroxybenzaldehyd.

In einer Folgestudie wurden die Schiff'schen Basen zu den korrespondierenden sekundären Aminen umgesetzt. Die erhaltenen Amine zeigten nun keine antifungale Aktivität mehr, sodass

geschlussfolgert wurde, dass die antifungale Aktivität dieser Coumarin-basierten Verbindungen auf die Iminfunktion zurückzuführen ist[7]. Makrozyklische Liganden und deren Kupferkomplexe, die aus der Kondensation von Diethylphthalat mit *ortho*-Phenylendiamin-basierten Schiff'schen Basen erhalten wurden, zeigten eine antifungale Aktivität gegen *C. albicans* und *A. niger*, welche vergleichbar oder teils besser war, als das kommerziell verwendete Nystatin. Auch hier waren die Metallkomplexe insgesamt aktiver als die freien Liganden[8]. Potente antifungale Eigenschaften besitzen ebenfalls Pyrazol-basierte Schiff'sche Basen. Mehrere Derivate von 3-(4-Chlorphenyl)-4-substituierten Pyrazolen (Abb. 5), insbesondere diejenigen, welche eine elektronenziehende Gruppe trugen, zeigten gleiche oder bessere Aktivität gegenüber *C. krusei, C. neoformans, A. niger* und *A. flavus* als die Referenzverbindungen Fluconazol und 5-Fluorocystein. Außerdem konnte eine sehr gute antituberkulöse Aktivität gegenüber dem Stamm H37Rv von *M. tuberculosis* beobachtet werden[9].

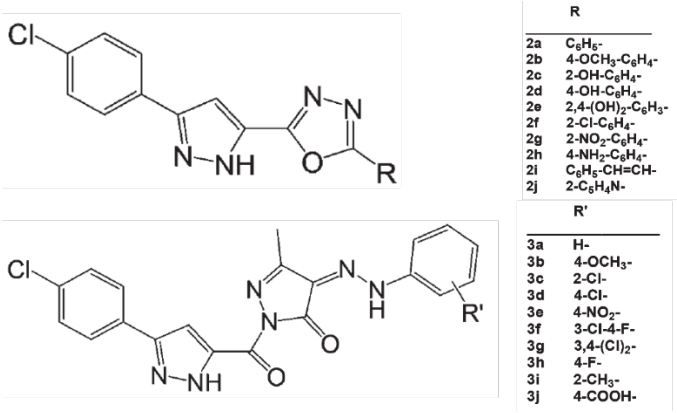

	R
2a	C_6H_5-
2b	4-OCH_3-C_6H_4-
2c	2-OH-C_6H_4-
2d	4-OH-C_6H_4-
2e	2,4-$(OH)_2$-C_6H_3-
2f	2-Cl-C_6H_4-
2g	2-NO_2-C_6H_4-
2h	4-NH_2-C_6H_4-
2i	C_6H_5-CH=CH-
2j	2-C_5H_4N-

	R'
3a	H-
3b	4-OCH_3-
3c	2-Cl-
3d	4-Cl-
3e	4-NO_2-
3f	3-Cl-4-F-
3g	3,4-$(Cl)_2$-
3h	4-F-
3i	2-CH_3-
3j	4-COOH-

Abbildung 5: Derivate von 3-(4-Chlorphenyl)-4-substituierten Pyrazolen mit potent antifungalen Eigenschaften[9].

Schiff'sche Basen, erhalten aus der Kondensation von *ortho*-Phthalaldehyd und *L*-Histidin bzw. *L*-Tryptophan, sowie deren mononukleare Co(II)-, Ni(II)- und Pd(II)-Komplexe zeigten exzellente antibakterielle Aktivität gegenüber grampositiven (*B. subtilis, S. aureus*) und gramnegativen *(E. coli, K. pneumoniai*) Bakterien. Die Aktivität der freien Schiff'schen Basen lag im Bereich der Referenzantibiotika Streptomycin und Ampicillin. Die Metallkomplexe zeigten allesamt eine deutlich höhere Aktivität als die freien Liganden. Am potentesten waren die getesteten Pd-Komplexe. Deren MIC-Werte lagen teilweise bis zu sechsmal niedriger, verglichen mit denen der Referenzverbindungen[10]. Eine zyklische Schiff'sche Base (Abb. 6), welche durch die Kondensation von Dibenzoyl und Triethylentetraamin erhalten werden kann, bildet mit verschiedensten Übergangsmetallionen mononukleare kationische Komplexe mit Chlorid als Gegenion. Bei Konzentrationen von 2.5 mg/L und höher zeigten sowohl die freie

Schiff'sche Base, als auch die Komplexe ähnliche Aktivitäten gegenüber *B. simplex, E. acetylicum, P. putida* und *E. coli* verglichen mit Cefepim. Bei einer Konzentration von 1 mg/L zeigte die freie Schiff'sche Base eine gleichbleibende Aktivität gegenüber *E. acetylicum*. Die Fe(III)- und UO_2(II)-Komplexe waren bei dieser Konzentration unverändert aktiv gegenüber *P. putida*. Außerdem besaßen die Zn(II)- und UO_2(II)-Komplexe gegenüber *B. simplex* eine höhere Aktivität im Vergleich mit Cefepim[(11)].

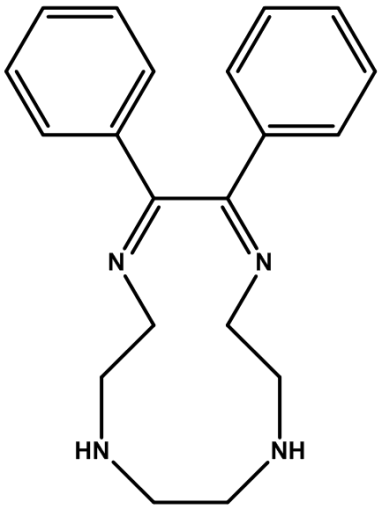

Abbildung 6: Zyklische Schiff'sche Base aus der Kondensation von Dibenzoyl und Triethylentetraamin.

Ein mononuklearer Cu(II)-Komplex mit einem Schiff'sche Base-Liganden aus Vanillin und *DL*-α-Aminobuttersäure besaß eine höhere Aktivität gegenüber *S. aureus, E. coli, K. pneumaniae, P. vulgaris* und *P. aeruginosa* als der Standard Amikacin. Die korrespondierenden Zn(II)- und (Ni(II)-Komplexe sowie der freie Ligand waren inaktiv. Lediglich der Co(II)-Komplex zeigt gegenüber *P. aeruginosa* noch eine moderate Aktivität[(12)].

Antiinflammatorische Eigenschaften konnten für eine Schiff'sche Base aus S-Benzyldithiocarbazat mit 3-Hydroxyacetophenon sowie den korrespondierenden Ni(II)- und Cu(II)-Komplexen beobachtet werden (Abb. 7). Zu diesem Zweck wurden mittels Carrageenen in Ratten Ödeme an den Pfoten induziert und die Größe der Schwellung gemessen[(13)]. Die untersuchten Verbindungen sowie Indomethacin als Standardtherapeutikum wurden in Dosen von 10 mg/kg Körpergewicht verabreicht. Sowohl die Komplexe als auch der freie Ligand konnten das Entstehen der Pfotenödeme signifikant inhibieren. Die antiinflammatorische Aktivität lag dabei im Bereich von Indomethacin. Auf Grund dieser Ergebnisse vermuten die Autoren einen ähnlichen Wirkmechanismus, nämlich die Hemmung der Cyclooxygenase[(14)].

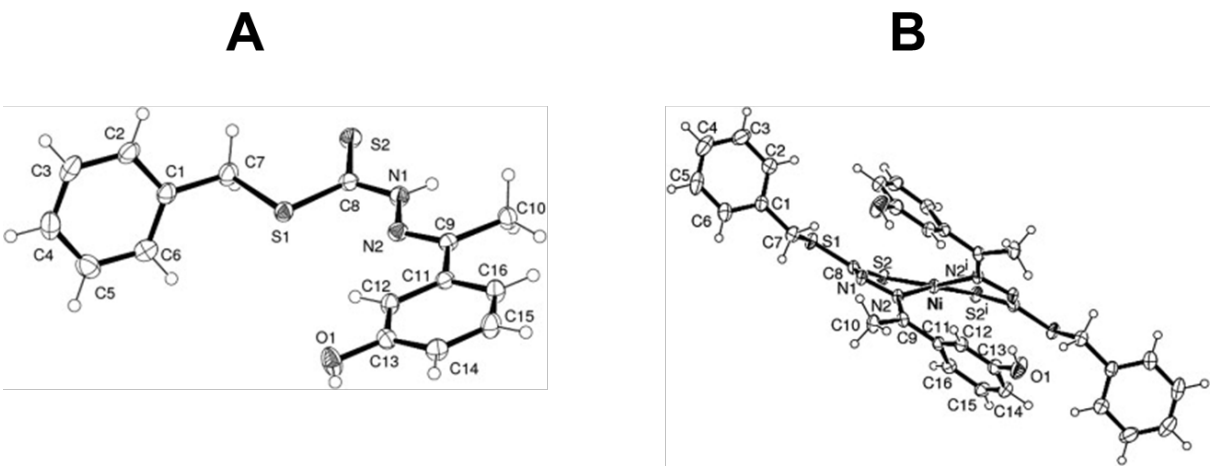

Abbildung 7: A) Kristallstruktur der Schiff'schen Base aus S-Benzyldithiocarbazat mit 3-Hydroxyacetophenon. B) Kristallstruktur des korrespondierenden Ni(II)-Komplex. Die Struktur des Cu(II)-Komplexes ist analog dazu[14].

Ebenfalls antiinflammatorische Eigenschaften besaßen heptakoordinierte Sn(IV)-Komplexe mit Liganden bestehend aus verschieden substituierten Aminophenolen und Pyridin-basierten Aldehyden. Von den 17 synthetisierten Sn(IV)-Komplexen konnte für fünf Verbindungen die Kristallstruktur bestimmt werden (Abb. 8). Für die Bestimmung des antiinflammatorischen Potenzials wurden lediglich die Butylzinn-Derivate 2a-2d verwendet, da deren Löslichkeit ausreichend hoch war. Die vier untersuchten Komplexe zeigten alle einen dosenabhängigen positiven Effekt auf die induzierte Entzündung, verglichen mit Indomethacin. Komplex 2c war dabei besonders potent und übertraf die Aktivität der Referenz um zwei Größenordnungen.

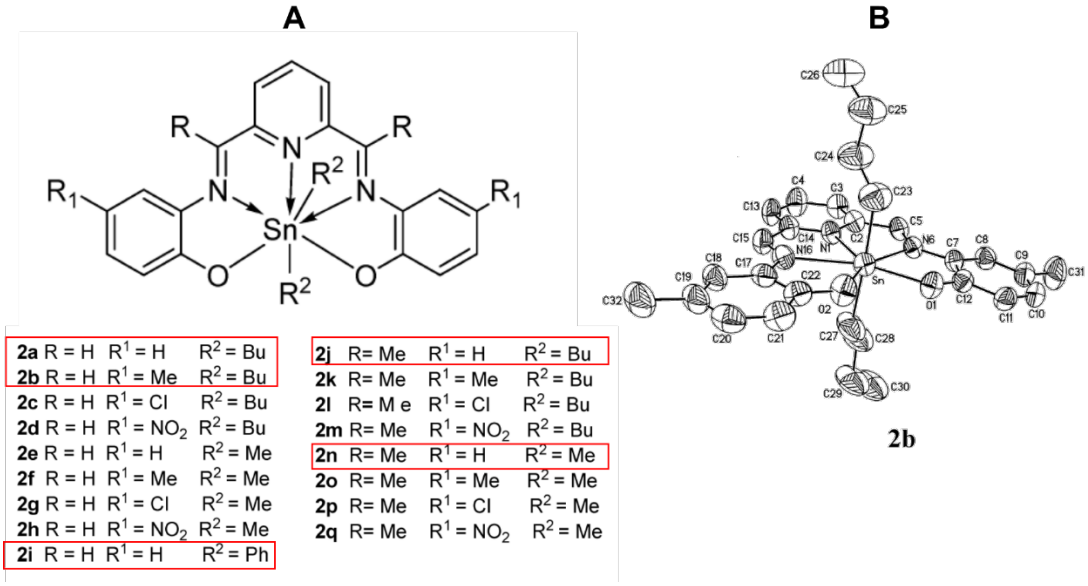

Abbildung 8: A) Übersicht über die erhaltenen Sn(IV)-Komplexe. Für die rot markierten Verbindungen konnte eine Kristallstruktur erhalten werden. B) Kristallstruktur des Sn(IV)-Komplex 2b[15].

Neben des eben beschriebenen antiinflammatorischen Potenzials zeigten die vier Komplexe *in vitro* ebenfalls ausgeprägte antiproliferative Eigenschaften. Verglichen mit dem Standard *Cis*-Platin besaßen alle Komplexe deutlich niedrigere IC_{50}-Werte gegenüber den sechs untersuchten Tumorzelllinien[15]. Eine Serie von monuklearen Cu(II)-Komplexen mit einem Schiff'sche Base-Ligand aus 2-Hydroxy-1-naphthaldehyd und 1-((2-Aminoethyl)amino)propan-2-ol und verschiedenen Co-Liganden (Abb. 9) zeigten potentes, dosenabhängiges antiproliferatives Verhalten gegenüber den zwei getesteten Tumorzelllinien HeLa und Hep G2. Der freie Ligand, die Co-Liganden, sowie die verwendeten Kupfersalze zeigten keinen antiproliferativen Effekt. Komplex 4 war am wirksamsten. Als Standard diente wiederum *Cis*-Platin[16].

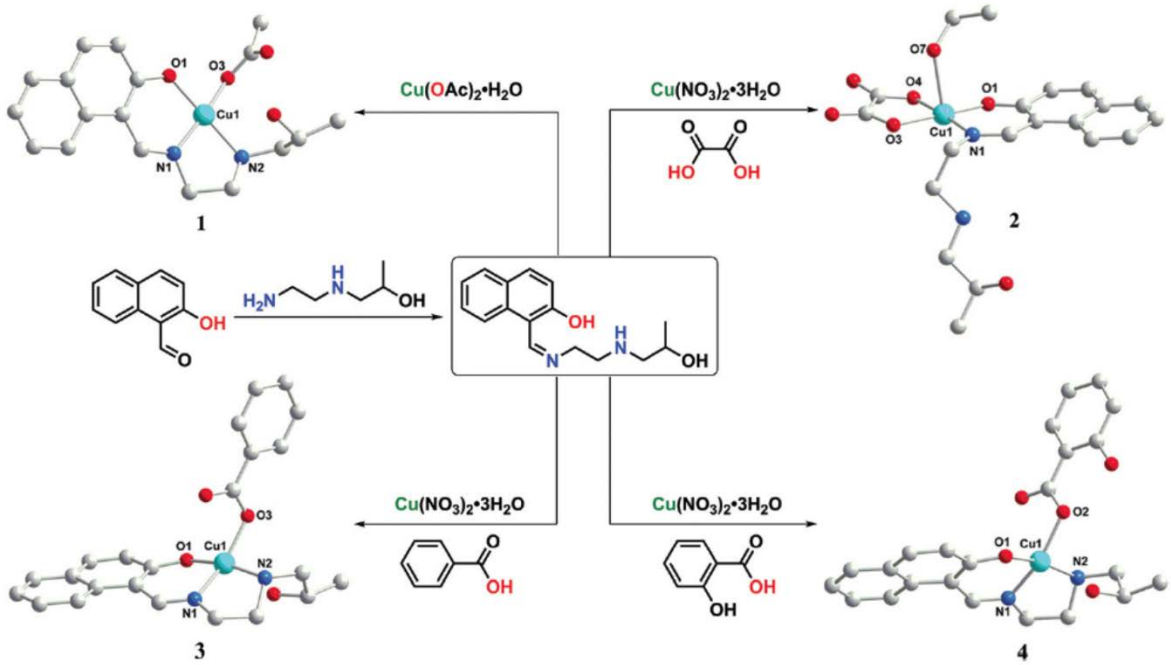

Abbildung 9: Syntheseschema und Kristallstrukturen der vier Cu(II)-Komplexe mit einem Schiff'sche Base-Ligand aus 2-Hydroxy-1-naphthaldehyd und 1-((2-Aminoethyl)-amino)propan-2-ol und verschiedenen Co-Liganden[16].

Schiff'sche Basen, welche eine strukturelle Verwandtschaft zu Chloroquin, einem Arzneistoff zur Therapie und Prophylaxe von Malaria, besitzen und deren Metallkomplexe zeigten in *in vitro*-Studien moderate bis sehr gute Antimalaria-Effekte. Die Aktivität der Schiff'schen Basen war allgemein höher als die der Iminanaloga. Die korrespondierenden Rhodiumkomplexe zeigten einen stärkeren Effekt als die Iridiumkomplexe[17]. Als Standardreferenz diente Chloroquin.

Ein weiteres Gebiet der Anwendung von Schiff'schen Basen ist deren Effekt auf das zentrale Nervensystem. Interessant sind dabei antikonvulsante und nootropische Effekte, geringe

Neurotoxizität, sowie ein möglicher Einsatz als Antidepressivum. Schiff'sche Basen bieten auch in diesem Bereich viele Möglichkeiten[18].

Schiff'sche Basen und deren Komplexe sind aber nicht nur im Bereich der bioaktiven Eigenschaften von Interesse. Sie sind ebenso Gegenstand der Forschung in der Katalyse[19–21], der elektrolumineszenten Materialien[22–24] oder von Fluoreszenzmaterialien[25–27]. Insbesondere zyklische Liganden führen zu Metallkomplexen, welche das Verhalten von SMMs aufweisen[28–32].

1.3 Metallkomplexe mit *ortho*-Vanillin

ortho-Vanillin (2-Hydroxy-3-methoxybenzaldehyd) als Aldehydquelle für die Synthese von Schiff'schen Basen ist selbst bioaktiv. Es ist ein schwacher Tyrosinase-Inhibitor[33] und zeigt sowohl antimutagene als auch comutagene Eigenschaften in *E. coli*[34, 35]. Eine hohe antifungale Aktivität gegenüber *C. neoformans* wurde für *ortho*-Vanillin nachgewiesen, ausgelöst durch oxidativen Stress in den Pilzzellen[36]. Außerdem konnte bei Patienten mit Sichelzellanämie eine Inhibition des Kaliumtransports in roten Blutzellen, sowie eine Reduktion der Na^+/K^+-Pumpe beobachtet werden[37]. Im Vergleich zum ebenfalls häufig eingesetzten Salicylaldehyd besitzt *ortho*-Vanillin durch die Methoxygruppe eine zusätzliche Stelle für die Koordination bzw. Verbrückung von Metallkationen (Abb. 10), was die Bildung von großen, polynuklearen Komplexen zulässt. Abhängig vom verwendet Metall und eventuellen Co-Liganden existiert für Komplexe mit *ortho*-Vanillin eine hohe strukturelle Vielfalt.

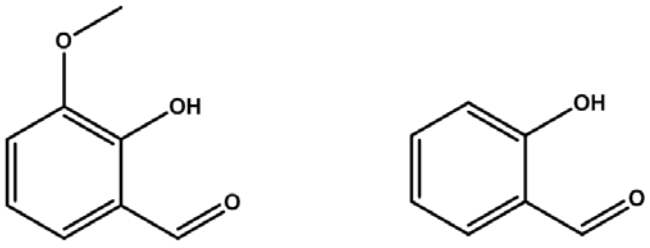

***ortho*-Vanillin** **Salicylaldehyd**

Abbildung 10: Strukturformeln von *ortho*-Vanillin und Salicylaldehyd.

1.3.1 Mononukleare Komplexe

Mononuklearen Komplexe ohne organische Co-Liganden sind literaturbekannt für Cu(II)[38–41], Ni(II)[42], Oxovanadium(IV)[43] und Fe(III)[44]. Der Fe(III)-Komplex ist zudem ein effektiver Katalysator für die Sulfoxidation. Strukturell verbindet alle diese Komplexe, dass das Zentralatom jeweils von zwei *ortho*-Vanillin-Molekülen koordiniert wird, die eine Ebene aufspannen. Zwei Wassermoleküle vervollständigen die Koordinationssphäre, sodass sich eine

oktaedrische Geometrie ergibt. Bei den Cu(II)-Komplexen entscheidet die Stellung der *ortho*-Vanillin-Liganden über die Koordinationsgeometrie: Im Kristall wird bei *cis*-Stellung eine quadratisch-pyramidale Geometrie (Abb. 11A) und bei *trans*-Stellung eine oktaedrische Geometrie erreicht (Abb. 11B). Ob die Liganden *cis* oder *trans* zueinander stehen, hängt wiederum von den Reaktionsbedingungen ab[(39)].

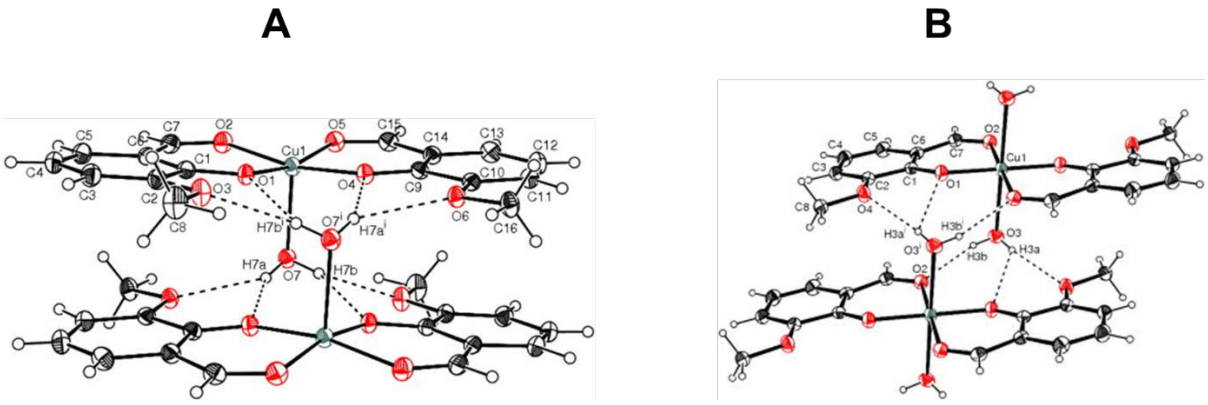

Abbildung 11: A) Mononuklearer $Cu(oVan)_2$-Komplex mit quadratisch-pyramidaler Koordinationsgeometrie. B) Mononuklearer $Cu(oVan)_2$-Komplex mit oktaedrischer Koordinationsgeometrie[(39)].

Unter Einsatz von Trimethylphosphin können oktaedrische, mononukleare Co(III)-Komplexe mit zwei *ortho*-Vanillin-Liganden und zwei $PhMe_3$-Liganden[(45)] oder einem *ortho*-Vanillin-Liganden, zwei $PhMe_3$-Liganden und zwei Methylgruppen am Cobaltzentrum[(46)] erhalten werden. Aromatische Co-Liganden führen ebenfalls zu mononuklearen Komplexen. So konnten Co(II)-Komplexe mit 2,9-Dimethyl-1,10–phenanthrolin[(47)] und 2,2′-Bipyridin[(48)] erhalten werden. Zn(II)-Komplexe wurden mit 2,2′-Bipyridin oder 2,2′-Dipyridylamin erhalten[(49)]. Alle Komplexe sind verzerrt oktaedrisch.

Dass die *cis-trans*-Stellung von Liganden nicht nur Einfluss auf die Koordinationsgeometrie, sondern auch auf das magnetische Verhalten haben kann, zeigt eine Serie von kationischen mononuklearen Dy(III)-Komplexen mit *ortho*-Vanillin und 2,4-Diamino-6-pyridyl-1,3,5-triazin. Alle drei Komplexe weisen eine quadratisch-antiprismatische Koordinationsumgebung um das Dysprosiumion auf. Bei den Komplexen 1 und 3 sind die Liganden in *trans*-Stellung zueinander orientiert, während sie sich bei Komplex 2 in *cis*-Stellung zueinander befinden (Abb. 12). Hervorgerufen wird dieser Effekt durch das jeweilige Gegenion (1: Br^-, 2: NO_3^-, 3: $CF^3SO_3^-$). Während die Gegenionen bei 1 und 3 außerhalb der Koordinationsebenen und relativ weit weg von der molekularen Einheit liegen, befindet sich das Nitration bei Komplex 2 zwischen den Ebenen und näher dran. Zwar zeigen alle drei Komplexe SMM-Verhalten, weisen aber auch gravierende Unterschiede auf. So liegt die effektive Energiebarriere U_{eff} mit 615 K

bei Komplex 2 wesentlich höher als bei den anderen Komplexen (U_{eff}(1) = 221 K, U_{eff}(3) = 120 K). Ebenso besitzt Komplex 2 mit 7 K eine höhere Blocking-Temperatur verglichen mit 4 K für Komplex 1 bzw. 3 K für Komplex 3[50].

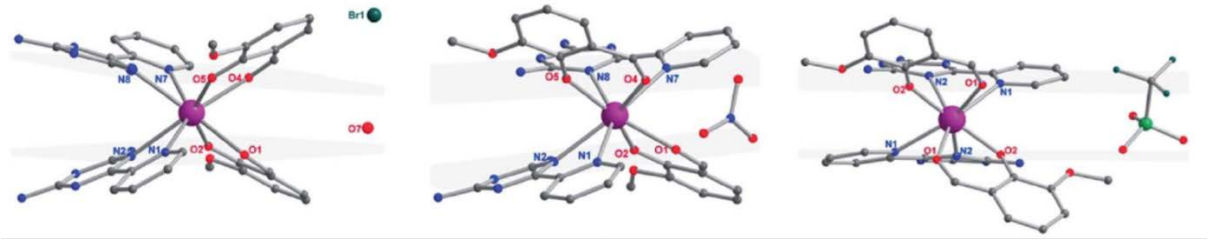

Abbildung 12: Mononukleare Dy(III)-Komplexe mit *ortho*-Vanillin und 2,4-Diamino-6-pyridyl-1,3,5-triazin als Liganden. Die grau dargestellten Ebenen repräsentieren die oberen und unteren Koordinationsebenen[50].

1.3.2 Dinukleare Komplexe

Während es nur ein literaturbekanntes Beispiel für homometallische dinukleare Komplexe, nämlich einen Cu(II)-Komplex mit Adamantanammoniumperchlorat als Gegenion gibt[51], sind heterometallische Komplexe etwas zahlreicher vertreten. Beschrieben wurden Cu(II)-Na-Komplexe mit Perchlorat[52] bzw. Antimonhexafluorid[53], sowie ein Cu(II)-Komplex mit Phosphorhexafluorid[53] als Gegenion, welche allesamt eindimensionale Kettenstrukturen bilden. Ein anderer Cu(II)-Na-Komplex mit Nitrat als Gegenion bildet hingegen Schichten aus[54]. Außerdem konnten verschiedene Lanthanid-Nickel-Komplexe (Ln = Gd, Y, Pr) mit Nitratanionen synthetisiert werden. In den Gd- und Pr-Komplexen ist das Lanthanidatom jeweils zehnfach koordiniert[55, 56]. Für den Y-Komplex beträgt die Koordinationszahl 9[56]. In allen beschriebenen Fällen sind jeweils zwei *ortho*-Vanillin-Moleküle an der Komplexbildung beteiligt.

1.3.3 Trinukleare Komplexe

Trinukleare Komplexe mit *ortho*-Vanillin sind bisher nur für die Lanthanide Yb, Gd und Dy bekannt. Alle Komplexe weisen ein identisches Kernmotiv, ein Dreieck aus Lanthanidatomen verbrückt durch deprotonierte Phenoxogruppen des *ortho*-Vanillins, auf. Die Koordinationszahl beträgt 8. Die Liganden bilden mit dem Dreiecksmotiv eine Ebene. Ansonsten unterscheiden sich die Komplexe lediglich durch die Anionen, Chlorid oder Nitrat. In allen Fällen koordiniert zusätzlich Wasser an die Zentralatome (Abb. 13).

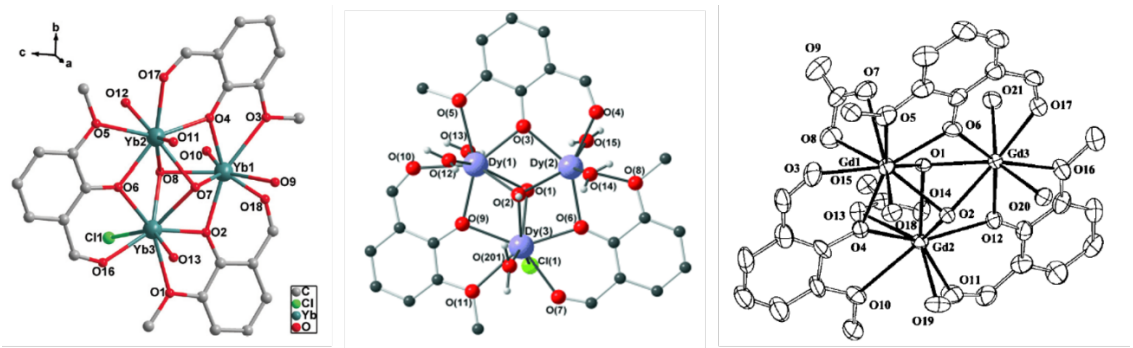

Abbildung 13: Kristallstrukturen der trinuklearen Komplexe von Yb[57], Dy[58] und Gd[59] mit *ortho*-Vanillin.

Der Yb-Komplex erwies sich als guter Katalysator für die Henry-Reaktion, der Kupplung von aliphatischen Nitroverbindungen mit Carbonylverbindungen[57]. Für den Dy-Komplex konnte SMM-Verhalten nachgewiesen werden[58].

1.3.4 Tetranukleare Komplexe

Alle bisher publizierten homometallische tetranukleare Ni(II)-Komplexe mit *ortho*-Vanillin besitzen allesamt die gleiche Struktur: Ein Hetereokubankern, aufgebaut aus Nickel und Sauerstoff bzw. Stickstoff. Im Falle der Ni-O-Heterokubane sind die Nickelatome μ_3-verbrückt durch Methanol[60–63]. Im Falle von Stickstoff wird die μ_3-Verbrückung mittels Azidionen erreicht[64]. Komplettiert wird die oktaedrische Koordinationssphäre des Nickels durch die deprotonierte Phenoxogruppe und die Carbonylgruppe. Zwischen den Nickelatomen existieren ferromagnetische Wechselwirkungen. Die in der Literatur beschriebenen homometallischen tetranuklearen Co(II)-Komplexe sind isostrukturell zu den oben beschriebenen Ni(II)-Komplexen[62, 65]. Allerdings konnte für die Cobaltverbindungen SMM-Verhalten nachgewiesen werden[62]. Zwei isostrukturelle Gd- und Dy-Komplexe mit einem planaren, tetranuklearen Butterfly-Kernmotiv sind in der Literatur beschrieben. Die Lanthanidatome sind durch zwei Hydroxidliganden μ_3-verbrückt, wodurch die Metallzentren eine Ebene aufspannen. Die inneren Lanthanidatome werden achtfach koordiniert von den Liganden und Pivalationen, was zu einer verzerrt quadratisch-antiprismatischen Geometrie führt. Die äußeren Lanthanidatome sind durch zusätzliche Nitrationen neunfach koordiniert, woraus eine dreifach-überkappte trigonal-prismatische Geometrie resultiert. Der Dy-Komplex zeigt SMM-Verhalten[66].

Ein Ni(II)-Na-Komplex ist das bisher einzige literaturbekannte Beispiel für einen heterometallischen tetranuklearen Nickel-Komplex. Die Verbindung kann als Dimer, bestehend aus Azid-verbrückten [NiNa(oVan)$_2$(N$_3$)(DMF)]-Einheiten, betrachtet werden. Das

Strukturmotiv sind zwei flächenverknüpfte Würfel, denen je eine Ecke fehlt. Ein Nickelatom ist jeweils oktaedrisch koordiniert von den μ_2-Phenoxo- und μ_2-Aldehydgruppen zweier Ligandmoleküle, sowie zweier μ_3-Azidionen. Das Natriumatom ist pseudo-oktaedrisch koordiniert von den μ_2-Phenoxo-, μ_2-Aldehyd- und den Methoxygruppen zweier Ligandmoleküle, sowie einem Solvensmolekül[67].

Bei den heterometallischen Cobaltverbindungen ist ein $[Co_2Na_2(oVan)_4(N_3)_2(DMF)]$-Komplex bekannt[68], welcher isostrukturell zum oben beschrieben Nickelanalogon ist. Des Weiteren sind drei Co_2Ln_2-Komplexe mit Ln = Gd, Tb, Y b beschrieben. Auch diese Komplexe besitzen das bekannte Strukturmotiv der flächenverknüpften Würfel mit jeweils einer fehlenden Ecke (Abb. 14). Zwei μ_3–Hydroxidgruppen verbrücken die Metallzentren und liegen jeweils über- bzw. unterhalb der der Ebene, welche durch die Metallzentren definiert wird. Die Cobaltatome sind verzerrt oktaedrisch von den μ_3–Hydroxidgruppen, je zwei Phenoxo-, einer Aldehyd- und einer Methoxygruppe koordiniert. Die Lanthanidzentren sind neunfach koordiniert von einer Hydroxidgruppe, zwei Phenoxogruppen, sowie einer Methoxy- und Aldehydgruppe. Letztere stammen von unterschiedlichen Ligandmolekülen. Abgesättigt wird die Koordinationssphäre von zwei Nitrationen. Aus dieser Serie zeigt nur der Co-Gd-Komplex SMM-Verhalten[69].

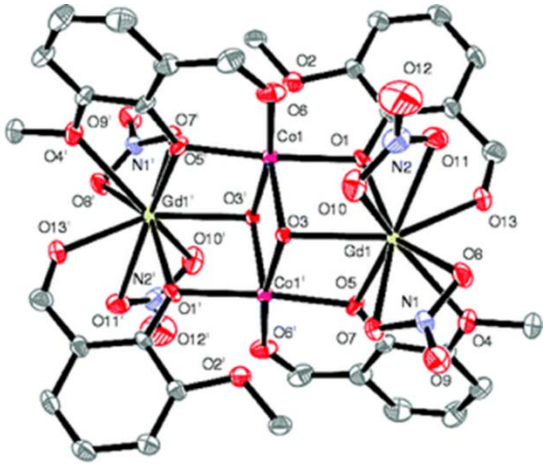

Abbildung 14: Kristallstruktur des Co-Gd-Komplexes. Die korrespondierenden Tb- und Y-Komplexe sind isostrukturell[69].

1.3.5 Hexanukleare Komplexe

Homometallische hexanukleare Verbindungen sind nur für Lanthanide bekannt. Durch zusätzliche Reaktanden lassen sich die in Kapitel 1.3.3 beschriebenen trinuklearen Dy-Einheiten mit Dreicksmotiv[58] zu hexanuklearen Dy-Komplexen verknüpfen (Abb. 15). Ein dazu isostruktureller Tm-Komplex wurde ebenfalls erhalten, allerdings unter anderen Reaktionsbedingungen. Ein Komplex mit gleichem Strukturmotiv kann ebenfalls bei

Verwendung von Dysprosiumnitrat hergestellt werden[70]. Die Dy_6-Komplexe zeigen SMM-Verhalten.

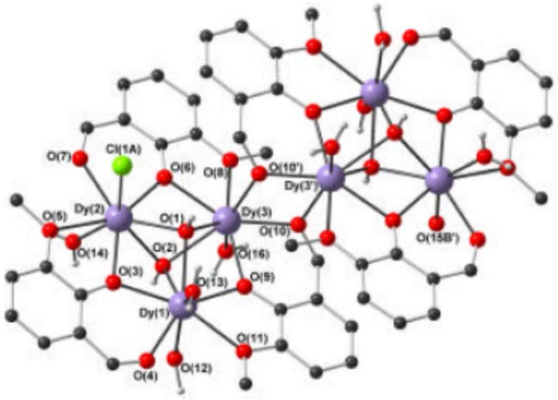

Abbildung 15: Kristallstruktur eines hexanuklearen Dy(III)-Komplexes[71], aufgebaut aus den bereits beschriebenen Dy_3-Einheiten[58]. Der ebenfalls erhaltene Tm_6-Komplex ist isostrukturell.

Bei Verwendung von Zink lassen sich isostrukturelle, heterometallische hexanukleare Komplexe mit Eu und Nd der Form $[Zn_4Ln_2]$ synthetisieren. Die Metallzentren werden von zwei Ligandmolekülen und einer μ_3-Hydroxidgruppe zu einer Zn_2Ln-Einheit verbrückt. Die beiden Zinkionen sind zusätzlich über ein Acetation verbrückt. Ein Nitration koordiniert an das Lanthanidatom. Dadurch ergeben sich drei unterschiedliche, käfigartige Koordinationsgeometrien: Das neunfach koordinierte Lanthanid ist verzerrt-trigonal-prismatisch von Sauerstoff umgeben, eines der Zinkionen wird verzerrt trigonal-bipyramidal von Sauerstoff koordiniert und das zweite Zinkion weist eine verzerrt quadratisch-pyramidale Koordinationsgeometrie auf. Die Verbrückung der Zn_2Ln-Einheiten geschieht über vier Acetationen. Dabei richten sich die Einheiten so zueinander aus, dass durch die Metallzentren zwei Zn_2Ln-Ebenen gebildet werden. Durch kurze intermolekulare C···H···O-Wechselwirkungen und π–π-Stacking zwischen den Aryleinheiten werden im Kristall zweidimensionale Schichten gebildet. Diese wiederum sind verlinkt durch C···H···O-Wechselwirkungen zwischen den Nitrationen und den Methoxygruppen. Dadurch wird ein dreidimensionales offenes Netzwerk mit Kanälen entlang der kristallographischen *b*-Achse generiert[72].

1.3.6 Heptanukleare Komplexe

Der homometallische Nickel-Komplex ist ein gemischt-valenter, dreifach positiv geladener scheibenartiger Komplex mit drei Perchloratanionen zum Ladungsausgleich (Abb. 16.). Alle

Ni(II)-Atome sind verzerrt oktaedrisch von μ_3-Hydroxidgruppe umgeben, welche die die peripheren Ni(II)-Atome mit dem zentralen Ni(III)-Atom verbinden.

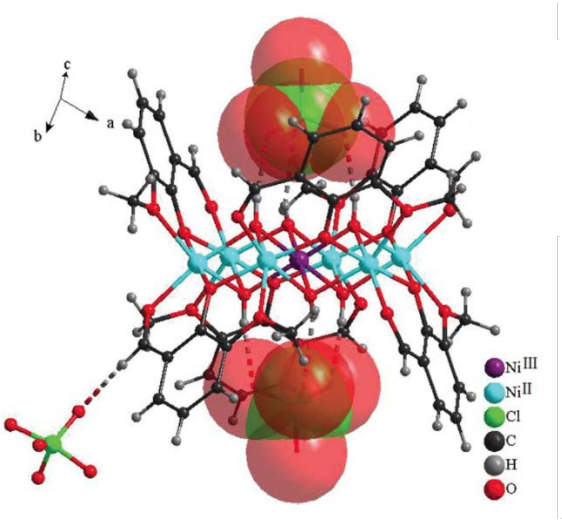

Abbildung 16: Kristallstruktur des heptanuklearen gemischt-valenten Komplexes $[Ni^{II}_6(OH)_6(oVan)_6Ni^{III}](ClO_4)_3$ [67].

Damit ergibt sich für das Ni(III)-Zentrum ebenfalls eine leicht verzerrt oktaedrische Koordinationsgeometrie. Die Liganden verbrücken ebenso die peripheren Ni(II)-Atome. Je drei Liganden liegen ober bzw. unterhalb der $Ni^{II}_6Ni^{III}$-Ebene.

Dadurch erhält der Komplex die Form einer doppelten Schüssel. Das Schüsselvolumen beträgt ungefähr 744 Å³. Zwei Perchloratgegenionen werden durch Wasserstoffbrückenbindungen innerhalb der Schüssel gehalten. Das dritte Perchloratanion, welches außerhalb liegt, verbindet durch schwache Wasserstoffbrückenbindungen insgesamt vier Doppelschüsseln miteinander, was zu einer supramolekularen dreidimensionalen Packung führt. Dieser heptanukleare Komplex zeigt dominante antiferromagnetische Wechselwirkungen [67].

Der heptanukleare heterometallische Komplex $[Fe_2(oVan)_8Na_5]\cdot 3OH\cdot 8H_2O$ (Abb. 17) kann als Dimer aus zwei unabhängigen Fe(III)-Einheiten betrachtet werden. Das Eisenzentrum ist verzerrt oktaedrisch von vier Liganden umgeben. Dabei können zwei unterschiedliche Koordinationsmodi beobachtet werden: Zwei der Liganden koordinieren ausschließlich über die Phenoxogruppe zum Eisen, während die anderen beiden chelatartig über die Phenoxo- und die Aldehydgruppe koordinieren. Die mono- und bidentaten Liganden befinden sich in *cis*-Position zueinander. Die beiden Eiseneinheiten sind verbunden durch eine von vier Natriumionen aufgespannte, stark verzerrte quadratische Ebene, in deren Zentrum sich das fünfte Natriumion befindet. Das zentrale Natriumatom ist umgeben von acht Sauerstoffatomen von den organischen Liganden. Die peripheren Natriumatome sind siebenfach von Sauerstoff

koordiniert. Sechs Sauerstoffatome stammen vom organischen Liganden und eines entweder von den Hydroxidgruppen oder Wasser[73].

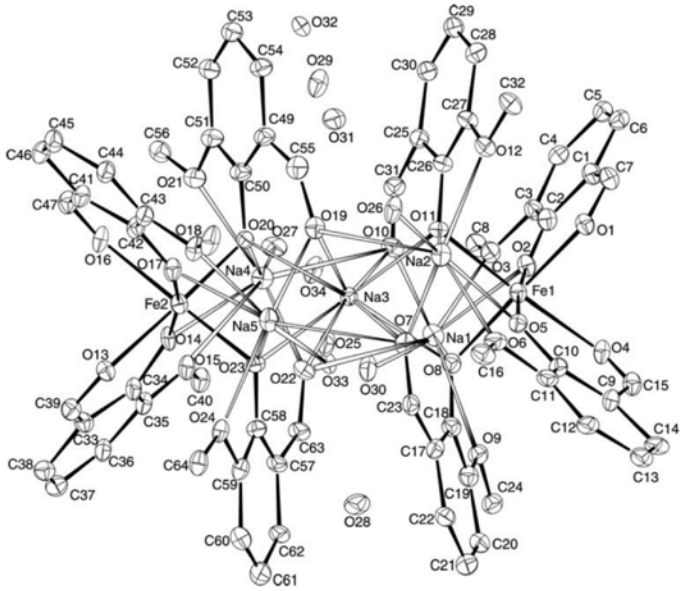

Abbildung 17: Kristallstruktur des heptanuklearen Komplexes $[Fe_2(oVan)_8Na_5]\cdot 3OH\cdot 8H_2O$[73].

1.4 Schiff'sche Basen mit *ortho*-Vanillin und deren Metallkomplexe

Obwohl mit *ortho*-Vanillin die Aldehydquelle festgelegt ist, ist die strukturelle Vielfalt an damit gewonnen Schiff'schen Basen dennoch sehr hoch. Diese Vielfalt spiegelt sich auch in deren Eigenschaften wieder. Nicht nur Metallkomplexe mit *ortho*-Vanillin sind hinsichtlich ihrer magnetischen Eigenschaften sehr interessant, gleiches gilt auch für Metallkomplexe mit auf *ortho*-Vanillin basierenden Schiff'schen Basen[74]. Darauf soll an dieser Stelle aber nicht näher eingegangen werden. Ebenfalls aus dem Bereich der Materialforschung wird über das katalytische Potenzial von Metallkomplexen auf *ortho*-Vanillin basierenden Schiff'schen Basen berichtet. Dinukleare Zink-Salen-Komplex mit Liganden, synthetisiert aus *ortho*-Vanillin und (±)-trans-1,2-Diaminocyclohexan (L1) oder 2,2-Dimethyl-1,3-propandiamin (L2) katalysieren die Ringöffnungscopolymerisation von Kohlenstoffdioxid und Cyclohexenoxid bzw. Kohlenstoffdioxid und Phthalsäureanhydrid sowie die Terpolymerisation von Kohlenstoffdioxid, Cyclohexenoxid und Phthalsäureanhydrid. Dabei erwies sich der Komplex mit L2 am potentesten[75]. Eine Serie von $Ni^{II}_2Ln^{III}_2$-Komplexen (Ln = Dy[76], Y, Sm, Eu, Gd, Tb[77]) mit einem Schiff'sche Base-Ligand aus *ortho*-Vanillin und 2-Aminophenol (L1, Abb. 18A) bzw. 3-Amino-2-napthol (L2, Abb. 18B) wurde hinsichtlich ihres Katalysepotenzials bei der Elektrozyklisierung untersucht. Lediglich vom Dy-Komplex mit L1 (Abb. 18C) und von dem Y-Komplex mit L2 konnte eine Kristallstruktur erhalten werden (Abb. 18D). Von den

anderen Lanthanid-Komplexen mit dem Liganden L1 wurden nur amorphe Pulver erhalten. Dennoch lassen die analytischen Daten darauf schließen, dass die Strukturen analog zum Dy-Komplex sind.

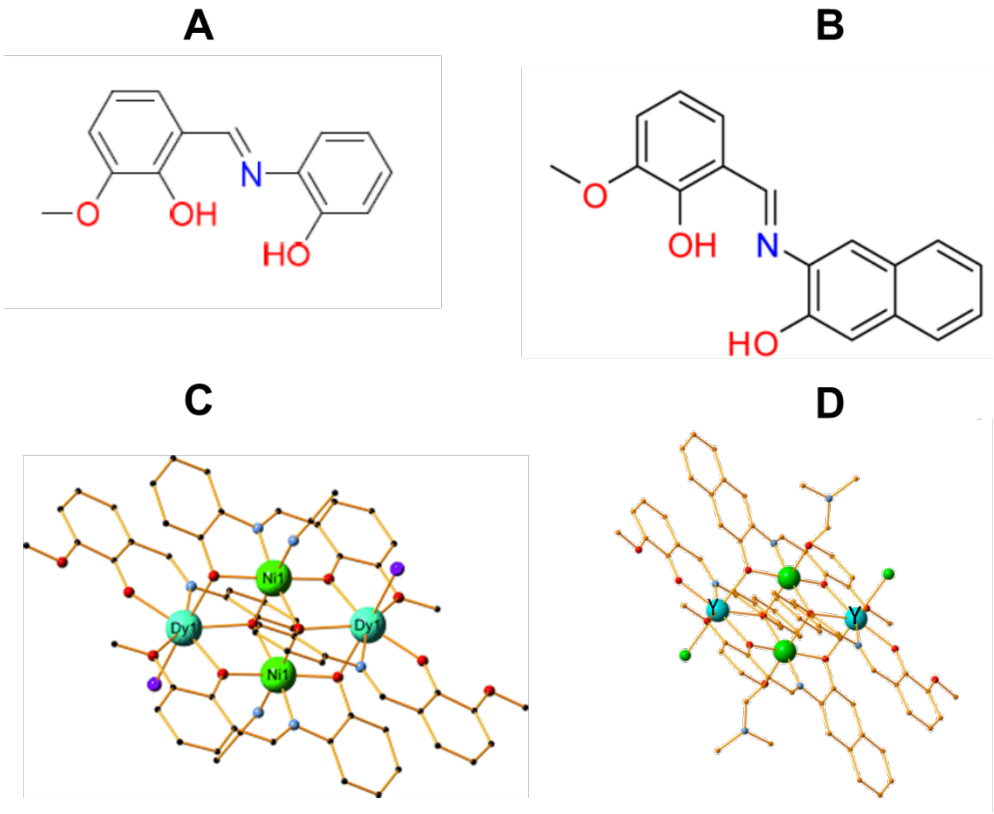

Abbildung 18: A) Ligand L1 aus *ortho*-Vanillin und 2-Aminophenol[77]. B) Ligand L2 aus *ortho*-Vanillin und 3-Amino-2-napthol[77]. C) Dy-Komplex mit L1[76]. D) Y-Komplex mit L2[77].

Als Prototyp, um das katalytische Potenzial der Komplexe einschätzen zu können, diente die Reaktion von Furan-2-aldehyd mit Morpholin. Verglichen mit simplen Ni- und Ln-Salzen konnten alle Komplexe die Prototypreaktion signifikant katalysieren. Der Dy(L1)- sowie der Y(L1)-Komplex stachen mit quantitativen Umsetzungen aus dieser Reihe hervor. Mit diesen beiden Komplexen, sowie dem Y(L2)-Komplexen und weiteren Y-Komplexen wurde weiterführend das katalytische Potenzial für die Reaktionen von Furan-2-aldehyd mit mehr oder weniger komplexen sekundären und primären Aminen untersucht. Für nahezu alle untersuchten Reaktionen wurden moderate bis quantitative Umsetzungen beobachtet. Insbesondere bei den substituierten Anilinen konnten mit den Y-Komplexen deutlich höhere Umsetzungen erzielt werden, verglichen mit dem Dy-Komplex[77].

Zwei Pd(II)-Komplexe wurden mit Schiff'schen Basen aus *ortho*-Vanillin und 4-Methylbenzylamin bzw. 4-Fluorobenzylamin (Abb. 19) erhalten. Ihr katalytisches Potenzial wurde für die Heck-Reaktion von Iodbenzol mit Acrylsäuremethylester untersucht. Mit einer

Beladung von 1 mmol% konnte nach 6 h bei 100 °C eine 100%ige Umsetzung beobachtet werden[78].

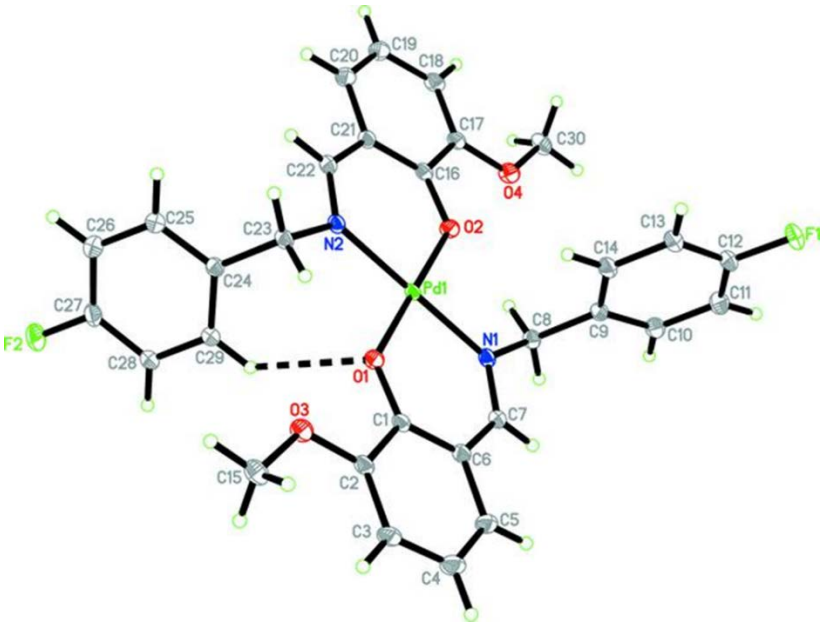

Abbildung 19: Kristallstruktur des Pd(II)-Komplexes mit einem Liganden aus *ortho*-Vanillin und 4-Fluorobenzylamin[79].

Fe(III)-Salen-Komplexe mit Liganden, synthetisiert aus *ortho*-Vanillin und 1,2-Phenylendiamin (Fe-SP)[80–82] (Abb. 20) bzw. Ethylendiamin[82], zeigten sich als hochwirksame anticancerogene Verbindungen. Insbesondere Fe-SP zeigte sich toxisch gegenüber Zelllinien verschiedensten Ursprungs, ist aber nicht selektiv für bestimme Tumortypen. Unter den getesteten Zelllinien befanden sich auch Zelllinien (OVCAR-3 und SKOV-3), welche eine Resistenz gegenüber klinisch relevanten Konzentrationen von gängigen Zytostatika wie Adriamycin, Melphalan und *Cis*-Platin aufweisen. Selbst bei diesen Zelllinien konnte eine Abnahme der Zellviabilität bis deutlich unter 20% bei einer Konzentration von 3 µM beobachtet werden. Erste *in vivo*-Studien an Ratten zeigten, dass Fe-SP keine systemische Toxizität verursacht, was die Verbindung für weitere *in vivo*-Studien interessant macht[80]. Die Fe(III)-Salen- und Salphen-Komplexe verursachen den Zelltod durch Induzierung von Apoptose über den mitochondrialen Pfad und die Caspase-Aktivierung[82]. Der freie Ligand hingegen weist keine signifikante Zytotoxizität auf.

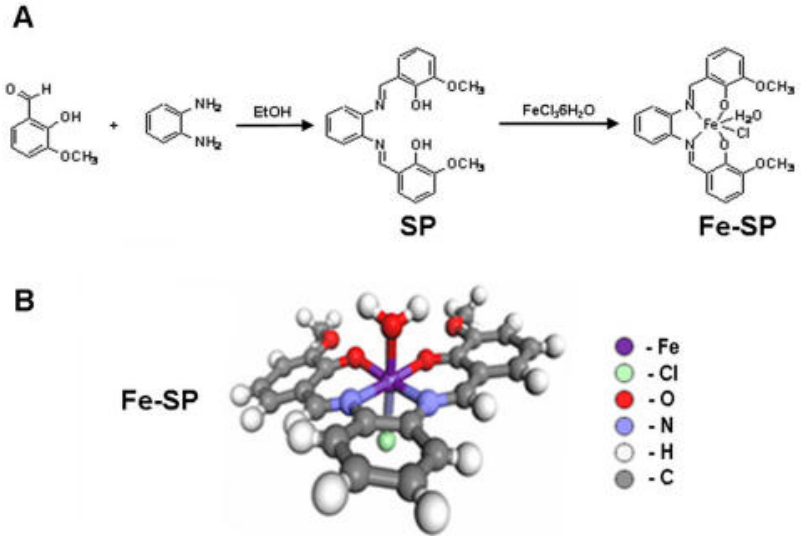

Abbildung 20: Syntheseschema und Kristallstruktur eines Fe(III)-Komplexes mit einem Salen-Liganden basierend auf *ortho*-Vanillin und 1,2-Phenylendiamin[80].

Ebenfalls potent zytotoxisch und antioxidativ sind Ru(III)-Salen-Komplexe mit Schiff'sche Base-Liganden aus *ortho*-Vanillin und S-Methylthiosemicarbazid, sowie Triphenylphosphin- bzw. Triphenylarsin-Co-Liganden. Zur Bestimmung des zytotoxischen Potenzials wurden nur die Triphenylarsin-haltigen Komplexe herangezogen. Gegenüber der Brustkrebszelllinie MCF-7 zeigte sich der auf *ortho*-Vanillin basierende Komplex mit einem IC_{50}-Wert von 0.90 µM am wirksamsten verglichen mit den anderen drei Komplexen, bei denen zur Generierung des Liganden Salicylaldehyd bzw. Derivate davon verwendet wurden und dem Standard *Cis*-Platin (IC_{50} = 12.33 µM). Mittels *in vitro*-Antioxidant-Assays wurde das Potenzial der Komplexe als Radikalfänger zu agieren für verschiedene, in Zellen vorkommende Radikale, untersucht. Alle untersuchten Komplexe (auch die Triphenylphosphin-haltigen) wiesen ein deutlich höheres Antioxidationsvermögen auf als die Standards Vitamin C und Butylhydroxytoluol (BHZ). Auch hierbei schnitt der *ortho*-Vanillin -haltige Komplex (Nr. 7) am besten ab[83].

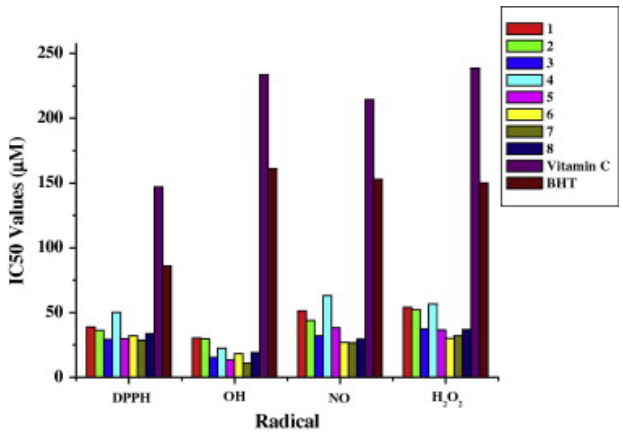

Abbildung 21: Antioxidant-Studie: IC_{50}-Werte von verschiedenen Ru(III)-Komplexen und Standardantioxidantien[83].

Auch Komplexe mit Nicht-Salen-Liganden sind potent zytotoxisch. Eine Serie mononuklearer Cu(II)-Komplexe mit einem Liganden aus *ortho*-Vanillin und 8-Aminochinon, sowie verschiedenen Bipyridinderivaten als Co-Liganden, sind hoch wirksam gegenüber vier getesteten Zelllinien. Die IC_{50}-Werte der Komplexe lagen mehr als das Zehnfache unter denen der Referenz *Cis*-Platin. Den stärksten zytotoxischen Effekt mit IC_{50} = 0.93 µM zeigte der Komplex mit Dipyridophenazin (dppz) als Co-Ligand. Der freie Schiff'sche Base-Ligand (IC_{50} = 4.04 µM) und dppz (IC_{50} = 3.00 µM) besaßen ebenfalls einen höheren antiproliferativen Effekt als *Cis*-Platin (IC_{50} = 12.06 µM) für die getestete Zelllinie SCC15[(84)]. Verschiedene mononukleare Organozinn(IV)-Komplexe (Abb. 22; Verbindungen 1, 2, 4) sowie ein supramolekularer Komplex, erzeugt durch intermolekulare Sn-N-Wechselwirkungen (Abb. 22; Verbindung 5), bei denen Pyridin-4-carbohydrazid die Aminquelle darstellt, wurden hinsichtlich ihres Effektes auf das Wachstum von fünf *Cis*-Platin-resistenten Zelllinien untersucht. Die organischen Reste sind dabei entscheidend. Die Verbindungen mit *n*-Buytl- bzw. Phenylresten am Zinn zeigten bei allen fünf Zelllinien einen stark hemmenden Effekt auf das Zellwachstum. Der Komplex mit den deutlich kleineren Methylresten zeigte zwar bei zwei der fünf Zelllinien einen signifikanten inhibitorischen Effekt, allerdings schwächer als die *n*-Butyl- und Phenyl-Spezies. Zu groß dürfen die Reste allerdings auch nicht sein, wie der Komplex mit Octylgruppen am Zinn beweist. Dieser Komplex ist wirksam gegen vier der fünf Zelllinien, aber signifikant schlechter als die *n*-Butyl- und Phenyl-Komplexe (Abb. 22; Tabelle)[(85)].

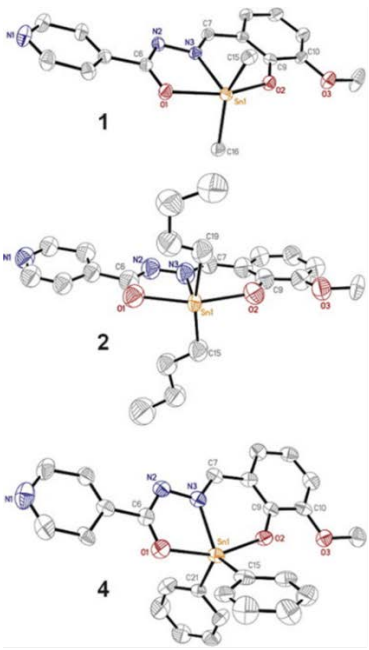

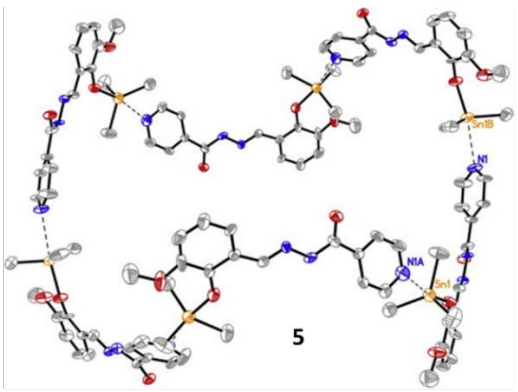

Compound	IC_{50} (µg/mL)				
	Caco-2	A549	HT-29	HCT-116	HL-60
1	>10	>10	4.73 ± 0.68	>10	2.58 ± 0.41
2	2.12 ± 0.33	1.23 ± 0.09	0.43 ± 0.36	0.57 ± 0.25	0.18 ± 0.75
3	>10	7.44 ± 0.87	3.79 ± 0.58	3.97 ± 0.60	0.69 ± 0.16
4	1.75 ± 0.24	1.61 ± 0.21	1.18 ± 0.07	1.09 ± 0.03	0.18 ± 0.74
5	>10	10.33 ± 1.01	5.37 ± 0.73	4.20 ± 0.62	1.79 ± 0.25
Cisplatin	>60	>60	>60	53	>60

Abbildung 22: Kristallstrukturen von verschiedenen Organozinn(IV)-Verbindungen mit einem Liganden aus *ortho*-Vanillin und Pyridin-4-carbohydrazid, sowie Ergebnisse des MTT-Assays[(85)].

Neben antiproliferativen Eigenschaften von *ortho*-Vanillin-basierten Schiff'schen Basen und korrespondierender Metallkomplexe sind auch antimikrobielle und antivirale Effekte bekannt. So zeigt beispielsweise eine Schiff'sche Base aus *ortho*-Vanillin und 1-(7-Methoxyquinolin-4-yl)-5-methyl-1H-1,2,3-triazol-4-carbohydrazid antibakterielle Aktivität gegenüber den getesteten Organsimen *B.subtilis, S. haemolytius, P. aeruginosa* und *K. pneumoniae*. Der inhibitorische Effekt auf das Wachstum liegt dabei etwas unter dem der Referenz Ciprofloxacin. Gegenüber den Pilzen *A. niger* und *C. albicans* erwies sich diese Schiff'sche Base ebenfalls als wirksam. Die Aktivität lag im Bereich der Referenz Fluconazol[(86)]. Aus einer Reihe Übergangsmetallkomplexe mit Liganden aus *ortho*-Vanillin und 2-Amino-3-hydroxypyridin zeigte der Fe(III)-Komplex gegenüber *F. oxysporum* antifungales Potenzial, welches im Bereich von Fluconazol lag [(87)]. Ein mononuklearer Oxovanadium(IV)-Komplex, bei dem der Ligand mit Benzohydrazid als Aminquelle synthetisiert wurde (Abb. 23), erwies sich als gleichermaßen aktiv gegen *B. cereus* und *S. aureus* wie die Referenz Ciprofloxacin[(88)].

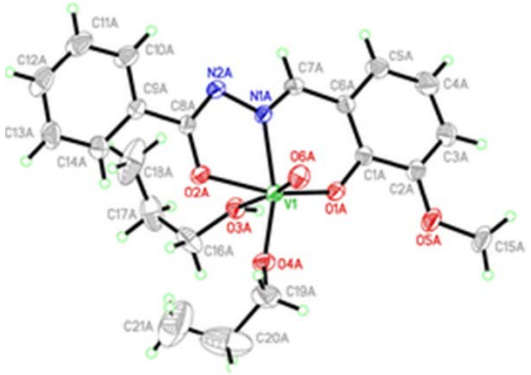

Abbildung 23: Kristallstruktur eines Oxovanadium-Komplexes mit einem Liganden aus *ortho*-Vanillin und Benzohydrazid[(88)].

Des Weiteren zeigen sowohl eine Schiff'sche Base, gewonnen aus *ortho*-Vanillin und Salicylhydrazid, sowie deren Mg-, Mn-, Co-, Ni-, Cu- und Zn-Komplexe mit variierenden Nuklearitäten antivirale Effekte gegenüber den Herpes-simplex-Viren HSV-1, HSV-2 und HSV-1/TK$^-$ (Acyclovir-resistent) und dem Vacciniavirus. Als Referenzen dienten insgesamt sechs verschiedene Virostatika. Am wirksamsten waren dabei die Mg-, Mn- und Zn-Komplexe. Bei HSV-1/TK$^-$ und dem Vacciniavirus lagen die EC_{50}-Werte im Bereich der Referenzvirostatika oder niedriger. Gegenüber RNA-Viren, wie z.B. dem HI-Virus, waren alle getesteten Verbindungen inaktiv[(89)]. Analgetisches, antipyretisches und antiinflammatorisches Potenzial wurde für mononukleare Zn- und Cu-Komplexe mit einem Liganden, bei dem 2-Aminobenzimidazol die Aminquelle darstellt, *in vivo* nachgewiesen. Verglichen mit den Standards Paracetamol und Diclofenac waren die Komplexe weniger aktiv[(90)].

1.5 Stand der Literatur – Schiff'sche Basen aus *ortho*-Vanillin und Aminosäuren und deren Metallkomplexe

Von den 20 proteinogenen Aminosäuren kommen bis auf Prolin alle als Aminquelle für die Synthese von Schiff'schen Basen mit *ortho*-Vanillin und korrespondierender Metallkomplexe in Frage. In diesem Kapitel soll der Stand der Forschung zu Beginn dieser Arbeit für die in dieser Arbeit behandelten Systeme dargelegt werden.

1.5.1 System *ortho*-Vanillin/*L*-Glutaminsäure

Beschrieben wurde die Synthese der Schiff'schen Base aus *ortho*-Vanillin und *L*-Glutaminsäure sowie deren Cobaltpentaamin- und tetraamin-Komplexe erstmals 1977[(91)]. Synthetisiert wurde der Ligand nach einer Vorschrift für das entsprechende Salicylaldehydanalogon[(92)]. Die Komplexe wurden in dieser und einer Folgestudie[(93)] mittels IR (vier Banden angegeben) charakterisiert und polarographisch untersucht. Aufgrund der IR-Daten schlussfolgerten die Autoren, dass es sich um mononukleare Co(III)-Komplexe handelt, bei denen der Ligand entweder monodentat (Pentaamin-Komplex) oder bidentat (Tetraamin-Komplex) ist. Aus den Polarogrammen in 0.1 *M* Essigsäure wurden Stabilitätskonstanten und die Parameter ΔH, ΔG und ΔS berechnet. Die *ortho*-Vanillin-Glutaminsäure-Komplexe besaßen eine niedrigere Stabilitätskonstante als die ebenfalls untersuchten Glycin- und Asparaginsäurekomplexe. Die untersuchten Tetraamin-Komplexe besaßen eine höhere Stabilitätskonstante als die Pentaamin-Komplexe.

Ebenfalls polarographisch untersucht wurde ein Chrom(III)-pentaamin-Komplex mit Perchlorat als Anion. Dieser Komplex wurde durch Elementaranalyse der Elemente Chrom, Kohlenstoff und Stickstoff, sowie IR (drei Banden angegeben) charakterisiert. Die maximale Absorption wurde mit 525 nm bestimmt. Außerdem wurde eine irreversible Reduktion zu Cr(II) beobachtet[(94)]. Das Reduktionsverhalten wurde in einer Folgepublikation tiefergehend untersucht[(95)].

Weiterhin erschienen Artikel zu diesem System in zwei chinesischsprachigen Magazinen. So wurden Cu(II)- und Zn(II)-Komplexe synthetisiert und charakterisiert. Das Potenzial des Cu(II)-Komplexes als Radikalfänger zu agieren wurde mittels ESR untersucht[(96)]. Cr(III)- und Mo(II)-Komplexe wurden synthetisiert und charakterisiert und die Interaktion mit DNA untersucht. Dabei wurde eine bathochrome Verschiebung beobachtet[(97)]. Außerdem wurde das Komplexierungsverhalten der Schiff'schen Base mit Co(II), Ni(II), Cu(II) und Zn(II) mittels

potentiometrischen Methoden untersucht. In 1:1-Komplexen bindet der Ligand tetradentat und tridentat in 1:2-Komplexen. Die Komplexstabilität folgt der Irving-Williams-Reihe[98].
Die drei zuletzt zitierten Publikationen waren im Rahmen der Literaturrecherche nicht zugänglich. Die genannten Resultate wurden den Abstracts entnommen.

1.5.2 System *ortho*-Vanillin/*L*-Glutamin

Nair *et al.* veröffentlichten die Synthese und Charakterisierung einer Serie von Co(II)-, Ni(II)-, Cu(II)- und Zn(II)-Komplexen mit Liganden, welche aus der Kondensation von *ortho*-Vanillin mit den Aminosäuren *L*-Valin, *L*-Glutamin und *L*-Histidin erhalten werden. Die erhaltenen Komplexe wurden mittels spektroskopischen Methoden, Elementaranalyse, molarer Leitfähigkeit und magnetischen Messungen charakterisiert. Darüber hinaus wurden Studien in Lösung vorgenommen und die antimikrobielle Aktivität bestimmt. Der Vergleich der IR-Daten zwischen den freien Liganden und den Komplexen zeigt eine Verschiebung der Banden der C=N-Streckschwingung zu niedrigeren Frequenzen und eine Verschiebung der phenolischen Sauerstoff-Streckschwingung zu höheren Frequenzen in den Komplexen. Außerdem werden neue Banden in den Regionen 438–410 cm^{-1} (M–O-Schwingung) und 516–505 cm^{-1} (M–N-Schwingung) beobachtet. Weiterhin konnten die Banden für die symmetrische und asymmetrische Schwingung der koordinierten Carboxylgruppe identifiziert werden. Dies lässt den Schluss zu, dass die Schiff'schen Basen über die Phenoxo-Gruppe, dem Stickstoffatom der Imingruppe und die Carboxygruppe an das Metallzentrum binden. Im Falle von Histidin wird das Metall zusätzlich über das Stickstoffatom der Imidazolgruppe koordiniert. Sowohl aus den magnetischen Messungen (μ_{eff} –Werte), als auch aus den UV/VIS-Spektren wird deutlich, dass die Nickelzentren eine tetraedrische und die Kupferzentren eine quadratisch-planare Koordinationsgeometrie aufweisen. Für die Cobalt-Komplexe ergibt sich mit dem Histidin-basierten Liganden eine quadratisch-planare und mit den beiden anderen Aminosäuren eine tetraedrische Koordinationsgeometrie. Aus der Elementaranalyse schlussfolgern die Autoren, dass es sich bei den synthetisierten Komplexen um mononukleare Komplexe handeln muss, wobei im Falle der Glutamin- und Valin-basierten Liganden ein zusätzliches Wassermolekül an das Metallzentrum koordiniert. Die molare Leitfähigkeit bei Raumtemperatur stand ebenfalls im Einklang mit der Erwartung eines neutralen Komplexes aus einem zweifach positiv geladenem Ion und einem dianionischen Ligand. Die Cu(II)-Komplexe sowie die freien Liganden wurden auf ihr antimikrobielles Potenzial gegenüber *S. aureus E. coli.* und *S. typhi* untersucht. Als Referenz diente Ampicillin. Die freien Liganden zeigten eine deutlich geringere antibakterielle Aktivität als die Metallkomplexe und Ampicillin. Die Metallkomplexe zeigten

allesamt eine höhere Aktivität als der Standard. Besonders aktiv war der Cu(II)-Komplex mit dem Glutamin-basierten Liganden[(99)].

In zwei Publikationen von Xiao *et al.*, die kurz nacheinander eingereicht wurden, wurde über die Synthese und die Eigenschaften eines trinuklearen Kupferkomplex mit einem Liganden aus *ortho*-Vanillin und *L*-Glutamin (GVC) berichtet. Die chronologisch frühere Veröffentlichung ist eine reine molekularbiologische Arbeit. Dabei wurde festgestellt, dass GVC bei einer Konzentration von 50 µM die Proliferation von MDA-MB-231-Zellen, einer humanen Brustkrebszelllinie, um ca. 75% inhibiert. Der freie Ligand inhibierte das Wachstum nur zu ca. 40%. Kupfer(II)-chlorid hatte nur einen sehr geringen Effekt. Um zu untersuchen, ob GVC in der Lage ist, die Proteasomaktivität von Tumorzellen zu hemmen, wurden Zellen der Linie MDA-MB-231 für 24 h mit GVC, dem freien Liganden oder Kupfer(II)-chlorid inkubiert. Anschließend wurden die Proteine extrahiert und die proteasomale Chymotrypsin-ähnliche Aktivität bestimmt. Dabei zeigt sich bei einer Konzentration 25 bzw. 40 µM eine Inhibition von 65% bzw. 80% bei GVC. Außerdem wurde eine Akkumulation von verschiedenen ubiquitinierten Proteinen beobachtet, ebenfalls ein Zeichen für die Inhibition der Proteasomaktivität. Der freie Ligand und Kupfer(II)-chlorid hatten keinen Effekt. Gleichsam zeigte sich bei Inkubation mit GVC eine Veränderung der zellulären apoptotischen Morphologie. Es konnte die Produktion von apoptotischen Nuklei in den Zellen festgestellt werden. GVC induzierte also konzentrationsabhängig die Inhibition der Proteasomaktivität und Apoptose. Daraufhin wurde der Zusammenhang zwischen Inhibition der Proteasomaktivität und Induzierung der Apoptose näher betrachtet. Die Zellen wurden mit GVC inkubiert und in verschiedenen Zeitintervallen über 24 h die Proteasominhibition und die Anzeichen für Apoptose untersucht. Nach 2 h konnte eine Inhibition von ca. 45% und die damit verbundene Akkumulation von ubiquitinierten Proteinen beobachtet werden, welche danach stabil blieb. Erst 16 h nach der Inkubation konnten zelluläre Apoptosemarker sowie eine Änderung der Zellmorpholgie beobachtet werden. Daraus schlussfolgerten die Autoren, dass die durch GVC induzierte Inhibition der Proteasomaktivität die Apoptose auslöst. Um zu überprüfen, ob dieser Effekt auch bei anderen Tumorarten auftritt, wurden die Versuche mit Zellen der Linie Jurkat (Akute T-Zell-Leukämie) wiederholt. Bei einer Konzentration von 50 µM an GVC lag die Zellviabilität <10%. DMSO, der freie Ligand und Kupfer(II)-chlorid hatten bei gleicher Konzentration keinen Effekt. Die Inhibition der Proteasomaktivität setzte bereits früher als 2 h nach der Inkubation ein. Apoptosemarker wurden nach 20 h beobachtet. Die Änderung der Zellmorphologie setzte bereits nach 8 h ein. Auch bei dieser Zelllinie wird die Apoptose durch die Inhibition der Proteasomaktivität, ausgelöst durch GVC, induziert. Bemerkenswerterweise

hatte GVC auf Nicht-Tumorzellen der Linie MCF-10A keinen Effekt. GVC erwies sich damit als selektiv für Tumorzellen[(100)].

In der zweiten Publikation von Xiao *et al.* wurde die Synthese der Schiff'schen Basen aus *ortho*-Vanillin mit *L*-Glutamin (GVC), sowie mit *L*-Asparagin als Lithiumsalz und die Synthese von korrespondierenden Kupfer-Komplexen beschrieben. Die erhaltenen Verbindungen wurden mittels molarer Leitfähigkeit, Elementaranalyse, UV/Vis- und IR-Spektroskopie, ^{1}H-NMR und TG-DTG charakterisiert. Die Geometrien der freien Schiff'schen Basen wurde mit der Hartree–Fock-Methode und elektronischer Absorptionspektroskopie untersucht. Außerdem wurde das antibakterielle und antiproliferative Potenzial der Verbindungen bestimmt. Da beide Aminosäuren je zwei Aminogruppen tragen, könnte die Kondensation mit *ortho*-Vanillin theoretisch an beiden Aminogruppen erfolgen. Allerdings ist die Aktivierung der jeweiligen Gruppe pH-abhängig. Daher wurde Lithiumhydroxid als Deprotonierungsreagenz gewählt, um nur die α-Aminogruppe zu aktivieren. Die terminale Aminogruppe benötigt zur Aktivierung einen pH-Wert von 10. Die Komplexsynthese erfolgte mit dem fertigen Liganden. Auf Grund der UV/Vis-Spektren wird für die Koordinationsgeometrie für den Komplex mit *L*-Glutamin eine verzerrte quadratische Pyramide und für den Komplex mit *L*-Asparagin ein verzerrter Oktaeder angenommen. Der Vergleich der IR-Spektren zwischen den freien Liganden und den Komplexen zeigt zum einen die bereits erwähnten Verschiebungen der Banden für die C=N-Streckschwingung zu niedrigeren Wellenzahlen und der phenolischen Sauerstoff-Streckschwingung zu höheren Wellenzahlen in den Komplexen. Auch die Verschiebungen für die symmetrischen und asymmetrischen Schwingungen der Carboxygruppen sind sichtbar. Ebenfalls beobachtet wurden zusätzliche Banden für die M–O-Schwingung und M–N-Schwingung. Die Schwingungen der terminalen Amino- und Methoxygruppen sind jeweils unverändert. Dies lässt schlussfolgern, dass die Koordination an das Metallzentrum über das Stickstoffatom der Iminfunktion, die Phenoxo- und die Carboxygruppe erfolgt. Die terminale Amino- und die Methoxygruppe sind nicht an der Koordination beteiligt. Im ^{1}H-NMR in DMSO sind ebenfalls Unterschiede in den Spektren zwischen dem freien *L*-Glutamin-basierten Liganden und dem korrespondierenden Kupfer-Komplex zu beobachten. Während der Ligand bei 14.23 ppm ein Signal aufweist, welches dem phenolischen Proton zugeordnet wird, verschwindet dieses Signal im Spektrum des Komplexes. Außerdem ist eine Tieffeldverschiebung der Signale der aromatischen Protonen und des Protons an der Imingruppe sichtbar. Die Lage des Signals der Methoxygruppe ist nahezu unverändert. Diese Ergebnisse lassen ebenfalls den Schluss zu, dass die Imninfunktion und die Phenoxogruppe, jedoch nicht die Methoxygruppe an der Koordination beteiligt sind. In den NMR-Spektren sind

jedoch keine Integrale angegeben. Die Ergebnisse der Rechnung nach der Hartree–Fock-Methode sind in Abbildung 24 dargestellt.

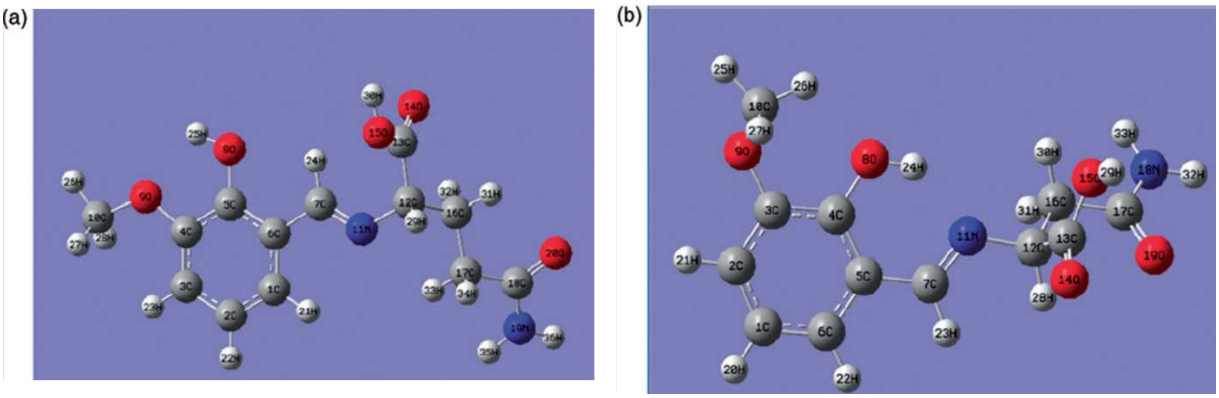

Abbildung 24: Berechnete stabile Geometrien der Schiff'schen Basen mit a) *L*-Glutamin und b) *L*-Asparagin[(101)].

Das Stickstoffatom im *L*-Glutamin-basierten Liganden ist nicht-planar mit dem Sauerstoffatom der Phenoxogruppe und dem aromatischen Ring, aber coplanar im Liganden mit *L*-Asparagin. Die zusätzliche Methylengruppe in *L*-Glutamin macht diesen Liganden empfänglich für eine von *L*-Asparagin verschiedene Koordination des Kupfers. Obwohl in der Publikation keine Daten der Elementaranalyse präsentiert wurden, schließen die Autoren daraus und den anderen analytischen Daten, dass sich mit dem *L*-Asparagin-basierten Liganden ein mononuklearer Komplex und mit dem *L*-Glutamin-basierten Liganden ein trinuklearer Komplex bildet (Abb. 24).

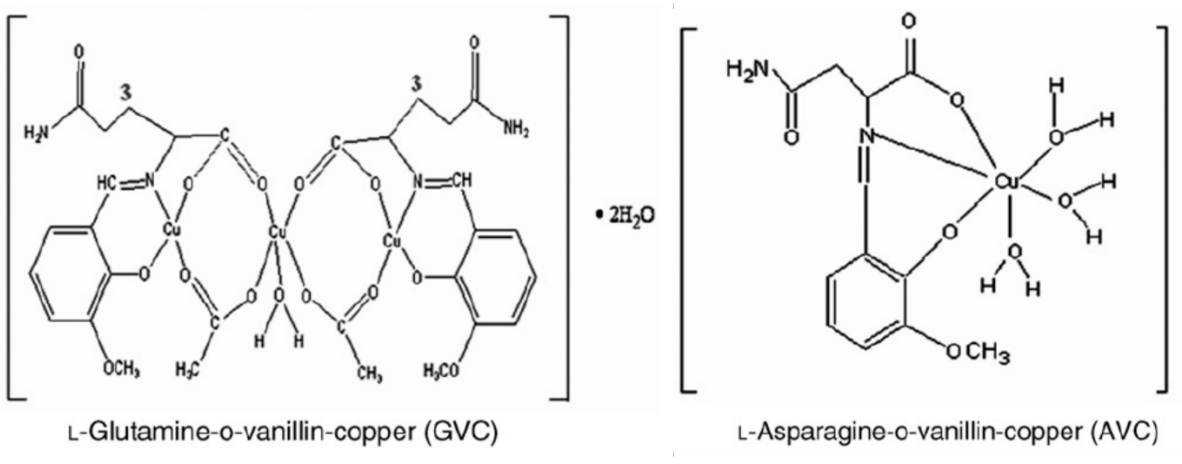

Abbildung 24: Strukturen der beschriebenen Cu(II)-Komplexe mit *L*-Glutamin und *L*-Asparagin-haltigen Liganden[(101)].

Das antibakterielle Potenzial der Liganden und der Komplexe wurde gegenüber *E. coli*, *P. aeruginosa*, *S. aureus* und *B. subtilis* untersucht. Laut den Autoren besaßen alle vier untersuchten Verbindungen antibakterielles Potetzial gegenüber allen Organismen. Dabei

zeigten die Komplexe eine höhere Aktivität als die freien Liganden. Die höchste antibakterielle Aktivität zeigte der Komplex mit dem *L*-Glutamin-basierten Liganden. Allerdings wurde kein Standard getestet, so dass nicht klar ist, wie aktiv die Verbindungen im Vergleich zu gängigen Antibiotika tatsächlich sind. Selbiges gilt auch für die antiproliferativen Eigenschaften gegenüber MDA-MB-231-Zellen. Der Komplex mit dem *L*-Glutamin-basierten Liganden inhibierte bei einer Konzentration von 50 µMol die Proliferation um ca. 80%, während es beim *L*-Asparagin-basierten Liganden nur ca. 40 % waren. Bei einer Konzentration von 10 µMol wurde die Proliferation nur zu ca. 20% bzw. 15% inhibiert. Auch beim Zytotoxizitätstest fehlte ein Standard[(101)].

Das bisher einzige kristallographisch belegte Beispiel für einen Komplex, welcher den Liganden aus *ortho*-Vanillin und *L*-Glutamin enthält, ist ein mononuklearer Nickel-Komplex mit 1,10-Phenanthrolin als Co-Ligand (Abb. 25). Ebenfalls in dieser Publikation enthalten ist die Kristallstruktur des entsprechenden Salicylaldehydanalogons.

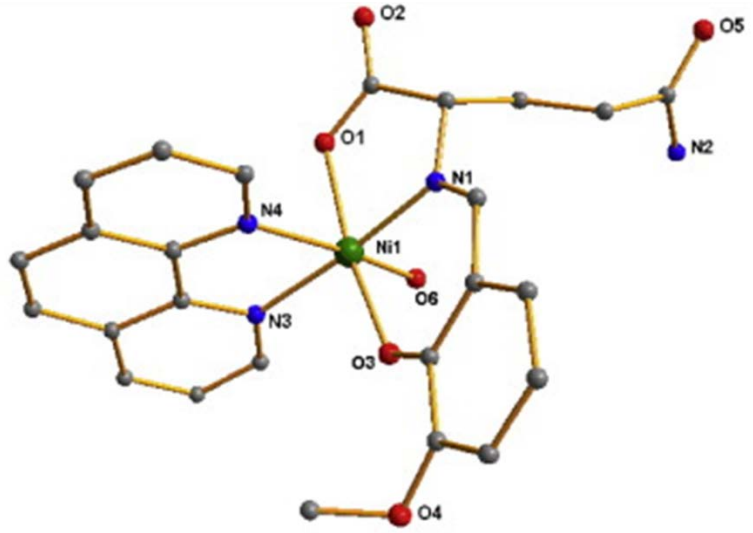

Abbildung 25: Kristallstruktur eines mononuklearen Ni(II)-Komplexes mit dem Liganden aus *ortho*-Vanillin und *L*-Glutamin[(102)].

Der Ligand wurde *in situ* synthetisiert und direkt mit Nickelacetat und 1,10-Phenanthrolin umgesetzt. Das Nickelzentrum ist oktaedrisch vom Stickstoffatom der Iminfunktion, den Stickstoffatomen des Phenanthrolins, der Phenoxogruppe und der Carboxygruppe koordiniert. Vervollständigt wird die Koordinationssphäre von einem Wassermolekül. Das Nickelatom liegt 0.03 Å über der äquatorialen Ebene. Durch intermolekulare N—H···O und O—H···O Wasserstoffbrückenbindungen wird ein supramolekulares 2D-Netzwerk entlang der kristallographischen *bc*-Ebene gebildet. Weiterhin wurde der Komplex durch IR und Elementaranalyse charakterisiert. Dabei entspricht Lage und Anzahl der relevanten Banden den

Erwartungen. Beide Komplexe wurden hinsichtlich ihrer Wechselwirkung mit DNA und BSA mittels UV-Absorption, Fluoreszenz- und CD-Spektroskopie und Viskositätsmessungen untersucht. Beide Komplexe binden über Interkalation an CT-DNA. Dabei zeigte der Komplex mit der Schiff'schen Base aus *ortho*-Vanillin eine stärkere Interaktion mit CT-DNA. Allerdings lagen die Bindungskonstanten niedriger als die des Referenzinterkalators Ethidiumbromid. Mittels CD-Spektroskopie konnte festgestellt werden, dass die Interkalation der Komplexe keinen signifikanten Einfluss auf die Helixkonformation hat. Beide Komplexe binden an BSA, wobei die Bindung einen Einfluss auf die Konformation des Proteins hat, was zu einem Verlust der α-Helix-Stabilität führt. Dabei zeigte wieder der Komplex mit der Schiff'schen Base aus *ortho*-Vanillin eine höhere Bindungsaffinität und eine stärkere Konformationsänderung. Außerdem zeigen beide Komplexe antioxidatives Potentzial[(102)].

1.5.3 System *ortho*-Vanillin/*L*-Tyrosin

Die Synthese, Charakterisierung und Proteinbindungseigenschaften des Liganden wurden 2011 von Gao *et al.* publiziert. Der Ligand wurde dabei als neutrale Verbindung, d.h. nicht als Salz, synthetisiert. Charakterisiert wurde der Ligand mittels Elementaranalyse, Schmelzpunktbestimmung und IR. Das Verhalten gegenüber BSA wurde mittels Fluoreszenzspektroskopie untersucht. Verglichen mit dem Liganden aus *ortho*-Vanillin und D-Phenylalanin zeigte der Tyrosin-haltige Ligand eine geringere Bindungsaffinität zu BSA. Im Vergleich mit dem Liganden, der *L*-3,4-Dihydroxyphenylalanin enthält, ist die Bindungsaffinität höher. Die verminderte Bindungsaffinität wird mit den Hydroxidgruppen am aromatischen Ring begründet. Durch diese wird nicht nur das π-Stacking behindert, sondern auch die elektrostatischen Wechselwirkungen zwischen Protein und Ligand vermindert. Die Bindung der Liganden erfolgt im Falle des Phenylalanin-basierten Liganden über die Tryptophanreste, bei den beiden anderen Liganden über die Tyrosinreste des Proteins[(103)].
Mit verschiedenen Lanthanidsalzen (La, Pr, Nd und Sm) wurden anionische Komplexe mit Kalium als Gegenion synthetisiert. Dieser Verbindungen wurden mittels Leitfähigkeitstitration, Bestimmung von μ_{eff}, Elementaranalyse, UV/VIS- und IR-Spektroskopie und thermischer Analyse charakterisiert. Aus den gewonnen Daten wurde geschlussfolgert, dass es sich um mononukleare Komplexe mit zwei Ligandmolekülen handelt[(104)].
Die Arbeitsgruppe um Dieter Reher veröffentlichte in mehreren Publikationen Synthesen und Kristallstrukturen von Oxovanadium-Komplexen mit Schiff'schen Basen aus Aminosäuren und verschiedenen substituierten Salicylaldehydderivaten. Dabei konnte u.a. die Struktur eines Oxovanadium(IV)-Komplexes mit einem Liganden aus *ortho*-Vanillin und *L*-Tyrosin erhalten

werden (Abb. 26). Die Synthese des Komplexes erfolgte in einer Eintopfreaktion in Methanol/Wasser. Der Komplex wurde mittels Elementaranalyse, IR- und UV/Vis-Spektroskopie, EPR und FAB-MS charakterisiert. Der Komplex weist eine beinahe ideale quadratisch-pyramidale Koordinationsgeometrie um das Metallzentrum auf. Dabei formen der tridentate Ligand und ein Wassermolekül die quadratische Ebene. Das doppelt gebundene Sauerstoffatom liegt in axialer Position und bildet die Spitze der Pyramide. Das Vanadiumatom liegt etwas oberhalb der Ebene. Durch Wasserstoffbrückenbindungen zwischen sauerstoffhaltigen Gruppen des Liganden, dem koordinierten Wassermolekül sowie weiteren Solvensmolekülen und π-π-Wechselwirkungen entsteht im Kristall ein supramolekulares Netzwerk[(105)].

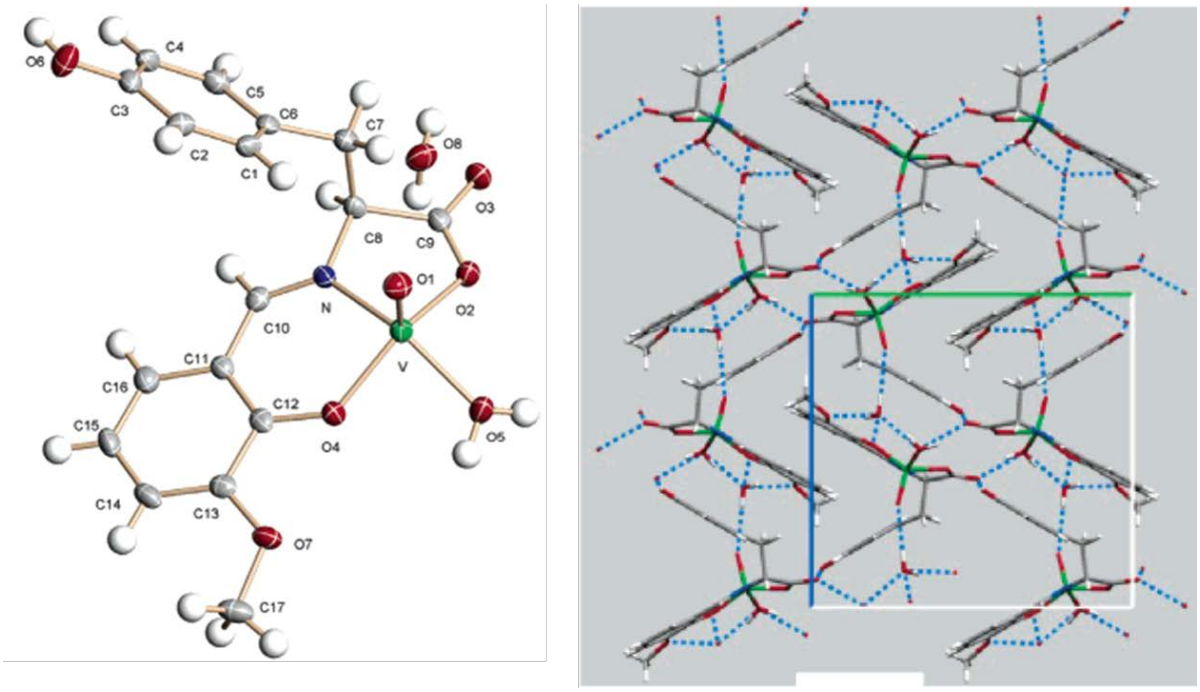

Abbildung 26: Kristallstruktur eines Oxovanadium-Komplexes mit einem Liganden aus *ortho*-Vanillin und *L*-Tyrosin und supramolekulare Packung[(105)].

In einer früheren Publikation wurden die Synthesen von Komplexen mit Ethanol und Wasser bzw. THF und Wasser als enthaltene Solventien beschrieben. Die Verbindungen wurden mittels Elementaranalyse, EPR und IR charakterisiert. Anhand dieser Daten wurde eine Struktur angenommen, wie in Abbildung 26 gezeigt[(106)]. Außerdem wurde über sie Synthese eines dinuklearen Oxovanadiumkomplexes berichtet. Dabei handelt es sich laut Strukturvorschlag um Sauerstoff-verbrückte mononukleare Einheiten. Das Vanadium ist jeweils sechsfach koordiniert. Dieser Strukturvorschlag wird gestützt durch eine Kristallstruktur eines Vanadiumkomplexes mit einem Liganden aus *ortho*-Vanillin und Serin. IR, ^{1}H- und ^{51}V-NMR und EPR stützen diese Annahme[(107)].

Rein kristallographisch beschrieben sind ein Vanadium- und ein Kupferkomplex mit aromatischen Co-Liganden. Bei dem Vanadiumkomplex handelt es sich um einen Oxovanadium(IV)-Komplex mit 2,2‘-Bipyridin als Co-Ligand (Abb.27). Das Metallzentrum wird verzerrt oktaedrisch von der tridentaten Schiff’schen Basen, dem bidentaten Co-Liganden und dem doppelt gebunden Sauerstoffatom koordiniert. Der Bipyridin-Ligand ist nicht planar, sondern die Ringe stehen in einem Winkel von 7.2 ° zueinander. Weiterhin befinden sich in der asymmetrischen Einheit ein Molekül Wasser und ein Molekül Methanol. Dadurch wird durch O—H···O-Wasserstoffbrückenbindungen und π-π-Wechselwirkungen zwischen den Bipyridin-Liganden ein dreidimensionales Netzwerk aufgebaut[(108)].

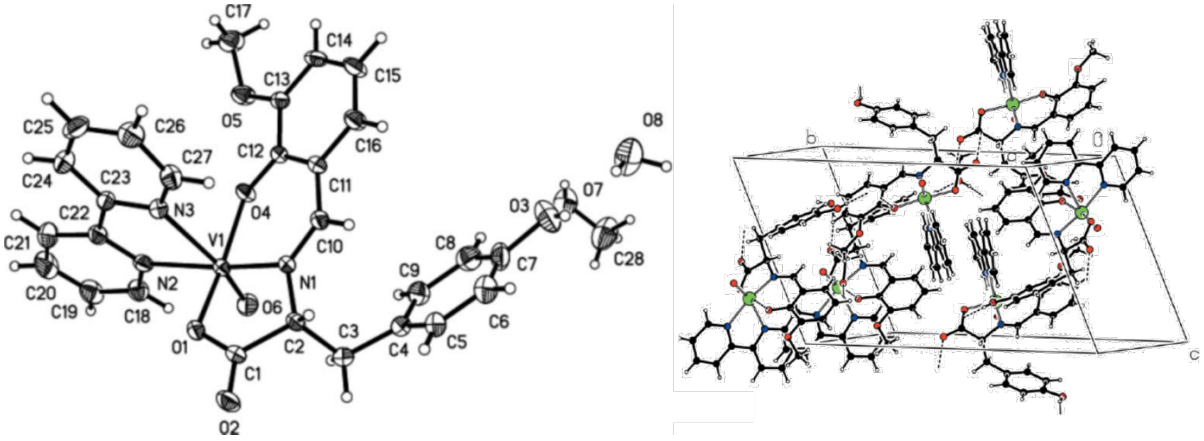

Abbildung 27: Kristallstruktur eines Oxovanadium-Komplexes mit einem Liganden aus *ortho*-Vanillin und *L*-Tyrosin und 2,2‘-Bipyridin als Co-Ligand und supramolekulare Packung[(108)].

Der Kristallstruktur des Cu(II)-Komplex wurde mit 1,10-Phenanthrolin als Co-Ligand erhalten (Abb. 28). Das Kupferzentrum ist fünffach koordiniert von der tridentaten Schiff’schen Base und den beiden Stickstoffatomen des 1,10-Phenanthrolins. Daraus ergibt sich eine verzerrte quadratisch-pyramidale Koordinationsgeometrie. Das Stickstoffatom der Schiff’schen Base befindet sich in der axialen Position. Außerdem ist in der asymmetrischen Einheit ein Wassermolekül enthalten. Durch intra- und intermolekulare Wechselwirkungen wird ein zweidimensionales Netzwerk im Festkörper erhalten[(109)].

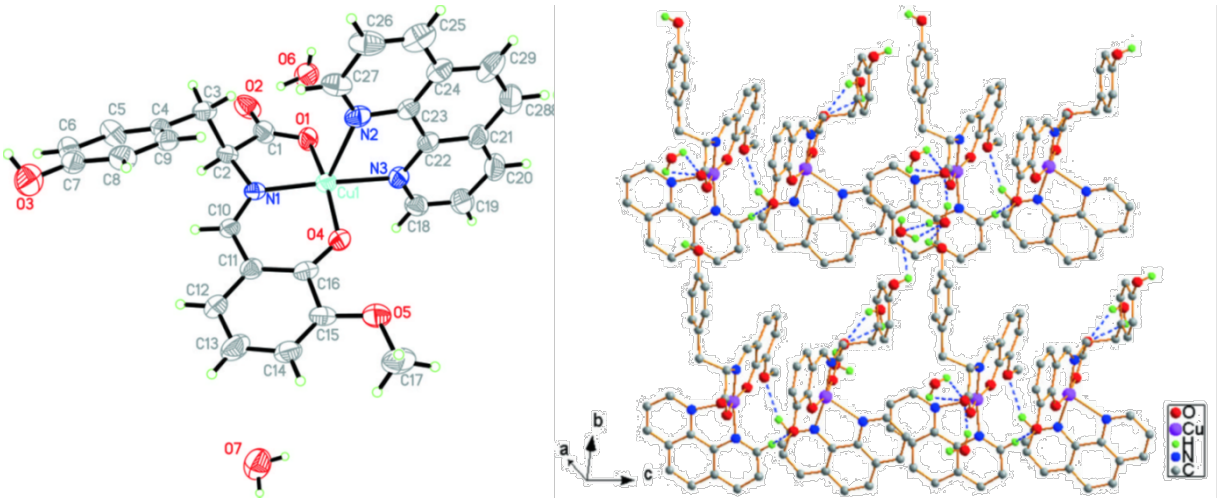

Abbildung 28: Kristallstruktur eines Cu(II)-Komplexes mit einem Liganden aus *ortho*-Vanillin und *L*-Tyrosin und 1,10-Phenanthrolin als Co-Ligand und supramolekulare Packung[(109)].

2. Motivation und Zielsetzung

Die verwendeten Edukte zur Konstruktion der Schiff'schen Basen, *ortho*-Vanillin und proteinogene Aminosäuren, bieten jedes für sich und insbesondere als Kombination eine Reihe von interessanten Eigenschaften und Möglichkeiten. Proteinogene Aminosäuren bieten sich als Aminquelle an, da sie natürlich vorkommende Verbindungen und nicht nur am Aufbau von Proteinen beteiligt sind, sondern auch im gesamten Metabolismus eine wichtige Rolle spielen. Sofern die Seitenketten nicht für den Aufbau von Metallkomplexen verwendet werden, ist eine Interaktion eben dieser mit biologischen *targets* denkbar. Darüber hinaus besteht die Vermutung, dass durch Naturstoffe in der Ligandsphäre eine verbesserte Resorbierbarkeit der daraus resultierenden Komplexe erzielt werden kann. Die Eigenschaften und Vorzüge von *ortho*-Vanillin wurden bereits in Kapitel 1.3 beschrieben. Die aus *ortho*-Vanillin und proteinogenen Aminosäuren resultierenden Schiff'schen Basen verfügen damit über mindestens fünf und maximal acht Koordinationsstellen zum Aufbau von Metallkomplexen, was die Synthese besonders großer Verbindung möglich werden lässt. Auf Grund der eben genannten Eigenschaften dieser Liganden ist es umso erstaunlicher, dass es bisher nur relativ wenige Publikationen auf diesem Feld gibt. Insbesondere das weitgehende Fehlen von Kristallstrukturen zu den bisher untersuchten Metallkomplexen stellt eine wesentliche Wissenslücke im Bereich der möglichen Strukturmotive dar.

Daher sollen in dieser Arbeit die Schiff'sche Base-Liganden von ausgewählten Aminosäuren in Reinform synthetisiert und charakterisiert werden. Die Liganden, entweder in Reinform oder *in situ* generiert, sollten anschließend mit verschiedenen Metallsalzen umgesetzt werden. Dabei soll es das Ziel sein, messbare Einkristalle der Komplexe zu erhalten, um eine eindeutige Strukturaufklärung zu ermöglichen. Die erhaltenen Liganden und Komplexe sollen, wenn angebracht, hinsichtlich ihres biologischen Potenzials untersucht werden.

3. Methodisches

Ein grundlegender Anspruch dieser Arbeit war es gewesen, jeden neu erhaltenen Komplex mit einer Kristallstruktur belegen zu können. Aufgrund der relativen Unempfindlichkeit der untersuchten Systeme ergibt sich eine Vielzahl an Parametern, mit denen sowohl die Reaktionen als auch das Wachstum von Kristallen beeinflusst werden können. Dazu zählen z.B. Reaktionstemperatur und -dauer, das/die verwendeten Lösungsmittel, Eduktzusammensetzung (stöchiometrische Verhältnisse, verschiedene Metallsalze, usw.), Additive, etc. Um möglichst viele Bedingungen auf einmal bei einem Ansatz regulieren zu können, wurde eine Screeningmethode zur Bestimmung der optimalen Kristallisationsbedingungen im Mikromaßstab für die untersuchten Systeme entwickelt. Mittels dieses Screenings können verschiedene Lösungsmittel und Lösungsmittelgemische, verschiedene Additive und unterschiedliche pH-Werte pro Ansatz bei gegebener Eduktzusammensetzung, Temperatur und Reaktionsdauer getestet werden.

Dazu wurden die in molekularbiologischen und biochemischen Laboratorien üblichen 96-*well*-Mikrotestplatten aus Polystyrol verwendet (Abb. 29).

Abbildung 29: 96-*well*-Mikrotestplatte mit Flachboden aus Polystyrol.

Das maximale Volumen pro *well* beträgt 300 µL. Im Rahmen dieser Arbeit wurde ein Arbeitsvolumen von 200 µL gewählt. Dieses setzte sich aus 50 µl Reaktionslösung und 150 µL Lösung der jeweiligen Bedingung zusammen. Abbildung 30 zeigt das Pipettierschema am Beispiel von Methanol als Hauptlösungsmittel. Weitere Screenings wurden auch mit Ethanol als Hauptlösungsmittel durchgeführt. Die Prozentangaben in den Reihen A bis C beziehen sich auf die Endkonzentration an Methanol im *well* nach Zugabe der Reaktionslösung. Die Angaben in den Reihen D bis F geben die Einwaage des jeweiligen Additives in mmol pro 25 mL Gesamtvolumen wieder. Die Endkonzentration an Methanol nach Zugabe der Reaktionslösung in diesen *wells* betrug 70%. Für NaOH und HCl ist der jeweilige Anteil einer 2 *M* wässrigen Lösung in µL pro *well* angegeben. Auch hier wurde eine Endkonzentration an Methanol nach Zugabe der Reaktionslösung von 70% erreicht. An dieser Stelle ist anzumerken, dass die ange-

strebten Endkonzentrationen nur erreicht werden, wenn die Reaktionslösung ausschließlich mit dem Hauptlösungsmittel angesetzt wird. Dies war nicht für alle verwendeten Aminosäuren möglich. Die genauen Zusammensetzungen der Bedingungslösungen befinden sich im Anhang. Die Wahl der Hauptlösungsmittel, Methanol oder Ethanol, beruht auf früheren Erfahrungen im Umgang mit der Schiff'schen Base aus Salicylaldehyd und (±)-2-Aminobutanol[(110)]. Im Zusammenhang mit dieser Publikation wurden auch bereits erste Versuche mit *ortho*-Vanillin durchgeführt, bei denen sich diese Solventien als geeignet erwiesen. Ebenfalls beruhend auf o.g. Vorarbeit wurde Acetonitril ins Portfolio aufgenommen. Dimethylformamid wurde auf Grund seiner hohen Polarität verwendet, um insbesondere bei Schiff'schen Base-Komplexen mit unpolaren Aminosäuren das Kristallwachstum zu fördern.

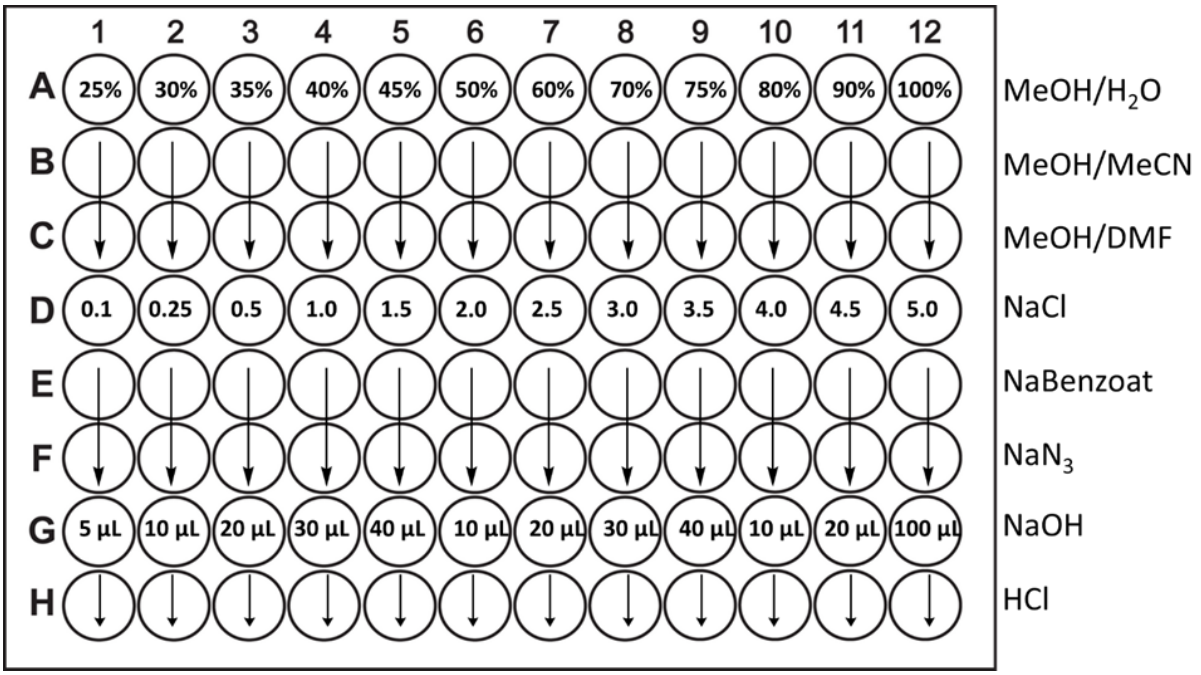

Abbildung 30: Pipettierschema für die Ansätze im Mikromaßstab am Beispiel von Methanol als Hauptlösungsmittel.

Analoges gilt für Natriumchlorid als Additiv. Hintergrund war die Annahme, dass die zunehmende Ionendichte und damit auch die Polarität in der wässrigen Phase beim Abdampfen des organischen Lösungsmittels das Kristallwachstum vom Komplexen mit unpolaren Aminosäuren anregt. Natriumbenzoat wurde bereits früher erfolgreich als Kristallisationszusatz eingesetzt, ohne selbst in der entstandenen Verbindung enthalten zu sein[(110)]. Die Zugabe von Natriumazid erhöht zum einen die Polarität der Lösung, zum anderen kann das Azidion aber auch verbrückend wirken, wodurch die Bildung von Kristallen begünstigt werden kann oder gar neue Strukturen erhalten werden können. Natronlauge und Salzsäure in verschiedenen

Konzentration ermöglichen die Untersuchung einer eventuellen pH-Abhängigkeit der Kristallisation bzw. der Produktsynthese.

In der Praxis wurden 150 µL der jeweiligen Bedingung vorgelegt und anschließend mittels einer 8-Kanal-Pipette je 50 µL der Reaktionslösung zugesetzt. Zum Schluss wurden beide Lösungen durch mehrmaliges Aufziehen und Ausstoßen gemischt und die Platte mit einer transparenten Folie versiegelt. Um ein Abdampfen des Lösungsmittels und damit die Kristallisation zu ermöglichen, wurde die Folie über jedem *well* mit einem kleinen Loch perforiert. Bei erfolgreichem Kristallwachstum wurde der Ansatz im Regelfall auf 1 mmol (Aminosäure, *ortho*-Vanillin, Metallsalz) bei 25 mL Gesamtvolumen der entsprechenden Bedingung hochskaliert. Allerdings funktionierte die 1:1-Hochskalierung nicht in allen Fällen, sodass teilweise eine weitere Feinjustierung der Bedingungen nötig war.

Dieses Screening bietet eine Reihe von Vorteilen: Da mit einem Reaktionsansatz bis zu 96 verschiedene Bedingungen für die Kristallisation getestet werden können, führt dies insbesondere bei teuren Edukten zu einer enormen Kostensenkung und einer drastischen Verringerung der Abfallmenge. Auf Grund des geringen Arbeitsvolumens erhält man, verglichen mit Ansätzen im Makromaßstab, Ergebnisse in relativer kurzer Zeit. Bei den mit diesem Screening untersuchten Systemen konnten Kristalle nach einem Zeitraum von wenigen Stunden bis zu einer Woche erhalten werden, während die Kristallisation im Makromaßstab bis zu 6 Wochen dauern kann. Weiterhin kann die Synthese gezielt optimiert werden, da der Rahmen für die ideale Kristallisationsbedingung durch die Vielzahl an getesteten Bedingungen stark eingegrenzt wird. Dieses Screening ist nicht nur auf die Arbeit mit Schiff‘schen Basen begrenzt, sondern lässt sich problemlos auf viele andere Systeme übertragen, bei denen die Kristallisation über die langsame Evaporation eines Solvens erreicht wird. Durch die Wahl des richtigen Equipments sind auch Screenings mit anderen Kristallisationstechniken, z.B. Überschichtung, realisierbar. Selbst Kristallisationsansätze unter Inertgasbedingungen wären durchführbar.

4. Kumulativer Teil

I "A chiral, low-cytotoxic Ni_{15}-wheel complex."
Muche, S.; Levacheva, I.; Samsonova, O.; Pham, L.; Christou, G.; Bakowsky, U.; Hołyńska, M. *Inorganic chemistry* **2014**, *53* (14), 7642–7649.

II "Synthesis, structure and stability of a chiral imine-based Schiff-base ligand derived from L-glutamic acid and its [Cu_4] complex."
Muche, S.; Levacheva, I.; Samsonova, O.; Biernasiuk, A., Malm, A. Lonsdale, R.; Popiołek, L., Bakowsky, U.; Hołyńska, M. *Journal of Molecular Structure* **2017**, *1127*, 231-236.

III "New insights into the coordination chemistry of Schiff bases derived from amino acids: Planar [Ni_4] complexes with tyrosine side-chains."
Muche, S.; Hołyńska, M. *Journal of Molecular Structure* **2017**, *1142*, 168–174.

IV "Synthesis, characterization and crystal structure of (2RS,4R)-2-(2-hydroxy-3-methoxyphenyl)thiazolidine-4-carboxylic acid**.**"
Muche, S.; Müller, M.; Hołyńska, M. *Journal of Molecular Structure*; Manuskript akzeptiert

V "A gap is filled: First structures of enantiopure iron(III) complexes with Schiff base ligands derived from *ortho*-vanillin and *L*-glutamine or *L*-glutamic acid."
Muche, S.; Harms, K.; Burghaus, O.; Hołyńska, M. *Polyhedron*; Manuskript eingereicht

VI "Novel Pd(II) Schiff Base complexes derived from *ortho*-vanillin and *L*-tyrosine or *L*-glutamic acid: Synthesis, characterization, crystal structures and biological properties."
Muche, S.; Biernasiuk, A. Malm, A; Popiołek, Ł.; Hordyjewska, A.; Olszewska, A.; Hołyńska, M.; *Manuskript in Vorbereitung*

I A chiral, low-cytotoxic Ni_{15}-wheel complex

Muche, S.; Levacheva, I.; Samsonova, O.; Pham, L.; Christou, G.; Bakowsky, U.; Hołyńska, M. *Inorganic chemistry* **2014**, *53* (14), 7642–7649.

A new chiral [Ni_{15}] complex with a Schiff-base ligand derived from o-vanillin and L-glutamic acid is presented, emphasizing the properties relevant for biology and materials science. The formation of the complex molecules in solution is confirmed by AFM and dynamic light scattering studies. The compound is weakly antiferromagnetic with considerable admixture of excited states, comprising negligibly interacting [Ni_3] units. Studies of the interactions with two cell lines indicate low cytotoxicity.

Inhalt: Die Synthese, Charakterisierung und Untersuchung von magnetischen und biologischen Eigenschaften eines pentadecanuklearen Ni(II)-Komplexes in Form eines Rades, welcher ein seltenes Beispiel für ungeradzahlige radförmige Ni(II)-Komplexe darstellt, wird präsentiert. Die Synthese des einkristallinen Produktes durch langsame Evaporation des Lösungsmittels aus einer Eintopfreaktion und die Kristallstruktur werden beschrieben. Als analytische Methoden zur Charakterisierung des [Ni_{15}]-Rades werden IR-Spektroskopie, Elementaranalyse, EDX und TGA herangezogen. Mittels IR-Spektroskopie wird außerdem gezeigt, dass der Komplex stabil in Methanol bzw. 95% Wasser/5% Methanol ist. AFM- und DLS-Studien in Methanol bzw. 95% Wasser/5% Methanol enthüllen zudem, dass zwei Hauptstrukturtypen vorliegen: Diskrete Komplexmoleküle und Agglomerate. LDH- und MTT-Assays mit zwei murinen Zelllinien und einer Exposition mit dem [Ni_{15}]-Rad über 4 h und 24 h belegen, dass der Komplex keine signifikante Zytotoxizität gegenüber den getesteten Zelllinien über die betrachteten Zeiträume besitzt. Die Untersuchung der magnetischen Eigenschaften zeigt ein dominantes antiferromagnetisches Verhalten, sowie intermolekulare Wechselwirkungen bei Temperaturen unterhalb von 24 K.

Eigener Anteil: Die Planung und Durchführung der Synthese sowie die Aufnahme und Auswertung der Basisanalytik wurde von mir durchgeführt unter Betreuung von Małgorzata Hołyńska. Die Röntgenstrukturanalyse wurde von der hauseigenen Serviceabteilung durchgeführt. Die Analyse der kristallographischen Daten sowie der Daten der magnetischen Messung erfolgte durch Małgorzata Hołyńska und Linh Pham aus der Arbeitsgruppe von George Christou. Irina Levacheva und Olga Samsonova aus der Arbeitsgruppe von Udo Bakowsky führten die MTT- und LDH-Assays, die AFM- und DLS-Studien durch und bereiteten die dazugehörigen Daten auf. Das Manuskript wurde von allen Autoren gemeinschaftlich verfasst.

Inorganic Chemistry

Article

pubs.acs.org/IC

A Chiral, Low-Cytotoxic [Ni_{15}]-Wheel Complex

Simon Muche,[†] Irina Levacheva,[‡] Olga Samsonova,[‡] Linh Pham,[§] George Christou,[§] Udo Bakowsky,[‡] and Małgorzata Hołyńska*[,†,§]

[†]Fachbereich Chemie and Wissenschaftliches Zentrum für Materialwissenschaften (WZMW), Philipps-Universität Marburg, Hans-Meerwein-Straße, D-35032 Marburg, Germany

[‡]Institut für Pharmazeutische Technologie & Biopharmazie, Philipps-Universität Marburg, Ketzerbach 63, D-35032 Marburg, Germany

[§]Department of Chemistry, University of Florida, Gainesville, Florida 32611-7200, United States

Supporting Information

ABSTRACT: A new chiral [Ni_{15}] complex with a Schiff-base ligand derived from *o*-vanillin and L-glutamic acid is presented, emphasizing the properties relevant for biology and materials science. The formation of the complex molecules in solution is confirmed by AFM and dynamic light scattering studies. The compound is weakly antiferromagnetic with considerable admixture of excited states, comprising negligibly interacting [Ni_3] units. Studies of the interactions with two cell lines indicate low cytotoxicity.

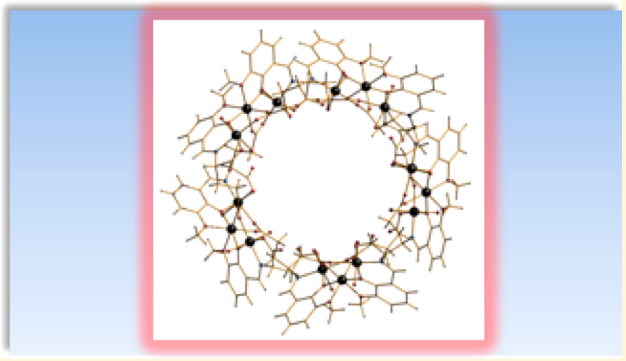

1. INTRODUCTION

Polynuclear metal complexes are of high importance in bioinorganic chemistry, yet their biological activity is scarcely explored due to the complexity of these systems and is limited mainly to Pt/Ru compounds.[1] In particular, simple complexes with Schiff-base ligands are known to often display antibacterial activity[2] and to act as models for enzymes.[3] At the same time, they often serve as magnetic materials, showing single-molecule magnet behavior.[4] Beside a wide variety of physical applications the wheel-like structures can play a significant role in many biochemical processes, such as micelle formation[5−8] and insertion of proteins into biological membranes.[9] It is assumed that large wheel-shaped molecules can be potentially used for DNA binding, due to the negative charge present on their surface.[10] Recent research focuses not only on antitumor activity of, for example, Pt(II) compounds, but also on introducing low-cytotoxic drug nanocarriers based on metal complexes.[1c] These compounds may play the role of "Trojan horses", delivering cytotoxic species into target tissue.[1c]

In this paper we report on the synthesis and properties of a chiral high-nuclearity [Ni^{II}_{15}] complex (**1**), incorporating a Schiff-base ligand derived from a natural amino acid. The compound is a rare example of an odd-number wheel-like Ni(II) cluster. Concomitantly the related compound was synthesized by Vittal et al.[11a] by a different method. The known even-numbered Ni(II) wheel-like molecules include the highest nuclearity [Ni_{24}] assemblies. Winpenny et al.[11b] contributed an [Ni_{24}] complex with a heterocyclic 3-methyl-3-pyrazolin-5-one ligand.[11b] Recently also an [Ni_{24}] wheel-like complex with isophthalate as a ligand, forming a 3D coordination polymer, has been reported by Tao et al.[11c] An [$Ni_{20}L_4(HL)_4(OAc)_{28}$] ($H_2L$ = 3-[benzyl(2-hydroxyethyl)-amino]-1-propanol) complex with a central [Ni_{12}] loop and four peripheral [Ni_2] fragments is also known.[11d] Other nuclearity Ni(II) wheels include [Ni_{16}],[11e] [Ni_{12}],[11f−i] [Ni_{11}],[11j] [Ni_{10}],[11k] and [Ni_6][11l,m] compounds. On the other hand, the [Ni_{15}] complexes displaying different topologies include a selenium-bridged [$Ni_{15}Se_{15}(PPh_3)_6$] cluster reported by Fenske and Ohmer,[12a] displaying a barrel-like structure. A sulfur-bridged analogue was introduced by Liu et al.,[12b] whereas a similar complex with a different phosphine ligand was synthesized by Midollini et al.[12c] Albano et al.[12d] synthesized an antimony-bridged nickel(II) carbonyl cluster, $[NEt_3CH_2Ph]_2[Ni_{15}(\mu_{12}\text{-}Sb)(CO)_{24}]$, with a distorted Sb-centered [$Ni_{12}(\mu_{12}$-Sb)] icosahedral moiety capped with three Ni atoms.

2. RESULTS AND DISCUSSION

2.1. Syntheses and Structure. The Schiff-base ligand, being a constituent of the title complex, is formed *in situ* in the reaction of *o*-vanillin and L-glutamic acid in the presence of sodium acetate (Scheme 1).

The ligand has been already mentioned in physicochemical studies on its metal complexes, however, with no crystal structure determinations.[13] The known reports on the metal

Received: April 25, 2014
Published: July 3, 2014

dx.doi.org/10.1021/ic500957y | *Inorg. Chem.* 2014, 53, 7642−7649

Scheme 1. Overview of the Procedure for Isolation of 1[a]

L-Glu + AcONa + *o*-vanillin + H_2O/MeOH
↓ $NiCl_2$, stirring at 80°C
$0.5[Ni_{15}(L)_{10}(H_2O)_{19}(MeOH)]\cdot 0.5[Ni_{15}(L)_{10}(H_2O)_{20}]$ (**1**) (30%)

[a] L-Glu = L-glutamic acid, H_3L = the Schiff-base ligand.

ion complexation include mainly spectroscopic, polarographic, potentiometric, or molecular modeling studies. An example is the report on polarographic behavior of chromium(III) complexes published by Malik et al.[13b] Our attempts to isolate the ligand in crystalline form have so far been unsuccessful. On the other hand, formation of an oily product can be confirmed. The title complex is an $[Ni_{15}]$ neutral chiral assembly with 10 bridging ligands, being a Schiff base derived from *o*-vanillin and L-glutamic acid. The Schiff-base ligand adopts the coordination mode illustrated in Scheme 2. The two carboxylate groups are mono/bidentately coordinated with *anti*/*syn*−*syn* mode (Scheme 2).

Scheme 2. Coordination Mode of the Schiff-Base Ligand in 1

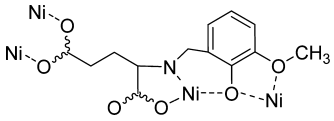

The oxidation state of the Ni^{2+} ions is confirmed by charge balance considerations and studies of the magnetic properties. Due to extensive disorder of the organic part/solvent in the crystal structure, only a limited discussion of the molecule's geometrical parameters is possible. The wheel-like assembly is of 11/24 Å of inner/outer diameter, respectively (Figure 1, top). In the complex molecule trinuclear $[Ni_3]$ units with Ni^{2+} ions at closest distances can be distinguished (at 3.42(1)−3.462(2) Å; see Table S3). Schematic structure of one of the $[Ni_3]$ units is presented in Figure 1 (bottom). The Ni^{2+} ion arrangement is linear, which suggests two equivalent pathways for magnetic interactions. A similar construction basis was observed by Winpenny et al.[11a] for their $[Ni_{24}]$ wheel-like complexes with a 3-methyl-3-pyrazolin-5-one ligand. In each $[Ni_3]$ unit in **1** two Ni^{2+} ions are linked by a double oxo-acetato bridge. The oxo part is the ligand *o*-vanillin part phenoxo atom; the acetate comes from the L-glutamic acid carboxylate group bonded to γ-C and coordinates in a *syn*, *syn* mode. Thus, two perpendicular rings are defined, joined by one Ni^{2+} ion. Each ring is slightly puckered with Ni−O−C−O torsion angles of, for example, 21(2)°, 26(2)° and 21(2)°, 25(2)° for the Ni1−Ni2 and the Ni2−Ni3 ring, respectively. The representative bond angles are highlighted in Figure 1 (bottom). Each thus defined unit is at ∼8.3−9.3 Å from the equivalent unit, magnetically isolated with the organic ligands. Each Ni^{2+} ion displays a distorted octahedral coordination environment. The central Ni^{2+} ion of each $[Ni_3]$ unit is surrounded solely by ligand O atoms. Four ligands are participating in this arrangement: two ligands are chelating through one methoxo and one phenoxo O atom; the other two ligands donate one acetate O atom each. The other two Ni^{2+} ions of the $[Ni_3]$ unit display coordination environments analogous to each other. Thus, in both cases two water ligands are coordinated to the central metal atom in a *trans* arrangement, where one ligand points outside and the second ligand points inside the molecule. The water ligand pointing inside should be involved

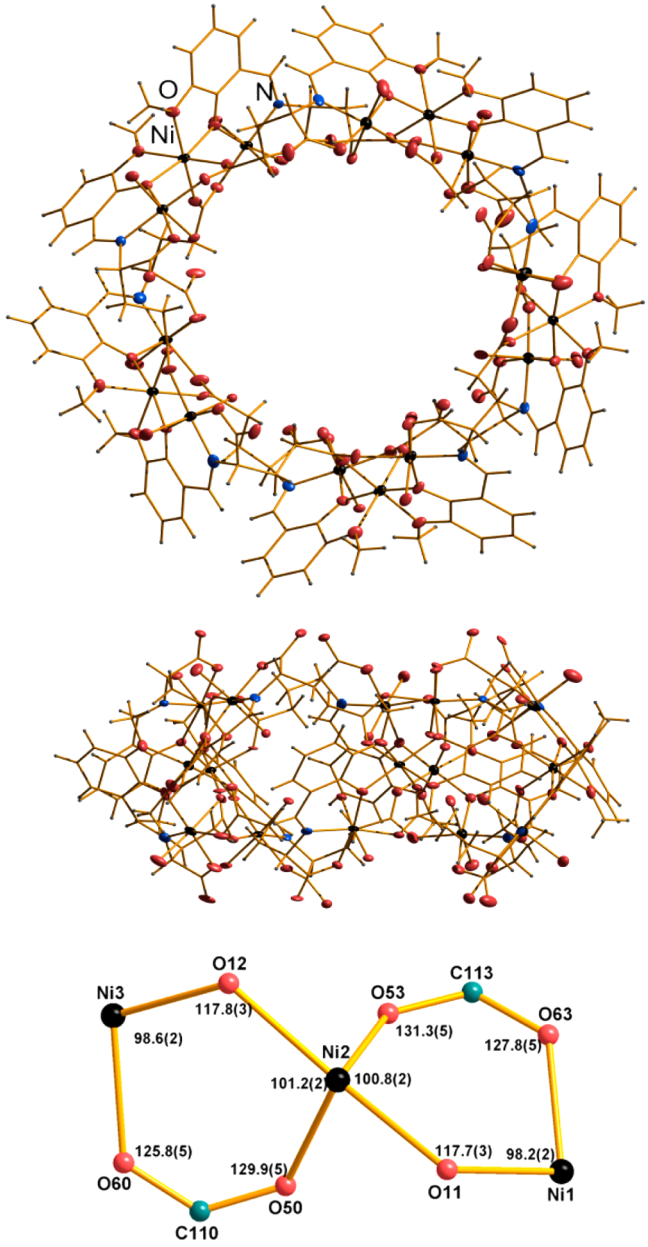

Figure 1. Molecular structure of the title complex (top), along with the side view (middle) and schematic structure of one of the $[Ni_3]$ units (bottom). Disordered part is omitted for clarity. Thermal ellipsoids of non-C/H atoms are plotted at the 20% probability level.

in intramolecular hydrogen bonds to the acetate O atoms available as acceptors. The coordination spheres are completed by two organic ligands: one donates a single acetate O atom; the second ligand chelates through phenoxo/methoxo O atoms and one N atom.

The complex molecules in the crystal structure form overlapping columns extending along [100] (Figure 2) with heavily disordered solvent molecules inside and outside the columns. A network of hydrogen bonding is present, which is difficult to describe in detail due to extensive disorder.

2.2. AFM Study. The high solubility of **1** in methanol can be utilized to prepare the AFM slides. In order to prepare a monolayer of the examined substance, the solution in methanol was deposited on a silicon wafer. The AFM studies (Figure 3) revealed two major types of structures: small rounded point-

dx.doi.org/10.1021/ic500957y | Inorg. Chem. 2014, 53, 7642−7649

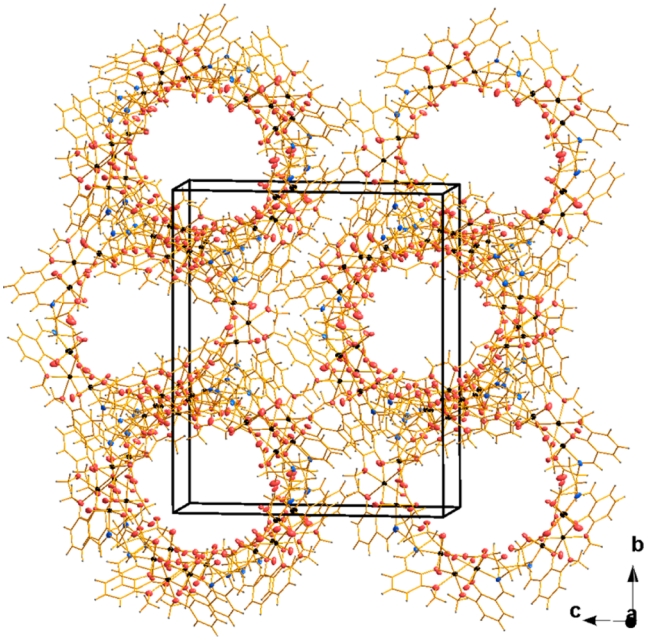

Figure 2. Packing of the complex molecules in **1**. Solvent molecules are omitted for clarity.

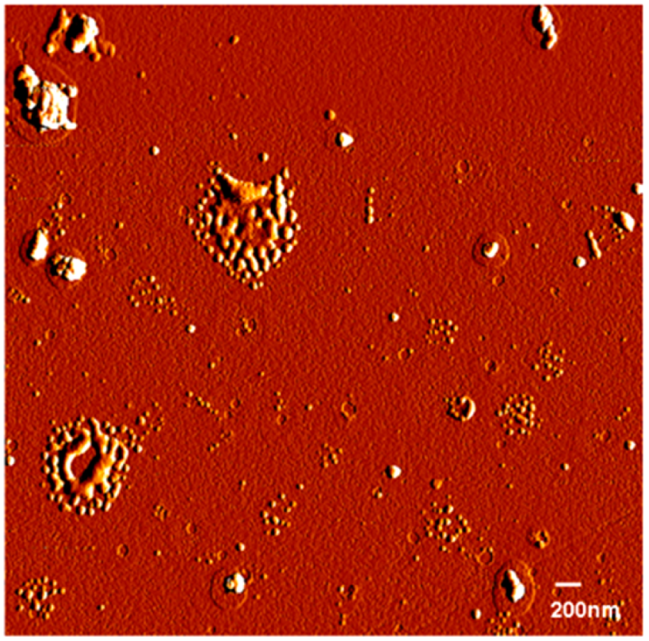

Figure 3. AFM image on deposition from the solution of **1** in methanol.

shaped structures under 10 nm size, which are assumed to be the molecules of **1**, along with larger round and irregular assemblies of 100−500 nm diameter assumed to be agglomerates of the complex molecules.

2.3. Dynamic Light Scattering Study. Studies of a 95% water/5% methanol solution of **1** were undertaken by dynamic light scattering (Figure S3). Interestingly, the obtained data correlate well with the AFM results for a solution in methanol. In both cases an aggregation is observed, most probably due to noncovalent interactions (see SI). Thus, larger aggregates of several hundred nanometer diameters can still be observed, along with a ∼2.7 nm size component corresponding to the complex molecules **1**. Simple IR studies for residues left upon evaporating the solutions support this conclusion (see SI). The peak assignable to species under 0.5 nm in size might indicate partial hydrolysis of the molecular wheels.

2.4. Cytotoxicity Study. The solution studied by dynamic light scattering (5% methanol/95% water) was examined for interaction with two cellular lines in order to assess the potential toxicity of **1**. The following cell lines were used: L929, subcutaneous connective mouse tissue; areolar and adipose, adherent cell line with fibroblast morphology (L929 is used by United States Pharmacopoeia for biocompatibility tests); B16, skin tissue, mouse melanoma, mixture of spindle-shaped and epithelial-like cells, adherent cell line (a fast growing cell line with intensive metabolism). With both *in vitro* assays (MTT and LDH) no IC_{50} (50% cellular toxicity) value could be reached in the tested concentration range. This means that **1** does not demonstrate any pronounced acute and long-term necrotic or apoptotic activity upon contact with the living cells in the given exposure time. Low-range inhibition of metabolism observed for L929 and B16 cell lines (Figures 4 and 5) cannot be assigned to a selective substance effect.

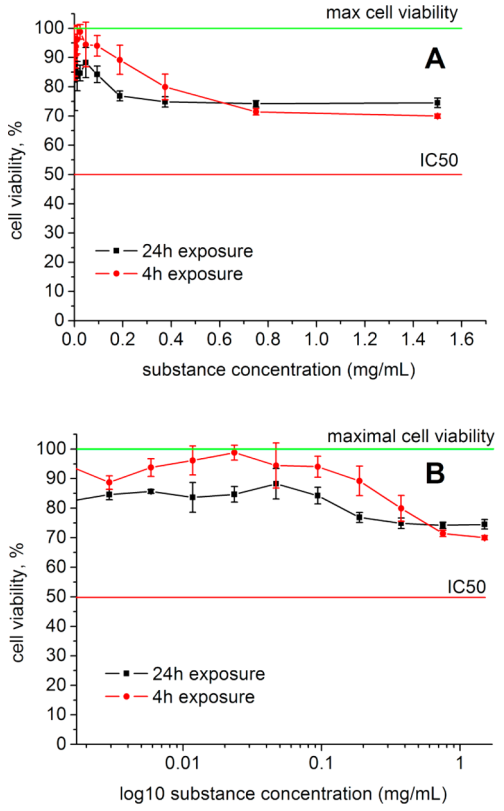

Figure 4. Mitochondrial activity of mouse melanoma with different exposure to the test substance **1**: (A) direct concentration dependence, (B) logarithmic dependence, which is used for the IC_{50} calculation.

It is interesting to note that the melanoma cells have a slightly more pronounced metabolism drop in a lower concentration range, which may be due to a faster accumulation in the cells, as these cells have a faster doubling time.[14] The difference in interactions with malignant and normal cells may be better distinguished at higher concentration ranges. For both cell lines the long-term exposure (24 h) had more impact on the cell metabolism, which is common for non-physiological substances and their accumulation in the tissue.[15]

dx.doi.org/10.1021/ic500957y | *Inorg. Chem.* 2014, 53, 7642−7649

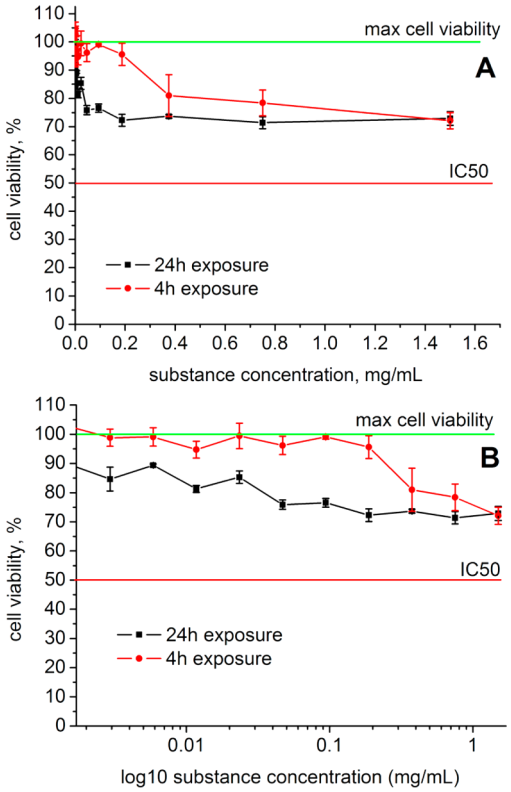

Figure 5. Mitochondrial activity of mouse fibroblasts with different exposure to the test substance **1**: (A) direct concentration dependence, (B) logarithmic dependence, which is used for IC_{50} calculation.

The LDH assay matches the results obtained for the MTT assay in the short- and long-term toxicity trend (Figure 6). The 24 h incubation with **1** leads to a stronger LDH-level expression for both cell lines, as expected. This was observed due to accumulation of the metabolites in the cell culture wells. Each cell line can reach up to 10% cellular toxicity under physiological conditions due to accumulation of the cell metabolism products over a longer exposure time. A toxic control with Triton-X led to complete cell lysis and developed 100% LDH toxicity. Our results allow us to define the analyzed substance as a promising agent of low cytotoxicity, as it does not reach the IC_{50} in both short- and long-term exposure times. On the other hand, both simple Ni(II) salts, such as acetate or chloride, and complex compounds, such as $[NEt_4]_2[NiCl_4]$, are cytotoxic already at concentrations of 100 μM (please see refs 16–27 and those for the compounds mentioned below). The majority of the studied complexes are mononuclear. Especially high cytotoxicity is displayed by mononuclear Ni(II) semicarbazone/thiosemicarbazone-functionalized chinone derivatives as ligands.[17] The analogous Pd/Cu complexes are weakly cytotoxic. Binuclear $[Ni_2]$ complexes with 3,3-dialkyl/aryl-1-benzoylthiourea as a ligand are cytotoxic toward T47D cell lines and have a higher effect than "cisplatin".[27] Polynuclear (tri- to pentanuclear) Ni(II) complexes derived from salicylhydroxamic acid interact with DNA and show antibacterial activity.[28] An interesting example is an $[Ni_4]$ complex with a biphenol-based ligand, inducing condensation of DNA, but no cleavage and no cytotoxicity.[29]

2.5. Magnetic Properties. $\chi_M T$ vs T curves recorded for **1** (Figure 7a) show dominating antiferromagnetic behavior (Figure 8, Weiss constant of −2.4 K in the linear region). The $\chi_M T$ value at room temperature is about 13.58 cm^3 K/mol, which is smaller than expected for 15 non-interacting Ni^{2+} ions (S = 1, 15.00 cm^3 K/mol). The decrease at low temperatures may be a combined effect of weak antiferromagnetic interactions and zero field splitting effects. The drop in the in-phase ac $\chi_M'T$ values at lower temperatures (Figure 9) suggests that the spin ground state is not well isolated, and the excited states are populated even at low temperatures, probably due to the weak magnetic interactions within the system. As a consequence, it was also not possible to provide a reasonable fit of the reduced magnetization data (Figure 10). The presence of low-lying excited states was also reported for the carboxylate-bridged $[Ni_{12}]$ complexes comprising three tetranuclear units stabilized by a central templating anion in a wheel-like arrangement.[30]

The complex molecules in **1** contain five $[Ni_3]$ units linked through carboxylate−phenoxido bridges. The units are essentially magnetically isolated by the organic ligand parts. Thus, for the first approximation, the fit of the magnetic data was based on a simple trinuclear model (Scheme 3) under the assumption that the trinuclear units do not interact. In this model the J' constant value (Scheme 3) is expected to be very low. The corresponding van Vleck equation is quoted in the SI.

For nickel(II) complexes the g values should be greater than 2.0, as expected for d^6–d^9 metals. On the basis of the reported exchange coupling parameters between two Ni^{2+} ions bridged by carboxylate and/or phenoxido ligands,[31] the J value is expected to be small, but still should remain higher than J'. Thus, constraints of $g > 2$ and also of $J < 10$, along with $J' > -10$, were applied. The TIP value was kept at 6.0×10^{-4} cm^3 mol^{-1}. Moreover, because of the weak coupling between the Ni centers, the effect of intermolecular interactions becomes more significant and cannot be ignored at very low temperatures.

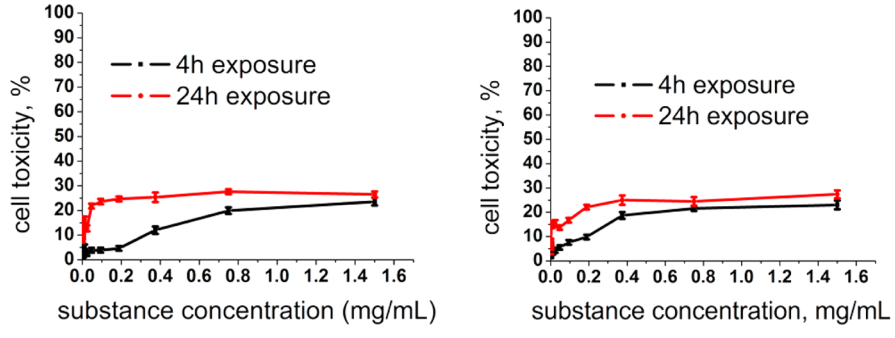

Figure 6. LDH cellular toxicity in mouse fibroblasts (left) and mouse melanoma (right) with different exposure times to the test substance **1**.

dx.doi.org/10.1021/ic500957y | Inorg. Chem. 2014, 53, 7642–7649

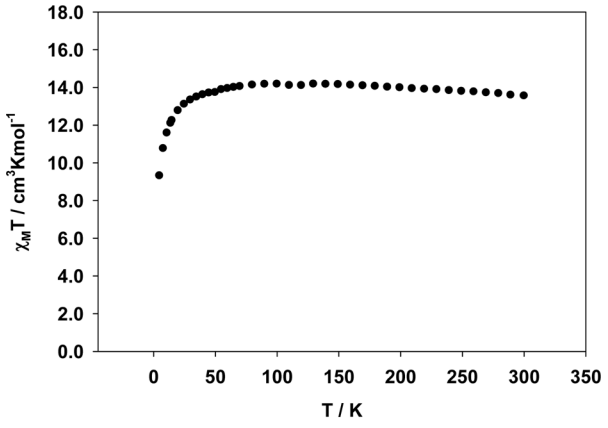

(a)

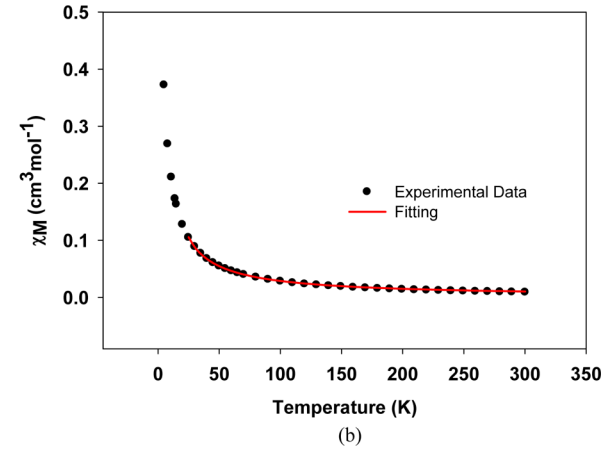

(b)

Figure 7. Plot of the (a) $\chi_M T$ vs T and (b) χ_M vs T dependence for **1** in a 0.1 T field (the solid line shows a fit to the corresponding van Vleck equation with the resulting parameters $J = -4.4(8)$, $J' = -0.3(4)$ cm^{-1}, $g = 2.00(5)$; goodness of fit coefficient $R^2 = 0.9992$).

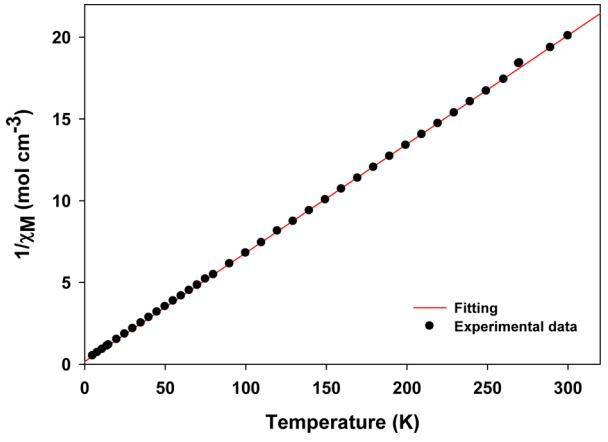

Figure 8. $1/\chi_M$ vs T dependence.

Therefore, only the data above 24 K were considered for the fit. Fitting of the experimental χ_M data led to $J = -4.4(8)$, $J' = -0.3(4)$ cm^{-1}, and $g = 2.00(5)$ (goodness of fit coefficient $R^2 = 0.9992$; Figure 7b). As expected, both couplings are weak, and the coupling between the two distant Ni centers is considerably smaller than the coupling between the two adjacent ones. Although the magnitude of the adjusted J value is considerably lower than the J value obtained from the van Vleck fit, it is still higher than the J' value by an approximate factor of 6, also

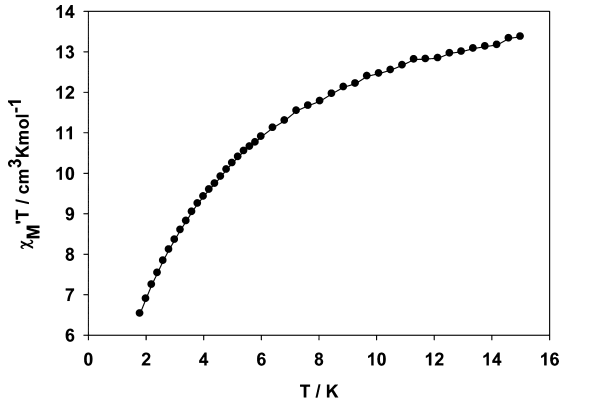

Figure 9. Alternating current $\chi_M' T$ vs T plot.

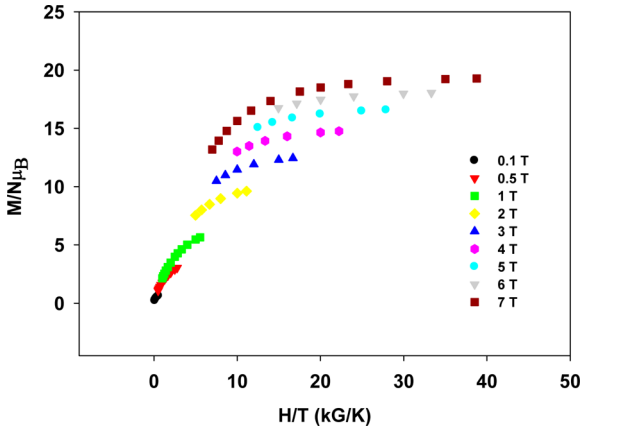

Figure 10. Plot of the reduced magnetization vs field.

Scheme 3. Model of Magnetic Exchange Interactions in 1

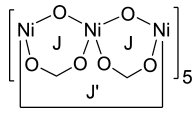

exhibiting weak antiferromagnetic interactions between the adjacent Ni centers. Employing the J and J' values from the van Vleck fit, the energies of the resulting spin states are plotted in Figure 11, indicating a ground state of $S = 1$ for each trinuclear unit. The first and the second excited state are $S = 0$ and $S = 1$, respectively, which is only 7.6 and 16.4 cm^{-1} above the ground

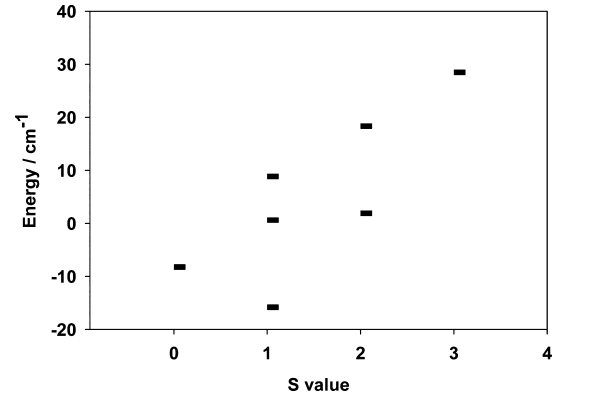

Figure 11. Energy of the states calculated based on the J parameters obtained from a van Vleck fit of the experimental data.

dx.doi.org/10.1021/ic500957y | Inorg. Chem. 2014, 53, 7642−7649

state. The presence of these low-lying excited states is consistent with the conclusions based on the dc, the in-phase ac, and the reduced magnetization analysis. The antiferromagnetic nature of both J and J' provides a potentially spin-frustrated system, but the very weak magnitude of J' vs J and the $S = 1$ ground state of the $[Ni_3]$ unit indicate that the magnetic properties are determined by J and the effect of J' is insignificant. Complex **1** is structurally a rare example of an odd-membered ring topology,[32] but magnetically it is best described as five separate $[Ni_3]$ units.

The trinuclear carboxylate−phenoxido-bridged $[Ni_3]$ unit seems to be unprecedented in the reported literature.[33] The most similar systems reported are trimetallic $[Ni_3]$ species with acetate−double phenoxido bridges.[30] The presence of antiferromagnetic coupling can be correlated with the values for the relevant bond angles greater than 90° (Figure 1, bottom).[30]

The ac out-of-phase component for **1** (Figure S4) shows no peak on its temperature dependence determined at 1000 Hz frequency of the oscillating field, which suggests no single-molecule magnet properties.

3. CONCLUSIONS

To sum up, a new wheel-like chiral $[Ni_{15}]$ complex was introduced with a Schiff-base derived from *o*-vanillin and L-glutamic acid acting as a ligand. The presence of the obtained complex molecules was confirmed in solution with methods such as dynamic light scattering and AFM studies on a silicon slide surface. Apart from uniform spherical constructs, the complex superpositioned elements were found in solution and on the AFM image. On the basis of preliminary biological studies low toxicity was confirmed, which are grounds for further, more detailed biological investigations, as only low-cytotoxic substances are candidates for applications such as gene transfer. In particular, the limitation of the preliminary studies was the low solubility in water, which we aim to overcome using nanocarriers, such as particles and liposomes. The host−guest chemistry of the complex itself may also bring new insights into its potential as a model system. Moreover, the specific molecular structure of substance **1** opens promising preconditions to examine its interaction with DNA.[34]

4. EXPERIMENTAL SECTION

4.1. Synthesis and Analytical Data. A 147 mg (1.0 mmol) amount of L-glutamic acid was dissolved in 10 mL of water. Then 408 mg (3.0 mmol) of sodium acetate was dissolved in 10 mL of methanol and added to the solution of L-glutamic acid. A 152 mg (1.0 mmol) portion of *o*-vanillin was dissolved in 5 mL of methanol and added to the stirred L-glutamic acid/sodium acetate solution. The resulting yellow solution was heated to 80 °C and stirred until the solid part was completely dissolved. Then 238 mg (1 mmol) of $NiCl_2{\cdot}6H_2O$ was added to the yellow solution. The solution color changed to green immediately. The solution was stirred for 30 min at 80 °C and was transferred to a 30 mL vial for crystallization by slow evaporation. Green crystals in the form of plates were obtained within 2 weeks in 30% yield.

Elemental analysis for the substance dried under vacuum for several hours, analyzed as $[C_{130.29}H_{160.58}N_{10}Ni_{15}O_{80}]{\cdot}4H_2O$: Calcd (found): C 38.17 (38.84), H 4.14 (4.56), N 3.42 (3.22). IR bands (cm^{-1}): 446.9 (m), 484.2 (m), 507.5 (vw), 532.5 (vw), 555.7 (vw), 584.7 (vw), 624.5 (vw), 654.0 (vw), 676.0 (vw), 738.2 (vw), 779.3 (m), 822.6 (vw), 852.4 (vw), 895.0 (vw), 962.5 (w), 1026.4 (vw), 1082.0 (m), 1108.2 (w), 1168.6 (vs), 1213.9 (w), 1240.1 (m), 1292.6 8 (vw), 1349.5 (s), 1386.0 (m), 1420.8 (s), 1441.0 (s), 1456.1 (vs), 1552.7 (vs), 1602.0 (w), 1645.0 (s), 1979.8 (vw), 2035.9 (vw), 2149.3 (vw), 2162.4 (vw), 2323.2 (vw), 2944.5 (vw).

4.2. Physical Measurements. *X-ray Measurement.* X-ray data were collected at 100(2) K on a Bruker Quest D8 diffractometer with a CMOS detector and Mo Kα radiation.[35]

Spectroscopy. IR spectra were collected with the aid of a Bruker Alpha-P infrared-spectrometer equipped with a platinum-ATR with a diamond crystal.

CHN Elemental Analyses. These were carried out on an Elementar Vario Microcube elemental analyzer in CHNS mode.

Energy-Dispersive X-ray spectroscopy (EDX). These measurements were performed on a CamScan 4DV + EDX Noran Instruments Voyager 4.0 with a Pioneer detector.

Thermal Behavior. The TGA diagram for an 11.2 mg sample of **1** was recorded on a Netzsch STA 409 CD device in the temperature range 25−1200 °C at a scanning rate of 5 K/min. The compound slowly released interstitial solvent already starting at room temperature in two steps with mass loss in total attributable to 94 molecules of H_2O or 37 molecules of methanol, which roughly corresponds to the solvent content assessed after application of the SQUEEZE procedure (see refinement details). Further on, a stepwise decomposition is observed (Figure S2), most probably involving release of solvent ligands coordinated to the Ni^{2+} ions in the first place.

Magnetic Measurements. Measurements of the magnetic properties were carried out on a Quantum Design MPMS XL SQUID magnetometer. The powdered microcrystalline sample was restrained in eicosane to prevent torquing. Two kinds of samples were examined: a sample directly after removal from the mother liquor and the sample dried in a vacuum for 2 h. The obtained temperature/field dependences were similar to those in the case of the "wet" sample. However, as clearly degradation of the crystalline phase was observed on drying, the data obtained for a "wet" sample were further evaluated. The molecular mass for the "wet" sample was estimated taking into account the solvent removed by the SQUEEZE procedure during the structure refinement.

Variable-temperature dc magnetic susceptibility measurements were performed in a 0.1 T field in the 5.0−300 K range. The susceptibility data were corrected with respect to the holder and the sample (estimated from Pascal's constants[36]) diamagnetic contribution. Studies for the reduced magnetization plots were carried out at the applied fields of 1000, 5000, 10 000, 20 000, 30 000, 40 000, 50 000, 60 000, and 70 000 Oe.

The temperature-dependent ac susceptibility measurement was performed at 1000 Hz frequency of the oscillating field.

AFM. Substance solution for AFM imaging was prepared in methanol, dropped onto an ultraflat silicon wafer (TED Pella Inc., Redding, CA, USA), and incubated at room temperature for 5 min for the substance to sediment and attach to the surface. To optimize the conditions for the AFM measurement, we have tested the different solutions and concentrations with DLS (see below). The excess methanol was subsequently removed, and the sample area was carefully dried with air. AFM measurements were performed as described previously[37] using NanoWizard (JPK Instruments, Berlin, Germany) in intermittent contact mode with commercially available silicon tips (NSC16 AlBS, Micromasch, Tallinn, Estonia). The image is presented in Figure 3 in the amplitude mode in a 5 × 5 μm frame.

Dynamic Light Scattering. For zeta potential measurements the solutions of substance **1** in 5% methanol/95% water (twice distilled, filtered) were used (see Figure S3). Two concentrations were applied: 2 mg/mL ("diluted") and 6 mg/mL ("concentrated").

The hydrodynamic diameter of the polyplexes was measured in the clear zeta cuvette (Malvern, Herrenberg, Germany) with a Zetasizer Nano ZS (Malvern, Herrenberg, Germany) at 25 °C with 173° backward scattering angle and analyzed using the Smoluchowski model. The number of runs and the attenuator position were adjusted automatically (8−11).

Studies of Stability in Solution by IR Spectrometry. A simple test was also conducted for the solutions of the $[Ni_{15}]$ complex in MeOH and in H_2O/MeOH (95/5). On evaporation of these solutions, a light green powder is obtained, which displays the same IR pattern as recorded for the pure crystalline compound (see Figure S1).

dx.doi.org/10.1021/ic500957y | Inorg. Chem. 2014, 53, 7642−7649

4.3. Studies of Biological Properties. *Details of the Cytotoxicity Assays. Materials.* MTT (3-(4,5-dimethylthiazol-2-yl)-2,5-diphenyltetrazolium bromide) was purchased from Sigma-Aldrich (Taufkirchen, Germany), and the LDH cytotoxicity detection kit was obtained from Roche Diagnostics (Mannheim, Germany).

Preparation of the Test Substance. The test substance was dissolved in methanol; subsequently distilled water was added to obtain the final solution with a 5% methanol content in water. The maximal test substance concentration was set at 1.5 mg/mL and subsequently diluted.

Cell Cultures. B16 mouse melanoma and L929 mouse fibroblasts were cultured in DMEM supplemented with 10% γ-inactivated fetal calf serum (PAA Laboratories, Cölbe, Germany) in a humidified atmosphere with 5% and 7.5% CO_2 at 37 °C, respectively. Subculturing was performed every several days upon 70−80% confluence to new Petri dishes with fresh medium.

I. MTT. The MTT cell proliferation assay[38] measures the cell proliferation rate as a function of metabolic activity in cell mitochondria. When metabolic events coupled with interaction of the test substance within cells lead to apoptosis or necrosis, the reduction in cell viability can be seen. The treated cells that suffer some toxic effect of the test substance have a diminished ability to metabolize the tetrazolium MTT to a substance with an absorption peak at 570 nm. The untreated cells are run as a blank control or a 100% cell viability. All values are related to this control.

B16 and L929 cells were seeded in 96-well plates at a density of 8000 cells/well in a full culture medium (Nunc, Wiesbaden, Germany), then maintained at normal cultivation conditions for 24 h to ensure sufficient cell adherence to the well bottom as reported previously.[39] After treatment with the test substance at different concentrations, starting from 1.5 mg/mL for 4 or 24 h, respectively, the medium was replaced by a serum-free medium containing MTT reagent and incubated again for 4 h. Cell viability was determined by measuring the absorbance of the enzymatically formed formazan at 570 nm with 690 nm background corrections; prior to measurement the cells were lysed in 200 μL of DMSO. The results are presented here as mean values of four replicates with standard deviation.

II. LDH Cytotoxicity Assay. Lactate dehydrogenase (LDH)[40] is a soluble cytosolic enzyme present in most eukaryotic cells and is released into the culture medium upon cell death due to damage of the plasma membrane. The plasma membrane may be damaged due to interactions with a test substance. The increase of the LDH activity in the culture supernatant is proportional to the number of cells with a damaged membrane or lysed cells. As a 100% toxicity control Triton-X can be used, as it is known to effectively lyse the cell membrane. Physiological cell metabolism leads to induction of LDH in the culture medium; at normal conditions untreated cells have up to 10% cellular toxicity assigned to that.

4.4. Details of Structure Refinement. The crystal structure **1** was solved with SHELXS97 and refined with SHELXL97 software.[41] On the basis of systematic absences the $P2_1$ space group type was chosen with absolute configuration consistent with pure enantiomer reagent used in the synthesis, as well as with X-ray diffraction studies. C-bonded H atoms were generated in their calculated positions with U_{eq} = 1.2/1.5U_{eq}(parent C atom) for aromatic, methylene/methyl H atoms, respectively. Other H atoms were not found on difference Fourier maps. Four ordered water molecules (O21W−O24W) were localized. Terminal solvent molecules bonded to Ni^{2+} ions were found to be water ligands, except for one site, where occupational disorder presence had to be assumed, with methanol/water components. The corresponding occupancies were refined and then constrained at the refined values (~0.29 for the methanol ligand; the O atom was assumed to retain its position in both components; a DFIX restraint was used for the C−O bond length). For the N18/N19/N10-containing ligands the AFIX 66 constraint had to be applied to the C18/C19/C10 phenyl rings. For the N18 ligand additional disorder of one $-CH_2COO$ moiety had to be assumed, causing difficulties even in localizing the corresponding atoms. The presence of two components was assumed (refined occupancies of 0.57(2)/0.43(2), respectively). For one component the DFIX restraint was used for the carboxyl O···O distance and a FLAT restraint was applied to the whole moiety. Moreover, the SAME restraint was used to make the geometrical parameters of the disordered moiety components coordinated to Ni^{2+} ions similar to that in the case of the ordered C123-containing moiety, coordinated to Ni4. For the N12/N13/N14 ligands the positions of the C12/C13/C14 aromatic rings were assumed to be disordered in two positions with half-occupancies, with isotropic temperature factors for most displaced atoms. AFIX 66 constraints were used to keep the right geometrical parameters for the corresponding phenyl rings. A combination of SIMU/ISOR/EADP restraints was also applied in some cases. The SQUEEZE procedure[42] had to be applied for the treatment of the remaining heavily disordered solvent molecules in voids between the molecules. In total, three voids were treated, of 7106, 4, and 4 Å^3 volume, containing 1782/4/4 electrons per unit cell, respectively. This should correspond approximately to either 50 methanol or 111 water molecules per asymmetric unit.

On the final difference Fourier map the highest peak of 0.80 e/Å^3 is located at the C88−C128 bond within the disordered ligand moiety, 2.96 Å to Ni12.

CCDC-972059 contains the supplementary crystallographic data for this paper. These data can be obtained free of charge from the Cambridge Crystallographic Data Centre via www.ccdc.cam.ac.uk/data_request/cif.

■ ASSOCIATED CONTENT

Ⓢ Supporting Information

Details of the physical property/stability measurements (magnetic properties, EDX, IR, DLS, TGA, crystallographic tables). This material is available free of charge via the Internet at http://pubs.acs.org.

■ AUTHOR INFORMATION

Corresponding Author

*E-mail: holynska@staff.uni-marburg.de.

Author Contributions

S.M. and M.H. performed syntheses and structural analyses; O.S. and I.L. performed the studies of biological properties/AFM, L.P., M.H., and G.C. performed magnetic measurements and their detailed analysis. All authors cowrote the paper.

Notes

The authors declare no competing financial interest.

■ ACKNOWLEDGMENTS

M.H. gratefully acknowledges the help of Prof. Dr. S. Dehnen (generous support and helpful discussions). The authors thank Dr. Eyas Dayyoub for technical support with AFM.

■ REFERENCES

(1) (a) Holm, R. H.; Kennepohl, P.; Solomon, E. I. *Chem. Rev.* **1996**, *96*, 2239. (b) Lippard, S. J.; Berg, J. M. In *Principles of Bioinorganic Chemistry*; University Science Books: Mill Valley, CA, 1994. (c) Therrien, B.; Süss-Fink, G.; Govindaswamy, P.; Renfrew, A. K.; Dyson, P. J. *Angew. Chem., Int. Ed.* **2008**, *47*, 3773.

(2) (a) Anbu, S.; Kamalraj, S.; Varghese, B.; Muthumary, J.; Kandaswamy, M. *Inorg. Chem.* **2012**, *51*, 5580. (b) Cimerman, Z.; Galic, N.; Bosner, B. *Anal. Chim. Acta* **1997**, *343*, 145.

(3) (a) Halcrow, M. A.; Christou, G. *Chem. Rev.* **1994**, *94*, 2421. (b) Fontecave, M.; Menage, S.; Duboc-Toia, C. *Coord. Chem. Rev.* **1998**, *178*, 1555. (c) Mukhopadhyay, S.; Mal, S. K.; Bhad-uri, S.; Armstrong, W. H. *Chem. Rev.* **2004**, *104*, 3981. (d) Nayak, S.; Nayek, H. P.; Dehnen, S.; Powell, A. K.; Reedijk, J. *Dalton Trans.* **2011**, *40*, 2699.

(4) (a) Bagai, R.; Christou, G. *Chem. Soc. Rev.* **2009**, *38*, 1011. (b) Leuenberger, M. N.; Loss, D. *Nature* **2001**, *410*, 789. (c) Aromi, G.; Brechin, E. K. *Struct. Bonding (Berlin)* **2006**, *122*, 1. (d) Gatteschi,

D.; Sessoli, R. *Angew. Chem., Int. Ed.* **2003**, *42*, 268. (e) Christou, G.; Gatteschi, D.; Hendrickson, D. N.; Sessoli, R. *MRS Bull.* **2000**, *25*, 66.
(5) Kauzmann, W. *Adv. Protein Chem.* **1959**, *14*, 1.
(6) Tanford, C. *Protein Sci.* **1997**, *6*, 1358.
(7) Tanford, C. *The Hydrophobic Effect: Formation of Micelles and Biological Membranes*, 2nd ed.; Wiley, New York, 1980.
(8) Tanford, C. *Science* **1978**, *200*, 1012.
(9) (a) Nelson, D. L.; Cox, M. M. In *Lehninger Principles of Biochemistry*, 4th ed.; Freeman: New York, 2005. (b) Baron, R.; Setny, P.; McCammon, J. A. *J. Am. Chem. Soc.* **2010**, *132*, 12091. (c) Ball, P. *Nature* **2011**, *478*, 467.
(10) Liu, T.; Diemann, E.; Li, H.; Dress, A. W. M.; Müller, A. *Nature* **2003**, *426*, 59.
(11) (a) Thio, Y.; Toh, S. W.; Xue, F.; Vittal, J. J. *Dalton Trans.* **2014**, *43*, 5998. (b) Dearden, A. L.; Parsons, S.; Winpenny, R. E. P. *Angew. Chem., Int. Ed.* **2001**, *40*, 152. (c) Li, J.; Tao, J.; Huang, R.-B.; Zheng, L.-S. *Inorg. Chem.* **2012**, *51*, 5988. (d) Nakajima, T.; Seto, K.; Horikawa, F.; Shimizu, I.; Scheurer, A.; Kure, B.; Kajiwara, T.; Tanase, T.; Mikuriya, M. *Inorg. Chem.* **2012**, *51*, 12503. (e) Brechin, E. K.; Gould, R. O.; Harris, S. G.; Parsons, S.; Winpenny, R. E. P. *J. Am. Chem. Soc.* **1996**, *118*, 11293. (f) Andres, H.; Basler, R.; Blake, A. J.; Cadiou, C.; Chaboussant, G.; Grant, C. M.; Güdel, H.-U.; Murrie, M.; Parsons, S.; Paulsen, C.; Semadini, F.; Villar, V.; Wernsdorfer, W.; Winpenny, R. E. P. *Chem.—Eur. J.* **2002**, *8*, 4867. (g) Cadiou, C.; Murrie, M.; Paulsen, C.; Villar, V.; Wernsdorfer, W.; Winpenny, R. E. P. *Chem. Commun.* **2001**, 2666. (h) Sydora, O. L.; Wolczanski, P. T.; Lobkovsky, E. B.; Rumberger, E.; Hendrickson, D. N. *Chem. Commun.* **2004**, 650. (i) Blake, A. J.; Grant, C. M.; Parsons, S.; Rawson, J. M.; Winpenny, R. E. P. *J. Chem. Soc., Chem. Commun.* **1994**, 2363. (j) Decker, A.; Fenske, D.; Maczek, K. *Angew. Chem., Int. Ed. Engl.* **1996**, *35*, 2863. (k) Zhang, C.; Matsumoto, T.; Samoc, M.; Petrie, S.; Meng, S.; Corkery, T. C.; Stranger, R.; Zhang, J.; Humphrey, M. G.; Tatsumi, K. *Angew. Chem., Int. Ed.* **2010**, *49*, 4209. (l) Zhang, S.; Zhen, L.; Xu, B.; Inglis, R.; Li, K.; Chen, W.; Zhang, Y.; Konidaris, K. F.; Perlepes, S. P.; Brechin, E. K.; Li, Y. *Dalton Trans.* **2010**, *39*, 3563. (m) Angamuthu, R.; Kooijman, H.; Lutz, M.; Spek, A. L.; Bouwman, E. *Dalton Trans.* **2007**, 4641.
(12) (a) Fenske, D.; Ohmer, J. *Angew. Chem., Int. Ed. Engl.* **1987**, *26*, 148. (b) Hong, M.; Huang, Z.; Liu, H. *J. Chem. Soc., Chem. Commun.* **1990**, 1210. (c) Berti, E.; Cecconi, F.; Ghilardi, C. A.; Midollini, S.; Orlandini, A. *Inorg. Chem. Commun.* **1999**, *2*, 146. (d) Albano, V. G.; Demartin, F.; Femoni, C.; Iapalucci, M. C.; Longoni, G.; Monari, M.; Zanello, P. *J. Organomet. Chem.* **2000**, *593*−*594*, 325.
(13) (a) Bembi, R.; Tandon, O. P. *J. Inorg. Nucl. Chem.* **1981**, *43*, 565. (b) Malik, W. U.; Bembi, R.; Bhargava, P. P.; Sushila; Tandon, O. P. *J. Ind. Chem. Soc.* **1980**, *57*, 455.
(14) Andreeff, M.; Goodrich, D. W.; Pardee, A. B. In *Holland-Frei Cancer Medicine*, 5th ed.; BC Decker: Hamilton (ON), 2000.
(15) Pelin, M.; Sosa, S.; Della Loggia, R.; Poli, M.; Tubaro, A.; Decorti, G.; Florio, C. *Food Chem. Toxicol.* **2012**, *50*, 206.
(16) Morita, H.; Umeda, M.; Ogawa, H. I. *Mut. Res.* **1991**, *261*, 131.
(17) Afrasiabi, Z.; Sinn, E.; Chen, J.; Ma, Y.; Rheingold, A. L.; Zakharov, L. N.; Rath, N.; Padhye, S. *Inorg. Chim. Acta* **2004**, *357*, 271.
(18) Afrasiabi, Z.; Sinn, E.; Padhye, S.; Dutta, S.; Padhye, S.; Newton, C.; Anson, C. E.; Powell, A. K. *J. Inorg. Biochem.* **2003**, *95*, 306.
(19) Afrasiabi, Z.; Sinn, E.; Lin, W.; Ma, Y.; Campana, C.; Padhye, S. *J. Inorg. Biochem.* **2005**, *99*, 1526.
(20) Liu, Y.-C.; Song, X.-Y.; Chen, Z.-F.; Gu, Y.-Q.; Peng, Y.; Liang, H. *Inorg. Chim. Acta* **2012**, *382*, 52.
(21) Datta, S.; Seth, D. K.; Gangopadhyay, S.; Karmakar, P.; Bhattacharya, S. *Inorg. Chim. Acta* **2012**, *392*, 118.
(22) Prabhakaran, R.; Kalaivani, P.; Huang, R.; Poornima, P.; Vijaya Padma, V.; Dallemer, F.; Natarajan, K. *J. Biol. Inorg. Chem.* **2013**, *18*, 233.
(23) Li, M. X.; Zhang, L. Z.; Zhang, D.; Ji, B. S.; Zhao, J. W. *Eur. J. Med. Chem.* **2011**, *46*, 4383.
(24) Zhong, X.; Yi, J.; Sun, J.; Wei, H.-L.; Liu, W.-S.; Yu, K.-B. *Eur. J. Med. Chem.* **2006**, *41*, 1090.
(25) Matkar, S. S.; Wrischnik, L. A.; Jones, P. R.; Hellmann-Blumberg, U. *Biochem. Biophys. Res. Commun.* **2006**, *343*, 754.
(26) Zhong, X.; Wei, H.-L.; Liu, W.-S.; Wang, D.-Q.; Wang, X. *Bioorg. Med. Chem. Lett.* **2007**, *17*, 3774.
(27) Selvakumaran, N.; Pratheepkumar, A.; Ng, S. W.; Tiekink, E. R. T.; Karvembu, R. *Inorg. Chim. Acta* **2013**, *404*, 82.
(28) Alexiou, M.; Tsivikas, I.; Dendrinou-Samara, C.; Pantazaki, A. A.; Trikalitis, P.; Lalioti, N.; Kyriakidis, D. A.; Kessissoglou, D. P. *J. Inorg. Biochem.* **2003**, *93*, 256.
(29) Dong, X.; Wang, X.; He, Y.; Yu, Z.; Lin, M.; Zhang, C.; Wang, J.; Song, Y.; Zhang, Y.; Liu, Z.; Li, Y.; Guo, Z. *Chem.—Eur. J.* **2010**, *16*, 14181.
(30) Pons-Balagu, A.; Piligkos, S.; Teat, S. J.; Sanchez Costa, J.; Shiddiq, M.; Hill, S.; Castro, G. R.; Ferrer-Escorihuela, P.; SaÇudo, E. C. *Chem.—Eur. J.* **2013**, *19*, 9064.
(31) (a) Mukherjee, P.; Drew, M. G. B.; Gomez-Garcia, C. J.; Ghosh, A. *Inorg. Chem.* **2009**, *48*, 4817. (b) Lu, J.-W.; Chen, C.-Y.; Kao, M.-C.; Cheng, C.-M.; Wie, H.-H. *J. Mol. Struct.* **2009**, *936*, 228.
(32) (a) Cannon, R. D.; White, R. P. *Prog. Inorg. Chem.* **1988**, *36*, 195. (b) Cage, B.; Cotton, F. A.; Dalal, N. S.; Hillard, E. A.; Rakvin, B.; Ramsey, C. M. *J. Am. Chem. Soc.* **2003**, *125*, 5270.
(33) CCDC ver. 5.34, November 2013.
(34) (a) Atkinson, H.; Chalmers, R. *Genetica* **2010**, *138*, 485. (b) Matulis, D.; Rouzina, I.; Bloomfield, V. A. *J. Mol. Biol.* **2000**, *296*, 1053.
(35) Bruker AXS. *APEX2* v2012.10-0; 2012.
(36) König, E. *Magnetic Properties of Coordination and Organometallic Transition Metal Compounds*; Hellwege, K. H.; Hellwege, A. M., Eds.; Springer: Berlin, 1966; pp 27−29
(37) Samsonova, O.; Glinca, S.; Biela, A.; Pfeiffer, C.; Dayyoub, E.; Sahin, D.; Klebe, G.; Kissel, T. *Acta Biomater.* **2013**, *9*, 4994.
(38) Zheng, M.; Liu, Y.; Samsonova, O.; Endres, T.; Merkel, O.; Kissel, T. *Int. J. Pharm.* **2012**, *1* (427), 80.
(39) Liu, Y.; Samsonova, O.; Sproat, B.; Merkel, O.; Kissel, T. *J. Controlled Release* **2011**, *163*, 262.
(40) Smith, S. M.; Wunder, M. B.; Norris, D. A.; Shellman, Y. G. *PLoS One* **2011**, *6*, e26908.
(41) Sheldrick, G. M. *SHELXTL 5.1*; Bruker AXS Inc.: Madison, WI, USA, 1997.
(42) Spek, A. L. *Acta Crystallogr.* **2009**, *D65*, 148.

A chiral, low-cytotoxic [Ni_{15}]-wheel complex

Simon Muche[a], Irina Levacheva[b], Olga Samsonova[b], Linh Pham[c], George Christou[c], Udo Bakowsky[b] and Małgorzata Hołyńska[a,c*]

[a]Fachbereich Chemie and Wissenschaftliches Zentrum für Materialwissenschaften (WZMW), Philipps-Universität Marburg, Hans-Meerwein-Straße, D-35032 Marburg, Germany.
[b]Institut für Pharmazeutische Technologie & Biopharmazie Philipps-Universität Marburg, Ketzerbach 63, D-35032 Marburg.
[c]Department of Chemistry, University of Florida, Gainesville, Florida 32611-7200, United States.

SUPPORTING INFORMATION

(Supplementary Material for Communication to *Inorg. Chem.*)

Experimental

Details of the studies of the magnetic properties

Van Vleck equation derived for the model assuming the presence of isolated [Ni_3] units (see the main article):

$$\chi_M = \frac{Ng^2\beta^2}{3kT} \cdot \frac{N}{D} + TIP$$

$$N = 6\exp(2m) + 6\exp(2n) + 30\exp(4m) + 6\exp(-4m) + 30\exp(6n) + 84\exp(6m)$$

$$D = 3\exp(2m) + \exp(-2m + 2n) + 3\exp(2n) + 5\exp(4m + 2n) + 3\exp(4m + 6n) + 5\exp(6n) + 7\exp(6m + 6n)$$

$$m = \frac{J}{kT} \qquad n = \frac{J'}{kT}$$

References for ESI

[S1] CIF core dictionary ver. 2.2 by Brown, I.D. (Brockhouse Institute for Materials Research, McMaster University, Hamilton, Ontario Canada).

Supplementary tables

Table S1 Basic crystallographic data for **1**.

	1
Formula	$C_{130.29}H_{160.58}N_{10}Ni_{15}O_{80}\cdot 4(H_2O)$
Formula weight	4099.46
Temperature [K]	100(2)
λ [Å]	0.71073
Crystal system	Monoclinic
Space group	$P2_1$
a [Å]	23.163 (6)
b [Å]	26.423 (7)
c [Å]	24.602 (7)
β [°]	112.74 (3)
V [Å^3]	13887 (6)
Z, ρ_{calc} [g cm^{-3}]	2, 0.980
μ [mm^{-1}]	1.05
F(000)	4225
Crystal size [mm]	0.25 × 0.23 × 0.10
θ range [º]	2.05-25.00
rflns: total/unique	124836/47738
R(int)	0.113
Abs. corr.	multi-scan
Min., max. transmission factors	0.539, 0.745
Data/restraints/params	47738/103/2012
GOF on F^2	1.03
R1 [I > 2σ(I)]	0.074
wR2 (all data)	0.152
Max., min. $\Delta\rho_{elect}$ [e Å^{-3}]	0.80, -1.11

Table S2 BVS calculations for metal ions in **1** [S1]. The quoted values are highly affected by the experimental errors connected with structure disorder.

	Ni^{2+}	**Ni^{3+}**
Ni1	2.15	2.75
Ni2	2.31	2.95
Ni3	2.12	2.71
Ni4	2.12	2.72
Ni5	2.28	2.92
Ni6	2.17	2.71
Ni7	2.08	2.67
Ni8	2.28	2.91
Ni9	2.12	2.71
Ni10	2.16	2.77
Ni11	2.22	2.83
Ni12	2.17	2.71
Ni13	2.05	2.63
Ni14	2.25	2.87
Ni15	2.15	2.76

Table S3 Ni…Ni distances in **1**.

Ni1 - Ni2	3.462(2)
Ni2 - Ni3	3.454(2)
Ni4 - Ni5	3.458(2)
Ni5 - Ni6	3.450(2)
Ni7 - Ni8	3.452(2)
Ni8 - Ni9	3.454(2)
Ni10 - Ni11	3.431(2)
Ni11 - Ni12	3.42(1)
Ni13 - Ni14	3.453(2)
Ni14 - Ni15	3.449(3)

Table S4 Selected geometrical parameters of the complex molecule in **1** [Å, °].

Ni1—O31	1.973 (5)	Ni8—O54	2.018 (6)
Ni1—N11	2.019 (7)	Ni8—O25	2.059 (7)
Ni1—O63	2.033 (6)	Ni8—O26	2.084 (6)
Ni1—O11	2.049 (5)	Ni9—N16	1.979 (7)
Ni1—O1W	2.108 (5)	Ni9—O16	2.013 (6)
Ni1—O2W	2.111 (5)	Ni9—O64	2.049 (6)
Ni2—O50	1.988 (5)	Ni9—O36	2.063 (6)
Ni2—O53	1.995 (6)	Ni9—O12W	2.089 (5)
Ni2—O11	1.996 (5)	Ni9—O11W	2.130 (6)
Ni2—O12	2.018 (5)	Ni10—N17	1.983 (8)
Ni2—O21	2.075 (6)	Ni10—O17	1.995 (6)
Ni2—O22	2.080 (6)	Ni10—O59	2.022 (7)
Ni3—N12	2.007 (7)	Ni10—O37	2.040 (7)
Ni3—O12	2.015 (6)	Ni10—O13W	2.119 (6)
Ni3—O60	2.044 (6)	Ni10—O14W	2.121 (6)
Ni3—O32	2.064 (5)	Ni11—O56	2.001 (6)
Ni3—O4W	2.082 (6)	Ni11—O18	2.014 (6)
Ni3—O3W	2.105 (6)	Ni11—O69	2.015 (6)
Ni4—N13	1.950 (8)	Ni11—O17	2.021 (6)
Ni4—O65	2.039 (7)	Ni11—O28	2.080 (6)
Ni4—O33	2.044 (6)	Ni11—O27	2.112 (6)
Ni4—O13	2.045 (7)	Ni12—N18	1.946 (11)
Ni4—O5W	2.122 (6)	Ni12—O18	1.983 (12)
Ni4—O6W	2.126 (5)	Ni12—O38	2.039 (10)
Ni5—O14	1.991 (6)	Ni12—O15W	2.094 (16)
Ni5—O52	1.999 (5)	Ni12—O66	2.104 (15)
Ni5—O55	2.014 (6)	Ni12—O16W	2.118 (15)
Ni5—O13	2.018 (6)	Ni13—N19	1.988 (8)
Ni5—O24	2.065 (7)	Ni13—O19	2.026 (6)
Ni5—O23	2.089 (7)	Ni13—O39	2.060 (7)
Ni6—N14	1.977 (9)	Ni13—O61	2.071 (7)
Ni6—O34	2.003 (6)	Ni13—O17W	2.121 (6)
Ni6—O62	2.023 (6)	Ni13—O18W	2.129 (6)
Ni6—O14	2.046 (6)	Ni14—O19	1.988 (6)
Ni6—O8W	2.101 (5)	Ni14—O58	1.991 (6)
Ni6—O7W	2.121 (6)	Ni14—O10	2.014 (6)
Ni7—O15	2.021 (6)	Ni14—O51	2.051 (6)
Ni7—O67	2.032 (6)	Ni14—O29	2.066 (6)
Ni7—N15	2.035 (7)	Ni14—O20	2.106 (6)
Ni7—O35	2.062 (6)	Ni15—N10	1.995 (8)
Ni7—O9W	2.104 (5)	Ni15—O10	2.019 (6)
Ni7—O10W	2.104 (6)	Ni15—O30	2.026 (6)
Ni8—O15	1.995 (6)	Ni15—O68	2.051 (7)
Ni8—O57	2.010 (6)	Ni15—O20W	2.091 (6)

Ni8—O16	2.011 (6)	Ni15—O19W	2.101 (7)
O31—Ni1—N11	83.3 (3)	O54—Ni8—O26	178.8 (2)
O31—Ni1—O63	88.0 (2)	O25—Ni8—O26	88.0 (3)
N11—Ni1—O63	170.0 (2)	N16—Ni9—O16	90.5 (3)
O31—Ni1—O11	173.7 (2)	N16—Ni9—O64	169.9 (3)
N11—Ni1—O11	90.7 (3)	O16—Ni9—O64	98.5 (2)
O63—Ni1—O11	98.2 (2)	N16—Ni9—O36	82.8 (3)
O31—Ni1—O1W	90.8 (2)	O16—Ni9—O36	173.1 (3)
N11—Ni1—O1W	88.8 (2)	O64—Ni9—O36	88.3 (3)
O63—Ni1—O1W	86.5 (2)	N16—Ni9—O12W	94.6 (2)
O11—Ni1—O1W	90.8 (2)	O16—Ni9—O12W	85.7 (2)
O31—Ni1—O2W	93.3 (2)	O64—Ni9—O12W	90.7 (2)
N11—Ni1—O2W	94.6 (2)	O36—Ni9—O12W	93.0 (2)
O63—Ni1—O2W	90.7 (2)	N16—Ni9—O11W	89.9 (3)
O11—Ni1—O2W	85.5 (2)	O16—Ni9—O11W	89.8 (2)
O1W—Ni1—O2W	175.0 (2)	O64—Ni9—O11W	85.6 (2)
O50—Ni2—O53	90.1 (2)	O36—Ni9—O11W	91.9 (2)
O50—Ni2—O11	86.2 (2)	O12W—Ni9—O11W	173.7 (2)
O53—Ni2—O11	100.8 (2)	N17—Ni10—O17	91.6 (3)
O50—Ni2—O12	101.2 (2)	N17—Ni10—O59	169.9 (3)
O53—Ni2—O12	85.6 (2)	O17—Ni10—O59	98.4 (3)
O11—Ni2—O12	170.3 (2)	N17—Ni10—O37	81.1 (3)
O50—Ni2—O21	91.3 (2)	O17—Ni10—O37	172.6 (3)
O53—Ni2—O21	177.3 (2)	O59—Ni10—O37	88.9 (3)
O11—Ni2—O21	76.9 (2)	N17—Ni10—O13W	90.0 (3)
O12—Ni2—O21	96.5 (2)	O17—Ni10—O13W	91.7 (2)
O50—Ni2—O22	178.5 (2)	O59—Ni10—O13W	88.1 (3)
O53—Ni2—O22	91.0 (2)	O37—Ni10—O13W	89.7 (2)
O11—Ni2—O22	94.6 (2)	N17—Ni10—O14W	91.9 (2)
O12—Ni2—O22	77.8 (2)	O17—Ni10—O14W	86.3 (2)
O21—Ni2—O22	87.8 (2)	O59—Ni10—O14W	90.4 (2)
N12—Ni3—O12	90.7 (3)	O37—Ni10—O14W	92.5 (2)
N12—Ni3—O60	169.9 (2)	O13W—Ni10—O14W	177.3 (2)
O12—Ni3—O60	98.6 (2)	O56—Ni11—O18	100.9 (3)
N12—Ni3—O32	82.4 (3)	O56—Ni11—O69	89.4 (3)
O12—Ni3—O32	173.0 (2)	O18—Ni11—O69	86.2 (2)
O60—Ni3—O32	88.4 (2)	O56—Ni11—O17	85.7 (2)
N12—Ni3—O4W	92.4 (2)	O18—Ni11—O17	170.8 (2)
O12—Ni3—O4W	85.0 (2)	O69—Ni11—O17	100.4 (2)
O60—Ni3—O4W	92.2 (2)	O56—Ni11—O28	178.7 (3)
O32—Ni3—O4W	94.1 (2)	O18—Ni11—O28	77.8 (3)
N12—Ni3—O3W	91.3 (2)	O69—Ni11—O28	90.5 (2)
O12—Ni3—O3W	91.3 (2)	O17—Ni11—O28	95.6 (3)
O60—Ni3—O3W	84.7 (2)	O56—Ni11—O27	92.0 (3)
O32—Ni3—O3W	90.0 (2)	O18—Ni11—O27	95.8 (3)
O4W—Ni3—O3W	174.8 (2)	O69—Ni11—O27	177.3 (3)
N13—Ni4—O65	164.6 (3)	O17—Ni11—O27	77.3 (2)
N13—Ni4—O33	78.8 (3)	O28—Ni11—O27	88.2 (2)
O65—Ni4—O33	86.3 (2)	N18—Ni12—O18	100.0 (9)
N13—Ni4—O13	96.2 (3)	N18—Ni12—O38	79.2 (6)
O65—Ni4—O13	98.8 (3)	O18—Ni12—O38	179.2 (11)
O33—Ni4—O13	174.6 (3)	N18—Ni12—O15W	87.4 (16)
N13—Ni4—O5W	89.1 (3)	O18—Ni12—O15W	92.1 (6)
O65—Ni4—O5W	87.0 (3)	O38—Ni12—O15W	87.5 (11)
O33—Ni4—O5W	91.1 (3)	N18—Ni12—O66	163.9 (10)
O13—Ni4—O5W	90.8 (3)	O18—Ni12—O66	95.2 (5)
N13—Ni4—O6W	92.9 (3)	O38—Ni12—O66	85.4 (8)
O65—Ni4—O6W	92.1 (2)	O15W—Ni12—O66	87.0 (6)
O33—Ni4—O6W	93.3 (2)	N18—Ni12—O16W	95.3 (16)

O13—Ni4—O6W	85.0 (2)	O18—Ni12—O16W	88.8 (5)
O5W—Ni4—O6W	175.5 (2)	O38—Ni12—O16W	91.7 (11)
O14—Ni5—O52	101.6 (2)	O15W—Ni12—O16W	176.9 (7)
O14—Ni5—O55	86.0 (2)	O66—Ni12—O16W	90.0 (6)
O52—Ni5—O55	90.3 (2)	N19—Ni13—O19	93.4 (3)
O14—Ni5—O13	171.0 (2)	N19—Ni13—O39	80.1 (3)
O52—Ni5—O13	84.9 (2)	O19—Ni13—O39	173.3 (3)
O55—Ni5—O13	100.3 (2)	N19—Ni13—O61	170.8 (3)
O14—Ni5—O24	77.3 (3)	O19—Ni13—O61	95.3 (3)
O52—Ni5—O24	178.1 (3)	O39—Ni13—O61	91.2 (3)
O55—Ni5—O24	91.2 (3)	N19—Ni13—O17W	88.3 (3)
O13—Ni5—O24	96.0 (3)	O19—Ni13—O17W	90.6 (2)
O14—Ni5—O23	97.4 (3)	O39—Ni13—O17W	90.7 (3)
O52—Ni5—O23	90.8 (3)	O61—Ni13—O17W	88.7 (3)
O55—Ni5—O23	176.2 (3)	N19—Ni13—O18W	93.7 (3)
O13—Ni5—O23	76.2 (3)	O19—Ni13—O18W	86.3 (2)
O24—Ni5—O23	87.8 (3)	O39—Ni13—O18W	92.7 (2)
N14—Ni6—O34	80.4 (3)	O61—Ni13—O18W	89.7 (2)
N14—Ni6—O62	169.4 (3)	O17W—Ni13—O18W	176.3 (3)
O34—Ni6—O62	89.5 (2)	O19—Ni14—O58	87.5 (2)
N14—Ni6—O14	92.7 (3)	O19—Ni14—O10	169.8 (3)
O34—Ni6—O14	172.9 (2)	O58—Ni14—O10	100.6 (3)
O62—Ni6—O14	97.5 (2)	O19—Ni14—O51	99.2 (2)
N14—Ni6—O8W	92.3 (3)	O58—Ni14—O51	90.7 (2)
O34—Ni6—O8W	93.2 (2)	O10—Ni14—O51	87.0 (2)
O62—Ni6—O8W	91.5 (2)	O19—Ni14—O29	79.0 (3)
O14—Ni6—O8W	85.4 (2)	O58—Ni14—O29	92.1 (3)
N14—Ni6—O7W	89.5 (3)	O10—Ni14—O29	94.3 (3)
O34—Ni6—O7W	90.0 (3)	O51—Ni14—O29	176.7 (3)
O62—Ni6—O7W	87.2 (3)	O19—Ni14—O20	93.5 (3)
O14—Ni6—O7W	91.7 (3)	O58—Ni14—O20	179.0 (3)
O8W—Ni6—O7W	176.6 (3)	O10—Ni14—O20	78.4 (3)
O15—Ni7—O67	99.0 (2)	O51—Ni14—O20	89.3 (2)
O15—Ni7—N15	90.9 (3)	O29—Ni14—O20	88.0 (2)
O67—Ni7—N15	169.1 (3)	N10—Ni15—O10	93.1 (3)
O15—Ni7—O35	172.1 (2)	N10—Ni15—O30	81.2 (3)
O67—Ni7—O35	88.5 (2)	O10—Ni15—O30	174.3 (3)
N15—Ni7—O35	81.9 (3)	N10—Ni15—O68	168.6 (3)
O15—Ni7—O9W	91.2 (2)	O10—Ni15—O68	97.6 (3)
O67—Ni7—O9W	86.0 (2)	O30—Ni15—O68	88.1 (3)
N15—Ni7—O9W	89.4 (2)	N10—Ni15—O20W	92.6 (2)
O35—Ni7—O9W	92.0 (2)	O10—Ni15—O20W	87.2 (2)
O15—Ni7—O10W	85.1 (2)	O30—Ni15—O20W	92.7 (2)
O67—Ni7—O10W	91.6 (2)	O68—Ni15—O20W	91.7 (3)
N15—Ni7—O10W	93.7 (2)	N10—Ni15—O19W	89.8 (3)
O35—Ni7—O10W	92.1 (2)	O10—Ni15—O19W	90.5 (3)
O9W—Ni7—O10W	175.2 (2)	O30—Ni15—O19W	89.7 (3)
O15—Ni8—O57	99.9 (2)	O68—Ni15—O19W	86.3 (3)
O15—Ni8—O16	171.5 (2)	O20W—Ni15—O19W	176.8 (2)
O57—Ni8—O16	86.5 (2)	Ni2—O11—Ni1	117.7 (3)
O15—Ni8—O54	85.7 (2)	Ni3—O12—Ni2	117.8 (3)
O57—Ni8—O54	89.0 (2)	Ni5—O13—Ni4	116.7 (3)
O16—Ni8—O54	100.2 (2)	Ni5—O14—Ni6	117.4 (3)
O15—Ni8—O25	78.0 (2)	Ni8—O15—Ni7	118.5 (3)
O57—Ni8—O25	177.8 (2)	Ni8—O16—Ni9	118.3 (3)
O16—Ni8—O25	95.5 (2)	Ni10—O17—Ni11	117.4 (3)
O54—Ni8—O25	91.6 (3)	Ni12—O18—Ni11	117.8 (5)
O15—Ni8—O26	95.2 (3)	Ni14—O19—Ni13	118.7 (3)
O57—Ni8—O26	91.5 (2)	Ni14—O10—Ni15	117.6 (3)

O16—Ni8—O26	78.9 (2)		

Supplementary Figures

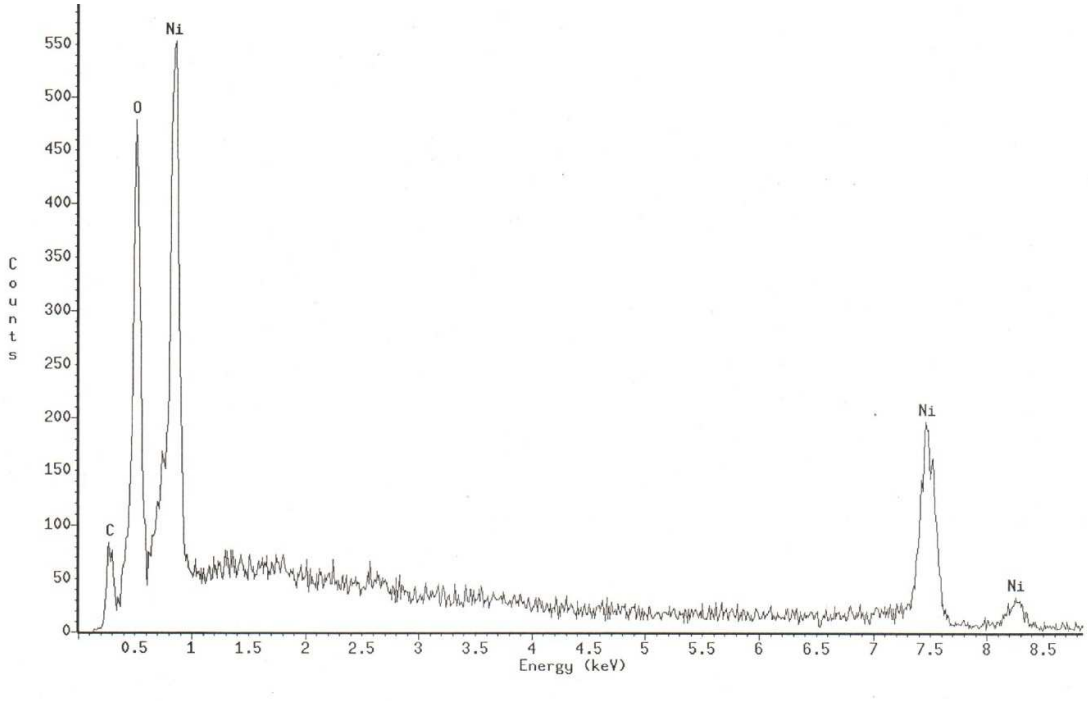

(a)

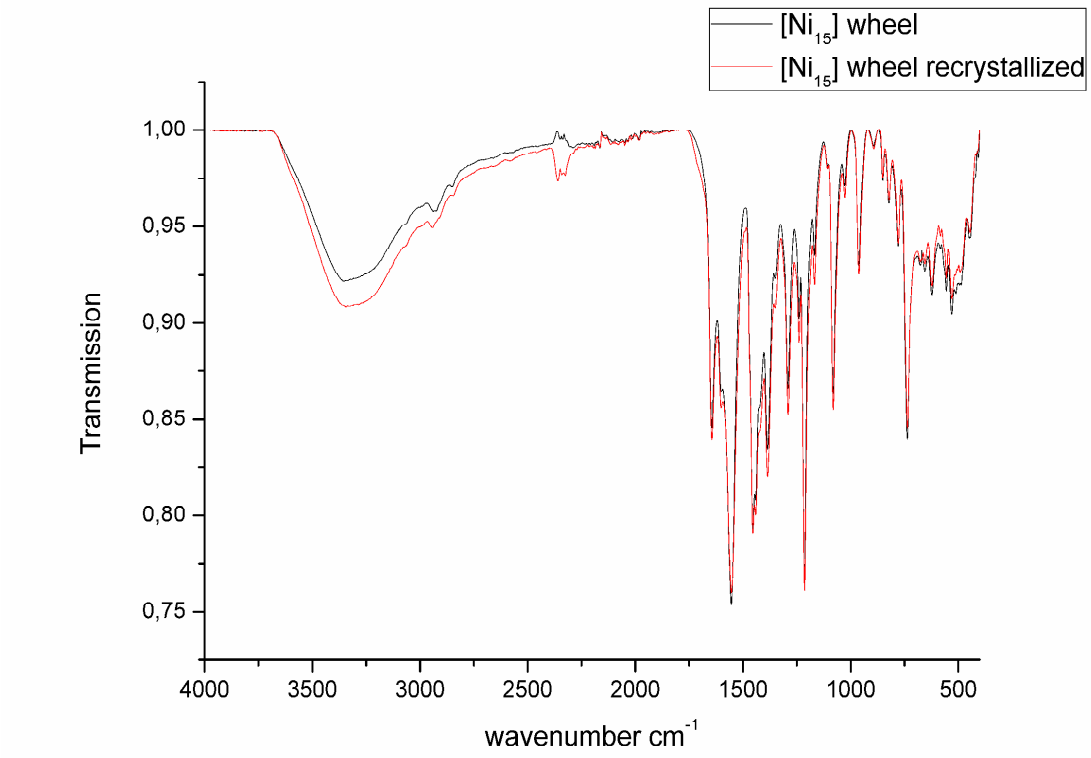

(b)

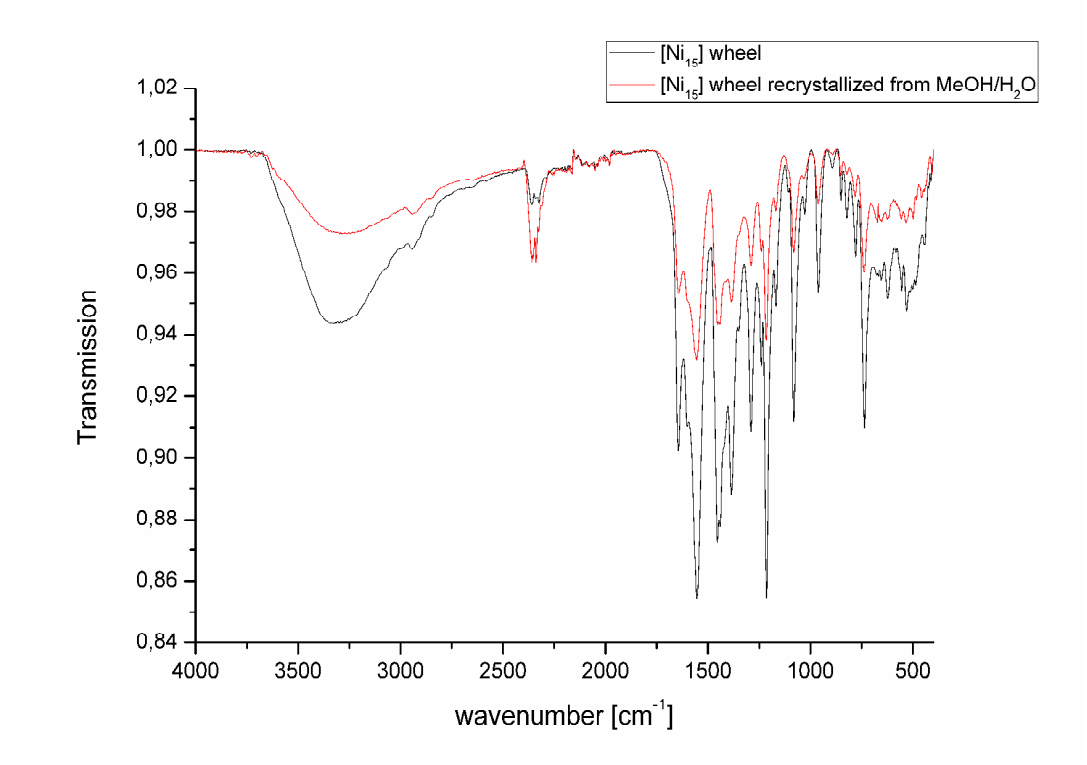

(c)

Figure S1 (a) The EDX spectrum collected for a sample of **1**. (b) Comparison of the IR spectrum of the crystalline product and of the residue obtained after evaporating its solution in methanol. (c) Comparison of the IR spectrum of the crystalline product and of the residue obtained after evaporating its solution in water/methanol (95/5).

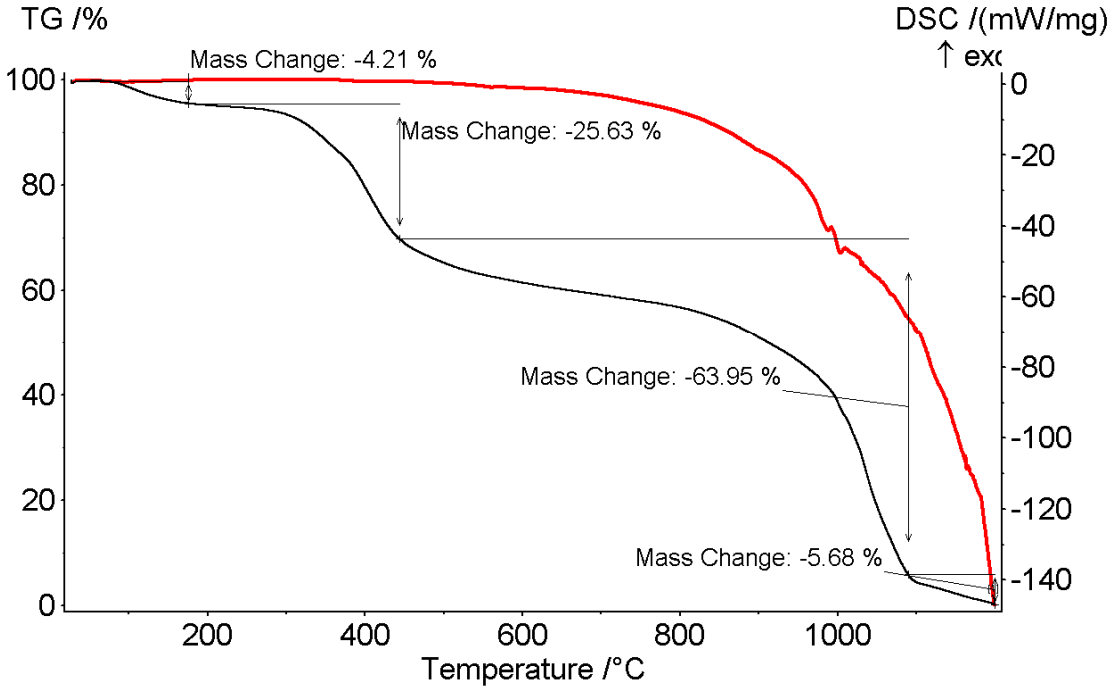

Figure S2 Thermogravimetric diagram collected for a sample of **1**.

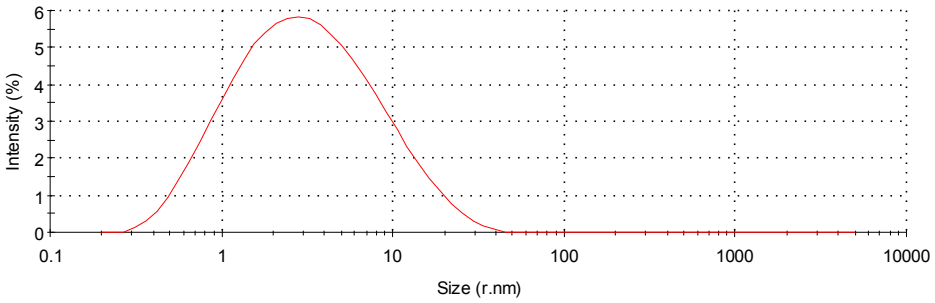
Intensity (%)
0
1
2
3
4
5
6
0.1
1
10
100
1000
10000
Size (r.nm)

(a)

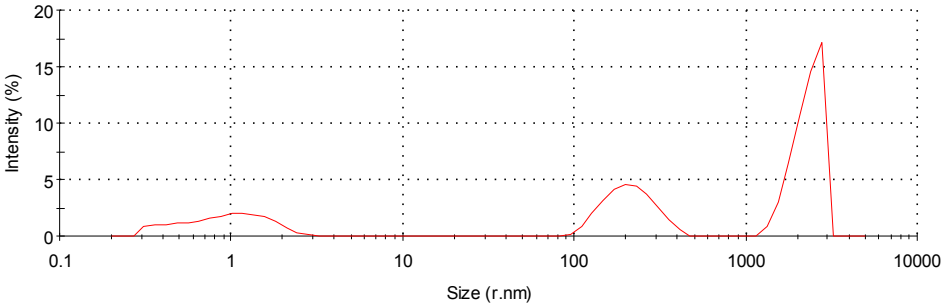
Intensity (%)
0
5
10
15
20
0.1
1
10
100
1000
10000
Size (r.nm)

(b)

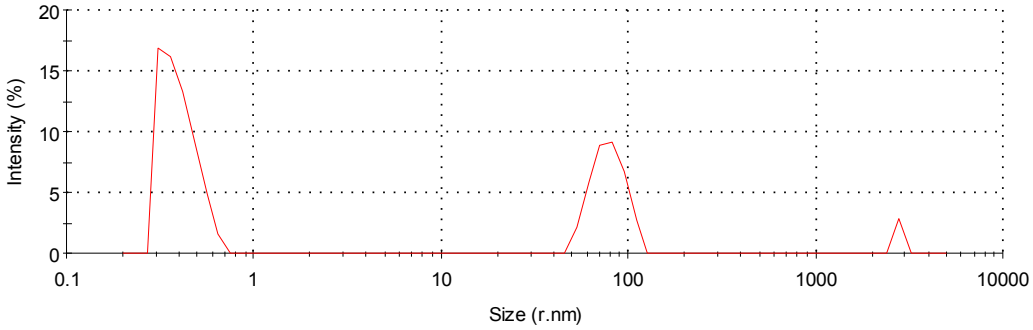
Intensity (%)
0
5
10
15
20
0.1
1
10
100
1000
10000
Size (r.nm)

(c)

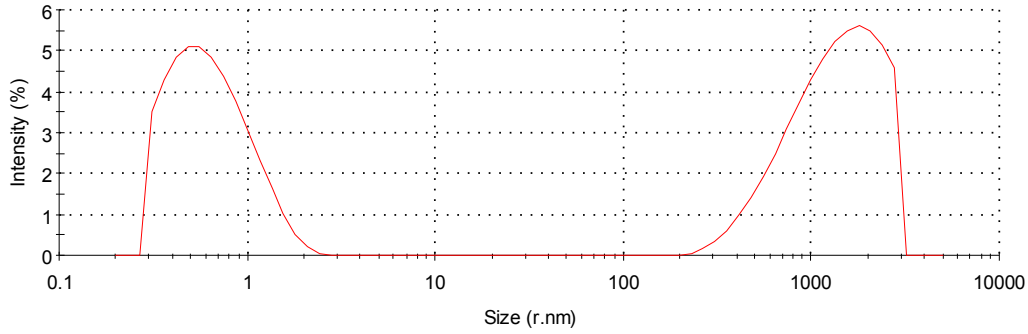
Intensity (%)
0
1
2
3
4
5
6
0.1
1
10
100
1000
10000
Size (r.nm)

(d)

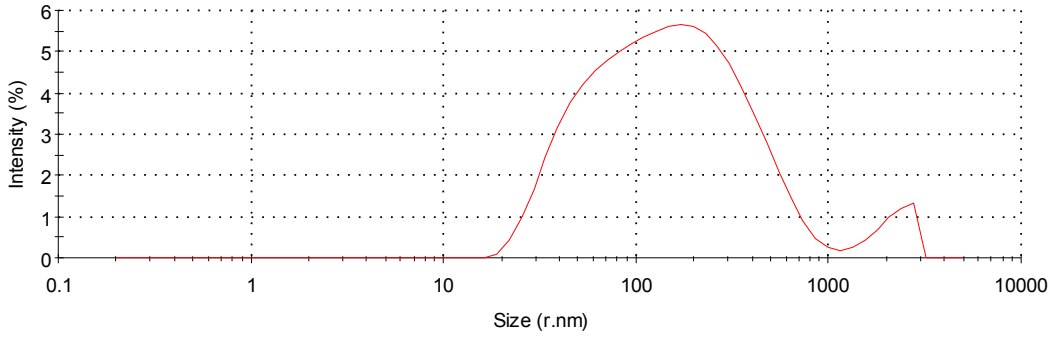

(e)

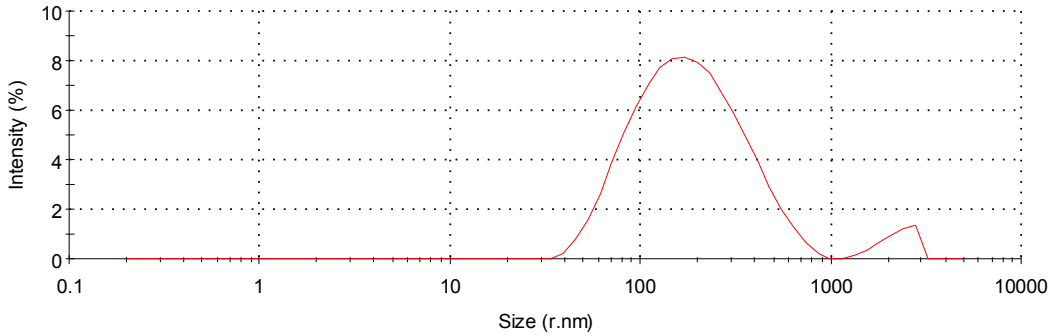

(f)

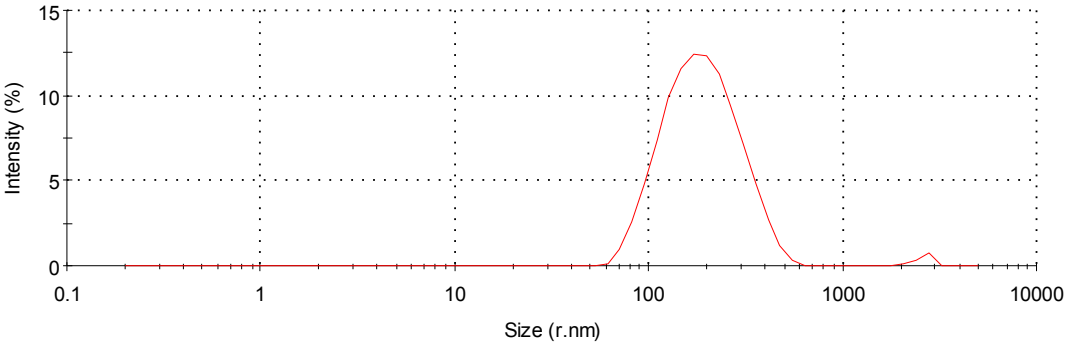

(g)

Figure S3 DLS results for the solutions of **1** (see Section 2 on dynamic light scattering for details): (a) freshly prepared in methanol ("diluted"), (b) freshly prepared in methanol ("concentrated"), (c) after 15 min. incubation in methanol ("diluted"), (d) after 1 h incubation in methanol ("diluted"), (e) freshly prepared in water/methanol ("diluted"), (f) in water/methanol after 15 min. ("diluted"), (g) in water/methanol after 1 h ("diluted"). Hydrodynamic Diameter [nm] / Intensity [%] – (a) peak: 4.6/100, (b) peak 1: agglomerates >2000/52.7, peak 2: 216.8/27.6, peak 3: 1.0/19.7, (c) peak 1: 0.4/61.7, peak 2: 78.7/35.4, peak 3: agglomerates >2000/2.9, (d) peak 1: >1400/55.4, peak 2: 0.7/44.6, (e) peak 1: 192.5/94.9, peak 2: agglomerates >2000/5.1, (f) peak 1: 212.3/95.4, peak 2: agglomerates >2000/4.6, (g) peak 1: 193.0/97.2, peak 2: >2000/2.8.

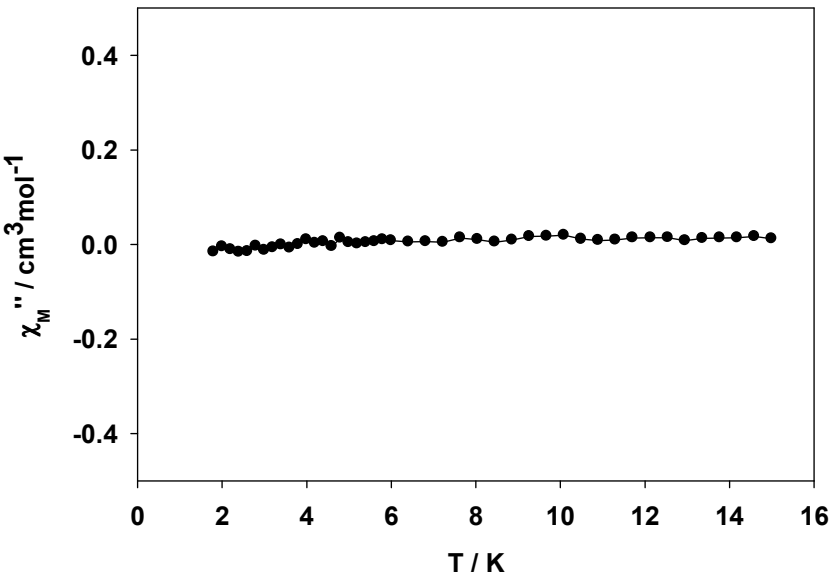

Figure S4 AC χ_M'' *vs.* T plot.

II Synthesis, structure and stability of a chiral imine-based Schiff-base ligand derived from L-glutamic acid and its [Cu_4] complex

Muche, S.; Levacheva, I.; Samsonova, O.; Biernasiuk, A., Malm, A. Lonsdale, R.; Popiołek, L., Bakowsky, U.; Hołyńska, M. *Journal of Molecular Structure* **2017**, *1127*, 231-236.

Studies of the stability of a ligand derived from *L*-glutamic acid and *ortho*-vanillin and its new [Cu_4] complex are presented. The [Cu_4] complex contains a heterocubane [$Cu^{II}_4O_4$] core and pendant carboxylic groups increasing its solubility in water, also under basic conditions. The stability of the complex in different solvents is confirmed with ESI-MS studies and such experiments as successful recrystallization. The complex is stable also under physiological conditions whereas the ligand is partly decomposed to *L*-glutamic acid and *ortho*-vanillin.

Inhalt: Berichtet werden die Synthesen, vollständige Charakterisierung und Untersuchungen zu den biologischen Eigenschaften eines Schiff'sche Base-Liganden aus *ortho*-Vanillin und *L*-Glutaminsäure als Dinatriumsalz, sowie eines korrespondierenden tetranuklearen Cu(II)-Komplexes, dessen Kristallstruktur ebenfalls beschrieben wird. Beide Verbindungen werden mittels IR, Elementaranalyse und ESI-MS charakterisiert. Für den Liganden werden zusätzlich NMR-Studien zur Stabilität unter physiologischen Bedingungen präsentiert. Dabei zeigt sich, dass der Ligand nahezu sofort teilweise (max. 23%) in seine Edukte zerfällt. Die Stabilität des Kupferkomplexes wird mittels IR-Spektroskopie bestimmt. Dieser ist über den betrachteten Zeitraum von 48 h stabil. Der Ligand zeigt keine signifikante Zytotoxizität gegenüber zwei getesteten murinen Zelllinien und der Kupferkomplex lediglich moderate Zytotoxizität. Aus antimikrobiellen Studien geht hervor, dass der Metallkomplex milde bis moderate antibakterielle Aktivität gegenüber grampositive Bakterien, sowie gute antifungale Aktivität gegen Organsimen der Gattung *Candida* besitzt. Der Ligand zeigt milde bis gute Aktivität gegenüber grampositiven und gramnegativen Bakterien und eine sehr starke Aktivität gegenüber Organismen der Gattung *Candida* sowie Fluconazol-resistenten Stämmen dieser Gattung. Allerdings ist dieses anfangs bemerkenswerte Ergebnis auf den Zerfall des Liganden zurückzuführen. Ebenfalls durchgeführte Tests mit *ortho*-Vanillin haben gezeigt, dass *ortho*-Vanillin dieselbe und teilweise auch höhere antifungale Aktivität besitzt wie der Ligand. *L*-Glutaminsäure ist dagegen inaktiv.

Eigener Anteil: Die Planung und Durchführung der Synthesen sowie die Aufnahme und Auswertung der Basisanalytik wurde von mir durchgeführt unter Betreuung von Małgorzata

Hołyńska. Die Röntgenstrukturanalyse wurde von der hauseigenen Serviceabteilung durchgeführt. Die Analyse der kristallographischen Daten erfolgte durch Małgorzata Hołyńska. Die NMR-Spektren zur Bestimmung der Stabilität des Liganden wurden von Cornelia Mischke aus der hauseigenen NMR-Abteilung aufgenommen und von mir ausgewertet. Irina Levacheva und Olga Samsonova aus der Arbeitsgruppe von Udo Bakowsky führten die MTT-Assays durch und bereiteten die dazugehörigen Daten auf. Die antimikrobiellen Studien wurden von Anna Biernasiuk, Anna Malm und Łukasz Popiołek durchgeführt und die dazugehörigen Daten aufbereitet. Richard Lonsdale half bei der Erstellung des Manuskriptes und teilweise bei der Datenanalyse und Simulation. Das Manuskript wurde von allen Autoren gemeinschaftlich verfasst.

Journal of Molecular Structure 1127 (2017) 231–236

Contents lists available at ScienceDirect

Journal of Molecular Structure

journal homepage: http://www.elsevier.com/locate/molstruc

Synthesis, structure and stability of a chiral imine-based Schiff-based ligand derived from L-glutamic acid and its [Cu_4] complex

Simon Muche [a], Irina Levacheva [b], Olga Samsonova [b], Anna Biernasiuk [c], Anna Malm [c], Richard Lonsdale [a, d], Łukasz Popiołek [e], Udo Bakowsky [b], Małgorzata Hołyńska [a, *]

[a] Fachbereich Chemie und Wissenschaftliches Zentrum für Materialwissenschaften, Philipps-Universität Marburg, Hans-Meerwein-Strasse, D-35043, Marburg, Germany
[b] Institut für Pharmazeutische Technologie & Biopharmazie, Philipps-Universität Marburg, Ketzerbach 63, D-35032, Marburg, Germany
[c] Department of Pharmaceutical Microbiology, Medical University, Chodźki 1, 20-093, Lublin, Poland
[d] Max-Planck-Institut für Kohlenforschung, Kaiser-Wilhelm-Platz 1, D-45470, Mülheim an der Ruhr, Germany
[e] Department of Organic Chemistry, Medical University of Lublin, Chodźki 4A, 20-093, Lublin, Poland

ARTICLE INFO

Article history:
Received 19 June 2016
Received in revised form
23 July 2016
Accepted 25 July 2016
Available online 27 July 2016

Keywords:
Copper (II)
Schiff-base
Stability
Crystal structure

ABSTRACT

Studies of the stability of a ligand derived from *L*-glutamic acid and *ortho*-vanillin and its new [Cu_4] complex are presented. The [Cu_4] complex contains a heterocubane [$Cu^{II}_4O_4$] core and pendant carboxylic groups increasing its solubility in water, also under basic conditions. The stability of the complex in different solvents is confirmed with ESI-MS studies and such experiments as successful recrystallization. The complex is stable also under physiological conditions whereas the ligand is partly decomposed to *L*-glutamic acid and *ortho*-vanillin.

1. Introduction

Oligonuclear metal complexes with Schiff-base ligands have been shown to often display antibacterial, antifungal, anti-inflammatory and antiviral activities [1]. In spite of these observations, attempts to rationalize them are scarcely available. For instance, Raman et al. [2a] studied Schiff bases derived from 1H-indole-2,3-dione (isatin) and 4-(2-aminoethyl)phenol (tyramine) and their Cu, Ni, Zn complexes interacting with the minor groove of CT-DNA. The increased antibacterial activity of the metal complexes was rationalized in terms of Tweedy's chelation theory on metal-ligand bonding enhancing the system's liphophilicity and, as a consequence, the ability to penetrate lipid membranes and to block the metal-binding sites of microbial enzymes. Moreover, the highest activity of the Cu(II) complex was explained in terms of the atomic radius/electronegativity of the Cu^{2+} ion leading to the conclusion that the antimicrobial properties are more promising for ions with higher electronegativities and large atomic radii. These considerations were completed with docking studies. Such theoretical reports rationalizing the interaction with DNA and proteasome inhibition of some Schiff-base complexes are available also for other systems [2b–f].

In particular, fungal infections (candidiasis) are a serious problem to civilization, increasing the mortality of infants and individuals suffering from decreased immunity. The administration of therapeutic doses of the currently available antimicrobial agents to patients leads to multiple side effects [3]. The most common adverse effects are allergic reactions, shifts in microflora balance and the generation of resistance in pathogenic species. After misbalancing of the natural defense system in the body, so follows the increase in the host vulnerability towards external pathogens, leading to a more aggressive disease progression [4,5]. To find the “golden ratio” in the interplay of host-drug-microbe means not only to improve the therapeutic efficacy but also to immensely improve the patients' life quality.

In this contribution we report on a sodium salt of a Schiff-base derived from *ortho*-vanillin and *L*-glutamic acid (**Na_2HL**, Scheme 1), as well as its [Cu_4] complex (**$[Cu_4(HL)_4]\cdot 4.6H_2O$**) featuring pendant carboxylic groups. It is shown that the ligand partly

* Corresponding author.
E-mail address: holynska@staff.uni-marburg.de (M. Hołyńska).

http://dx.doi.org/10.1016/j.molstruc.2016.07.100
0022-2860/

decomposes under physiological conditions. On the other hand, the copper(II) complex displays significant stability, even in its aqueous solution (Fig. 1). This is part of our project on the coordination chemistry of Schiff-base ligands containing biologically relevant moieties which already yielded a biologically compatible wheel-like [Ni_{15}] complex, reported elsewhere [6]. Apart from that study, the title copper(II) complex is the second example of a metal complex with this ligand system.

2. Results and discussion

2.1. Syntheses and stability

Although the reported ligand has been known for many decades [7], no analytical data are available, except for the stability constants of its metal complexes.

Herein the ligand **H_3L** (Scheme 1) was synthesized in the form of a sodium salt **Na_2HL** by modification of a method reported by Heinert and Martell [8] for the potassium salt of the vanillin analogue. Formation of a disodium salt of the organic ligand is consistent with the elemental analysis results (see SI).

Under ESI conditions the exact mass peaks were found. The ^{1}H NMR spectrum in MeOD (Fig. S2) shows all of the expected signals, except for the proton from the phenolic −OH group, which is due to a fast exchange with the solvent. In D_2O partial decomposition takes place as evidenced by the presence of a new peak at 9.97 p.m., attributed to the aldehyde H atom of *ortho*-vanillin.

Attempts to crystallize the ligand in its neutral form **H_3L** were unsuccessful and usually led to yellow oily phases.

The corresponding complex **$[Cu_4(HL)_4]\cdot 4.6H_2O$** was crystallized from a system where the organic ligand was generated *in situ* (see Scheme 2 for the ligand coordination mode). Subsequent protonation of the side chains is essential for crystal growth of the **$[Cu_4(HL)_4]\cdot 4.6H_2O$** complex. Addition of hydrochloric acid to the reaction mixture from the beginning hampers crystallization.

$[Cu_4(HL)_4]\cdot 4.6H_2O$ is soluble in polar solvents, e.g. water, ethanol, methanol and isopropanol and slightly soluble in dichloromethane. Compound **Na_2HL** dissolves immediately with partial decomposition in water. Furthermore, **Na_2HL** is soluble in methanol and DMSO and sparingly in ethanol.

$[Cu_4(HL)_4]\cdot 4.6H_2O$ displays molecular peaks under ESI-MS conditions in its aqueous and dichloromethane solutions. On drying in vacuum for 6 h neither the color nor the solubility changes. The vacuum-dried and air-dried samples of **$[Cu_4(HL)_4]\cdot 4.6H_2O$** show identical IR spectra (see SI). These observations confirm a reasonable stability of both **$[Cu_4(HL)_4]\cdot 4.6H_2O$** and **$Na_2HL$** in solution and in solid state.

To investigate the behavior in solution and, at the same time, the potential of **Na_2HL** and **$[Cu_4(HL)_4]\cdot 4.6H_2O$** for application in biological systems, their stability under physiological conditions was investigated. Due to the paramagnetic nature of the complex, measurement by standard NMR was not possible. Therefore the stability for **$[Cu_4(HL)_4]\cdot 4.6H_2O$** was investigated mainly with IR spectroscopy. Fig. 1 shows the IR spectra in the relevant range from 1800 cm^{-1} to 400 cm^{-1} for the complex as-synthesized and the remaining dried solids after various time spans of shaking the dissolved compound in phosphate-buffered saline (PBS) at 37 °C. All spectra show no significant discrepancy compared to the spectra of the as-synthesized **$[Cu_4(HL)_4]\cdot 4.6H_2O$** (black line). These results are conform with our unsuccessful efforts to explore the reactivity of the carboxylic groups of **$[Cu_4(HL)_4]\cdot 4.6H_2O$**. Furthermore, we could recrystallize the complex from a sample prepared in the same manner like for the stability test without any structural changes. Crystal growth on the inner face of the tube was observed at 4 °C within 2 weeks. Cell constants/full X-ray diffraction measurements confirmed that these crystal structures are identical as for the copper complex.

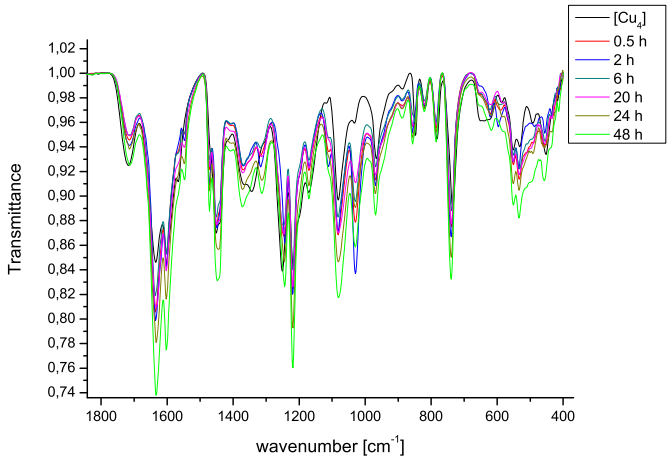

Fig. 1. IR spectra of **$[Cu_4(HL)_4]\cdot 4.6H_2O$** as synthesized (black line) and after various time spans.

The same experimental setting as for **$[Cu_4(HL)_4]\cdot 4.6H_2O$** was also performed for **Na_2HL**. The spectra of the remaining solid after drying showed significant differences compared to the spectra of **Na_2HL** as-synthesized. Furthermore, the color of the solution changed to brown after around 20 h. Based on these results and the fact, that the NMR spectra recorded in D_2O show a decomposition of **Na_2HL** to *ortho*-vanillin, we performed short- and long-term NMR measurement to determine the stability of **Na_2HL** under physiological conditions. Fig. 2 shows the relevant signals for *ortho*-vanillin (10.17 ppm, CO*H*) and the **Na_2HL** (8.44 ppm, *HC*═N) in the

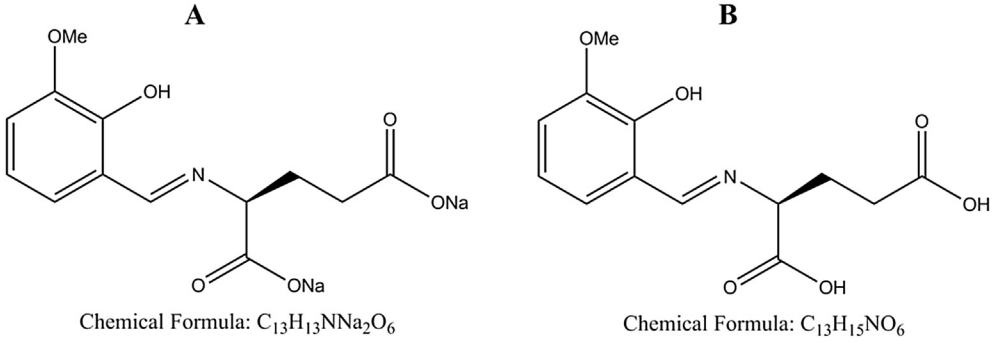

Scheme 1. Structural and chemical formula of the ligand as disodium salt (A; abbrev. **Na_2HL**) and its neutral form (B; abbrev. **H_3L**).

recorded spectra. The *ortho*-vanillin/ligand ratio was determined by the integrals, which should give 1 in total. The spectrum A was recorded immediately after mixing **Na_2HL** with the NMR solvent (t_0). The spectra B–F were recorded in steps of 2 min. The spectra G and H were recorded 2 h and 24 h after t_0. All spectra show decomposition of **Na_2HL** in PBS/D_2O into *ortho*-vanillin. At t_0 15% of compound **Na_2HL** is decomposed into *ortho*-vanillin. This value increases up to 23% during the next 10 min, where it remains stable. After 24 h the value persists at 23%. Furthermore, after 24 h the solution turned to light brown and a new signal appeared at 8.59 ppm. Identification of the new signal was not possible. However, the spectrum F resembles the other spectra.

2.2. Structural aspects

$[Cu_4(HL)_4]\cdot 4.6H_2O$ was obtained in crystalline form and found suitable for single crystal X-ray diffraction studies. The compound crystallizes in the $P2_1$ space group type (see Experimental and SI for the details of the crystal structure determination). The complex molecules lie in general positions and comprise 4 doubly deprotonated ligands and four Cu^{2+} ions (Fig. 3). A central distorted-cubane $[Cu_4O_4]$ motif is created by the involvement of phenoxo O, imino N and carboxylate O atoms from each ligand. Each ligand thus chelates two Cu^{2+} ions in three modes: O,O and 2(O,N). Such a motif is common in Cu(II) chemistry. Selected parameters of the complex core are listed in Table S2. In each organic ligand the second carboxylic group remains protonated, pointing outside the complex core. Two of these groups are disordered in two positions. Unexpectedly, only the carboxylic O atom (O55) is involved in *O*–H···O hydrogen bonds as donor. The acceptor is the symmetry-related coordinated O33 carboxylate atom. Thus hydrogen-bonded chains are formed along [010] (Fig. 4). Water molecules are located between the chains in a layered-like arrangement.

3. Conclusions

The title compound **Na_2HL** derived from *L*-glutamic acid and *ortho*-vanillin isolated as a disodium salt was shown to undergo partial decomposition under physiological conditions. Initial studies show its potential for applications as an antifungal agent (see SI).

Na_2HL can be used as a precursor of a tetranuclear copper(II) complex **$[Cu_4(HL)_4]\cdot 4.6H_2O$** with pendant carboxylic groups and lower antibacterial/antifungal activity but increased cytotoxicity, as shown by the first tests (see SI). The carboxylic functional groups of **$[Cu_4(HL)_4]\cdot 4.6H_2O$** allow to tune its solubility and our studies confirm its high stability in solution. Inclusion of biologically relevant moieties in **$[Cu_4(HL)_4]\cdot 4.6H_2O$** and **$Na_2HL$** seems to increase their biological compatibility as confirmed with studies of cytotoxicity.

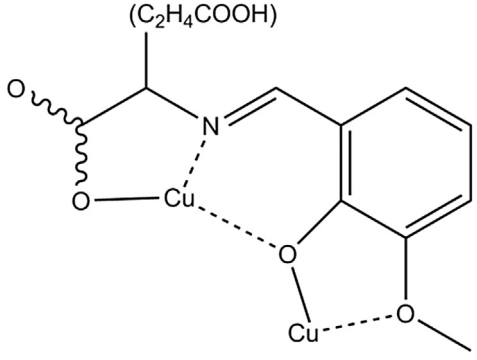

Scheme 2. Coordination mode of **HL** in **$[Cu_4(HL)_4]\cdot 4.6H_2O$** (stereochemistry not shown).

4. Experimental section

4.1. Syntheses

The ligand **Na_2HL**: 320 mg (8 mmol) of NaOH was dissolved in 60 mL of warm methanol. 588 mg (4 mmol) of *L*-glutamic acid was added and stirred until the solid was dissolved completely. 608 mg (4 mmol) of *ortho*-vanillin was added and the yellow solution was stirred for 1 h at room temperature. Addition of 150 mL of diethyl ether led to precipitation of the yellow product **Na_2HL**. The solid was filtered off, washed with diethyl ether and dried under air for 12 h. The resulting product was dried for 2 h under high vacuum.

IR bands for **Na_2HL** (cm^{-1}): 471.9 (vw), 512.7 (vw), 559.2 (vw), 576.4 (m), 605.6 (vw), 638.6 (vw), 664.0 (w), 735.6 (s), 776.5 (m), 794.0 (w), 844.6 (s), 930.1 (w), 973.1 (m), 1012.4 (vw), 1074.2 (m), 1170.3 (w), 1254.1 (s), 1280.01 (w), 1316.4 (vw), 1336.6 (w), 1413.6 (s), 1455.4 (s), 1575.4 (vs), 1632.5 (m).

^{1}H NMR (ppm, MeOD-d_4):8.31 (s, 1H), 6.86 (d, 2H, $3J = 8.27$ Hz), 6.48 (t, 1H,, $3J = 7.73$ Hz; 8.03 Hz), 4.06–4.11 (m, 1H), 3.81 (s, 1H), 2.10–2.39 (m, 4H).

Elemental analysis for the substance dried under vacuum for 2 h, analysed as $C_{13}H_{13}NO_6Na_2$ (see SI for details): Calcd (found): C 48.01 (47.24), H 4.03 (4.00), N 4.31 (4.23), O 29.52 (29.76).

ESI-MS: Molecular peak was found at $m/z = 282.1$ (ESI+; $[M + H]^+$) and 280.1 (ESI-; $[M - H]^-$) in methanol.

The complex **$[Cu_4(HL)_4]\cdot 4.6H_2O$**: 147 mg (1.0 mmol) of *L*-glutamic acid and 408 mg (3.0 mmol) of sodium acetate was dissolved in 3.5 mL of water and 5 mL of methanol and heated to 80 °C. When the solid part was completely dissolved, 152 mg (1.0 mmol) of *ortho*-vanillin was added to the stirred *L*-glutamic acid/sodium acetate solution. To the resulting yellow solution 250 mg (1 mmol) of $CuSO_4\cdot 5H_2O$ was added. The solution color changed to green immediately. The solution was stirred for 30 min at 80 °C and afterwards combined with a solution containing 11.5 mL of water, 6 mL of methanol and 0.6 mL of 2 M hydrochloric acid. The solution was stirred for one minute and transferred into a 30 mL vial for crystallization by slow evaporation. Green crystals in form of plates were obtained within one day. Crystallization is finished after few days depending on evaporation rate. Yield: average 147 mg per sample.

IR bands for **$[Cu_4(HL)_4]\cdot 4.6H_2O$** ($cm^{-1}$): 463.38 (w), 534.03 (w), 651.98 (w), 740.59 (m), 785.20 (w), 812.55 (w), 846.58 (w), 966.57 (m), 1083.14 (w), 1085.77 (m), 1216.71 (s), 1251.56 (s), 1348.50 (m), 1453.65 (m), 1565.89 (w), 1602.37 (s), 1634.46 (s), 1694.58 (m), 2335.63 (vw), 2362.63 (vw), 2842.87 (vw), 2908.44 (vw), 2947.02 (vw), 2985.59 (vw).

Elemental analysis: Elemental analysis for the substance dried under vacuum for 6 h, analysed as $C_{52}H_{52}N4O_{24}Cu_4\cdot 4H_2O$: Calcd (found): C 43.28 (43.37), H 4.18 (4.19), N 3.88 (3.86).

ESI-MS: Molecular peak was found at $m/z = 1394$ (ESI+; dichloromethane; $[M+Na]^+$) and 1372 (ESI+; water and small amount of sodium acetate trihydrate; $[M+H]^+$).

4.2. Physicochemical measurements

Elemental analyses were carried out on an Elementar Vario Microcube elemtal analyzer in CHNS mode. Oxygen content analysis was carried out on an Elemental rapid OXY Cube elemental analyzer.

IR spectra were recorded using a Bruker Alpha-P Infrared-spectrometer equipped with a Platinum-ATR with a diamond crystal.

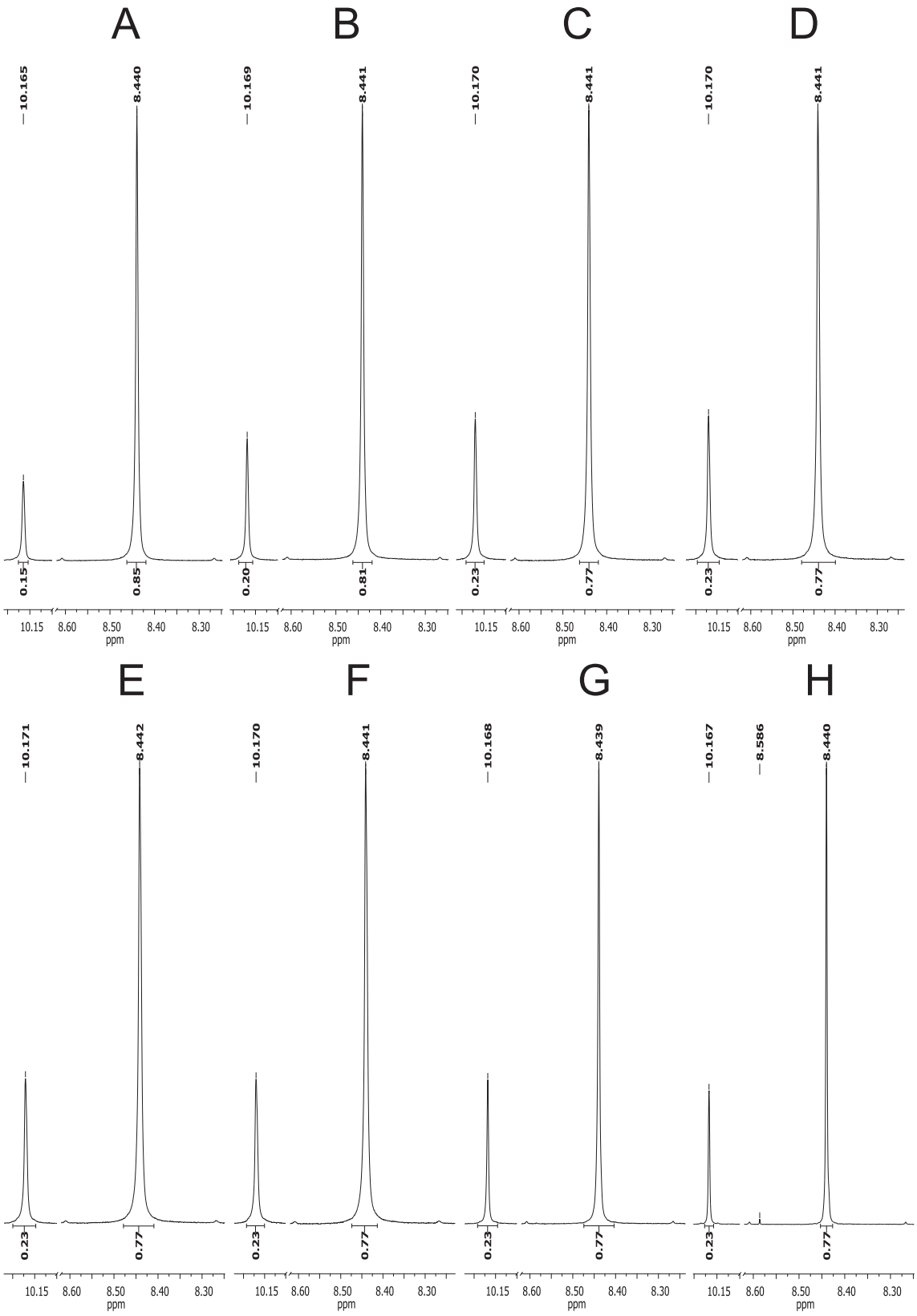

Fig. 2. NMR spectra of **Na_2HL** dissolved in PBS/D_2O (90:10) recorded after various time spans (see text). The relevant signals and integrals are shown only for the ligand and *ortho*-vanillin.

Optical absorption spectra were recorded with a Varian Cary 5000 spectrometer. Samples prepared as solutions in methanol and water with small amount of sodium acetate trihydrate were used. **1** displays three absorption maxima in both, methanol and a slightly

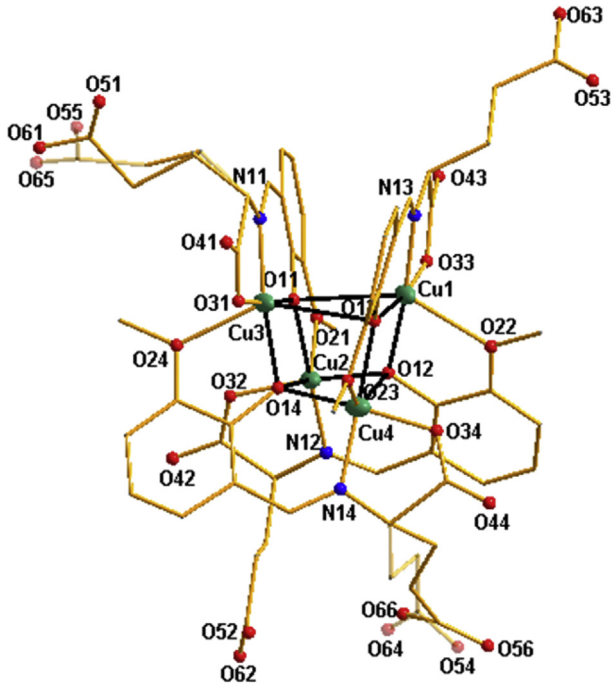

Fig. 3. The molecular structure of **[Cu$_4$(HL)$_4$]·4.6H$_2$O** with atom labelling scheme (thermal ellipsoids of the non-C/H atoms are plotted at 30% probability level). C atoms are shown as sticks and H atoms are omitted for clarity. Disorder components are distinguished with different transparencies.

basic aqueous solution. For methanol as solvent the maxima are at 382 nm, 275 nm and 238 nm. The maxima for the slightly basic aqueous solution are at 371 nm, 277 nm and 237 nm.

^{1}H NMR spectra for **Na$_2$HL** were recorded in methanol-d4 with a Bruker DRX 300 MHz spectrometer at room temperature. Chemical shifts were quoted in ppm relative to the residual protons of deuterated solvents.

Electrospray ionization mass spectrometry (ESI-MS) was performed on a Finnigan LTQ-FT spectrometer by Thermo Fischer Scientific in the positive and negative ion mode with solvent as carrier gas.

4.2.1. X-ray diffraction studies

Single crystal of **[Cu$_4$(HL)$_4$]·4.6H$_2$O** was mounted on an IPDS2 diffractometer equipped with an image plate detector and graphite-monochromated MoK_α radiation. Problems with weak X-ray scattering and solvent loss had to be faced.

4.3. Refinement details

Two $(CH_2)_2(COO)$ moieties were found to be disordered in two positions. The positions were refined with fixed half-occupancies setting restraints on C–C (1.54(5) Å), C–O (1.25(5) Å) bond lengths and O···O distances (2.25(5) Å). EADP constraints were applied to the corresponding atoms displacement factors. Anti-bumping restraints were applied to the H10F···H96B, H13A … H54 A at −x+1, y−0.5, −z (1.90(5) Å) and O63···O1W (2.60(1) Å) distances. The C11-phenyl ring was treated as a rigid hexagon. 6 water molecules of solvation were localized. The occupancies refined to 1.0 for O1W, O3W, to 0.8 for O2W, O4W, O5W, to 0.2 for O6W and were subsequently fixed. The remaining solvent molecules were heavily disordered and required application of a SQUEEZE procedure removing 0.6–6 water molecules from four voids of 31–195 Å^3 volume. On the difference Fourier map the highest maximum of 0.86 e/Å^3 was found at 2.15 Å from the H13B atom, attributable to additional solvent molecules of low occupancy which could not be assigned a reasonable model.

4.4. Stability tests

The stability of the complex **[Cu$_4$(HL)$_4$]·4.6H$_2$O** under physiological conditions was determined by IR spectroscopy. 144 mg (0.1 mmol) of the copper complex was dissolved in 10 mL PBS. The green solution was aliquoted (1 mL) and transferred to micro tubes. With a thermal shaker the tubes were heated to 37 °C and shook at 300 rpm. After 0.5 h, 2 h, 6 h, 20 h, 24 h and 48 h the particular tube was removed from the shaker, the solution was dried *in vacuo* to dryness and the remaining green solid was analyzed by IR spectroscopy.

The stability of the ligand **Na$_2$HL** under physiological conditions was determined by NMR spectroscopy. 10 mg of the ligand was dissolved in a NMR tube in 0.7 mL PBS/D$_2$O (90:10) preheated to 37 °C and the measurement was started immediately. Further measurements were done in 2 min-steps for 10 min, after 2 h and

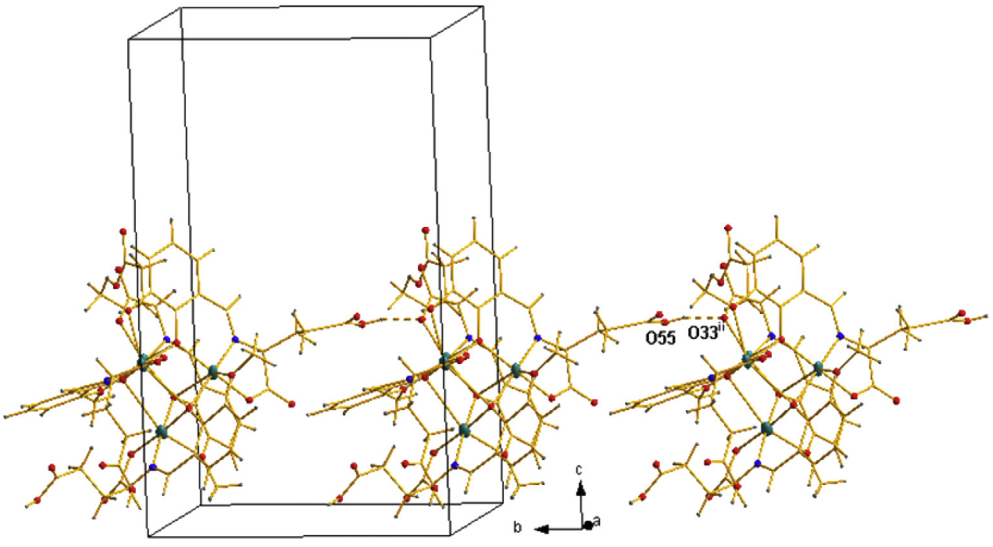

Fig. 4. Hydrogen-bonded chains along [010] in **[Cu$_4$(HL)$_4$]·4.6H$_2$O**.

24 h. After 24 h a color change of the solution to brown was observed. The *ortho*-vanillin/ligand ratio was determined from the integrals of the particular signals. Baseline and phase corrections were done with Bruker TopSpin 3.5 pl2. Integration and images were done with MestReNova 6.0.2–5475.

Appendix A. Supplementary data

Supplementary data related to this article can be found at http://dx.doi.org/10.1016/j.molstruc.2016.07.100.

References

[1] (a) S. Anbu, S. Kamalraj, B. Varghese, J. Muthumary, M. Kandaswamy, A series of oxyimine-based macrocyclic dinuclear zinc(ii) complexes enhances phosphate ester hydrolysis, DNA binding, DNA hydrolysis, and lactate dehydrogenase inhibition and induces apoptosis, Inorg. Chem. 51 (2012) 5580–5592;
(b) Z. Cimerman, N. Galic, B. Bosner, The Schiff bases of salicylaldehyde and aminopyridines as highly sensitive analytical reagents, Anal. Chim. Acta 343 (1997) 145–153;
(c) M.A. Halcrow, G. Christou, Biomimetic chemistry of nickel, Chem. Rev. 94 (1994) 2421–2481;
(d) M. Fontecave, S. Menage, C. Duboc-Toia, Functional models of non-heme diiron enzymes, Coord. Chem. Rev. 178 (1998) 1555–1572;
(e) S. Mukhopadhyay, S.K. Mal, S. Bhaduri, W.H. Armstrong, Manganese clusters with relevance to photosystem II, Chem. Rev. 104 (2004) 3981–4026;
(f) S. Nayak, H.P. Nayek, S. Dehnen, A.K. Powell, J. Reedijk, Trigonal propeller-shaped $Mn^{III}_3M^{II}Na$ complexes (M = Mn, Ca): structural and functional models for the dioxygen evolving centre of PSII, Dalton Trans. 40 (2011) 2699–2702.
[2] (a) N. Raman, S. Sobha, L. Mitu, Synthesis, structure elucidation, DNA interaction, biological evaluation, and molecular docking of an isatin-derived tyramine bidentate Schiff base and its metal complexes, Monatsh. Chem. 143 (2012) 1019–1030;
(b) R. Miri, N. Razzaghiasl, M.K. Mohammadi, QM study and conformational analysis of an isatin Schiff base as a potential cytotoxic agent, J. Mol. Model 19 (2013) 727–735;
(c) M.C. Heffern, J.W. Kurutz, T.J. Meade, Spectroscopic elucidation of the inhibitory mechanism of Cys_2His_2 zinc finger transcription factors by cobalt(III) Schiff base complexes, Chem. Eur. J. 19 (2013) 17043–17053;
(d) R. Alizadeh, M. Afzal, F. Arjmand, *In vitro* DNA binding, pBR322 plasmid cleavage and molecular modeling study of chiral benzothiazole Schiff-base-valine Cu(II) and Zn(II) complexes to evaluate their enantiomeric biological disposition for molecular target DNA, Spectrochim. Acta Part A Mol. Biomol. Spectrosc. 131 (2014) 625–635;
(e) J. Zuo, C. Bi, Y. Fan, D. Buac, C. Nardon, K.G. Daniel, Q. Ping Dou, Cellular and computational studies of proteasome inhibition and apoptosis induction in human cancer cells by amino acid Schiff base–copper complexes, J. Inorg. Biochem. 118 (2013) 83–93;
(f) S. Tabassum, S. Yadav, I. Ahmad, Heterobimetallic o-vanillin functionalized complexes: *in vitro* DNA binding validation, cleavage activity and molecular docking studies of $Cu^{II}–Sn^{IV}_2$ analogs, J. Organomet. Chem. 752 (2014) 17–24.
[3] F. Rafii, J.B. Sutherland, C.E. Cerniglia, Effects of treatment with antimicrobial agents on the human colonic microflora, Ther. Clin. Risk. Manag. 4 (2008) 1343–1358.
[4] F. Javed, L.P. Samaranayake, G.E. Romanos, Treatment of oral fungal infections using antimicrobial photodynamic therapy: a systematic review of currently available evidence, Photochem. Photobiol. Sci. 13 (2014) 726–734.
[5] R.F. Donnelly, P.A. McCarron, M.M. Tunney, Antifungal photodynamic therapy, Microbiol. Res. 163 (2008) 1–12.
[6] D. Sanglard, F.C. Odds, Resistance of Candida species to antifungal agents: molecular mechanisms and clinical consequences, Lancet. Infect. Dis. 2 (2002) 73–85.
[7] W.U. Malik, R. Bembi, Thermodynamic study (polarographically) of the reaction between cobalt (III) ammines and some Schiff-bases derived from amino-acids, J. Indian Chem. Soc. 56 (1979) 776–778.
[8] D. Heinert, A.E. Martell, Pyridoxine and Pyridoxal Analogs V. Syntheses and infrared spectra of Schiff bases, J. Am. Chem. Soc. 84 (1962) 3257–3263.

Synthesis, structure and stability of a chiral imine-based Schiff-based ligand derived from L-glutamic acid and its [Cu_4] complex

Simon Muche,[a] Irina Levacheva,[b] Olga Samsonova,[b] Anna Biernasiuk,[c] Anna Malm,[c] Richard Lonsdale,[a,d] Łukasz Popiołek,[e] Udo Bakowsky,[b] and Małgorzata Hołyńska[*a]*

[a] Fachbereich Chemie and Wissenschaftliches Zentrum für Materialwissenschaften, Philipps-Universität Marburg, Hans-Meerwein-Strasse, D-35043 Marburg, Germany. E-Mail: holynska@staff.uni-marburg.de

[b] Institut für Pharmazeutische Technologie & Biopharmazie, Philipps-Universität Marburg, Ketzerbach 63, D-35032 Marburg, Germany.

[c] Department of Pharmaceutical Microbiology, Medical University, Chodźki 1, 20-093 Lublin, Poland.

[d] Max-Planck-Institut für Kohlenforschung, Kaiser-Wilhelm-Platz 1, D-45470, Mülheim an der Ruhr, Germany.

[e] Department of Organic Chemistry, Medical University of Lublin, Chodźki 4A, 20-093 Lublin, Poland.

SUPPORTING INFORMATION

1. Analytical data

Fitting of the elemental analysis data

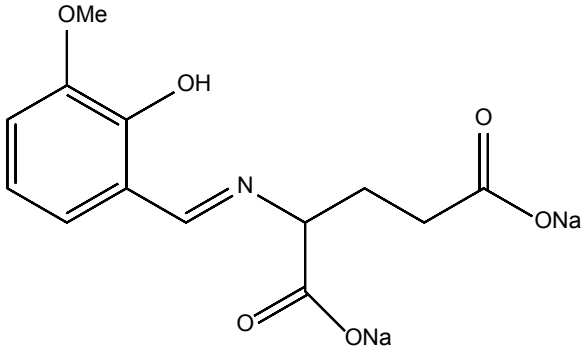

Chemical Formula: $C_{13}H_{13}NNa_2O_6$

Elemental Analysis: C, 48.01; H, 4.03; N, 4.31; Na, 14.14; O, 29.52

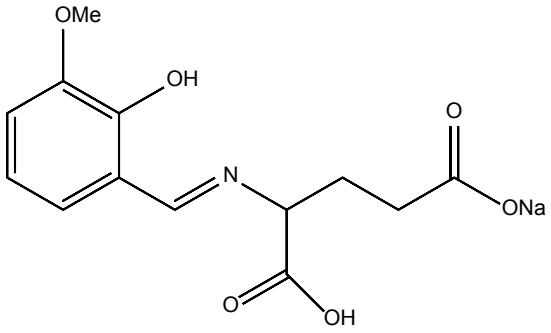

Chemical Formula: $C_{13}H_{14}NNaO_6$

Elemental Analysis: C, 51.49; H, 4.65; N, 4.62; Na, 7.58; O, 31.66

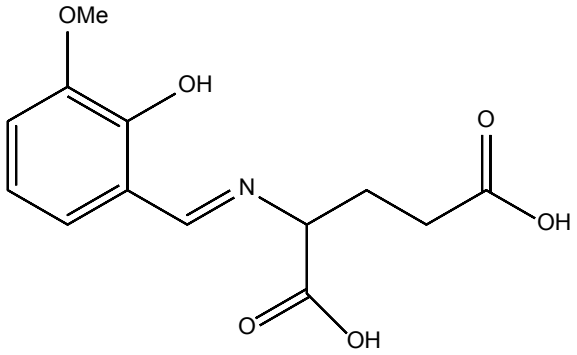

Chemical Formula: $C_{13}H_{15}NO_6$

Elemental Analysis: C, 55.51; H, 5.38; N, 4.98; O, 34.13

Found: C, 47.24; H, 4.00; N, 4.23 → Disodium salt

2. Supplementary figures

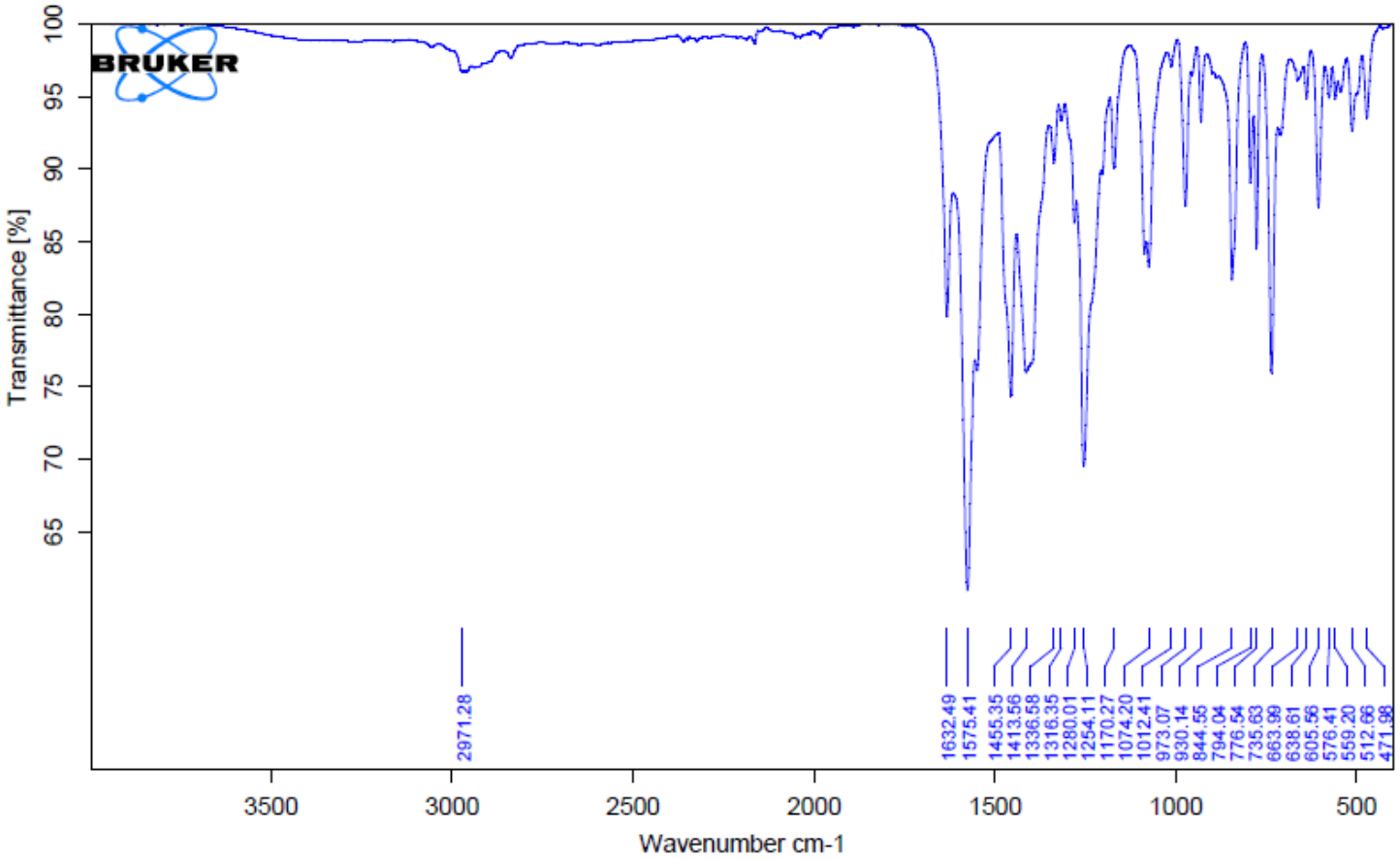

Figure S1 IR spectrum for the ligand dried for several hours under high vacuum.

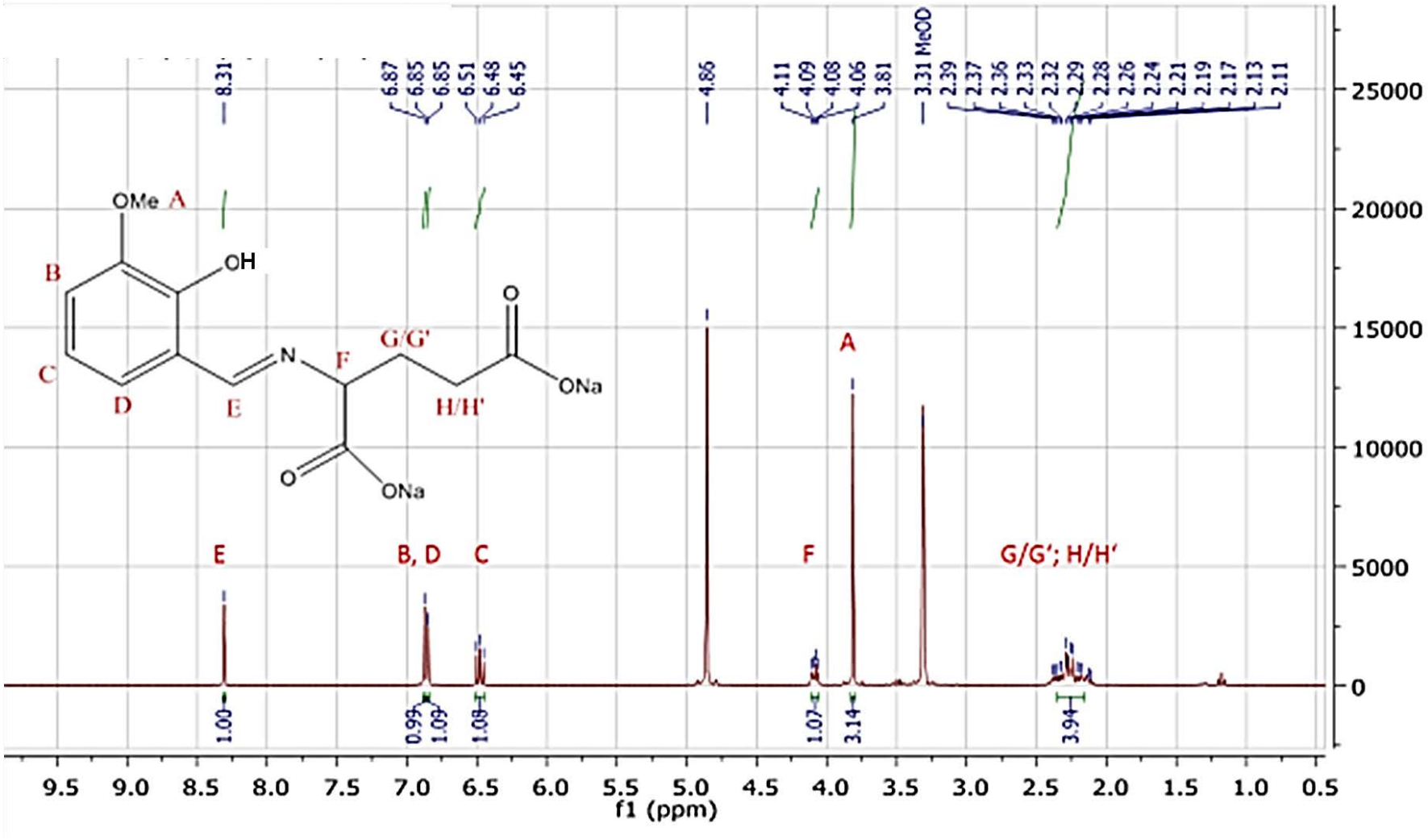

Figure S2 ^{1}HNMR spectrum for the ligand **Na_2HL** in MeOD.

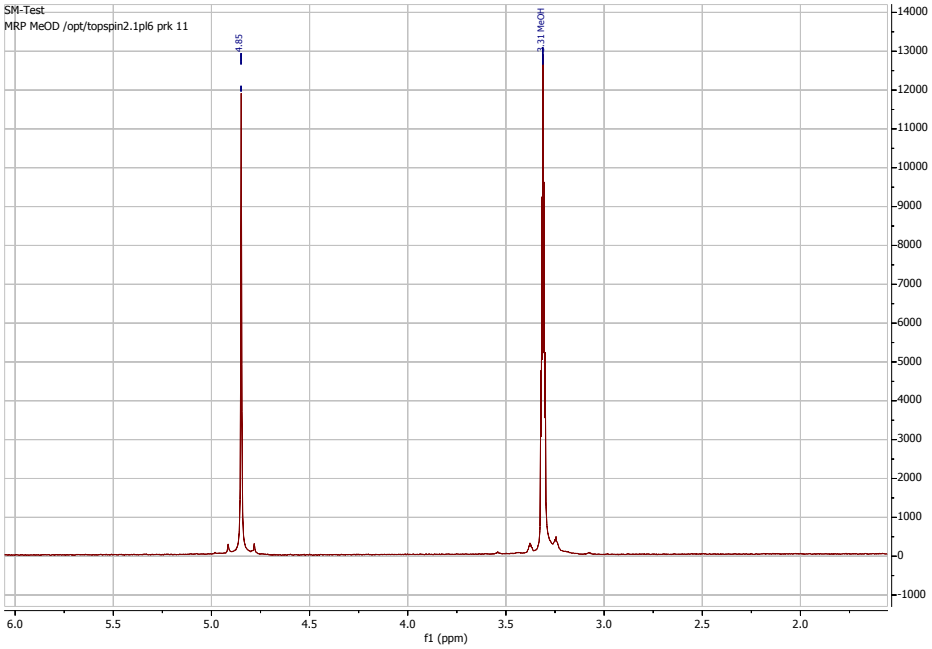

Figure S3 [1]HNMR spectrum of MeOD explaining origin of the peak at 4.86 ppm in Figure S2.

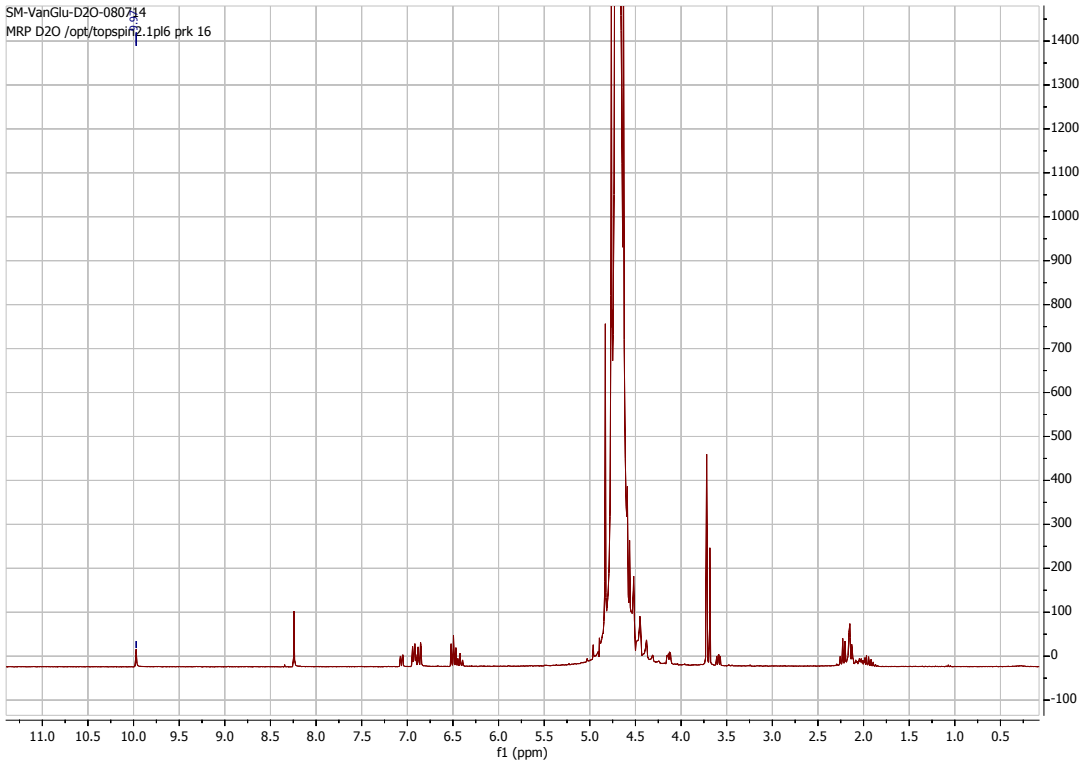

Figure S4 [1]HNMR of **Na_2HL** in D_2O.

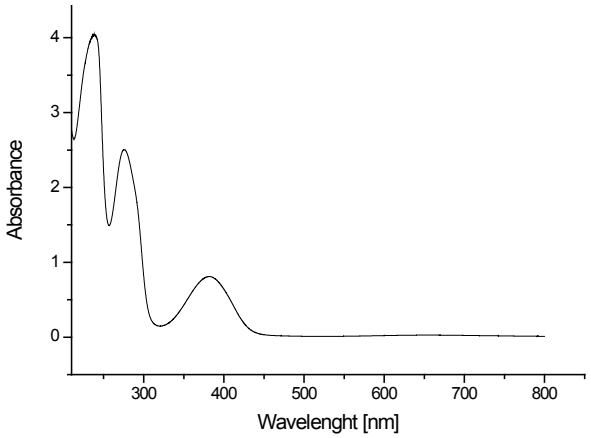

(a)

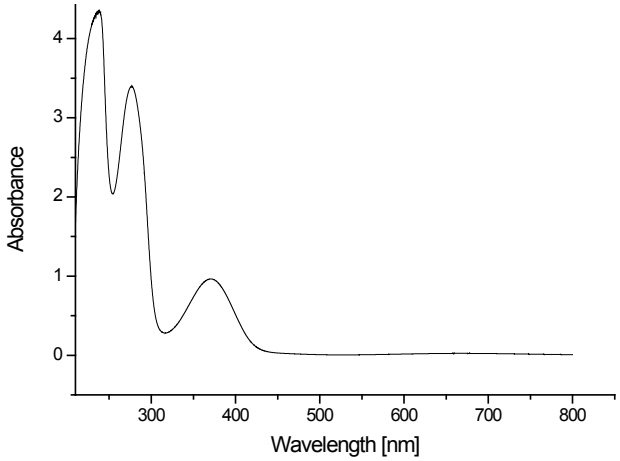

(b)

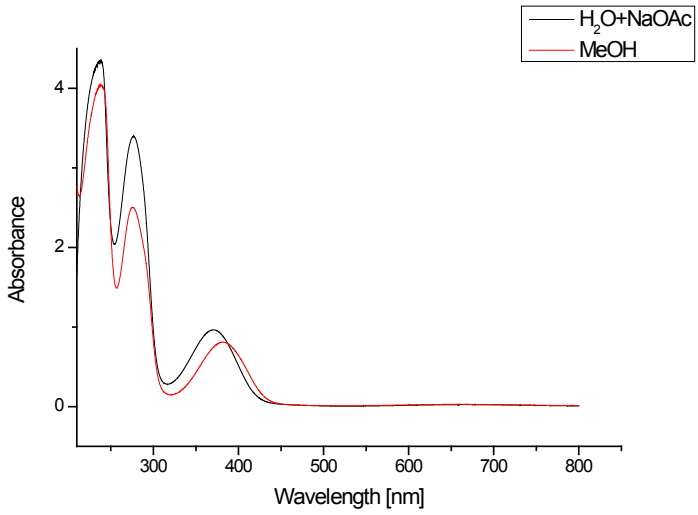

(c)

Figure S5 UV-Vis spectra of **[Cu$_4$(HL)$_4$]·4.6H$_2$O** in (a) MeOH, (b) H_2O with addition of sodium acetate, (c) overlap of (a) and (b).

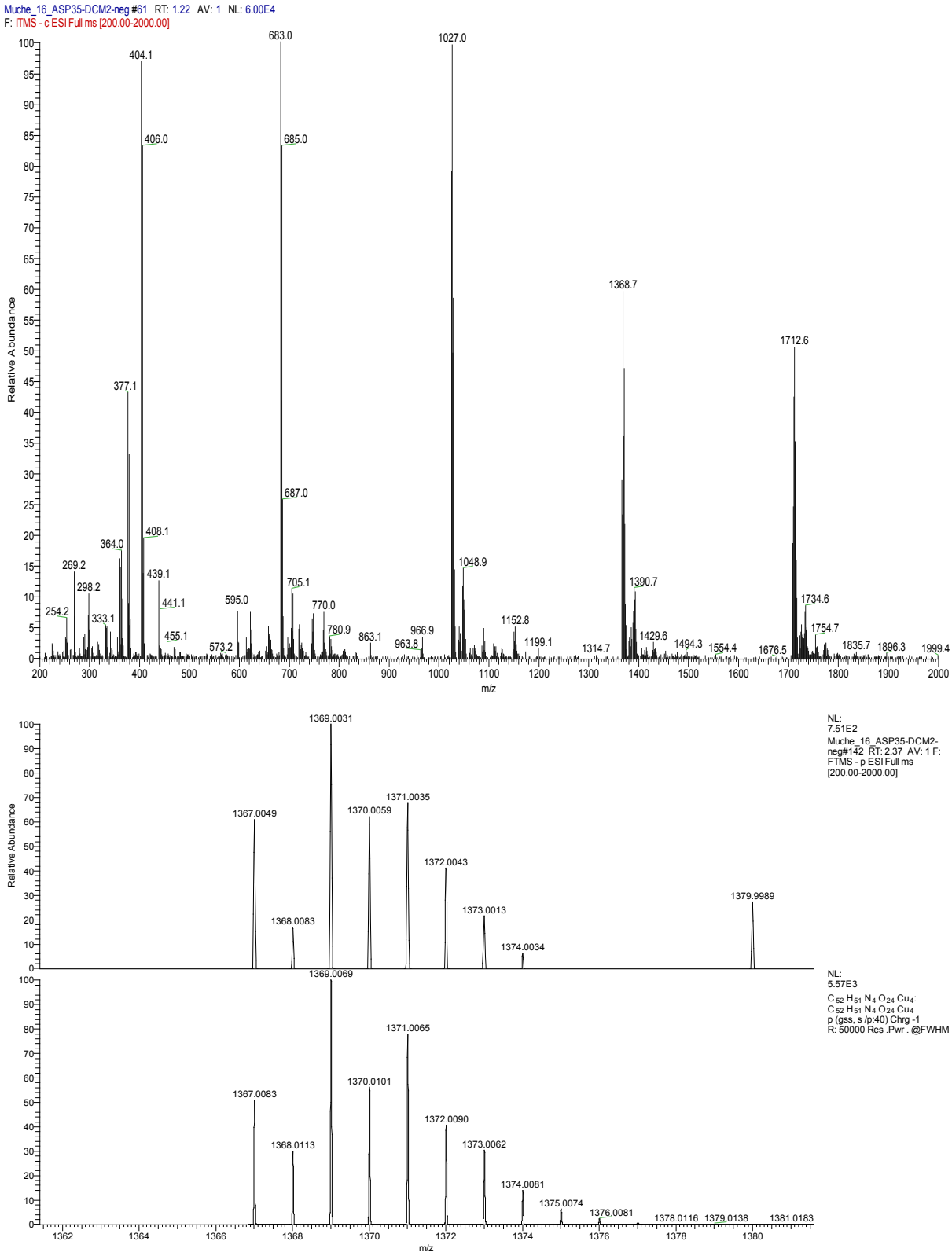

Figure S6 ESI-MS spectrum of **$[Cu_4(HL)_4]\cdot 4.6H_2O$** in dichloromethane with simulation of the molecular peak.

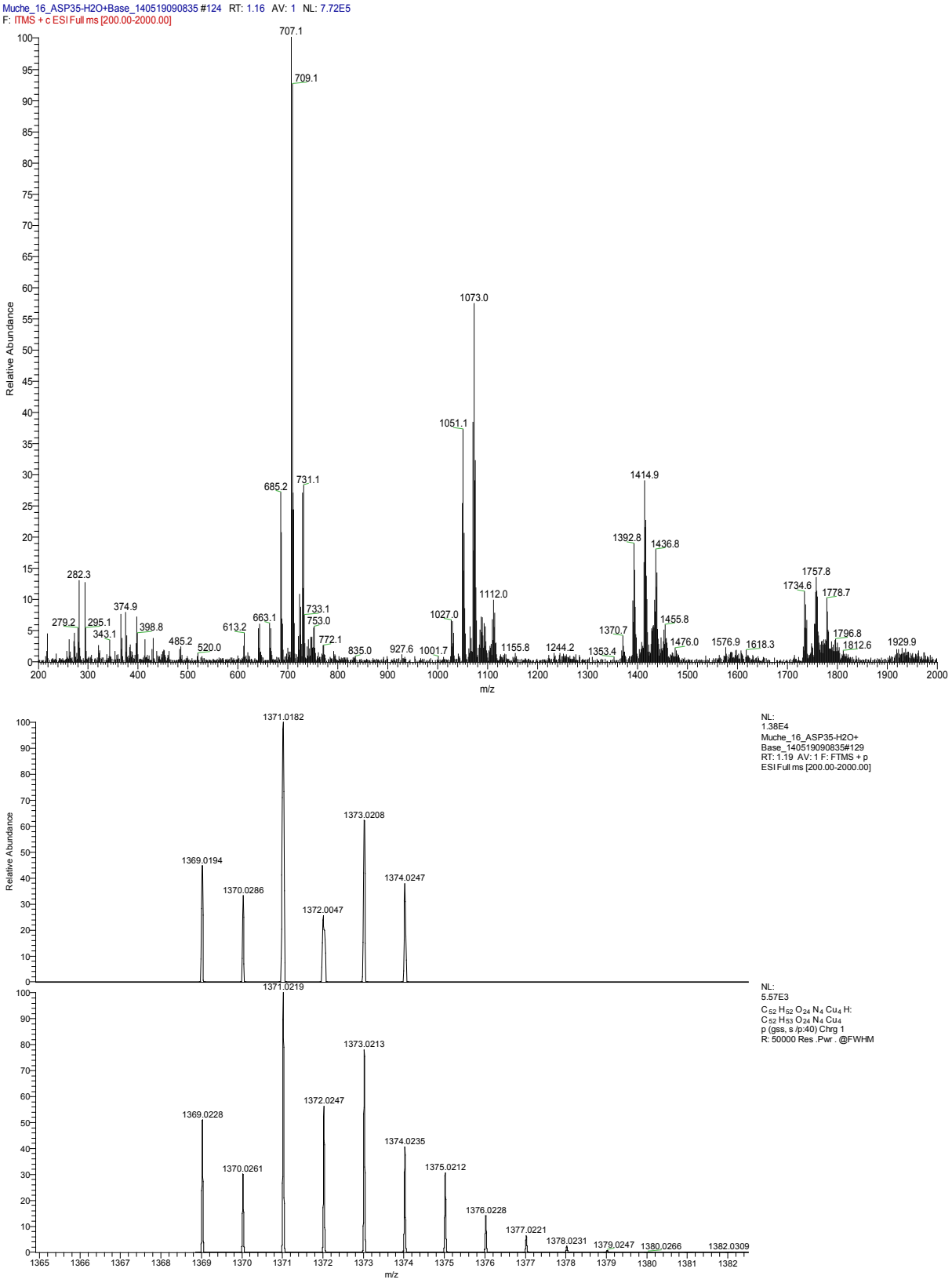

Figure S7 ESI-MS spectrum of **$[Cu_4(HL)_4]\cdot 4.6H_2O$** in water with small amount of sodium acetate trihydrate with simulation of the molecular peak.

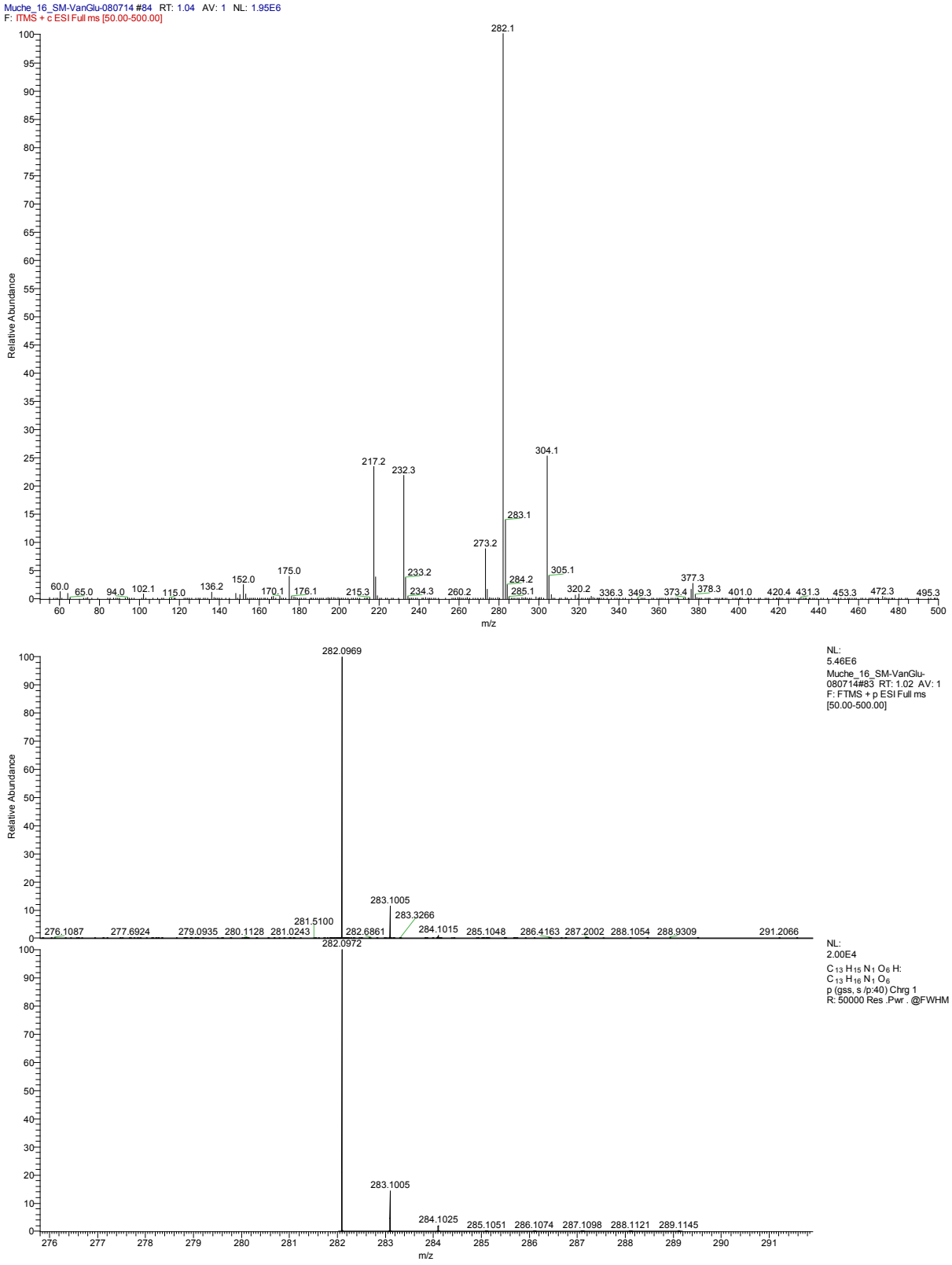

Figure S8 ESI(+)-MS spectrum of **Na_2HL** in methanol with simulation of the molecular peak.

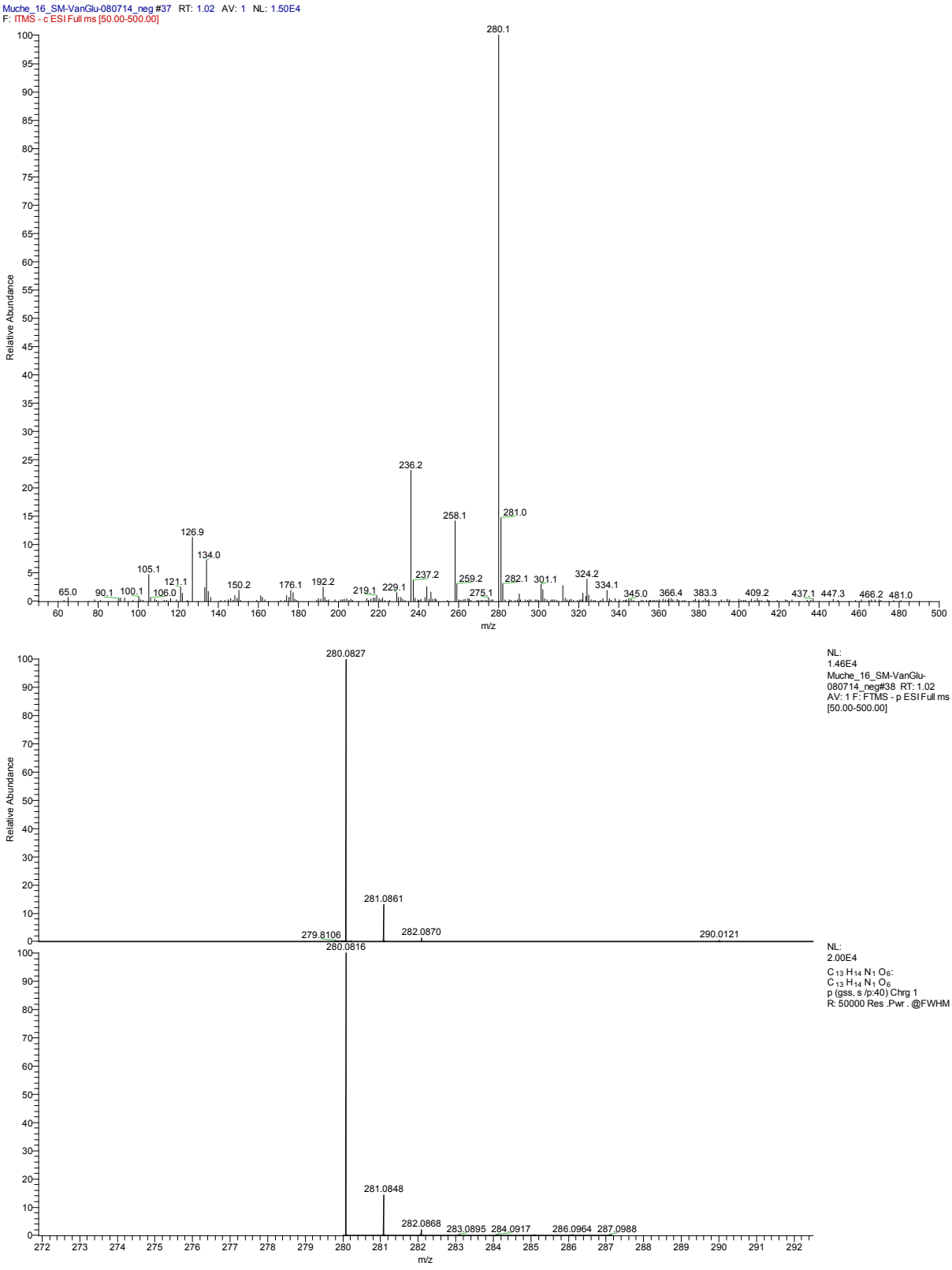

Figure S9 ESI(-)-MS spectrum of **Na_2HL** in methanol with simulation of the molecular peak.

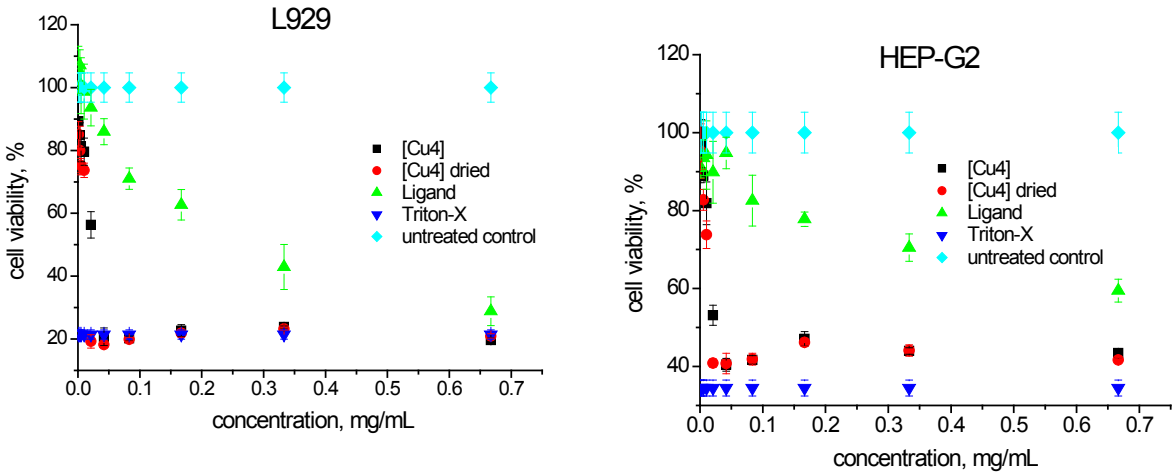

Figure S10 Biocompatibility assay for L929 fibroblasts and Hep-G2 hepatocytes, exposition to tested substances – 24 h.

3. Supplementary tables

Table S1. Selected crystallographic data for **[Cu$_4$(HL)$_4$]·4.6H$_2$O**.

Formula	$C_{52}H_{52}Cu_4N_4O_{24}$, 4.6($H_2O$)
Formula weight	1454.01
Temperature [K]	100(2)
λ [Å]	0.71073
Crystal system	monoclinic
Space group	$P2_1$
a [Å]	12.616(2)
b [Å]	12.595(2)
c [Å]	20.837(3)
β [°]	95.16(3)
V [Å^3]	3297.6(9)
Z, ρ_{calc} [g cm^{-3}]	2, 1.464
μ [mm^{-1}]	1.36
F(000)	1492
Crystal size [mm]	0.46x0.32x0.04
θ range [º]	1.62-25.00
rflns: total/unique	16360/9750
R(int)	0.0782
Abs. corr.	numerical
Min., max. transmission factors	0.572, 0.898
Data/restraints/params	9750/21/748
GOF on F^2	1.038
R1 [I > 2σ(I)]	0.0614
wR2 (all data)	0.1159
Max., min. $\Delta\rho_{elect}$ [e Å^{-3}]	0.86, -0.39

Table S2. Selected bond lengths and angles (Å, °) for **[Cu$_4$(HL)$_4$]·4.6H$_2$O**.

Cu1—N13	1.927 (8)	Cu3—O31	1.923 (9)
Cu1—O13	1.930 (8)	Cu3—N11	1.927 (9)
Cu1—O33	1.933 (8)	Cu3—O11	1.968 (8)
Cu1—O12	1.985 (7)	Cu3—O14	1.973 (8)
Cu1—O22	2.297 (8)	Cu3—O24	2.278 (7)
Cu2—N12	1.923 (8)	Cu4—N14	1.925 (10)
Cu2—O12	1.934 (8)	Cu4—O34	1.928 (9)
Cu2—O32	1.951 (7)	Cu4—O14	1.991 (8)
Cu2—O11	1.999 (7)	Cu4—O13	2.007 (7)
Cu2—O21	2.313 (8)	Cu4—O23	2.292 (9)
N13—Cu1—O13	92.8 (4)	O31—Cu3—N11	84.8 (4)
N13—Cu1—O33	83.2 (4)	O31—Cu3—O11	176.0 (3)
O13—Cu1—O33	171.7 (3)	N11—Cu3—O11	92.3 (4)
N13—Cu1—O12	173.0 (4)	O31—Cu3—O14	93.3 (4)
O13—Cu1—O12	89.5 (3)	N11—Cu3—O14	172.1 (4)
O33—Cu1—O12	93.6 (3)	O11—Cu3—O14	89.2 (3)
N13—Cu1—O22	111.4 (3)	O31—Cu3—O24	88.0 (3)
O13—Cu1—O22	94.3 (3)	N11—Cu3—O24	113.4 (4)
O33—Cu1—O22	93.9 (3)	O11—Cu3—O24	95.8 (3)
O12—Cu1—O22	74.9 (3)	O14—Cu3—O24	74.1 (3)
N12—Cu2—O12	95.0 (3)	N14—Cu4—O34	84.4 (5)
N12—Cu2—O32	83.0 (3)	N14—Cu4—O14	92.9 (4)
O12—Cu2—O32	170.7 (4)	O34—Cu4—O14	173.1 (4)
N12—Cu2—O11	173.2 (4)	N14—Cu4—O13	176.1 (4)
O12—Cu2—O11	87.7 (3)	O34—Cu4—O13	96.1 (4)
O32—Cu2—O11	95.3 (3)	O14—Cu4—O13	87.1 (3)

N12—Cu2—O21	98.4 (3)	N14—Cu4—O23	99.1 (4)
O12—Cu2—O21	101.8 (3)	O34—Cu4—O23	87.0 (4)
O32—Cu2—O21	87.4 (3)	O14—Cu4—O23	99.8 (3)
O11—Cu2—O21	74.9 (3)	O13—Cu4—O23	77.0 (3)

Table S3. Hydrogen bonding parameters (Å, °) for **[Cu$_4$(HL)$_4$]·4.6H$_2$O**.

D—H···*A*	*D*—H	H···*A*	*D*···*A*	*D*—H···*A*
O52—H52K···O5W	0.84	2.24	2.846(18)	129
O55—H55···O33^{ii}	0.84	1.97	2.778(19)	160
C71—H71···O43^{i}	0.95	2.63	3.498(14)	152
O51—H51A···O33^{ii}	0.84	2.28	3.013(16)	146
C52—H52···O41^{iii}	0.95	2.60	3.344(14)	136
C82—H82···O53^{iv}	1.00	2.29	3.285(17)	175
C73—H73···O42^{v}	0.95	2.37	3.243(12)	153
C103—H10J···O43	0.99	2.37	3.090(14)	129
C134—H5C···O63^{i}	0.98	2.31	3.163(19)	146
Symmetry codes: (i) −*x*+2, *y*−1/2, −*z*+1; (ii) *x*, *y*−1, *z*; (iii) *x*, *y*+1, *z*; (iv) *x*−1, *y*, *z*; (v) *x*+1, *y*, *z*.				

Table S4. The values of MIC and MBC or MFC [µg/ml] of L-glutamic acid and *ortho*-vanillin against the reference strains of microorganisms.

. **Species**		**MIC (MBC or MFC) [µg/ml]** of the tested compounds	
		L-glutamic acid	***ortho*-vanillin**
Gram-positive bacteria	*Staphylococcus aureus* ATCC 6538	-	500 (>1000)
	Staphylococcus aureus ATCC 25923	-	500 (>1000)
	Staphylococcus aureus ATCC 43300	-	500 (>1000)
	Staphylococcus aureus NIM 1	-	1000 (>1000)
	Staphylococcus aureus NIM 2	-	500 (>1000)
	Staphylococcus epidermidis ATCC 12228	-	250 (500)
	Micrococcus luteus ATCC 10240	-	125 (500)
	Bacillus subtilis ATCC 6633	-	250 (250)
	Bacillus cereus ATCC 10876	-	500 (1000)
	Streptococcus pneumoniae ATCC 49619	-	1000 (>1000)
	Streptococcus pyogenes ATCC 19615	-	1000 (>1000)
	Streptococcus mutans ATCC 25175	-	1000 (>1000)
Gram-tive bacteria	*Klebsiella pneumoniae* ATCC 13883	-	250 (>1000)
	Proteus mirabilis ATCC 12453	-	500 (>1000)
	Bordetella bronchiseptica	-	125

	ATCC 4617		(500)
	Salmonella typhimurium ATCC 14028	-	1000 (>1000)
	Escherichia coli ATCC 25922	-	250 (>1000)
	Escherichia coli ATCC 3521	-	500 (>1000)
	Pseudomonas aeruginosa ATCC 9027	-	1000 (>1000)
	Enterobacter cloacae NIM	-	1000 (>1000)
Fungi	*Candida albicans* ATCC 2091	500 (1000)	7.81 (31.25)
	Candida albicans ATCC 10231	500 (1000)	31.25 (31.25)
	Candida parapsilosis ATCC 22019	1000 (>1000)	31.25 (125)

Table S5. The values of MIC and MFC [µg/ml] of L-glutamic acid and *ortho*-vanillin against the fluconazole sensitive (strains 1 – 13) and fluconazole resistant *Candida* spp. (strains 14 – 20) isolated from clinical specimens.

Species		**MIC (MFC) [µg/ml]** of the tested compounds	
		L-glutamic acid	***ortho*-vanillin**
1.	*C. albicans*	1000 (>1000)	62.5 (62.5)
2.	*C. parapsilosis*	-	62.5 (125)
3.	*C. sake*	1000 (>1000)	31.25 (62.5)
4.	*C. kefyr*	1000 (>1000)	62.5 (125)
5.	*C. pulcherrima*	-	62.5 (250)
6.	*C. lambica*	-	62.5 (125)
7.	*C. dubliniensis*	1000 (>1000)	62.5 (62.5)
8.	*C. inconspicua*	-	125 (250)
9.	*C. famata*	1000 (>1000)	62.5 (62.5)
10.	*C. maris*	-	62.5 (125)
11.	*C. lusitaniae*	-	125 (125)
12.	*C. glabrata*	-	62.5 (125)
13.	*C. tropicalis*	-	62.5

			(250)
14.	*C. albicans* (I)	1000 (>1000)	62.5 (125)
15.	*C. albicans* (II)	1000 (>1000)	62.5 (125)
16.	*C. krusei* (I)	-	125 (250)
17.	*C. krusei* (II)	-	125 (250)
18.	*C. krusei* (III)	-	125 (500)
19.	*C. glabrata*	-	62.5 (250)
20.	*C. inconspicua*	-	125 (500)

Table S6. The values of MIC and MBC or MFC [μg/mL] of the [Cu_4] complex (**[$Cu_4(HL)_4$]·4.6H_2O**) and ligand (**Na_2HL**) against the reference strains of microorganisms. The standard antibiotics used as positive controls: ciprofloxacin (CIP) or vancomycin (VA*) for bacteria and fluconazole (FLU**) for fungi.

Species		**MIC (MBC or MFC) [μg/mL]** of the tested compounds		
		[Cu_4] complex	**Ligand**	**CIP/VA*/ FLU****
Gram-positive bacteria	*Staphylococcus aureus* ATCC 6538	1000 (1000)	500 (>1000)	0.244
	Staphylococcus aureus ATCC 25923	1000 (1000)	125 (>1000)	0.488
	Staphylococcus aureus ATCC 43300	500 (1000)	250 (>1000)	0.244
	Staphylococcus aureus NIM 1	500 (500)	500 (1000)	0.488
	Staphylococcus aureus NIM 2	500 (500)	250 (1000)	0.122
	Staphylococcus epidermidis ATCC 12228	1000 (1000)	125 (1000)	0.122

	Micrococcus luteus ATCC 10240	250 (500)	62.5 (1000)	0.976
	Bacillus subtilis ATCC 6633	1000 (1000)	62.5 (250)	0.031
	Bacillus cereus ATCC 10876	1000 (1000)	125 (>1000)	0.061
	Streptococcus pneumoniae ATCC 49619	1000 (1000)	1000 (>1000)	3.907*
	Streptococcus pyogenes ATCC 19615	1000 (1000)	500 (>1000)	0.976*
	Streptococcus mutans ATCC 25175	1000 (1000)	1000 (>1000)	0.488*
Gram-negative bacteria	*Klebsiella pneumoniae* ATCC 13883	-	1000 (>1000)	
	Proteus mirabilis ATCC 12453	-	250 (1000)	
	Bordetella bronchiseptica ATCC 4617	-	500 (1000)	
	Salmonella typhimurium ATCC 14028	-	125 (1000)	
	Escherichia coli ATCC 25922	-	1000 (>1000)	
	Escherichia coli ATCC 3521	-	250 (>1000)	
	Pseudomonas aeruginosa *ATCC* 9027	-	500 (>1000)	
	Enterobacter cloacae NIM	-	1000 (>1000)	
Fun	*Candida albicans*	125	7.81	0.245**

	ATCC 2091	(250)	(15.62)	
	Candida albicans ATCC 10231	125 (>1000)	15.62 (15.62)	0.976**
	Candida parapsilosis ATCC 22019	250 (>1000)	7.81 (31.25)	1.953**

Table S7. The values of MIC and MFC [μg/mL] of the [Cu_4] complex and ligand **Na_2HL** against the fluconazole sensitive (strains 1 – 13) and fluconazole resistant *Candida* spp. (strains 14 –20) isolated from clinical specimens.

Species		**MIC (MFC) [μg/mL]** of the tested compounds	
		[Cu_4] complex (1)	**Ligand (1a)**
1.	*C. albicans*	250 (500)	62.5 (62.5)
2.	*C. parapsilosis*	250 (>1000)	62.5 (1000)
3.	*C. sake*	500 (>1000)	15.62 (125)
4.	*C. kefyr*	500 (>1000)	62.5 (125)
5.	*C. pulcherrima*	1000 (>1000)	62.5 (125)
6.	*C. lambica*	500 (>1000)	62.5 (250)
7.	*C. dubliniensis*	250 (500)	62.5 (62.5)
8.	*C. inconspicua*	1000 (>1000)	250 (1000)

9.	*C. famata*	500 (1000)	62.5 (125)
10.	*C. maris*	250 (500)	31.25 (125)
11.	*C. lusitaniae*	1000 (1000)	125 (125)
12.	*C. glabrata*	1000 (1000)	62.5 (125)
13.	*C. tropicalis*	1000 (1000)	125 (500)
14.	*C. albicans*	250 (500)	15.62 (62.5)
15.	*C. albicans*	250 (500)	62.5 (62.5)
16.	*C. krusei*	-	125 (500)
17.	*C. krusei*	1000 (1000)	250 (1000)
18.	*C. krusei*	1000 (1000)	125 (500)
19.	*C. glabrata*	1000 (1000)	125 (125)
20.	*C. inconspicua*	1000 (1000)	125 (250)

4. Initial studies of antibacterial and antifungal activity

The results of our study indicated that the examined compounds **$[Cu_4(HL)_4]\cdot 4.6H_2O$** and partly decomposed **Na_2HL** display an inhibitory effect on the growth of the reference strains of microorganisms, both bacteria and yeasts.

According to the data presented in Table S6, on the basis of minimal inhibitory concentration values obtained by the broth microdilution method, it was shown that **$[Cu_4(HL)_4]\cdot 4.6H_2O$** exhibited mild or moderate bactericidal activity against all of the tested strains of Gram-positive bacteria, both pathogenic staphylococci, i.e. *Staphylococcus aureus* ATCC and NIM with MIC (Minimum Inhibitory Concentration) = 500 – 1000 μg/mL and opportunistic bacteria, such as *Staphylococcus epidermidis* ATCC 12228, *Micrococcus luteus* ATCC 10240, *Bacillus subtilis* ATCC 6633 and *Bacillus cereus* ATCC 10876 with MIC = 250 – 1000 μg/mL. The minimal bactericidal concentration values ranged from 500 to 1000 μg/mL and MBC (Minimum Bactericidal Concentration)/MIC = 1 – 2. The bacteria belonging to the reference streptococci (*Streptococcus* spp. ATTC) were also sensitive to the $[Cu_4]$ complex with MIC = MBC = 1000 μg/mL and MBC/MIC = 1.

Compound **$[Cu_4(HL)_4]\cdot 4.6H_2O$** had no inhibitory effect on the growth of the strains of Gram-negative bacteria even at the maximal concentration used (1000 μg/mL) by the preliminary agar dilution method. At the same time, **Na_2HL** was found to be active against these reference strains of bacteria with MIC = 125 – 1000 μg/mL and MBC ≥ 1000 μg/mL (Table S6).

On the other hand, **Na_2HL** and its decomposition products showed good or mild bactericidal or bacteriostatic activity against all of the tested strains of Gram-positive bacteria with MIC = 62.5 – 1000 μg/mL and MBC = 250 – > 1000 μg/mL. Minimum concentrations of the mixture **Na_2HL**, which inhibited the growth of staphylococci ranged from 125 μg/mL to 500 μg/mL and MBC ≥ 1000 μg/mL, streptococci – from 500 to 1000 μg/mL and MBC >1000 μg/mL.

Bacillus spp. ATCC and *Micrococcus luteus* ATCC 10240 were especially sensitive to **Na_2HL** (MIC = 62.5 μg/mL and MBC = 250 – 1000 μg/mL) (Table S6).

Both compounds inhibited the growth of the reference strains of yeasts belonging to the *Candida* species. Compound **$[Cu_4(HL)_4]\cdot 4.6H_2O$** showed a good bioactivity against both *Candida albicans* ATCC strains (MIC = 125 μg/mL) with fungicidal effect towards *Candida albicans* ATCC 2091 (MFC = 250 μg/mL and MFC/MIC = 2) and fungistatic activity against *Candida albicans* ATCC 10231 (MFC > 1000 μg/mL, MFC/MIC > 4). The fungistatic activity towards *Candida parapsilosis* ATCC 22019 was moderate (MIC = 250 μg/mL and MFC > 1000 μg/mL) (Table S6). However, the mixture **Na_2HL** showed much higher bioactivity with fungicidal effect (MFC/MIC = 1 – 4) against the reference strains of fungi belonging to *Candida* spp. ATTC. Minimum concentrations, inhibiting their growth ranged from 7.81 μg/mL to 15.62 μg/mL and MFC = 15.62 – 31.25 μg/mL (Table S6).

As mentioned above, the decomposition products of **Na_2HL** are *ortho*-vanillin and *L*-glutamic acid. As control the antibacterial and antifungal studies were performed for both *ortho*-vanillin and *L*-glutamic acid. The results show that *L*-glutamic acid had no inhibitory effect on the growth of all reference strains of bacteria. On the basis of minimal inhibitory concentration values, it was shown that this acid showed moderate or mild influence on the growth of fungi *Candida albicans* ATTC (MIC = 500 μg/ml, MFC = 1000 μg/ml) and *Candida parapsilosis* ATCC 22019 (MIC = 1000 μg/ml, MFC > 1000 μg/ml), respectively (Table S4).

In accordance with the data presented in Table S4, it was shown that *ortho*-vanillin indicated activity against all tested bacteria. Among them, *Micrococcus luteus* ATCC 10240 and *Bordetella bronchiseptica* ATCC 4617 were the most sensitive to this compound at MIC = 125 μg/ml and MBC = 500 μg/ml. It had moderate or mild activity towards the remaining bacteria (MIC = 250 – 1000 μg/ml, MBC = 250 – ≥ 1000 μg/ml).

In turn, minimum concentrations of *ortho*-vanillin, which inhibited the growth of reference yeasts ranged from 7.81 μg/ml for *Candida albicans* ATTC 2091 to 31.25 μg/ml for other *Candida* spp. ATTC and MFC = 31.25 – 125 μg/ml (Table S4). In the case of clinical strains of *Candida* spp., the activity of this substance was good for all isolates with MIC = 31.25 – 125 μg/ml and MBC = 62.5 – 500 μg/ml. It exhibited fungicidal activity (MFC/MIC = 1 – 4) against the all tested strains of *Candida* spp. (Table S5).

Based on the *in vitro* antimicrobial activity screening we can conclude that the antibacterial activity of the ligand was comparable to the activity of *ortho*-vanillin. Only in the case of activity against: *S. aureus* ATCC 25923, *S. aureus* ATCC 43300, *M. luteus* ATCC 10240, *B. subtilis* ATCC 10876 and *B. cereus* ATCC 10876 the values of MIC for the ligand were significantly lower than the corresponding values for *ortho*-vanillin. Considering reference strains of *Candida* spp. the activity of the ligand was slightly higher than the activity of *ortho*-vanillin, especially against *C. parapsilosis* ATCC 22019 (ligand: MIC = 7.81 μg/mL; *ortho*-vanillin: MIC = 31.25 μg/mL).

4.1 Studies on the fluconazole-resistant fungi

4.1.1. Studies on the fungi isolated from clinical specimens

In accordance with Tables S6 and S7, on the basis of minimal inhibitory concentration values obtained by the broth microdilution method, it was shown that the tested compounds, **$[Cu_4(HL)_4]\cdot 4.6H_2O$** and **$Na_2HL$**, had slightly lower activity against the strains of *Candida* spp. isolated from the clinical specimens.

The isolates belonging to the *Candida* spp. strains, i.e. *C. albicans, C. parapsilosis, C. sake, C. kefyr, C. lambica, C. dubliniensis, C. famata* and *C. maris* were subject to moderate bioactivity of compound **$[Cu_4(HL)_4]\cdot 4.6H_2O$** with MIC = 250 – 500 μg/mL and MFC = 500 – ≥ 1000 μg/mL. The activity against other isolates was mild (Table S7).

In the case of mixture **Na_2HL**, the activity was higher than the activity of compound **$[Cu_4(HL)_4]\cdot 4.6H_2O$**. MIC values ranged from 15.62 to 250 μg/mL and MFC = 62.5 – 1000 μg/mL (MFC/MIC = 1 – 16). The antifungal activity of this compound against most of the strains was good. *C. sake* was especially sensitive to the mixture **Na_2HL** with MIC = 15.62 μg/mL (Table S7).

The activity of these compounds was similar against the fluconazole resistant *Candida* spp. strains. Minimum concentrations of **$[Cu_4(HL)_4]\cdot 4.6H_2O$** and **$Na_2HL$**, which inhibited the growth of these yeasts, ranged from 250 to 1000 μg/mL and 15.62 to 250 μg/mL, respectively. Both compounds indicated a fungicidal effect (MFC/MIC = 1 – 4). One of the isolates of *C. krusei* was insensitive to compound **$[Cu_4(HL)_4]\cdot 4.6H_2O$** (Table S7).

The *L*-glutamic acid showed slightly lower activity against strains of *Candida* spp. isolated from clinical specimens (MIC = 1000 μg/ml and MFC > 1000 μg/ml) or had no inhibitory effect against these microorganisms (Table S5).

As for the clinical *Candida* strains the antifungal activity of **Na_2HL**, except 4 cases, was almost the same as the activity of *ortho*-vanillin. The growth of *C. sake* and *C. maris* was inhibited stronger by the **Na_2HL** than by *ortho*-vanillin. To the contrary the antifungal activity of *ortho*-vanillin towards *C. inconspicua* and *C. tropicalis* was higher than the activity of **Na_2HL**. In addition to this activity against fluconazole resistant *Candida* species in case of *Candida albicans* (I) was higher for **Na_2HL** than for *ortho*-vanillin. *Ortho*-vanillin exhibited higher activity than **Na_2HL** towards *C. krusei* (II) and *C. glabrata*. In other cases the activity of **Na_2HL** was equal to the activity of *ortho*-vanillin (Table S5).

4.2 Studies of cytotoxicity – biocompatibility *in vitro*

To study the biocompatibility of **$[Cu_4(HL)_4]\cdot 4.6H_2O$** and its components *in vitro* we have chosen two cell lines. The L929 fibroblast cell line is routinely used by Unites States

Pharmacopoeia for cytotoxicity test regulations and in ISO 10993-5 for the assessment of biological risks. The hepatocyte Hep-G2 cell line is an appropriate model to evaluate the potential adverse drug/metabolite effects occurring during the first-pass through the liver during systemic application.

Samples of **$[Cu_4(HL)_4]\cdot 4.6H_2O$** and dried **$[Cu_4(HL)_4]\cdot 4.6H_2O$** (under vacuum for 2 h) did not show any significant difference over the whole range of tested concentrations. That could serve as a proof of the stability of **$[Cu_4(HL)_4]\cdot 4.6H_2O$**, remaining intact over the processes of drying and re-solution, otherwise the separated components may have had a deviating impact on the mitochondrial activity of cells. As for instance shown for the **Na_2HL** – it possesses lower toxic potential for mammalian cells in comparison to **$[Cu_4(HL)_4]\cdot 4.6H_2O$** (Figure S10). The concentration range of 0.001-0.01 mg/mL of **$[Cu_4(HL)_4]\cdot 4.6H_2O$** can be considered as biocompatible both in L929 and Hep-G2, here the treated cells retain over 70% viability. **Na_2HL** is biocompatible over a broader concentration range: up to 0.083 mg/mL in L929, and up to 0.33 mg/mL in Hep-G2. Though the Hep-G2 line is considered to be more sensitive to the toxic effects as also demonstrated on the Triton-X control, **Na_2HL** has here a milder effect in comparison to L929. The interval with 70% and higher cell viability values has a good predisposition for the drug application without significant side effects for the host organism.

4.3 Cell culture and biocompatibility assay (MTT)

For cultivation both cell lines, L929 fibroblasts and Hep-G2 hepatocytes, were incubated at 95% air and 5% carbon dioxide in DMEM high glucose medium supplemented with 10% fetal bovine serum, and subcultivated 2-3 times a week at 80-90% confluence.

For experiment the L929 were seeded at a density of 10 000 and Hep-G2 at 15 000 and incubated for 24h, after that fresh medium was replaced and 24h-treatment with different concentrations of test substance (0.0015 – 0.667 mg/mL) was started. Later the treated cells

and untreated controls were supplemented with MTT-reagent (3-(4,5-dimethylthiazol-2-yl)-2,5-diphenyltetrazoliumbromide) in serum free medium to be metabolized in mitochondria. Triton-X 4% served as toxic control aggressive to cell membranes. After 4 h formed formazan crystals were dissolved in DMSO and analyzed at 570 nm, results presented as mean values of 4 replicates with standard deviation.

4.4 Antimicrobial and antifungal activity

The examined compounds **$[Cu_4(HL)_4]\cdot 4.6H_2O$** and **$Na_2HL$**, L-glutamic acid and *ortho*-vanillin were screened *in vitro* for antibacterial and antifungal activities using the broth microdilution method according to European Committee on Antimicrobial Susceptibility Testing (EUCAST)[S1] and Clinical and Laboratory Standards Institute guidelines (CLSI).[S2] In this study were applied reference strains of microorganisms from American Type Culture Collection (ATCC), routinely used for the evaluation of antimicrobials and strains from National Medicines Institute in Warsaw (NIM), including Gram-positive bacteria (*Staphylococcus aureus* ATCC 6538, *Staphylococcus aureus* ATCC 25923, *Staphylococcus aureus* ATCC 43300, *Staphylococcus aureus* NIM 1, *Staphylococcus aureus* NIM 2, *Staphylococcus epidermidis* ATCC 12228, *Streptococcus pyogenes* ATCC 19615, *Streptococcus pneumoniae* ATCC 49619, *Streptococcus mutans* ATCC 25175, *Bacillus subtilis* ATCC 6633, *Bacillus cereus* ATCC 10876, *Micrococcus luteus* ATCC 10240), Gram-negative bacteria (*Escherichia coli* ATCC 3521, *Escherichia coli* ATCC 25922, *Klebsiella pneumoniae* ATCC 13883, *Proteus mirabilis* ATCC 12453, *Salmonella typhimurium* ATCC 14028, *Enterobacter cloacae* NIM, *Pseudomonas aeruginosa* ATCC 9027, *Pseudomonas aeruginosa* ATCC 27853 and *Bordetella bronchiseptica* ATCC 4617) and fungi belonging to yeasts (*Candida albicans* ATCC 2091, *Candida albicans* ATCC 10231, *Candida parapsilosis* ATCC 22019).

In the second study of antifungal activity of the tested compounds, 20 clinical strains of fungi from *Candida* species were used. Among them were: *C. albicans, C. parapsilosis, C. sake, C. kefyr, C. pulcherrima, C. lambica, C. dubliniensis, C. inconspicua, C. famata, C. maris, C. lusitaniae, C. glabrata, C. tropicalis* and fluconazole-resistant isolates: *C. krusei* (3 isolates), *C. albicans* (2 isolates), *C. inconspicua* and *C. glabrata*. The isolates belonging to *C. krusei* have natural resistance to fluconazole, which is a standard antifungal agent from triazole antifungal medication.

These yeasts were isolated by the authors (from the Department of Pharmaceutical Microbiology of Medical University in Lublin, Poland) from different clinical materials, e.g. from upper respiratory tract of hospitalized patients including cancer persons (i.e. with non-small cell lung cancer or hematological malignancies). Some of them were after pre- or post-operative chemotherapy. The isolates were also obtained from patients with chronic hepatitis C (undergoing peginterferon and ribavirin therapy or without antiviral therapy), patients with diabetes, elderly people, aged of 65 years old or older, staying in close population, such as a care centre and people staying outside the home care.

The Ethical Committee of the Medical University of Lublin approved the study protocol (No. KE-0254/75/2011). All isolates were identified by standard diagnostic methods – biochemical microtest, e.g.: ID 32 C, API 20 C AUX, API Candida (bioMérieux) on the basis of assimilation of various substrates.

The microbial cultures were subcultured on nutrient agar or Sabouraud agar at 35 °C for 18-24 h or 30 °C for 24-48 h for bacteria and fungi, respectively. The surface of Mueller-Hinton agar or Mueller-Hinton agar with 5% sheep blood (for bacteria) and RPMI 1640 with MOPS (for fungi) were inoculated with the suspensions of bacterial or fungal species. Microbial suspensions were prepared in sterile 0.85% NaCl with an optical density of McFarland standard scale 0.5 – approximately 1.5 x 10^8 CFU (Colony Forming Units)/mL for bacteria and 0.5 McFarland standard scale – approximately 5 x 10^5 CFU/mL for fungi.[S1-S3]

Sample containing 50 mg of examined compound was first dissolved in 1 mL dimethyl sulphoxide (DMSO) and then appropriately diluted. Furthermore, bacterial and fungal suspensions were put onto Petri dishes with solid media containing 1000 μg/mL of the tested compounds **$[Cu_4(HL)_4]\cdot 4.6H_2O$** and **$Na_2HL$** followed incubation under similar conditions as previously. The inhibition of microbial growth was judged by comparison with a control culture prepared without any sample tested. Ciprofloxacin (for *Staphylococcus* spp., *Micrococcus* spp., *Bacillus* spp. and Gram-negative bacteria), vancomycin (for *Streptococcus* spp.) or fluconazole (for *Candida* spp.) were used as a reference antimicrobial compounds (Sigma-Aldrich).[S1-S3]

Subsequently MIC (Minimal Inhibitory Concentration), defined as the lowest concentration of the samples showing complete bacterial or fungal growth inhibition, was examined by the microdilution broth method using their two-fold dilutions from 1000 to 0.488 μg/mL, in Mueller-Hinton broth or Mueller-Hinton broth with 5% sheep blood (for bacteria) and RPMI 1640 broth with MOPS (for fungi) prepared in 96-well microtiter plates. Next 2 μL of each bacterial or fungal suspension with an optical density of 0.5 McFarland standard, was added to each well containing 200 μL broth with various concentrations of the examined compounds. The microplates were incubated at suitable conditions (37 °C or 30 °C, 24 h for bacteria or fungi, respectively) and then MIC was assessed spectrophotometric. Appropriate DMSO, growth and sterile controls were carried out. The medium with no tested substances was used also as control.[S1-S3]

The MBC (Minimal Bactericidal Concentration) or MFC (Minimal Fungicidal Concentration) are described as the lowest concentration of the compounds that is required to kill a particular bacterial or fungal species. MBC or MFC was determined by removing 20 μL of the culture using for MIC determinations from each well and spotting onto appropriate agar medium. After incubation (37 °C or 30 °C, 24 h for bacteria or fungi, respectively), the lowest compounds concentrations with no visible growth observed was assessed as a

bactericidal/fungicidal concentration. All the experiments were performed three times and representative data are presented.[S1-S3]

In this study, no bioactivity was defined as a MIC > 1000 μg/mL, mild bioactivity as a MIC in the range 501 – 1000 μg/mL, moderate bioactivity with MIC from 126 to 500 μg/mL, good bioactivity as a MIC in the range 26 – 125 μg/mL, strong bioactivity with MIC between 10 and 25 μg/mL and very strong bioactivity as a MIC < 10 μg/mL. The MBC/MIC or MFC/MIC ratios were calculated in order to determine bactericidal/fungicidal (MBC/MIC ≤ 4, MFC/MIC ≤ 4) or bacteriostatic/fungistatic (MBC/MIC > 4, MFC/MIC > 4) effect of the tested compounds.[S3,S4]

References for SI

[S1] European Committee for Antimicrobial Susceptibility Testing (EUCAST) (2003). Determination of minimum inhibitory concentrations (MICs) of antibacterial agents by broth dilution. EUCAST discussion document E. Dis 5.1, *Clin. Microbiol. Infect.* **2003**, *9*, 1-7.

[S2] Clinical and Laboratory Standards Institute. Reference method for broth dilution antifungal susceptibility testing of yeasts. M27-S4. Clinical and Laboratory Standards Institute, Wayne, PA, USA, **2012**.

[S3] Łączkowski K. Z., Misiura K., Biernasiuk A., Malm A., Siwek A., Plech T. Synthesis, Antimicrobial Activities and Molecular Docking Studies of Novel 6-Hydroxybenzofuran-3(2H)-one Based 2,4-Disubstituted 1,3-Thiazoles. *Lett. Drug Des. Discov.* **2013**, *10*, 798-807.

[S4] O'Donnell F., Smyth T. J., Ramachandran V. N., Smyth W. F. A study of the antimicrobial activity of selected synthetic and naturally occurring quinolines. *Int. J. Antimicrob. Agents.* **2010**, *35*, 30-38.

III New insights into the coordination chemistry of Schiff bases derived from amino acids: Planar [Ni_4] complexes with tyrosine side-chains

Muche, S.; Hołyńska, M. *Journal of Molecular Structure* **2017**, *1142*, 168–174.

Structure and properties of a rare metal complex of the chiral Schiff base ligand derived from *ortho*-vanillin and *L*-tyrosine are presented. This study is a continuation of research on ligands containing biologically compatible moieties. The ligand is also fully characterized in form of a sodium salt, in particular in solution, for the first time. The metal complex contains a unique bowl-shaped [Ni_4] core. Its structure is investigated both in solution (ESI-MS, NMR) and in solid state (X-ray diffraction studies). Under certain conditions the complex can be isolated as crystalline DMF solvate which is studied in solid state.

Inhalt: Die Synthesen und vollständige Charakterisierung eines Schiff'sche Base-Liganden aus *ortho*-Vanillin und *L*-Tyrosin als Dinatriumsalz und zwei korrespondierenden tetranuklearen Ni(II)-Komplexen werden präsentiert. Bei beiden Komplexen handelt es sich um isostrukturelle Solvate (DMF bzw. Methanol), von denen die Kristallstrukturen beschrieben werden. Hierbei ist anzumerken, dass messbare Kristalle des DMF-Solvates nur aus Ansätzen in 96-*well*-Platten gewonnen werden konnten. Während die meisten tetranuklearen Nickelkomplexe, bei denen die Metallzentren durch Sauerstoff verbrückt sind, einen Heterokuban als Strukturmotiv besitzen, stellen die gezeigten Verbindungen eine der seltenen Ausnahmen dar: Die sauerstoffverbrückten Metallzentren formen eine schüsselartige Struktur. Alle Tyrosinreste der vier an der Komplexbildung beteiligten Liganden sind frei zugänglich, sodass sich die Möglichkeit bietet, über weitere Metallionen [Ni_4L_4]-Einheiten zu dreidimensionalen Netzwerken zu verknüpfen. Weiterhin wird die Stabilität der beiden Solvate in Lösung und im festen Zustand nachgewiesen.

Eigener Anteil: Die Planung und Durchführung der Synthesen sowie die Aufnahme und Auswertung der Basisanalytik wurde von mir durchgeführt unter Betreuung von Małgorzata Hołyńska. Die Röntgenstrukturanalyse wurde von der hauseigenen Serviceabteilung durchgeführt. Die Analyse der kristallographischen Daten erfolgte durch Małgorzata Hołyńska. Das Manuskript wurde von beiden Autoren gemeinschaftlich verfasst.

Journal of Molecular Structure 1142 (2017) 168–174

Contents lists available at ScienceDirect

Journal of Molecular Structure

journal homepage: http://www.elsevier.com/locate/molstruc

New insights into the coordination chemistry of Schiff bases derived from amino acids: Planar [Ni_4] complexes with tyrosine side-chains

Simon Muche, Małgorzata Hołyńska*

Fachbereich Chemie and Wissenschaftliches Zentrum für Materialwissenschaften, Philipps-Universität Marburg, Hans-Meerwein-Strasse, D-35043, Marburg, Germany

ARTICLE INFO

Article history:
Received 22 October 2016
Received in revised form
7 April 2017
Accepted 11 April 2017
Available online 15 April 2017

Keywords:
Nickel(II)
Schiff-base
Amino acid
Crystal structure
Stability

ABSTRACT

Structure and properties of a rare metal complex of the chiral Schiff base ligand derived from *ortho*-vanillin and *L*-tyrosine are presented. This study is a continuation of research on ligands containing biologically compatible moieties. The ligand is also fully characterized in form of a sodium salt, in particular in solution, for the first time. The metal complex contains a unique bowl-shaped [Ni_4] core. Its structure is investigated both in solution (ESI-MS, NMR) and in solid state (X-ray diffraction studies). Under certain conditions the complex can be isolated as crystalline DMF solvate which is studied in solid state.

1. Introduction

Ortho-vanillin is known as a precursor of new magnetic materials, for instance a trinuclear dysprosium complex, that shows SMM behaviour [1] or a heterometallic [Co_2Gd_2] complex [2]. Not only *ortho*-vanillin itself forms materials with highly interesting magnetic properties, but also Schiff-base ligands derived from *ortho*-vanillin are known as precursors of new magnetic materials [3–7].

Introduction of amino acids to such ligands allows for increase in their coordination capabilities, now involving more coordination sites, and in their biological compatibility. Schiff bases containing L-tyrosine and their metal complexes exhibit a variety of interesting properties. Antimicrobial activity against gram-positive and gram-negative bacteria was reported for Schiff bases containing indole-3-carboxaldehyde and their transition metal (Cu, Ni, Co) complexes [8,9]. The metal complexes, in particular those bearing nitrate as counter-ion, showed the highest antimicrobial activity. Cinnamon aldehyde and its derivates used as aldehyde sources lead to Schiff bases, which are potentially antibacterial and antifungal. In some cases their activity was higher compared to the standard reference drugs [10]. A salicylaldehyde-based Schiff base strongly inhibits growth of *E. coli* in the same range like Ampicillin. Measurements of the genes associated with expression of metabolism suggest that the growth is inhibited probably through down-regulation of *cysB* and *tsh* gene leading to an interference in cysteine biosynthetic pathway and to inhibiting the biosynthesis of temperature-sensitive hemagglutinin [11]. The same compound was identified as a potent non-competitive α-glucosidase inhibitor. The free ligand exhibits a higher inhibitory activity compared to its corresponding silver(I) complex [12]. A mononuclear copper(II) complex with a Schiff base derived from 5-bromosalicylaldehyde and *L*-tyrosine mimics ascorbate oxidase activity [13]. Catalytic activity was reported for ruthenium(II) complexes with substituted salicylaldehydes [14], homogenous and heterogeneous binuclear manganese(II) complexes with salicylaldehyde [15] and an encapsulated binuclear manganese(II) complex with salicylaldehyde in zeolite Y [16].

In our previous work we introduced studies of stability and biological properties of a Schiff-base ligand derived from *ortho*-vanillin and *L*-glutamic acid, along with its [Cu_4] complex [17]. The pendant carboxylic group featured by the [Cu_4] complex resulted in its remarkable solubility, also in aqueous solutions and stability in phosphate buffer. We also showed that this ligand system is capable of forming large wheel-like [Ni_{15}] complexes [18].

While for tetranuclear nickel complexes bridged by oxygen

* Corresponding author.
E-mail address: holynska@staff.uni-marburg.de (M. Hołyńska).

http://dx.doi.org/10.1016/j.molstruc.2017.04.036
0022-2860/

atoms the cubane-like core is the most common motif, examples with a planar core are rare. In the literature some examples of planar or nearly planar tetranuclear nickel-containing core are known. A complex formed by 1,3-bis(benzoylacetoneimine)-propan-2-ol, a pentadentate Schiff-base ligand, possesses a twisted-chair core [19]. Surrounded by a macrocyclic ligand, a bowl-like complex with a planar core is formed [20]. Further complexes with a planar core, but bridged by acetate and/or methoxo ligands on both sides of the plane, are formed involving other macrocyclic ligands [21,22]. Planar cores bridged outside the plane are formed by non-macrocyclic ligands too [23,24]. The planar core motif can be also found in heptanuclear nickel complexes [25,26].

In this contribution we report on new [Ni_4] complexes of a ligand derived from *L*-tyrosine and *ortho*-vanillin. The structure of the green needle-shaped crystals was confirmed with X-ray diffraction studies and it was found that the central metal ion's coordination sphere is distorted octahedral. Two of metal centers are chelated by three ligand molecules, whereas two solvent molecules complete the coordination sphere of the other two metal ions. The ligand can form complexes in a pentadentate or tridentate manner. The complex units are linked due to intermolecular hydrogen bonds involving the solvent molecules present in the crystal structure. Although the complexes bear aromatic moieties, π-π interactions do not play any role in the crystal structure packing. The ligand has been mentioned in literature, but only herein the first full chemical characterization is provided. The [Ni_4] complexes display a unique planar core and the presence of tyrosine hydroxyl side-chains.

2. Results and discussion

2.1. Synthesis and characterization

The title ligand **H_2L** was mentioned in some publications but never full characteristics was reported in spite of the synthetic procedures that yield its monopotassium salt published in 1990 [27] and for the neutral form, but with lack of basic analyses, e. g. NMR and mass spectrometry [28]. The ligand was usually generated *in situ* as precursor of vanadyl complexes used e. g. for modelling of active centers of peroxidases or phosphatases [29–31]. Furthermore, mononuclear vanadium and copper complexes with co-ligands are known [32,33]. It is a Schiff-base derived from *ortho*-vanillin and *L*-tyrosine (Fig. 1).

Herein the ligand **H_2L** was synthesized in the form of a disodium salt **Na_2L** (Fig. 1) following the procedure recently reported by us for the *L*-glutamic acid derivate [17]. Formation of a disodium salt of the organic ligand is consistent with the elemental analysis results (see SI for more information) and the synthesis procedure (usage of 2 eq NaOH), the ESI(+) mass spectrum shows the molecular peak for $[H_2L+H^+]^+$ (m/z = 316.12; Fig. S1).

The ^{1}HNMR spectrum in MeOD (Fig. 2) shows all of the expected signals, except for the proton from the phenolic –OH group which is due to a fast exchange with the solvent. Integration of the signal at 3.35 ppm gives a value of 0.57 only instead of the expected integral of 1 due to overlapping of the signal with the solvent peak. The NMR spectra also show residues of diethyl ether which could not be removed.

When the NMR spectrum was recorded in D_2O, additional sets of signals appeared. Similar as previously reported for the ligand derived from *ortho*-vanillin and *L*-glutamic acid [17], **Na_2L** (black boxes in Fig. S2) partly decomposes to *ortho*-vanillin (red boxes in Fig. S2) and *L*-tyrosine (blue boxes in Fig. S2). Hereby the signal at 7.15–7.20 ppm with an integral of 1.05 results from overlapping of the signals of the aromatic protons from *ortho*-vanillin and *L*-tyrosine. The signal at 3.08 ppm with an integral of 4.04 results from overlapping of the signals of the methoxy groups from *ortho*-vanillin and **Na_2L**. The multiplet at 2.96–3.05 ppm with an integral of 1.40 originates from the overlapping of the signals from the ligand and protons of the *L*-tyrosine methylene group. The *ortho*-vanillin/**Na_2L** ratio was determined by the integrals which should give 1 in total and showed decomposition of 23%. **Na_2L** is soluble in polar solvents such as water and methanol.

The corresponding complex **[Ni_4(L)$_4$]-MeOH** was crystallized from a system where the organic ligand was generated *in situ*. **[Ni_4(L)$_4$]-MeOH** displays molecular peaks under ESI-MS conditions in methanolic solution in both positive (m/z = 1485.12) and negative mode (m/z = 1483.11) (Figs. S4 and S5). These results indicate the stability of **[Ni_4(L)$_4$]-MeOH** in solution. On drying in vacuum for several hours the color of the solid complex changes slightly to olive green. However, the vacuum-dried and air-dried samples of **[Ni_4(L)$_4$]-MeOH** show identical IR spectra (Fig. 3). These observations additionally confirm a reasonable stability of the complex in solid state. The complex dissolves very well in DMSO resulting in a yellow color of the solution. In methanol **[Ni_4(L)$_4$]-MeOH** is less soluble but the color of the solution is green. **[Ni_4(L)$_4$]-MeOH** also dissolves in water but formation of colourless to light green residues is observable. Due to the paramagnetic nature of the complex NMR studies are limited, so that it remains unclear if the complex decomposes in water and DMSO.

The DMF solvate of **[Ni_4(L)$_4$] ([Ni_4(L)$_4$]-DMF)** is synthesized in the same manner but with addition of DMF at the end (see Experimental section). Synthesis of the complex in a macroscale sample (25 mL; 1 mmol) did not lead to crystals suitable for X-ray analysis. Suitable crystals were obtained from a microscale sample (150 μL; 1/96 mmol). However, the elemental analysis shows a significant increase of nitrogen content compared to the methanol solvate. Comparison of the IR spectra of the DMF and methanol solvate of **[Ni_4(L)$_4$]** reveals a difference in the peaks in the relevant region between 400 cm^{-1} and 1800 cm^{-1} (Fig. 4). This difference is

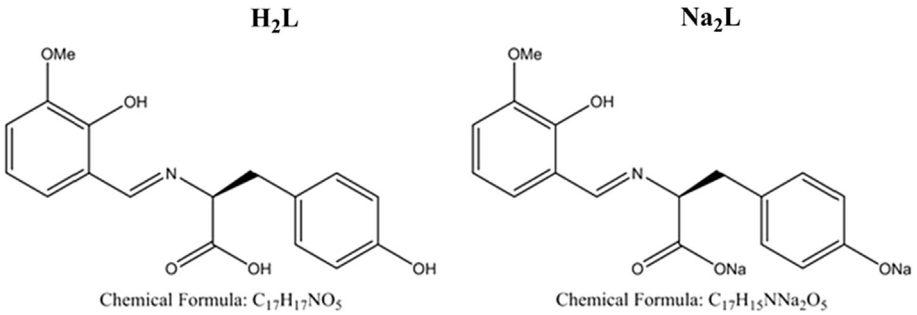

Fig. 1. Structural and chemical formula of the ligand in its neutral form **H_2L** and as disodium salt **Na_2L**.

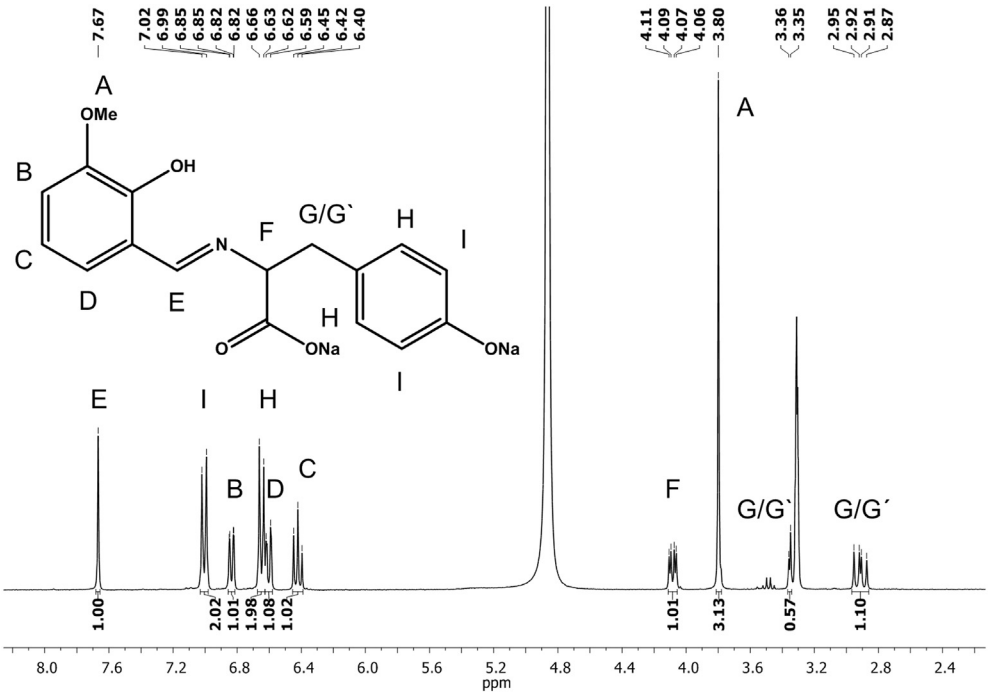

Fig. 2. ^{1}HNMR spectrum for **Na_2L** in MeOD.

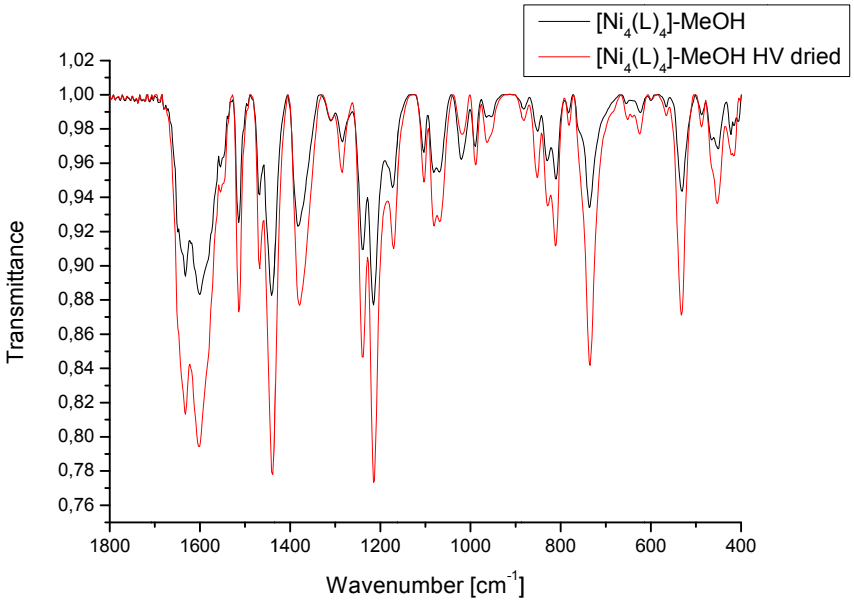

Fig. 3. IR spectra of **[$Ni_4(L)_4$]-MeOH** dried under air (black line) and under HV (high vacuum, red line). (For interpretation of the references to colour in this figure legend, the reader is referred to the web version of this article.)

due to the DMF content. The ESI mass spectra in both positive and negative mode show the molecular peak found for **[$Ni_4(L)_4$]-MeOH** and the same fragmentation pattern (Figs. S8 and S9). The vacuum-dried and air-dried samples of **[$Ni_4(L)_4$]-DMF** show identical IR spectra (Fig. S12), which additionally confirm a reasonable stability of **[$Ni_4(L)_4$]-DMF** in solid state, as well as for **[$Ni_4(L)_4$]-MeOH**. The ESI mass spectra in both positive and negative mode obtained for crystals from the microscale sample show the molecular peak found for both complexes as described above and the same fragmentation pattern (Figs. S13 and S14). The IR spectra for crystals from the macro- and microscale sample are identical (Fig. S16).

The syntheses for both solvates are reproducible.

2.2. Crystal structures

The two Ni complexes isolated for the title ligand system are “bowl-shaped” with a close-to-planar [Ni_4] core. The two complexes are isostructural but they differ in the solvent content and the pattern of terminal ligands of the “bowl” inner part (three water molecules and one methanol molecule in the case of **[$Ni_4(L)_4$]-**

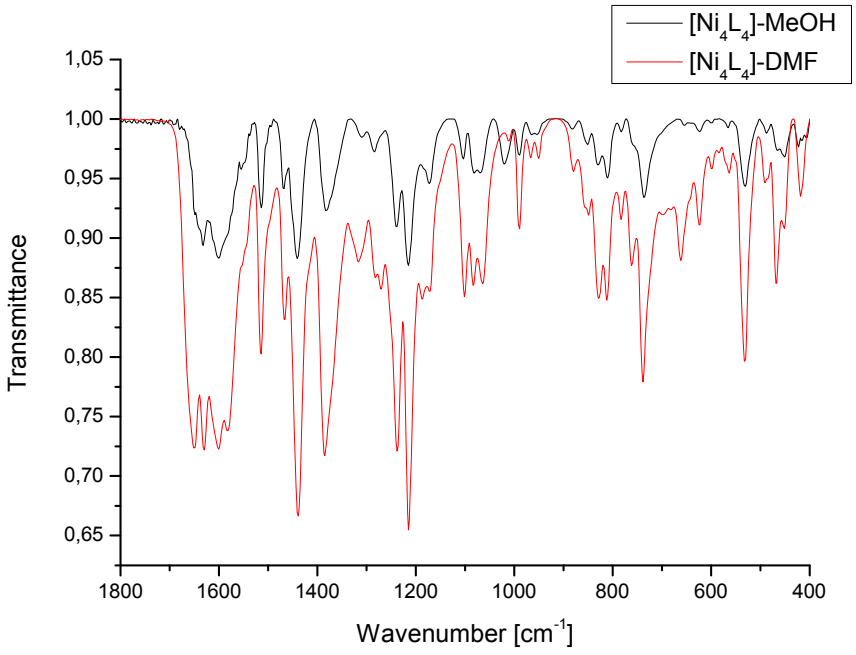

Fig. 4. IR spectra of air-dried samples of **[Ni$_4$(L)$_4$]-MeOH** and **[Ni$_4$(L)$_4$]-DMF** in the region between 400 cm^{-1} and 1800 cm^{-1}.

MeOH and four water molecules in the case of **[Ni$_4$(L)$_4$]-DMF**). Crystallographic data for both complexes are given in Table 1. Morphology of the crystals is visualized in Fig. S17.

The **[Ni$_4$(L)$_4$]-MeOH** complex molecule comprises four Ni^{2+} ions joined in a close-to-planar dumbbell-like arrangement by two ligand molecules (Fig. 5). Each of these ligands is doubly deprotonated and chelates two Ni^{2+} ions in its methoxo-phenoxo and nitrogen-carboxylate pockets, respectively. The coordination sphere of the central "dumbbell" Ni^{2+} ions is completed with three terminal water molecules (Ni–O bond lengths at 2.109(3) to 2.134(3) Å) and one terminal methanol molecule (Ni–O1M bond of 2.082(3) Å length). The water H atoms could not be localized from difference Fourier maps, but the O···O distances indicate that there should be one hydrogen bond (O2W···O3W of 2.741(5) Å). The O1W···O1M distance on the other side of the "dumbbell" is longer (3.346(8) Å). The tyrosine hydroxyphenyl moiety forms a side-chain. Interplanar angles between the tyrosyl and vanillin phenyl rings are of 43.4(3) and 33.4(2)° for the C414/C124 and C411/C121 rings, respectively. Moreover, each of the two Ni^{2+} ions in the methoxo-phenoxo pockets is further triply chelated with phenoxo/carboxylate O atoms and an N atom from terminal Schiff-base ligands (Fig. 6). For these ligands the interplanar angles between the planes of phenyl rings are different (81.5(3) and 54.6(2)° for the C413/C123 and C412/C122 rings, respectively). This underlines the

Table 1
Selected X-ray data for **[Ni$_4$(L)$_4$]-MeOH**/**[Ni$_4$(L)$_4$]-DMF**.

	[Ni$_4$(L)$_4$]-MeOH	[Ni$_4$(L)$_4$]-DMF
Formula	$C_{68}H_{68}N_4Ni_4O_{24}\cdot 5.84(CH_4O)$	$C_{68}H_{68}N_4Ni_4O_{24}\cdot 4.6(H_2O)\cdot 2(CH_4O)\cdot 3(C_3H_7NO)$
Formula weight	1747.17	1926.29
Temperature [K]	115(2)	115(2)
λ [Å]	0.71073	0.71073
Crystal system	Orthorhombic	Orthorhombic
Space group	$P2_12_12_1$	$P2_12_12_1$
a [Å]	14.393 (2)	14.757 (2)
b [Å]	23.017 (3)	23.279 (3)
c [Å]	24.719 (3)	26.220 (3)
β [°]		
V [Å^3]	8189.0 (18)	9007 (2)
Z, ρ_{calc} [g cm^{-3}]	4, 1.429	4, 1.421
μ [mm^{-1}]	0.99	0.91
F(000)	3684	4040
Crystal size [mm]	0.33 × 0.33 × 0.13	0.27 × 0.18 × 0.11
θ range[°]	1.86–25.00	2.08–25.00
rflns: total/unique	77449/14417	69414/15866
R(int)	0.0503	0.0779
Abs. corr.	numerical	numerical
Min., max. transmission factors	0.745, 0.919	0.805, 0.950
Data/restraints/params	14417/17/1061	69414/0/1144
GOF on F^2	1.03	1.02
R1 [I > 2σ(I)]	0.039	0.046
wR_2 (all data)	0.120	0.118
Max., min. $\Delta\rho_{elect}$ [e Å^{-3}]	0.97, −0.60	0.52, −0.41

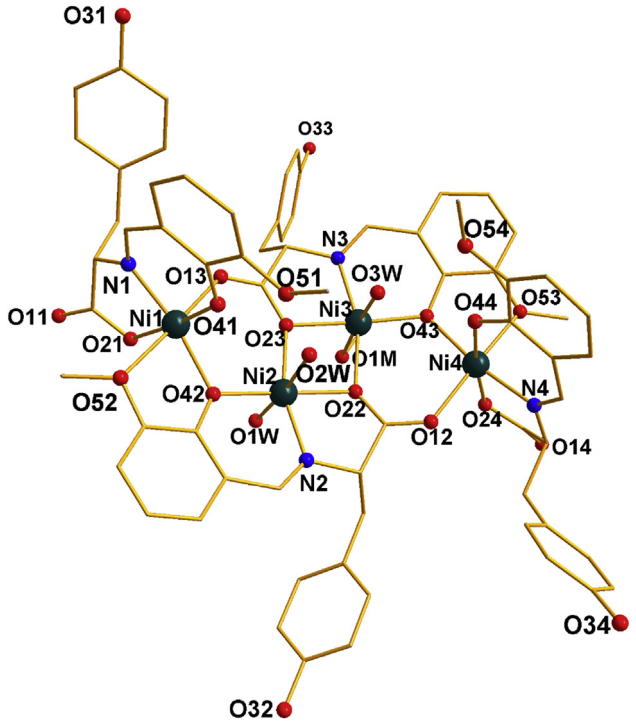

Fig. 5. Molecular structure of **[Ni$_4$(L)$_4$]-MeOH** (**[Ni$_4$(L)$_4$]-DMF** is a different solvate of **[Ni$_4$(L)$_4$]-MeOH**) with atom labeling scheme. C atoms are show as sticks/H atoms are omitted for clarity.

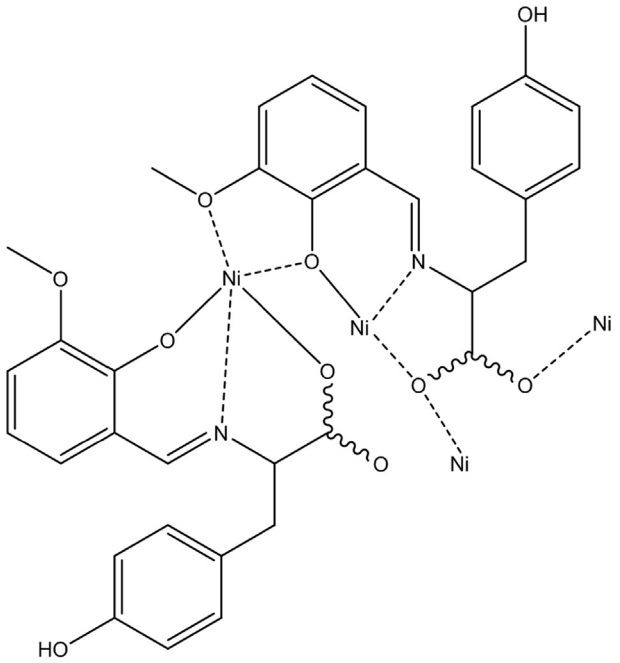

Fig. 6. Coordination mode of **L** in **[Ni$_4$(L)$_4$]-MeOH** (stereochemistry not shown).

ligand flexibility and potential of the side-chain hydroxyl groups to further participate in coordination to additional metal ions.

In the **[Ni$_4$(L)$_4$]-MeOH** complex the water O2W and O3W terminal ligands pointing inside of the "bowl" are at a hydrogen bonding distance whereas the water O1W and methanol O1M ligands pointing on the other side are separated by ca. 3.34 Å. The structure contains multiple partly disordered methanol molecules of solvation, some of which are at hydrogen bonding distance to the O atoms of the terminal ligands. The complex molecules form columns along the [100] direction (Fig. 7).

In the **[Ni$_4$(L)$_4$]-DMF** complex all terminal solvent ligands are water molecules but they follow the same pattern with respect to hydrogen bonding distances as in the case of **[Ni$_4$(L)$_4$]-MeOH** with one "shorter" distance (O2W···O4W at 2.782(7) Å) and one "longer" distance (O1W···O3W at 3.269(7) Å). Thus the organic part is the driving force for the overall "bowl-like" arrangement of the complex molecules. Obviously the solvent part affects also the organic ligands conformation as the interplanar angles between planes of the vanillin and tyrosyl rings differ with respect to **[Ni$_4$(L)$_4$]-MeOH** (in **[Ni$_4$(L)$_4$]-DMF**: 34.50(3) and 38.6(4)° for the C414/C124 and C411/C121 rings, respectively; 42.3(2) and 59.9(3)° for the C413/C123 and C412/C122 rings, respectively). The **[Ni$_4$(L)$_4$]-DMF** complex contains ca. 5 water, 2 methanol and 5 DMF molecules of solvation per complex molecule. These molecules surround the complex molecules in some cases engaging in hydrogen bonds to the available O atoms. Possible hydrogen-bonded contacts, including weak hydrogen bonding with C atoms as donors, are listed and quantified in Tables S3 and S4.

3. Conclusion and outlook

In perspective, we anticipate that the rich field of Schiff-bases derived from amino acids will yield many more examples of interesting coordination chemistry and biological compatibility.

A thorough characterization of the ligands scattered in literature seems to be needed and will be undertaken.

In this study we presented the full characterization of the Schiff-base ligand derived from *L*-tyrosine and *ortho*-vanillin, as well as a rare example of planar tetranuclear nickel complexes and the first example of a nickel complex containing this Schiff-base ligand. Furthermore, we could verify the stability of the complexes in solution and in solid state by IR-spectroscopy and ESI-MS studies. The presented crystal structures reveal flexible unbound side chains of the used amino acid and the effect of the surroundings on the ligand conformation. This fact allows the possibility either to connect [Ni$_4$L$_4$]-units to three-dimensional networks via metal ions or to introduce further functional groups on the side chain.

4. Experimental

4.1. Synthesis

4.1.1. Ligand Na_2L

At 80 °C 240 mg (6 mmol) of sodium hydroxide were dissolved in 30 ml of methanol. 544 mg *L*-tyrosine (3 mmol) were added to the methanolic solution. When the *L*-tyrosine was dissolved completely, 456 mg (3 mmol) of *ortho*-vanillin were added. The color of the solution changed to yellow immediately. The solution was stirred for 1 h at 80 °C. After the solution was cooled down to room temperature 150 ml aliquots of diethyl ether were added. A yellow precipitate appeared. The yellow precipitate was separated from the solution, washed several times with diethyl ether and dried *in vacuo*. Yield (average): 743.7 mg (69%).

Elemental analysis for the substance dried under vacuum for several hours, analysed as $C_{17}H_{15}NO_5Na_2 \bullet 0.22Et_2O$: Calcd (found): C 57.18 (58.49), H 4.62 (4.97), N 3.73 (3.93).

IR bands (cm^{-1}) for **Na$_2$L** dried *in vacuo*: 426.9 (w), 490.9 (w), 530.1 (m), 737.4 (w), 808.8 (w), 828.9 (w), 848.4 (w), 982.6 (vw), 1092.4 (w), 1168.9 (m), 1221.1 (s), 1365.2 (m), 1410.1 (w), 1452.4 (w), 1513.5 (m), 1611.8 (s) [C=N].

^{1}H NMR (300 MHz, MeOD) δ 7.67 (s, 1H), 7.01 (d, J = 8.4 Hz, 2H),

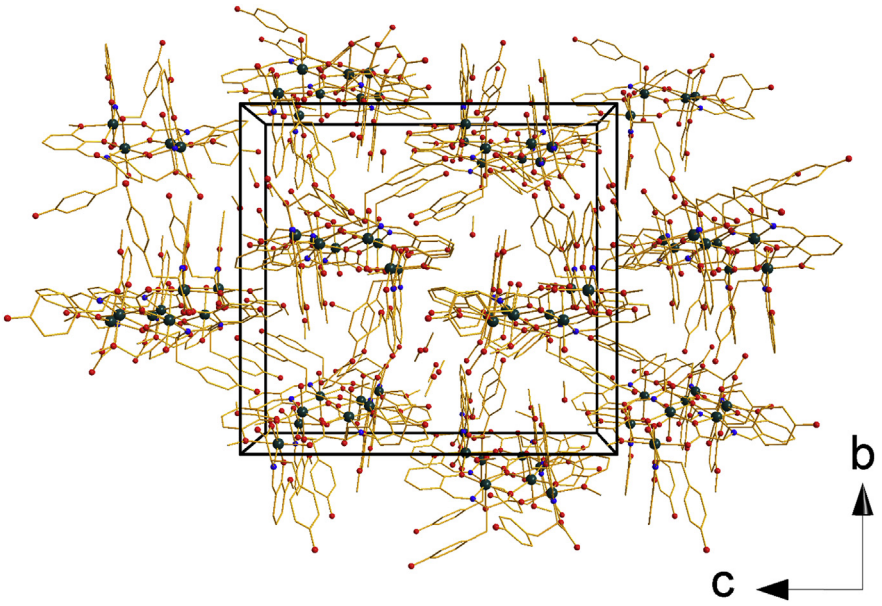

Fig. 7. Columnar arrangement of the complex molecules along [100] in **[Ni$_4$(L)$_4$]-MeOH**.

6.84 (dd, J = 7.6, 1.1 Hz, 1H), 6.65 (d, J = 8.4 Hz, 2H), 6.61 (d, J = 8.2 Hz, 1H), 6.42 (t, J = 7.9 Hz, 1H), 4.08 (dd, J = 9.9, 3.8 Hz, 1H), 3.80 (s, 3H), 3.35 (d, J = 3.3 Hz, 0.5H), 2.91 (dd, J = 13.8, 10.0 Hz, 1H).

^{1}H NMR (300 MHz, D_2O) δ 7.69 (s, 1H), 7.10 (d, J = 8.5 Hz, 2H), 6.96 (dd, J = 7.6, 1.2 Hz, 1H), 6.79 (d, J = 8.5 Hz, 2H), 6.66 (dd, J = 8.2, 1.3 Hz, 1H), 6.48 (t, J = 7.9 Hz, 1H), 4.30 (dd, J = 9.3, 4.1 Hz, 1H), 3.80 (s, 4H), 3.33 (dd, J = 13.7, 3.9 Hz, 1H), 3.06–2.95 (m, 1H).

ESI(+) (MeOH): Molecular peak was found at m/z = 316.12 ($[H_2L+H^+]^+$). Further identified peak: m/z = 338.10 ($[H_1LNa_1+H^+]^+$).

4.1.2. Complex [Ni$_4$(L)$_4$]-MeOH

At 80 °C 80 mg (2 mmol) of sodium hydroxide were dissolved in 20 ml of methanol. 181 mg of *L*-tyrosine (1 mmol) were added to the methanolic solution. When *L*-tyrosine was dissolved completely, 152 mg (1 mmol) of *ortho*-vanillin were added. The color of the solution changed to yellow immediately. To the yellow solution 238 mg (1 mmol) of $NiCl_2 \cdot 6H_2O$ were added and the green solution was stirred for 30 min at 80 °C. The solution was transferred to 30 mL vial for crystallization by slow evaporation. First green crystals appeared after one week. Crystallization was finished after 11 days. The crystals were filtered off and dried under air for ca. 12 h. Yield (average): 328.4 mg (0.188 mmol; 18.8%).

Elemental analysis for the substance dried under vacuum for several hours, analysed as $C_{68}H_{68}N4O_{24}Ni_4 \cdot 3.5$ MeOH: Calcd (found) C 51.39 (51.8), H 4.94 (4.93), N 3.35 (3.41), O 26.31 (26.11).

IR bands (cm^{-1}) **[Ni$_4$(L)$_4$]-MeOH** dried *in vacuo*: 415.9 (vw), 453.0 (w), 487.7 (vw), 531.9 (m); 625.0 (w), 735.2 (m), 781.6 (vw), 811.2 (w), 851.9 (w), 963.3 (w), 988.6 (w), 1018.5 (w), 1081.0 (w), 1102.9 (w), 1170.6 (w), 1214.3 (s), 1239.2 (m), 1285.2 (w), 1379.1 (m), 1439.5 (s), 1468.0 (w), 1513.4 (m), 1601.9 (s), 1632.3 (s).

ESI(+) (MeOH): molecular peak was found at m/z = 1485.12: $[Ni_4(L)_4]+H^+$.

Further peaks: m/z = 743.06: $[Ni_2(L)_2]+H^+$; 765.05: $[Ni_2(L)_2]+Na^+$; 1114.09: $[Ni_3(L)_3]+H^+$; 11136.09: $[Ni_3(L)_3]+Na^+$; 1507.11: $[Ni_4(L)_4]+Na^+$.

ESI(−) (MeOH): molecular peak was found at m/z = 1483.11: $[Ni_4(L)_4]^-$. Further peaks m/z = 685.13: $[Ni(L)(HL)]^-$, 741.05: $[Ni_2(L)_2]$-H^+; 1056.17: $[Ni_2(L)_2(HL)]^-$; 1112.08: $[Ni_3(L)_3]^-$; 1427.19: $[Ni_3(L)_3(HL)]^-$.

4.1.3. Complex [Ni$_4$(L)$_4$]-DMF

At 80 °C 80 mg (2 mmol) of sodium hydroxide were dissolved in 15 ml of methanol. 181 mg of *L*-tyrosine (1 mmol) were added to the methanolic solution. When *L*-tyrosine was dissolved completely, 152 mg (1 mmol) of *ortho*-vanillin were added. The color of the solution changed to yellow immediately. To the yellow solution 238 mg (1 mmol) $NiCl_2 \cdot 6H_2O$ were added and the green solution was stirred for 30 min at 80 °C. Finally 5 mL DMF were added, stirred vigorously for 1 min, then the solution was transferred to 30 mL vial for crystallization by slow evaporation. First green crystals appeared after one week. The crystals were filtered off after 13 days and dried under air overnight. Yield (average): 314 mg (16.3%).

The obtained crystals had no sufficient quality for X-ray measurement. Suitable crystals were obtained from a 150 μL microscale sample in a 96-well polystyrene microtiter plate.

Elemental analysis for the substance dried under vacuum for several hours, analysed as $C_{68}H_{68}N4O_{24}Ni_4 \cdot 2.7$ DMF$\cdot$1.3 MeOH$\cdot 2H_2O$: Calcd (found) C 50.66 (50.56), H 5.28 (5.20), N 5.11 (5.12), O 26.16 (26.95).

IR bands (cm^{-1}) **[Ni$_4$(L)$_4$] DMF** dried *in vacuo*: 412.2 (vw), 416.8 (w), 426.7 (w), 450.4 (w); 467.7 (vw), 483.1 (w), 491.0 (w), 530.4 (m), 538.0 (vw), 564.5 (w), 600.6 (vw), 623.6 (w), 640.9 (w), 663.1 (s), 682.6 (w), 738.6 (s), 761.3 (w), 781.7 (w), 809.7 (m), 828.6 (m), 848.9 (w), 857.8 (w), 881.5 (w), 950.7 (w), 966.7 (w), 989.6 (w), 1010.7 (w), 1062.1 (m), 1083.7 (m), 1101.4 (m), 1168.7 (m), 1215.9 (s), 1238.6 (s), 1270.7 (m), 1284.8 (m), 1307.1 (w), 1317.0 (w), 1364.0 (vw), 1385.3 (m), 1435.0 (vw), 1441.8 (s), 1468.0 (m), 1514.6 (m), 1543.0 (vw), 1580.1 (vw), 1601.52 (s), 1631.4 (s), 1650.4 (s), 1669.0 (vw), 2831.3 (w), 2926.7 (w).

Bands at 848.9, 1083.7, 1238.6, 1385.2 1669.0, 2831.3 and 2926.7 can be identified as DMF bands.

ESI(+) (MeOH): molecular peak was found at m/z = 1485.12: $[Ni_4(L)_4]+H^+$.

Further peaks: m/z = 743.06: $[Ni_2(L)_2]+H^+$; 765.05: $[Ni_2(L)_2]+Na^+$; 1114.09: $[Ni_3(L)_3]+H^+$; 11136.09: $[Ni_3(L)_3]+Na^+$; 1507.11: $[Ni_4(L)_4]+Na^+$.

ESI(−) (MeOH): molecular peak was found at m/z = 1483.11: $[Ni_4(L)_4]^-$. Further peaks m/z = 685.13: $[Ni(L)(HL)]^-$, 741.05: $[Ni_2(L)_2]$-H^+; 1056.17: $[Ni_2(L)_2(HL)]^-$; 1112.08: $[Ni_3(L)_3]^-$; 1427.19:

$[Ni_3(L)_3(HL)]^-$.

4.2. Physicochemical measurements

Elemental analyses were carried out on an Elementar Vario Microcube elemental analyzer in CHNS mode. Oxygen content analysis was carried out on an Elementa rapid OXY Cube elemental analyzer.

IR spectra were recorded using a Bruker Alpha-P Infrared-spectrometer equipped with a Platinum-ATR with a diamond crystal.

^{1}H NMR spectra for **Na_2L** were recorded in methanol-d_4 and D_2O with a Bruker DRX 300 MHz spectrometer at room temperature. Chemical shifts were quoted in ppm relative to the residual protons of deuterated solvents.

Electrospray ionization mass spectrometry (ESI-MS) was performed on a Finnigan LTQ-FT spectrometer by Thermo Fischer Scientific in the positive and negative ion mode with solvent as carrier gas.

X-ray diffraction experiment: A single crystal of **$[Ni_4(L)_4]$-MeOH**/**$[Ni_4(L)_4]$-DMF** was mounted on a Bruker D9 Quest diffractometer equipped with CMOS detector and MoK_α radiation source. Basic crystallographic details are collected in Table 1.

Details on structure refinement: The crystal structures were solved by direct methods with SHELXS97 software and refined in SHELXL97 [34]. Where possible, H atoms were placed in their calculated positions and refined with a riding model. Water H atoms were not localized.

For **$[Ni_4(L)_4]$-MeOH** part of the methanol molecules of solvation were refined as disordered (for two molecules occupancies were refined and fixed at the achieved values of 0.4 and 0.6, for one molecule the occupancy was refined to ca. 0.84 as a free variable). On the final difference Fourier map the highest maximum of 0.97 e/Å^3 is localized near to the disordered solvent site.

For **$[Ni_4(L)_4]$-DMF** SQUEEZE procedure had to be applied to remove spurious disordered solvent effect. For three disordered water molecules occupancies were refined and fixed at 0.7, 0.7 and 0.2, respectively. On the final difference Fourier map the highest maximum of 0.52 e/Å^3 is localized near to the disordered solvent site.

Acknowledgement

S. M. acknowledges help of Helena Helm with the synthesis of metal complexes.

Appendix A. Supplementary data

Supplementary data related to this article can be found at http://dx.doi.org/10.1016/j.molstruc.2017.04.036.

References

[1] J. Tang, I. Hewitt, N.T. Madhu, G. Chastanet, W. Wernsdorfer, C.E. Anson, C. Benelli, R. Sessoli, A.K. Powell, Angew. Chem. 45 (2006) 1729–1733 (International ed. in English).
[2] J.-P. Costes, L. Vendier, W. Wernsdorfer, Dalton Trans. 40 (2011) 1700–1706 (Cambridge, England 2003).
[3] N. Ahmed, C. Das, S. Vaidya, S.K. Langley, K.S. Murray, M. Shanmugam, Chem. Weinheim der Bergstrasse, Ger. 20 (2014) 14235–14239.
[4] H. Ke, W. Zhu, S. Zhang, G. Xie, S. Chen, Polyhedron 87 (2015) 109–116.
[5] S. Saha, S. Pal, C.J. Gómez-García, J.M. Clemente-Juan, K. Harms, H.P. Nayek, Polyhedron 74 (2014) 1–5.
[6] C.-B. Tian, D.-Q. Yuan, Y.-H. Han, Z.-H. Li, P. Lin, S.-W. Du, Inorg. Chem. Front. 1 (2014) 695–704.
[7] N. Ahmed, C. Das, S. Vaidya, A.K. Srivastava, S.K. Langley, K.S. Murray, M. Shanmugam, Dalton Trans. 43 (2014) 17375–17384 (Cambridge, England 2003).
[8] Z.H. Chohan, M. Praveen, A. Ghaffar, Metal-based drugs 4 (1997) 267–272.
[9] Z.H. Chohan, M. Praveen, A. Ghaffaf, Synth. React. Inorg. Metal-Organic Chem. 28 (1998) 1673–1687.
[10] H. Wang, H. Yuan, S. Li, Z. Li, M. Jiang, Bioorg. Med. Chem. Lett. 26 (2016) 809–813.
[11] L. Xia, Y.-F. Xia, L.-R. Huang, X. Xiao, H.-Y. Lou, T.-J. Liu, W.-D. Pan, H. Luo, Eur. J. Med. Chem. 97 (2015) 83–93.
[12] J. Zheng, L. Ma, Bioorg. Med. Chem. Lett. 25 (2015) 2156–2161.
[13] Z. Moradi-Shoeili, Z. Amini, D.M. Boghaei, B. Notash, Polyhedron 53 (2013) 76–82.
[14] R. Kureshy, N. Khan, S. Abdi, S. Patel, P. Iyer, J. Mol. Catal. A Chem. 150 (1999) 175–183.
[15] M. Ghorbanloo, M. Jaworska, P. Paluch, G.-D. Li, L.-J. Zhou, Transit. Met. Chem. 38 (2013) 511–521.
[16] M. Ghorbanloo, S. Rahmani, H. Yahiro, Transit. Met. Chem. 38 (2013) 725–732.
[17] S. Muche, I. Levacheva, O. Samsonova, A. Biernasiuk, A. Malm, R. Lonsdale, Ł. Popiołek, U. Bakowsky, M. Hołyńska, J. Mol. Struct. 1127 (2017) 231–236.
[18] S. Muche, I. Levacheva, O. Samsonova, L. Pham, G. Christou, U. Bakowsky, M. Hołyńska, Inorg. Chem. 53 (2014) 7642–7649.
[19] M. Mikuriya, K. Minowa, N. Nagao, Inorg. Chem. Commun. 4 (2001) 441–443.
[20] K. Ikeda, K. Matsufuji, M. Ohba, M. Kodera, H. Okawa, BCSJ 77 (2004) 733–739.
[21] X.-B. Wan, C.-M. Jin, Z.-W. Shi, G.-Y. Lu, J. Chem. Crystallogr. 34 (2004) 57–60.
[22] P.E. Kruger, V. McKee, Chem. Commun. (1997) 1341–1342.
[23] A.D. Katsenis, V.G. Kessler, G.S. Papaefstathiou, Dalton Trans. 40 (2011) 4590–4598 (Cambridge, England 2003).
[24] A.M. Barrios, S.J. Lippard, J. Am. Chem. Soc. 121 (1999) 11751–11757.
[25] S.T. Meally, C. McDonald, G. Karotsis, G.S. Papaefstathiou, E.K. Brechin, P.W. Dunne, P. McArdle, N.P. Power, L.F. Jones, Dalton Trans. 39 (2010) 4809.
[26] S.T. Meally, G. Karotsis, E.K. Brechin, G.S. Papaefstathiou, P.W. Dunne, P. McArdle, L.F. Jones, CrystEngComm 12 (2010) 59–63.
[27] R. Roy, M.C. Saha, P.S. Roy, Transit. Met. Chem. 15 (1990) 51–57.
[28] J. Gao, Y. Guo, J. Wang, Z. Wang, X. Jin, C. Cheng, Y. Li, K. Li, Spectrochim. acta. Part A, Mol. Biomol. Spectrosc. 78 (2011) 1278–1286.
[29] D. Rehder, M. Ebel, C. Wikete, G. Santoni, J. Gätjens, Pure Appl. Chem. 77 (2005).
[30] M. Ebel, D. Rehder, Inorg. Chem. 45 (2006) 7083–7090.
[31] C. Grüning, D. Rehder, J. Inorg. Biochem. 80 (2000) 185–189.
[32] B.-Q. Jing, L.-Z. Li, D.-Q. Wang, T. Xu, Acta Crystallogr. E Struct. Rep. Online 61 (2005) m2106–m2108.
[33] X. Pu, L. Li, J. Dong, B. Jing, Acta Crystallogr. Sect. E, Struct. Rep. online 67 (2011) m465–6.
[34] G.M. Sheldrick, SHELXTL 5.1, Bruker AXS Inc, 6300 Enterprise Lane, Madison, WI 53719–1173, USA, 1997.

New insights into the coordination chemistry of Schiff bases derived from amino acids: planar [Ni_4] complexes with tyrosine side chains

Simon Muche[a] *and Małgorzata Hołyńska*[*a]

[a] Fachbereich Chemie and Wissenschaftliches Zentrum für Materialwissenschaften, Philipps-Universität Marburg, Hans-Meerwein-Strasse, D-35043 Marburg, Germany. E-Mail: holynska@staff.uni-marburg.de

SUPPORTING INFORMATION

1. Analytical data

Fitting of the elemental analysis data

H_2L

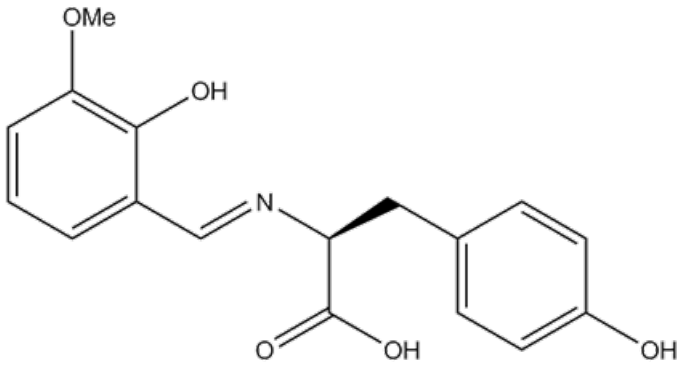

Chemical Formula: $C_{17}H_{17}NO_5$

Molecular Weight: 315,33

Elemental Analysis: C, 64.75; H, 5.43; N, 4.44; O, 25.37

NaHL

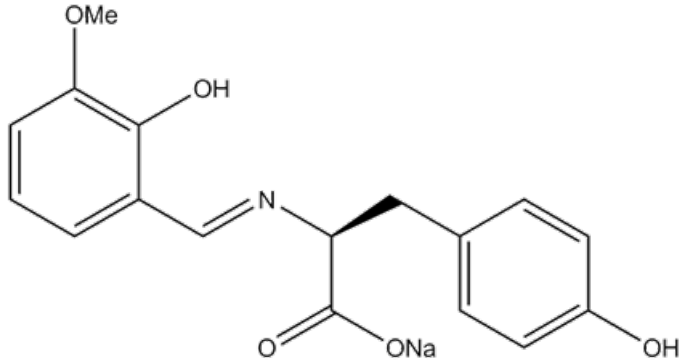

Chemical Formula: $C_{17}H_{16}NNaO_5$

Molecular Weight: 337,31

Elemental Analysis: C, 60.53; H, 4.78; N, 4.15; Na, 6.82; O, 23.72

Na_2L

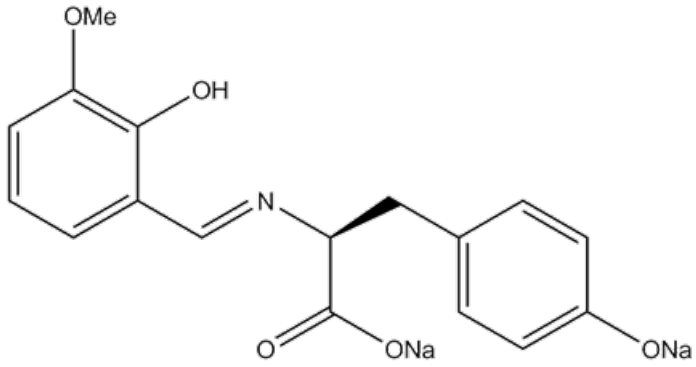

Chemical Formula: $C_{17}H_{15}NNa_2O_5$

Molecular Weight: 359,29

Elemental Analysis: C, 56.83; H, 4.21; N, 3.90; Na, 12.80; O, 22.26

2. Supplementary figures

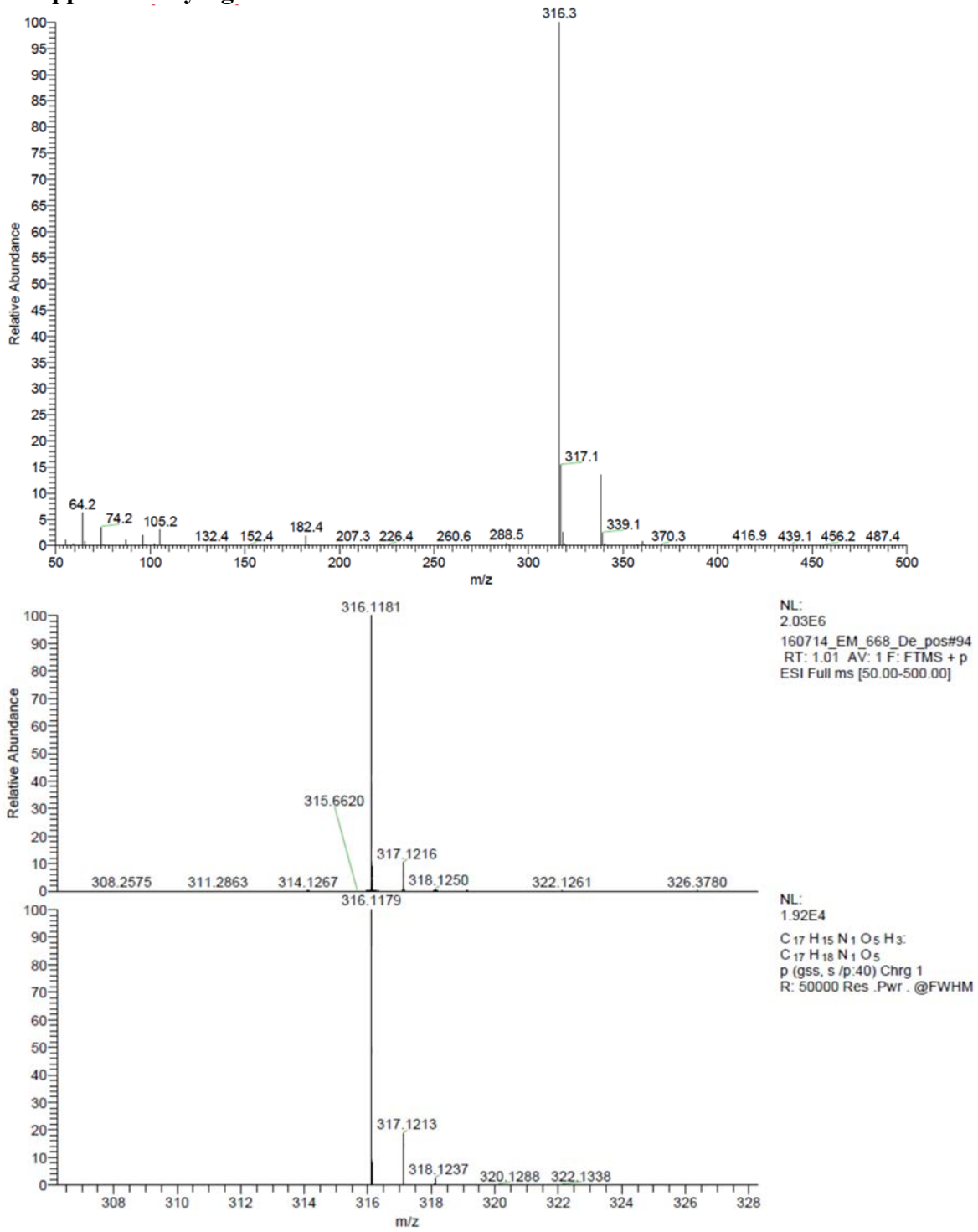

Figure S1. ESI-MS spectrum of **Na_2L** in methanol with simulation of the molecular peak.

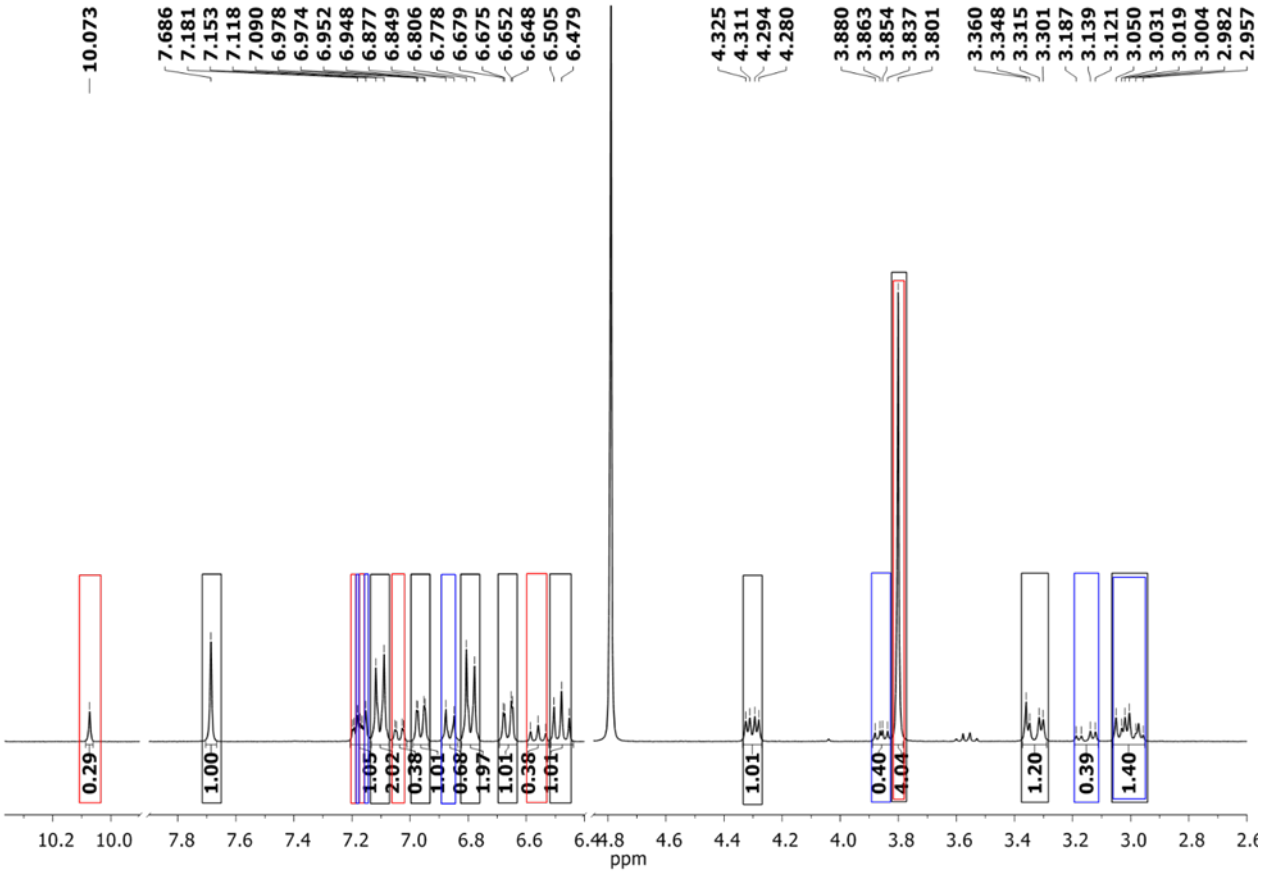

Figure S2. [1]HNMR spectrum for **Na$_2$L** in D_2O. Visible signals: **Na$_2$L** (black boxes), *ortho*-vanillin (red boxes) and *L*-tyrosine (blue boxes).

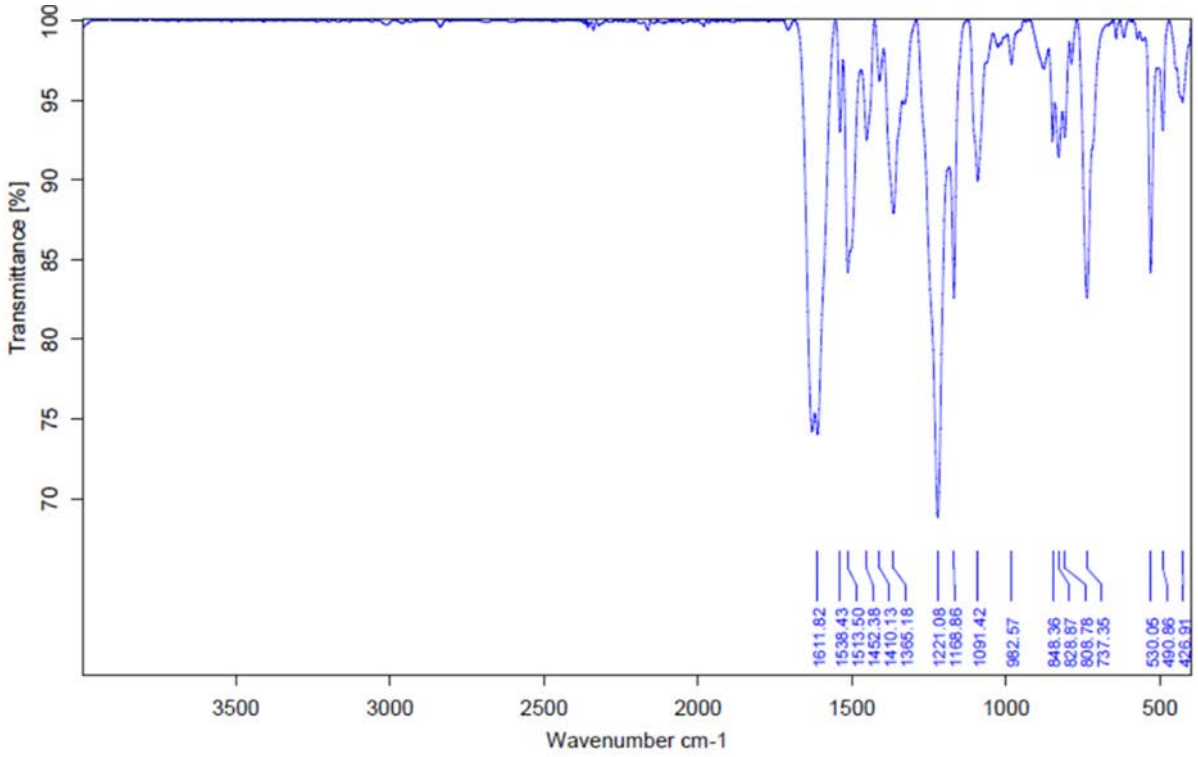

Figure S3. IR spectrum of **Na$_2$L** dried *in vacuo*.

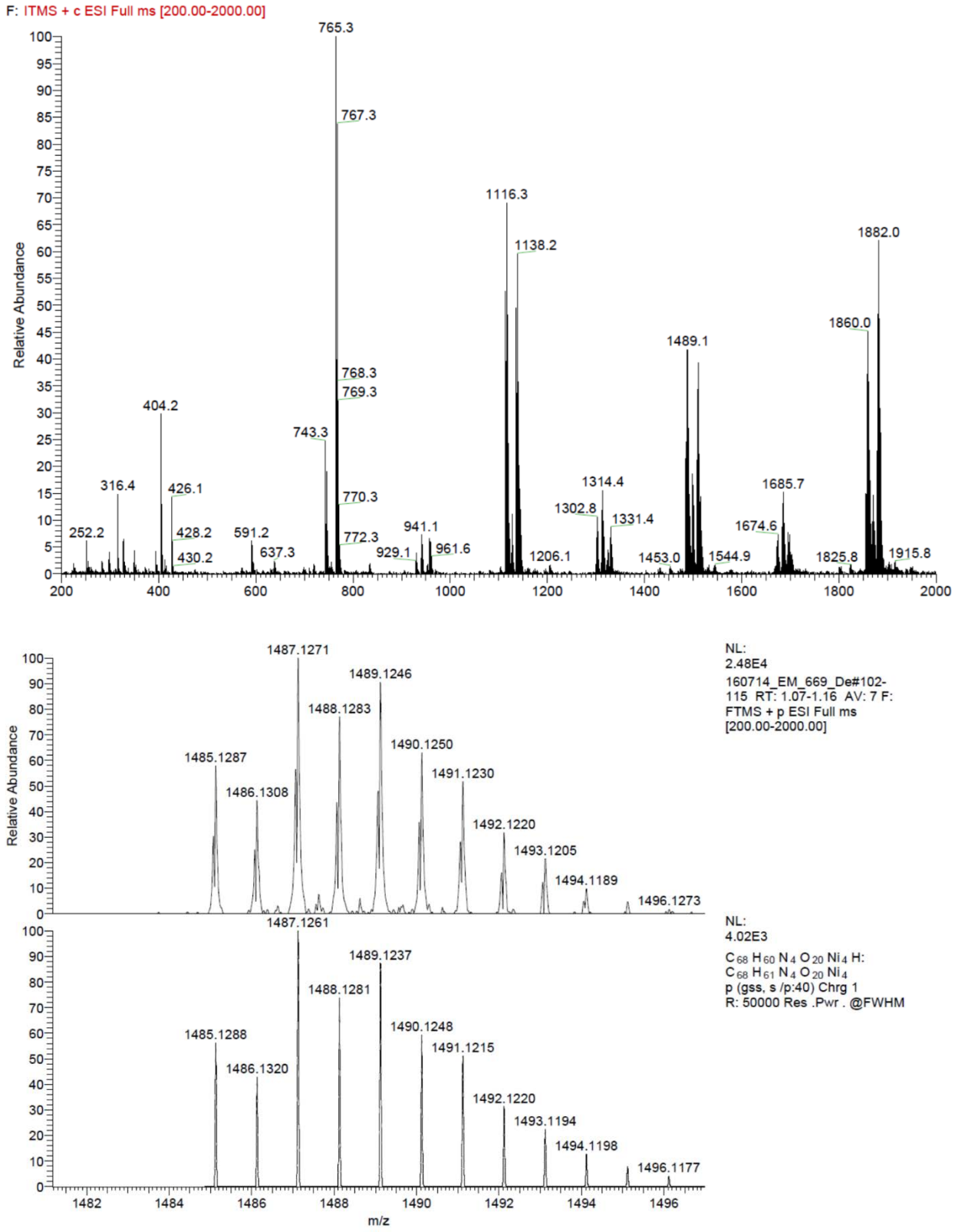

Figure S4. ESI(+)-MS spectrum of **[Ni$_4$(L)$_4$]-MeOH** in methanol with simulation of the molecular peak.

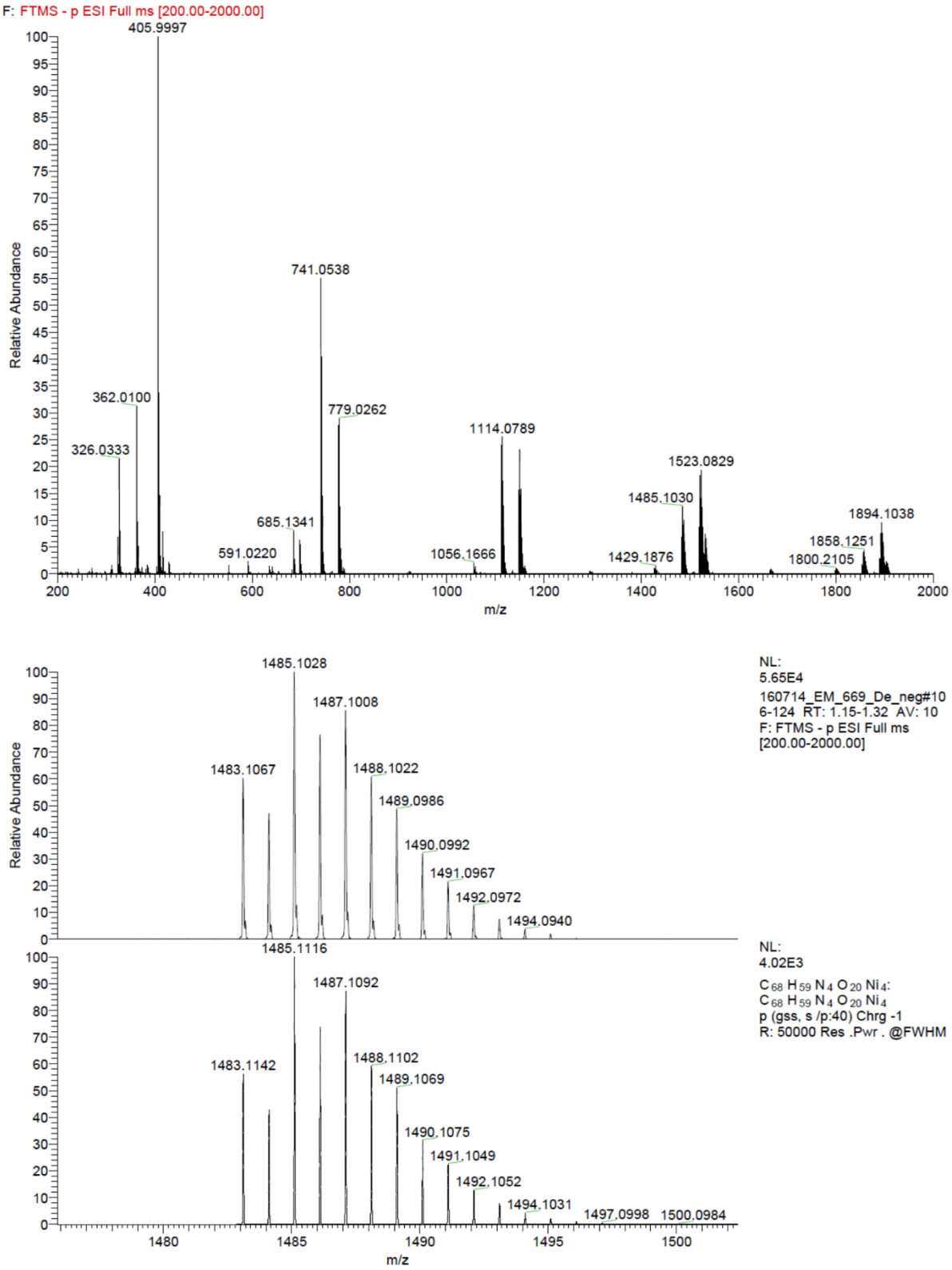

Figure S5. ESI(-)-MS spectrum of **[Ni$_4$(L)$_4$]-MeOH** in methanol with simulation of the molecular peak.

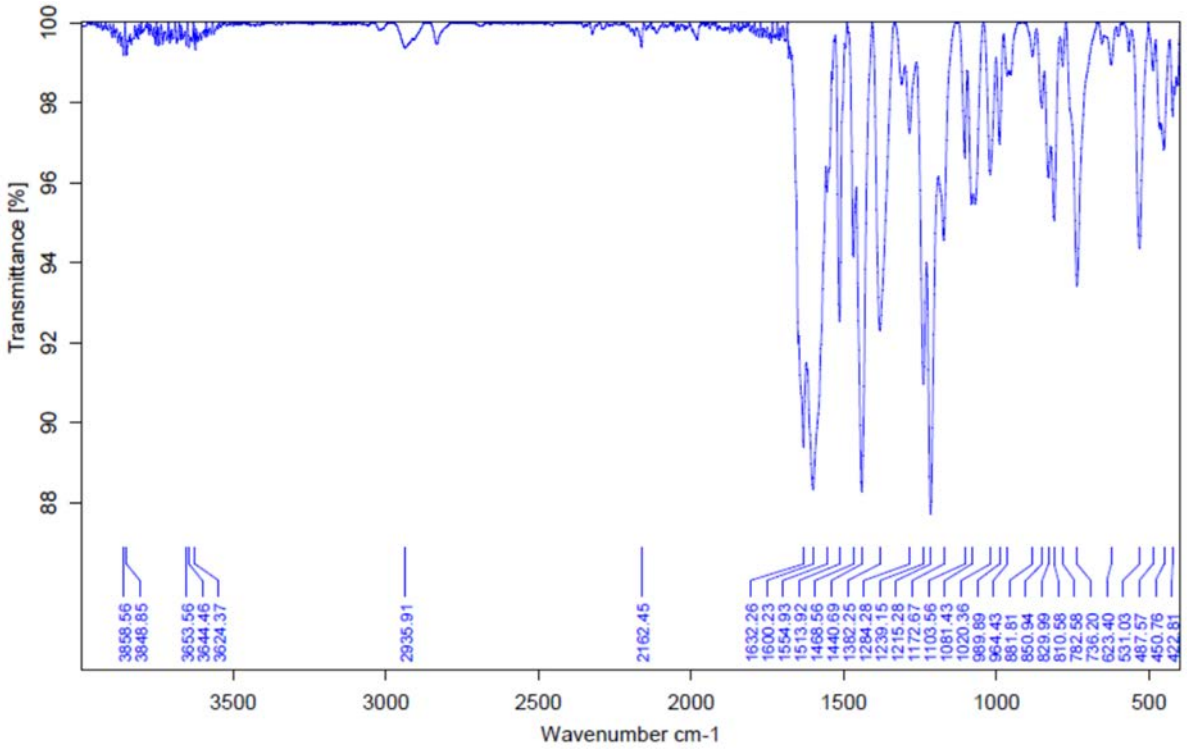

Figure S6. IR spectrum of **[Ni$_4$(L)$_4$]-MeOH** dried under air.

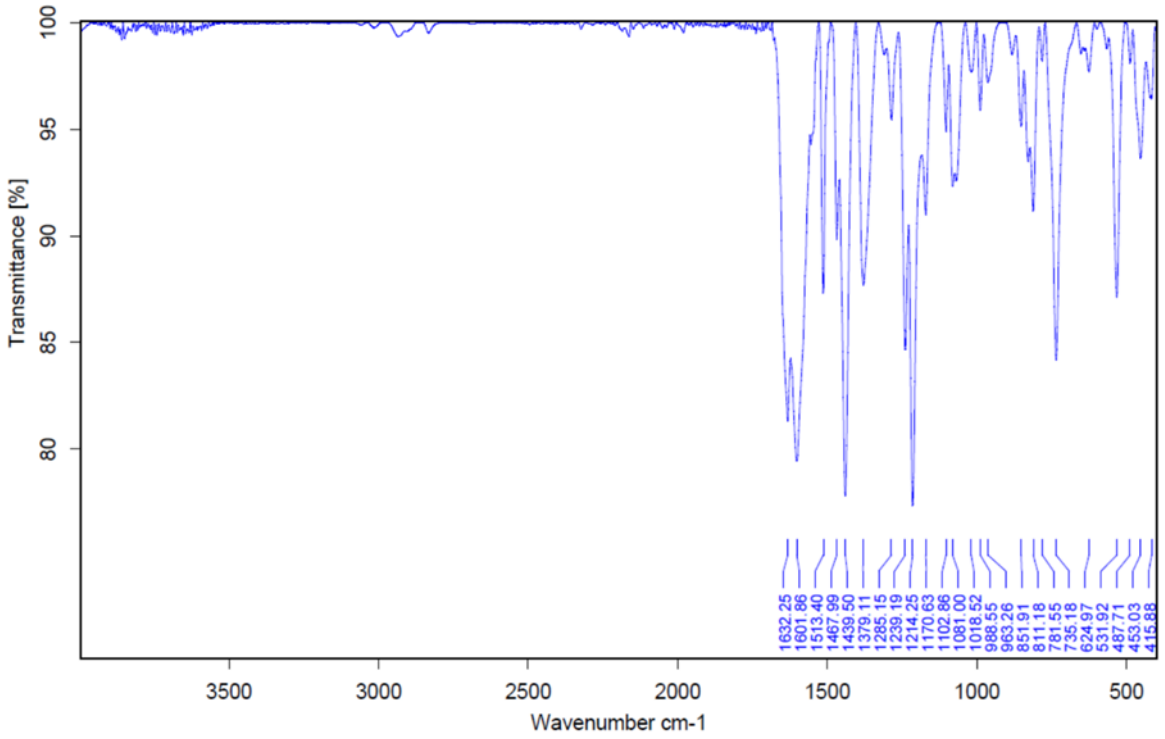

Figure S7. IR spectrum of **[Ni$_4$(L)$_4$]-MeOH** dried *in vacuo*.

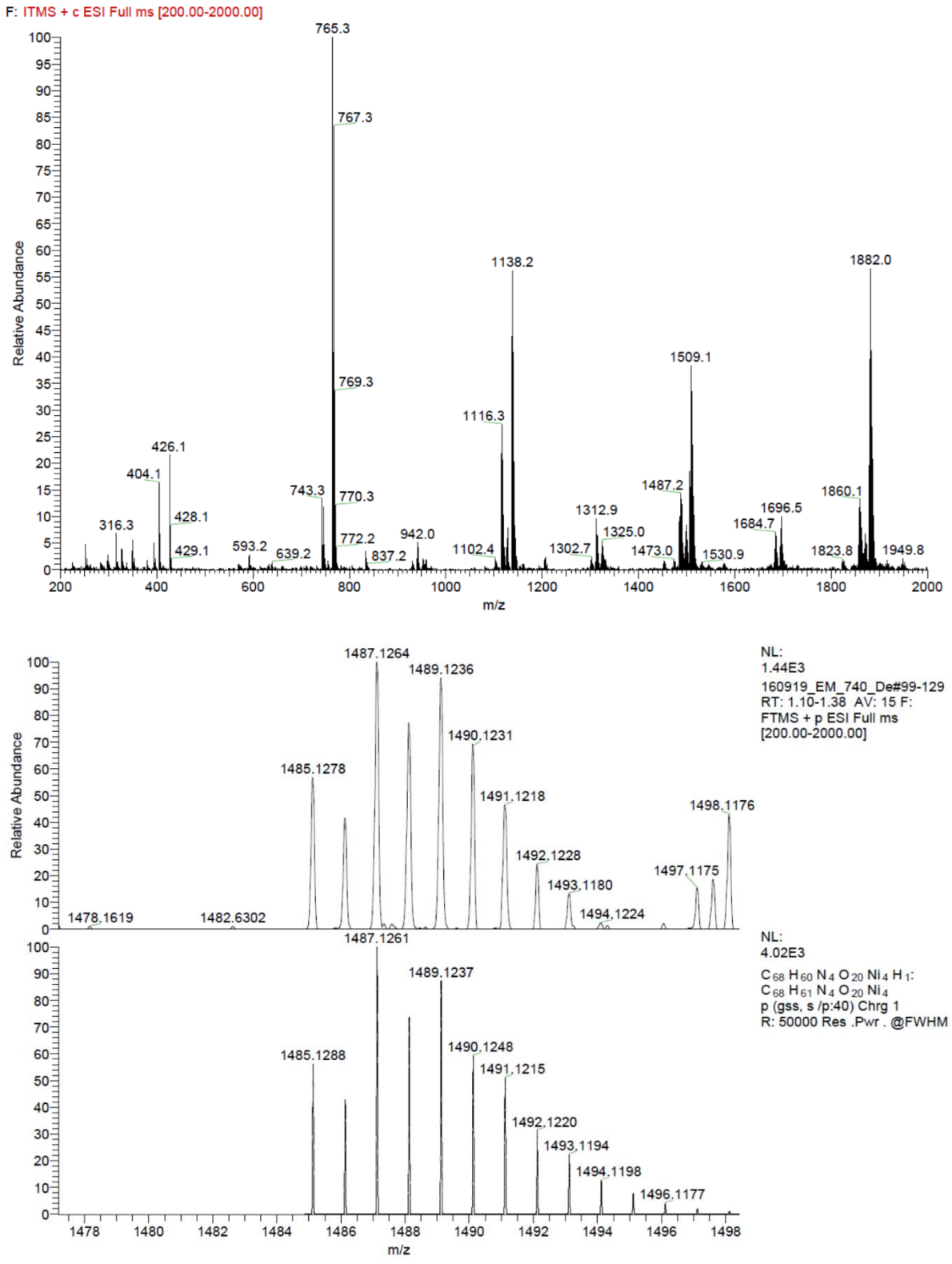

Figure S8. ESI(+)-MS spectrum of **[Ni$_4$(L)$_4$]-DMF** (macroscale sample) in methanol with simulation of the molecular peak.

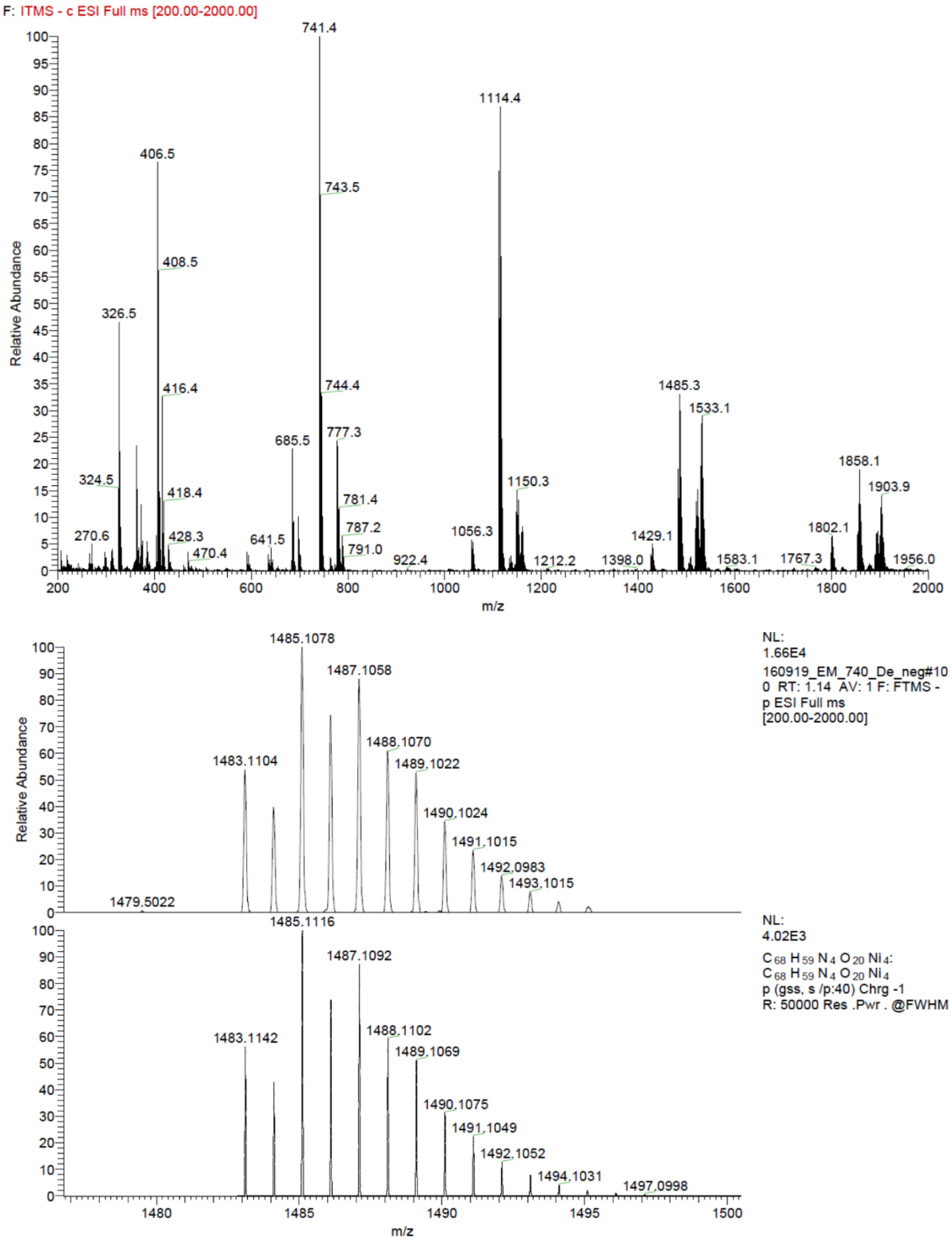

Figure S9. ESI(-)-MS spectrum of **[Ni$_4$(L)$_4$]-DMF** (macroscale sample) in methanol with simulation of the molecular peak.

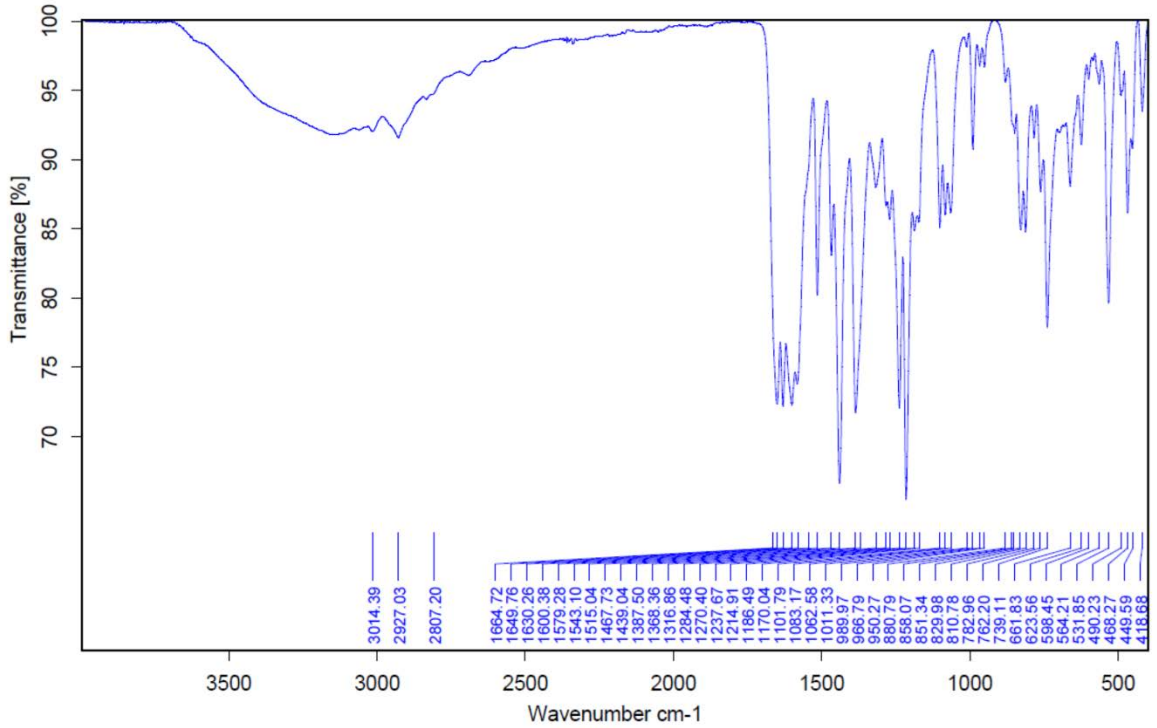

Figure S10. IR spectrum of **[Ni$_4$(L)$_4$]-DMF** dried under air.

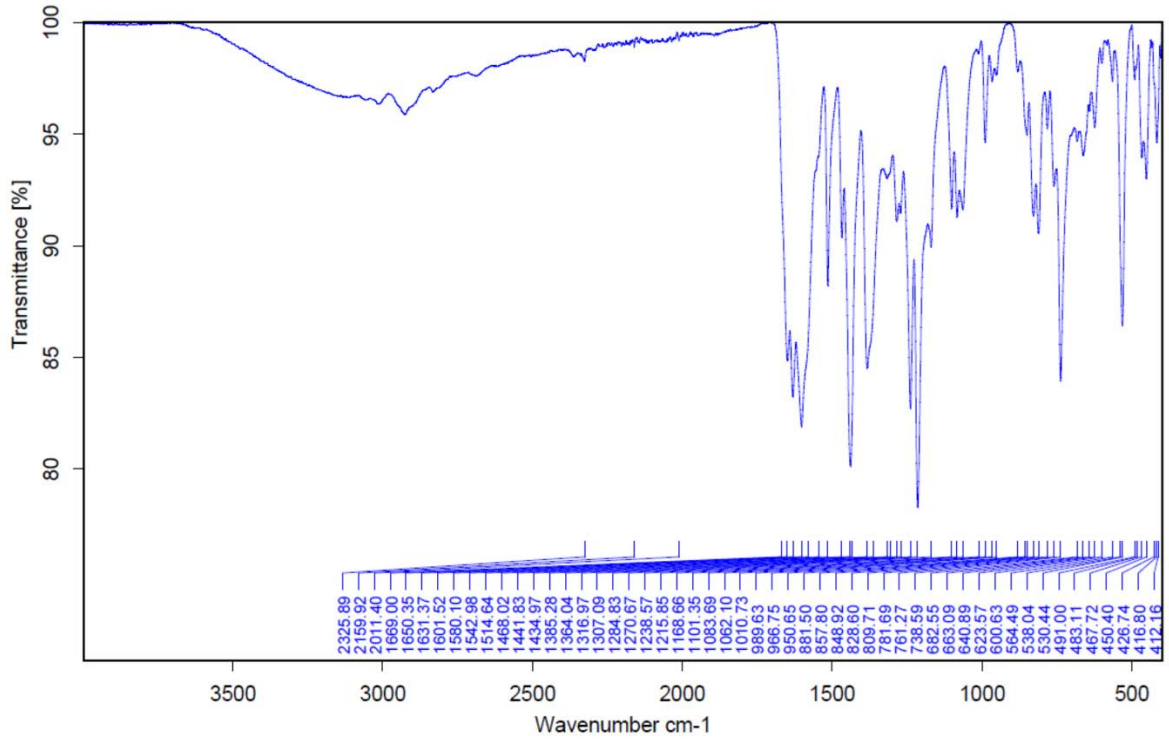

Figure S11. IR spectrum of **[Ni$_4$(L)$_4$]-DMF** dried *in vacuo*.

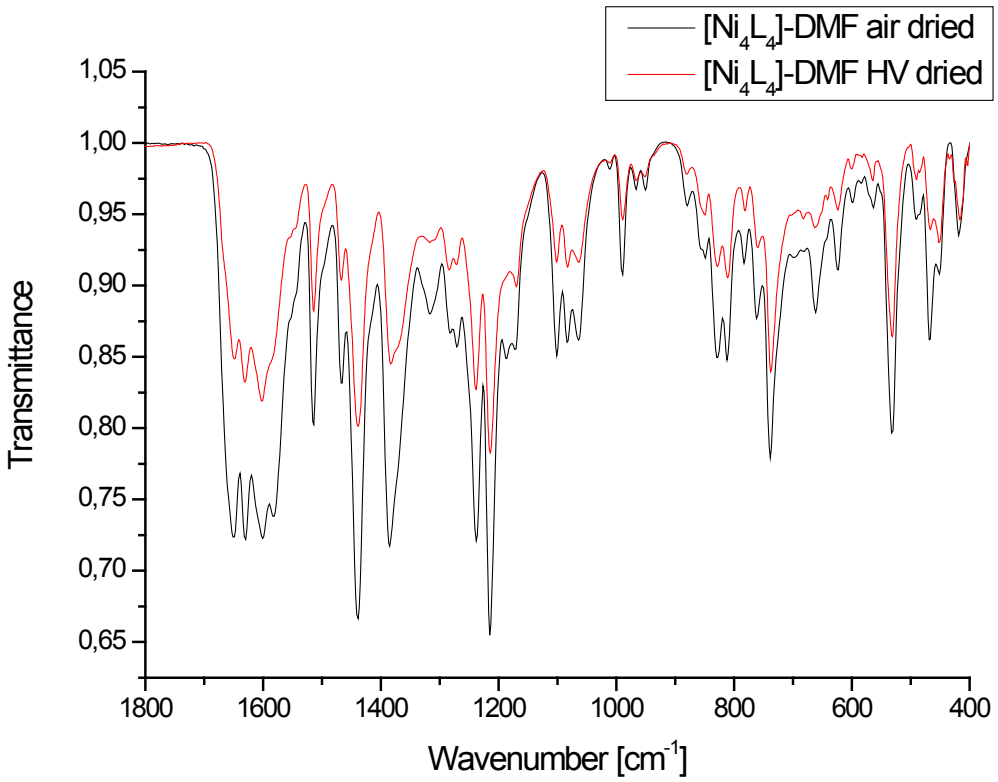

Figure S12. IR spectra of air dried and HV (high vacuum) dried samples of **[Ni$_4$(L)$_4$]-DMF** in the region between 400 cm^{-1} and 1800 cm^{-1}.

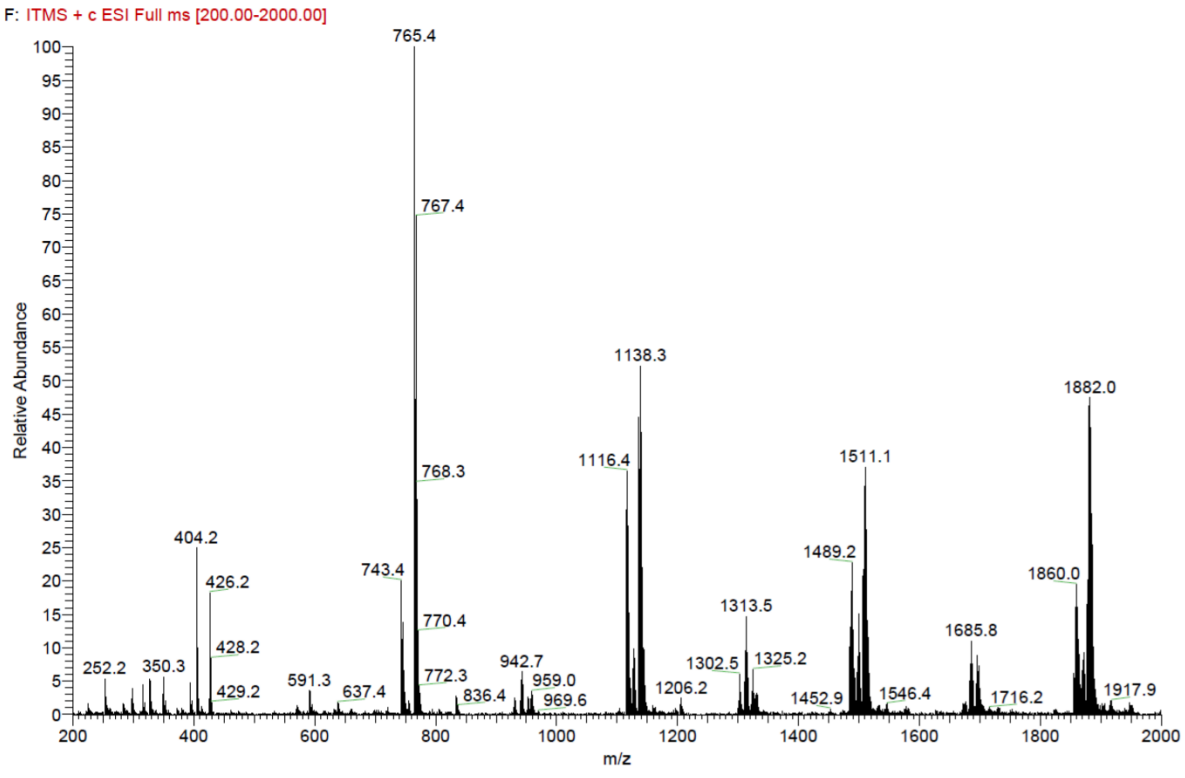

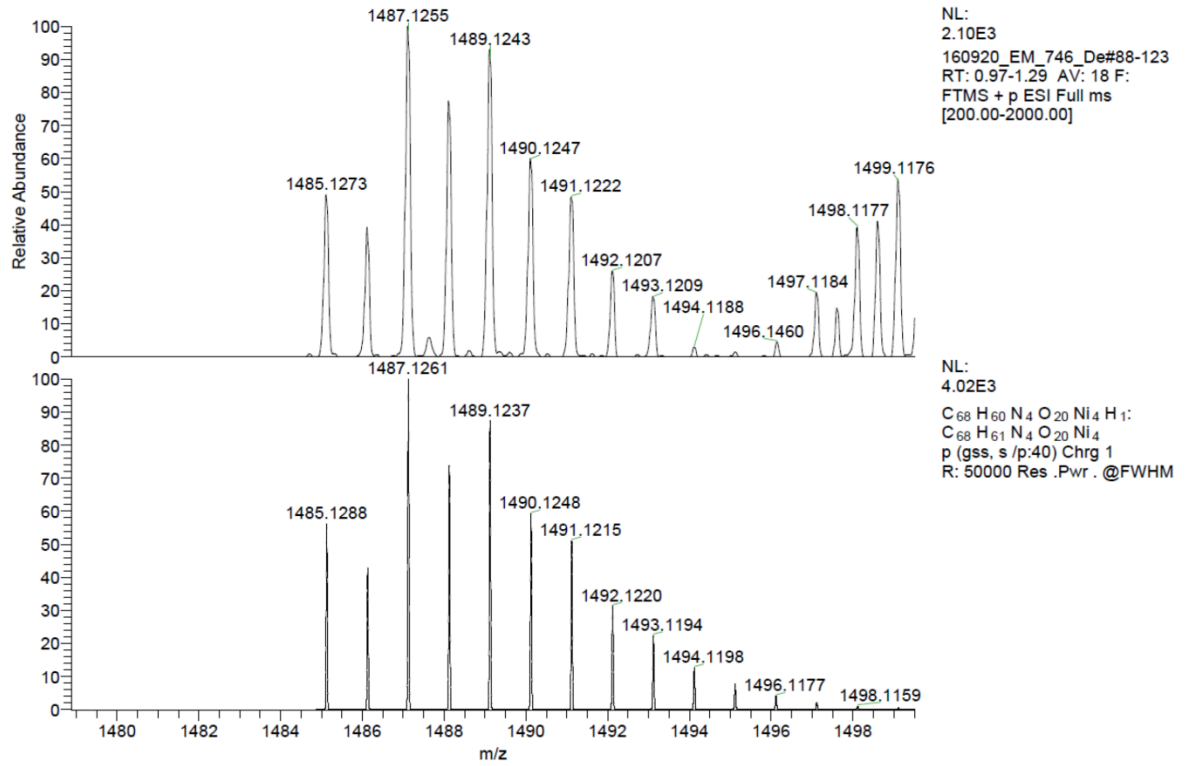

Figure S13. ESI(+)-MS spectrum of **[Ni$_4$(L)$_4$]-DMF** (microscale sample) in methanol with simulation of the molecular peak.

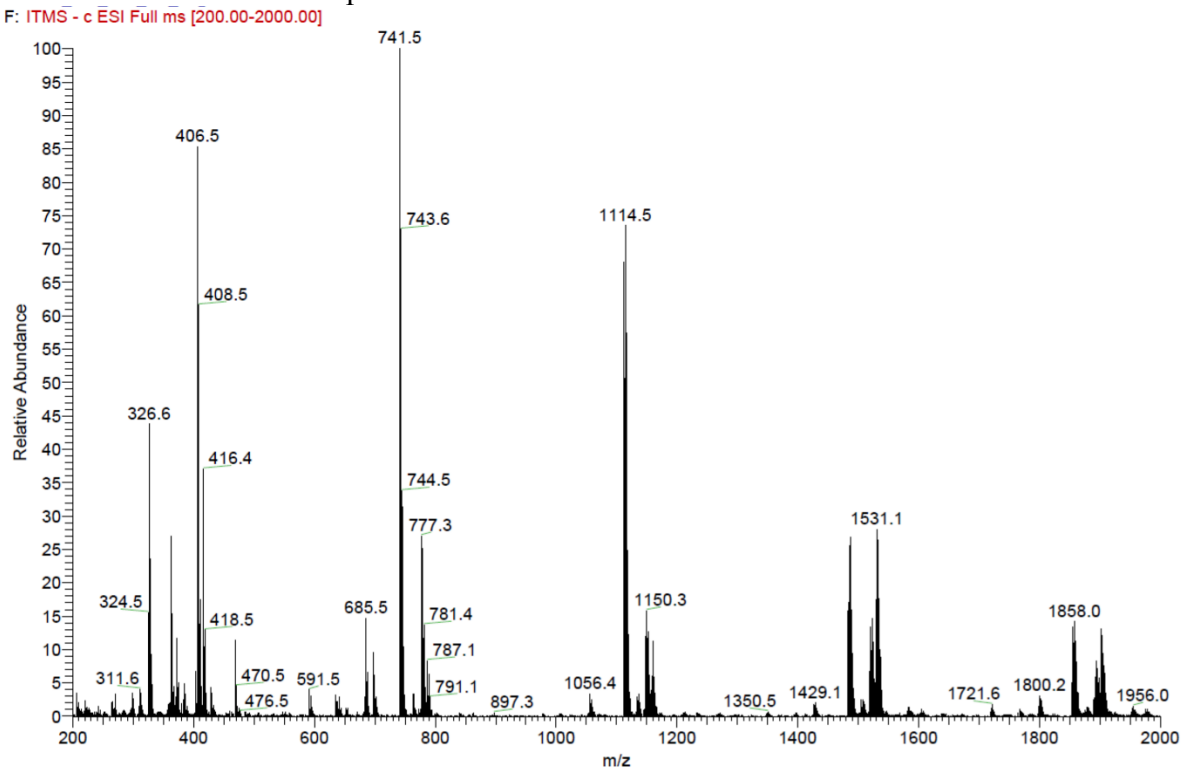

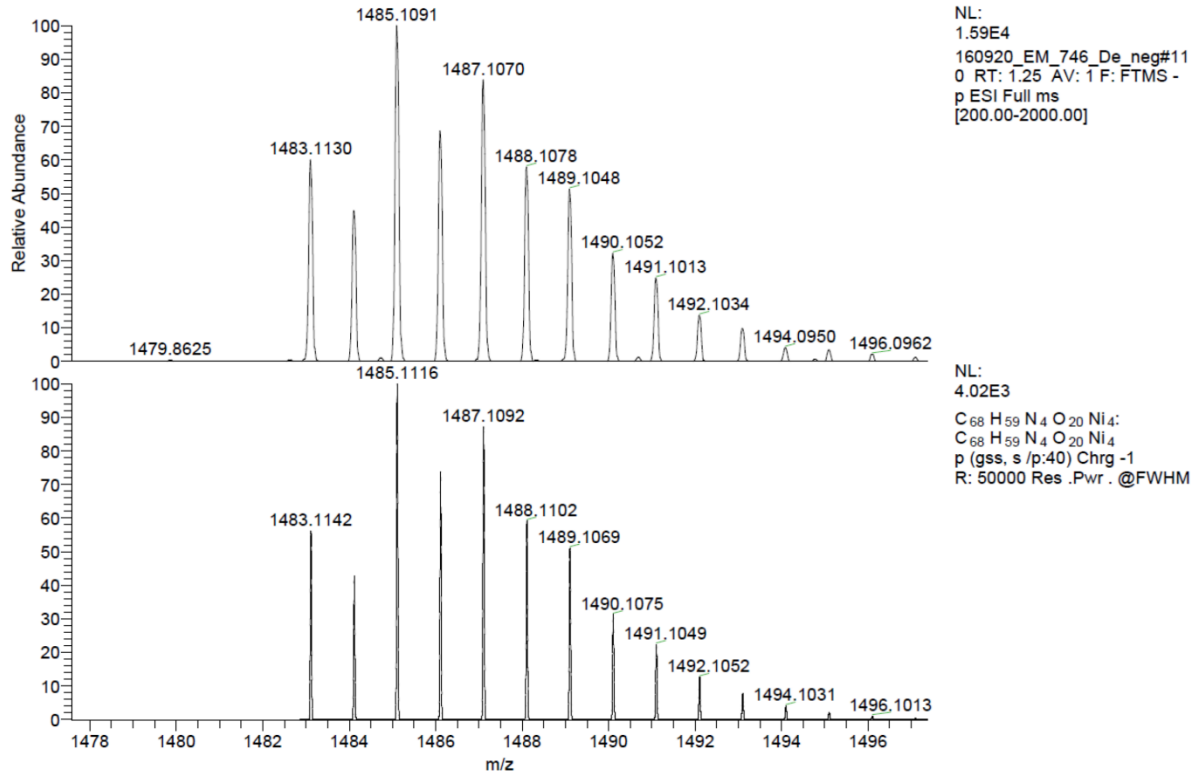

Figure S14. ESI(-)-MS spectrum of **[Ni$_4$(L)$_4$]-DMF** (microscale sample) in methanol with simulation of the molecular peak.

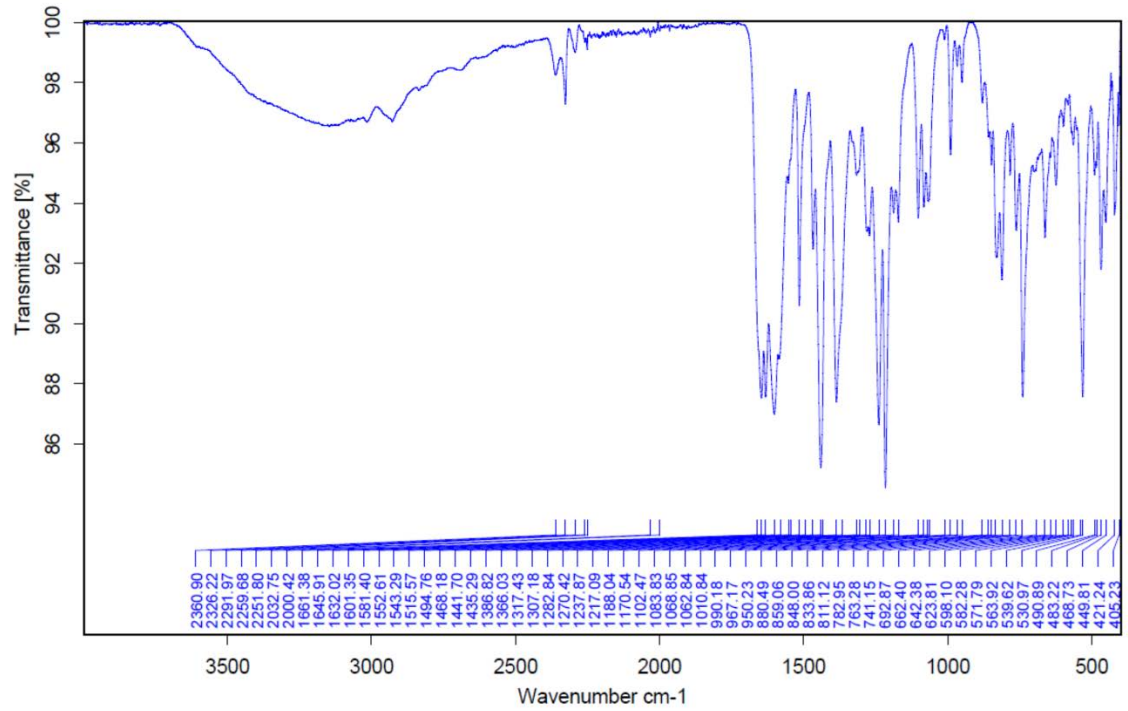

Figure S15. IR spectrum of **[Ni$_4$(L)$_4$]-DMF** microscale sample dried under air.

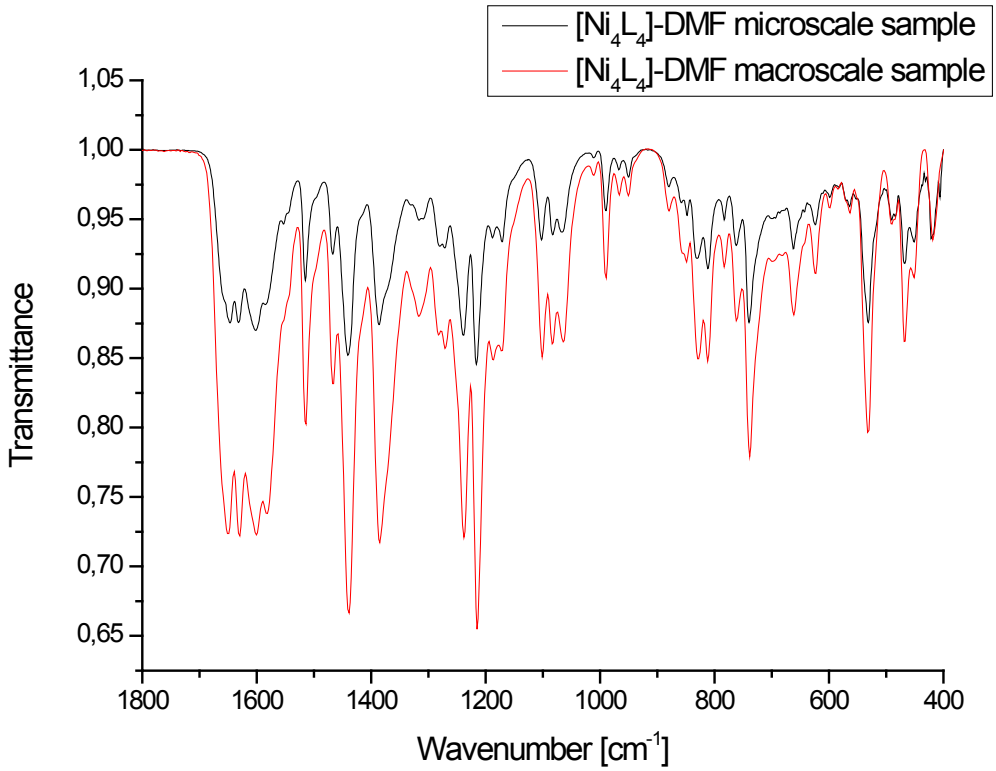

Figure S16. IR spectra of air-dried samples of **[Ni4(L)4]-DMF** derived from macro- and microscale samples in the region between 400 cm^{-1} and 1800 cm^{-1}.

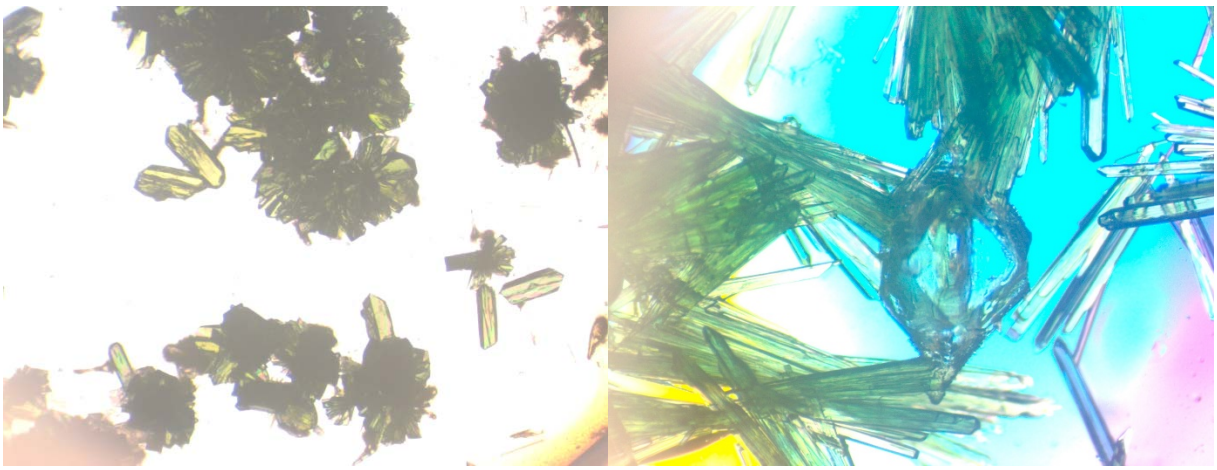

Figure S17. Images of the crystalline samples: (left) **[Ni4(L)4]-MeOH**, (right) **[Ni4(L)4]-DMF**.

3. Supplementary tables

Table S1. Selected geometric parameters [Å, °] for **[$Ni_4(L)_4$]-MeOH**.

Ni1—N1	1.977 (3)	Ni3—O43	1.972 (3)
Ni1—O41	1.980 (3)	Ni3—N3	1.977 (3)
Ni1—O42	2.050 (3)	Ni3—O22	2.031 (3)
Ni1—O21	2.067 (3)	Ni3—O23	2.043 (3)
Ni1—O13	2.137 (3)	Ni3—O1M	2.082 (3)
Ni1—O52	2.213 (3)	Ni3—O3W	2.127 (3)
Ni2—O42	1.972 (3)	Ni4—O44	1.975 (3)
Ni2—N2	1.975 (4)	Ni4—N4	1.999 (3)
Ni2—O23	2.035 (3)	Ni4—O24	2.045 (3)
Ni2—O22	2.048 (3)	Ni4—O43	2.061 (3)
Ni2—O1W	2.109 (3)	Ni4—O12	2.127 (3)
Ni2—O2W	2.134 (3)	Ni4—O53	2.181 (3)
N1—Ni1—O41	93.40 (12)	O43—Ni3—N3	96.98 (12)
N1—Ni1—O42	167.74 (12)	O43—Ni3—O22	102.61 (11)
O41—Ni1—O42	86.70 (11)	N3—Ni3—O22	160.39 (12)
N1—Ni1—O21	81.65 (12)	O43—Ni3—O23	175.65 (11)
O41—Ni1—O21	174.94 (11)	N3—Ni3—O23	81.21 (12)
O42—Ni1—O21	97.92 (10)	O22—Ni3—O23	79.18 (11)
N1—Ni1—O13	85.69 (12)	O43—Ni3—O1M	92.86 (11)
O41—Ni1—O13	90.98 (11)	N3—Ni3—O1M	95.79 (13)
O42—Ni1—O13	106.57 (10)	O22—Ni3—O1M	84.39 (12)
O21—Ni1—O13	89.69 (11)	O23—Ni3—O1M	91.26 (11)

N1—Ni1—O52	93.01 (12)	O43—Ni3—O3W	87.43 (11)
O41—Ni1—O52	95.05 (11)	N3—Ni3—O3W	90.54 (12)
O42—Ni1—O52	74.78 (10)	O22—Ni3—O3W	89.28 (11)
O21—Ni1—O52	84.22 (11)	O23—Ni3—O3W	88.64 (10)
O13—Ni1—O52	173.90 (11)	O1M—Ni3—O3W	173.58 (12)
O42—Ni2—N2	97.52 (13)	O44—Ni4—N4	93.22 (13)
O42—Ni2—O23	102.41 (11)	O44—Ni4—O24	173.35 (12)
N2—Ni2—O23	159.84 (12)	N4—Ni4—O24	81.90 (13)
O42—Ni2—O22	176.49 (11)	O44—Ni4—O43	86.95 (11)
N2—Ni2—O22	80.95 (13)	N4—Ni4—O43	170.27 (13)
O23—Ni2—O22	78.98 (11)	O24—Ni4—O43	97.09 (12)
O42—Ni2—O1W	89.46 (13)	O44—Ni4—O12	93.98 (11)
N2—Ni2—O1W	95.25 (15)	N4—Ni4—O12	85.06 (13)
O23—Ni2—O1W	87.97 (14)	O24—Ni4—O12	90.12 (12)
O22—Ni2—O1W	93.82 (13)	O43—Ni4—O12	104.64 (11)
O42—Ni2—O2W	88.15 (10)	O44—Ni4—O53	91.85 (11)
N2—Ni2—O2W	90.49 (12)	N4—Ni4—O53	94.83 (13)
O23—Ni2—O2W	87.19 (10)	O24—Ni4—O53	84.10 (12)
O22—Ni2—O2W	88.70 (10)	O43—Ni4—O53	75.44 (11)
O1W—Ni2—O2W	174.02 (13)	O12—Ni4—O53	174.17 (12)

Table S2. Selected geometric parameters [Å, °] for **[$Ni_4(L)_4$]-DMF**.

Ni1—O41	1.972 (3)	Ni3—N3	1.955 (3)
Ni1—N1	1.976 (3)	Ni3—O43	1.972 (3)

Ni1—O21	2.035 (3)	Ni3—O22	2.015 (3)
Ni1—O42	2.063 (3)	Ni3—O23	2.037 (3)
Ni1—O13	2.141 (3)	Ni3—O3W	2.112 (3)
Ni1—O52	2.208 (3)	Ni3—O4W	2.140 (3)
Ni2—O42	1.969 (3)	Ni4—O44	1.969 (3)
Ni2—N2	1.975 (3)	Ni4—N4	2.004 (4)
Ni2—O23	2.020 (3)	Ni4—O43	2.052 (3)
Ni2—O22	2.053 (3)	Ni4—O24	2.066 (3)
Ni2—O1W	2.099 (3)	Ni4—O12	2.101 (3)
Ni2—O2W	2.111 (3)	Ni4—O53	2.193 (3)
O41—Ni1—N1	93.56 (14)	N3—Ni3—O43	97.79 (14)
O41—Ni1—O21	175.02 (13)	N3—Ni3—O22	160.90 (13)
N1—Ni1—O21	82.19 (14)	O43—Ni3—O22	101.30 (12)
O41—Ni1—O42	88.80 (12)	N3—Ni3—O23	81.21 (13)
N1—Ni1—O42	165.48 (14)	O43—Ni3—O23	177.35 (13)
O21—Ni1—O42	94.67 (13)	O22—Ni3—O23	79.69 (11)
O41—Ni1—O13	91.83 (13)	N3—Ni3—O3W	92.78 (14)
N1—Ni1—O13	86.81 (14)	O43—Ni3—O3W	92.40 (13)
O21—Ni1—O13	90.53 (13)	O22—Ni3—O3W	87.13 (13)
O42—Ni1—O13	107.45 (11)	O23—Ni3—O3W	90.10 (13)
O41—Ni1—O52	91.71 (14)	N3—Ni3—O4W	91.78 (13)
N1—Ni1—O52	90.72 (14)	O43—Ni3—O4W	87.36 (12)
O21—Ni1—O52	85.77 (14)	O22—Ni3—O4W	88.43 (12)
O42—Ni1—O52	74.89 (11)	O23—Ni3—O4W	90.21 (12)

O13—Ni1—O52	175.79 (13)	O3W—Ni3—O4W	175.43 (12)
O42—Ni2—N2	96.35 (14)	O44—Ni4—N4	91.50 (14)
O42—Ni2—O23	103.59 (11)	O44—Ni4—O43	89.43 (12)
N2—Ni2—O23	159.66 (13)	N4—Ni4—O43	167.17 (15)
O42—Ni2—O22	175.10 (13)	O44—Ni4—O24	173.58 (12)
N2—Ni2—O22	80.63 (13)	N4—Ni4—O24	82.10 (14)
O23—Ni2—O22	79.20 (11)	O43—Ni4—O24	96.70 (12)
O42—Ni2—O1W	91.74 (13)	O44—Ni4—O12	91.64 (13)
N2—Ni2—O1W	95.23 (13)	N4—Ni4—O12	87.33 (14)
O23—Ni2—O1W	88.21 (13)	O43—Ni4—O12	105.43 (12)
O22—Ni2—O1W	92.37 (13)	O24—Ni4—O12	88.59 (12)
O42—Ni2—O2W	87.47 (13)	O44—Ni4—O53	94.35 (13)
N2—Ni2—O2W	90.49 (13)	N4—Ni4—O53	92.48 (14)
O23—Ni2—O2W	86.47 (12)	O43—Ni4—O53	74.69 (11)
O22—Ni2—O2W	88.70 (12)	O24—Ni4—O53	85.46 (13)
O1W—Ni2—O2W	174.28 (12)	O12—Ni4—O53	174.01 (13)

Table S3. Hydrogen bonding parameters [Å, °] for **[Ni$_4$(L)$_4$]-MeOH**. Symmetry codes: (i) −x, y−1/2, −z+3/2; (ii) x−1/2, −y+3/2, −z+2; (iii) x+1, y, z; (iv) −x−1/2, −y+1, z−1/2; (v) −x+1/2, −y+1, z+1/2.

D—H···A	D—H	H···A	D···A	D—H···A
O31—H31···O24^{i}	0.84	1.89	2.723 (6)	174
O33—H33···O5M^{ii}	0.84	1.87	2.651 (9)	154
O2M—H2M···O6M^{iii}	0.84	1.90	2.637 (11)	146
O4M—H4M···O14^{ii}	0.84	1.75	2.580 (8)	171
O5M—H5M···O4M	0.84	1.91	2.630 (11)	143
O6M—H6M···O7M	0.84	1.86	2.664 (8)	160
O7M—H7M···O3W	0.84	1.95	2.768 (6)	166
O8M—H8M···O3M	0.84	1.88	2.708 (9)	167
C211—H211···O33^{iv}	1.00	2.54	3.407 (8)	145
C311—H31A···O13	0.99	2.46	3.231 (7)	135
C611—H611···O14^{i}	0.95	2.39	3.324 (8)	169

C721—H721···O33^{iv}	0.95	2.66	3.245 (7)	121
C523—H523···O41^{v}	0.95	2.65	3.499 (7)	149
C314—H31G···O12	0.99	2.49	3.289 (7)	137
C814—H814···O11^{iii}	0.95	2.47	3.386 (9)	162

Table S4. Hydrogen bonding parameters [Å, °] for **[Ni$_4$(L)$_4$]-DMF**. Symmetry codes: (i) x+1/2, −y+1/2, −z+2; (ii) −x+3/2, −y+1, z+1/2; (iii) x+1/2, −y+1/2, −z+1; (iv) −x+3/2, −y, z+1/2; (v) −x+2, y−1/2, −z+3/2.

D—H···A	D—H	H···A	D···A	D—H···A
O31—H31···O11i	0.84	1.88	2.688 (8)	161
O32—H32···O6W	0.84	1.83	2.647 (9)	162
O33—H33···O14ii	0.84	1.88	2.673 (7)	158
O34—H34···O24iii	0.84	1.94	2.667 (7)	145
O1M—H1M···O9W	0.84	1.87	2.568 (16)	139
O2M—H2M···O5W	0.84	1.95	2.759 (10)	163
C211—H211···O32iv	1.00	2.64	3.489 (9)	143
C811—H811···O11i	0.95	2.54	3.243 (9)	131
C721—H721···O32iv	0.95	2.47	3.166 (10)	130
C722—H722···O1Dv	0.95	2.65	3.287 (9)	125
C613—H613···O14ii	0.95	2.49	3.192 (9)	131
C314—H31G···O12	0.99	2.39	3.208 (8)	140
C814—H814···O14iii	0.95	2.60	3.522 (9)	164
C3D—H3D1···O14ii	0.98	2.48	3.421 (11)	162
C4D—H4D···O24	0.95	2.55	3.477 (10)	164

IV Synthesis, characterization and crystal structure of (2RS,4R)-2-(2-hydroxy-3-methoxyphenyl)thiazolidine-4-carboxylic acid

Muche, S.; Müller, M.; Hołyńska, M. *Journal of Molecular Structure*, Manuskript akzeptiert

The condensation reaction of *ortho*-vanillin and *L*-cysteine leads to formation of a racemic mixture of (2RS,4R)-2-(2-hydroxy-3-methoxyphenyl)thiazolidine-4-carboxylic acid and not, as reported in the available literature, to a Schiff base. The racemic mixture was fully characterized by 1D- and 2D-NMR techniques, ESI-MS and X-ray diffraction. Addition of $ZnCl_2$ led to formation of crystals in form of colorless needles, suitable for X-ray diffraction studies. The measured crystals were identified as the diastereomer (2R,4R)-2-(2-hydroxy-3-methoxyphenyl)thiazolidine-4-carboxylic acid **1**. The bulk material is racemic. Thazolidine exists as zwitterion in solid state, as indicated by the crystal structure.

Inhalt: Präsentiert wird die Synthese und vollständige Charakterisierung der racemischen (2RS,4R)-2-(2-hydroxy-3-methoxyphenyl)thiazolidin-4-Carboxylsäure aus *ortho*-Vanillin und *L*-Cystein. Ursprünglich sollte, wie in diversen Publikationen dargestellt, auf diesem Weg die entsprechende Schiff'sche Base erhalten werden. Allerdings zeigen alle analytischen Daten, insbesondere 1D- und 2D-NMR, dass bei der Kondensationsreaktion der Edukte nur das Thiazolidin erhalten wird. Durch Zugabe von Metallsalzen sollten entweder Metallkomplexe des Thiazolidins erhalten oder eine Ringöffnung bewirkt und damit die Synthese von Metallkomplexen der korrespondierenden Schiff'schen Base ermöglicht werden. Mit den verwendeten Übergangsmetallsalzen wird aber lediglich wieder das Thiazolidin erhalten, wobei die Zugabe von $ZnCl_2$ zu einem kristallinen Präzipitat führt, aus dem messbare Kristalle isoliert werden können. Bei mehreren Messungen wird immer die Struktur des (2R,4R)-Diastereomers erhalten, obwohl das NMR des Präzipitats klar zeigt, dass es sich um das Racemat handelt. Im Kristall liegt das (2R,4R)-Thiazolidin als Zwitterion vor, welches durch Wasserstoffbrückenbindungen stabilisiert wird.

Eigener Anteil: Die Planung der Synthesen wurde von mir vorgenommen unter Betreuung von Małgorzata Hołyńska. Matthias Müller führte die Experimente aus und war für die Aufnahme und Auswertung der Basisanalytik im Rahmen seiner Vertiefung unter meiner Betreuung verantwortlich. Die Röntgenstrukturanalyse wurde von der hauseigenen Serviceabteilung durchgeführt. Die Analyse der kristallographischen Daten erfolgte durch Małgorzata Hołyńska und mich. Das Manuskript wurde bis auf die kristallographischen Teile von mir ausgearbeitet. Małgorzata Hołyńska verfasste die kristallographischen Teile. Die Überarbeitung erfolgte gemeinsam.

Synthesis, characterization and crystal structure of (2RS,4R)-2-(2-hydroxy-3-methoxyphenyl)thiazolidine-4-carboxylic acid

Simon Muche[a], Matthias Müller[a], Małgorzata Hołyńska[a]*

[a]Fachbereich Chemie und Wissenschaftliches Zentrum für Materialwissenschaften, Philipps-Universität Marburg, Hans-Meerwein-Strasse, D-35043, Marburg, Germany.

E-Mail: holynska@staff.uni-marburg.de

Abstract

The condensation reaction of *ortho*-vanillin and *L*-cysteine leads to formation of a racemic mixture of (2RS,4R)-2-(2-hydroxy-3-methoxyphenyl)thiazolidine-4-carboxylic acid and not, as reported in the available literature, to a Schiff base. The racemic mixture was fully characterized by 1D- and 2D-NMR techniques, ESI-MS and X-ray diffraction. Addition of $ZnCl_2$ led to formation of crystals in form of colorless needles, suitable for X-ray diffraction studies. The measured crystals were identified as the diastereomer (2R,4R)-2-(2-hydroxy-3-methoxyphenyl)thiazolidine-4-carboxylic acid **1**. The bulk material is racemic. Thazolidine exists as zwitterion in solid state, as indicated by the crystal structure.

Key Words

ortho-vanillin•L-cysteine• Thiazolidine•NMR•crystal structure

Highlights

- Characterization of (2RS,4R)-2-(2-hydroxy-3-methoxyphenyl)thiazolidine-4-carboxylic acid with 1D- and 2D-NMR techniques
- Crystal structure of (2R,4R)-2-(2-hydroxy-3-methoxyphenyl)thiazolidine-4-carboxylic acid **1**
- Zwitterionic form of **1**

Graphical abstract

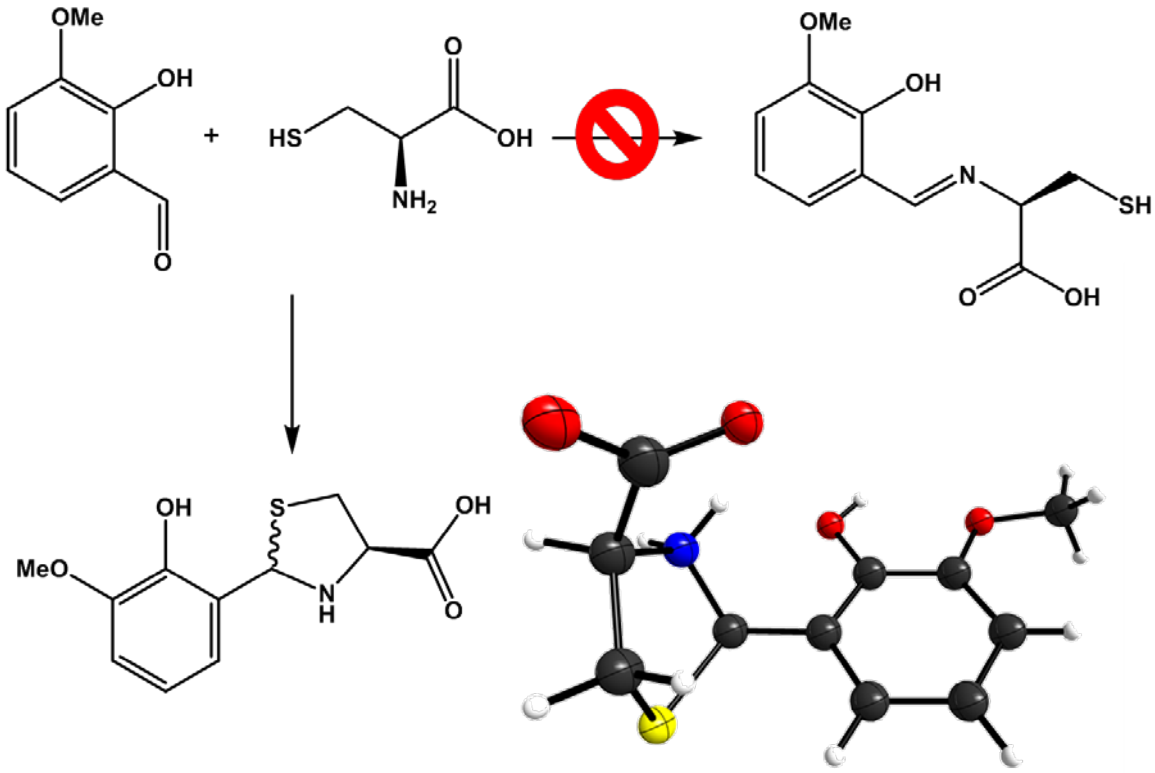

Introduction

Thiazolidines possess a 5-membered saturated ring with a thioether group and an amine group in the 1 and 3 positions as characteristic functional groups. These compounds can be seen as *N,S*-acetals. Thiazolidine derivatives show a range of biological properties. *N*-[4-(4'-Chlorophenyl)thiazol-2-yl] thiosemicarbazide can be condensed with isatin and its 5-chloro and 5-bromo derivatives which results in Schiff and Mannich bases showing interesting antimicrobial properties[(1)]. Several N-[(4-oxo-2-substituted aryl-1, 3-thiazolidine)-acetamidyl]-5-nitroindazoles, synthesized by conventional and microwave-assisted synthesis, possess moderate till strong activity against bacteria and fungi[(2)]. Antibacterial activity and activity against *Mycobacterium tuberculosis* were reported for N-{4-[(4-amino-5-sulfanyl-4H-1,2,4-triazol-3-yl)methyl]-1,3-thiazol-2-yl}-2-substituted-amide derivatives[(3)].
Furthermore, antibacterial activity was proved for thiazolidines derived from L-cysteine and various aromatic aldehydes, which were in a further step treated with *t*-butyloxycarbonyl anhydride. Crystal structure was determined for (4R)-2-(5-Fluoro-2-hydroxyphenyl)thiazolidine-4-carboxylic acid[(4)]. 3-tert-butoxycarbonyl-2-arylthiazolidine-4-carboxylic acid derivatives were also found to be potential antibacterial agents. Among these derivatives, crystal structure could be determined for (2R,4R)-3-(tert-butoxycarbonyl)-2-(4-methoxyphenyl)thiazolidine-4-carboxylic acid[(5)]. Antiproliferative activity against prostate cancer was observed for 2-aryl-4-oxo-thiazolidin-3-yl-amides[(6)]. From a series of thiazolidin-4-ones bearing a lipophilic adamantyl substituent at position 2, (R)-(+)-2-Adamantan-1-yl-3-(4,6-dimethyl-pyridin-2-yl)-thiazolidin-4-one was found to be active against HIV-1 and HIV-2 in the investigated cell culture[(7)]. Side-chain-modified 4-aminoquinoline derivatives, particularly 2-(4-chloro-phenyl)-3-[2-(7-chloroquinolin-4-ylamino)-ethyl]-2,3-dihydrobenzoe[1,3]-thiazin-4-one, showed very strong antiplasmodial activity *in vitro* and antimalarial activity in mice[(8)]. Furthermore, it was shown that thiazolidines are potential angiotensin-converting enzyme inhibitors[(9, 10)].
The racemic mixture of the title compound was found to be a moderate inhibitor of the influenza virus neuraminidase[(11)]. Furthermore, the stability of this thiazolidine was studied by titration and HPLC experiments[(12)]. NMR studies and conformation analysis, as well as studies of the influence of thiazolidines on the reaction of acetophenone with diphenylsilane in the presence of $[Rh(COD)Cl]_2$, were performed[(13)]. In this work we present the crystal structure of (2R,4R)-2-(2-hydroxy-3-methoxyphenyl)thiazolidine-4-carboxylic acid **1** and characterization of its racemic mixture. We also show that contrary to the previously published work no Schiff base is formed in the applied reaction system.

Results and discussion

Synthesis and characterization

In our previous work, we characterized some Schiff bases derived from *ortho*-vanillin and amino acids and synthesized the corresponding metal complexes[(14–16)]. In this study our original goal was the synthesis of the Schiff base derived from *ortho*-vanillin and *L*-cystein. As a result of the simple condensation of both starting materials the formation of a thiazolidine product is expected. Our literature inquiry did not result in a known procedure to synthesize the pure Schiff base. Surprisingly, for salicylaldehyde as starting compound, several synthetic procedures leading to the pure Schiff base ligand were reported with, more or less, detailed characterization and presentation of analytical data[(17–22)]. All reported procedures are simple condensation reactions and differ only in reaction time, temperature and composition of the used solvents. Application of these procedures to our system led to white to pale yellow solids. The obtained solids were investigated with NMR and all samples showed ^{1}H-NMR spectra equivalent to the one presented in Figure 1.

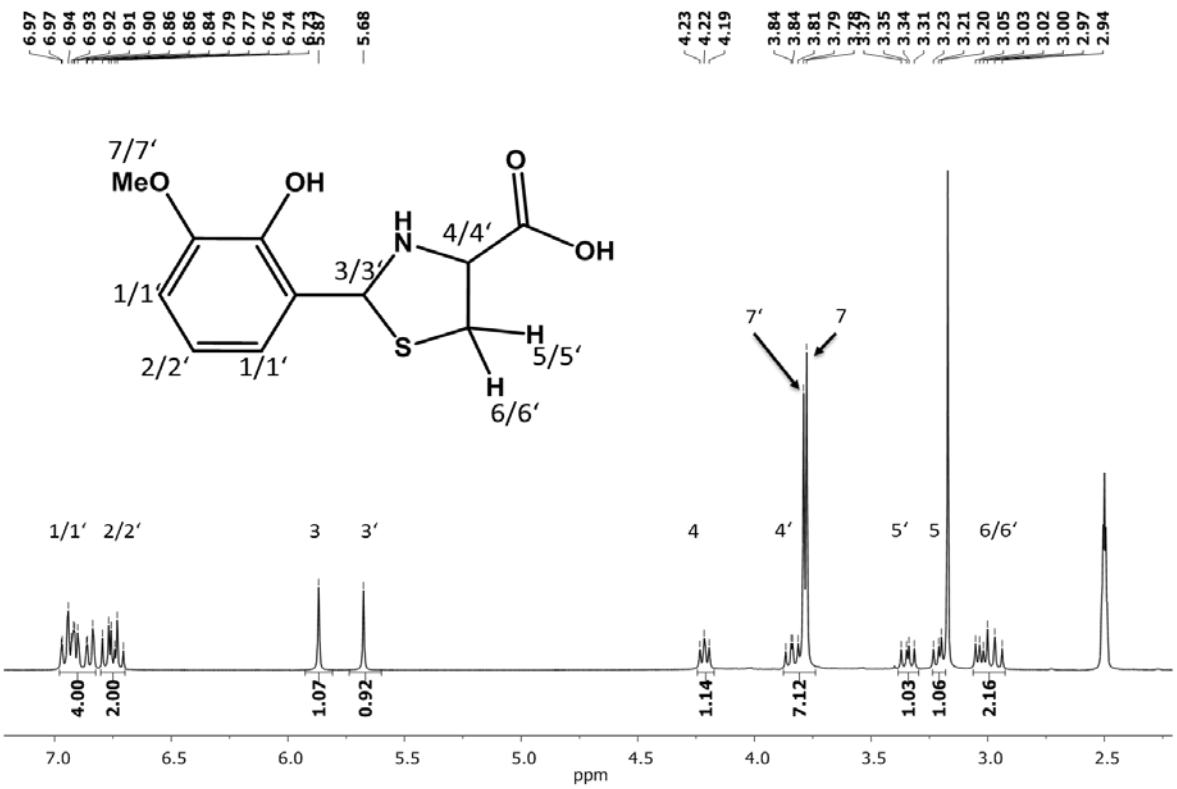

Figure 1: [1]H-NMR of racemic (2RS,4R)-2-(2-hydroxy-3-methoxyphenyl)thiazolidine-4-carboxylic acid and assignment of the signals.

The typical singlet at >8 ppm for the proton at the C-N double bond, like reported for other amino acid containing Schiff bases, is absent. Instead, two signals at 5.87 ppm and 5.67 ppm appear. The synthesized compound was definitely not a Schiff base. As expected, the compound could be identified as a racemic mixture of (2RS,4R)-2-(2-hydroxy-3-methoxyphenyl)thiazolidine-4-carboxylic acid and the described signals belong to the protons of the two diastereomeres at the position 2 of the thiazolidine ring. This result is additionally supported by COSY spectra (Fig. 2).

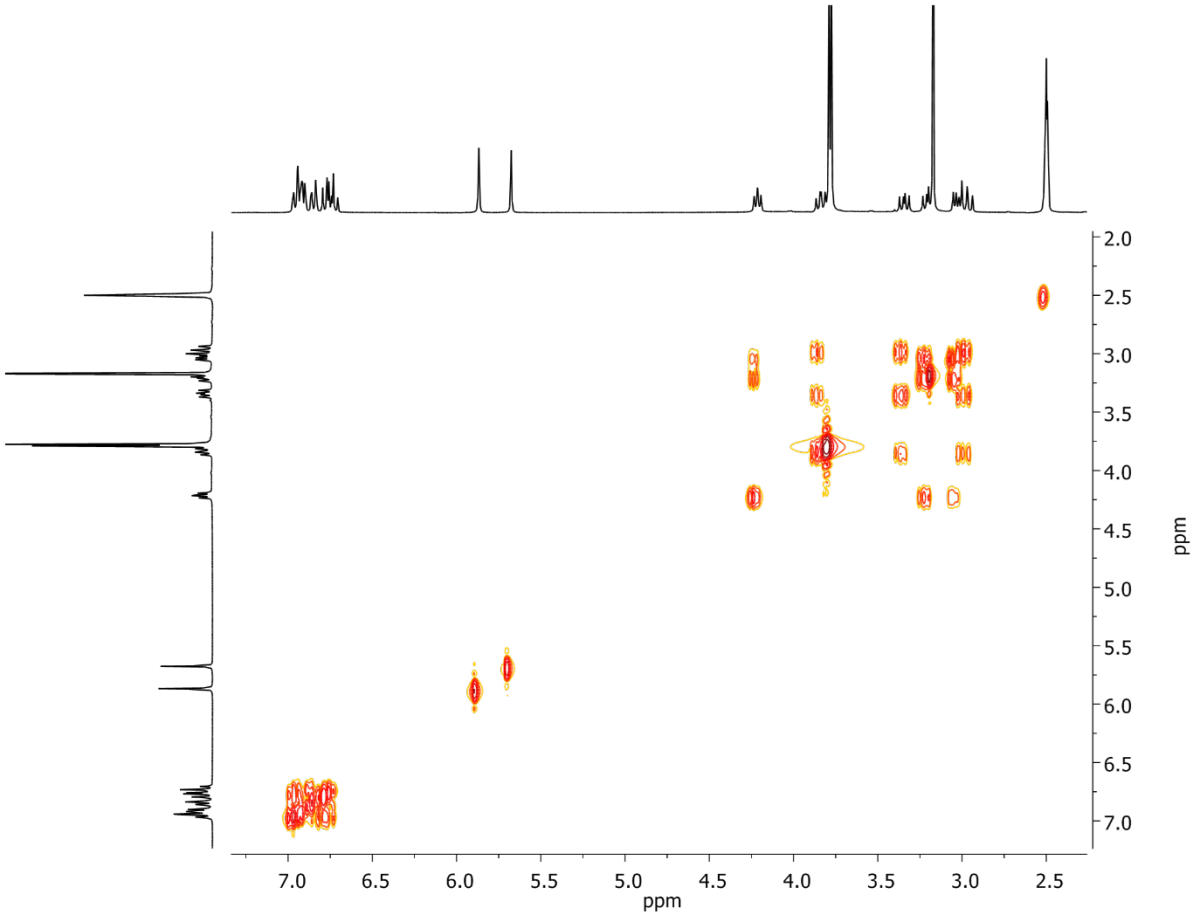

Figure 2: ^{1}H-COSY-NMR of racemic (2RS,4R)-2-(2-hydroxy-3-methoxyphenyl)thiazolidine-4-carboxylic acid and assignment of the signals.

It is notable that the signals of the methoxy groups overlap the signal of the proton at position 4 of the thiazolidine ring. Therefore the signals are not separately integrated. Furthermore, the remaining methanol signals overlap the signal of one of the methylene protons at the position 5. Our data and the ratio of (2*R*, 4*R*)- and (2*S*, 4*R*)-diastereomers of about 7:8 totally agree with the data of Skvortsov *et al.*[13], so that a further discussion of the ^{1}H-NMR spectra could be retrieved from that paper. The ^{13}C-NMR spectrum shows, as expected, 22 signals for the racemic compound (Fig. 3). Based on the HMQC-NMR spectrum (Fig. 4) it was possible to assign some of the signals from the ^{13}C-NMR spectrum.

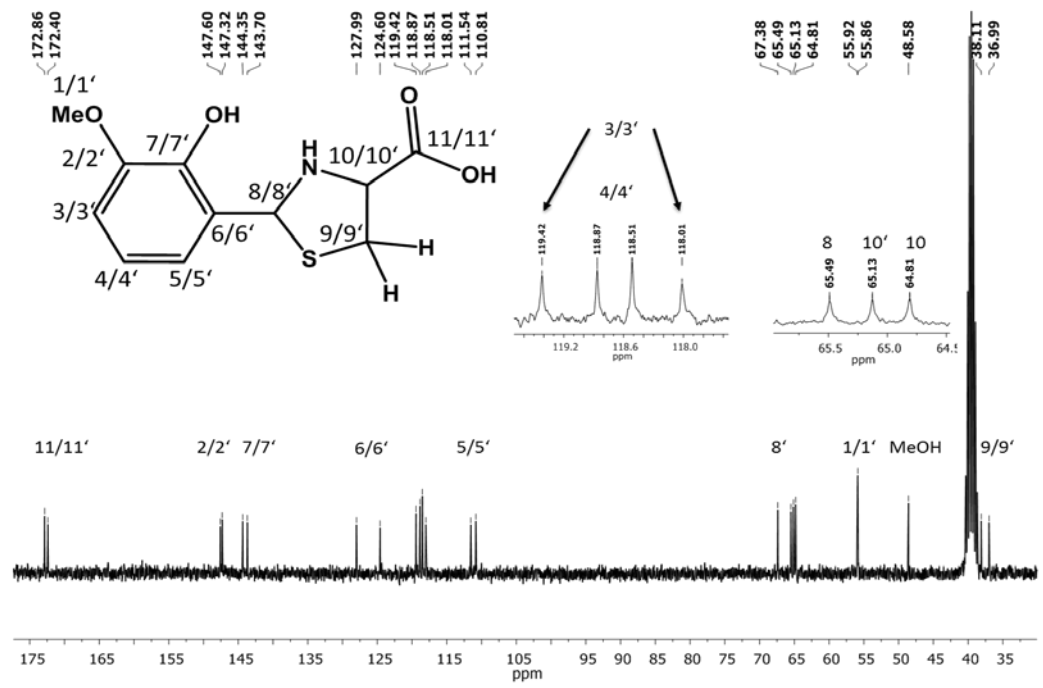

Figure 3: ^{13}C-NMR spectrum of the racemic (2RS,4R)-2-(2-hydroxy-3-methoxyphenyl)thiazolidine-4-carboxylic acid and assignment of the signals.

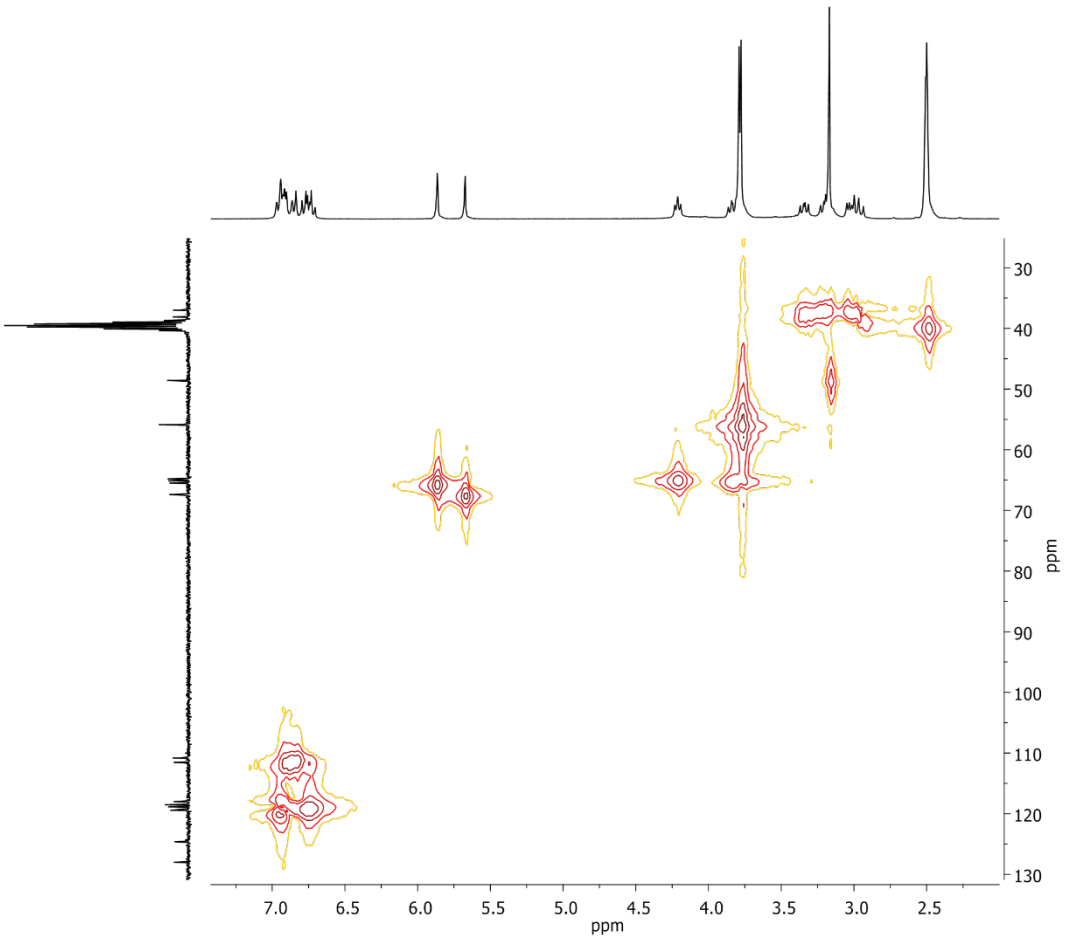

Figure 4: HMQC-NMR spectrum of the racemic (2RS,4R)-2-(2-hydroxy-3-methoxyphenyl)thiazolidine-4-carboxylic acid and assignment of the signals.

The original synthetic procedures were reported for salicylaldehyde as substrate. To check if the reported procedures led in this case to the desired Schiff base, we repeated the syntheses with salicylaldehyde. The obtained ^{1}H-NMR spectra of the products in form of white solids showed in all cases again singlets at 5.84 ppm and 5.65 ppm, respectively, and not the expected singlet at >8 ppm (Fig. S1). Apparently, the use of salicylaldehyde also leads to the formation of a thiazolidine product. Thus, the reported syntheses and the presented analytical data based on a condensation reaction could not be reproduced and did not lead to Schiff bases but to thiazolidines.

Crystal structure

In many previous reports it was assumed based on analytical data that metal complexes were formed with a Schiff base ligand derived from *L*-cysteine and *ortho*-vanillin[23] or salicylaldehyde[17–22, 24–26]. So far one crystal structure of an aluminum complex containing a Schiff base derived from *L*-cysteine has been published[27]. In this case, probably addition of metal ions prevent the formation of a thiazolidine product or the metal ion is able to reopen the thiazolidine ring. For this reason we performed several syntheses where the ligand was generated *in situ* and different metal salts (Ni, Zn, Mn(II) and Fe(III)) were added. A crystalline product **1** with crystals in form of colorless needles suitable for X-ray diffraction was obtained only from the system where $ZnCl_2$ was added (Table S1). Figure 5 shows the crystal structure of the diastereomer **1**.

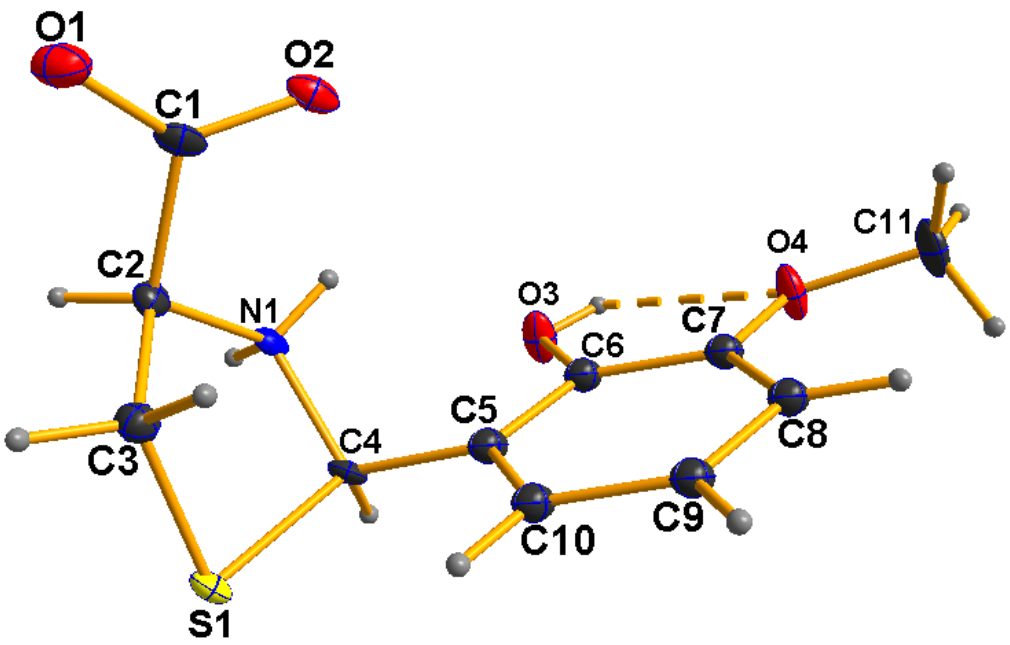

Figure 5 Molecular structure of (2R,4R)-2-(2-hydroxy-3-methoxyphenyl)thiazolidine-4-carboxylic acid **1**. Thermal ellipsoids are plotted at 50% probability level. Intramolecular hydrogen bond is depicted with dashed line.

The compound crystalizes in the non-centrosymmetric monoclinic space group type $P2_1$. The asymmetric unit contains one thiazolidine molecule and solvent molecules (Figure 5, Table 1). The solvent molecules site is occupied in 30% by a water and in 70% by a methanol molecule. Compound **1** exists in form of a zwitterion, where the N1 atom is double protonated and thus with positive charge, whereas carboxylate group is negatively charged. In the moiety derived from *ortho*-vanillin the hydroxyl

group acts as donor to an intramolecular hydrogen bond with the methoxo O atom acting as acceptor (Figure 5, Table 2). Additionally, the N-bonded H1 atom participates in a short contact to the methoxo O3 atom (N1…O3 distance at 2.917(4) Å and the N1-H1…O3 angle at 120(3)°).

The carboxylate C-O bond lengths are similar (1.241(4) and 1.259(4) Å, respectively) which confirms charge delocalization over this moiety. The thiazolidine ring adopts an envelope conformation with the C3-C2-N1-C4 torsion angle of -2.4(4)°. Table 1 contains selected bond lengths and bond angles. All these parameters are in the range published for other thiazolidines containing an aryl group bonded to the C4 atom [4, 5, 9, 10, 28–34].

One N-bonded H atom (H11) participates in an N-H…O hydrogen bond with symmetry-related carboxyl O2 atom acting as acceptor. Thus hydrogen-bonded chains are created, extending along the *b* axis (Figure 6a). Arrangement of the chains in the crystal structure is shown in Figure 6b, no significant stacking interactions occur between the aromatic rings. The disordered solvent molecules are located in voids between the chains. These solvent molecules participate in hydrogen bonds involving the *ortho*-vanillin hydroxyl group / carboxylate O atom as donor / acceptor (Table 2). Numerous C-H…O weak hydrogen bonds can be also distinguished (see Table 2).

The ^{1}H-NMR of the bulk material showed spectra shown in Figure 1, indicating a racemic mixture. Although several crystals from the same sample were investigated with X-ray diffraction studies, only the presented diastereomer was found.

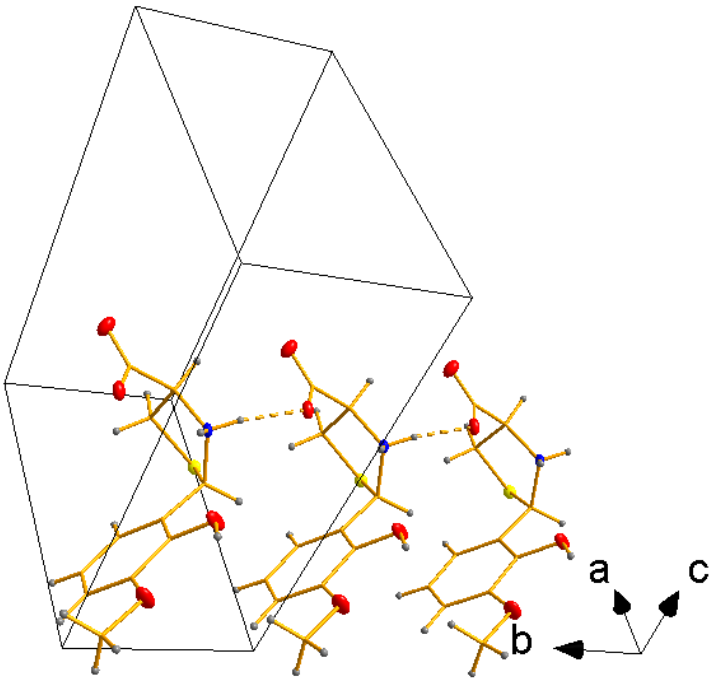

(a)

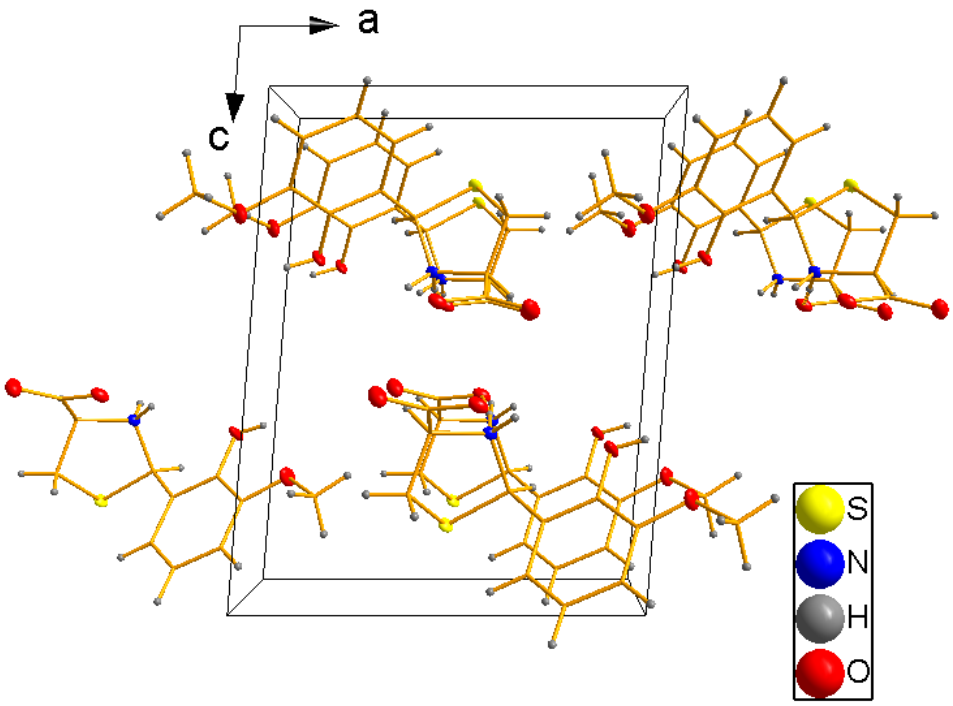

(b)

Figure 6 (a) One of the hydrogen-bonded chains extending along the *b* axis. (b) Arrangement of the hydrogen-bonded chains in the crystal structure. Hydrogen bonds are shown with dashed lines. For clarity, C atoms are shown as sticks and the disordered solvent is omitted.

Conclusion

In this contribution it could be verified that the condensation of *ortho*-vanillin and *L*-cysteine led to the formation of a racemic mixture of (2RS,4R)-2-(2-hydroxy-3-methoxyphenyl)thiazolidine-4-carboxylic acid **1** and not a Schiff base product. Results obtained with 1D- and 2D-NMR techniques support this conclusion. By addition of $ZnCl_2$ to the reaction mixture, colorless needles of **1**, suitable for X-ray diffraction studies, were obtained. In the crystal structure the thiazolidine compound exists as a zwitterion stabilized through intramolecular hydrogen bonds and adopting an envelope conformation. Hydrogen-bonded chains extending along the *b* direction are formed through N-H…O hydrogen bonds. The investigated crystal was a 2R-diastereomer, but the bulk material is racemic.

Experimental section

General

All syntheses were performed under air atmosphere. HPLC-grade methanol (HiperSolv Chromanorm, VWR BDH Prolabo) was used. All chemicals were purchased from commercial sources and used without further purification.

Synthesis of (2RS,4R)-2-(2-hydroxy-3-methoxyphenyl)thiazolidine-4-carboxylic acid

121 mg (1.0 mmol) of *L*-cysteine dissolved in a mixture of 10 mL water and 15 mL methanol. 152 mg (1 mmol) of *ortho*-vanillin was added to the stirred solution. The resulting pale yellow solution was heated to 80 °C and stirred until the solid part was dissolved completely. Then 136 mg (1.0 mmol) of

$ZnCl_2$ was added to the yellow solution. The solution was stirred for 10 min. at 80 °C and was transferred to a 30 mL vial for crystallization by slow evaporation. Colorless needles suitable for X-ray diffraction measurement were obtained within 1 day in quantitative yield.

Analytical data

IR bands (cm^{-1}): 416 (vw), 490 (m), 522 (w), 562 (vw), 604 (vw), 664 (s), 671 (s), 710 (s), 739 (s), 769 (m), 802 (s), 836 (w), 933 (m), 985 (vw), 1021 (s), 1052 (m), 1080 (m), 1181 (vw), 1241 (s), 1274 (s), 1372 (m), 1447 (w), 1481 (m), 1631 (m), 2518 (vw), 2349 (vw), 2843 (w), 2985 (w), 3136 (w).

Elemental analysis for the substance analyzed as $C_{11}H_{13}NO_4S$•0.7 MeOH•0.3H_2O: Calc (found) C 49.63 (49.25) H 5.84 (5.66) N 4.95 (4.95) O 28.26 (29.29) S 11.33 (11.11).

ESI(+): Molecular peak in methanol was found at *m/z* = 256.0637 ($[M+H^+]^+$).

NMR:

(2S, 4R)-Isomer

^{1}H-NMR (300 MHz, DMSO, δ in ppm): 3.03 (dd, ^3J = 5.18, 10.11, 1H), 3.22 (dd, ^3J = 6.83, 10.17, 1H), 3.78 (s, 3H, OCH_3), 4.21 (t, ^3J = 5.89, 1H), 5.87 (s, 1H), 6.70 – 6.97 (m, 3H, Aryl-H).

(2R, 4R)-Isomer

^{1}H-NMR (300 MHz, DMSO, δ in ppm): 2.95 (dd, ^3J = 9.27, 9.61, 1H), 3.34 (dd, ^3J = 7.01, 9.91, 1H), 3.79 (s, 3H, OCH_3), 3.84 (dd, ^3J = 7.26, 8.72, 1H,), 5.67 (s, 1H,), 6.70 – 6.97 (m, 3H, Aryl-H).

^{13}C-NMR (300 MHz, DMSO, δ in ppm): 36.88/38.11 (C9/9'), 55.86/55.92 (C1/1', O*C*H_3), 64.81 (C10), 65.13 (C10'), 65.49 (C8), 67.38 (C8'), 110.84/115.54 (C5/5'), 118.01/119.42 (C3/3'), 118.51/118.87 (C10/10'), 124.60/127.99 (C6/6'), 143.70/144.35 (C7/7'), 147.32/147.60 (C2/2'), 172.40/172.86 (C11/11').

Physicochemical measurements

Elemental analysis was carried out on an Elementar Vario Microcube elemental analyzer in CHNS mode. Oxygen content analysis was carried out on an Elementa rapid OXY Cube elemental analyzer.

IR spectra were recorded using a Bruker Alpha-P Infrared-spectrometer equipped with a Platinum-ATR with a diamond crystal.

All NMR spectra were recorded in DMSO-d_4 with a Bruker DRX 300 MHz spectrometer at room temperature. Chemical shifts were quoted in ppm relative to the residual protons of deuterated solvents.

Electrospray ionization mass spectrometry (ESI-MS) was performed on a Finnigan LTQ-FT spectrometer from Thermo Fischer Scientific in the positive and negative ion mode with solvent as carrier gas.

X-ray diffraction experiment

A single crystal of **1** was mounted on a Bruker D8 Quest diffractometer equipped with a CMOS detector and Mo$K_{\alpha 3}$radiation source. Basic crystallographic details are collected in Table 1. The structure was

solved by direct methods with SHELXS and refined against F^2 by full-matrix-least-square method using SHELXL-2014[35]. Multiscan absorption correction was applied.

Refinement details

EADP restraint was applied to the phenyl ring C atoms (C5 to C10), as well as methoxo O4 and C11 atoms and methanol C1M, O1M atoms. The N-bonded H atoms were found on difference Fourier maps and refined with DFIX restraints setting N-H bond lengths at 0.860(2) Å.

Additional maximum occurring near the methanol solvent molecule was interpreted as substitutionally disordered water molecule. The occupancies of both disorder components were refined and subsequently constrained at 0.7 and 0.3 for methanol and water molecules, respectively. Water H atoms were not located.

On the final difference Fourier map the highest maximum of 0.62 e/Å^3 is located at 1.31 Å from H1 of the protonated N1 atom, between the thiazolidine derivative molecule and the solvent site. Probably this indicates minor additional solvent content, but no refinable model could be proposed.

Acknowledgment

S. M. acknowledges Niklas Rinn for his assistance in this study.

References

1. Pandeya, S. N.; Sriram, D.; Nath, G.; DeClercq, E. *European Journal of Pharmaceutical Sciences* **1999,** *9* (1), 25–31.
2. Upadhyay, A.; Srivastava, S. K.; Srivastava, S. D. *European journal of medicinal chemistry* **2010,** *45* (9), 3541–3548.
3. Shiradkar, M. R.; Murahari, K. K.; Gangadasu, H. R.; Suresh, T.; Kalyan, C. A.; Panchal, D.; Kaur, R.; Burange, P.; Ghogare, J.; Mokale, V.; Raut, M. *Bioorganic & medicinal chemistry* **2007,** *15* (12), 3997–4008.
4. Song, Z.-C.; Ma, G.-Y.; Zhu, H.-L. *RSC Adv* **2015,** *5* (32), 24824–24833.
5. Song, Z.-C.; Ma, G.-Y.; Lv, P.-C.; Li, H.-Q.; Xiao, Z.-P.; Zhu, H.-L. *European journal of medicinal chemistry* **2009,** *44* (10), 3903–3908.
6. Gududuru, V.; Hurh, E.; Dalton, J. T.; Miller, D. D. *Bioorganic & medicinal chemistry letters* **2004,** *14* (21), 5289–5293.
7. Balzarini, J.; Orzeszko, B.; Maurin, J. K.; Orzeszko, A. *European journal of medicinal chemistry* **2007,** *42* (7), 993–1003.
8. Solomon, V. R.; Haq, W.; Srivastava, K.; Puri, S. K.; Katti, S. B. *J. Med. Chem.* **2007,** *50* (2), 394–398.
9. In, Y.; Shibata, M.; Doi, M.; Ishida, T.; Inoue, M.; Sasaki, Y.; Morimoto, S. *J. Chem. Soc., Chem. Commun. [Online]* **1986,** No. 6, 473.
10. Oya, M.; Kato, E.; Iwao, J.-I.; Yasuoka, N. *Chem. Pharm. Bull.* **1982,** *30* (2), 484–493.
11. Liu, Y.; Jing, F.; Xu, Y.; Xie, Y.; Shi, F.; Fang, H.; Li, M.; Xu, W. *Bioorganic & medicinal chemistry* **2011,** *19* (7), 2342–2348.
12. Butvin P., Al-Ja'afreh J., Světlík J., Havránek E. *Chemical Papers* **1999,** *53* (5), 315–322.
13. Skvortsov, A. N.; Uvarov, V. M.; Vekki, D. A. de; Studentsov, E. P.; Skvortsov, N. K. *Russ J Gen Chem* **2010,** *80* (10), 2007–2021.
14. Muche, S.; Levacheva, I.; Samsonova, O.; Pham, L.; Christou, G.; Bakowsky, U.; Hołyńska, M. *Inorg. Chem.* **2014,** *53* (14), 7642–7649.

15. Muche, S.; Levacheva, I.; Samsonova, O.; Biernasiuk, A.; Malm, A.; Lonsdale, R.; Popiołek, Ł.; Bakowsky, U.; Hołyńska, M. *Journal of Molecular Structure* **2017,** *1127*, 231–236.

16. Muche, S.; Hołyńska, M. *Journal of Molecular Structure* **2017,** *1142*, 168–174.

17. MacDonald, L. G.; Brown, D. H.; Morris, J. H.; Smith, W. E. *Inorganica Chimica Acta* **1982,** *67*, 7–12.

18. Pillai, M.R.A.; Kothari, K.; Banerjee, S.; Samuel, G.; Suresh, M.; Sarma, H. D.; Jurisson, S. *Nuclear Medicine and Biology* **1999,** *26* (5), 555–561.

19. Chohan, Z. H.; Arif, M.; Sarfraz, M. *Appl. Organometal. Chem.* **2007,** *21* (4), 294–302.

20. Wang, M.; Meng, Z.; Fu, J. *Applied radiation and isotopes* **2006,** *64* (2), 235–240.

21. Saha, U.; Mukherjea, K. K. *RSC Adv* **2015,** *5* (114), 94462–94473.

22. Maurya, M. R.; Kumar, U.; Correia, I.; Adão, P.; Costa Pessoa, J. *Eur. J. Inorg. Chem.* **2008,** *2008* (4), 577–587.

23. Grüning, C.; Rehder, D. *Journal of inorganic biochemistry* **2000,** *80* (1-2), 185–189.

24. Wang, Z.; Qin, Y.; Wang, C.; Sun, L.; Lu, X.; Lu, X. *Applied Surface Science* **2012,** *258* (6), 2017–2021.

25. Jursík, F.; Hájek, B. *Inorganica Chimica Acta* **1975,** *13*, 169–173.

26. Taqui Khan, M. M.; Kureshy, R. I.; Khan, N. H. *Tetrahedron: Asymmetry* **1991,** *2* (10), 1015–1020.

27. Ma, X.; Hao, P.; Li, J.; Roesky, H. W.; Yang, Z. *Z. anorg. allg. Chem.* **2013,** *639* (3-4), 493–496.

28. Balakrishnan, C.; Theetharappan, M.; Natarajan, S.; Thalamuthu, S.; Neelakantan, M. A. *RSC Adv* **2015,** *5* (127), 105453–105463.

29. Pinho e Melo, T. M. V. D.; Gomes, C. S. B.; Soares, M. I. L.; Gonsalves, A. M. d.'A. R.; Paixão, J. A.; Beja, A. M.; Silva, M. R. *Journal of Heterocyclic Chemistry* **2004,** *41* (4), 493–497.

30. Parthasarathy, R.; Paul, B.; Korytnyk, W. *J. Am. Chem. Soc.* **1976,** *98* (21), 6634–6643.

31. Pinho e Melo, T. M.V.D.; Santos, C. I.A.; Rocha Gonsalves, A. M.d.'A.; Paixão, J. A.; Beja, A. M. *Tetrahedron* **2004,** *60* (18), 3949–3955.

32. Bell, R. A.; Britten, J. F.; Howard-Lock, H. E.; Lock, C.J.L.; Schmidt, M. *Can. J. Chem.* **1994,** *72* (7), 1621–1624.

33. Song, Z.-C.; Guo, Y.; Liu, W.-H.; Hu, L.-C.; Cai, S.-N. *Acta Crystallogr E Struct Rep Online* **2010,** *66* (Pt 11), o2934.

34. Jagtap, R. M.; Rizvi, M. A.; Dangat, Y. B.; Pardeshi, S. K. *Journal of Sulfur Chemistry* **2016,** *37* (4), 401–425.

35. G.M. Sheldrick. *SHELXTL 5.1, Bruker AXS Inc, 6300 Enterprise Lane, Madison, WI 53719-1173, USA (1997)*.

Tables

Table 1 Selected bond lengths and bond angles (Å, °).

S1—C4	1.811 (3)	O2—C1	1.259 (4)
S1—C3	1.816 (4)	O3—C6	1.353 (4)
N1—C2	1.511 (4)	O4—C7	1.365 (4)
N1—C4	1.514 (4)	O4—C11	1.430 (4)
O1—C1	1.241 (4)		
C4—S1—C3	89.72 (15)	C2—C3—S1	105.5 (2)
C2—N1—C4	112.7 (2)	N1—C4—C5	112.6 (2)
N1—C2—C3	107.5 (3)	N1—C4—S1	103.1 (2)
N1—C2—C1	110.8 (3)	C5—C4—S1	115.6 (2)

Table 2 Main hydrogen bonds parameters (Å, °). Symmetry codes: (i) x, y−1, z; (ii) x−1, y, z; (iii) −x+1, y−1/2, −z+1; (iv) x+1, y, z; (v) −x, y−1/2, −z+1.

D—H···*A*	*D*—H	H···*A*	*D*···*A*	*D*—H···*A*
N1—H11···O2^{i}	0.86 (1)	1.88 (1)	2.710 (4)	162 (3)
O3—H3*A*···O4	0.84	2.22	2.674 (3)	114
O1*M*—H1*M*···O1^{ii}	0.84	2.02	2.822 (5)	160
O3—H3*A*···O1*M*	0.84	1.87	2.667 (4)	158
O3—H3*A*···O1*W*	0.84	1.96	2.709 (9)	149
C2—H2···O2^{iii}	1.00	2.65	3.156 (4)	111
C2—H2···O1*M*^{iv}	1.00	2.59	3.202 (5)	120
C11—H11*A*···O1^{ii}	0.98	2.58	3.432 (5)	145
C1*M*—H1*M*2···O3^{v}	0.98	2.55	3.175 (7)	121
C1*M*—H1*M*3···O2^{v}	0.98	2.61	3.391 (6)	137

Synthesis, characterization and crystal structure of (2RS,4R)-2-(2-hydroxy-3-methoxyphenyl)thiazolidine-4-carboxylic acid

Simon Muche,[a] *Matthias Müller*[a]*, Małgorzata Hołyńska*[*a]

[a] Fachbereich Chemie and Wissenschaftliches Zentrum für Materialwissenschaften, Philipps-Universität Marburg, Hans-Meerwein-Strasse, D-35043 Marburg, Germany. E-Mail: holynska@staff.uni-marburg.de

SUPPORTING INFORMATION

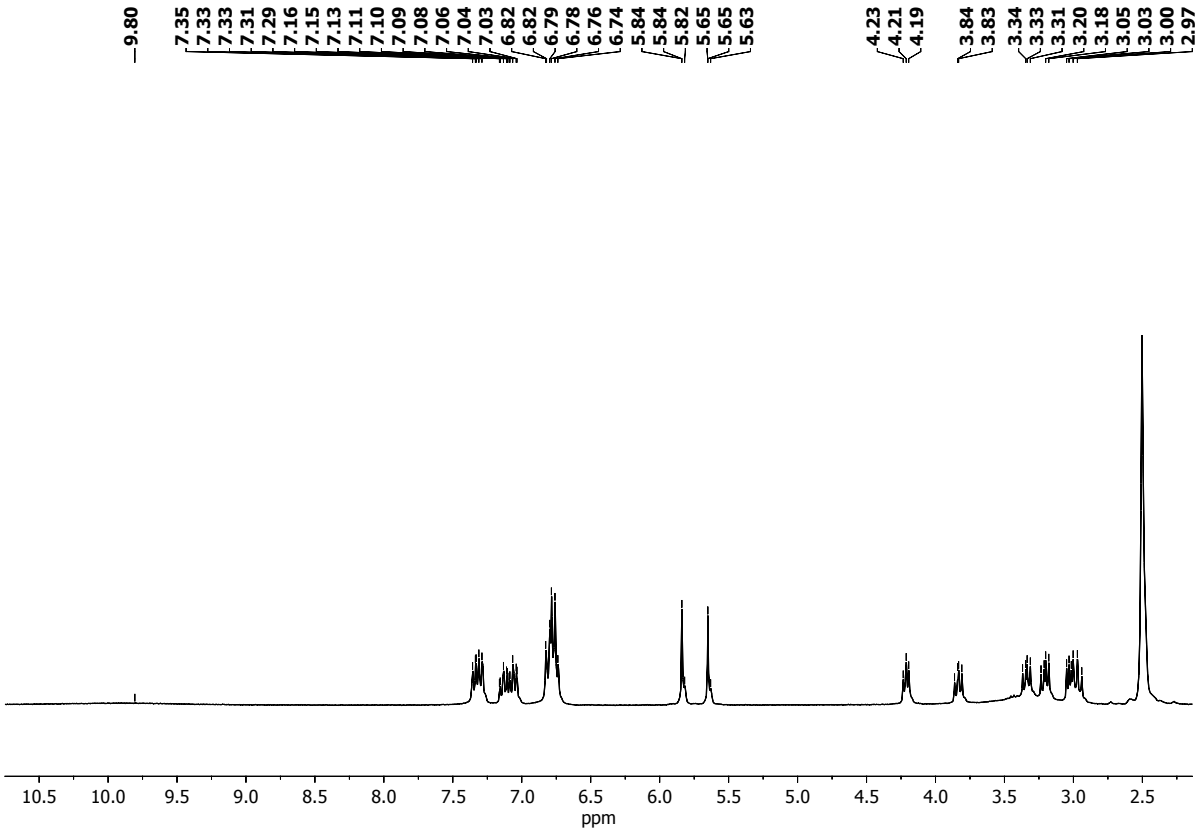

Figure S1. Representative ^{1}H-NMR spectrum for the product obtained in reaction of salicylaldehyde and L-cysteine, following several reported procedures[(1–6)].

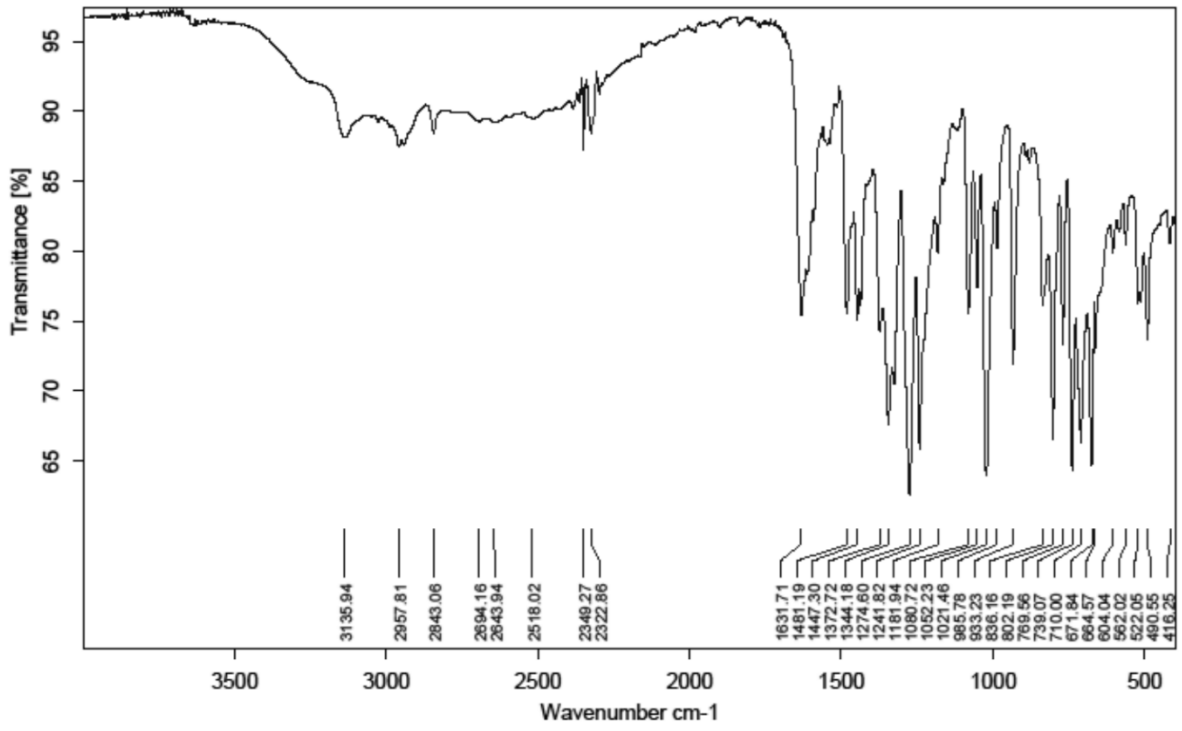

Figure S2. IR spectrum of the racemic (2R/S,4R)-2-(2-hydroxy-3-methoxyphenyl)thiazolidine-4-carboxylic acid.

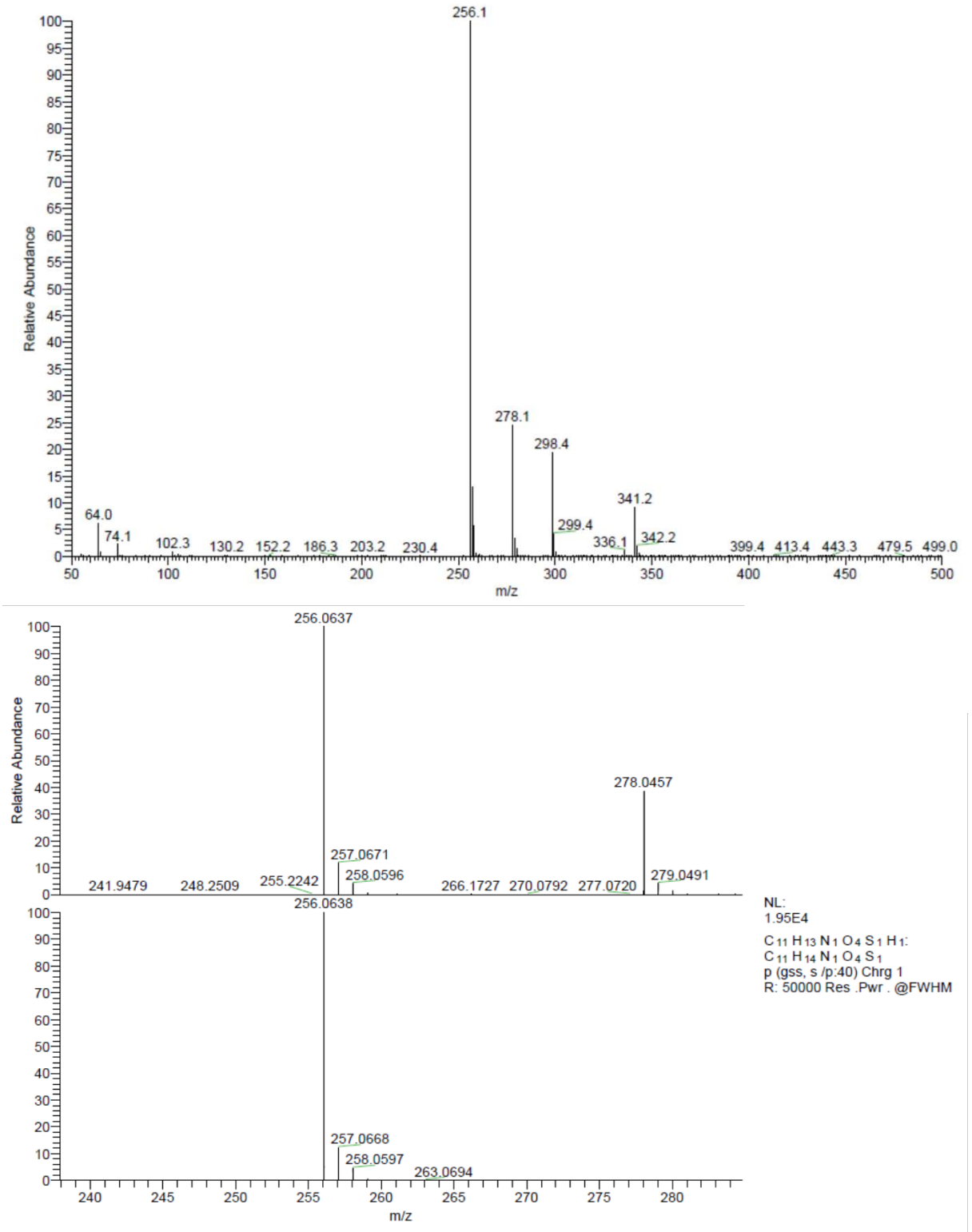

Figure S3. ESI(+) spectra of the racemic (2R/S,4R)-2-(2-hydroxy-3-methoxyphenyl)thiazolidine-4-carboxylic acid recorded in methanol and simulation of the molecular peak.

Table S1 Basic crystallographic data.

	1
Empirical formula	$C_{11.70}H_{16.40}NO_5S$
Formula weight	283.12
Temperature/K	100(2)
Crystal system	monoclinic
Space group	$P2_1$
a/Å	9.784 (3)
b/Å	5.120 (2)
c/Å	12.412 (4)
β/°	94.54 (3)
Volume/Å^3	619.8 (4)
Z, ρ_{calc}g/cm^3	2, 1.517
μ/mm^{-1}	0.28
F(000)	299
Crystal size/mm^3	0.70 × 0.06 × 0.05
Radiation	MoK_α (λ = 0.71073)
2Θ range for data collection/°	2.6-25.0
Data/restraints/parameters	2162/3/143
Goodness-of-fit on F^2	1.00
Final R indexes [I>=2σ (I)]	R = 0.033, wR = 0.080
Final R indexes [all data]	R = 0.034, wR = 0.081
Largest diff. peak/hole / e Å^{-3}	0.62, -0.30

References

1. MacDonald, L. G.; Brown, D. H.; Morris, J. H.; Smith, W. E. *Inorganica Chimica Acta* **1982,** *67*, 7–12.
2. Pillai, M.R.A.; Kothari, K.; Banerjee, S.; Samuel, G.; Suresh, M.; Sarma, H. D.; Jurisson, S. *Nuclear Medicine and Biology* **1999,** *26* (5), 555–561.
3. Chohan, Z. H.; Arif, M.; Sarfraz, M. *Appl. Organometal. Chem.* **2007,** *21* (4), 294–302.
4. Wang, M.; Meng, Z.; Fu, J. *Applied radiation and isotopes* **2006,** *64* (2), 235–240.
5. Saha, U.; Mukherjea, K. K. *RSC Adv* **2015,** *5* (114), 94462–94473.
6. Maurya, M. R.; Kumar, U.; Correia, I.; Adão, P.; Costa Pessoa, J. *Eur. J. Inorg. Chem.* **2008,** *2008* (4), 577–587.

V A gap is filled: First structures of enantiopure iron(III) complexes with Schiff base ligands derived from *ortho*-vanillin and *L*-glutamine or *L*-glutamic acid

Muche, S.; Harms, K.; Burghaus, O.; M. Hołyńska, M. *Polyhedron*, Manuskript akzeptiert

A series of new Fe(III) complexes, [Fe(OVGln)$_2$]Na **(1)**, [Fe(OVGln)$_2$]K **(2)**, [Fe(OVGlu)$_2$]Na **(3)** and [Fe(OVGlu)$_2$]K **(4)**, bearing a Schiff base ligand derived from *ortho*-vanillin (OV) and *L*-glutamine (Gln) or *L*-glutamic acid (Glu) is presented. The complexes are extensivly characterized by mass spectrometry, IR spectroscopy, X-ray powder diffraction, EPR and elemental analysis. Three complexes are additionally characterized by X-ray diffraction structure analysis. The mononuclear complexes are negatively charged with sodium or potassium as counter ions. Depending on the nature of the amino acid within the ligands and the counter ions, varying arrangements of the complex anions in the crystal structures can be observed. Also provided are the synthesis and full characterization for the applied ligand in form of its disodium salt

Inhalt: Durch die Kondensation von *ortho*-Vanillin mit *L*-Glutamin wird der entsprechende Schiff'sche-Base-Ligand als Dinatriumsalz erhalten und dessen vollständige Charakterisierung präsentiert. Durch die *in situ*-Reaktion von *ortho*-Vanillin mit *L*-Glutamin bzw. *L*-Glutaminsäure und Natrium- bzw Kaliumacetat und anschließender Zugabe von Eisen(III)-perchlorat können die vier mononuklearen Komplexe [Fe(OVGln)$_2$]Na **(1)**, [Fe(OVGln)$_2$]K **(2)**, [Fe(OVGlu)$_2$]Na **(3)** und [Fe(OVGlu)$_2$]K **(4)** erhalten werden. Im Falle der *L*-Glutamin-basierten Komplexe ist außerdem der Zusatz von Natrium bzw. Kaliumazid für das Kristallwachstum notwendig. Die Charakterisierung erfolgt durch Massenspektrometrie, IR, XRPD und Elementaranalyse. EPR-Studien der Komplexe in Lösung und im Festkörper zeigen, dass das Eisenzentrum in der Oxidationsstufe +III mit einem Spin von S = 5/2 vorliegt. Publikationsfähige kristallographische Daten wurden für die Komplexe **1**-**3** erhalten. Das gemeinsame Strukturmotiv ist ein von zwei Ligandmolekülen oktaedrisch koordiniertes Eisen(III)-Zentrum mit leicht verzerrter Geometrie, welches insgesamt einfach negativ geladen ist. Die Ladung wird kompensiert von den Alkalimetallkationen. **1** und **3** sind isostrukturell. Superstruktureffekte verhinderten eine zufriedenstellende Verfeinerung des Datensatzes von **4**. Basierend auf den analytischen Daten, insbesondere der Röntgenpulverdiffraktogramme, kann aber davon ausgegangen werden, dass **4**, trotz Kalium als Gegenion, isostrukturell zu **1** und **3** ist. Die erhalten Eisenkomplexe könnten als interessante Präkusoren für die Synthese von höherkernigen Komplexen dienen.

Eigener Anteil: Die Planung und Durchführung der Synthesen sowie die Aufnahme und Auswertung der Basisanalytik wurde von mir durchgeführt unter Betreuung von Małgorzata Hołyńska. Die EPR-Daten wurden von Olaf Burghaus aufgenommen und ausgewertet. Die Röntgenstrukturanalyse wurde von der hauseigenen Serviceabteilung durchgeführt. Die Analyse der kristallographischen Daten erfolgte durch Klaus Harms. Das Manuskript wurde von mir ausgearbeitet. Der EPR-Teil wurde von Olaf Burghaus verfasst. Die kristallographischen Teile wurden von mir und Małgorzata Hołyńska gemeinsam verfasst. Die Überarbeitung erfolgte gemeinsam.

A gap is filled: First structures of enantiopure iron(III) complexes with Schiff base ligands derived from *ortho*-vanillin and *L*-glutamine or *L*-glutamic acid

*Simon Muche[a], Klaus Harms[a], Olaf Burghaus[a], Małgorzata Hołyńska[a]**

[a]Fachbereich Chemie und Wissenschaftliches Zentrum für Materialwissenschaften, Philipps- Universität Marburg, Hans-Meerwein-Strasse, D-35043, Marburg, Germany.

E-Mail: holynska@staff.uni-marburg.de

A series of new Fe(III) complexes, $[Fe(OVGln)_2]Na$ **(1)**, $[Fe(OVGln)_2]K$ **(2)**, $[Fe(OVGlu)_2]Na$ **(3)** and $[Fe(OVGlu)_2]K$ **(4)**, bearing a Schiff base ligand derived from *ortho*-vanillin (OV) and *L*-glutamine (Gln) or *L*-glutamic acid (Glu) is presented. The complexes are extensivly characterized by mass spectrometry, IR spectroscopy, X-ray powder diffraction, EPR and elemental analysis. Three complexes are additionally characterized by X-ray diffraction structure analysis. The mononuclear complexes are negatively charged with sodium or potassium as counter ions. Depending on the nature of the amino acid within the ligands and the counter ions, varying arrangements of the complex anions in the crystal structures can be observed. Also provided are the synthesis and full characterization for the applied ligand in form of its disodium salt.

KEYWORDS: Schiff Base•amino acid•metal complex•iron(III)•crystal structure

Synthesis, characterization and crystal structures of an ligand derived from *ortho*-vanillin and *L*-glutamine as well as four novel high spin iron(III) complexes derived from *ortho*-vanillin and *L*-glutamine or *L*-glutamic acid. Crystal structures provided for three complexes.

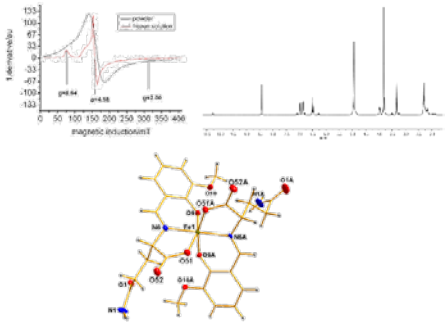

Highlights:

- Synthesis and full characterization of Schiff base ligand derived from *ortho*-vanillin and *L*-glutamine
- Four new iron(III) complexes with ligands derived from *ortho*-vanillin and *L*-glutamine or *L*-glutamic acid
- Crystal structures for three complexes
- Distorted octahedral geometry; S = 5/2

Introduction

Schiff bases and their metal complexes are highly interesting classes of compounds because of their large variety of properties, e.g. antibacterial, antimicrobial, antitumor or catalytic activity, described in a multitude of research articles. Schiff bases containing amino acid as amine source are of special interest due to the availability of a bioactive fragment from the amino acid. Combined with *ortho*-vanillin as aldehyde source which itself possesses biological activity[1–5], a powerful class of Schiff bases with many coordination sides for metal complexation is obtained.

For this type of Schiff bases iron complexes with known crystal structures are published only for salicylaldehyde as aldehyde source: when glycine is used the formation of ferrate complexes is reported. The iron center within the complex can be Fe(III)[6] or Fe(II)[7]. In both cases hexaaquairon(II) acts as counter ion. Monomeric [Fe(sal-gly)$_2$] units are bridged by two Na(H_2O)$^+$ ions. With an excess of salicylaldehyde and NaOH the dimer can be transformed to a dinuclear iron complex where a second salicylaldehyde molecule binds to the former ligand. The iron centers are bridged by oxygen-containing groups from the additional salicylaldehyde molecule[8]. Use of methionine and phenylalanine leads to monomeric Fe(III) complexes with triethylammonium as counter-ion. These complexes show good protein-binding activity and photoinduced cleavage activity[9]. With lysine a hexafluorophosphate salt of a mononuclear iron (III) complex could be isolated. During complexation this compound undergoes a racemization process[10]. Crystal structures of different metal complexes containing single *L*-glutamine[11–13] or tolylsulfonyl-substituted *L*-glutamine[14–16] are known. For the Schiff base derived from *ortho*-vanillin and *L*-glutamine crystal structure is known only for a nickel complex additionally containing phenanthroline, which displays DNA and protein binding abilities[17]. Mononuclear complexes of Co(II), Cu(II) and Ni(II), complexed by one ligand derived from *ortho*-vanillin and *L*-glutamine and one water molecule, in which the copper complex displays antibacterial activity against *S. aureus, E. coli* and *S. typhi*, were published by Nair et.al[18]. The structures of the complexes were predicted based on analytical data. Furthermore a trinuclear copper complex was described by Xiao et al.[19], displaying proteasome-inhibitory activity with respect to human breast cancer and leukemia cells[20]. The structure of this complex was calculated by Hartree–Fock method, taking into account its electronic absorption spectra.

Whereas for the Schiff base derived from *L*-glutamic acid and salicylaldehyde a large number of crystallographically characterized mono- and dinuclear copper complexes are known[21–27], less examples were published for the system containing *ortho*-vanillin but the ability to form polynuclear metal complexes was reported. Thus a pentadecanuclear low-cytotoxic nickel complex[28,29] and a tetranuclear copper complex with investigation of its biological activity[30] were published. Mononuclear complexes are so far unknown for this system.

The present study is a continuation of our work in the area of Schiff base ligands derived from *ortho*-vanillin and amino acids and their corresponding metal complexes, wherein we report a series of new mononuclear Fe(III) complexes bearing a Schiff base ligand derived from *ortho*-vanillin and *L*-glutamine or *L*-glutamic acid. Where possible, the complexes are characterized by X-ray diffraction structure analysis, mass spectrometry, IR spectroscopy, X-ray powder diffraction, EPR and elemental analysis. Furthermore, we present the synthesis and provide full characterization for the glutamine-based Schiff base ligand in form of its disodium salt.

Materials and methods

Synthesis

All syntheses were performed under air. HPLC-grade methanol (HiperSolv Chromanorm, VWR BDH Prolabo) was used. All chemicals were purchased from commercial sources and used without further purification.

Caution: Although no problems were encountered during the course of this work, attention is drawn to the potentially explosive nature of perchlorates.

***L*-Glutamine-based compounds**

Ligand OVGlnHNa$_2$: At 80 °C 400 mg (10 mmol) of sodium hydroxide were dissolved in 60 ml of methanol. 735 mg *L*-glutamine (5 mmol) were added to the methanolic solution. When the *L*-glutamine was dissolved completely, 760 mg (5 mmol) *ortho*-vanillin were added. The color of the solution changed to yellow immediately. The solution was stirred for 1 hour at 80 °C. After the solution was cooled down to room temperature, 150 ml aliquots of diethyl ether were added. A yellow precipitate appeared. The yellow precipitate was separated from the solution, washed several times with diethyl ether and dried *in vacuo*. Yield: 1.455 g (90%).
Elemental analysis: the substance dried under vacuum, analyzed as $C_{13}H_{14}N_2O_5Na_2$•0.1MeOH•0.05Et_2O•0.8H_2O: Calc (found) C 46.23 (46.22) H 4.81 (5.01) N 8.11 (8.19).
IR bands for **OVGlnHNa$_2$** dried under vacuum (cm^{-1}): 458.2 (vw), 536.8 (w), 571.8 (vw), 639.8 (w), 735.3 (m), 788.8 (vw), 810.0 (vw), 850.7 (w), 976.1 (w), 993.5 (vw), 1081.3(m), 1166.4 (w), 1208.1 (vs), 1317.3 (w), 1343.3 (vw), 1386.3 (m), 1448.8 (s), 1470.8 (m), 1535.6 (w), 1589.9 (s), 1624.1 (s), 1666.1 (m), 1980.5 (vw), 2050.3 (vw), 2325.1 (vw), 2833.7 (w), 2935.6 (w), 3050.3 (w), 3183.4 (w), 3344.1 (w).
^{1}H NMR (300 MHz, MeOD): δ 8.40 (s, 1H), 6.96 (dd, *J* = 8.0, 1.3 Hz, 1H), 6.85 (dd, *J* = 7.7, 1.2 Hz, 1H), 6.48 (t, *J* = 7.9 Hz, 1H), 3.95 (dd, *J* = 7.4, 4.3 Hz, 1H), 3.80 (s, 3H), 2.37 – 2.08 (m, 4H).
ESI-MS:
ESI(+) (MeOH): Molecular peak was found at *m/z* = 325.07: ([OVGlnHNa$_2$]+H^+). Further identified peaks: m/z = 303.09 ([OVGlnH$_2$Na]+H^+), 281.11 ([OVGlnH$_3$]+H^+).
ESI(-) (MeOH): Molecular peak was found at m/z = 279.1: [OVGlnH$_2$]$^-$.

Complex 1 [Fe(OVGln)$_2$]Na: 146 mg (1.0 mmol) of *L*-glutamine and 272 mg (2 mmol) of sodium acetate were dissolved in 3.5 mL of water and 3.5 mL of methanol and heated to 80 °C. When the solid part was completely dissolved, 152 mg (1.0 mmol) of *ortho*-vanillin was added to the stirred *L*-glutamine/sodium acetate solution. To the resulting yellow solution 354 mg (1 mmol) $Fe(ClO_4)_3$•xH_2O was added. The solution color changed to dark violet immediately. The solution was stirred for 30 min. at 80 °C and afterwards combined with a solution containing 10.8 mL of methanol, 7.2 mL of water and 195 mg (3 mmol) sodium azide. The solution was stirred for one minute and transferred into a 30 mL vial for crystallization by slow evaporation. Crystals in form of black/brown blocks appear after 4-6 weeks depending on the evaporation rate. The crystals were filtered off, washed with acetonitrile and dried under air for 12 h. Yield (average): 201 mg (30.14%). Without addition of sodium azide no crystal growth was observed.
Elemental analysis: the substance **1** dried under vacuum for 4 h, analyzed as $C_{26}H_{28}N_4O_{10}FeNa_1$•1.75$H_2O$: Calc (found) C 46.83 (46.37) H 4.76 (4.79) N 8.40 (8.48) O 28.19 (29.54).
IR bands for **1** dried under vacuum for 4 h (cm^{-1}): 413.9 (w), 450.3 (w), 547.3 (m), 618.8 (vw), 647.6 (w), 742.2 (m), 786.9 (w), 813.3 (w), 854.2 (w), 973.0 (w), 1078.2 (m), 1169.9 (w), 1221.3 (s), 1243.2 (s), 1296.1 (s), 1334.7 (m), 1410.7 (w), 1436.5 (s), 1469.7 (m), 1550.7 (w), 1596.3 (vs), 1615.5 (vs), 1981.0 (vw), 2069.2 (w), 2325.3 (vw), 2358.7 (vw), 2835.1 (vw), 2934.4 (w), 3188.2 (vw), 3327.0 (vw).
ESI-MS:
ESI(+) (MeOH or H_2O): Molecular peak was found at *m/z* = 636.11: ([Fe(OVGln)$_2$Na]+H^+).
ESI(-) (MeOH or H_2O): Molecular peak was found at *m/z* = 612.12: [Fe(OVGln)$_2$)]$^-$
Further identified peaks are presented in the Supporting information.

Complex 2 [Fe(OVGln)$_2$]K: 146 mg (1.0 mmol) of *L*-glutamine and 196 mg (2 mmol) of potassium acetate was dissolved in 10 mL of water and 15 mL of methanol and heated to 80 °C. When the solid part was completely dissolved, 152 mg (1.0 mmol) of *ortho*-vanillin was added to the stirred *L*-glutamic acid/potassium acetate solution. To the

resulting yellow solution 354 mg (1 mmol) $Fe(ClO_4)_3 \bullet xH_2O$ was added. The solution color changed to dark violet immediately. The solution was stirred for 30 min. at 80 °C and afterwards combined with a solution containing 10.8 mL of methanol, 7.2 mL of water and 243 mg (3 mmol) potassium azide. During stirring a fine dark precipitate appears. The solution was left at RT for minimum 2 h. During this time a colorless solid appeared. This solid supposed to be potassium perchlorate. The solution was filtered off into a 30 mL vial for crystallization by slow evaporation. Crystals in form of black/brown blocks appear after 4-6 weeks depending on evaporation rate. The crystals were filtered off, washed with ethyl acetate and dried under air over night. Yield (average): 182 mg (25.80%).
Elemental analysis: the substance **2** dried under vacuum for 4 h analyzed as $C_{26}H_{28}N_4O_{10}FeK_1 \bullet 3H_2O$: Calc (found) C 44.26 (43.86) H 4.86 (4.78) N 7.94 (7.98) O 29.48 (30.44).
IR bands for **2** dried under vacuum for 4 h (cm^{-1}): 414.9 (w), 450.4 (w), 499.7 (vw), 549.6 (w), 587.8 (w), 648.7 (vw), 742.4 (m), 737.1 (m), 785.4 (w), 812.9 (w), 855.5 (w), 898.8 (vw), 965.5 (w), 992.8 (vw), 1007.7 (vw), 1077.4 (m), 1124.4 (vw), 1171.9 (vw), 1223.0 (s), 1244.7 (s), 1296.0 (s), 1315.2 (m), 1334.9 (m), 1356.5 (m), 1384.6 (vw), 1439.3 (s), 1471.1 (m), 1549.9 (m), 1599.9 (vs), 1615.4 (vs),1655.6 (m), 2035.4 (w), 2324.4 (vw), 2838.0 (w), 2934.4 (w), 3332.0 (w).
ESI-MS:
ESI(+) (MeOH or H_2O): Molecular peak was found at *m/z* = 652.09: ($[Fe(OVGln)_2K]+H^+$).
ESI(-) (MeOH or H_2O): Molecular peak was found at *m/z* = 612.12: $[Fe(OVGln)_2]^-$**.**
Further identified peaks are presented in the Supporting Information.

***L*-Glutamic acid-based compounds**

Complex 3 [Fe(OVGlu)$_2$]Na: 147 mg (1.0 mmol) of *L*-glutamic acid and 408 mg (3.0 mmol) of sodium acetate were dissolved in 10 mL of water and 15 mL of methanol and heated to 80 °C. When the solid part was completely dissolved, 152 mg (1.0 mmol) of *ortho*-vanillin was added to the stirred *L*-glutamic acid/sodium acetate solution. To the resulting yellow solution 354 mg (1 mmol) $Fe(ClO_4)_3 \bullet xH_2O$ was added. The solution color changed to dark violet immediately. The solution was stirred for 30 min at 80 °C. During stirring a fine dark precipitate appeared. The solution was filtered off into a 30 mL vial for crystallization by slow evaporation. Crystals in form of black blocks were obtained within 12 days. Crystallization was finished after 3 weeks. The crystals were filtered off, washed with acetonitrile and dried under air for 12 h. Yield (average): 210 mg (29.23%).
Elemental analysis: the substance **3** dried under vacuum for 4 h analyzed as $C_{26}H_{26}N_2O_{12}FeNa_1 \bullet 4.5H_2O$: Calc (found) C 43.47 (43.83) H 4.91 (4.91) N 3.90 (3.94) O 36.75 (37.05).
IR bands for **3** dried under vacuum for 4 h (cm^{-1}): 416.0 (w), 452.6 (m), 481.6 (w), 549.8 (m), 591.3 (w), 747.9 (s), 786.9 (m), 852.9 (m), 886.8 (w), 936.7 (w), 975.0 (m), 1076.7 (s), 1168.9 (w), 1221.7 (s), 1241.1 (s), 1290.6 (s), 1399.2 (w), 1438.1 (m), 1470.4 (m), 1550.0 (w), 1596.6 (s), 1615.4 (vs), 1762.7 (m), 2162.4 (vw), 2353.8 (vw), 2939.2 (vw). 3397.5 (w).
ESI-MS:
ESI(+) (MeOH or H_2O): Molecular peak was found at *m/z* = 638.08: ($[Fe(OVGlu)_2]Na+H^+$). ESI(-) (MeOH or H_2O): Molecular peak was found at *m/z* = 614.08: $[Fe(OVGlu)_2]^-$
Further identified peaks are presented in the Supporting Information.

Complex 4 [Fe(OVGlu)$_2$]K: 147 mg (1.0 mmol) of *L*-glutamic acid and 294 mg (3.0 mmol) of potassium acetate were dissolved in 10 mL of water and 15 mL of methanol and heated to 80 °C. When the solid part was completely dissolved, 152 mg (1.0 mmol) of *ortho*-vanillin was added to the stirred *L*-glutamic acid/potassium acetate solution. To the resulting yellow solution 354 mg (1 mmol) $Fe(ClO_4)_3 \bullet xH_2O$ was added. The solution color changed to dark violet immediately. The solution was stirred for 30 min. at 80 °C. During stirring a fine dark precipitate appears. The solution was left at RT for minimum 2 h. During this time a colorless solid appeared. This solid supposed to be potassium perchlorate. The solution was filtered off into a 30 mL vial for crystallization

by slow evaporation. Crystals in form of small black blocks were obtained within 4 days. Crystallization was finished after 4 weeks. The crystals were filtered off, washed with ethyl acetate and dried under air for 12 h. Yield (average): 136 mg (18.52%).
Elemental analysis: the substance **4** dried under vacuum for 4 h analyzed as $C_{26}H_{26}N_2O_{12}FeK_1 \bullet 4.5H_2O$: Calc (found) C 43.04 (42.92) H 4.72 (4.63) N 3.86 (3.84) O 35.28 (35.44).
IR bands for **4** dried under vacuum for 4 (cm^{-1}): 416.3 (m), 452.2 (m), 483.8 (vw), 549.6 (m), 591.6 (w), 628.7 (vw), 662.7 (vw), 669.4 (vw), 748.3 (s), 787.3 (m), 813.5 (vw), 852.5 (m), 887.5 (w), 935.7 (w), 975.1 (m), 1077.5 (s), 1108.4 (vw), 1169.3 (w), 1193.3 (w), 1221.7 (s), 1240.7 (s), 1291.2 (s), 1315.4 (vw), 1367.7 (w), 1397.5 (w), 1438.3 (s), 1470.5 (m), 1550.1 (w), 1596.5 (s), 1615.1 (vs), 1730.1 (m), 1981.4 (vw), 2163.0 (vw), 2325.6 (w), 2641.8 (w), , 2939.2 (vw).3412.9 (w).
ESI-MS:
ESI(+) (MeOH or H_2O): Molecular peak was found at *m/z* = 654.00: ($[Fe(OVGlu)_2K+H^+$).
ESI(-) (MeOH or H_2O): Molecular peak was found at *m/z* = 614.08: $[Fe(OVGlu)_2]^-$
Further identified peaks are presented in the Supporting Information.

Physicochemical measurements

Elemental analyses were carried out on an Elementar Vario Microcube elemental analyzer in CHNS mode. Oxygen content analysis was carried out on an Elementa rapid OXY Cube elemental analyzer.
IR spectra were recorded using a Bruker Alpha-P Infrared-spectrometer equipped with a Platinum-ATR with a diamond crystal.
^{1}H NMR spectra for **OVGlnHNa$_2$** were recorded in methanol-d_4 with a Bruker DRX 300 MHz spectrometer at room temperature. Chemical shifts were quoted in ppm relative to the residual protons of deuterated solvents.
Electrospray ionization mass spectrometry (ESI-MS) was performed on a Finnigan LTQ-FT spectrometer by Thermo Fischer Scientific in the positive and negative ion mode with solvent as carrier gas.
EPR measurements were performed with a Bruker ESP300E X-band spectrometer. A Varian square wave TE102 resonator was used, equipped with a helium cryostat (Oxford 900). Microwave power was adjusted 6 dB below maximum signal to avoid any saturation broadening. The modulation amplitude was 2.4 mT at 100 kHz modulation frequency. No distortion, broadening or over filtering of EPR signals could be detected. Time constant was set to 655 mS with a sweep time of 167.7 sec for 400 mT scan width.
EDX spectra were recorded with a JEOL JIB-4610F device and a Bruker XFlash 5010 EDX detector. Data analysis was performed using Bruker Esprit 2.1 software.
EPR measurements were performed with a Bruker ESP300E X-band spectrometer. A Varian square wave TE102 resonator was used, equipped with a helium cryostat (Oxford 900). Microwave power was adjusted 6 dB below maximum signal to avoid any saturation broadening. The modulation amplitude was 2.4 mT at 100 kHz modulation frequency. No distortion, broadening or over-filtering of EPR signals could be detected. Time constant was set to 655 mS with a sweep time of 167.7 sec for 400 mT scan width.
X-ray powder diffraction (PXRD) patterns were measured at room temperature using an X'Pert Pro PW 3064/60 diffractometer (PANalytical) operating in Bragg–Brentano geometry with CoK_α radiation. The scans covered 10–110° with a step size of 0.026° in 2θ. The diffracted X-rays were recorded using a PIXel detector. A plate cut from a single crystal of silicon served as a sample holder which rotated during measurement. Simulation of the theoretical patterns from CIF-files and comparison with the experimental patterns were carried out employing the X'Pert Plus software.

X-ray crystallography

1, 3: X-ray diffraction data was collected with a STOE STADIVARI diffractometer equipped with CuKα radiation (γ = 1.54178 Å), a graded multilayer mirror monochromator and a DECTRIS PILATUS 300K detector using oil-coated shock-cooled crystals at 100(2) K. Absorption effects were corrected semi-empirical using multi-scanned reflexions (X-Area Integrate 1.71.0.0 (STOE, 2016) X-Area LANA

1.68.2.0 (STOE, 2016)). All structures were solved by direct methods by using the program XT V2014/1 (Bruker AXS Inc., 2014) and refined by full matrix least squares procedures on F^2 using SHELXL-2017/1 (Sheldrick, 2017). The non-hydrogen atoms were refined anisotropically, carbon bonded hydrogen atoms were included at calculated positions and refined using the 'riding model' with isotropic temperature factors at 1.2 times (for CH_3 groups 1.5 times) that of the preceding carbon atom. CH_3 groups were allowed to rotate about the bond to their next atom to fit the electron density. Nitrogen-bonded hydrogen atoms were located and allowed to refine isotropically, oxygen bonded hydrogen atoms were not located and not included into the refinement. Disorder of the carboxylate group of 1 was refined using restraints for the geometry and the displacement parameters. Occupancies of disordered solvent water were fixed in the range 0.25 to 0.75. Mixed occupancies (O/Na) was introduced into the refinement of 1.
2: X-ray diffraction data was collected with a Bruker D8 QUEST area detector diffractometer equipped with with MoKα radiation, a graded multilayer mirror monochromator (λ = 0.71073 Å) and a PHOTON-100 CMOS detector using an oil-coated shock-cooled crystal at 110(2) K. Absorption effects were corrected semi-empirical using multi-scanned reflexions (SADABS (Bruker AXS Inc., 2015)). Cell constants were refined using 9704 of observed reflections of the data collection. The structure was solved by direct methods by using the program XT V2014/1 (Bruker AXS Inc., 2014) and refined by full matrix least squares procedures on F^2 using SHELXL-2017/1 (Sheldrick, 2017). The non-hydrogen atoms have been refined anisotropically, carbon bonded hydrogen atoms were included at calculated positions and refined using the 'riding model' with isotropic temperature factors at 1.2 times (for CH_3 groups 1.5 times) that of the preceding carbon atom. CH_3 groups were allowed to rotate about the bond to their next atom to fit the electron density. Nitrogen or oxygen bonded hydrogen atoms also were calculated. NH_2 and H_2O were refined as rigid groups. The structure was twinned according to twin matrix (-1 0 0 0 -1 0 1 0 1 2) with ratio 70/30. Disorder of a side chain was refined with restraints for both the geometry and the displacement parameters.
4: Problems with super-structure effects which could not be resolved were faced, therefore crystallographic data for **4** is not presented.

Results and discussion

Synthesis and characterization

Ligand OVGlnHNa$_2$

Although the synthesis of the ligand was described in literature before, it was never fully characterized[18,19]. The title ligand **OVGlnHNa$_2$** (Fig. 1) was synthesized according to the procedure reported for the system *ortho*-vanillin/*L*-tyrosine[31]. The formation of a disodium salt was confirmed by elemental analysis (see SI for more information). The ESI(+) mass spectrum, recorded in methanol, shows the molecular peak for **OVGlnHNa$_2$** at *m/z* = 325.07 ($[OVGlnHNa_2+H^+]^+$, while the peak with the highest intensity at *m/z* = 303.09 could be identified as $[OVGlnH_2Na+H^+]^+$. The ESI(-) spectrum did not show the molecular peak for **OVGlnHNa$_2$**, however, the peak with the highest intensity at *m/z* = 279.09 could be identified as $[OVGlnH_2]^-$. The ^{1}HNMR spectrum in MeOD shows all of the expected signals and the integrals are in the expected range, except for the proton from the phenolic –OH group and the proton from the terminal amine group, which is due to a fast exchange with the solvent. The NMR spectrum also shows residues of diethyl ether, which could not be removed completely. The spectrum also contains signals from *ortho*-vanillin. Either residues of *ortho*-vanillin could not be removed even due to exhaustive washing with diethyl ether or the amount of water within the NMR-solvent is high enough to decompose the ligand. The latter would be consistent with the findings for the ligands derived from *ortho*-vanillin and *L*-tyrosine/*L*-glutamic acid and would explain the increased integral of 5.16 for the multiplet from 2.11 ppm to 2.32 ppm instead of the expected 4 (Fig S3). The ^{1}HNMR spectrum recorded in D_2O (Fig. S4) shows a significant decomposition of the ligand in its starting materials.

This is in accordance with the observed decomposition in water for the systems containing *L*-tyrosine/*L*-glutamic acid.

L-glutamine–based iron complexes

Crystals were obtained from a system where the organic ligand **OVGlnHNa$_2$** was generated *in situ* by applying sodium acetate as base in case of **1** and potassium acetate in case of **2**. At the end of the synthesis sodium azide or potassium azide were added, respectively. This is crucial for the formation of proper quality crystals, even though there were no azide ions observable in the crystal structures. During the preparation of **2** within hours after the reaction the solution cooled down to RT, a colourless solid appeared. This solid is slightly soluble potassium perchlorate and must be removed by filtration. Further precipitation of potassium perchlorate is also observed during solvent evaporation and it needs to be removed at this stage too. The choice of the metal salt is significant for successful crystal growth. Use of $FeCl_3$ did not lead to crystal growth. The presence of the weak coordinating anion ClO_4^- seems to play a functional role. Crystallization led to large crystals for both compounds. Interestingly it is possible to grow very large crystals of **1** with a size up to 14 × 5 × 3 mm (Fig. 2). The humid crystals are black and shiny, but when getting dry, the surface color turns to matt brown for **1** or matt black-brown for **2**. EDX data reveal a Na:Fe ratio of 47.92%:52.08% for **1** (Fig. S10) and a K:Fe ratio of 55.94%:44.06% for **2** (Fig. S17), which is close to an equimolar ratio. Elemental analyses data support these results and are consistent with the crystallographic results, indicating the presence of a single counter alkali metal ion per complex molecule. **1** and **2** dissolve very well in polar solvents, e. g. water , methanol and DMSO. In acetonitrile **2** possesses a higher solubility compared to **1**, so that it is necessary to wash the received crystals with ethyl acetate to avoid dilution and decrease of the yield. **1** and **2** display under ESI-MS conditions in methanolic solution, as well as in water, intensive peaks at *m/z* = 690.04, 674.07, 658.10 and 652.09 in positive mode with varying intensities and a less intensive peak at 636.11. The molecular peak for **1** was identified at *m/z* = 636.11 ($[Fe(OVGln)_2]Na+H^+$) and for **2** at *m/z* = 652.09 ($[Fe(OVGln)_2]K+H^+$). The remaining peaks are identified as the iron complex with varying composition and a number of potassium and sodium ions (see supporting information). Due to the ubiquitous presence of alkali metal ions, an exchange of the counter-ions is not unusual. In literature different examples are described where the affinity for coordination to alkali metal ions investigated by mass spectrometry is depending on the nature of the coordinating compound [32–34]. In negative mode in both solvents one intensive peak is visible at *m/z* = 612.12, which can be identified as $[Fe(OVGln)_2]^-$. Furthermore, the spectra show an identical fragmentation pattern with fragment peaks at *m/z* = 289.03, 321.05 and 333.02 (see supporting information). The ESI-MS results indicate the stability of **1** and **2** in polar solvents even under harsh ESI-MS conditions. Furthermore, a coordination mode of the ligand molecules like presented in Figure 3 is probable. At one hand, this mode is typical for the N_2O_4 coordination scheme. At the other hand, this assumption will be underpinned through IR spectra of the ligand and the corresponding complexes (Fig. 4A). The intensive band at 1208 cm^{-1}, which can be identified as the C-O vibration of the phenol group, is absent in the spectra of the complexes. Instead of those, two bands at 1221 cm^{-1} and 1243 cm^{-1} for the complex **1** and 1223 cm^{-1} and 1224 cm^{-1} for the complex **2** with almost the same intensity are visible. The appearance of two bands could be supposable explained by a distorted octahedral environment. Due to the paramagnetic nature of the complex, NMR studies were not possible for further confirmation of the stability in solution. Over months, no optical changes in shape or color of the crystals could be observed and IR-spectra of identical samples, measured in an interval of several months, showed no changes (Fig. S11+12 and S18+S19) so that we conclude that both compounds are stable in solid form too.

L-glutamic acid–based iron complexes

Crystals were obtained from a system where the organic ligand **OVGluHNa$_2$** (Fig. 1) was generated *in situ* by applying sodium acetate as base in case of **3** and potassium acetate in case of **4**. Synthesis of the ligand was already reported [30]. The use of iron(III)

perchlorate is again crucial for the crystal growth. These compounds crystallize without an addition of azide source. Similarly as reported above, during the preparation of **4** also within hours after the reaction and cooling down of the solution to RT, during solvent evaporation, a colourless solid appears. This solid is slightly soluble potassium perchlorate and must be removed by filtration. Crystals of **3** and for **4** are black and shiny, even after drying. The obtained crystals can have size up to 2 mm. EDX data reveal an Na:Fe ratio of 47.71%:52.29% for **3** (Fig. S24) and a K:Fe ratio of 47.67%:52.33% for **4** (Fig. S31), which is close to an equimolar ratio. The results are supported with the elemental analyses data and are consistent with the crystallographic results indicating the presence of a single alkali metal counterion for the glutamic acid based-compounds as well as for the glutamine-based compounds. Similar to the *L*-glutamine-based complexes, **3** and **4** dissolve very well in polar solvents and **4** possesses a higher solubility in acetonitrile than **3**. Under ESI-MS conditions in methanolic solution in positive mode **3** displays intensive peaks at *m/z* = 682.05, 660.06, and 638.05 which can be identified as the molecular peak at *m/z* = 638.08 ($[Fe(OVGlu)_2]Na+H^+$) and the analogues with two and three sodium ions. A corresponding potassium species is only detectable in water at *m/z* = 676.05 (see supporting information). For **4** the molecular peak in both solvents in positive mode is identified at *m/z* = 654.05 ($[Fe(OVGlu)_2K]+H^+$). The remaining peaks are identified as the iron complex with varying composition and a number of potassium and sodium ions. Additionally, several fragments could be identified below *m/z* = 400. In negative mode in both solvents for compound **3** and **4** one intensive peak is visible at *m/z* = 614.08 which can be identified as $[Fe(OVGlu_2]^-$. Fragments can be found below *m/z* = 400 (see supporting information). Similar to the L-glutamine based compounds a coordination mode shown in Figure 3 is supported by the available data and literature. The IR spectra support this assumption in the same manner like for the complexes **1** and **2**. The phenolic C-O vibration for the ligand appears at 1253 cm^{-1}. The spectra of the complexes show similar shaped bands like for **1** and **2** at 1222 cm^{-1} and 1241 cm^{-1} for both **3** and **4**, respectively (Fig. 4B). Due to the paramagnetic nature of the complexes NMR studies were not possible for further confirmation of their stability in solution. Over months, no optical changes in shape or color of the crystals could be observed and IR-spectra of identical samples, measured in an interval of several months, showed no changes (Fig. S24+25 and S32+S33) so that we conclude that both compounds are stable in solid form too.

EPR studies

Figure 5 depicts the high spin S=5/2 EPR spectra of **1** with the typical features suggesting zero field splitting much larger than the $h \cdot \nu$ value at X band (9.18 GHz). The powder (black line) shows the usual broadening due to intermolecular magnetic interactions of the neighboring molecules. These effects are not present for the frozen solution, which permits the determination of two distinct g_{eff} values. The g_z value around g=2.00 is not visible probably because of the extended angle dependent broadening. All investigated substances show very similar EPR spectra. Only small deviations in line width are noticeable. From the two low-field g_{eff} values it is possible to estimate the rhombicity (η=E/D), using the methods given by W.R. Hagen et al., to $\eta \sim 0.2$[35].

PXRD studies

The PXRD patterns of the bulk material for the complexes **1**–**4**, displayed in Figure 6, show similar patterns indicating that compounds **1**, **3** and **4** are isostructural. The fitted patterns derived from CIF-files match very well with the empirical patterns. The absence of significant additional reflections of potential impurities proves the phase purity of the synthesized compounds. The pattern for complex **2** is different from the other patterns, suggesting a structural difference. Unfortunately, it was not possible to fit the calculated pattern from the CIF-file to the empirical pattern with the available software. Therefore, we cannot draw any conclusion about the purity of complex **2**.

Crystal structures

Crystallographic data obtained for **1**-**3** are consistent with the analytical data for the bulk material and for the single crystals investigated with EDX. For **4** superstructure effects did not allow to determine the crystal structure.
The anionic complexes **1**-**3** are mononuclear (Figure 7) with distorted octahedral coordination environment of the central Fe atom (see Tables 2-4 for the selected bond lengths and bond angles). The observed bond lengths around the iron center range from 2.087-2.105 Å for Fe-N, 1.915-1.952 Å for Fe-O(hydroxo) and 2.029-2.069 Å for Fe-O(carboxyl). These results are consistent with the values for prior published iron complexes with an N_2O_4 coordination scheme and Schiff Base ligands, containing an amino acid and a hydroxylated aromatic aldehyde ligand (2.075-2.138 Å for Fe-N, 1.890-1.938 Å for Fe-O(hydroxo), 2.022-2.101 Å for Fe-O(carboxyl))[6–10,36].
1 and **3** are isostructural but differ in the organic ligand amino acid moiety which is glutamine in the case of **1** and glutamic acid in the case of **3**. Complex anions in **1**, **3** lie in special positions at a two-fold symmetry axis through the central Fe atom, resulting in an asymmetric unit which contains a half complex anion and the sodium ion with an occupancy of 0.5 (Fig. S34). Each central Fe atom is chelated by two organic ligands through their carboxyl and hydroxo O atoms and imine N. The methoxo group from the *ortho*-vanilin moiety and the side chain from the amino acid part remain pendant. O atoms from the pendant terminal carbonyl groups from two independent anions coordinate the sodium counter-ions and thus chains are formed along the *c* axis. The coordination sphere of each sodium cation is further saturated with disordered water molecules. In **3**, contrary to **1**, the amino acid carboxyl group is disordered in two positions, sodium cations are highly disordered and seem to be positionally disordered with water molecules. Furthermore, the packing diagram (Fig. S34) reveals formation of channels along the *c* axis. The channels with a three-fold screw axis are formed through helical arrangement of the complex anions. Inside the channels the sodium ions are located. The phenomenon of delocalisation of alkali metal ions in channels was observed for iron complexes before [37–40].
In **2** the anions are analogous to those in **1** and **2**, but the amino acid moiety in one of the constituent organic ligand molecules is disordered in two positions differing with respect to the ethylene moiety location. Potassium counter-ions form a dimeric assembly in the asymmetric unit through K-O coordination bonds (Fig. S35). One potassium ion is coordinated by two carboxylate moieties from one complex anion, the amide group of the second complex anion and three water molecules. In coordination sphere of the second potassium ion the phenolate and the methoxy group from one ligand molecule and the amide group of the same complex anion are involved. Two water molecules and a carboxylate group of the second complex anion complete the coordination sphere. The amide group and one of the water molecules bridge both potassium ions. Thus, chains extending along the *c* direction are created.
The received X-ray diffraction datasets for **4** were of poor quality and additional superstructure effects did not allow to determine a meaningful crystal structure. In particular, the refinement of the potassium counter-ion was problematic. However, based on the analytical data and the empirical powder pattern with appearance similar to **1** and **3**, it can be supposed that **4** possesses the same structure like **1** and **3**.

Conclusions

In summary, the synthesis and full characterization of a Schiff base ligand, derived from *ortho*-vanillin and *L*-glutamine as a disodium salt was presented. With this ligand and another L-glutamic acid-based ligand, four new mononuclear anionic iron(III) complexes, with potassium or sodium as counter-ion, were synthesized and characterized, three of them with a crystal structure. The metal centers of the complex anions are complexed by two ligand molecules and possess a distorted octahedral geometry of their coordination sphere. The side chains of the ligands remain pendant. The arrangement of the complex anions is driven by the amino acid side chain and the nature of the counter-ion. The presented mononuclear complexes could be useful precursors for the generation of complexes with higher nuclearity under basic conditions or with addition of further equivalents of *ortho*-vanillin, like it was described for other iron(III) complexes before[8,41]. Variation of the incorporated metallic counter-ions

could allow for the synthesis of new heterometallic complexes with new properties, not necessarily only with single charged metal ions, e. g. gold, silver or thallium, as indicated by our preliminary studies. Therefore the uncoordinated methoxy group at the aromatic moiety could play a key role in further reactivity of the precursor complexes.

Notes and references

[1] I. Kubo, I. Kinst-Hori, Tyrosinase Inhibitory Activity of the Olive Oil Flavor Compounds, J. Agric. Food Chem. 47 (11) (1999) 4574–4578.

[2] K. Watanabe, T. Ohta, Y. Shirasu, Enhancement and inhibition of mutation by o-vanillin in Escherichia coli, Mutation research 218 (2) (1989) 105–109.

[3] K. Takahashi, M. Sekiguchi, Y. Kawazoe, A specific inhibition of induction of adaptive response by o-vanillin, a potent comutagen, Biochemical and biophysical research communications 162 (3) (1989) 1376–1381.

[4] J.H. Kim, H.-O. Lee, Y.-J. Cho, J. Kim, J. Chun, J. Choi, Y. Lee, W.H. Jung, A vanillin derivative causes mitochondrial dysfunction and triggers oxidative stress in Cryptococcus neoformans, PloS one 9 (2) (2014) e89122.

[5] A. Hannemann, U.M.C. Cytlak, O.T. Gbotosho, D.C. Rees, S. Tewari, J.S. Gibson, Effects of o-vanillin on K(+) transport of red blood cells from patients with sickle cell disease, Blood cells, molecules & diseases 53 (1-2) (2014) 21–26.

[6] R. Hämäläinen, U. Turpeinen, M.S. Lehmann, M. Sjöström, S. Wold, E. Colacio, A.M. Mulichak, T. Alminger, M. Erickson, I. Grundevik, I. Hagin, K.-J. Hoffman, S. Johansson, S. Larsson, I. Löfberg, K. Ohlson, B. Persson, I. Skånberg, L. Tekenbergs-Hjelte, The Structure, Thermal and Magnetic Properties of Hexaaquairon(II) bis[bis(N-salicylideneglycinato)ferrate(III)] Dihydrate, Acta Chem. Scand. 43 (1989) 15–18.

[7] J. Han, Y.H. Xing, F.Y. Bai, X.J. Zhang, X.Q. Zeng, M.F. Ge, Synthesis and characterization of three ionic pairs of Fe(II) and Co(II) complexes with tridentate salicylideneglycine, Journal of Coordination Chemistry 62 (16) (2009) 2719–2727.

[8] G.-l. Liu, S.-f. He, S. Zhang, H. Li, In situ ligand and complex transformation of an iron(III) Schiff base complex: structural evidence and theoretical calculations, Dalton Trans. 41 (20) (2012) 6256–6262.

[9] Mohammed S. Ameerunisha Begum, Sounik Saha, Munirath Nethaj, Akhil R. Chakravartyi, Synthesis, crystal structures and protease activity of amino acid Schiff base iron(III) complexes, Indian J.Chem., Sect.A:Inorg., Bio-inorg., Phys., Theor. Anal. Chem. (48A) (2009) 473–479.

[10] M.S. Ameerunisha Begum, S. Saha, M. Nethaji, A.R. Chakravarty, Iron(III) Schiff base complexes of arginine and lysine as netropsin mimics showing AT-selective DNA binding and photonuclease activity, Journal of inorganic biochemistry 104 (4) (2010) 477–484.

[11] C. Zheng, R. Shi, X. Jin, Q. Qiu, H. Li, Three complexes with helical frameworks based on l-glutamine and l-asparagine: Crystal structures and circular dichroism properties, Inorganic Chemistry Communications 65 (2016) 16–20.

[12] A.K. Patra, S. Roy, A.R. Chakravarty, Synthesis, crystal structures, DNA binding and cleavage activity of l-glutamine copper(II) complexes of heterocyclic bases, Inorganica Chimica Acta 362 (5) (2009) 1591–1599.

[13] J.M. Schveigkardt, A.C. Rizzi, O.E. Piro, E.E. Castellano, R.C.d. Santana, R. Calvo, C.D. Brondino, Structural and Single Crystal EPR Studies of the Complex Copper L-Glutamine: A Weakly Exchange-Coupled System with syn-anti Carboxylate Bridges, Eur. J. Inorg. Chem. 2002 (11) (2002) 2913–2919.

[14] G. Lusvardi, L. Menabue, M. Saladini, Cadmium(II) N-(p-Tolylsulfonyl)glutaminate, Acta Crystallogr C Cryst Struct Commun 51 (11) (1995) 2287–2289.

[15] S. Brückner, L. Menabue, M. Saladini, M. Tolazzi, Coordination behaviour of Ar-SO2-N-amino acids toward the Mn(II) ion. Crystal and molecular structure of [Mn(tsgln)2] and [Mn(tS-DL-α-ala)2(H2O)]·2.78H2O·0.92CH3OH, Inorganica Chimica Acta 214 (1-2) (1993) 185–191.

[16] G. Lusvardi, L. Menabue, M. Saladini, Coordination properties of sulfonyl-N-aminoacids: Crystal and molecular structure of the [Zn(II) (N-(p-toluenesulfonyl)-L-glutaminate)2(H2O)2] complex, J Chem Crystallogr 25 (11) (1995) 713–716.

[17] Q. Wei, J. Dong, P. Zhao, M. Li, F. Cheng, J. Kong, L. Li, DNA binding, BSA interaction and SOD activity of two new nickel(II) complexes with glutamine Schiff base ligands, Journal of photochemistry and photobiology. B, Biology 161 (2016) 355–367.
[18] M. Sivasankaran Nair, S. Suda Kumari, M.A. Neelakantan, Studies on some novel Schiff-base complexes in solution and solid state, Journal of Coordination Chemistry 60 (12) (2007) 1291–1302.
[19] Y. Xiao, C. Bi, Y. Fan, S. Liu, X. Zhang, D. Zhang, Y. Wang, R. Zhu, Synthesis, characterization and bioactivity of Schiff base copper(II) complexes derived from L -glutamine and L -asparagine, Journal of Coordination Chemistry 62 (18) (2009) 3029–3039.
[20] Yan Xiao, Caifeng Bi, Yuhua Fan, Cindy Cui, Xia Zhang, Q. Ping Dou, L-glutamine Schiff base copper complex as a proteasome inhibitor and an apoptosis inducer in human cancer cells, int J Oncol 33 (2008) 1073–1079.
[21] J. Krätsmár-Šmogrovič, F. Pavelčik, J. Soldánová, J. Sivýa, V. Seressová, and M. Žemlička, The Crystal and Molecular Structure and Properties of Diaqua[N-salicylidene—(S)—(+)—glutamato]copper(II) Monohydrate, Zeitschrift für Naturforschung B 46 (1991) 1323–1327.
[22] V. Langer, D. Gyepesova, M. Kohutova, A. Valent, Dimeric (isoquinoline)(N-salicylidene-D,L-glutamato)copper(II) ethanol solvate, Acta crystallographica. Section C, Crystal structure communications 65 (Pt 5) (2009) m208-10.
[23] V. Langer, E. Scholtzová, D. Gyepesová, M. Kohútová, A. Valent, (1-Methylimidazole)(N -salicylidene-rac -glutamato)copper(II), Acta Crystallogr E Struct Rep Online 59 (12) (2003) m1181-m1183.
[24] V. Langer, E. Scholtzová, D. Gyepesová, M. Kohútová, A. Valent, (N -Salicylidene- D L -glutamato)(2-methylimidazole)copper(II), Acta Crystallogr E Struct Rep Online 60 (1) (2004) m129-m132.
[25] V. Langer, P. Mach, D. Gyepesova, L. Andrezalova, M. Kohutova, X-ray and DFT studies of a mono- and binuclear copper(II) ionic compound containing a Schiff base, Acta crystallographica. Section C, Crystal structure communications 68 (Pt 11) (2012) m326-8.
[26] X. Feng, C.-Z. Xie, L.-Y. Wang, Y.-F. Wang, L.-F. Ma, Synthesis and Crystal Structures of Ternary Copper(II) Complex Containing Salicylaldehyde Schiff Base and 4,4′-Bipyridine, J Chem Crystallogr 38 (8) (2008) 619–624.
[27] K. Korhonen, R. Hämäläinen, U. Turpeinen, Structure of catena-tetraaqua-di-μ3-(N-salicylidene-DL-glutamato)-tricopper(II) heptahydrate [Cu3(C12H10NO5)2(H2O)4].7H2O, Acta Crystallogr C Cryst Struct Commun 40 (7) (1984) 1175–1177.
[28] S. Muche, I. Levacheva, O. Samsonova, L. Pham, G. Christou, U. Bakowsky, M. Holynska, A chiral, low-cytotoxic Ni15-wheel complex, Inorganic chemistry 53 (14) (2014) 7642–7649.
[29] Y. Thio, S.W. Toh, F. Xue, J.J. Vittal, Self-assembly of a 15-nickel metallamacrocyclic complex derived from the L-glutamic acid Schiff base ligand, Dalton transactions (Cambridge, England 2003) 43 (16) (2014) 5998–6001.
[30] S. Muche, I. Levacheva, O. Samsonova, A. Biernasiuk, A. Malm, R. Lonsdale, Ł. Popiołek, U. Bakowsky, M. Hołyńska, Synthesis, structure and stability of a chiral imine-based Schiff-based ligand derived from L-glutamic acid and its [Cu4] complex, Journal of Molecular Structure 1127 (2017) 231–236.
[31] S. Muche, M. Hołyńska, New insights into the coordination chemistry of Schiff bases derived from amino acids: Planar [Ni 4] complexes with tyrosine side-chains, Journal of Molecular Structure 1142 (2017) 168–174.
[32] J. Kurek, W. Boczoń, P. Przybylski, B. Brzezinski, ESI MS, spectroscopic and PM5 semiempirical studies of Colchicine complexes with lithium, sodium and potassium salts, Journal of Molecular Structure 846 (1-3) (2007) 13–22.
[33] C. Wang, S.H. Yang, J. Wang, P. Kroll, K.A. Schug, D.W. Armstrong, Study of complexation between cyclofructans and alkali metal cations by electrospray ionization mass spectrometry and density functional theory calculations, International Journal of Mass Spectrometry 291 (3) (2010) 118–124.
[34] R. Colton, W. Kläui, Complexes in solution formed by an organometallic tripodal oxygen ligand with monovalent, divalent and trivalent metal ions: An electrospray mass spectrometric study, Inorganica Chimica Acta 211 (2) (1993) 235–242.
[35] W.R. Hagen, Biomolecular EPR spectroscopy, CRC Press, Boca Raton FL., op. 2009.
[36] M.D. Godbole, M.P. Puig, S. Tanase, H. Kooijman, A.L. Spek, E. Bouwman, Iron complexes of chiral phenol-oxazoline ligands: Structural studies and oxidation catalysis, Inorganica Chimica Acta 360 (6) (2007) 1954–1960.

[37] N.A. Bailey, D. Cummins, E.D. McKenzie, J.M. Worthington, The crystal and molecular structure of iron(III) compounds of the sexadentate ligand N,N′-ethylene-bis-(o-hydroxyphenylglycine), Inorganica Chimica Acta 18 (1976) L13-L14.
[38] N.A. Bailey, D. Cummins, E.D. McKenzie, J.M. Worthington, Iron(III) compounds of phenolic ligands. The crystal and molecular structure of iron(III) compounds of the sexadentate ligand N,N′-ethylene-bis-(o-hydroxyphenylglycine), Inorganica Chimica Acta 50 (1981) 111–120.
[39] S.K. Larsen, B.G. Jenkins, N.G. Memon, R.B. Lauffer, Structure-affinity relationships in the binding of unsubstituted iron phenolate complexes to human serum albumin. Molecular structure of iron(III) N, N'-bis(2-hydroxybenzyl)ethylenediamine-N,N'-diacetate, Inorg. Chem. 29 (6) (1990) 1147–1152.
[40] P.E. Riley, V.L. Pecoraro, C.J. Carrano, K.N. Raymond, Siderophilin metal coordination. 3. Crystal structures of the cobalt(III), gallium(III), and copper(II) complexes of ethylenebis[(o-hydroxyphenyl)glycine], Inorg. Chem. 22 (21) (1983) 3096–3103.
[41] A.K. Powell, S.L. Heath, D. Gatteschi, L. Pardi, R. Sessoli, G. Spina, F. Del Giallo, F. Pieralli, Synthesis, Structures, and Magnetic Properties of Fe2, Fe17, and Fe19 Oxo-Bridged Iron Clusters: The Stabilization of High Ground State Spins by Cluster Aggregates, J. Am. Chem. Soc. 117 (9) (1995) 2491–2502.

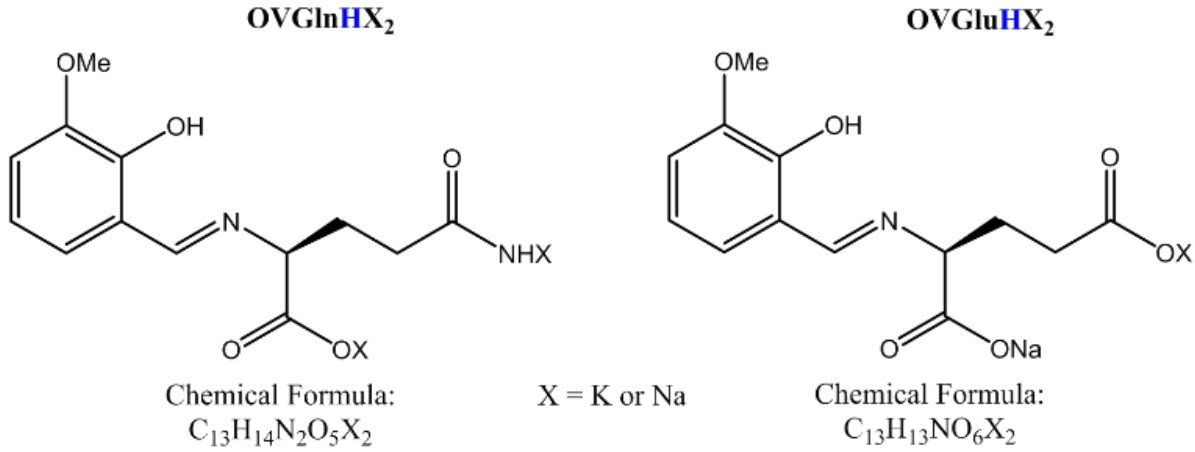

Figure 1. Structural and chemical formula of the ligands as disodium or dipotassium salts **OVGlnHX2** (*ortho*-vanillin + *L*-glutamine) and **OVGluHX2** (*ortho*-vanillin + *L*-glutamic acid).

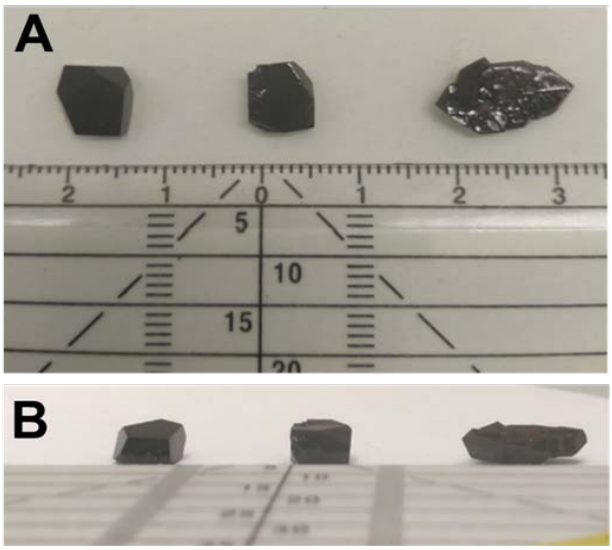

Figure 2. Large size crystals of **(1)** derived from different samples. A) top view; B) side view.

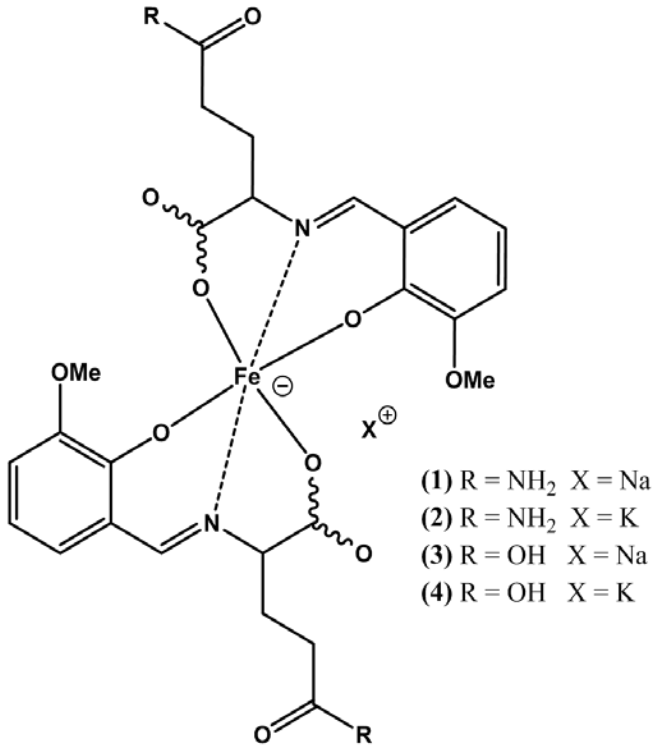

Figure 3. Coordination mode of **OVGlnHX$_2$** and **OVGluHX$_2$** in their corresponding iron complexes **1**-**4** (stereochemistry not shown).

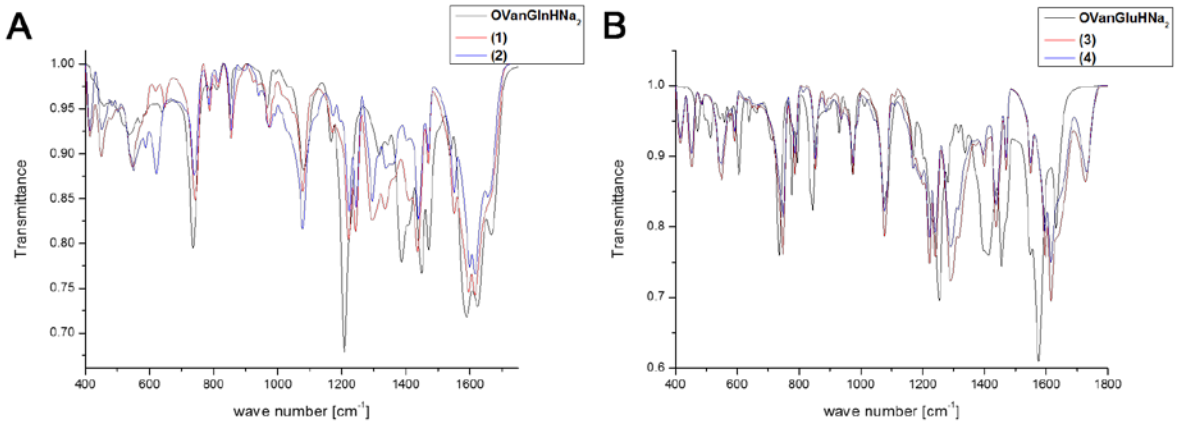

Figure 4: IR spectra of the ligands **OVanGlnHNa$_2$** and **OVanGluHNa$_2$** and their corresponding iron complexes **1** – **4.**

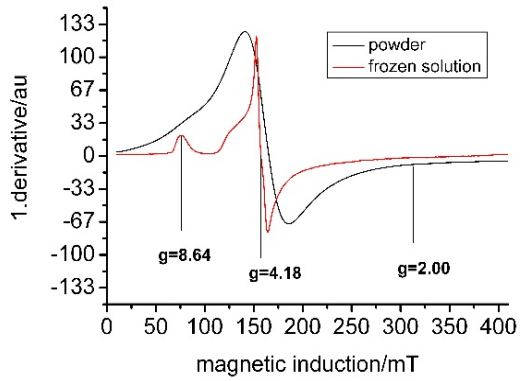

Figure 5.: X band EPR spectrum of **1**. Black: fine ground powder at 4K. Red: shock frozen solution of **1** 1 mmol dissolved in methanol at 4K. EPR-spectra for **2**-**4** are similar.

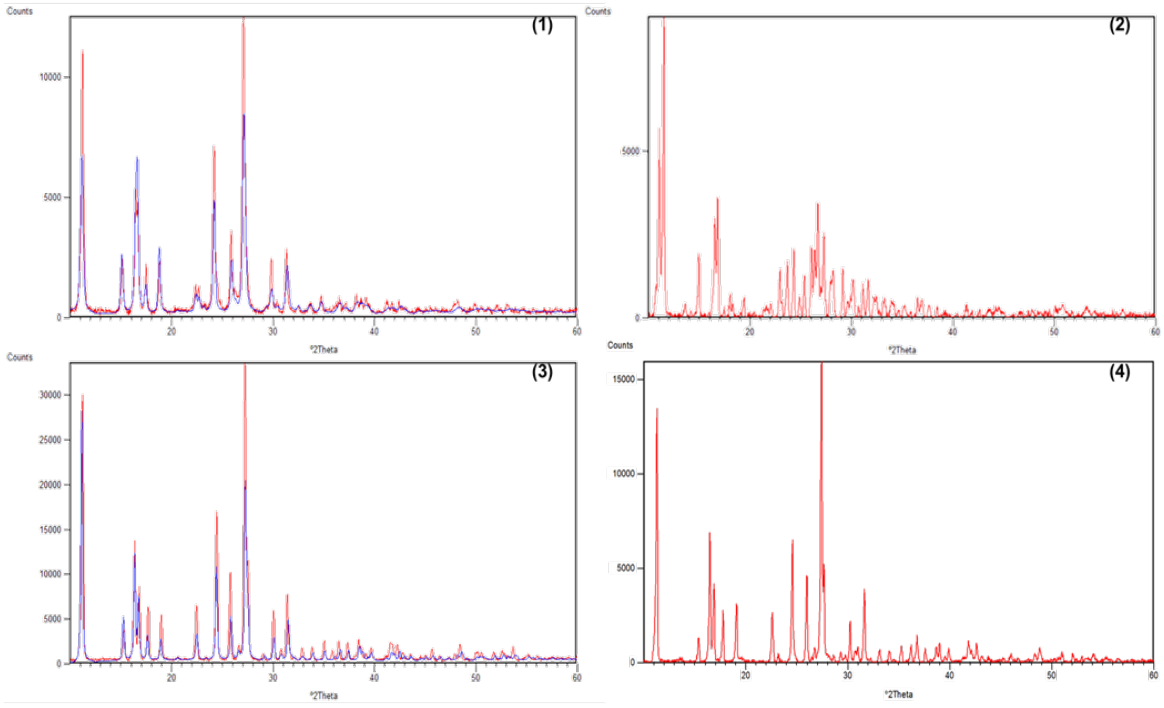

Figure 6.: PXRD patterns of the complexes **1**–**4**. Red line: Measured patterns. Blue line: Fitted patterns derived from CIF-files. Only the region from 10 till 60° 2θ is shown.

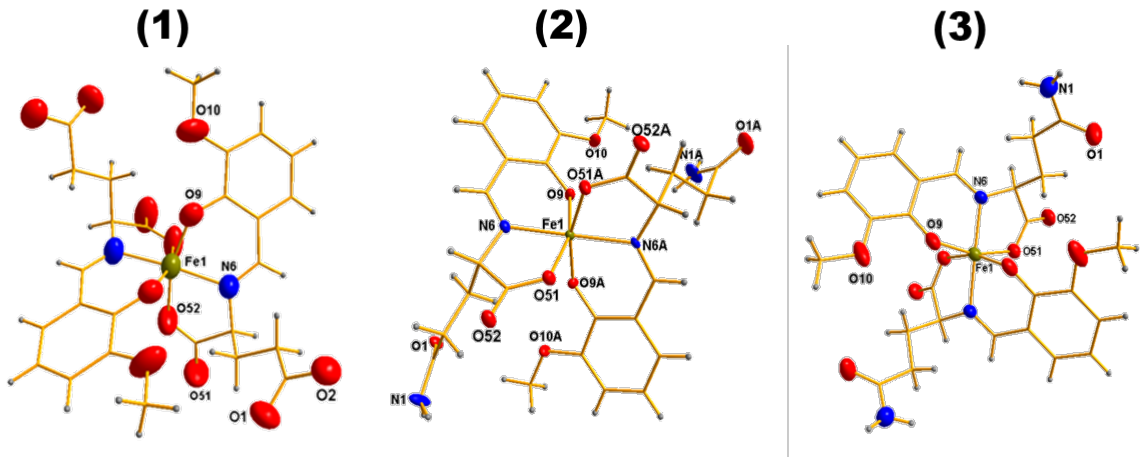

Figure 7: Molecular structures of **1**-**3**. For clarity, solvent molecules and alkali metal atoms, as well as any disordered part, are omitted, whereas C atoms are denoted as sticks. The symmetry-independent part is labelled. Thermal ellipsoids are plotted at 50% probability level.

Table 1. Basic crystallographic data for complexes **1-3**.

	1	**2**	**3**
Empirical formula	$C_{26}H_{40}FeN_4NaO_{16}$	$C_{52}H_{88}Fe_2K_2N_8O_{36}$	$C_{26}H_{36}FeN_2NaO_{17}$
Formula weight	743.46	1591.2	715.31
Temperature/K	100(2)	100(2)	100(2)
Crystal system	Trigonal	Monoclinic	Trigonal
Space group	P3221	P21	P3221
a/Å	a = 13.7445(2)	a = 13.0628(8)	a = 13.4602(2) Å
b/Å	b = 13.7445(2)	b = 21.4644(11)	b = 13.4602(2) Å
c/Å	c = 14.7085(4)	c = 14.1993(8)	c = 14.9215(4) Å
α, β,γ/°	90, 90, 120	90, 117.299(2), 90	90, 90, 120
Volume/Å3	2406.34(10)	3537.9(4)	2341.24(9)
Z, ρcalcg/cm3	3, 1.539	2, 1.494	3, 1.522
μ/mm-1	4.62	0.625	4.742
F(000)	1167	1668	1101
Crystal size/mm3	0.19 × 0.13 × 0.12	0.31 x 0.28 x 0.10	0.10 x 0.07 x 0.07
Radiation/ Å	CuKα (λ = 1.54178)	MoKα (λ = 0.71073)	CuKα (λ = 1.54178)
2Θ range for data collection/°	3.71 to 71.81	2.49 to 28.37	3.79 to 69.65
Data/restraints/parameters	3111 / 60 / 254	17632 / 63 / 939	2937 / 90 / 265
Goodness-of-fit on F2	1.066	1.044	1.036
Final R indexes [I>=2σ (I)]	R = 0.0556, wR = 0.1399	R = 0.0454, wR = 0.1121	R = 0.0524 , wR = 0.1437
Final R indexes [all data]	R = 0.0626, wR = 0.1436	R = 0.0505, wR = 0.1152	R = 0.0684 , wR = 0.1567
Largest diff. peak/hole /e Å-3	0.29, -0.34	0.99, -0.69	0.36, -0.23

Table 2. Selected geometric parameters of **1** [Å, °]. Symmetry operations used to generate equivalent atoms: #1 y,x,-z+1; #2 y,x,-z.

Fe1-O9	1.939(4)	Fe1-O51	2.069(4)	Fe1-N6	2.086(5)
C4-N6	1.479(7)	C1-O1	1.237(8)	C1-N1	1.316(9)
O9#1-Fe1-O9	98.0(3)	O51-Fe1-N6	76.87(17)	O9-Fe1-O51	162.42(17)
O9#1-Fe1-O51	90.42(17)	O51#1-Fe1-N6	92.12(18)	O51-Fe1-O51#1	85.9(2)
O9#1-Fe1-N6	103.80(18)	N6-Fe1-N6#1	165.1(3)	C7-N6-Fe1	124.5(4)
O9-Fe1-N6	86.10(18)	C9-O9-Fe1	125.1(4)	C4-N6-Fe1	113.9(4)
C5-O51-Fe1	119.9(4)				

Table 3. Selected geometric parameters of **2** [Å, °].

Fe1-O9	1.928(4)	Fe1-O51A	2.041(4)	Fe1-N6	2.091(4)
Fe1-O9A	1.930(4)	Fe1-O51	2.061(4)	Fe1-N6A	2.097(4)
Fe2-O9B	1.925(4)	Fe2-O51B	2.029(4)	Fe2-N6B	2.097(5)
Fe2-O9'	1.953(4)	Fe2-O51'	2.030(4)	Fe2-N6'	2.105(5)
N6-C7	1.284(7)	N6'-C7'	1.278(8)	N6A-C7A	1.282(7)
C1-O1	1.233(7)	C1'-O1'	1.263(8)	C1A-O1A	1.235(8)

C1-N1	1.352(7)	C1'-N1'	1.340(9)	C1A-N1A	1.338(9)
C1B-O1B	1.236(8)	C1B-N1B	1.312(9)		
O9-Fe1-O9A	95.11(17)	O9A-Fe1-O51A	161.25(16)	O9A-Fe1-O51	90.17(16)
O9-Fe1-O51A	94.65(18)	O9-Fe1-O51	161.77(16)	O51A-Fe1-O51	85.49(17)
O9-Fe1-N6	85.31(17)	O51A-Fe1-N6	97.83(17)	O9-Fe1-N6A	99.63(17)
O9A-Fe1-N6	98.88(17)	O51-Fe1-N6	76.62(17)	O9A-Fe1-N6A	85.95(16)
O51A-Fe1-N6A	76.66(17)	O51-Fe1-N6A	98.14(17)	N6-Fe1-N6A	172.80(18)
O9B-Fe2-O9'	91.10(16)	O51B-Fe2-O51'	89.7(2)	O9B-Fe2-N6'	105.48(18)
O9B-Fe2-O51B	164.57(19)	O9B-Fe2-N6B	87.04(18)	O9'-Fe2-N6'	84.62(17)
O9'-Fe2-O51B	91.53(18)	O9'-Fe2-N6B	101.25(18)	O51B-Fe2-N6'	89.9(2)
O9B-Fe2-O51'	92.43(18)	O51B-Fe2-N6B	77.5(2)	O51'-Fe2-N6'	77.73(19)
O9'-Fe2-O51'	162.31(19)	O51'-Fe2-N6B	96.2(2)	N6B-Fe2-N6'	166.18(19)
C7-N6-Fe1	126.1(4)	C4-N6-Fe1	114.4(3)	C5-O51-Fe1	119.7(3)
C7'-N6'-Fe2	123.5(4)	C4'-N6'-Fe2	113.3(4)	C5'-O51'-Fe2	119.7(4)
C7A-N6A-Fe1	124.4(3)	C4A-N6A-Fe1	113.8(3)	C5B-O51B-Fe2	120.4(4)
C7B-N6B-Fe2	125.4(4)	C4B-N6B-Fe2	114.7(5)	C5A-O51A-Fe1	120.6(4)
C9-O9-Fe1	129.6(4)	C9'-O9'-Fe2	124.7(3)	C9A-O9A-Fe1	127.3(3)
C9B-O9B-Fe2	129.2(4)				

Table 4. Selected geometric parameters of **3** [Å, °]. Symmetry operations used to generate equivalent atoms: #1 y,x,-z+1; #2 y,x,-z; #3 x-y,-y,-z+1/3; #4 -x,-x+y,-z+2/3.

Fe1-O9	1.916(4)	Fe1-O52	2.066(5)	Fe1-N6	2.089(4)
N6-C7	1.286(7)	C1-O1	1.198(10)	C1-O2	1.305(9)
C1-O2A	1.607(19)	C1-O1A	1.35(3)		
O9#1-Fe1-O9	96.4(3)	O9#1-Fe1-O52	91.7(2)	O9-Fe1-O52	162.46(16)
O52-Fe1-O52#1	84.8(3)	O9#1-Fe1-N6	102.31(19)	O9-Fe1-N6	86.46(17)
O52-Fe1-N6	76.63(16)	O52#1-Fe1-N6	93.6(2)	O9#1-Fe1-N6#1	86.46(17)
O9-Fe1-N6#1	102.32(19)	N6-Fe1-N6#1	166.9(3)	C7-N6-Fe1	125.0(4)
C4-N6-Fe1	113.3(4)	C5-O52-Fe1	119.3(4)	C9-O9-Fe1	126.8(4)

A gap is filled: First structures of enantiopure iron(III) complexes with Schiff base ligands derived from *ortho*-vanillin and *L*-glutamine or *L*-glutamic acid†

Simon Muche[a], *Klaus Harms*[a], *Olaf Burghaus*[a], *Małgorzata Hołyńska*[a]*

[a] Fachbereich Chemie and Wissenschaftliches Zentrum für Materialwissenschaften, Philipps-Universität Marburg, Hans-Meerwein-Strasse, D-35043 Marburg, Germany. E-Mail: holynska@staff.uni-marburg.de

SUPPORTING INFORMATION

1. Analytical data

Fitting of the elemental analysis data

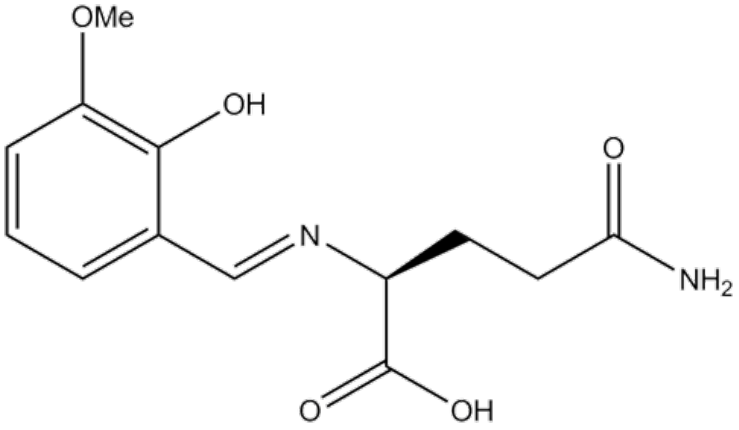

Chemical Formula: $C_{13}H_{16}N_2O_5$

Elemental Analysis: C, 55.71; H, 5.75; N, 10.00; O, 28.54

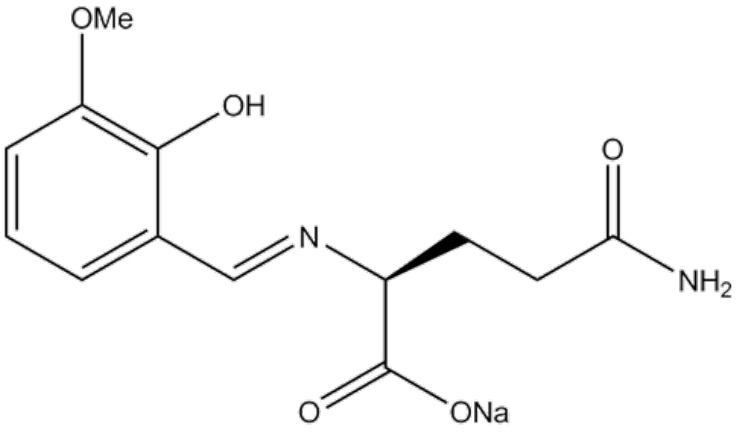

Chemical Formula: $C_{13}H_{15}N_2NaO_5$

Elemental Analysis: C, 51.66; H, 5.00; N, 9.27; Na, 7.61; O, 26.47

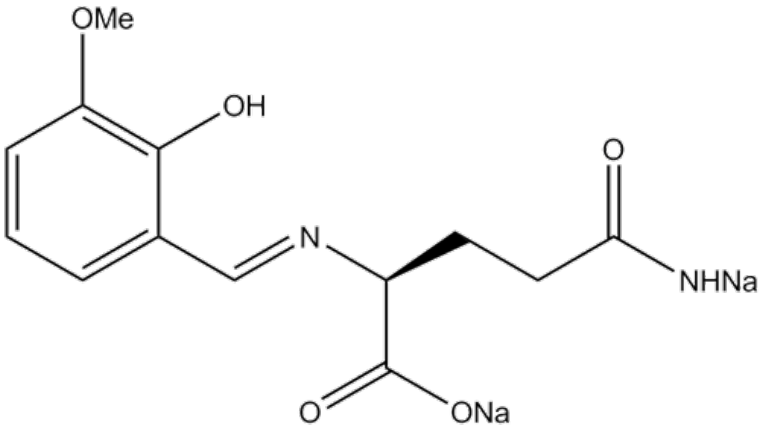

Chemical Formula: $C_{13}H_{14}N_2Na_2O_5$

Elemental Analysis: C, 48.16; H, 4.35; N, 8.64; Na, 14.18; O, 24.67

2. Supplementary figures

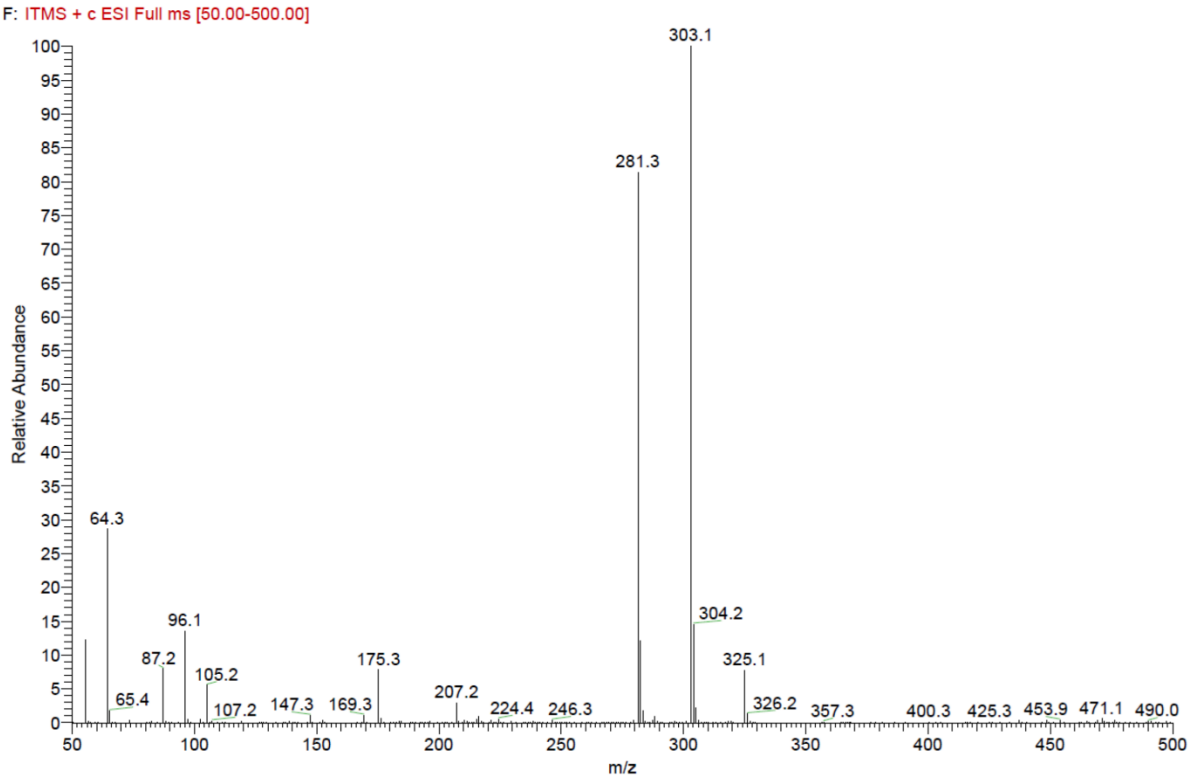

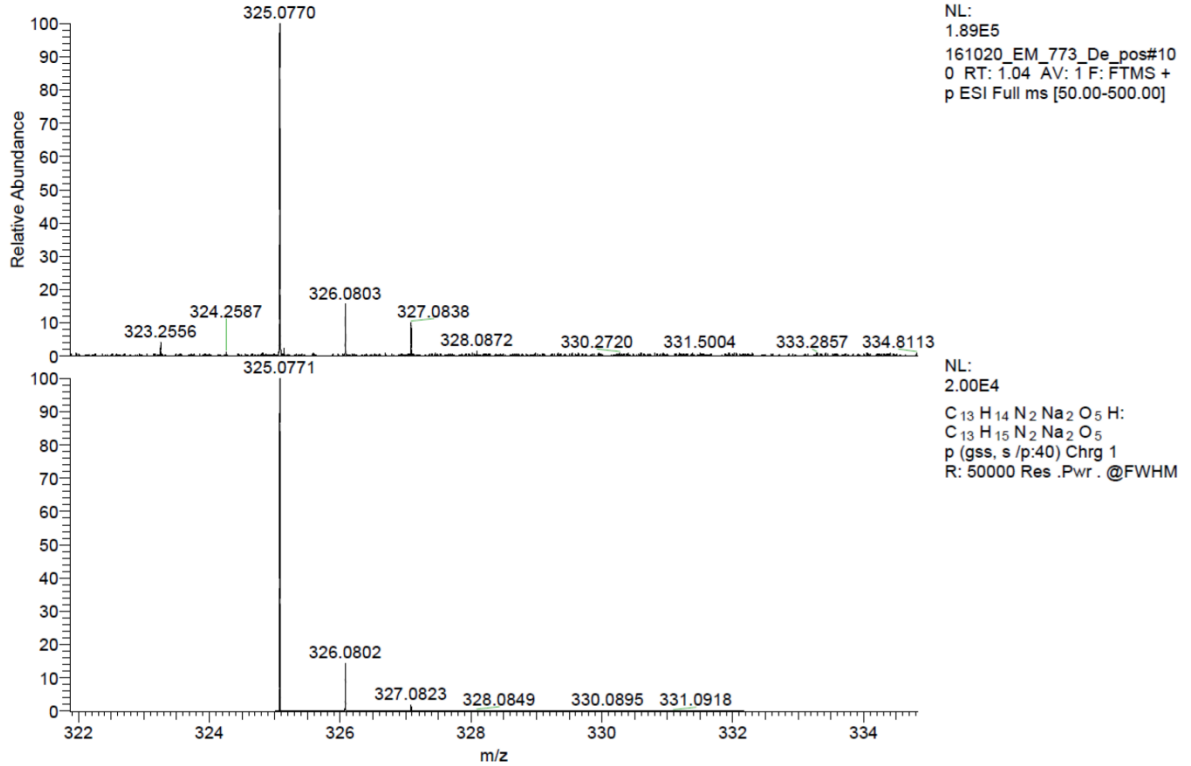

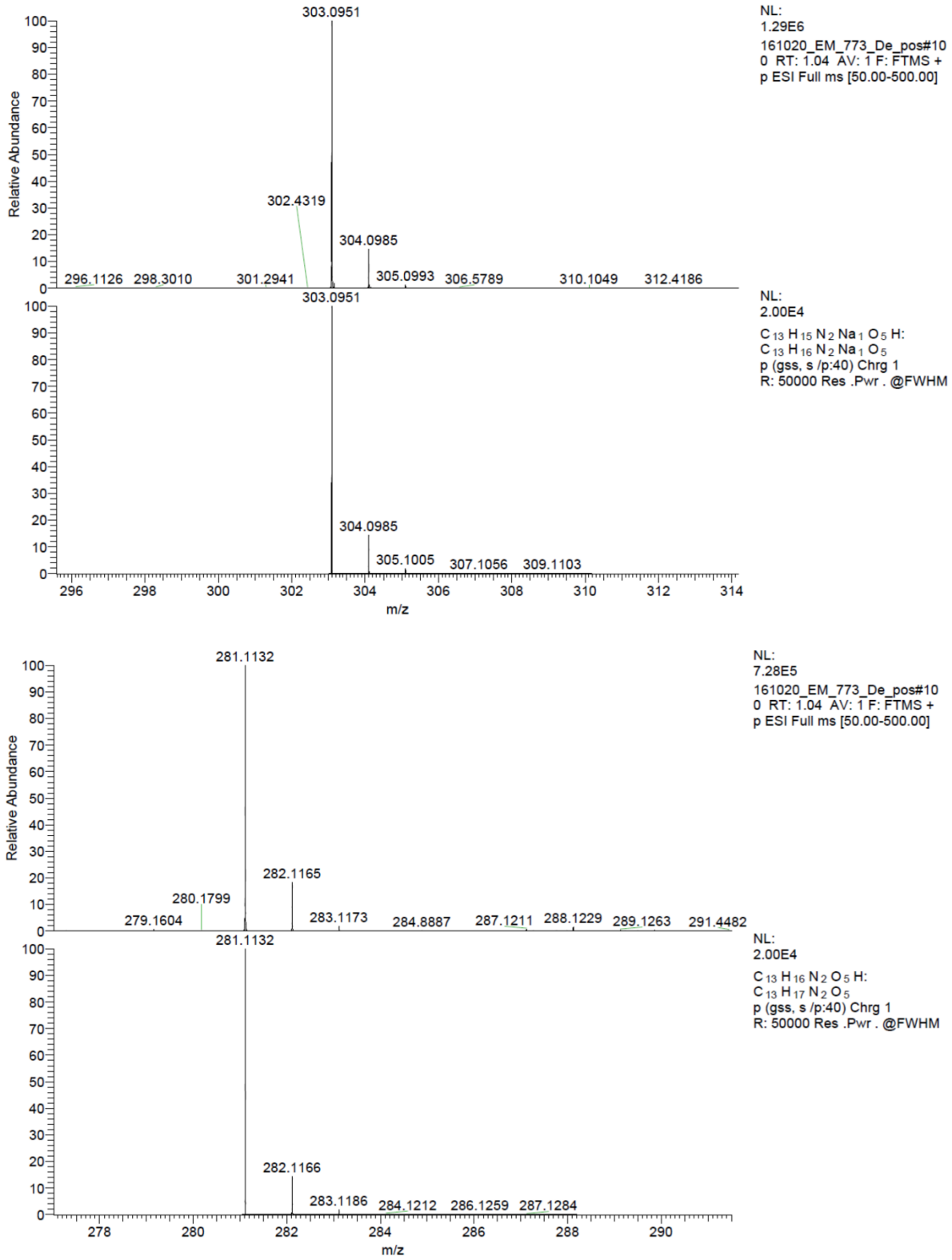

Figure S1. ESI(+)-MS spectrum of **OVGlnHNa$_2$** in methanol with simulation of the identified peaks.

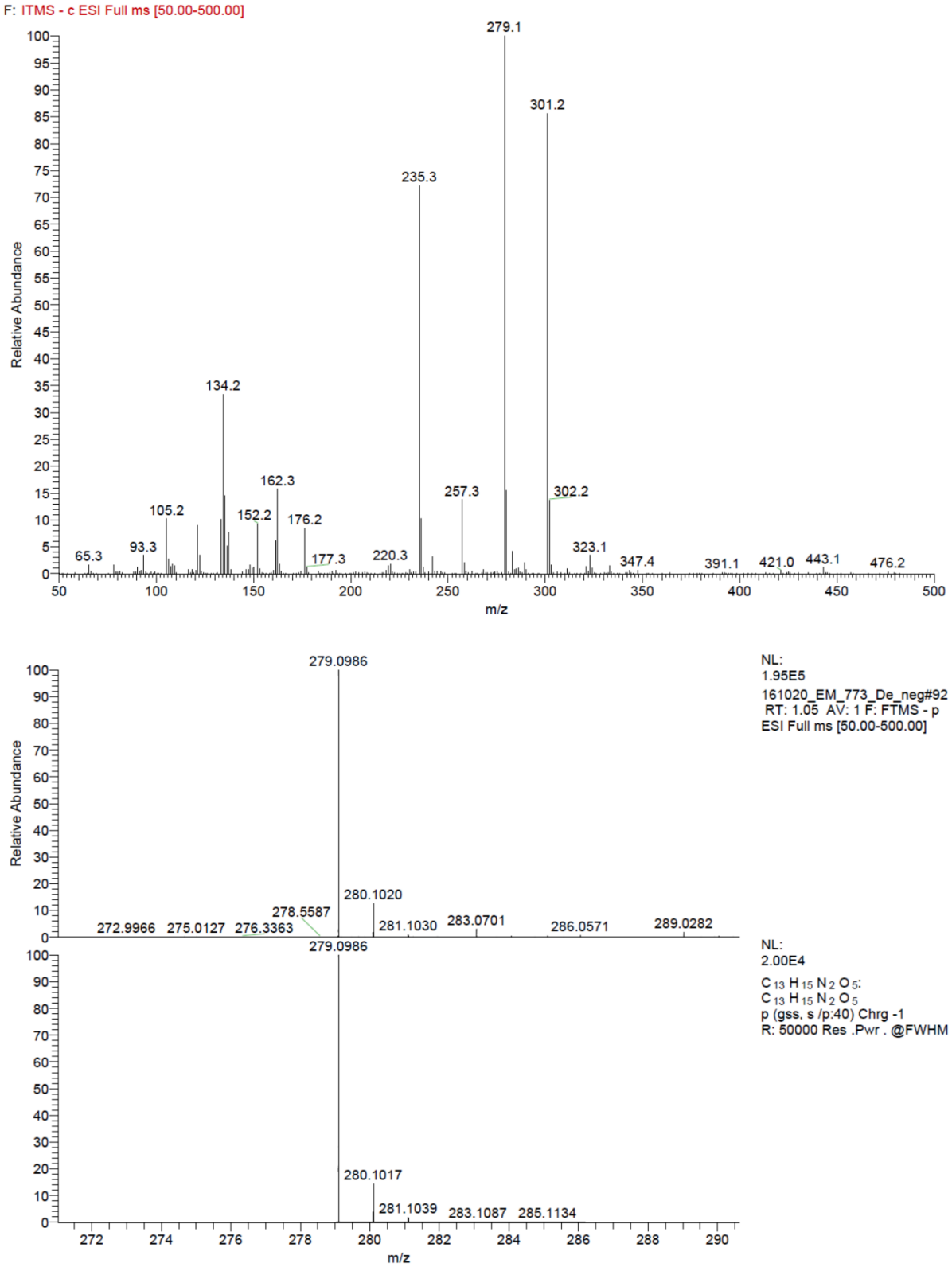

Figure S2. ESI(-)-MS spectrum of **OVGlnHNa$_2$** in methanol with simulation of the identified peaks.

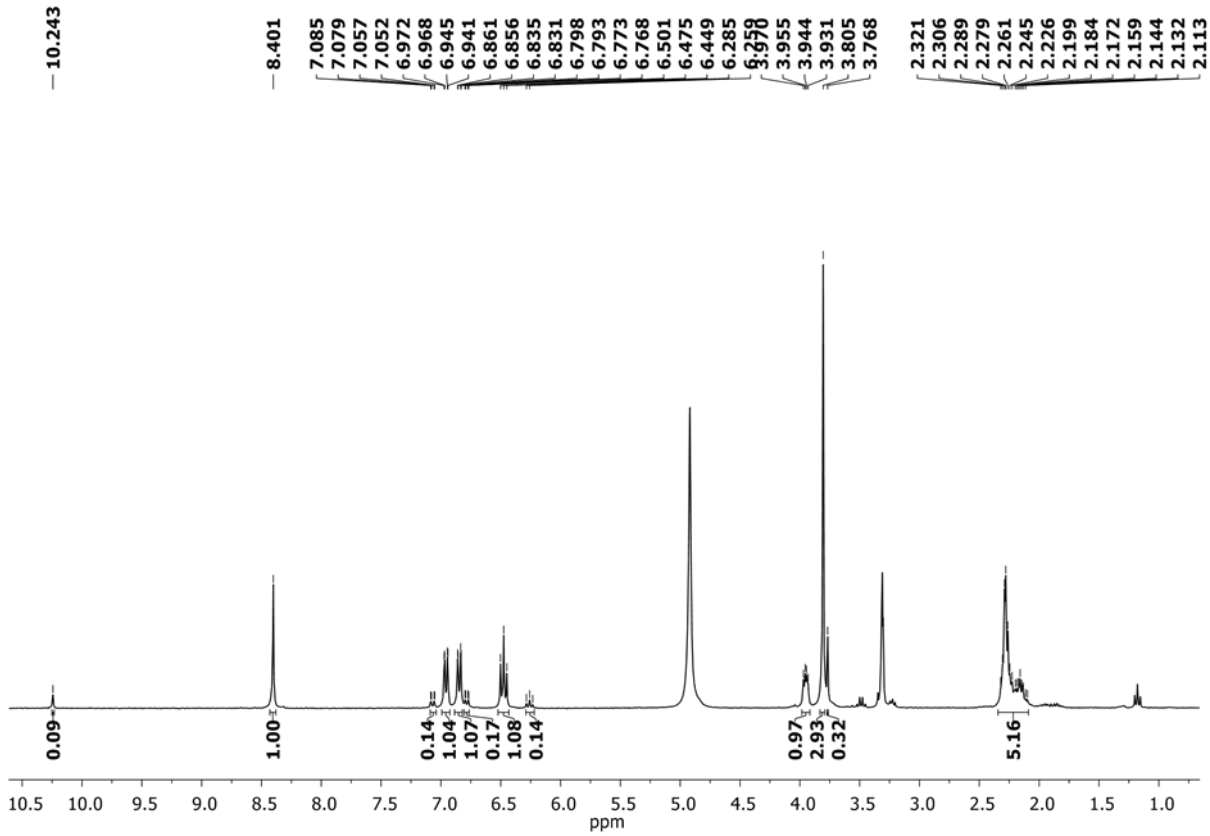

Figure S3. [1]HNMR spectrum for **OVGlnHNa$_2$** in MeOD.

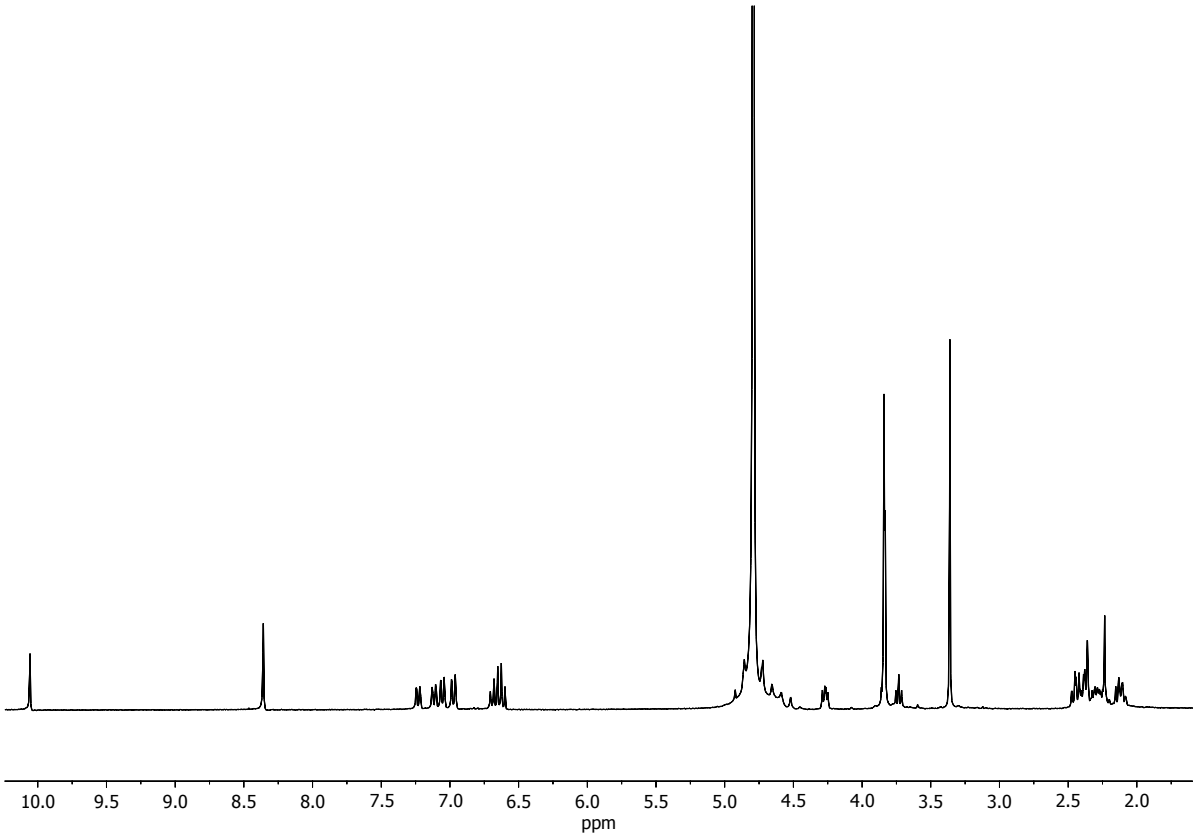

Figure S4. [1]HNMR spectrum for **OVGlnHNa$_2$** in D_2O.

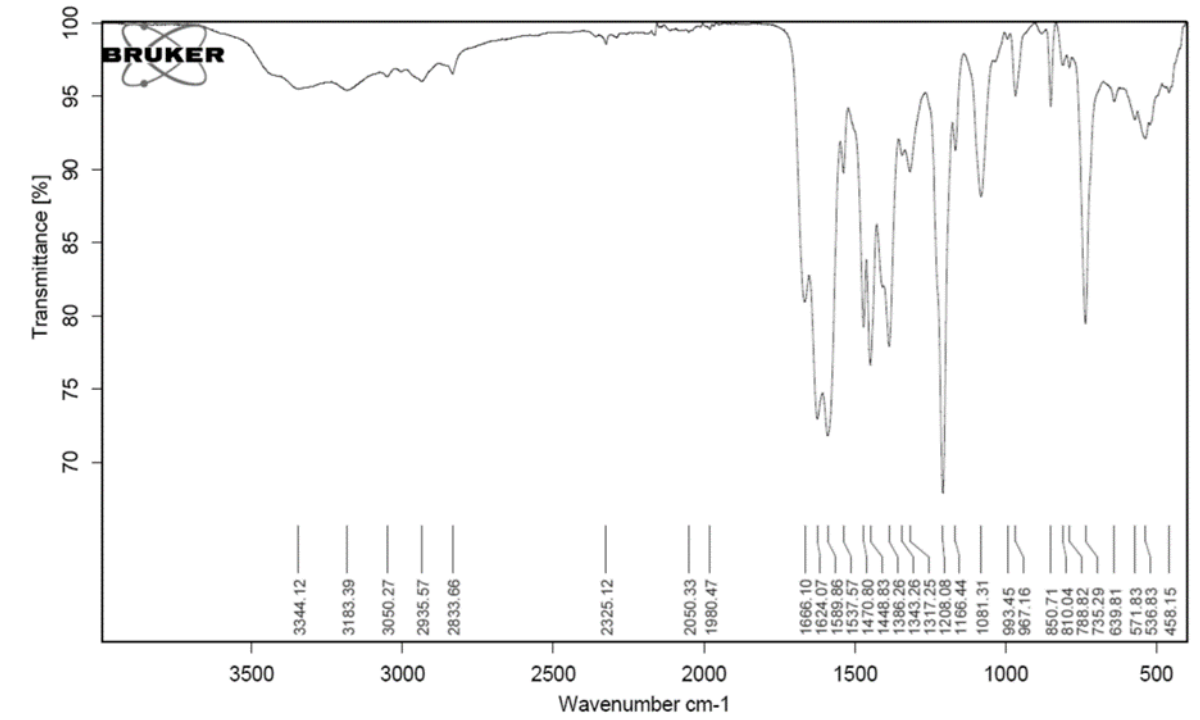

Figure S5. IR-spectra spectrum for **OVGlnHNa$_2$** dried *in vacuo*.

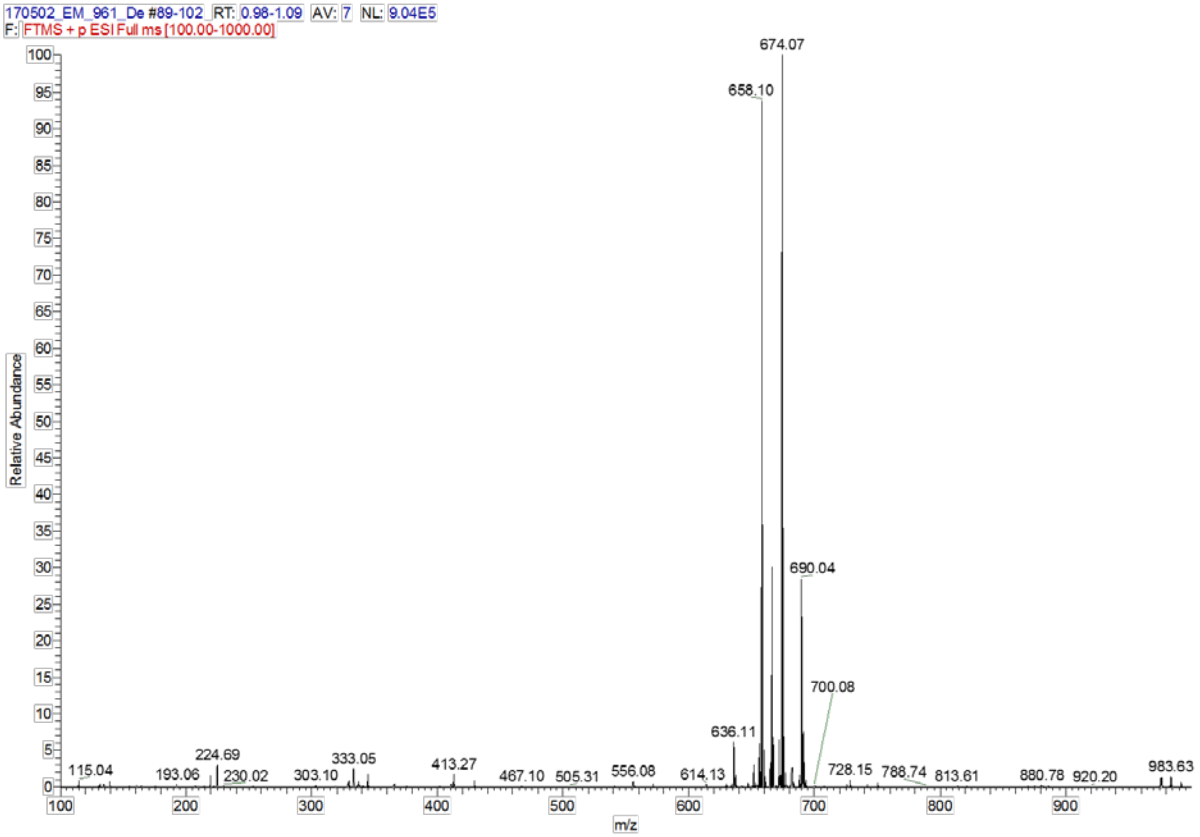

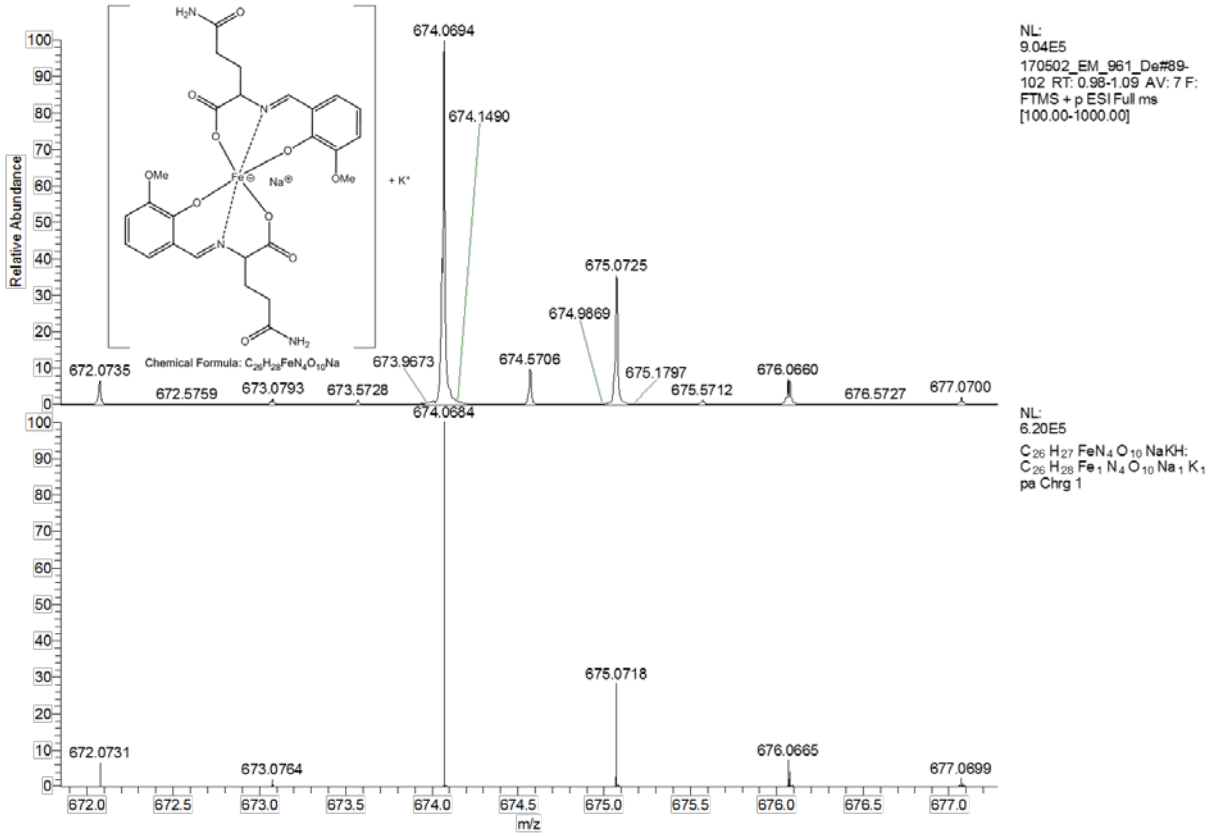
NL:
9.04E5
170502_EM_961_De#89-102 RT: 0.98-1.09 AV: 7 F: FTMS + p ESI Full ms [100.00-1000.00]
Relative Abundance
674.0694
674.1490
675.0725
674.9869
674.5706
673.9673
675.1797
676.0660
672.0735
672.5759
673.0793
673.5728
675.5712
676.5727
677.0700
674.0684
Chemical Formula: C26H28FeN4O10Na
+ K+
NL:
6.20E5
C26 H27 FeN4 O10 NaKH: C26 H28 Fe1 N4 O10 Na1 K1 pa Chrg 1
675.0718
672.0731
673.0764
676.0665
677.0699
672.0
672.5
673.0
673.5
674.0
674.5
675.0
675.5
676.0
676.5
677.0
m/z

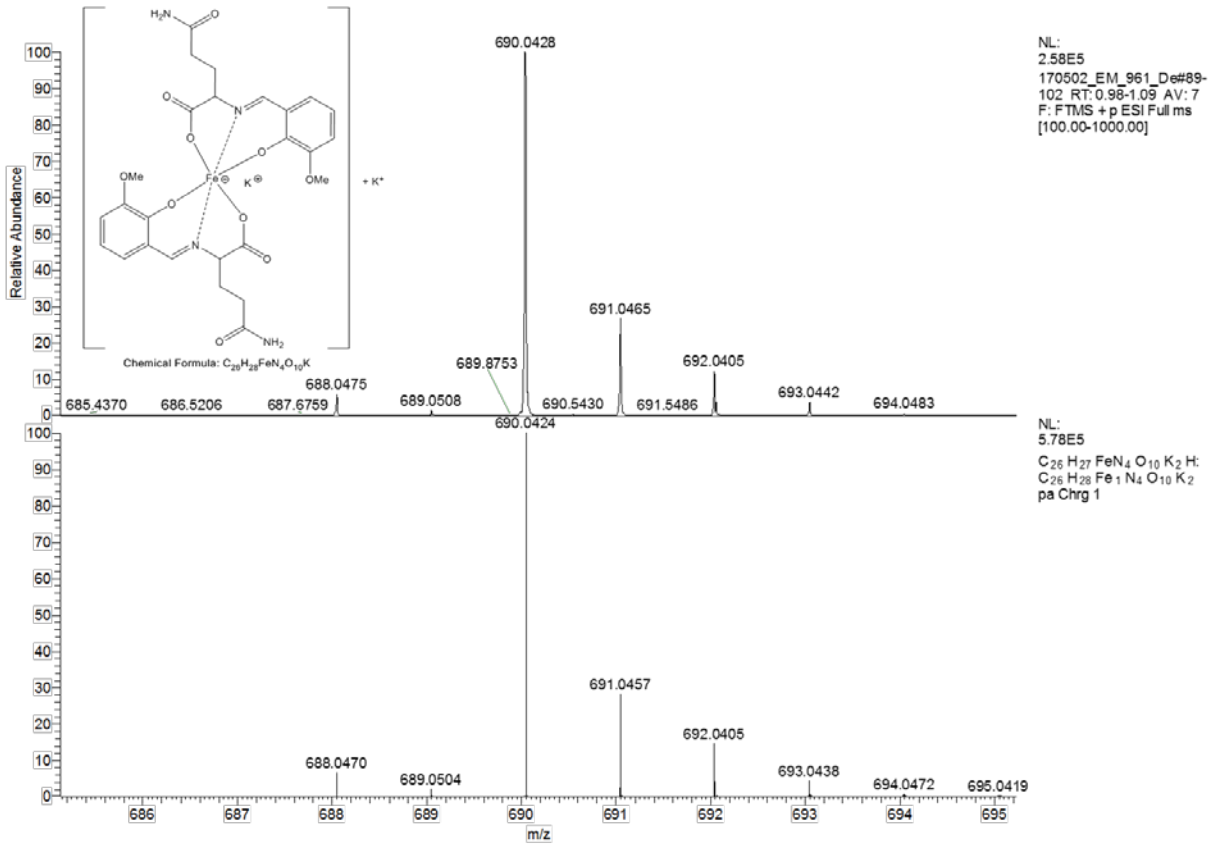
NL:
2.58E5
170502_EM_961_De#89-102 RT: 0.98-1.09 AV: 7 F: FTMS + p ESI Full ms [100.00-1000.00]
Relative Abundance
690.0428
691.0465
689.8753
692.0405
688.0475
693.0442
685.4370
686.5206
687.6759
689.0508
690.5430
691.5486
694.0483
690.0424
Chemical Formula: C26H28FeN4O10K
+ K+
NL:
5.78E5
C26 H27 FeN4 O10 K2 H: C26 H28 Fe1 N4 O10 K2 pa Chrg 1
691.0457
692.0405
688.0470
689.0504
693.0438
694.0472
695.0419
686
687
688
689
690
691
692
693
694
695
m/z

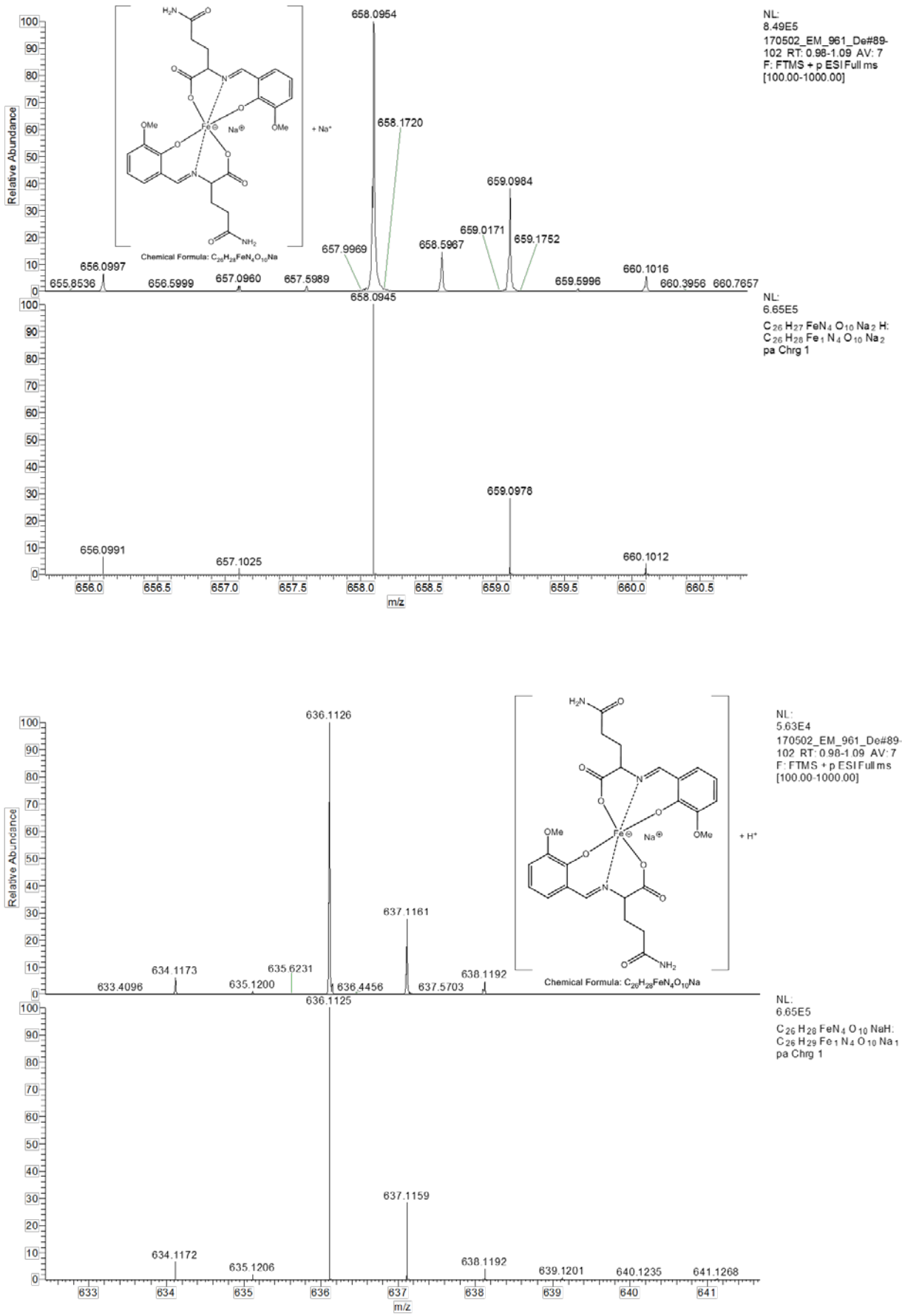

Figure S6. ESI(+)-MS spectrum of **1** in methanol with simulation of the identified peaks and structure suggestions.

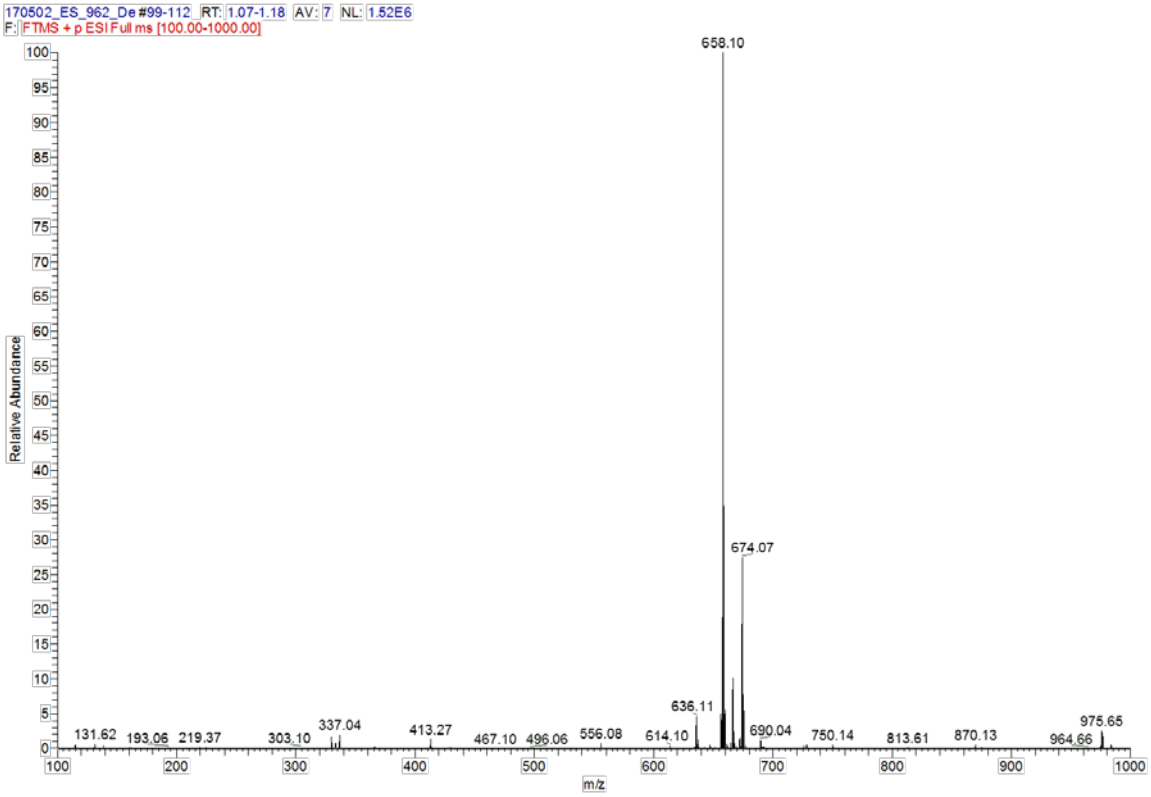

Figure S7. ESI(+)-MS spectrum of **1** in water. Due to the similar set of signals compared to the spectrum in methanol, simulations of the identified peaks are not shown.

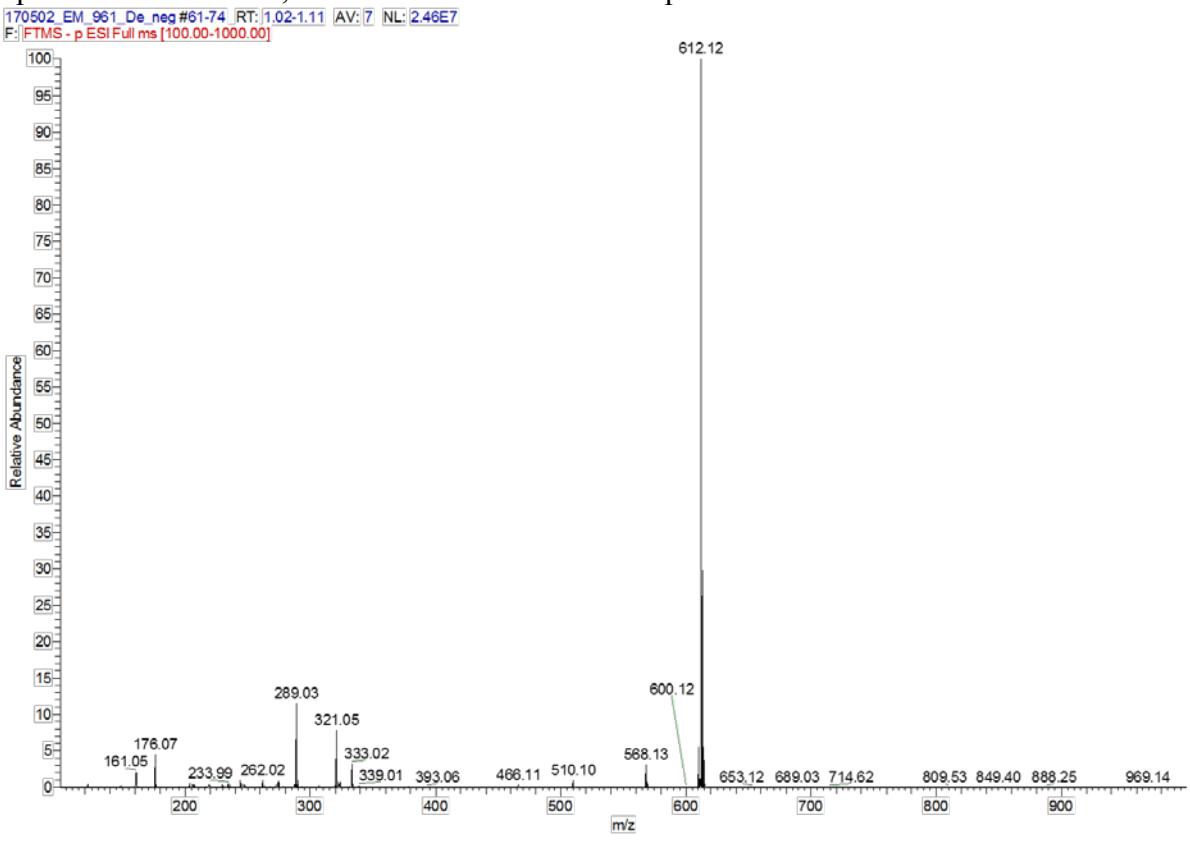

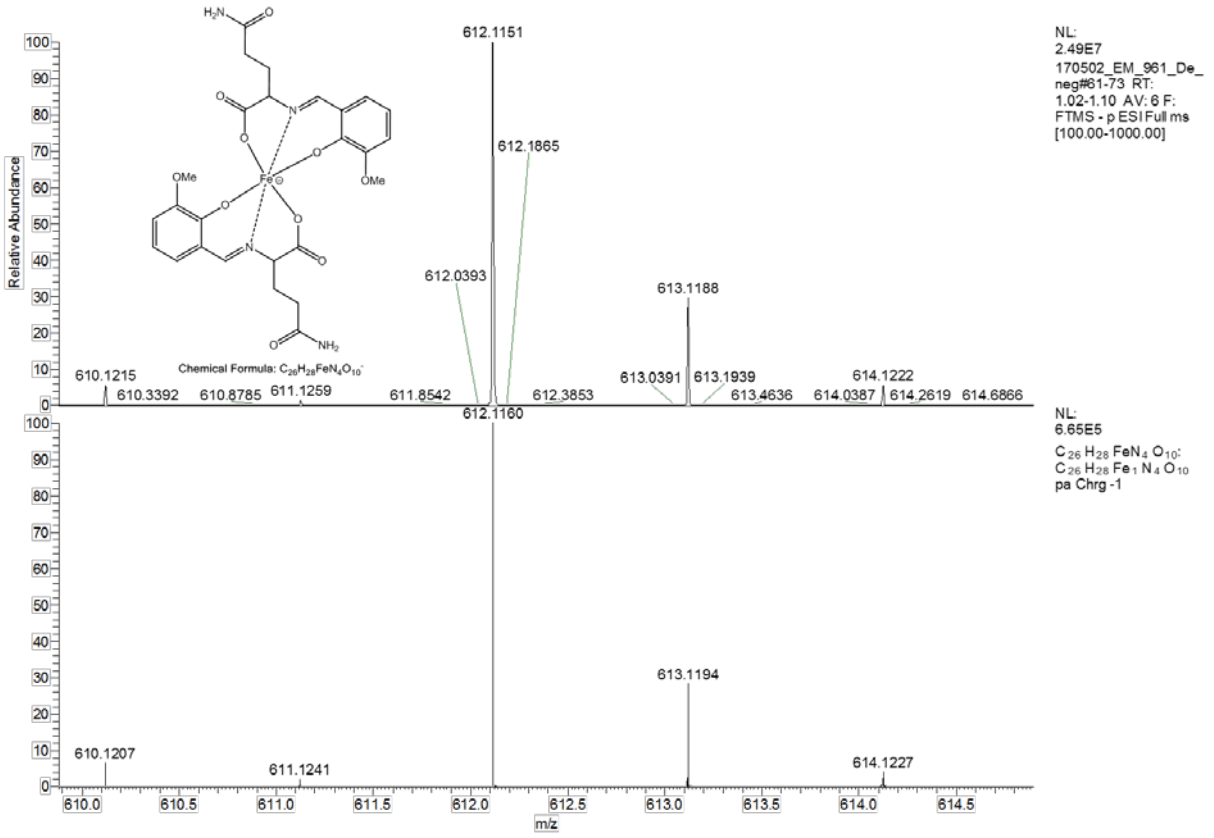
612.1151
612.1865
612.0393
613.1188
610.1215
610.3392
610.8785
611.1259
611.8542
612.1160
612.3853
613.0391
613.1939
613.4636
614.0387
614.1222
614.2619
614.6866
Chemical Formula: C26H28FeN4O10-
Relative Abundance
m/z
NL:
2.49E7
170502_EM_961_De_
neg#61-73 RT:
1.02-1.10 AV: 6 F:
FTMS - p ESI Full ms
[100.00-1000.00]
NL:
6.65E5
C26 H28 FeN4 O10:
C26 H28 Fe1 N4 O10
pa Chrg -1
613.1194
610.1207
611.1241
614.1227

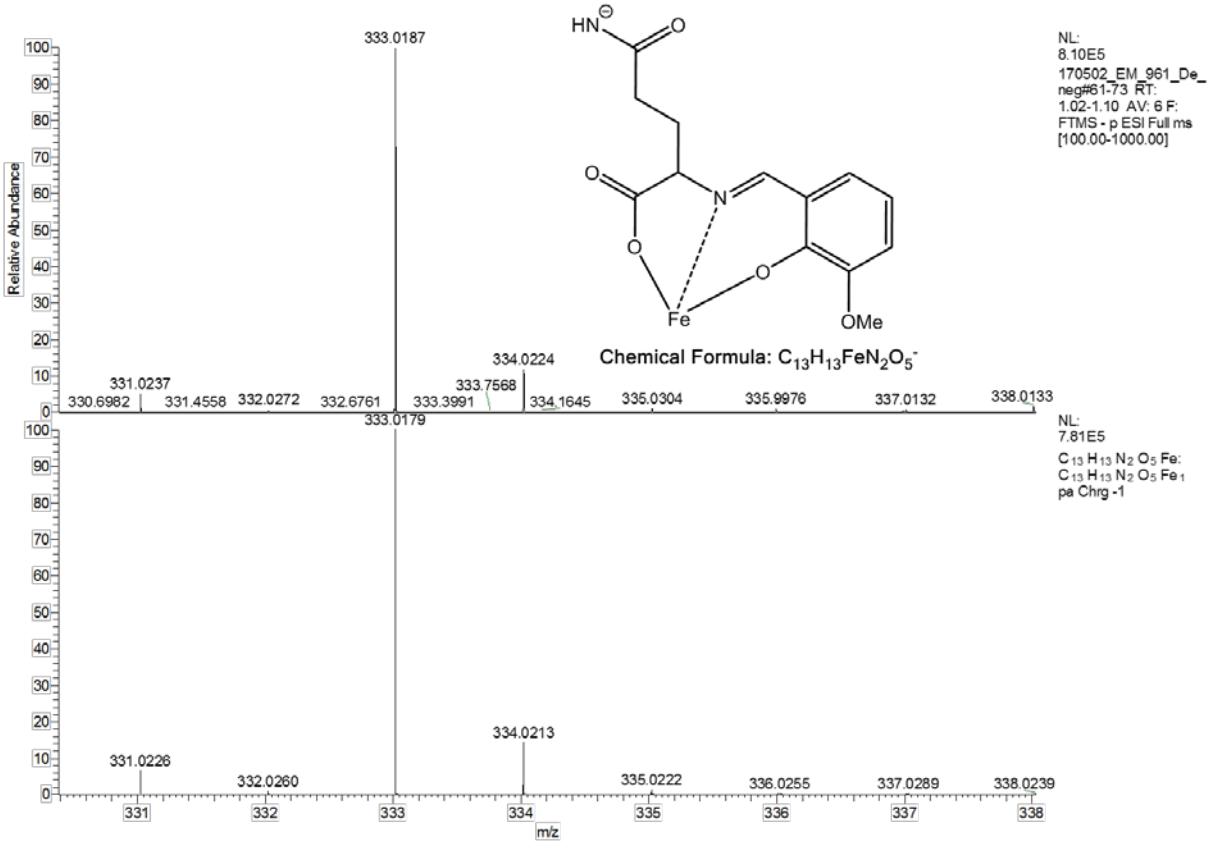
333.0187
334.0224
331.0237
330.6982
331.4558
332.0272
332.6761
333.3991
333.7568
334.1645
335.0304
335.9976
337.0132
338.0133
333.0179
Chemical Formula: C13H13FeN2O5-
Relative Abundance
m/z
NL:
8.10E5
170502_EM_961_De_
neg#61-73 RT:
1.02-1.10 AV: 6 F:
FTMS - p ESI Full ms
[100.00-1000.00]
NL:
7.81E5
C13 H13 N2 O5 Fe:
C13 H13 N2 O5 Fe1
pa Chrg -1
334.0213
331.0226
332.0260
335.0222
336.0255
337.0289
338.0239

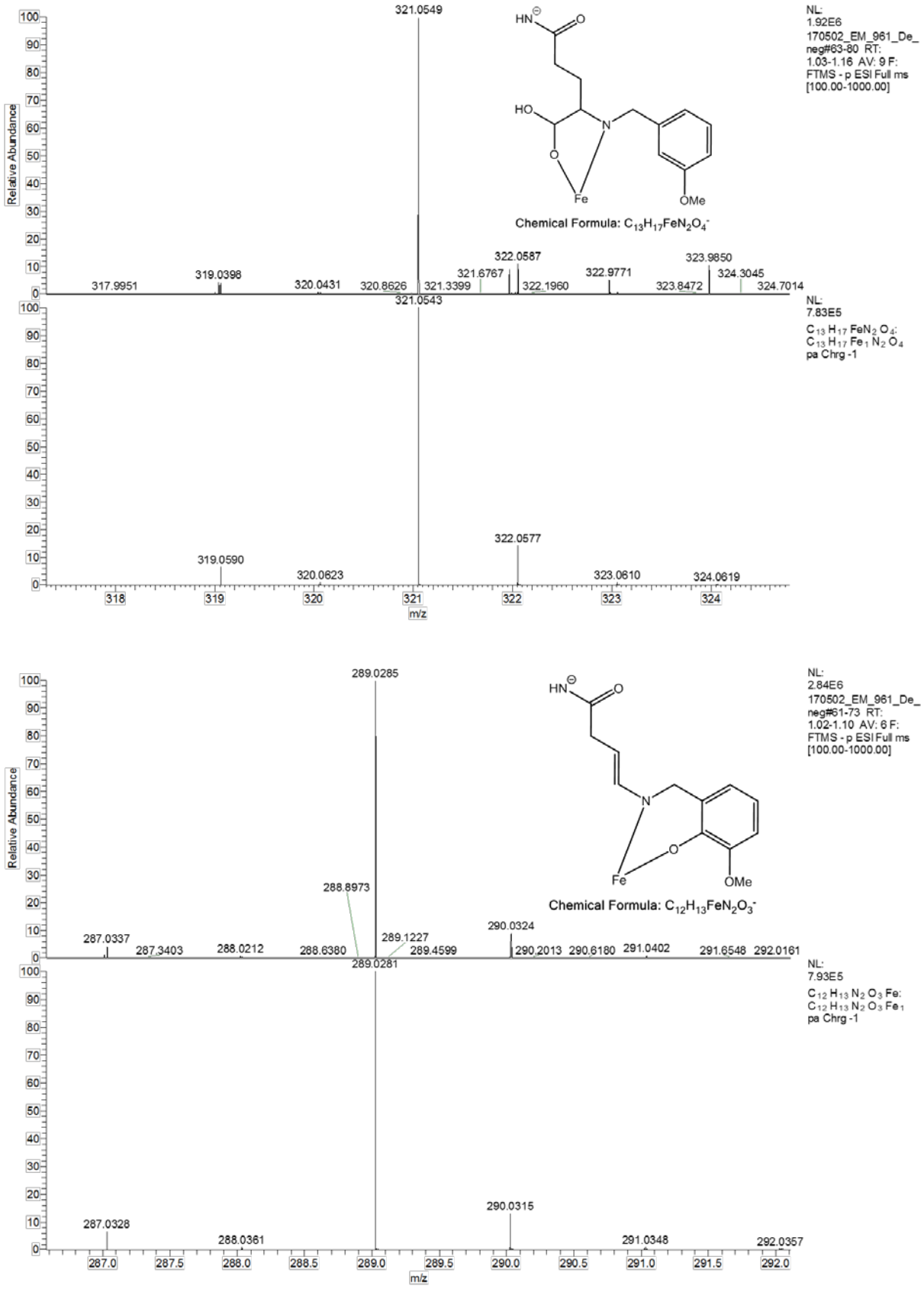

Figure S8. ESI(-)-MS spectrum of **1** in methanol with simulation of the identified peaks and structure suggestion.

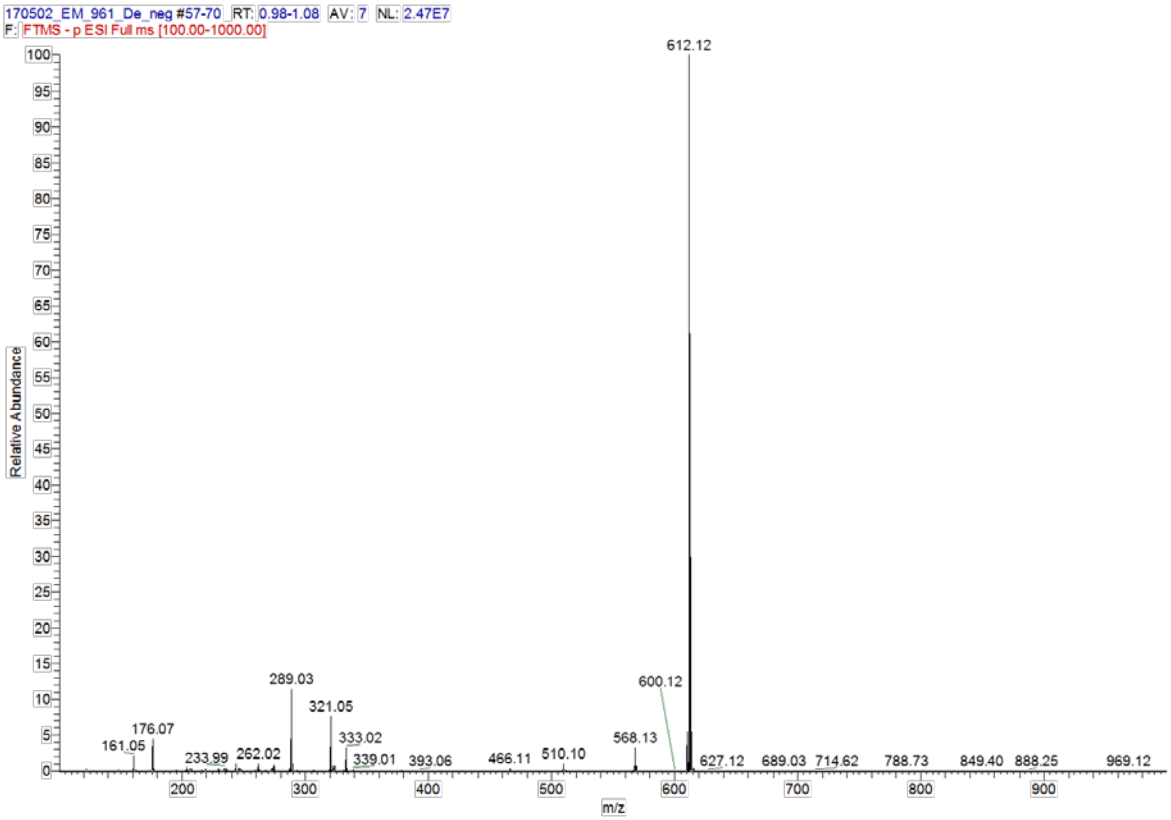

Figure S9. ESI(-)-MS spectrum of **1** in water. Due to the similar set of signals compared to the spectrum in methanol, simulations of the identified peaks are not shown.

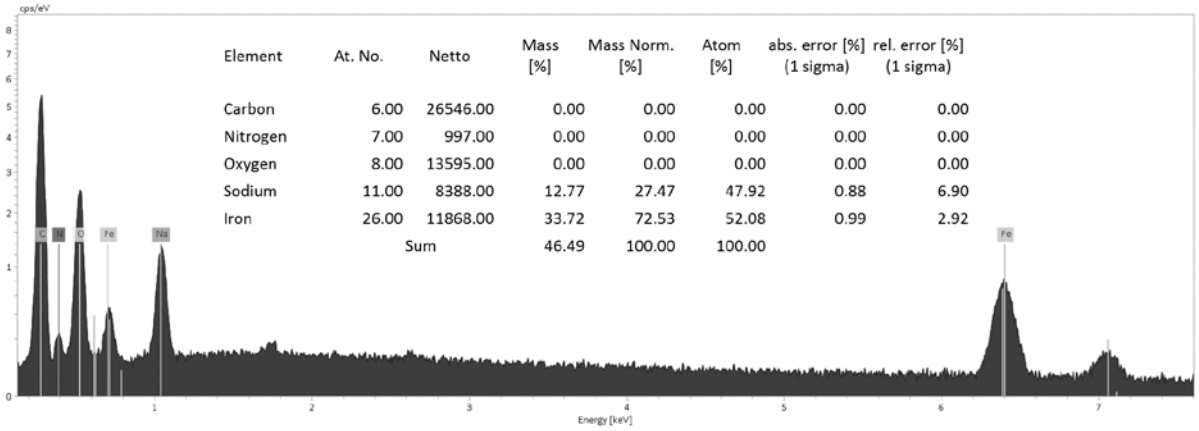

Element	At. No.	Netto	Mass [%]	Mass Norm. [%]	Atom [%]	abs. error [%] (1 sigma)	rel. error [%] (1 sigma)
Carbon	6.00	26546.00	0.00	0.00	0.00	0.00	0.00
Nitrogen	7.00	997.00	0.00	0.00	0.00	0.00	0.00
Oxygen	8.00	13595.00	0.00	0.00	0.00	0.00	0.00
Sodium	11.00	8388.00	12.77	27.47	47.92	0.88	6.90
Iron	26.00	11868.00	33.72	72.53	52.08	0.99	2.92
Sum			46.49	100.00	100.00		

Figure S10. EDX spectrum of **1** and the resulting Fe:Na ratio.

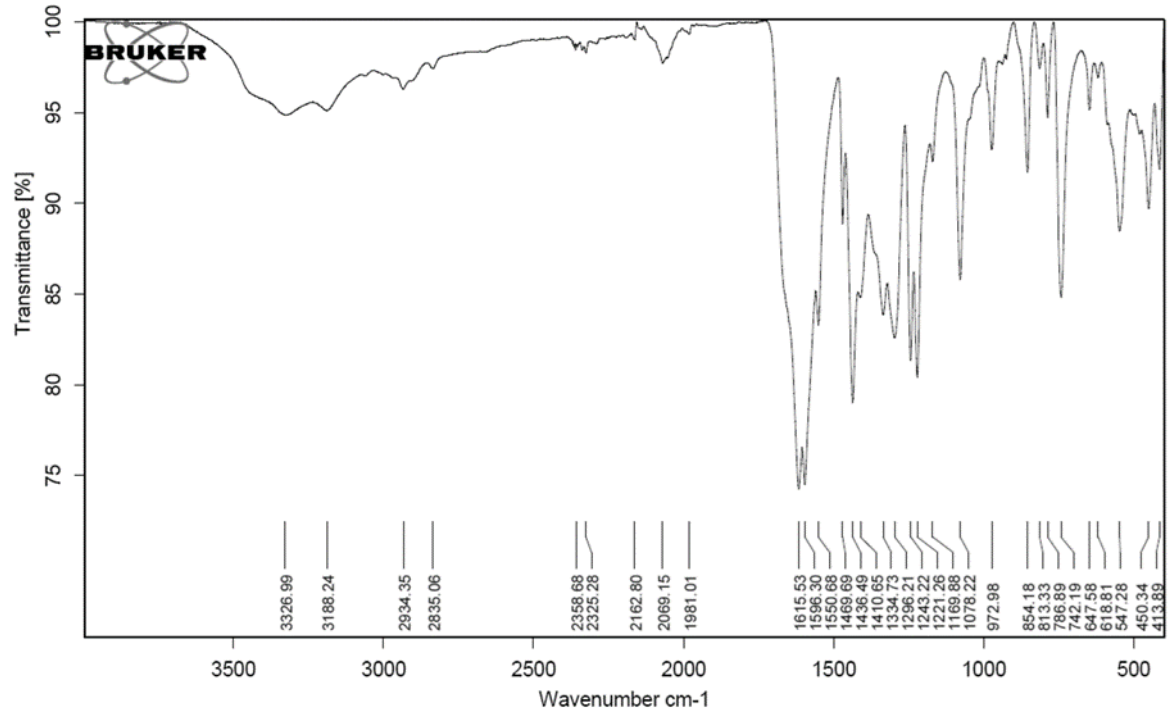

Figure S11. IR-spectrum for **1**, dried *in vacuo* and recorded directly after synthesis.

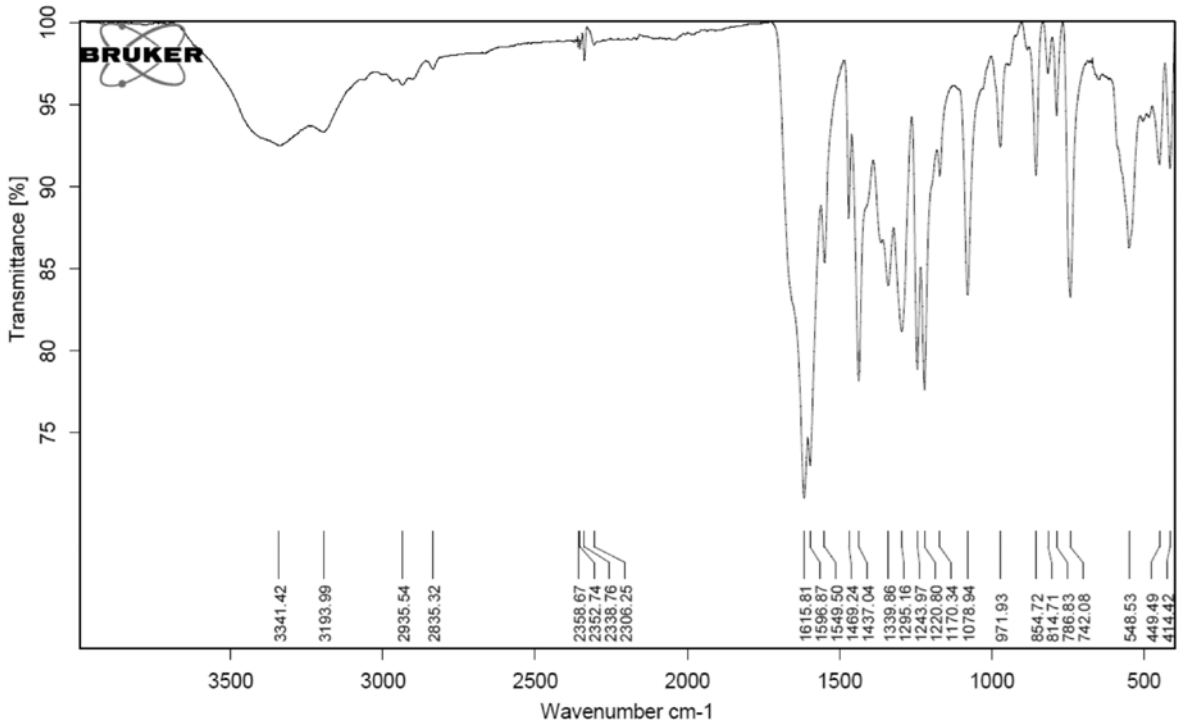

Figure S12. IR-spectrum for **1** dried *in vacuo* and recorded several months after synthesis.

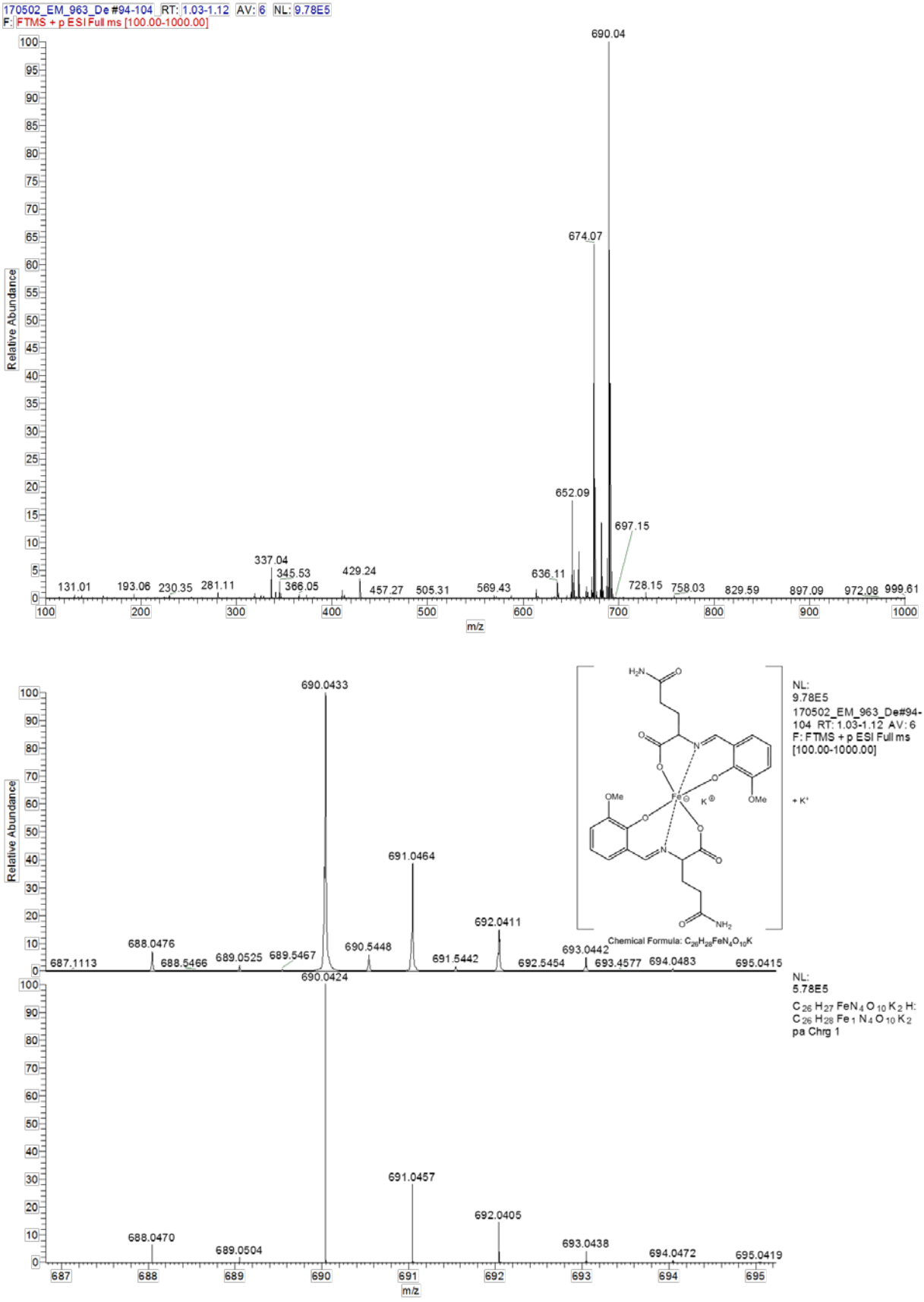
170502_EM_963_De #94-104 RT: 1.03-1.12 AV: 6 NL: 9.78E5
F: FTMS + p ESI Full ms [100.00-1000.00]
Relative Abundance
m/z
690.04
674.07
652.09
697.15
337.04
345.53
429.24
636.11
131.01
193.06
230.35
281.11
366.05
457.27
505.31
569.43
728.15
758.03
829.59
897.09
972.08
999.61
690.0433
691.0464
692.0411
688.0476
690.5448
687.1113
688.5466
689.0525
689.5467
691.5442
692.5454
693.0442
693.4577
694.0483
695.0415
690.0424
691.0457
692.0405
688.0470
689.0504
693.0438
694.0472
695.0419
Chemical Formula: C26H28FeN4O10K
NL:
9.78E5
170502_EM_963_De#94-104 RT: 1.03-1.12 AV: 6
F: FTMS + p ESI Full ms [100.00-1000.00]
+ K+
NL:
5.78E5
C26 H27 FeN4 O10 K2 H:
C26 H28 Fe1 N4 O10 K2
pa Chrg 1

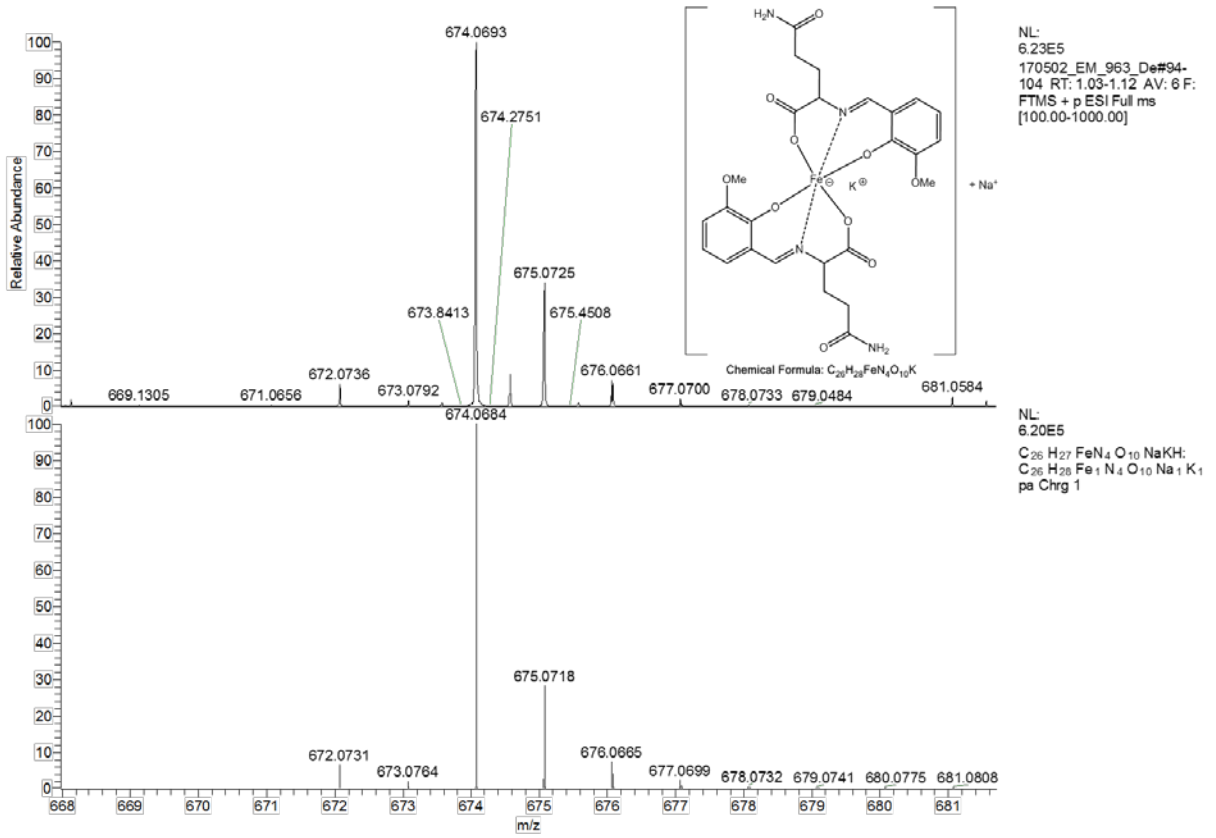
674.0693
674.2751
675.0725
673.8413
675.4508
672.0736
676.0661
669.1305
671.0656
673.0792
674.0684
677.0700
678.0733
679.0484
681.0584
Relative Abundance
NL:
6.23E5
170502_EM_963_De#94-104 RT: 1.03-1.12 AV: 6 F: FTMS + p ESI Full ms [100.00-1000.00]
Chemical Formula: C26H28FeN4O10K
+ Na+
NL:
6.20E5
C26 H27 FeN4 O10 NaKH: C26 H28 Fe1 N4 O10 Na1 K1 pa Chrg 1
675.0718
672.0731
673.0764
676.0665
677.0699
678.0732
679.0741
680.0775
681.0808
668
669
670
671
672
673
674
675
676
677
678
679
680
681
m/z

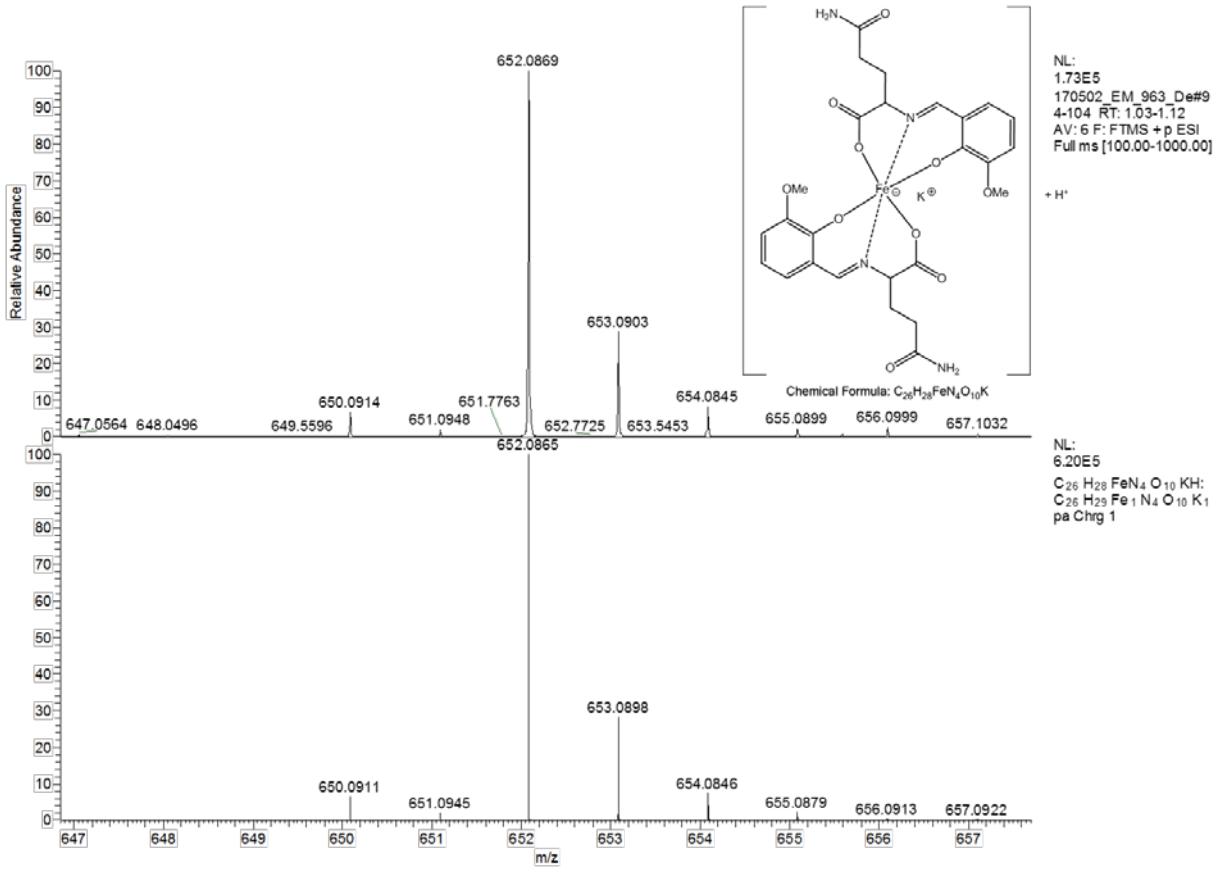
652.0869
653.0903
650.0914
651.7763
654.0845
647.0564
648.0496
649.5596
651.0948
652.7725
653.5453
655.0899
656.0999
657.1032
652.0865
Relative Abundance
NL:
1.73E5
170502_EM_963_De#94-104 RT: 1.03-1.12 AV: 6 F: FTMS + p ESI Full ms [100.00-1000.00]
Chemical Formula: C26H28FeN4O10K
+ H+
NL:
6.20E5
C26 H28 FeN4 O10 KH: C26 H29 Fe1 N4 O10 K1 pa Chrg 1
653.0898
650.0911
651.0945
654.0846
655.0879
656.0913
657.0922
647
648
649
650
651
652
653
654
655
656
657
m/z

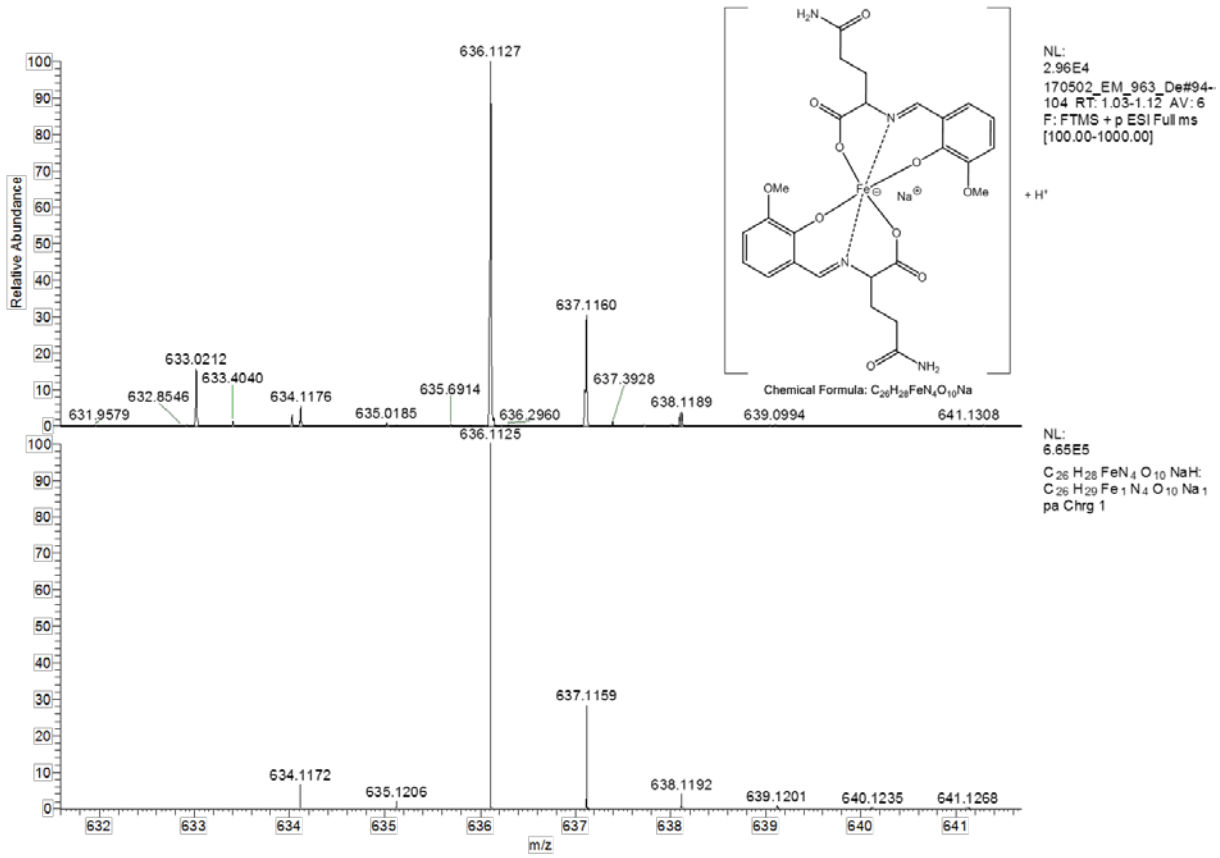

Figure S13. ESI(+)-MS spectrum of **2** and in methanol with simulation of the identified peaks and structure suggestions.

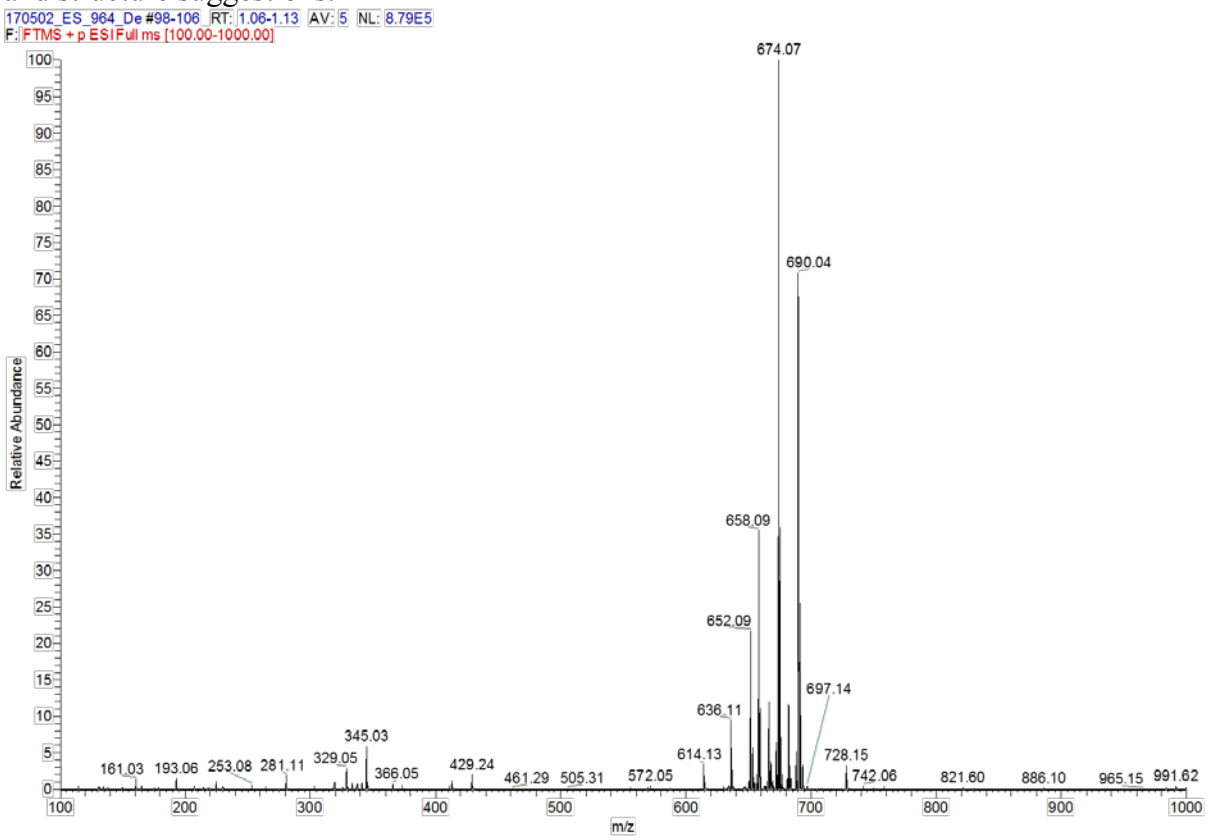

Figure S14. ESI(+)-MS spectrum of **2** in water. Due to the similar set of signals compared to the spectrum in methanol, simulations of the identified peaks are not shown.

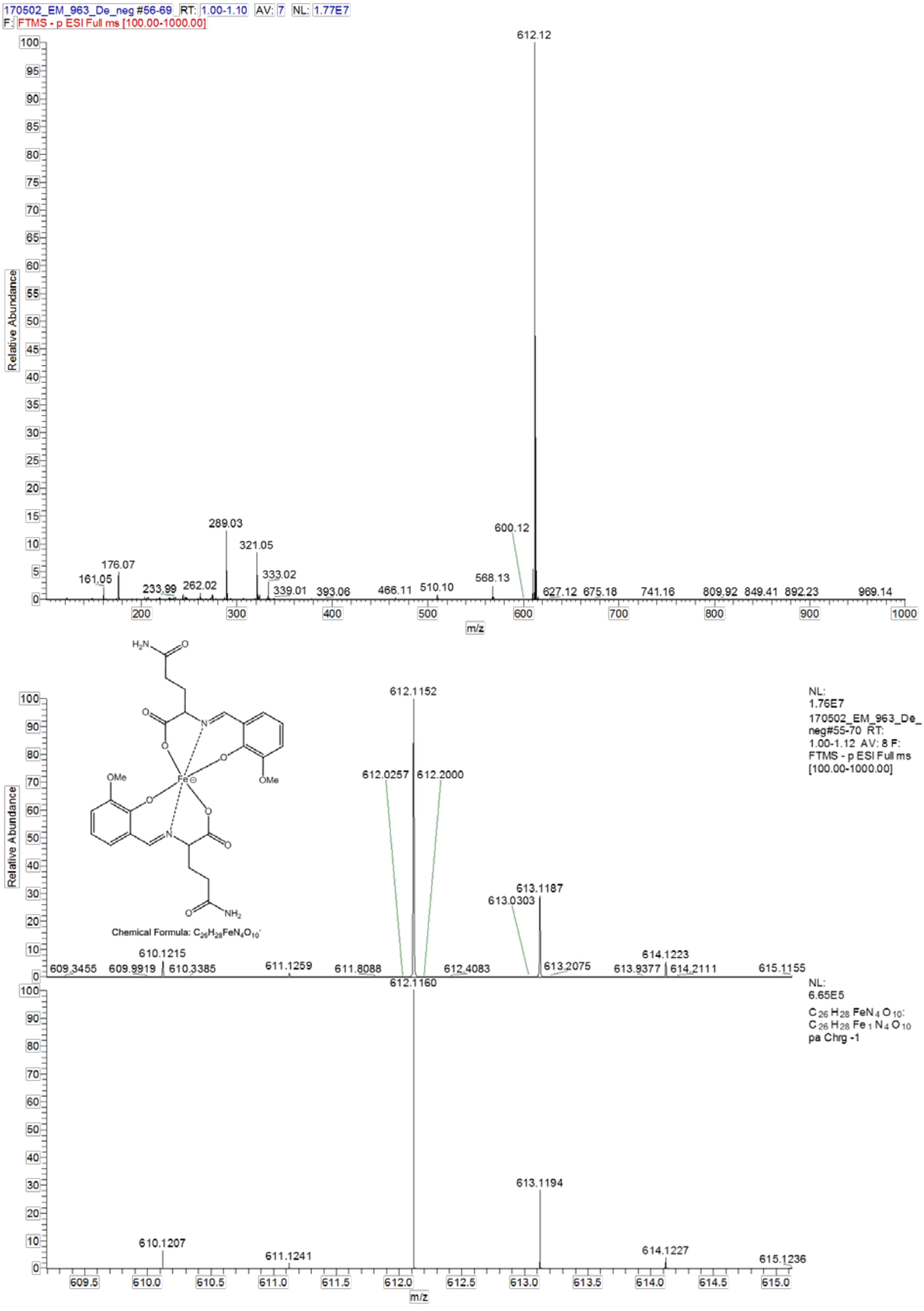
170502_EM_963_De_neg #56-69 RT: 1.00-1.10 AV: 7 NL: 1.77E7
F: FTMS - p ESI Full ms [100.00-1000.00]
612.12
289.03
321.05
176.07
161.05
333.02
600.12
568.13
233.99
262.02
339.01
393.06
466.11
510.10
627.12
675.18
741.16
809.92
849.41
892.23
969.14
Relative Abundance
m/z
Chemical Formula: C26H28FeN4O10
612.1152
612.0257
612.2000
613.1187
613.0303
610.1215
609.3455
609.9919
610.3385
611.1259
611.8088
612.4083
613.2075
614.1223
613.9377
614.2111
615.1155
612.1160
NL:
1.76E7
170502_EM_963_De_neg#55-70 RT:
1.00-1.12 AV: 8 F:
FTMS - p ESI Full ms
[100.00-1000.00]
NL:
6.65E5
C26 H28 FeN4 O10:
C26 H28 Fe1 N4 O10
pa Chrg -1
613.1194
610.1207
611.1241
614.1227
615.1236

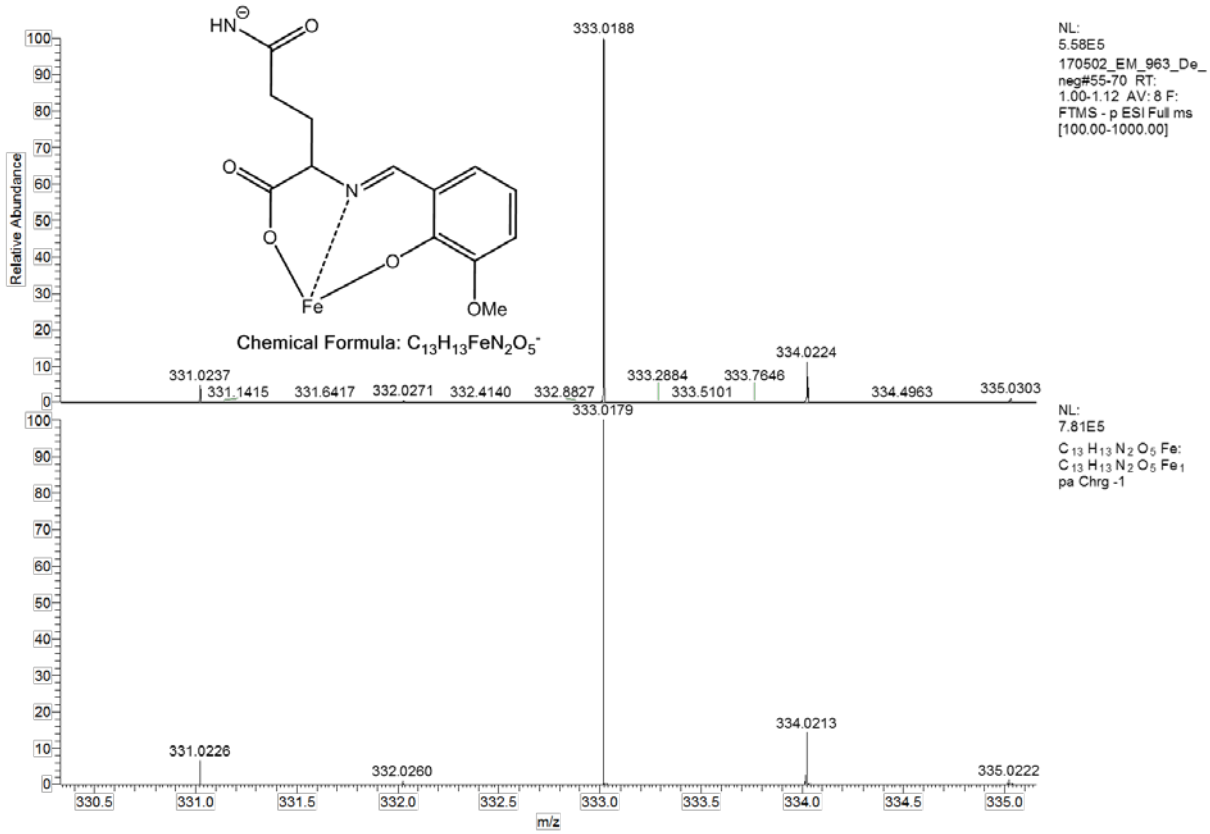
HN
O
O
O
N
O
O
Fe
OMe
Chemical Formula: $C_{13}H_{13}FeN_2O_5^-$
333.0188
NL:
5.58E5
170502_EM_963_De_
neg#55-70 RT:
1.00-1.12 AV: 8 F:
FTMS - p ESI Full ms
[100.00-1000.00]
Relative Abundance
331.0237
331.1415
331.6417
332.0271
332.4140
332.8827
333.2884
333.5101
333.7646
334.0224
334.4963
335.0303
333.0179
NL:
7.81E5
C 13 H 13 N 2 O 5 Fe:
C 13 H 13 N 2 O 5 Fe 1
pa Chrg -1
331.0226
332.0260
334.0213
335.0222
330.5
331.0
331.5
332.0
332.5
333.0
333.5
334.0
334.5
335.0
m/z

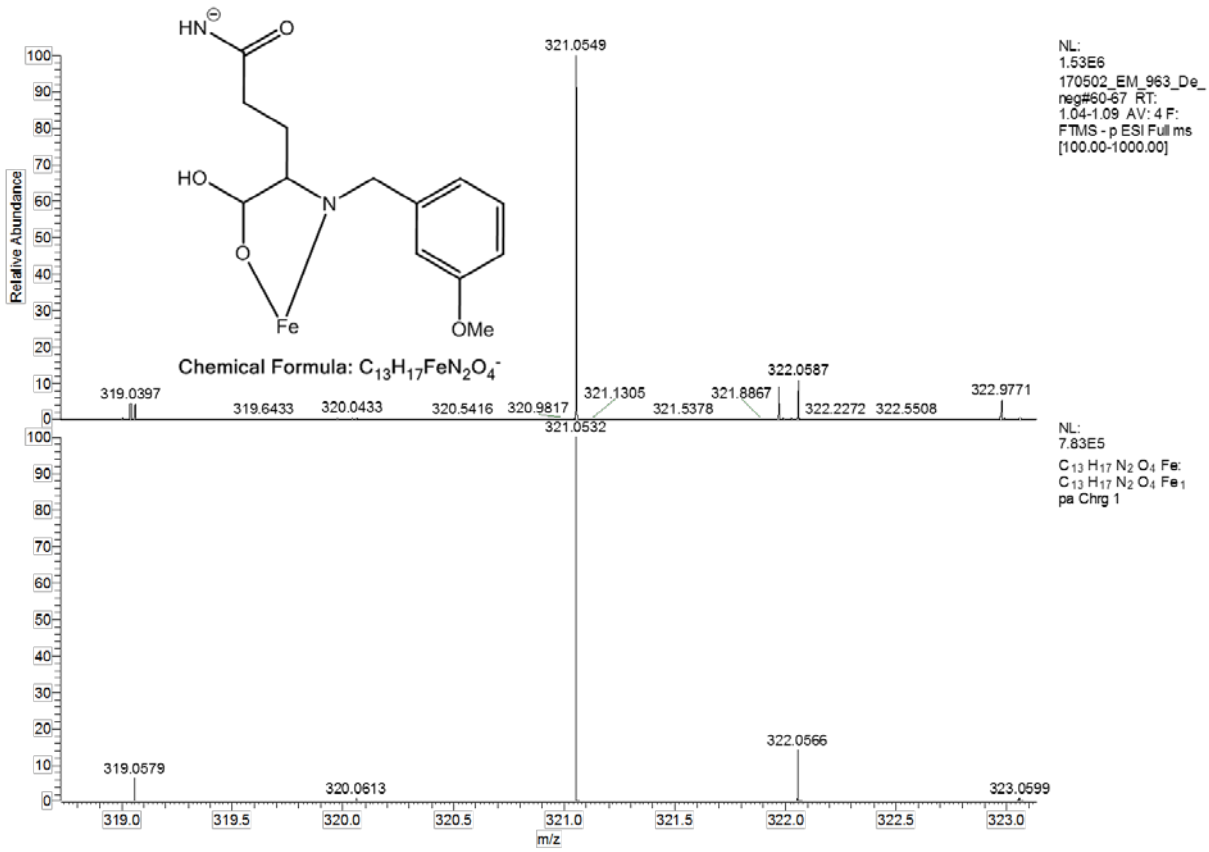
HN
O
HO
N
O
Fe
OMe
Chemical Formula: $C_{13}H_{17}FeN_2O_4^-$
321.0549
NL:
1.53E6
170502_EM_963_De_
neg#60-67 RT:
1.04-1.09 AV: 4 F:
FTMS - p ESI Full ms
[100.00-1000.00]
Relative Abundance
319.0397
319.6433
320.0433
320.5416
320.9817
321.1305
321.5378
321.8867
322.0587
322.2272
322.5508
322.9771
321.0532
NL:
7.83E5
C 13 H 17 N 2 O 4 Fe:
C 13 H 17 N 2 O 4 Fe 1
pa Chrg 1
319.0579
320.0613
322.0566
323.0599
319.0
319.5
320.0
320.5
321.0
321.5
322.0
322.5
323.0
m/z

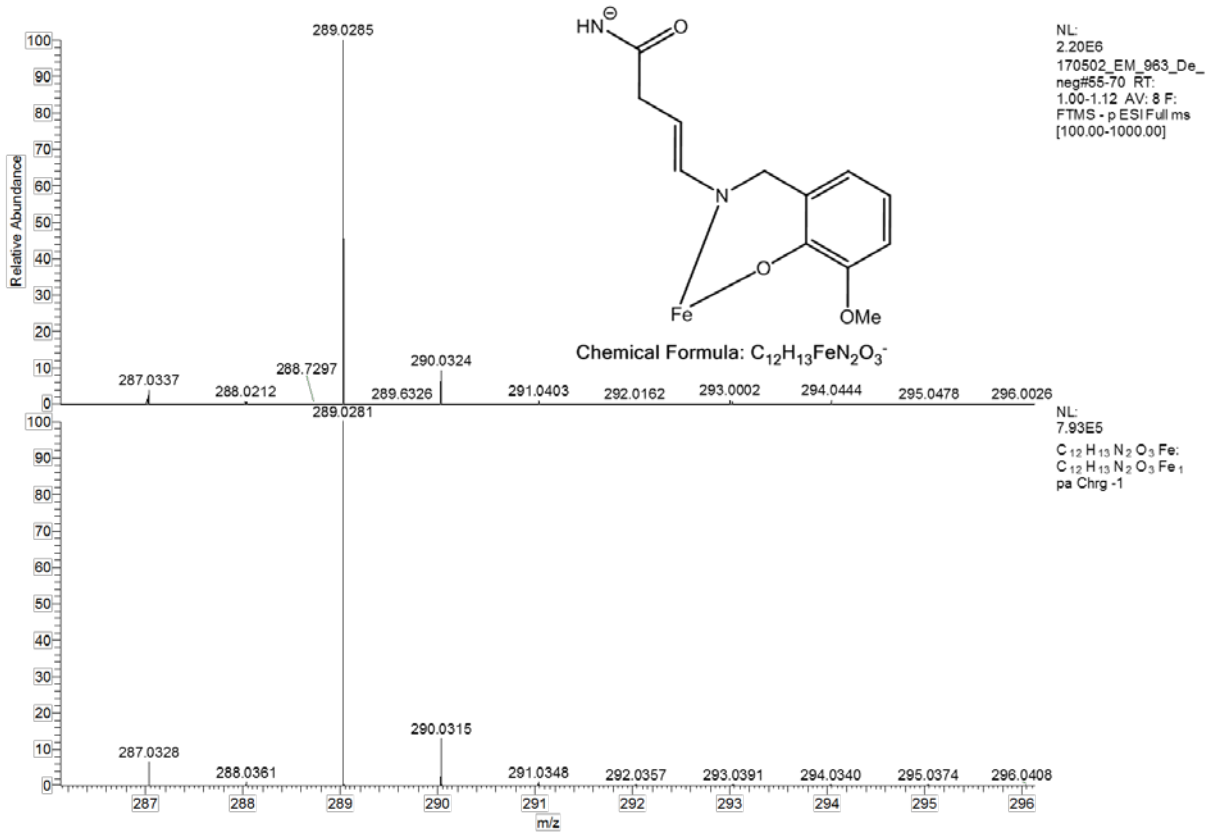

Figure S15. ESI(-)-MS spectrum of **2** in methanol with simulation of the identified peaks and structure suggestions.

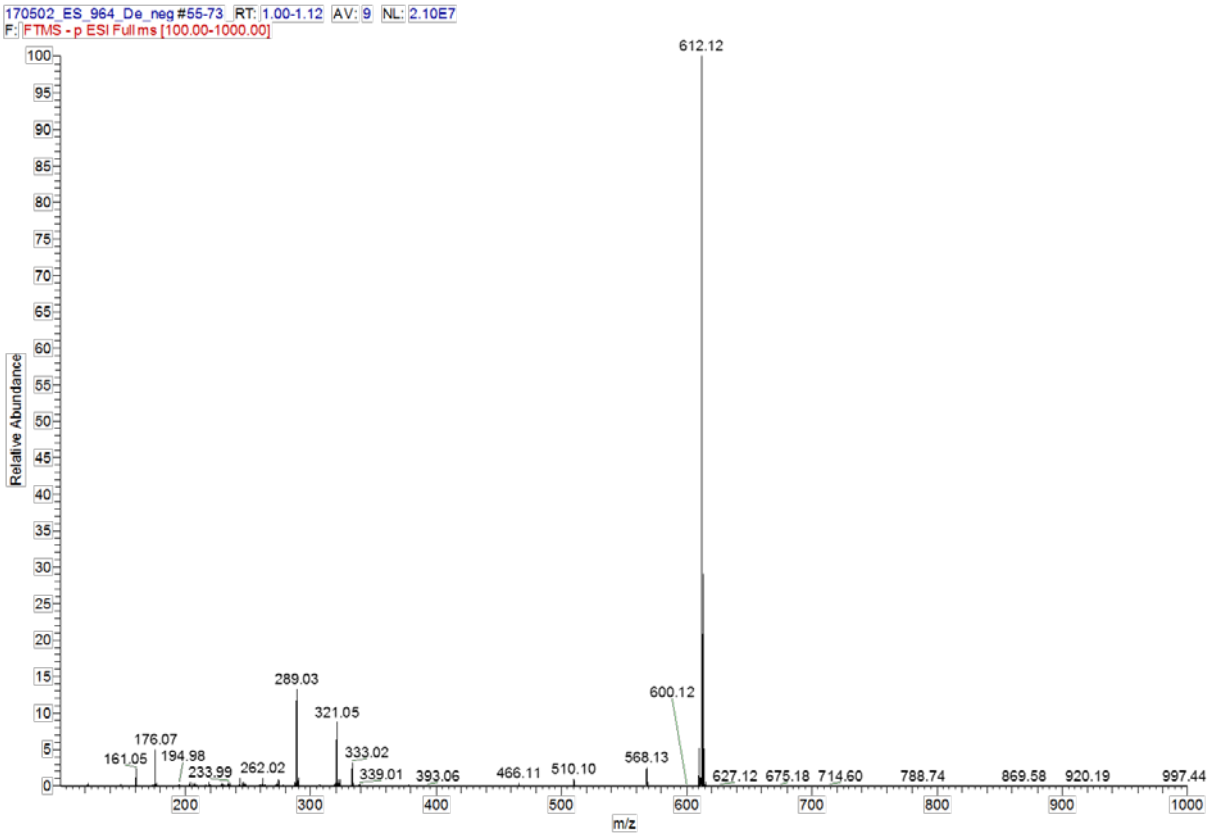

Figure S16. ESI(-)-MS spectrum of **2** in water. Due to the similar set of signals compared to the spectrum in methanol, simulations of the identified peaks are not shown.

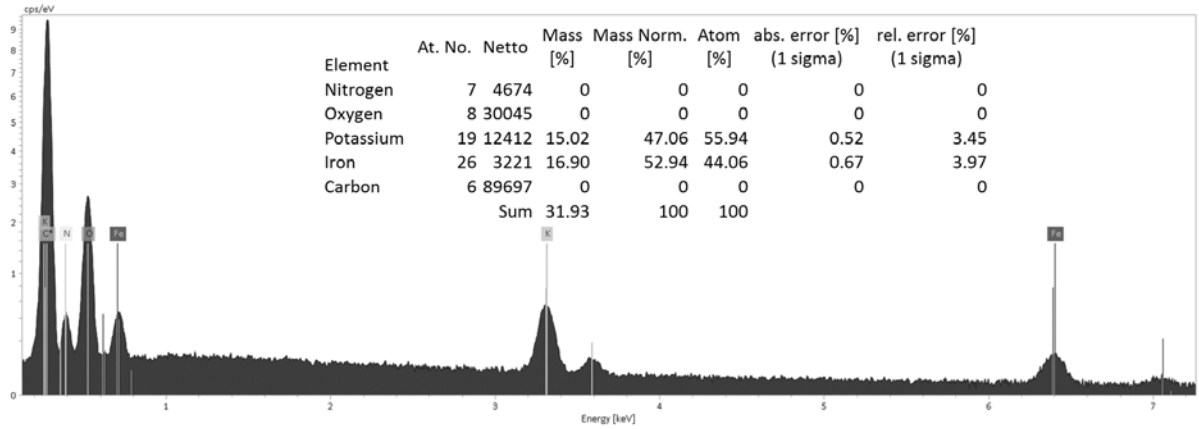

Figure S17. EDX spectrum of **2** and the resulting Fe:K ratio.

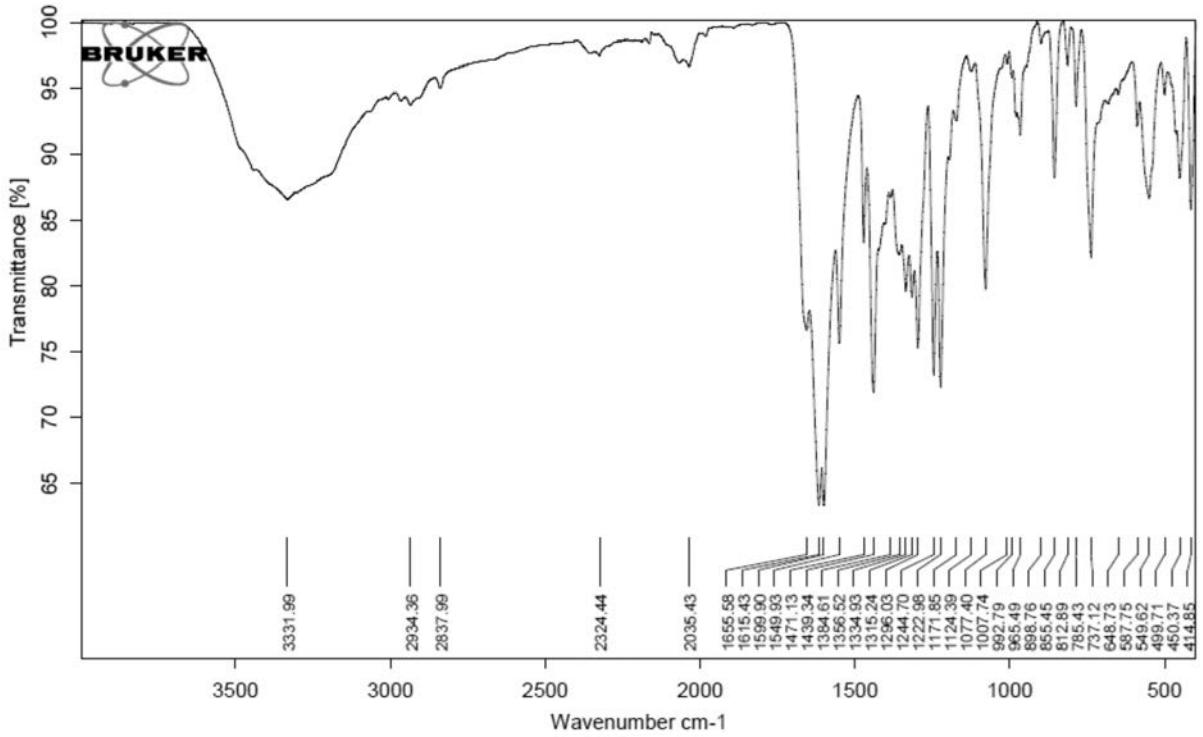

Figure S18. IR spectrum for **2** dried *in vacuo* and recorded recently after synthesis.

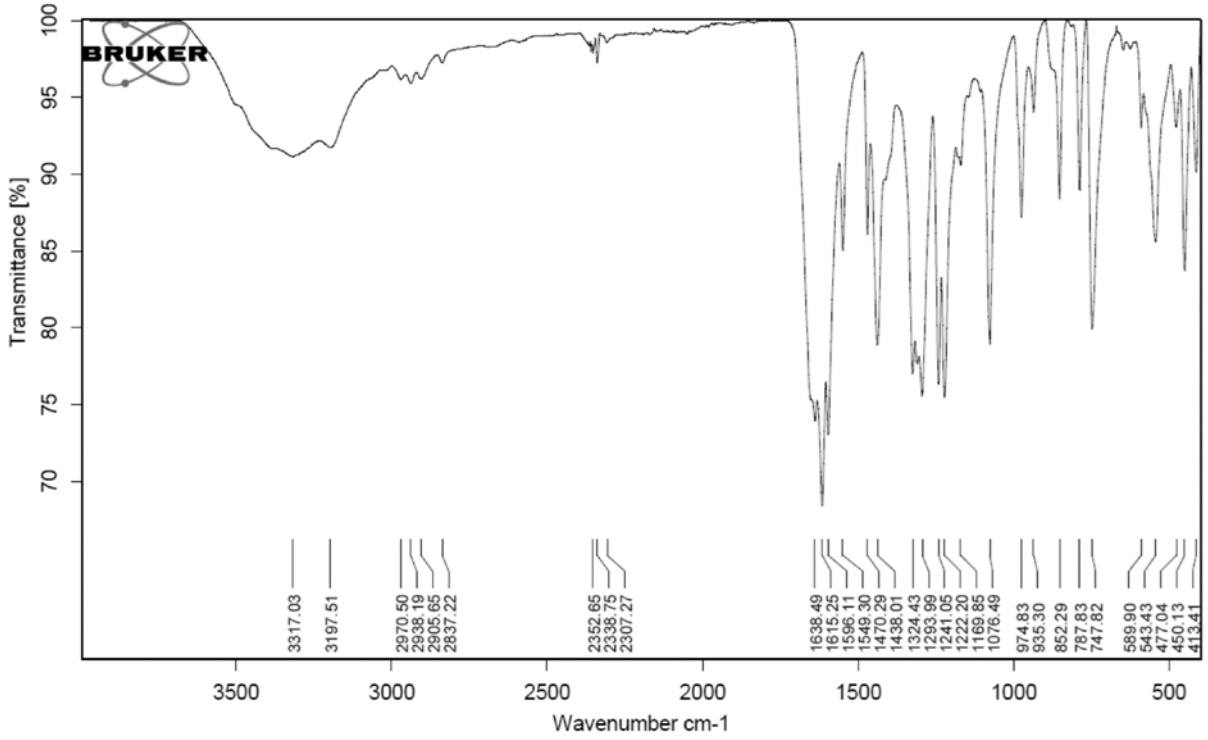

Figure S19. IR spectrum for **2** dried *in vacuo* and recorded several months after synthesis.

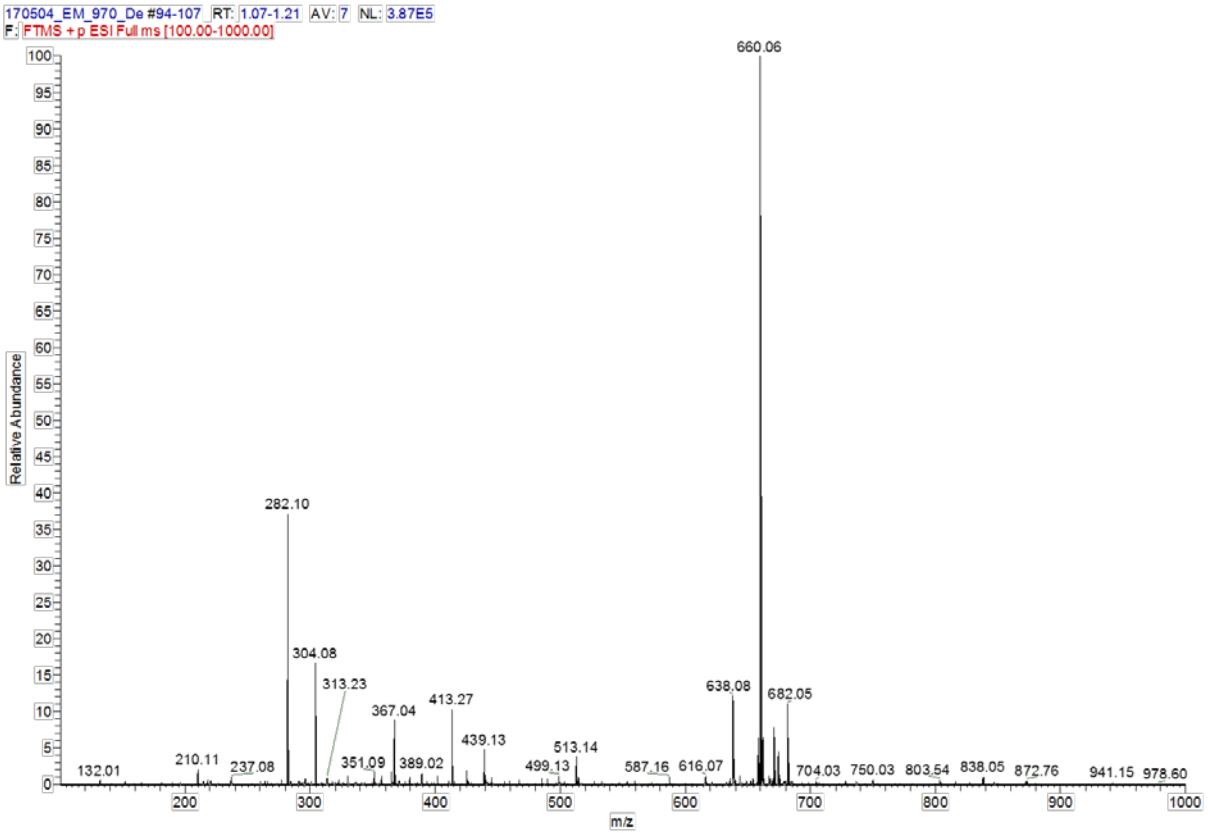

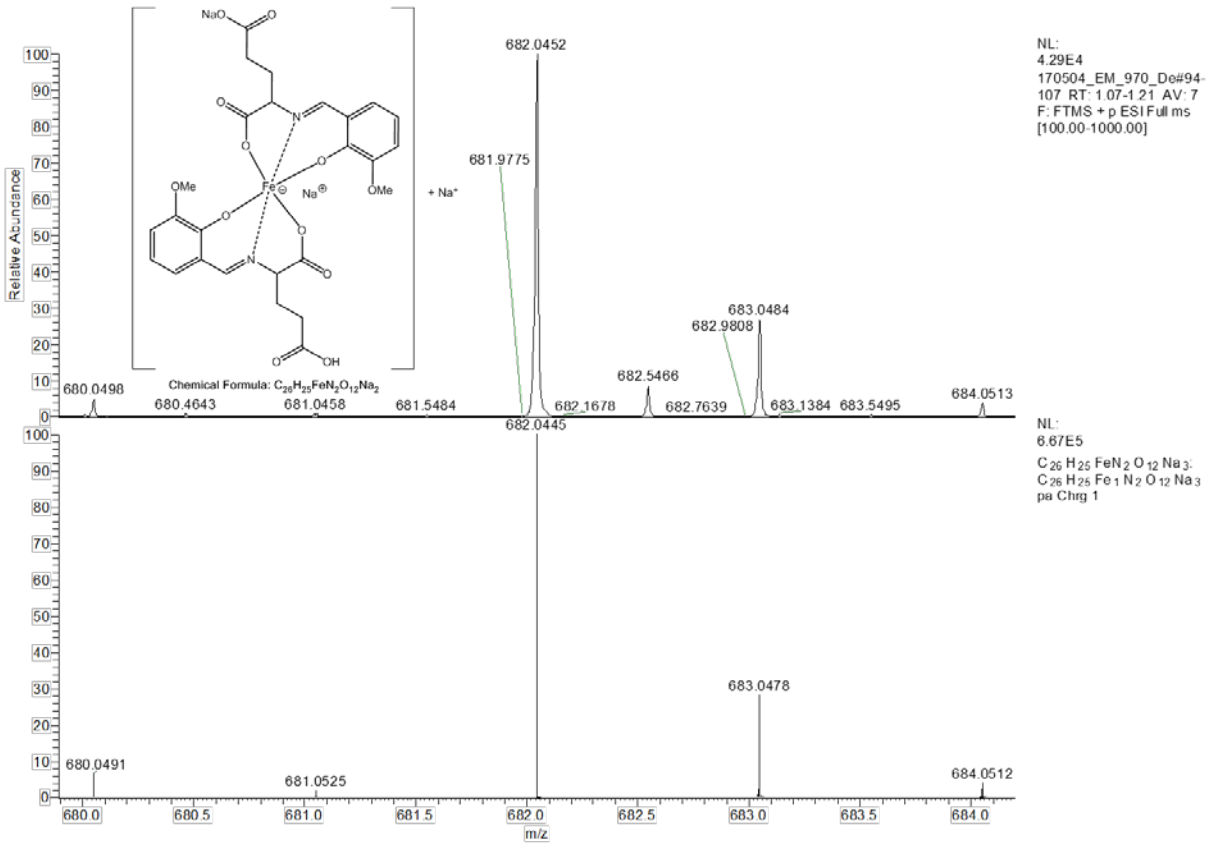
Relative Abundance
682.0452
681.9775
683.0484
682.9808
682.5466
680.0498
680.4643
681.0458
681.5484
682.1678
682.7639
683.1384
683.5495
684.0513
682.0445
+ Na+
Chemical Formula: C26H25FeN2O12Na2
NL:
4.29E4
170504_EM_970_De#94-107 RT: 1.07-1.21 AV: 7
F: FTMS + p ESI Full ms
[100.00-1000.00]
NL:
6.67E5
C26 H25 FeN2 O12 Na3:
C26 H25 Fe1 N2 O12 Na3
pa Chrg 1
683.0478
680.0491
681.0525
684.0512
m/z

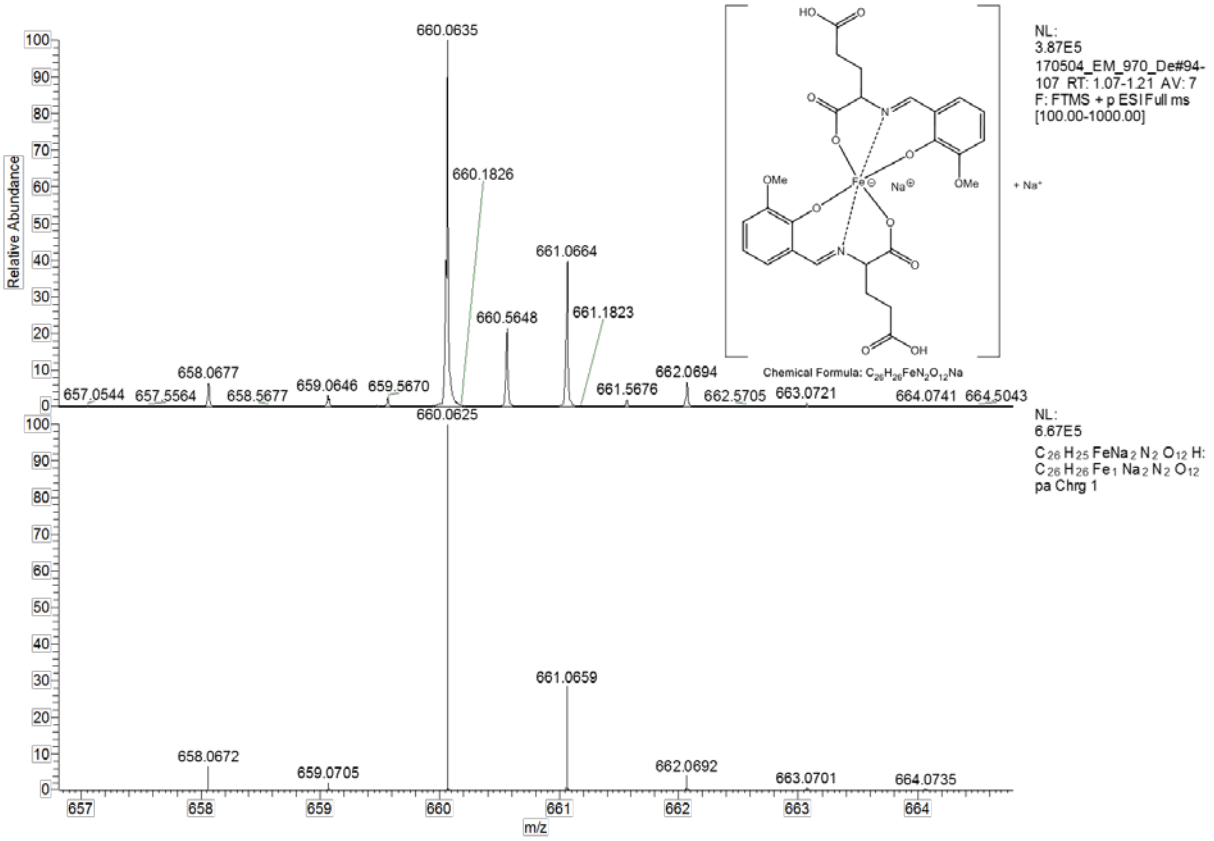
Relative Abundance
660.0635
660.1826
661.0664
660.5648
661.1823
658.0677
657.0544
657.5564
658.5677
659.0646
659.5670
661.5676
662.0694
662.5705
663.0721
664.0741
664.5043
660.0625
Chemical Formula: C26H26FeN2O12Na
+ Na+
NL:
3.87E5
170504_EM_970_De#94-107 RT: 1.07-1.21 AV: 7
F: FTMS + p ESI Full ms
[100.00-1000.00]
NL:
6.67E5
C26 H25 FeNa2 N2 O12 H:
C26 H26 Fe1 Na2 N2 O12
pa Chrg 1
661.0659
658.0672
659.0705
662.0692
663.0701
664.0735
m/z

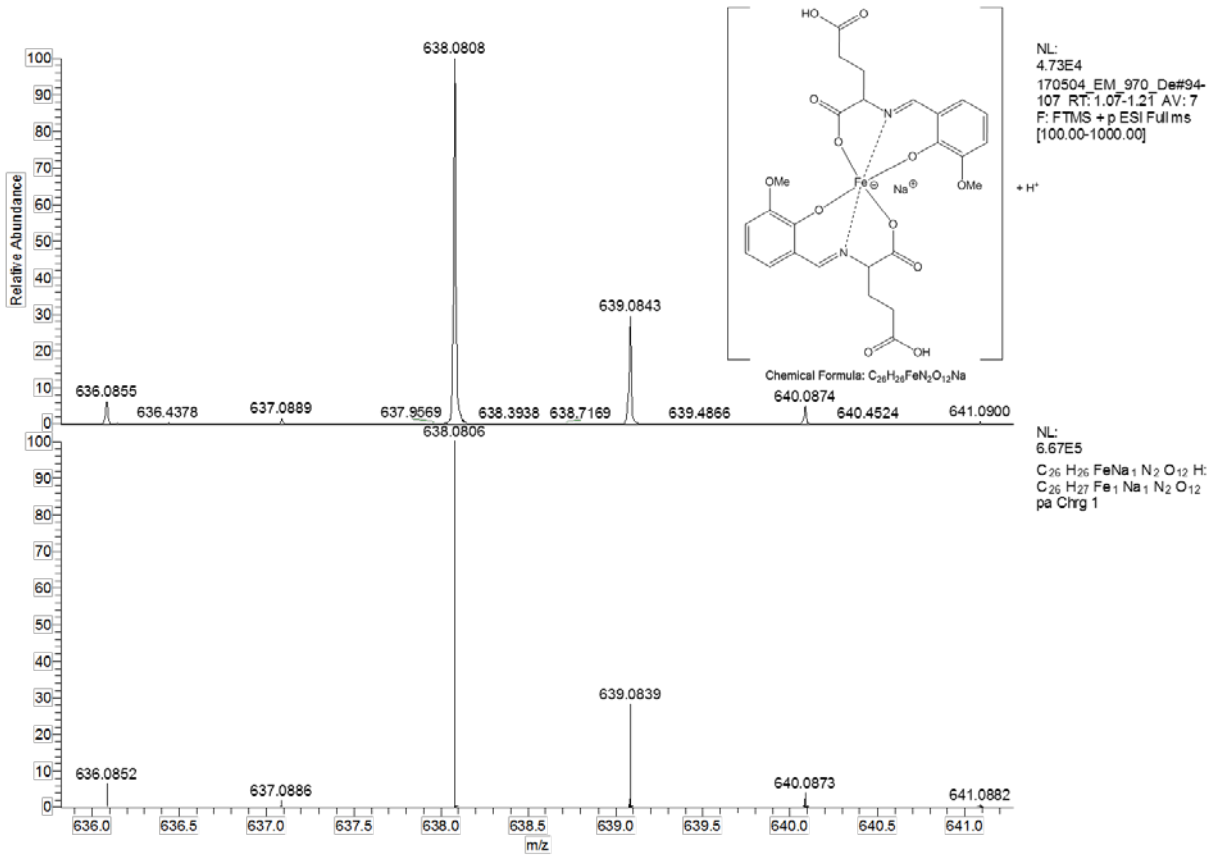
638.0808
639.0843
636.0855
636.4378
637.0889
637.9569
638.3938
638.7169
639.4866
640.0874
640.4524
641.0900
638.0806
639.0839
636.0852
637.0886
640.0873
641.0882
Relative Abundance
m/z
Chemical Formula: C26H28FeN2O12Na
+ H+
NL:
4.73E4
170504_EM_970_De#94-107 RT: 1.07-1.21 AV: 7
F: FTMS + p ESI Full ms
[100.00-1000.00]
NL:
6.67E5
C26 H26 FeNa1 N2 O12 H:
C26 H27 Fe1 Na1 N2 O12
pa Chrg 1

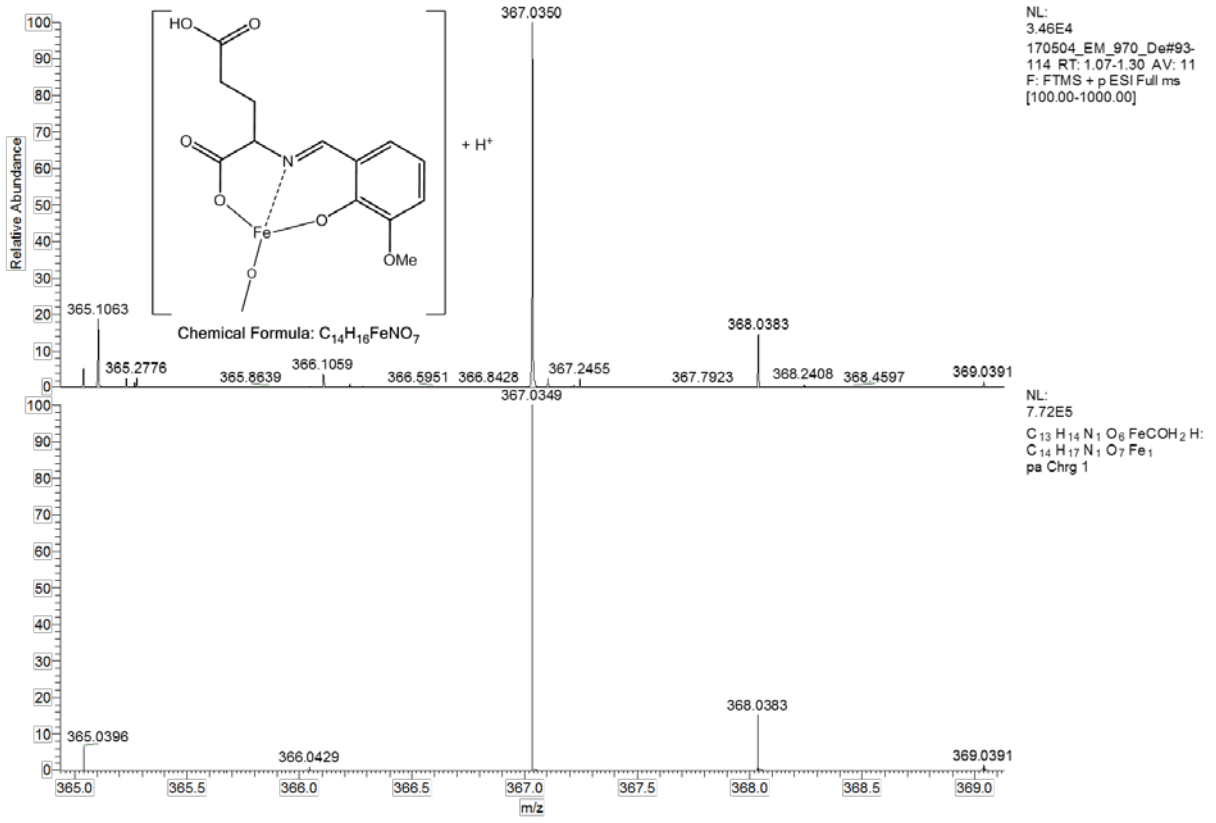
367.0350
365.1063
368.0383
365.2776
365.8639
366.1059
366.5951
366.8428
367.2455
367.7923
368.2408
368.4597
369.0391
367.0349
365.0396
366.0429
368.0383
369.0391
Relative Abundance
m/z
Chemical Formula: C14H16FeNO7
+ H+
NL:
3.46E4
170504_EM_970_De#93-114 RT: 1.07-1.30 AV: 11
F: FTMS + p ESI Full ms
[100.00-1000.00]
NL:
7.72E5
C13 H14 N1 O6 FeCOH2 H:
C14 H17 N1 O7 Fe1
pa Chrg 1

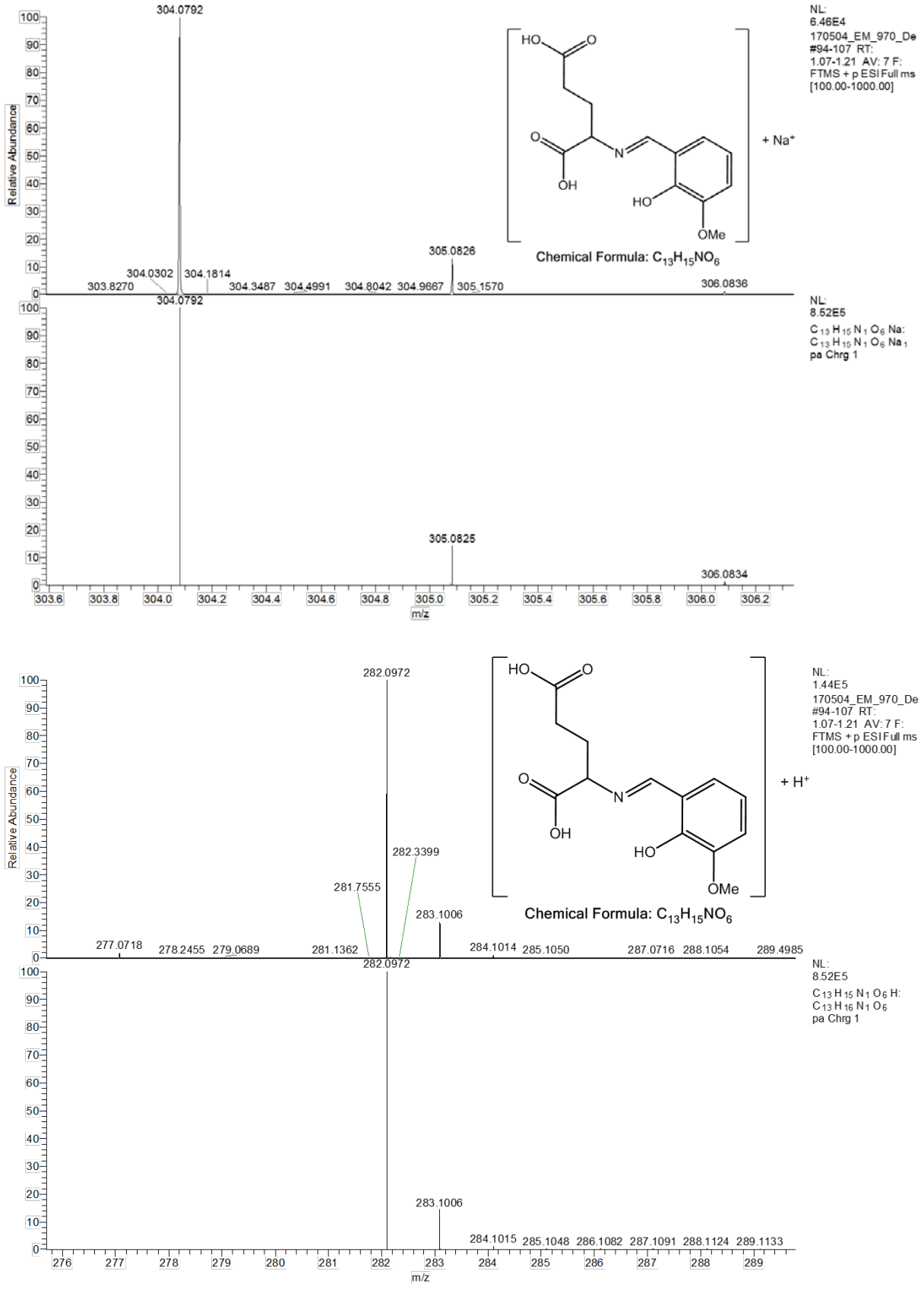

Figure S20. ESI(+)-MS spectrum of **3** in methanol with simulation of the identified peaks and structure suggestion.

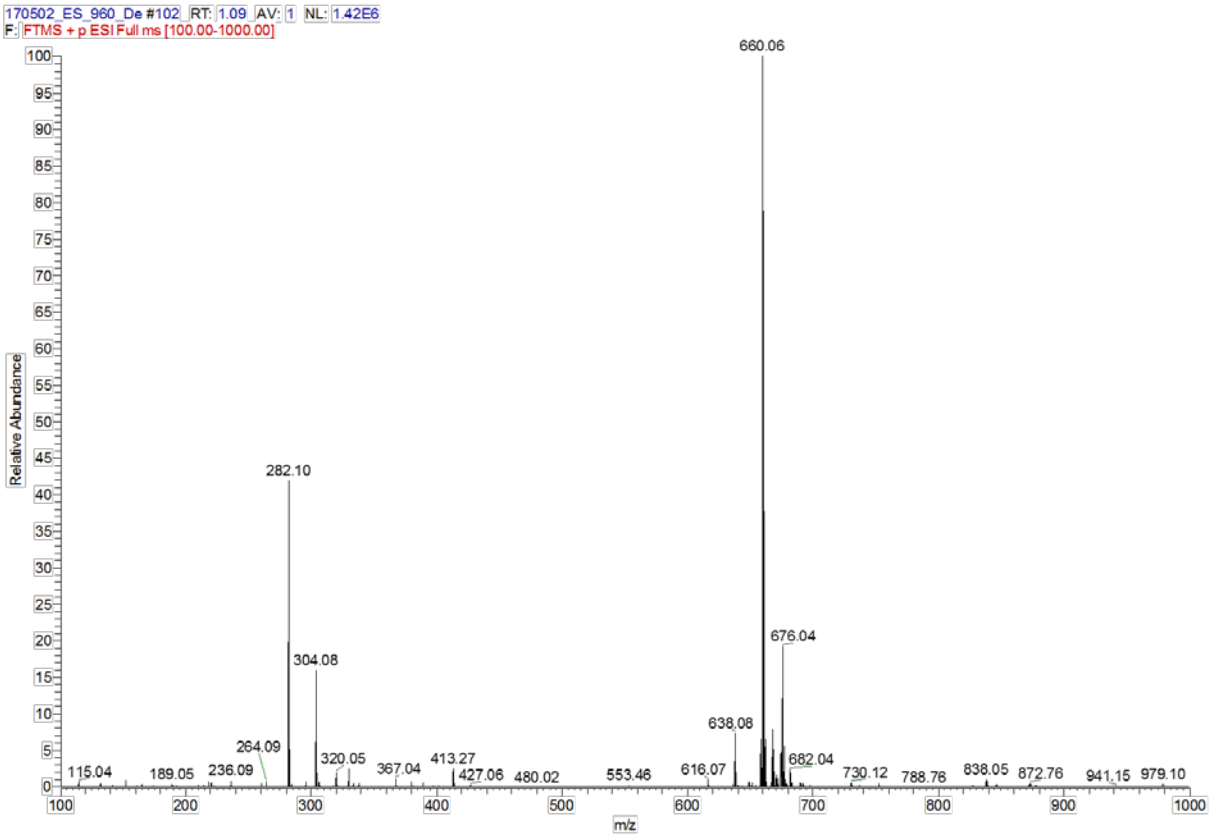

Figure S21. ESI(+)-MS spectrum of **3** in water. Due to the similar fragmentation pattern compared to the spectrum in methanol, simulation of the identified peaks is not shown.

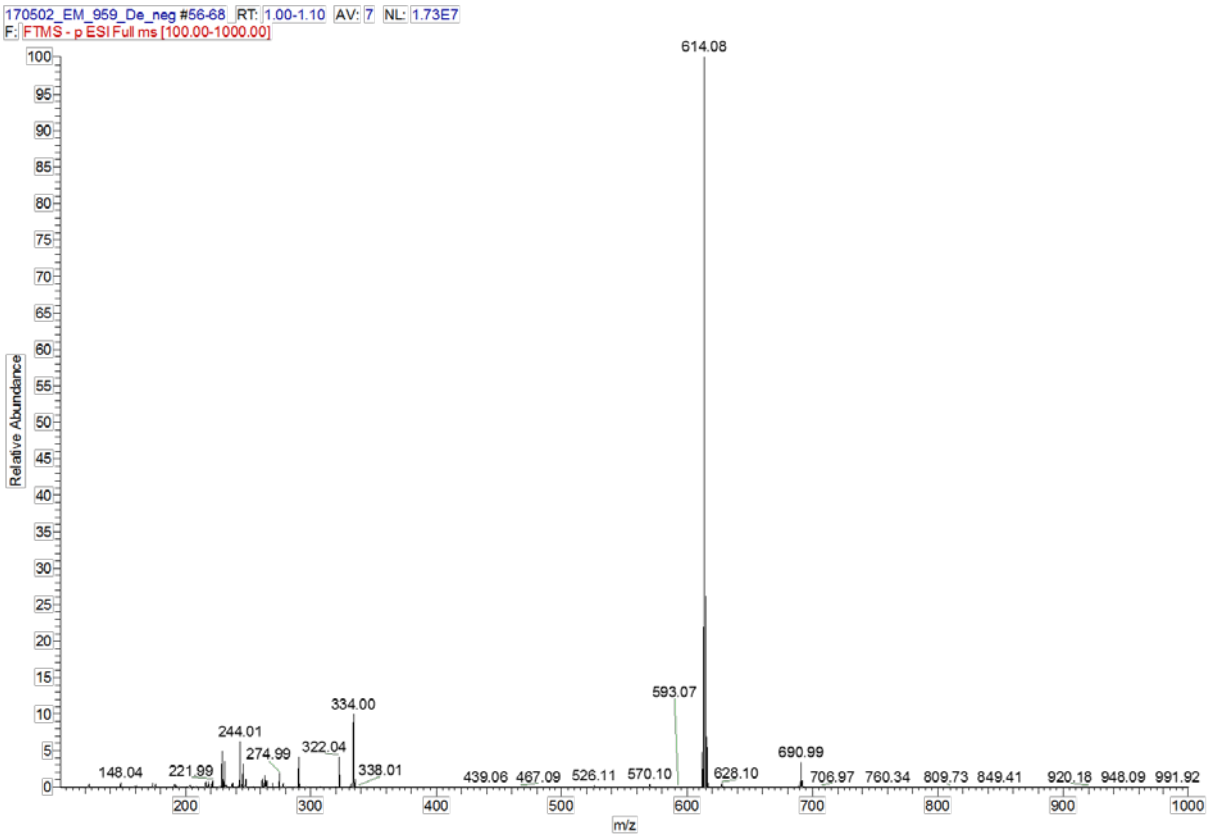

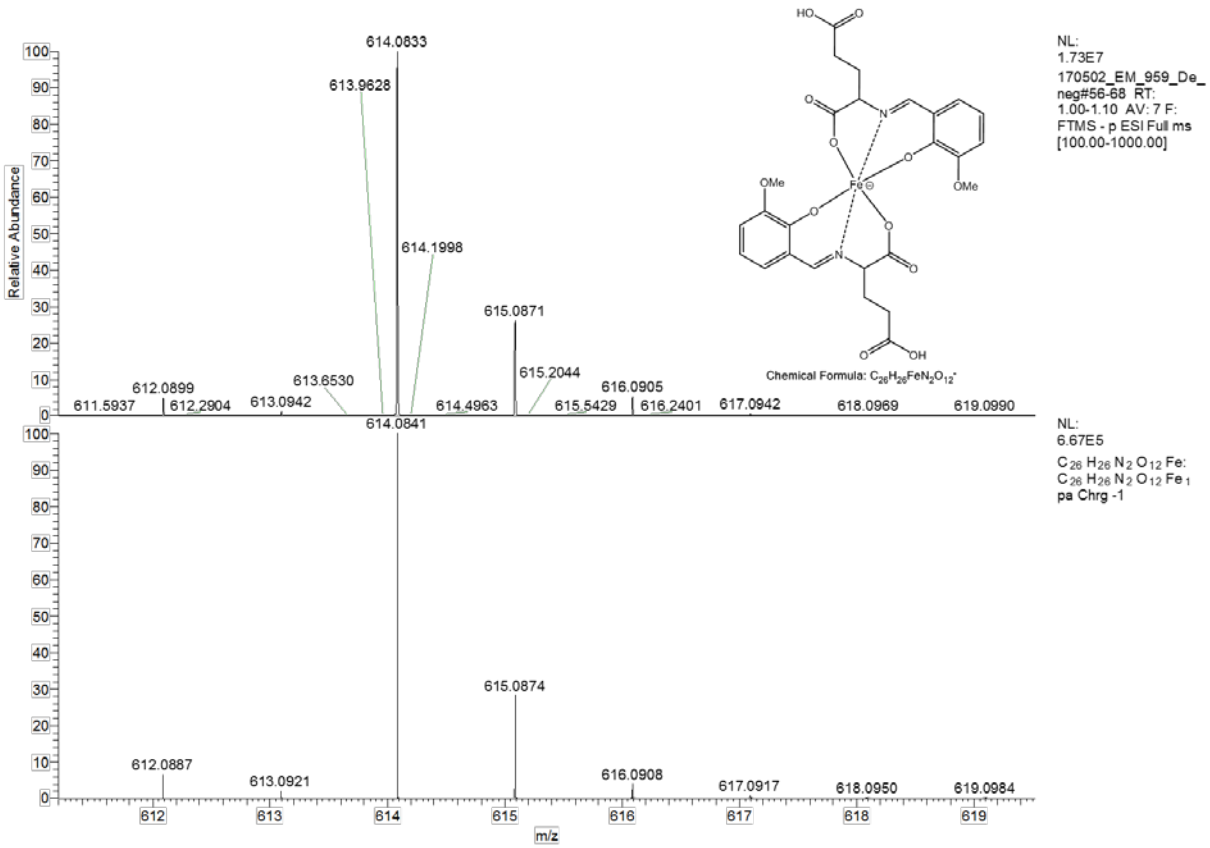
614.0833
613.9628
614.1998
615.0871
615.2044
612.0899
611.5937
612.2904
613.6530
613.0942
614.4963
615.5429
616.0905
616.2401
617.0942
618.0969
619.0990
614.0841
Relative Abundance
NL:
1.73E7
170502_EM_959_De_
neg#56-68 RT:
1.00-1.10 AV: 7 F:
FTMS - p ESI Full ms
[100.00-1000.00]
Chemical Formula: C26H26FeN2O12-
NL:
6.67E5
C26 H26 N2 O12 Fe:
C26 H26 N2 O12 Fe1
pa Chrg -1
615.0874
612.0887
613.0921
616.0908
617.0917
618.0950
619.0984
m/z

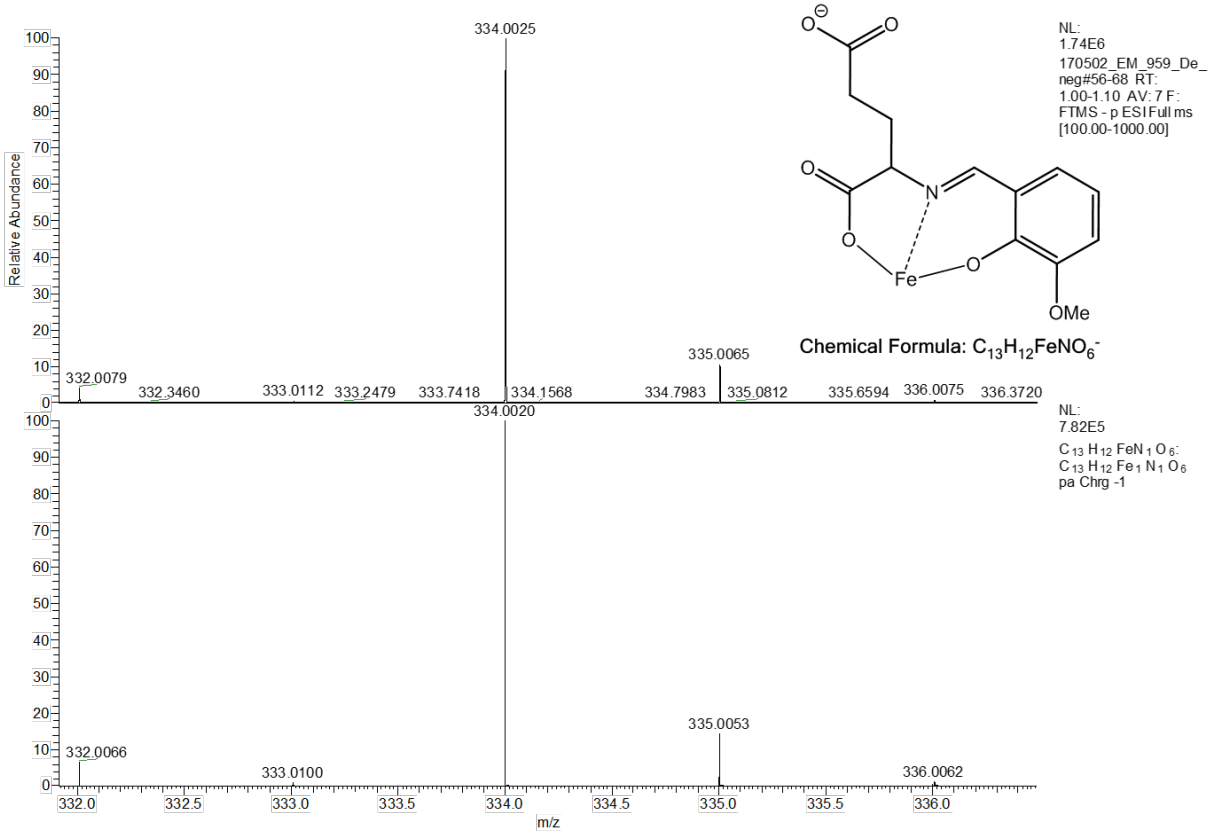
334.0025
335.0065
332.0079
332.3460
333.0112
333.2479
333.7418
334.1568
334.7983
335.0812
335.6594
336.0075
336.3720
334.0020
Relative Abundance
NL:
1.74E6
170502_EM_959_De_
neg#56-68 RT:
1.00-1.10 AV: 7 F:
FTMS - p ESI Full ms
[100.00-1000.00]
Chemical Formula: C13H12FeNO6-
NL:
7.82E5
C13 H12 FeN1 O6:
C13 H12 Fe1 N1 O6
pa Chrg -1
335.0053
332.0066
333.0100
336.0062
m/z

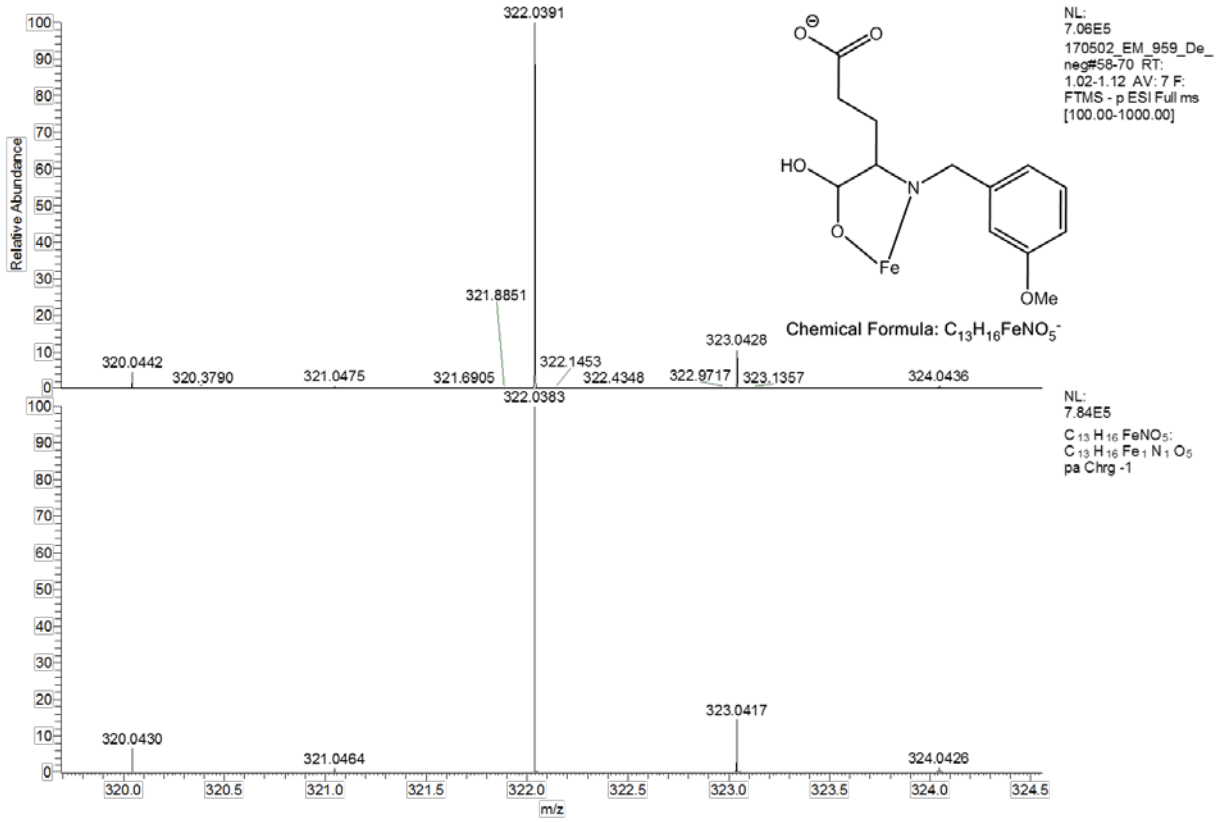

Figure S22. ESI(-)-MS spectrum of **3** in methanol with simulation of the identified peaks and structure suggestions.

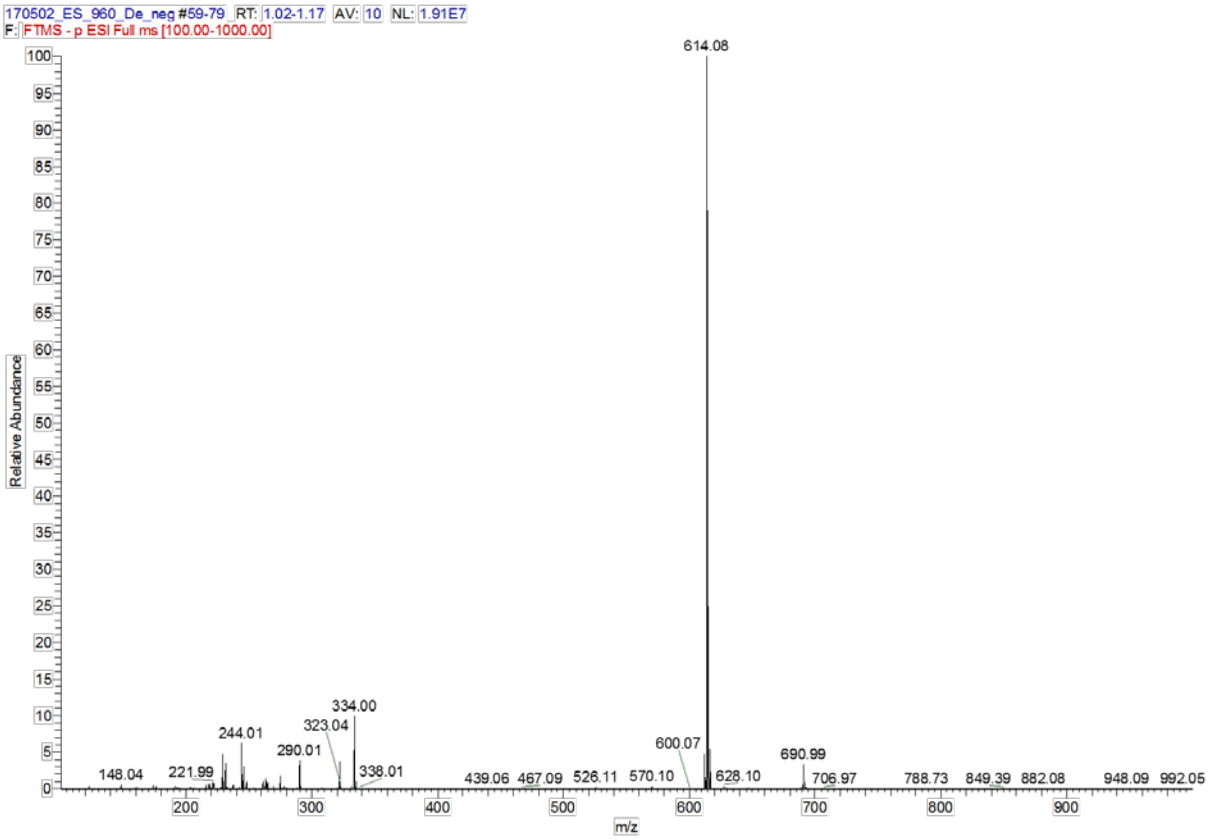

Figure S23. ESI(-)-MS spectrum of **3** in water. Due to the similar fragmentation pattern compared to the spectrum in methanol, simulation of the identified peaks is not shown.

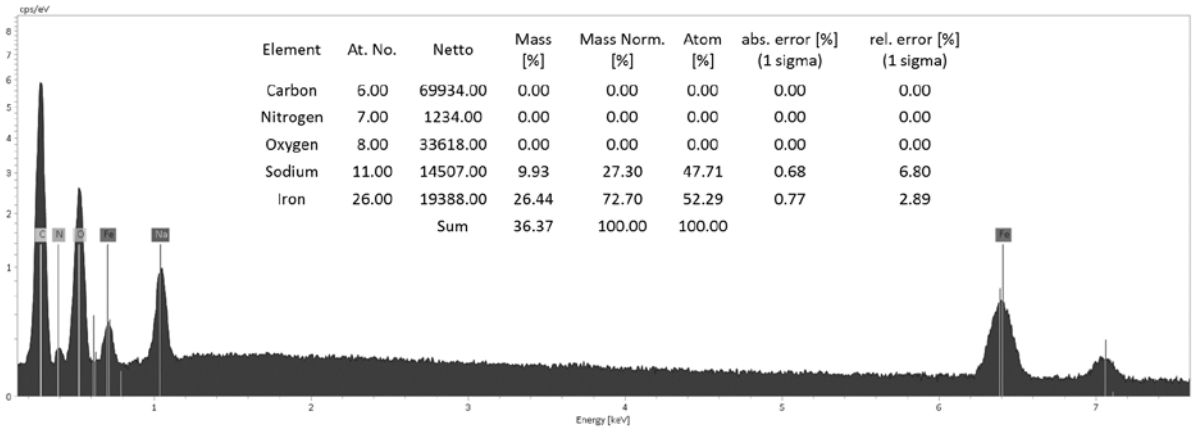

Figure S24. EDX spectrum of **3** and the resulting Fe:Na ratio.

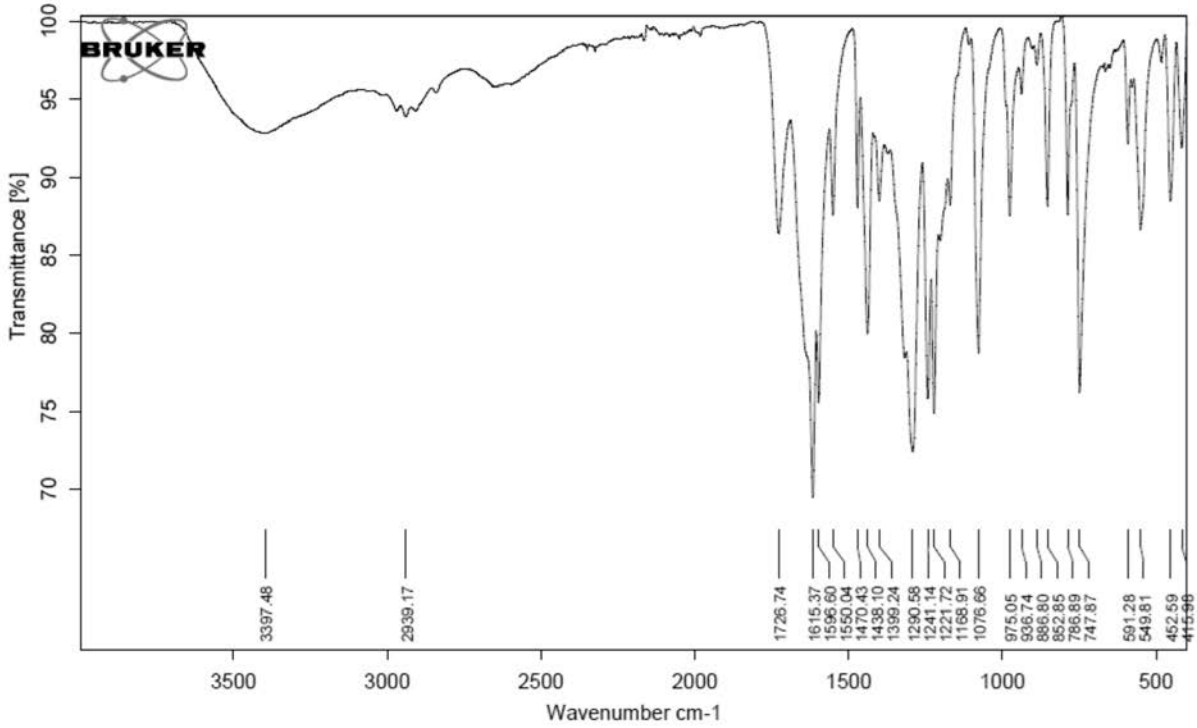

Figure S25. IR spectrum for **3** dried *in vacuo* and recorded directly after synthesis.

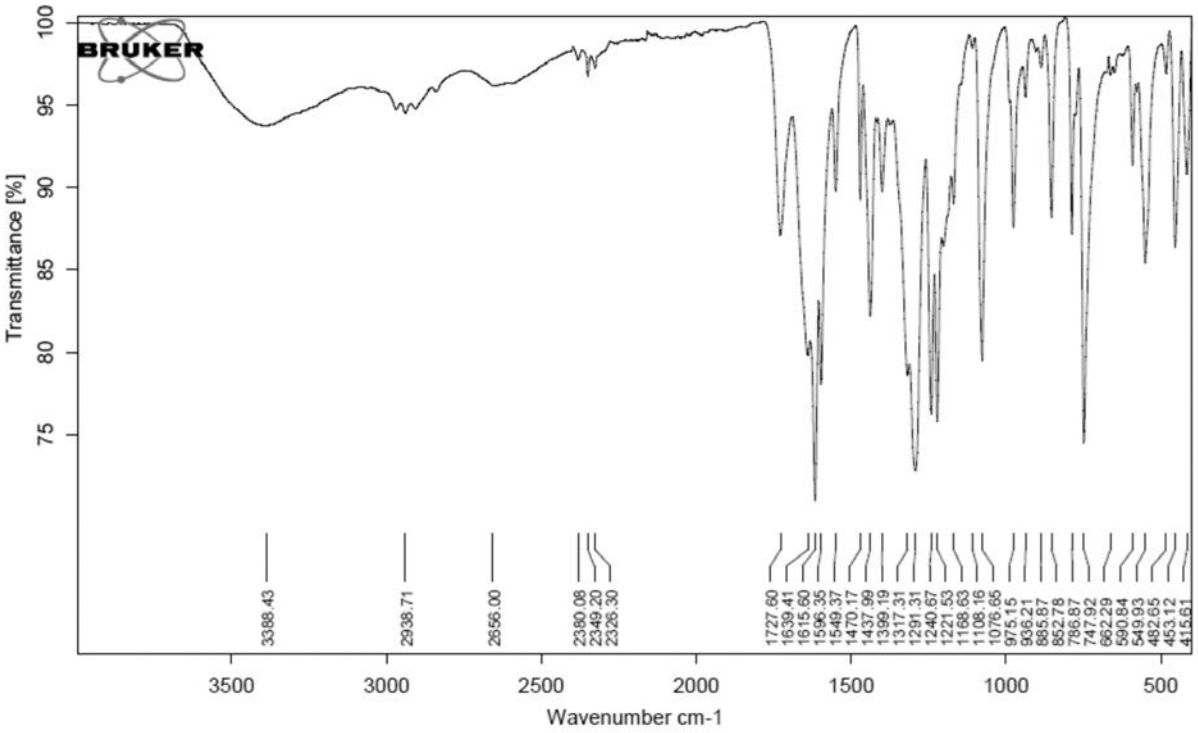

Figure S26. IR spectrum for **3** dried *in vacuo* and recorded several months after synthesis.

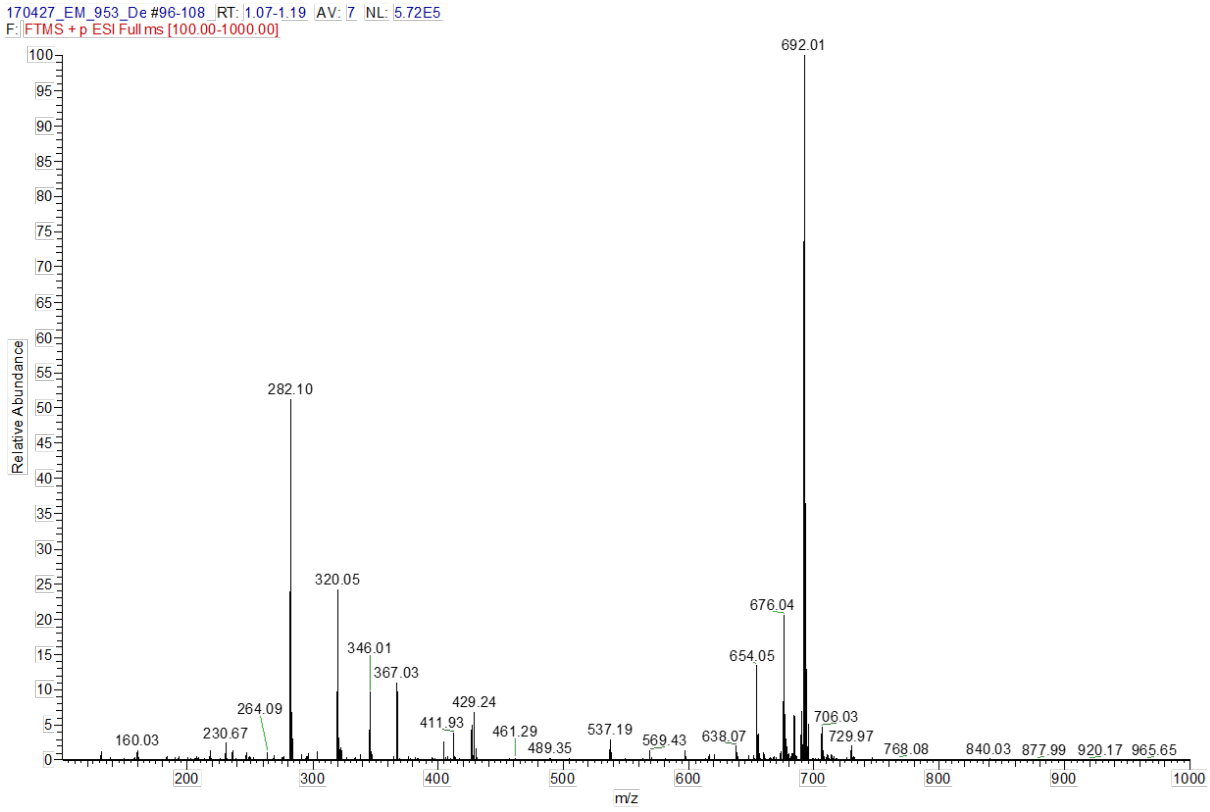

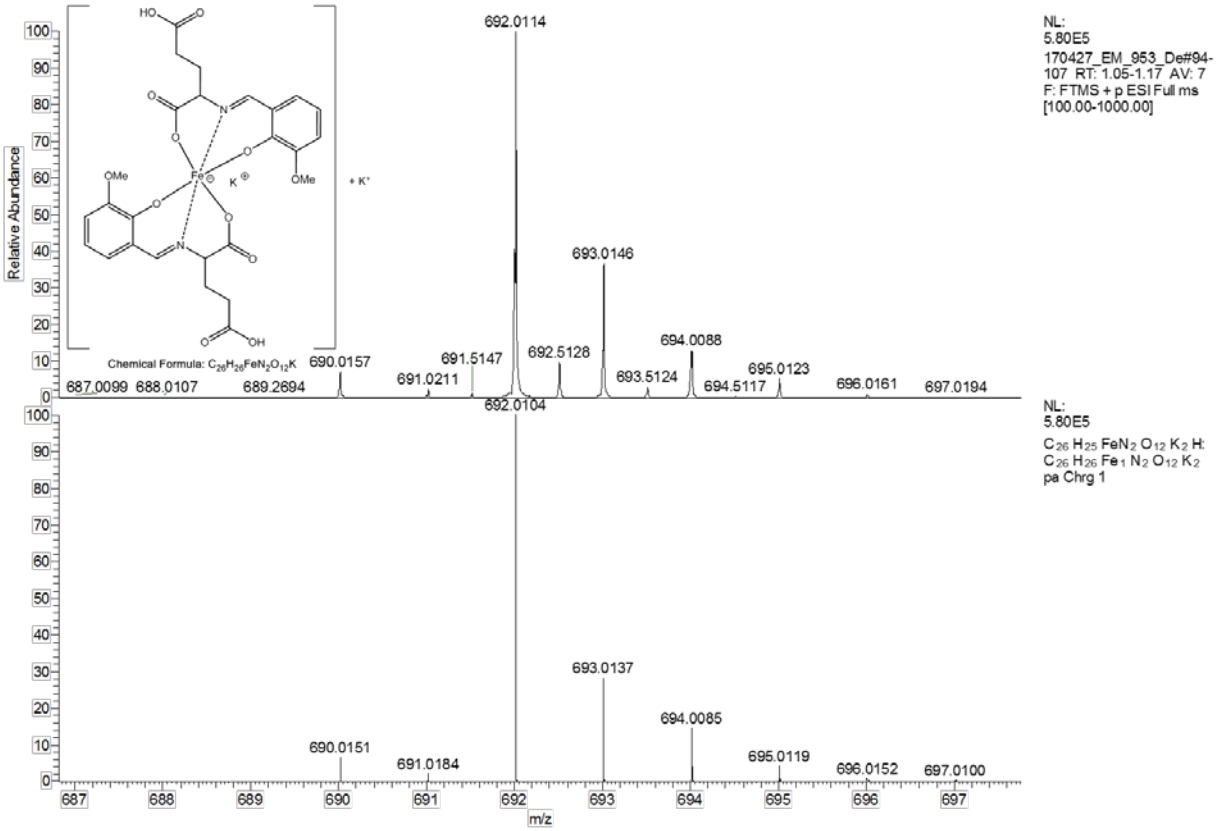
692.0114
693.0146
694.0088
695.0123
690.0157
691.5147
692.5128
691.0211
693.5124
694.5117
696.0161
697.0194
687.0099
688.0107
689.2694
+ K+
Chemical Formula: C26H26FeN2O12K
NL:
5.80E5
170427_EM_953_De#94-107 RT: 1.05-1.17 AV: 7 F: FTMS + p ESI Full ms [100.00-1000.00]
692.0104
693.0137
694.0085
690.0151
691.0184
695.0119
696.0152
697.0100
NL:
5.80E5
C26 H25 FeN2 O12 K2 H: C26 H26 Fe1 N2 O12 K2 pa Chrg 1
Relative Abundance
m/z

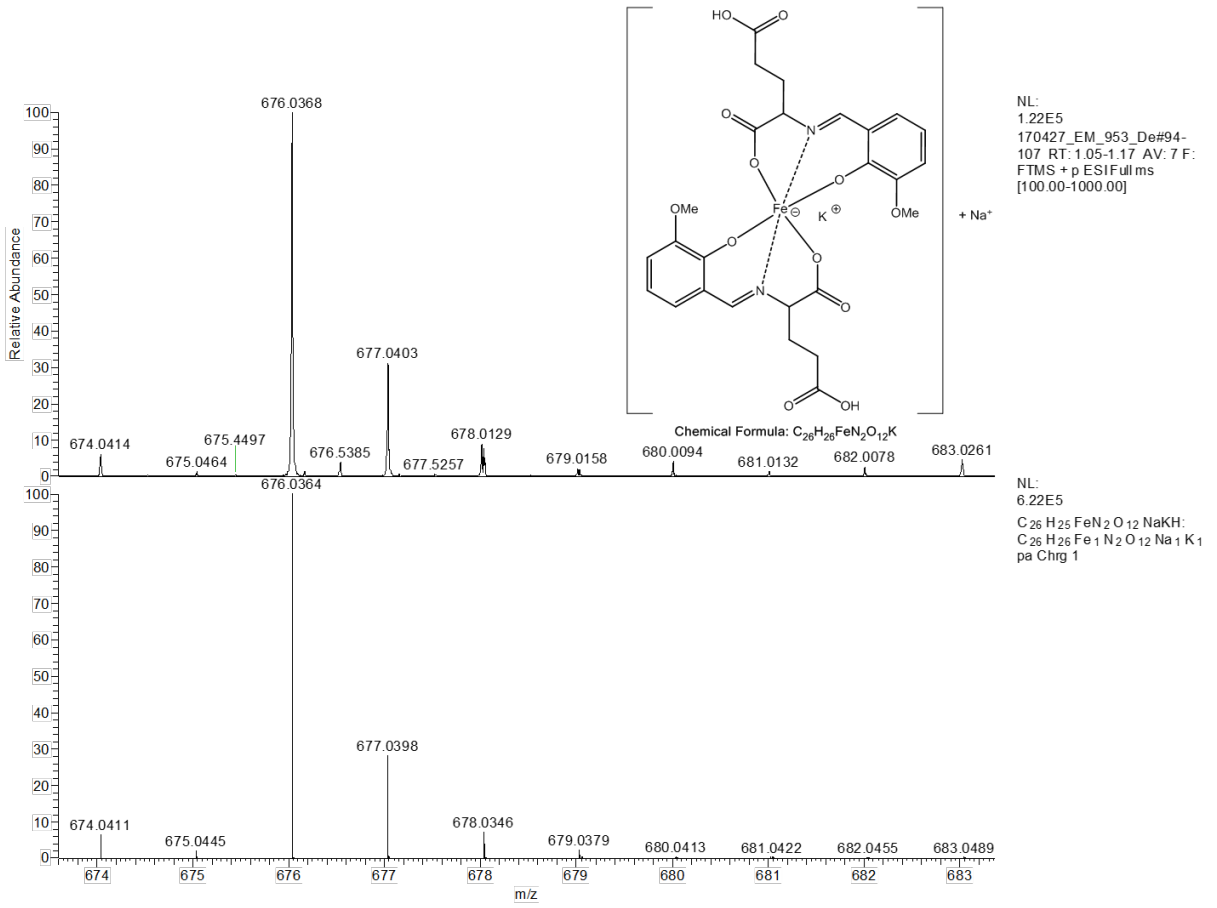
676.0368
677.0403
674.0414
675.4497
675.0464
676.5385
677.5257
678.0129
679.0158
680.0094
681.0132
682.0078
683.0261
+ Na+
Chemical Formula: C26H26FeN2O12K
NL:
1.22E5
170427_EM_953_De#94-107 RT: 1.05-1.17 AV: 7 F: FTMS + p ESI Full ms [100.00-1000.00]
676.0364
677.0398
674.0411
675.0445
678.0346
679.0379
680.0413
681.0422
682.0455
683.0489
NL:
6.22E5
C26 H25 FeN2 O12 NaKH: C26 H26 Fe1 N2 O12 Na1 K1 pa Chrg 1
Relative Abundance
m/z

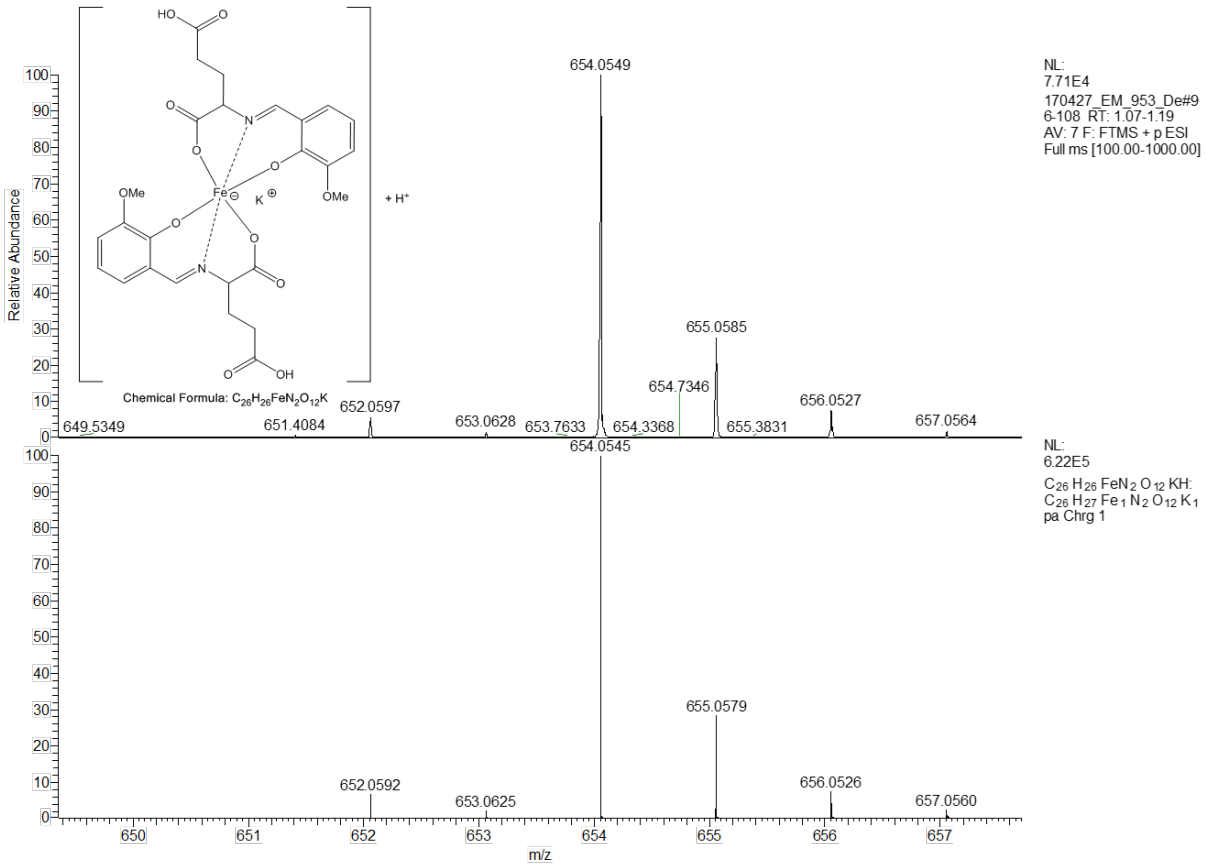
Relative Abundance
m/z
654.0549
655.0585
654.7346
656.0527
652.0597
649.5349
651.4084
653.0628
653.7633
654.3368
655.3831
657.0564
+ H+
Chemical Formula: C26H26FeN2O12K
NL:
7.71E4
170427_EM_953_De#9
6-108 RT: 1.07-1.19
AV: 7 F: FTMS + p ESI
Full ms [100.00-1000.00]
654.0545
655.0579
652.0592
653.0625
656.0526
657.0560
NL:
6.22E5
C26 H26 FeN2 O12 KH:
C26 H27 Fe1 N2 O12 K1
pa Chrg 1

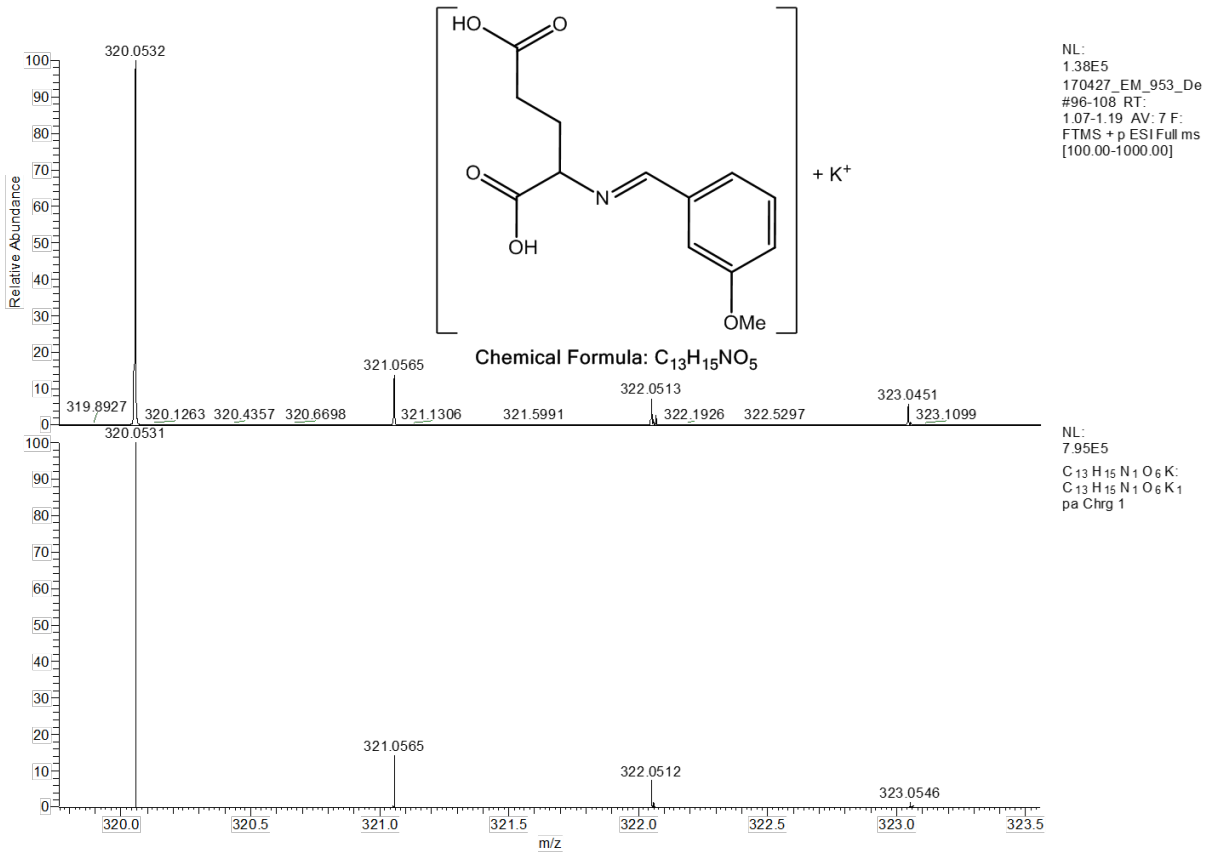
Relative Abundance
m/z
320.0532
321.0565
322.0513
319.8927
320.1263
320.4357
320.6698
321.1306
321.5991
322.1926
322.5297
323.0451
323.1099
+ K+
Chemical Formula: C13H15NO5
NL:
1.38E5
170427_EM_953_De
#96-108 RT:
1.07-1.19 AV: 7 F:
FTMS + p ESI Full ms
[100.00-1000.00]
320.0531
321.0565
322.0512
323.0546
NL:
7.95E5
C13 H15 N1 O6 K:
C13 H15 N1 O6 K1
pa Chrg 1

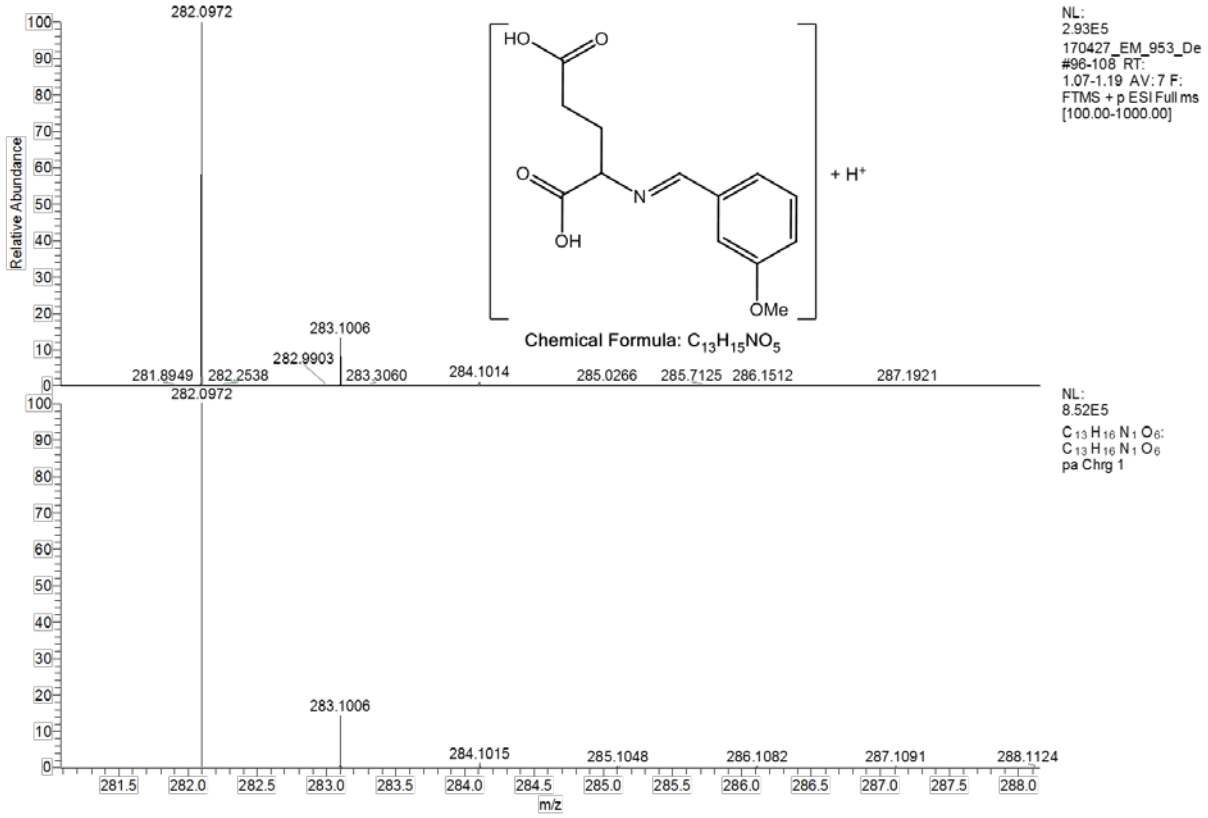

Figure S27. ESI(+)-MS spectrum of **4** in methanol with simulation of the identified peaks and structure suggestion.

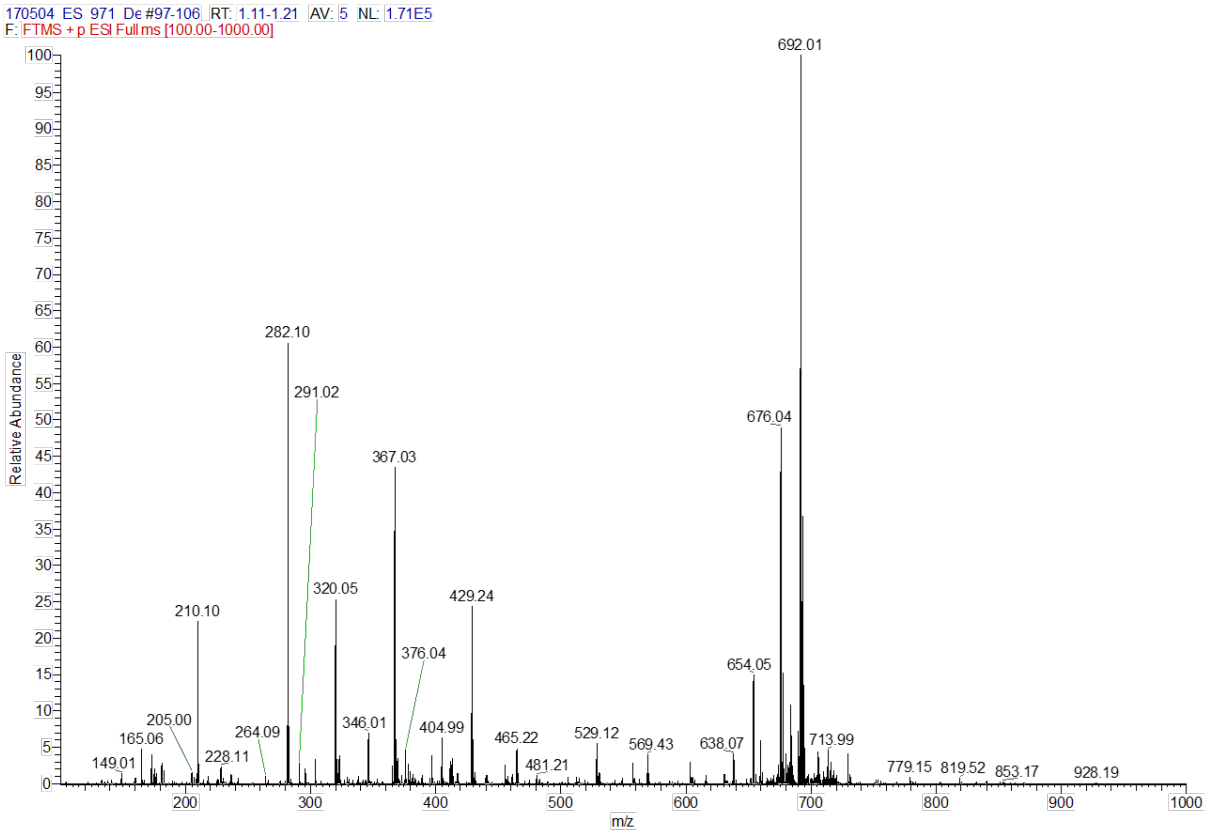

Figure S28. ESI(+)-MS spectrum of **4** in water. Due to the similar fragmentation pattern compared to the spectrum in methanol, simulation of the identified peaks is not shown.

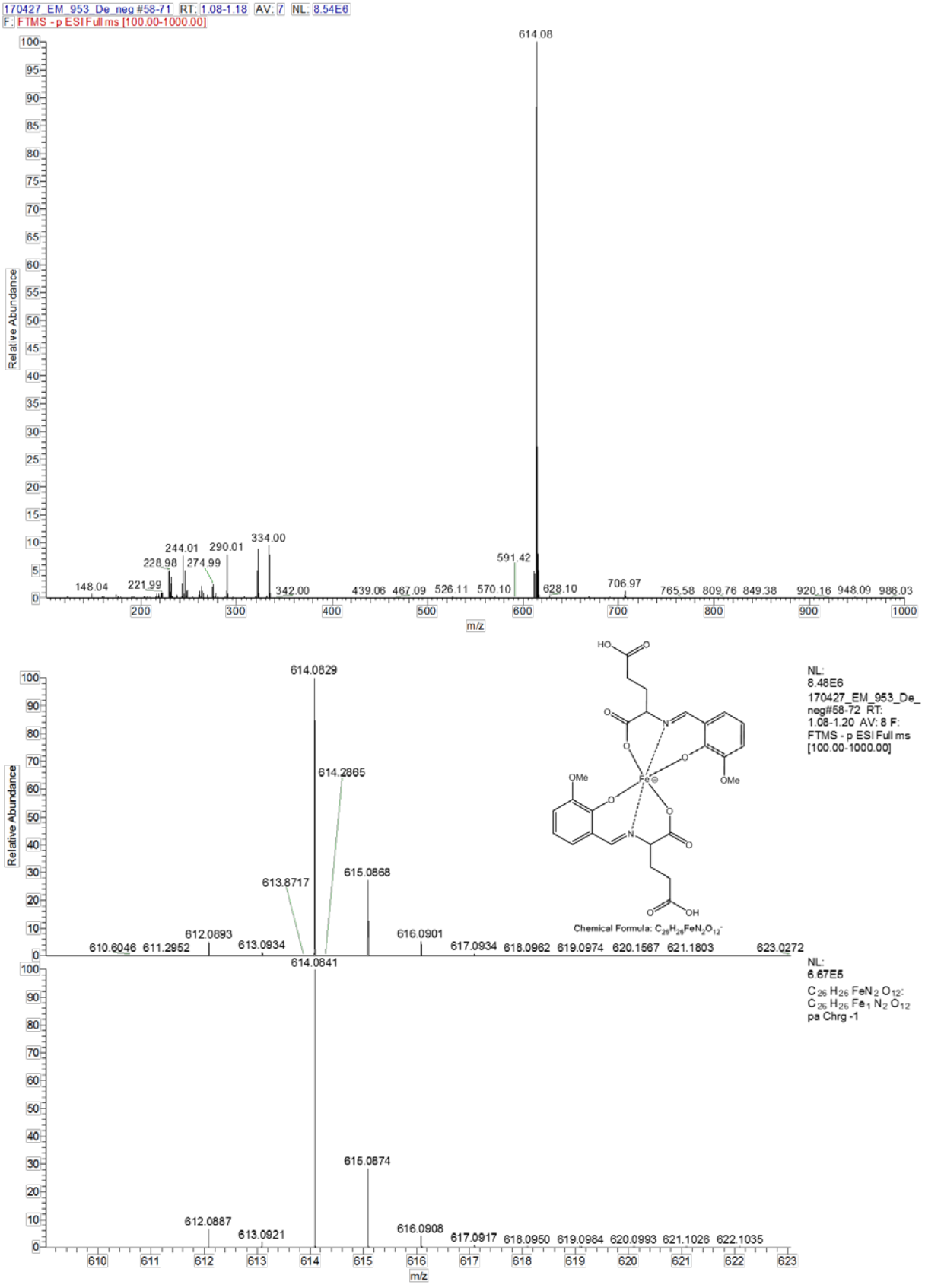
170427_EM_953_De_neg #58-71 RT: 1.08-1.18 AV: 7 NL: 8.54E6
F: FTMS - p ESI Full ms [100.00-1000.00]
614.08
591.42
334.00
290.01
244.01
228.98
274.99
148.04
221.99
342.00
439.06 467.09 526.11 570.10
628.10
706.97
765.58 809.76 849.38
920.16 948.09 986.03
Relative Abundance
m/z
614.0829
614.2865
613.8717
615.0868
612.0893
610.6046 611.2952
613.0934
616.0901
617.0934 618.0962 619.0974 620.1567 621.1803
623.0272
614.0841
615.0874
612.0887
613.0921
616.0908
617.0917 618.0950 619.0984 620.0993 621.1026 622.1035
OMe
OMe
Fe
OH
Chemical Formula: C26H26FeN2O12-
NL:
8.48E6
170427_EM_953_De_
neg#58-72 RT:
1.08-1.20 AV: 8 F:
FTMS - p ESI Full ms
[100.00-1000.00]
NL:
6.67E5
C26 H26 FeN2 O12:
C26 H26 Fe1 N2 O12
pa Chrg -1

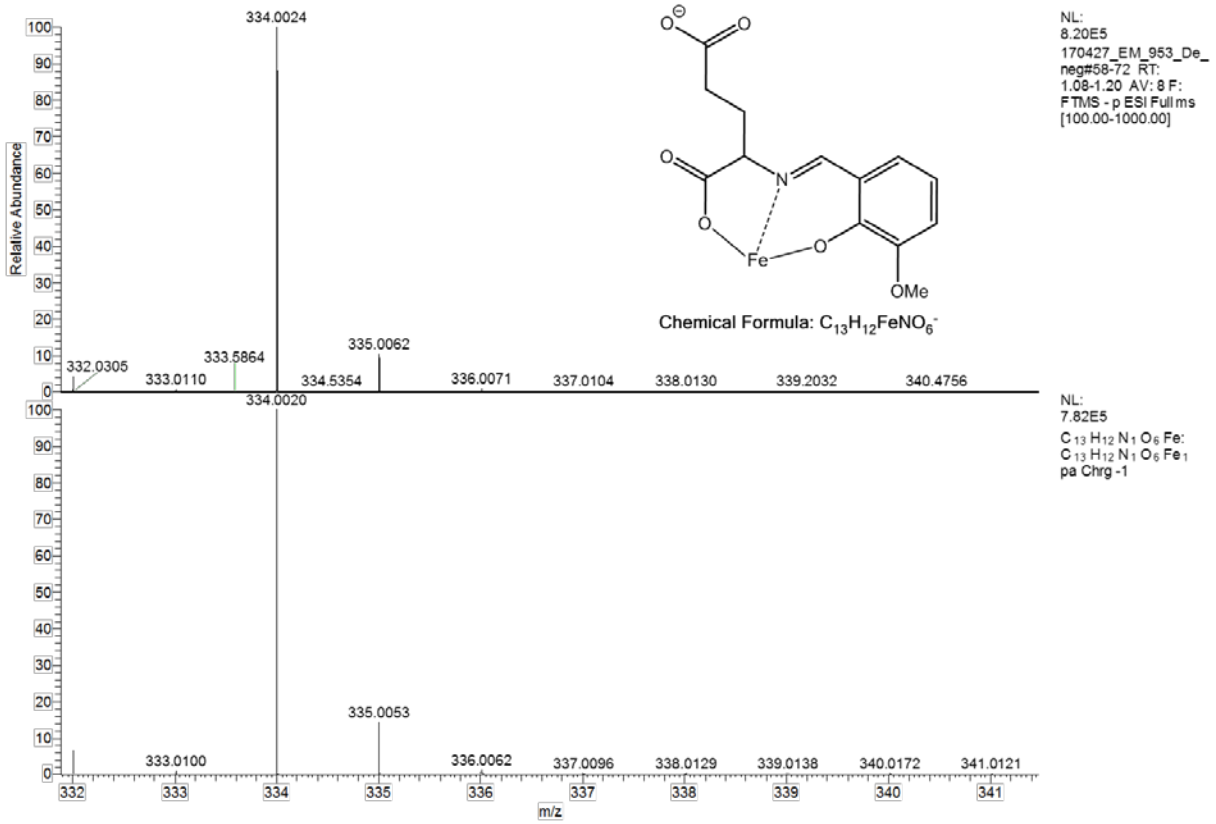
334.0024
Relative Abundance
332.0305
333.0110
333.5864
334.5354
335.0062
336.0071
337.0104
338.0130
339.2032
340.4756
334.0020
335.0053
333.0100
336.0062
337.0096
338.0129
339.0138
340.0172
341.0121
m/z
Chemical Formula: C13H12FeNO6-
NL:
8.20E5
170427_EM_953_De_
neg#58-72 RT:
1.08-1.20 AV: 8 F:
FTMS - p ESI Full ms
[100.00-1000.00]
NL:
7.82E5
C13 H12 N1 O6 Fe:
C13 H12 N1 O6 Fe1
pa Chrg -1

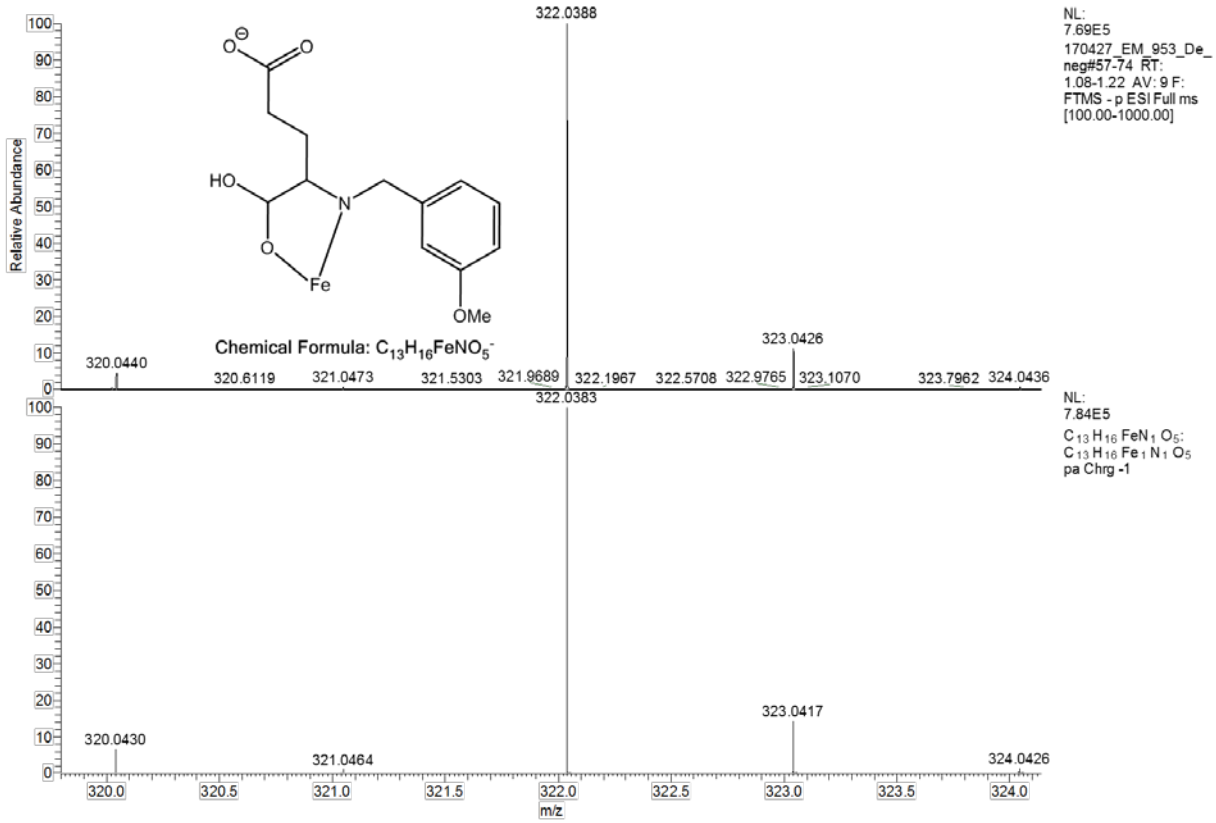
322.0388
Relative Abundance
320.0440
320.6119
321.0473
321.5303
321.9689
322.0383
322.1967
322.5708
322.9765
323.0426
323.1070
323.7962
324.0436
320.0430
321.0464
323.0417
324.0426
m/z
Chemical Formula: C13H16FeNO5-
NL:
7.69E5
170427_EM_953_De_
neg#57-74 RT:
1.08-1.22 AV: 9 F:
FTMS - p ESI Full ms
[100.00-1000.00]
NL:
7.84E5
C13 H16 Fe N1 O5:
C13 H16 Fe1 N1 O5
pa Chrg -1

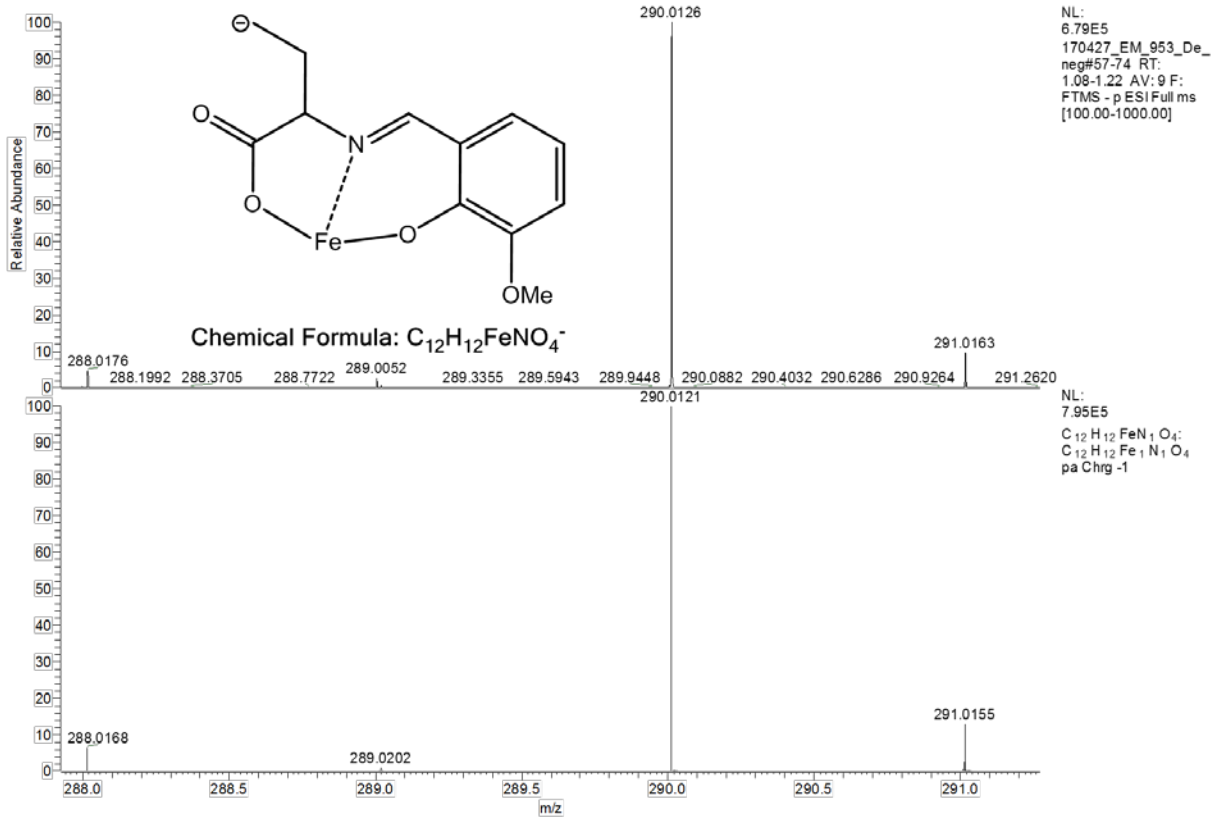

Figure S29. ESI(-)-MS spectrum of **4** in methanol with simulation of the identified peaks and structure suggestion.

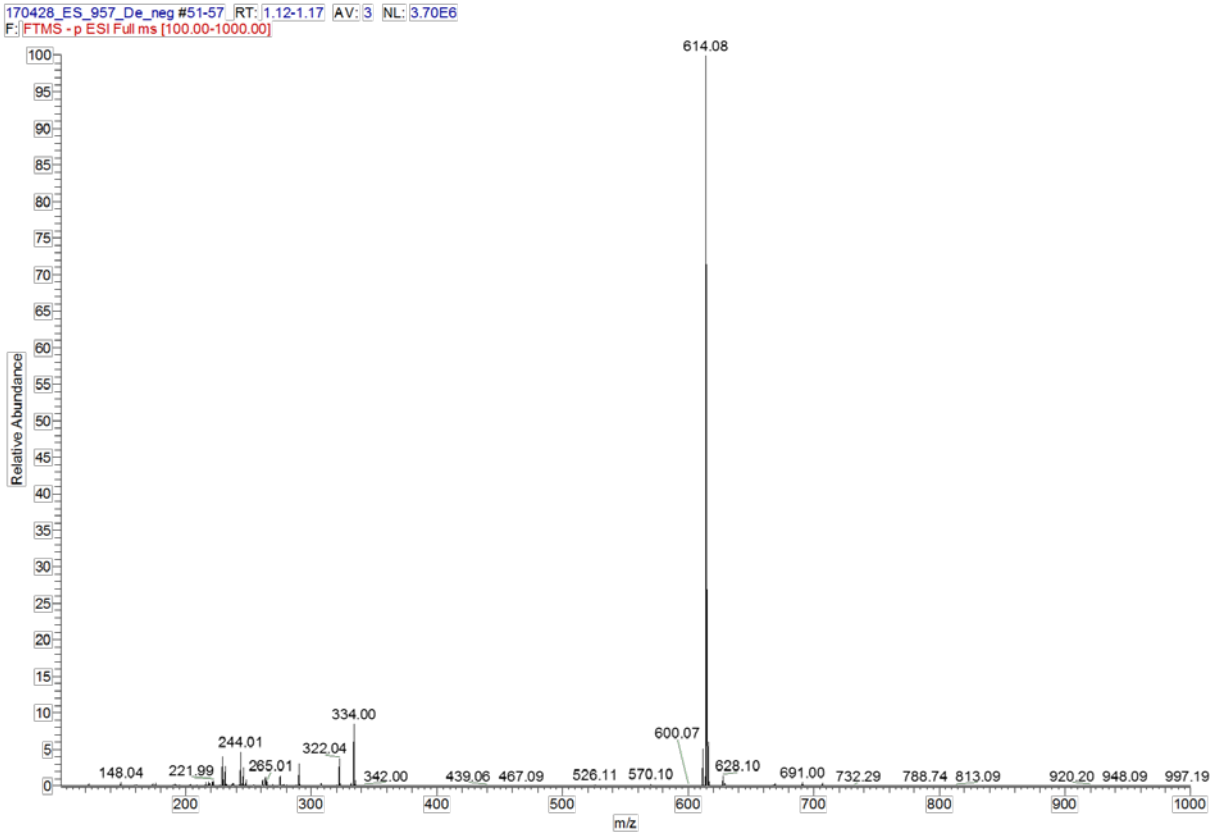

Figure S30. ESI(-)-MS spectrum of **4** in water. Due to the similar set of signals compared to the spectrum in methanol, simulations of the identified peaks are not shown.

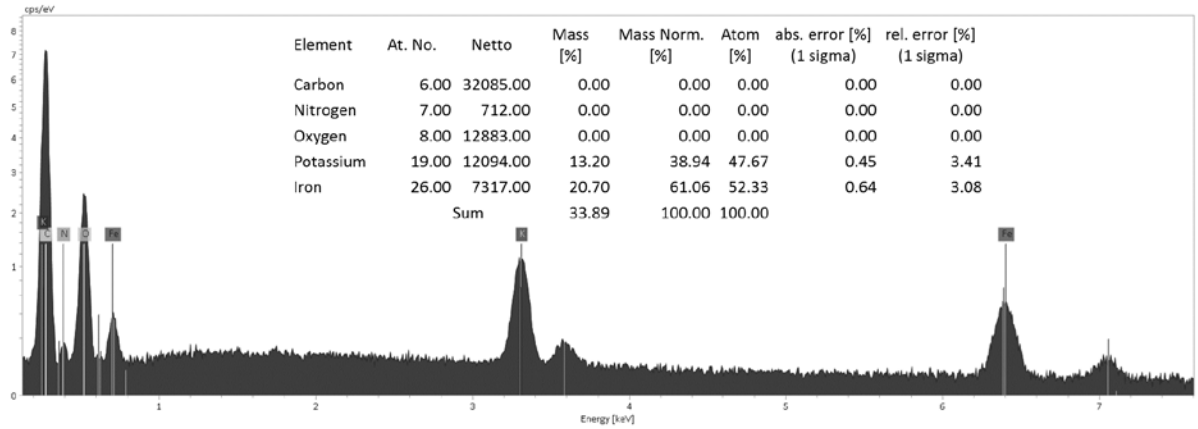

Element	At. No.	Netto	Mass [%]	Mass Norm. [%]	Atom [%]	abs. error [%] (1 sigma)	rel. error [%] (1 sigma)
Carbon	6.00	32085.00	0.00	0.00	0.00	0.00	0.00
Nitrogen	7.00	712.00	0.00	0.00	0.00	0.00	0.00
Oxygen	8.00	12883.00	0.00	0.00	0.00	0.00	0.00
Potassium	19.00	12094.00	13.20	38.94	47.67	0.45	3.41
Iron	26.00	7317.00	20.70	61.06	52.33	0.64	3.08
Sum			33.89	100.00	100.00		

Figure S31. EDX spectrum of **4** and the resulting Fe:K ratio.

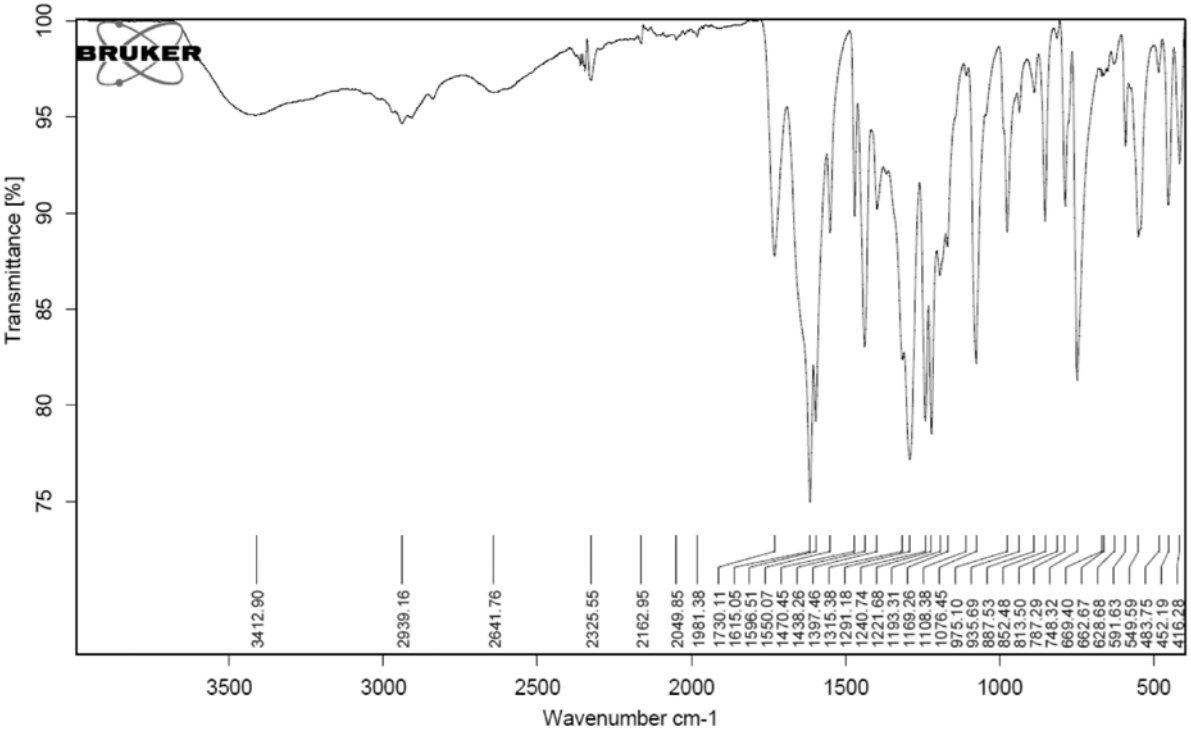

Figure S32. IR spectrum for **4** dried *in vacuo* and recorded directly after synthesis.

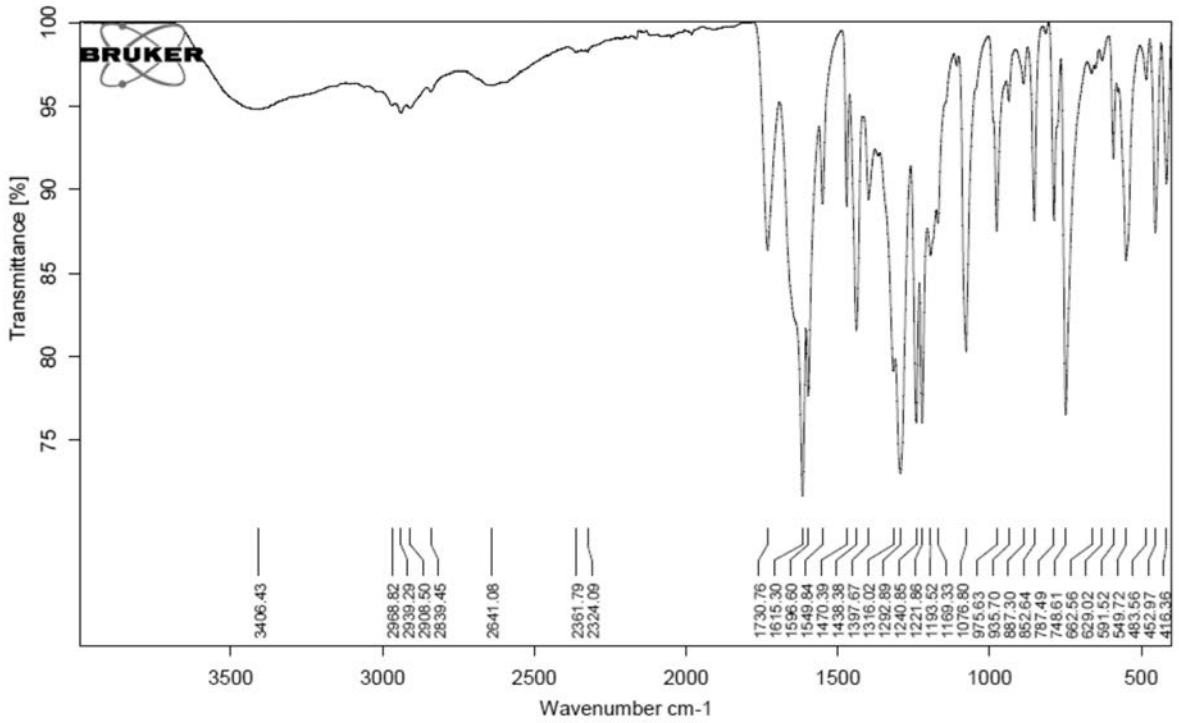

Figure S33. IR spectrum for **4** dried *in vacuo* and recorded several months after synthesis.

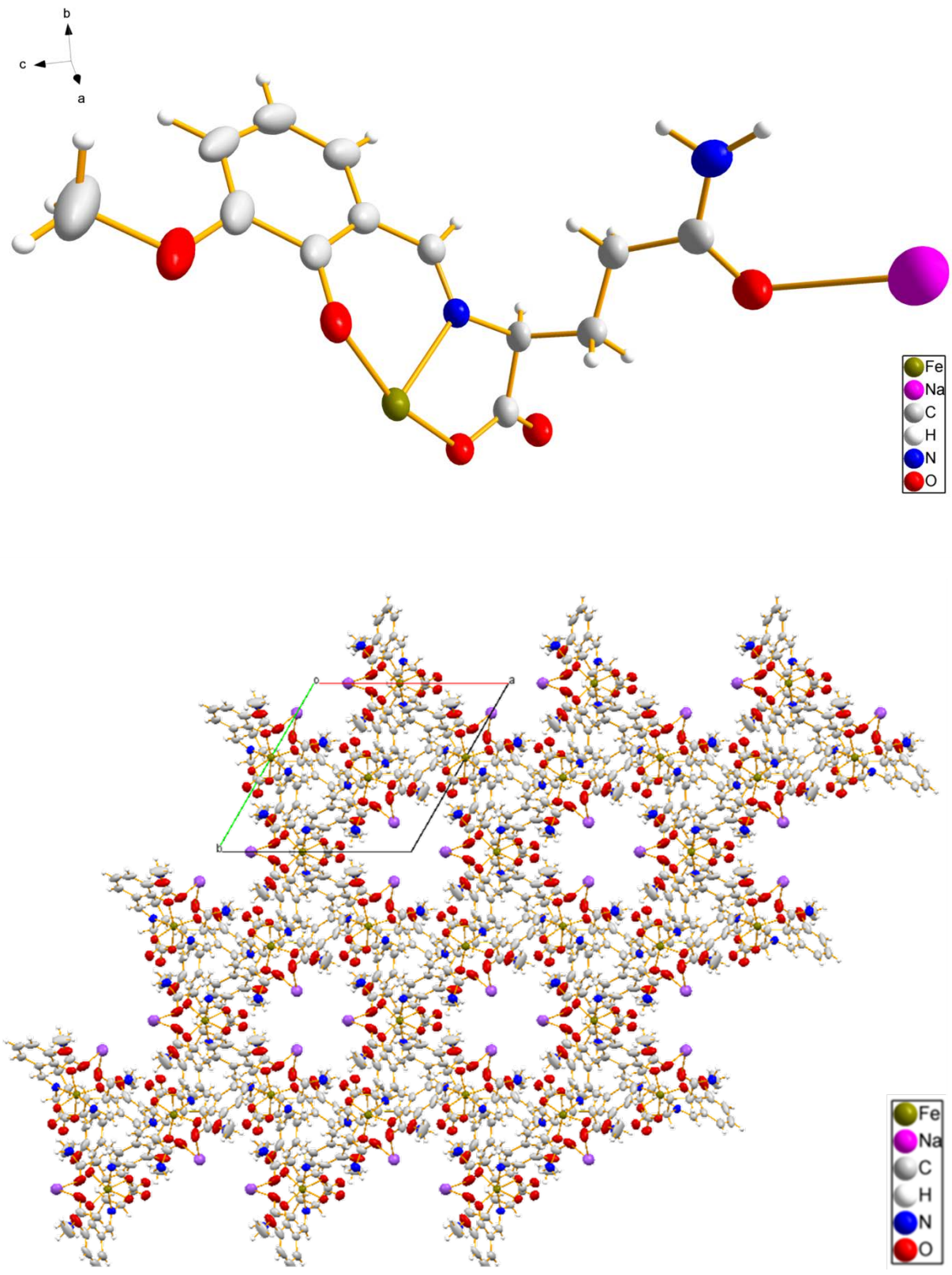

Figure S34. Asymmetric unit and packing diagram (view along *c* axis) of **1**. Compound **3** shows same asymmetric unit and packing diagram. The disordered solvent molecules around the sodium counter ion are omitted. Thermal ellipsoids are plotted at 50% probability level.

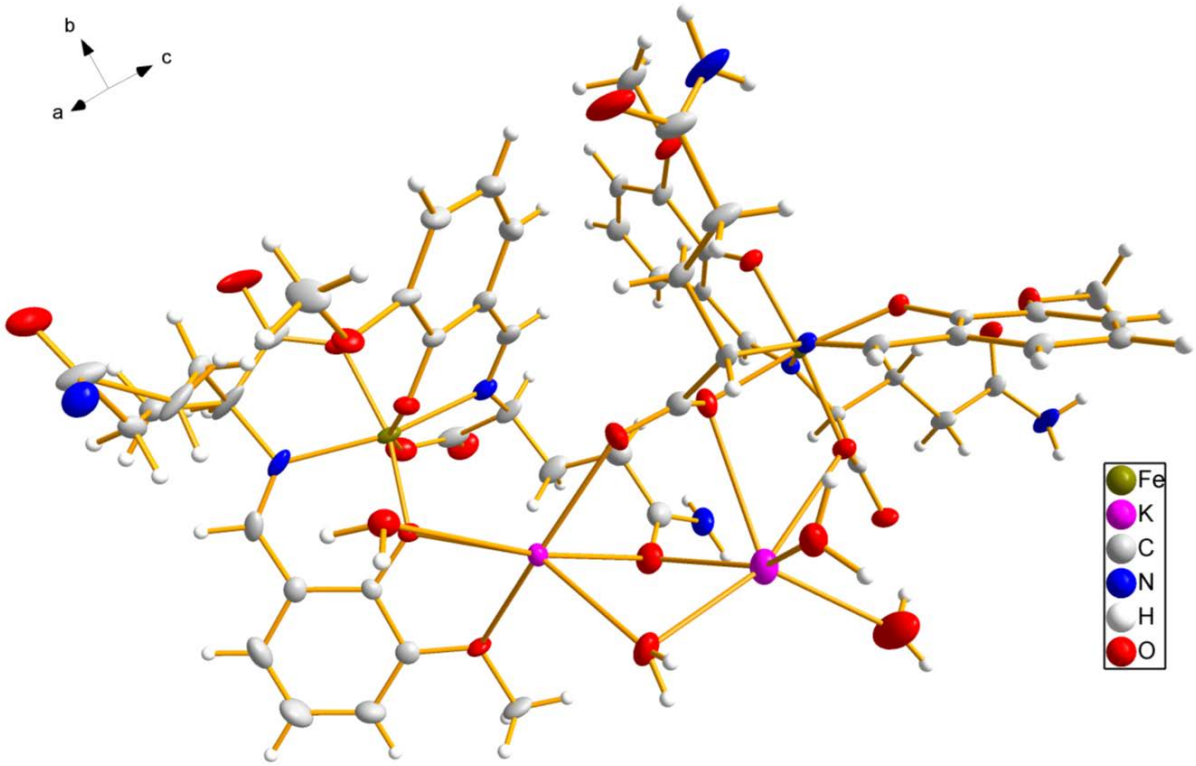

Figure S35. Asymmetric unit and the packing diagram (view along *c* axis) of **2**. Thermal ellipsoids are plotted at 50% probability level. Non-coordinating solvent molecules in the outer sphere of the complex anion are omitted for clarity.

VI Novel Pd(II) Schiff Base complexes derived from *ortho*-vanillin and *L*-tyrosine or *L*-glutamic acid: Synthesis, characterization, crystal structures and biological properties.

Muche, S.; Biernasiuk, A. Malm, A; Popiołek, Ł.; Hordyjewska, A.; Olszewska, A.; Hołyńska, M.; *Manuskript in Vorbereitung*

Presented are four novel Pd(II) complexes, [Pd(L1)(Cl)]K **(1)**, [Pd(L1)(Cl)]Na **(2)**, [Pd(L2)(Cl)]Na **(3)** and [Pd(L2)(H_2O)] **(4)**, where the ligands are derived from *ortho*-vanillin and either *L*-glutamic acid **(L1)** or *L*-tyrosine **(L2)**. The complexes were characterized by X-ray crystallography, ESI-MS, IR, NMR, XRPD and elemental analysis. Complexes **1**,**2** and **4** were found to stable in DMSO over 72 h. Complex **3** undergoes decomposition and rearrangement and seems to be in equilibrium with **4**. Investigation of bioactivity for the complexes and ligand **L2** revealed moderate to good antimicrobial activity for the complexes, whereas the ligand is inactive. In cytotoxicity studies with L929 cells all compounds displayed no cytotoxic properties up to a concentration of 200 µM.

Inhalt: Die Synthese und Charakterisierung von vier neuen Pd(II)-Komplexen, [Pd(L1)(Cl)]K **(1)**, [Pd(L1)(Cl)]Na **(2)**, [Pd(L2)(Cl)]Na **(3)** und [Pd(L2)(H_2O)] **(4)** wird präsentiert, bei denen die Liganden aus *ortho*-Vanillin und *L*-Glutaminsäure **(L1)** oder *L*-Tyrosin **(L2)** gewonnen wurden. Zur Synthese der Komplexe werden die Liganden entweder *in situ* generiert oder als fertiger Ligand eingesetzt, mit einem Ligand:Pd-Verhältnis von 1:1. Die Charakterisierung der Komplexe erfolgt durch ^{1}H-NMR, IR, Massenspektrometrie, Elementaranalyse und Röntgenstrukturanalyse. Außerdem wird mittels ^{1}H-NMR-Spektroskopie die Stabilität in DMSO über einen 72 h betrachtet. Dabei zeigt sich, dass alle Komplexe bis auf **3** stabil sind. **3** zerfällt sofort teilweise in seine Edukte. Außerdem können Signale von **4** beobachtet werden, was für die Ausbildung eines Gleichgewichts spricht. Die mononuklearen Komplexe besitzen eine verzerrte quadratisch-planare Geometrie um das Pd-Zentrum. Während die Verbindungen **1**-**3** anionisch sind und die negative Ladung durch ein Alkalimetallkation (Na oder K) kompensiert wird, ist **4** durch die Koordination eines Wassermoleküls anstatt eines Chloridions neutral. Die finale Verfeinerung der Kristallstruktur von **3** steht noch aus, da durch Fehlordnung die Position eines der beiden Natriumionen in der asymmetrischen Einheit bisher nicht eindeutig bestimmt werden konnte. Antimikrobielle Studien für **1**, **3**, **4** und **L2** zeigten für die Komplexe moderate bis gute Aktivität, während **L2** inaktiv ist. In Zytotoxizitätstest an Zellen der Linie L929 zeigte keine der getesteten Verbindungen zytotoxisches Potenzial bis zu einer Konzentration von 200 µM. Studien an weiteren humanen Krebszelllinien sind derzeit in Bearbeitung.

Eigener Anteil: Die Planung und Durchführung der Synthesen sowie die Aufnahme und Auswertung der Basisanalytik wurde von mir durchgeführt unter Betreuung von Małgorzata Hołyńska. Die Analyse der kristallographischen Daten erfolgte durch mich, Klaus Harms und Małgorzata Hołyńska. Łukasz Popiołek, Anna Hordyjewska und Anna Olszewska führten die MTT-Assays durch und bereiteten die dazugehörigen Daten auf. Die antimikrobiellen Studien wurden von Anna Biernasiuk und Anna Malm durchgeführt und die dazugehörigen Daten aufbereitet. Das Manuskript wurde von allen Autoren gemeinschaftlich verfasst.

New Pd(II) Schiff Base complexes derived from *ortho*-vanillin and *L*-tyrosine or *L*-glutamic acid: Synthesis, characterization, crystal structures and biological properties.

*Simon Muche[a], Klaus Harms, Anna Biernasiuk[b], Anna Malm[b], Łukasz Popiołek[c], Anna Hordyjewska[d], Anna Olszewska[e], Małgorzata Hołyńska[a]**

[a] Fachbereich Chemie und Wissenschaftliches Zentrum für Materialwissenschaften, Philipps-Universität Marburg, Hans-Meerwein-Strasse, D-35043, Marburg, Germany.

[b] Department of Pharmaceutical Microbiology, Medical University of Lublin, Chodźki 1, 20-093 Lublin, Poland.

[c] Department of Organic Chemistry, Medical University of Lublin, Chodźki 4A, 20-093, Lublin, Poland

[d] Department of Medicinal Chemistry, Medical University of Lublin, Chodźki 4A, 20-093, Lublin, Poland

[e] Department of Human Physiology, Medical University of Lublin, Chodźki 4A, 20-093, Lublin, Poland

Abstract

Four new Pd(II) complexes are presented, [Pd(L1)(Cl)]K **(1)**, [Pd(L1)(Cl)]Na **(2)**, [Pd(L2)(Cl)]Na **(3)** and [Pd(L2)(H_2O)] **(4)**, where the ligands are derived from *ortho*-vanillin and either *L*-glutamic acid **(L1)** or *L*-tyrosine **(L2)**. The complexes were characterized by X-ray diffraction studies, ESI-MS, IR NMR, XRPD and elemental analysis. Complexes **1**, **2** and **4** were found to stable in DMSO over 72 h. Complex **3** undergoes decomposition and rearrangement and seems to be in equilibrium with **4** in solution. Investigation of bioactivity for the complexes and the ligand **L2** revealed moderate until good antimicrobial activity of the complexes, whereas the ligand is inactive. In cytotoxicity studies with L929 cells all compounds displayed no cytotoxic properties up to a concentration of 200 μM.

Introduction

Metal-based compounds, in particular platinum-based compounds with their best known representative cisplatin ([$Pt(NH_3)_2Cl_2$]), are widely used in cancer therapy. Unfortunately, serious side effects such as neurotoxicity and nephrotoxicity, as well as the presence or acquisition of resistance and the limited spectrum of tumors combined with a lack of selectivity restrict the use of cisplatin[1, 2]. Therefore, Pd(II) compounds are in focus of research as an alternative to Pt(II) compounds with its origin in the 70's of the last century[3]. Pd(II) seems to be a good alternative due to similar chemical properties to Pt(II). Both can be classified as soft Lewis acids resulting in stronger bonds to soft bases, e. g. N- and S-donor ligands than to hard

bases like O-donors. Coordination of Pd(II) to heterobidentate P,As- and P,N-coordinating ligands was also reported[4]. Pt(II) and Pd(II) preferably form complexes with square-planar geometry. However, Pt(II) complexes possess an increased thermodynamic and kinetic stability in comparison to Pd(II) complexes. Hydrolysis and ligand exchange reactions of Pd(II) are 10^5 times faster compared to Pt(II)[5]. Most of the bioactive Pd(II) compounds contain N- and S-based ligands, like thiosemicarbazones, thiocarbazates-thiodamides, sulfur-containing Schiff bases etc.[1, 5–8]. Other ligands like oximes[9], N-heterocyclic carbenes[10], pyrazoles[11] or selenosemicarbazones[12] also result in bioactive Pd(II) complexes. Extensively studied for anti-cancer activity were the complexes [PdCl(terpy)](sac)•$2H_2O$ and [Pd(sac)(terpy)](sac)•$4H_2O$ (sac = saccharinate, and terpy = 2,2':6',2''-terpyridine)[13]. Both complexes show a very strong activity against various cell lines *in vitro*, even against cis-platin-resistant cell lines, as well as against breast cancer *in vivo*. The complexes initiate apoptosis or necrosis[14–20]. Furthermore, anti-viral[21], anti-inflammatory[22] anti-malarial[23] and anti-oxidant[24] properties of Pd(II) complexes were reported. In addition, Pd(II) complexes are potential inhibitors of enzyme alkaline phosphatase[25], an enzyme that catalyzes the transfer of phosphate groups to water or alcohol[26]. Besides the mononuclear Pd(II) complexes, di- , tri- and tetranuclear complexes also exhibit bioactivity[2, 27–30]. A further field of high importance is the usage of Pd(II) complexes in cross-coupling reactions[31] and oligomerization reactions[32]. Schiff bases and their metal complexes are interesting for research due to their large spectrum of properties, both in biological applications and catalysis. For instance, a series of mononuclear Pd(II) complexes of tridentate Schiff bases derived from salicylaldehyde and an amino- or thiophenol, saturated with triphenylphosphine demonstrated cytotoxic and antitumor activity, as well as interaction with DNA through intercalative mode[33].
In this paper we report on a series of new Pd(II) complexes with Schiff-base ligand derived from *ortho*-vanillin and *L*-tyrosine or *L*-glutamic acid.

Results and discussion

Synthesis and characterization

For the syntheses of complexes **1-4**, the tetrachloropalladate as palladium source was generated *in situ* by stirring $PdCl_2$ with an excess of NaCl or, in case of **1**, with KCl in methanol for 12 h. The ligands were either generated *in situ* or used as sodium salts, prepared following the previously reported procedures[34, 35]. In all cases a ligand:Pd ratio of 1:1 was chosen, resulting in mononuclear anionic Pd(II) complexes, coordinated by one ligand molecule and chloride or a neutral complex, where the chloride ligand is replaced by one solvent molecule, respectively (Fig.1).
Compounds **1** and **2** were synthesized with the ligand derived from *ortho*-vanillin and *L*-glutamic acid (**L1**), differing only in the counter ion and arrangement in solid state (see X-ray crystallography section below). For the synthesis of **1** the ligand was generated *in situ* and the reaction was performed in methanol following addition of HCl in a water/methanol mixture at the end, resulting in a final MeOH/H_2O ratio of approx. 1.5:1. Crystals of **1** suitable for X-ray diffraction studies were obtained only if $PdCl_2$ was stirred with KCl. This is proven by EDX, which reveals the presence of potassium, although a sodium source in form of sodium acetate was available. EDX showed a slightly increased amount of palladium, resulting in a Pd:Cl:K

ratio of 1.2:1:1. On the contrary, for the compound **2**, where the preformed ligand was used and the reaction was performed in pure methanol, crystals suitable for X-ray diffraction studies were obtained by using sodium only. Efforts to use potassium ions too did not lead to crystals suitable for X-ray diffraction studies. Addition of HCl at the end of the reaction is not necessary. EDX measurement revealed an equimolar Pd:Cl:Na ratio. The ^{1}H-NMR spectra for both in methanol-d_4 are similar to each other and show all expected signals with adequate integrals. The ESI-MS spectra in positive mode recorded in methanol show a high number of signals with varying intensities. For **1** intensive signals can be identified as the complex $[Pd(L1)(Cl)]^{-}$ with either potassium or sodium as counter-ion and variable amounts of sodium or potassium to generate the positive charge. In case of **2** intensive signals could be identified as the complex bears sodium in variable amounts only. Furthermore, in both spectra a signal was found which was determined as the complex and a coordinated methanol molecule instead of chlorine and sodium to generate the positive charge (*m/z* = 440). In addition intensive signals in the region of *m/z* > 780 are noticeable, indicating the formation of dimers and/or multimers. Due to the complexity of these signals, a reliable identification was not possible. In contrast, the spectra in negative mode show in both cases only one intensive signal around m/z = 420, identified as $[Pd(L1)(Cl)]^{-}$.

Compounds **3** and **4** were synthesized using the ligand derived from *ortho*-vanillin and *L*-tyrosine (**L2**). For the synthesis of compound **3** the ligand was generated *in situ*, resulting in a mononuclear anionic complex with sodium as counter-ion. The reaction was performed in methanol following addition of HCl in a water/methanol mixture at the end. The final MeOH/H_2O ratio was 1:1. EDX showed a Pd.Cl:Na ratio of nearly 1:1:1. For the synthesis of compound **4** the preformed ligand was used and the reaction was performed in methanol, following addition of water without HCl. The final MeOH/H_2O ratio was 1:3. Unfortunately, the EDX shows also sodium and chlorine with a ratio of 1:1 as minor impurities (Fig. S16). Either the precipitated crystals contain sodium chloride as impurity despite exhaustive rinsing with water or sodium chloride co-crystallizes with **4**, but cannot be found within the crystal structure. In the elemental analysis, chlorine was not detectable, which means the amount is below 1%. The ^{1}H-NMR spectrum of **3** in DMSO-d_6 shows a high number of signals, indicating decomposition and rearrangement (Fig. S12). Assignment and integration of the signals was not possible. On the contrary, the ^{1}H-NMR spectrum of **4** is very clear and shows only the expected signals with sufficient integrals. The stacked spectra of **3**, **4** and *ortho*-vanillin clearly reveal that **3** partially rearranges to **4** and decomposes into *ortho*-vanillin and *L*-tyrosine (Fig. S18). An equilibrium of **3** and **4** is also possible, underpinned by the observation that after filtration of the crystals of **3** needle-shaped crystals like those observed for **4** precipitated from the remaining solution. Determination of the cell constants for the needles confirms formation **4** from the reaction residue. The ESI(+) spectrum of **3** recorded in methanol shows a high number of signals over the whole measurement range. The product peak was found at *m/z* = 501.96, identified as $[Pd(L2)(Cl)]Na+Na^{+}$. Furthermore, two signals were found which were determined as the complex and a coordinated methanol molecule instead of chlorine (*m/z* = 474.01) and without any ligand coordinated to palladium (*m/z* = 441.99), both with sodium ions to generate the positive charge. The intensive peak at m/z = 292.09 can be identified as the neutral ligand without its methoxy group and a sodium ion to generate the positive charge. The product peaks for **4** were found at *m/z* = 474.01 and 452.03. Instead of a water molecule, a methanol molecule is coordinated to the Pd center and Na^{+} or H^{+} ion generates the positive

charge. Intensive peaks containing chlorine were not identified. In both spectra the formation of dimers/multimers is observed too in the range of $m/z > 800$. Again, reliable identification was not possible due to the complexity of these signals. The ESI(-) spectrum of **3** shows only one intensive signal at $m/z = 453.97$ which can be identified as $[Pd(L2)(Cl)]^-$. Interestingly, the same signal appears as in the spectrum of **4**. Probably the chlorinated species is formed during the measurement by chloride within the equipment or from the detected impurity described above and is as a result the only detectable species.

X-ray crystallography

Crystal structures of all compounds were determined by means of X-ray diffraction studies. Figure 2 shows the molecular structures of complexes **1** and **2**. Core motif is a square-planar coordinated Pd center with slightly distorted geometry. The metal center in each complex is coordinated by one molecule of **L1** by the nitrogen atom of the imine group, the oxygen atoms of the phenoxo and carboxyl group and one chloride ion. The side chains of the *L*-glutamic acid moiety remains pendant. The alkali metal counter ions are located next to the metal center and are coordinated by the methoxo and phenoxo group and the chloride ion. The asymmetric unit of **1** contains two discrete complex molecules, which are bridge by one potassium ion. The coordination sphere of the potassium ion is saturated by one molecule of water. The potassium ions are located above respectively below the plane spanned through the Pd center and its coordination sphere. In contrary, the asymmetric unit of **2** contains only one complex molecule and the sodium counter ion lies in plane with the coordinated Pd center. (…)

In figure 3 the molecular structures of **3** and **4** with the ligand **L2** are presented. In complex **3** the Pd center is coordinated in the same manner like described for **1** and **2**. The asymmetric unit contains two complex molecules which are bridged by one sodium ion. The sodium ion is coordinated by the methoxo and phenoxo groups and the chloride ions leading to orthogonally positions of the complex molecules around the counter ion. The *L*-tyrosine side chains remains pendant. One of them shows single disordering for the aromatic moiety.

In complex **4** the metal center is also coordinated by one molecule of **L2** in the described manner, but instead a chloride ion the coordination sphere is filled by a water molecule, resulting in an uncharged complex. The asymmetric unit contains two complex molecules and two molecules of water. (…)

Stability test

Prior to the tests for the antimicrobial and cytotoxic potential the new Pd(II) complexes the stability in solution was studied with ^{1}H-NMR. DMSO was chosen as solvent, because all complexes are soluble in DMSO and the resulting solutions can be easily diluted. For further studies the testing compounds were dissolved in DMSO. Spectra were recorded over 72 h in intervals of 24 h. The spectra of compounds **1**, **2** and **4** remain unaltered over the whole period. The spectra of **3** show an alteration of the signal intensity over the time. The amount of *ortho*-vanillin increases, indicated by the increasing intensity of the signal at 10.26 ppm which is assigned to the aldehyde proton (Fig. S22-S25).

Antimicrobial studies

Pd(II) complexes of Schiff Base are known to possess antimicrobial potential. Pd(II) and Ni(II) complexes with a Schiff base ligand derived from either salicylaldehyde (L^1H) or 2'-hydroxy acetophenone (L^2H) and 2-(3,4-dimethoxyphenyl)ethanamine, a dimethyl derivative of dopamine, which is the starting material for many neurotransmitting agents and other biologically important compounds, were investigated for their antimicrobial potential. $[Pd(L^1)_2]$ showed the highest antibacterial and antifungal potential[36]. Novel *N*-(salicylidene)-sulfaguanidines bearing ionic liquid moieties and their Pd(II)Cl(H_2O) complexes were synthesized by Schiff base condensation of ionic liquid-functionalized salicylaldehydes and sulfaguanidine and investigated for their antimicrobial properties. Both the free ligands and the Pd(II) complexes exhibited significant antibacterial and potential inhibitory activity against S. *aureus*. Thereby this activity is modulated by the nature of the ionic liquid core as well as the counter-ion[37].–Mononuclear Pd(II) complexes with tetradentate Schiff base ligands derived from o-phthalaldehyde and L-tryptophan or L-histidine showed excellent activity against *Bacillus subtilis, Staphylococcus aureus, Escherichia coli* and *Klebsiella pneumonia* even higher than for the tested standard drugs streptomycin and ampicillin. The corresponding Co(II), Ni(II) and (Cu) complexes were highly active too, but less active than the Pd(II) complexes. The antibacterial activity is due to the presence of indole and imidazole moieties[38]. Complexes with the formula $[PdL_2]Cl_2$, where L is the ligand derived from salicylaldehyde and *L*-glycine, *L*-alanine, *L*-methionine, *L*-valine or *L*-serine, were tested for their antibacterial activity. All complexes showed a remarkable activity against *Staphylococcus aureus* and *Escherichia coli,* similar or better than the references ampicillin and streptomycin. The highest activity was determined for the complexes containing *L*-alanine and *L*-glycine[39]. Therefore we tested our new synthesized complexes for their antimicrobial activity. Compound **2** was not tested separately, because of the identic structure with **1**. Investigation for the bioactivity of **L1** was published earlier[34].

Antibacterial activity

According to the data presented in Table 1, the newly synthesized compounds **1, 3, 4** and **L2** showed some antimicrobial activity towards reference bacteria. The microorganisms, such as *Staphylococcus epidermidis* ATCC 12228, *Micrococcus luteus* ATCC 10240 and *Bacillus subtilis* ATTC 6633 belonging to Gram-positive bacteria or *Bordetella bronchiseptica* ATTC 4617 from the Gram-negative bacteria were particularly sensitive to these substances with MIC = 125 – 500 μg/ml and MBC = 500 – 2000 μg/ml. The compounds showed good or moderate activity and bactericidal effect (MBC/MIC = 2 – 4) towards these microorganisms. The activity against remaining reference strains of bacteria was lower with moderate or mild effect (MIC = 250 – 1000 μg/ml and MBC = 500 – > 2000 μg/ml). The ligand **L2** had no inhibitory effect on the growth of some strains of bacteria belonging to staphylococci: *S. aureus* ATTC 43300 or *S. aureus* ATTC 6538 and *P. aeruginosa* 9027.

Antifungal activity

The tested compounds showed also good bioactivity against fungi belonging to yeasts *C. albicans* ATTC 2091, *C. albicans* ATTC 10231 and *C. parapsilosis* ATTC 22019 with MIC = 62.5 – 125 μg/ml. The minimal fungicidal concentration (MFC) values of these substances ranged from 125 μg/ml to 250 μg/ml. In turn, the minimal inhibitory concentration of all compounds which inhibited growth of *C. glabrata* ATTC 90030 and *C. krusei* ATTC 14243

was the same – 250 µg/ml and MFC = 500 – 1000 µg/ml. These compounds exhibited moderate effect against the tested microbes. The compounds showed fungicidal effect (MFC/MIC = 2 – 4) towards all reference *Candida* spp. strains (Table 1).

Cytotoxicity studies

Since several years, our group focuses on Schiff bases containing *ortho*-vanillin and amino acids and their metal complexes. This combination provides ligands with a large number of coordination sites depending on the amino acid and allows for synthesis of complexes with varying nuclearity from pentadecanuclear till mononuclear depending on the used metal and amino acid[40, 34, 35]. By the incorporation of amino acids as biologically relevant fragments into the ligands we expect an interaction with biological targets resulting in bioactivity of the ligands and the complexes. Pd(II) complexes with 2,2'-bipyridine and a variety of amino acids as ligands were tested for their growth inhibition of different cell lines and it was found, that some of the complexes show the same activity or are more potent than cisplatin[41]. In another study Pd(II) and Pt(II) complexes with amino acids and 2,2'-bipyridine or 1,10-phenanthroline were tested for the inhibitory potential of transcription. It was found that the Pd(II) complexes were more effective inhibitors than the corresponding Pt(II) complexes[42]. Pd(II) and Pt(II) complexes of substituted o-hydroxyacetophenone-glycine, including a derivative of ortho-vanillin, with a ligand:metal ratio of 2:1 were also synthesized. The ligands, as well as their Pd(II) and Pt(II) complexes, exhibit potent cytotoxic activity against Ehrlich ascites tumor cells *in vitro*, but appear to be more active *in vivo*[43]. Another approach to mediate the anticancer activity and selectivity is the incorporation of sugar-boronate esters. Pd(II) complexes were prepared with Schiff base ligand derived from 3-aminophenyl boronate ester of 1,2-O-isopropylidene-α-D-xylofuranose, 1,2-O-cyclohexylidene-α-D-xylofuranose, 1-O-benzyl-2,3-O-isopropylidene-α-L-sorbofuranose, 1,2:5,6-di-O-isopropylidene-D-mannitol and 1,2:5,6-di-O-cyclohexylidene-D-mannitol and 2-pyridinecarboxaldehyde, followed by the addition of Pd(cod)Cl_2. The resulting Pd(II) complexes are stable under physiological conditions and show moderate to good cytotoxicity against two cancer cell lines and are less to toxic to model non-tumorigenic human embryonic kidney cells compared to cisplatin. Furthermore it was found that the complexes intercalate with DNA[44].

The studied compounds displayed no cytotoxic properties up to the concentration of 200 µM in the tested cell line. The viability of L929 cells was in the range of 75% - 90%.

Conclusion

Experimental section

General

Synthesis of the Pd(II) complexes

[Pd(L1)(Cl)]K **(1):**

177 mg (1 mmol) $PdCl_2$ and 186 mg (2.5 mmol) potassium chloride were stirred in 5 mL of water overnight to generate the tetrachloropalladate substrate *in situ.*
147 mg (1.0 mmol) of *L*-glutamic acid and 408 mg (3.0 mmol) of sodium acetate was dissolved in 3.5 mL of water and 15.5 mL of methanol and heated to 60 °C. When the solid part was completely dissolved, 152 mg (1.0 mmol) of *ortho*-vanillin was added to the stirred *L*-glutamic acid/sodium acetate solution. To the resulting yellow solution the clear dark red palladium solution was added. An orange solid appeared immediately. 0.6 mL 2M HCl were added to the solution and stirred for 30 min at 60 °C. During stirring the solution turned clear. The clear orange solution was transferred into a 30 mL vial for crystallization by slow evaporation. Dark orange plate shaped crystals were obtained after 6 days. The crystals were filtered off after 12 days, washed with cold ethanol and dried on air in 12 h. Yield (average): 305.6 mg (63.06%).

Elemental analysis for the substance **1** dried under vacuum, analyzed as $C_{13}H_{13}NO_6PdClK$•1 H_2O•0.2 MeOH: Calc (found) C 32.71 (32.56) H 3.29 (3.35) N 2.89 (2.93) O 23.77 (25.25).

^{1}H NMR (300 MHz, DMSO) δ 12.19 (s, 1H), 7.84 (s, 1H), 6.97 (d, *J* = 7.7 Hz, 1H), 6.83 (d, *J* = 7.2 Hz, 1H), 6.46 (t, *J* = 7.7 Hz, 1H), 4.28 (s, 1H), 3.68 (s, 3H), 2.31 – 2.04 (m, 4H).

IR bands (cm^{-1}) for **1** dried *in vacuo*: 410 (m), 439 (vw), 459. (m), 471 (w), 497 (m), 512.0 (m), 545 (m), 580 (w), 641 (m), 746 (s), 788 (s), 819 (w), 859 (w), 902 (w), 939 (w), 971 (m), 991 (m), 1033(w), 1073 (m), 1112 (vw), 1172.4 (m), 1186 (w), 1204 (s), 1218 (s), 1240 (s), 1245.0 (vw),1272 (m), 1296 (m), 1336 (m), 1355 (m), 1405 (m), 1441 (s), 1471 (m), 1545 (m), 1605 (vs), 1630 (s), 1692 (s), 1717 (m), 2530 (vw), 2607 (vw), 2651 (vw), 2834 (w), 2929 (w), 3304.52 (w), 3508.26 (vw).

[Pd(L1)(Cl)]Na **(2):**

89 mg (0.5 mmol) $PdCl_2$ and 73 mg (1.25 mmol) sodium chloride were stirred in 5 mL of methanol for 12 h to generate the tetrachloropalladate *in situ.*
177 mg (0.5 mmol) of the Schiff Base composed of *L*-glutamic acid and *ortho*-vanillin, synthesized as previously reported[(34)], was dissolved in 20 mL of methanol and heated to 60 °C. To the resulting yellow solution the clear dark red palladium solution was added. The clear orange solution was stirred for 30 min at 60 °C and transferred into a 30 mL vial for crystallization by slow evaporation. Clusters of orange needles were obtained after 1 day. The crystals were filtered off after 6 days, washed with cold ethanol and dried under air for 12 h. Yield (average): 169.3 mg (73.12%).

Elemental analysis for the substance **2** dried under vacuum, analyzed as $C_{13}H_{13}NO_6PdClNa$•0.7 H_2O•0.2 MeOH: Calc (found) C 34.23 (34.22) H 3.31 (3.31) N 3.02 (3.07) O 23.84 (25.11).

^{1}H NMR (300 MHz, DMSO) δ 12.21 (s, 1H), 7.84 (s, 1H), 6.97 (d, *J* = 7. Hz, 1H), 6.82 (d, *J* = 7.23 Hz, 1H), 6.45 (t, *J* = 7.8 Hz, 1H), 4.28 (s, 1H), 3.67 (s, 3H), 2.32 – 2.04 (m, 4H).

IR bands (cm^{-1}) for **2** dried *in vacuo*: 447 (m), 490 (m), 529.4 (m), 552(s), 590 (w), 612 (w), 650 (m), 731 (vs), 775 (m), 816 (w), 858 (m), 890 (w), 969 (m), 1030 (m), 1083 (s), 1111 (w), 1171 (m), 1216 (vs), 1243 (vs), 1301 (vs), 1339 (m), 1371 (m), 1437 (s), 1468 (m), 1548 (m), 1605 (s), 1621 (s), 1659 (s), 1720 (m), 1980 (vw), 2164 (vw), 2322 (vw), 2836 (vw), 2933 (w), 2975 (vw), 3000 (vw), 3060 (vw), 3524 (vw).

[Pd(L2)(Cl)]Na **(3)**:

177 mg (1 mmol) $PdCl_2$ and 146 mg (2.5 mmol) sodium chloride were stirred in 2.5 mL of methanol for 12 h to generate the tetrachloropalladate substrate *in situ.*
At 60 °C 80 mg (2 mmol) of sodium hydroxide were dissolved in 4 mL of methanol. 181 mg *L*-tyrosine (1 mmol) were added to the methanolic solution. When *L*-tyrosine was dissolved completely 152 mg (1 mmol) *ortho*-vanillin were added. To the resulting yellow solution the clear dark red palladium solution was added. The cloudy orange solution was stirred for 30 min. at 60°C, followed by addition of a solution containing 11.4 ml of water, 6 mL of methanol and 0.6 mL 2M HCl. The clear orange solution was transferred into a 30 mL vial for crystallization by slow evaporation. Orange plate shaped crystals were obtained after 8 days. The crystals were filtered off after 12 days, washed with cold ethanol and dried under air for 12 h. Yield (average): 177 mg (33.88%).

Elemental analysis for the substance **3** dried under vacuum, analyzed as $C_{17}H_{15}NO_5PdClNa$•0.75 H_2O•0.25 MeOH: Calc (found) C 41.46 (42.26) H 3.53 (3.56) N 2.8 (2.83) O 19.21(20.57).

IR bands (cm^{-1}) for **3** dried *in vacuo*: 453 (m), 494 (w), 540 (s), 570 (m), 596 (w), 646 (w), 735 (s), 779 (w), 812 (m), 860 (m), 890 (w), 972 (m), 999 (w), 1066 (m), 1082 (m), 1106 (m), 1173 (s), 1213 (vs), 1245 (vs), 1268 (s), 1303 (s), 1355 (m), 1438 (s), 1469 (s), 1514 (s), 1546 (m), 1605 (vs), 1627 (vs), 1748 (m), 1889 (vw), 2051 (vw), 2838 (vw), 2935 (w), 3021 (vw), 3061 (vw), 3370 (w).

[Pd(L2)(H_2O)] **(4):**

89 mg (0.5 mmol) $PdCl_2$ and 146 mg (1.25 mmol) sodium chloride were stirred in 2.5 mL of methanol for 12 h to generate the tetrachloropalladate substrate *in situ.*
169 mg (0.5 mmol) of the Schiff Base composed of *L*-tyrosine and *ortho*-vanillin, synthesized as previously reported[(35)] was dissolved in 4 mL of methanol and heated to 60 °C. To the resulting yellow solution the clear dark red palladium solution was added. The resulting clear orange solution was stirred for 30 min at 60 °C, followed by addition of 18.5 mL of water and transferred into a 30 mL vial for crystallization by slow evaporation. Large orange needles were obtained after 1 day. The crystals were filtered off after 12, washed with cold ethanol and dried on air for 12 h. Yield (average): 117.3 mg (52.26%).

Elemental analysis: Elemental analysis for the substance **4** dried under vacuum, analyzed as $C_{17}H_{17}NO_6Pd$•0.35 H_2O•0.15 MeOH: Calc (found) C 45.89 (45.56) H 4.11 (4.11) N 3.12 (3.12) O 23.17 (24.99).

^{1}H NMR (300 MHz, DMSO) δ 9.28 (s, 1H,), 7.53 (s, 1H), 6.93 – 6.84 (m, 4H), 6.65 (d, *J* = 8.4 Hz, 2H), 6.56 (t, *J* = 7.8 Hz, 1H), 4.61 (s, 1H), 3.70 (s, 3H), 3.07 – 3.00 (dd, *J* = 13.9, 6.0 Hz, 1H).

IR bands (cm^{-1}) **4** dried *in vacuo* 450 (m), 539 (s), 570 (m), 641 (w), 733 (s), 778 (w), 811 (m), 856 (m), 888 (w), 973 (w), 1071(m), 1105 (w), 1172 (m), 1216 (vs), 1246 (vs), 1305 (s), 1358 (m), 1437 (s), 1467 (s), 1514 (s), 1544 (w), 1603 (vs), 1630 (s), 1888 (vw), 2834 (w), 2935 (w), 3016 (vw), 3170 (w).

In vitro antimicrobial assay

The examined compounds **L2**, **1**, **3** and **4** were screened *in vitro* for antibacterial and antifungal activities using the broth microdilution method according to European Committee on Antimicrobial Susceptibility Testing (EUCAST)[45] and Clinical and Laboratory Standards Institute guidelines[46] against a panel of reference strains of microorganisms, including Gram-positive bacteria (*Staphylococcus aureus* ATCC 25923, *Staphylococcus aureus* ATCC 43300, *Staphylococcus aureus* ATCC 6538, *Staphylococcus epidermidis* ATCC 12228, *Bacillus subtilis* ATCC 6633, *Bacillus cereus* ATCC 10876, *Micrococcus luteus* ATCC 10240), Gram-negative bacteria (*Bordetella bronchiseptica* ATCC 4617, *Escherichia coli* ATCC 25922, *Proteus mirabilis* ATCC 12453, *Klebsiella pneumoniae* ATCC 13883, *Salmonella typhimurium* ATCC 14028, *Pseudomonas aeruginosa* ATCC 9027) and fungi belonging to yeasts (*Candida albicans* ATCC 2091, *Candida albicans* ATCC 10231, *Candida parapsilosis* ATCC 22019, *Candida glabrata* ATTC 90030 and *Candida krusei* ATTC 14243). These microorganisms came from American Type Culture Collection (ATCC), routinely used for the evaluation of antimicrobials[47, 34]. All the used microbial cultures were first subcultured on nutrient agar or Sabouraud agar at 35°C for 18-24 h or 30°C for 24-48 h for bacteria and fungi, respectively. The surface of Mueller-Hinton agar (for bacteria) and RPMI 1640 with MOPS (for fungi) were inoculated with the suspensions of bacterial or fungal species. Microbial suspensions were prepared in sterile saline (0.85% NaCl) with an optical density of McFarland standard scale 0.5 – approximately 1.5 x 10^8 CFU (Colony Forming Units)/ml for bacteria and 0.5 McFarland standard scale – approximately 5 x 10^5 CFU/ml) for fungi[47, 34, 48]. Samples containing examined compounds were dissolved in 1 ml dimethyl sulphoxide (DMSO). Furthermore, bacterial and fungal suspensions were put onto Petri dishes with solid media containing 2 mg/ml of the tested compounds, followed by incubation at 37°C for 24 h and 30°C for 48 h for bacteria and fungi, respectively. The inhibition of microbial growth was judged by comparison with a control culture prepared without any sample tested. Ciprofloxacin or nystatin (Sigma) were used as reference antibacterial or antifungal compounds, respectively[47, 34, 48]. Subsequently, MIC (Minimal Inhibitory Concentration) of the compounds was examined by the microdilution broth method, using their two-fold dilutions in Mueller-Hinton broth (for bacteria) and RPMI 1640 broth with MOPS (for fungi) prepared in 96-well polystyrene plates. The final concentrations of the compounds ranged from 2000 to 0.98 µg/ml. Microbial suspensions were prepared in sterile saline (0.85% NaCl) with an optical density of 0.5 McFarland standard. Next 2 µl of each bacterial or fungal suspension was added per each well containing 200 µl broth and various concentrations of the examined compounds. After incubation (37°C, 24 – 48 h) the

MIC was assessed spectrofotometrically as the lowest concentration of the samples showing complete bacterial or fungal growth inhibition. Appropriate DMSO, growth and sterile controls were carried out. The medium with no tested substances was used as control[47, 34, 48]. The MBC (Minimal Bactericidal Concentration) or MFC (Minimal Fungicidal Concentration) are defined as the lowest concentration of the compounds that is required to kill a particular bacterial or fungal species. MBC/MFC was determined by removing 10 µl of the culture used for MIC determinations from each well and spotted onto appropriate agar medium. The plates were incubated for 37°C for 24 h and 30°C for 48 h for bacteria and fungi, respectively. The lowest compounds concentrations with no visible growth observed were assessed as a bactericidal/fungicidal concentration. All the experiments were repeated three times and representative data are presented[47, 34, 48]. In this study no bioactivity was defined as MIC > 1000 µg/ml, mild bioactivity as MIC in the range 501 – 1000 µg/ml, moderate bioactivity with MIC from 126 to 500 µg/ml, good bioactivity as a MIC in the range 26 – 125 µg/ml, strong bioactivity with MIC between 10 and 25 µg/ml and very strong bioactivity as a MIC < 10 µg/ml[49]. The MBC/MIC or MFC/MIC ratios were calculated in order to determine bactericidal/fungicidal (MBC/MIC ≤ 4, MFC/MIC ≤ 4) or bacteriostatic/fungistatic (MBC/MIC > 4, MFC/MIC > 4) effect of the tested compounds.

MTT assay and cytotoxicity

Cytotoxic properties of the newly synthetized compounds were assessed *in vitro* using MTT Assay Kit (Cayman Chemicals, USA) according to the manufacturer's protocol. In brief, L929 cells, to enable proper cell attachment, were seeded out at 1×10^4 cells per well onto a 96-well flat-bottom plate and cultured overnight in Eagle's medium (supplemented with fetal bovine serum and with antibiotics) at standard conditions (37°C, 5% CO_2, 90% humidity). Then the cells were incubated with the tested compounds at the concentration of 200 µM, 100 µM, 50 µM and 25 µM for 24, 48 and 72 h. The control groups were the cells untreated with tested compounds. The assay was terminated by adding MTT reagent (10 µl/well) and after four hours later by adding MTT detergent reagent (100 µl/well). After the incubation for 12 h, the absorbance was measured at 570 nm using ELx800 plate reader.

Physicochemical measurements

Elemental analyses were carried out on an Elementar Vario Microcube elemental analyzer in CHNS mode. Oxygen content analysis was carried out on an Elementa rapid OXY Cube elemental analyzer.

IR spectra were recorded using a Bruker Alpha-P Infrared-spectrometer equipped with a Platinum-ATR with a diamond crystal.

^{1}H NMR spectra were recorded in methanol-d_4 or DMSO-d_6 with a Bruker DRX 300 MHz spectrometer at room temperature. Chemical shifts were quoted in ppm relative to the residual protons of deuterated solvents.

Electrospray ionization mass spectrometry (ESI-MS) was performed on a Finnigan LTQ-FT spectrometer by Thermo Fischer Scientific in the positive and negative ion mode with solvent as carrier gas.

EDX spectra were recorded with a JEOL JIB-4610F device and a Bruker XFlash 5010 EDX detector. Data analysis was performed using Bruker Esprit 2.1 software.

Figures

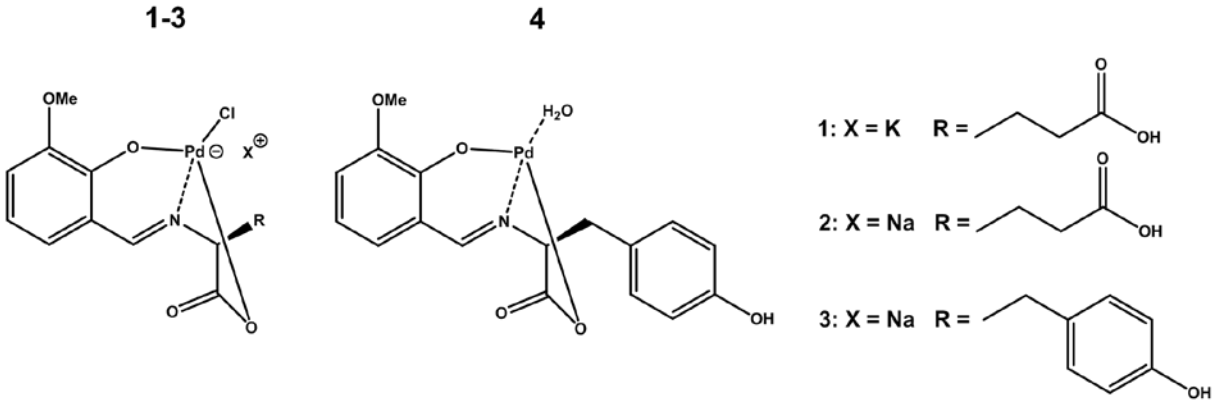

Fig. 1. Coordination scheme for compounds **1**-**4**.

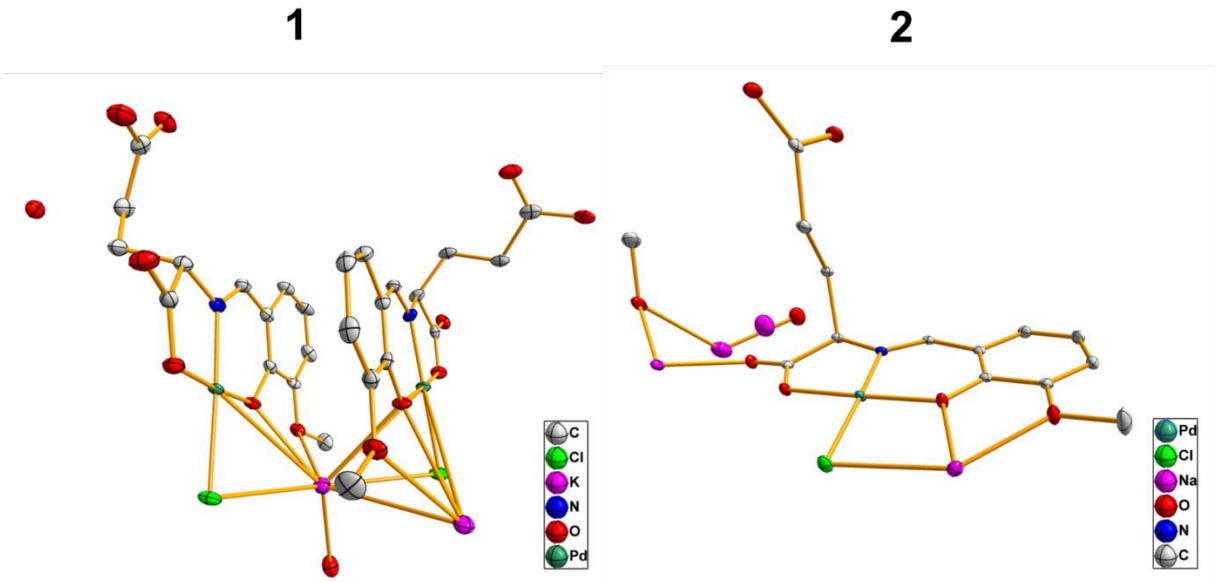

Fig. 2. Molecular structures of the asymmetric unit of complexes **1** and **2**. Thermal ellipsoids are plotted at 30% probability level. Hydrogen atoms are omitted for clarity.

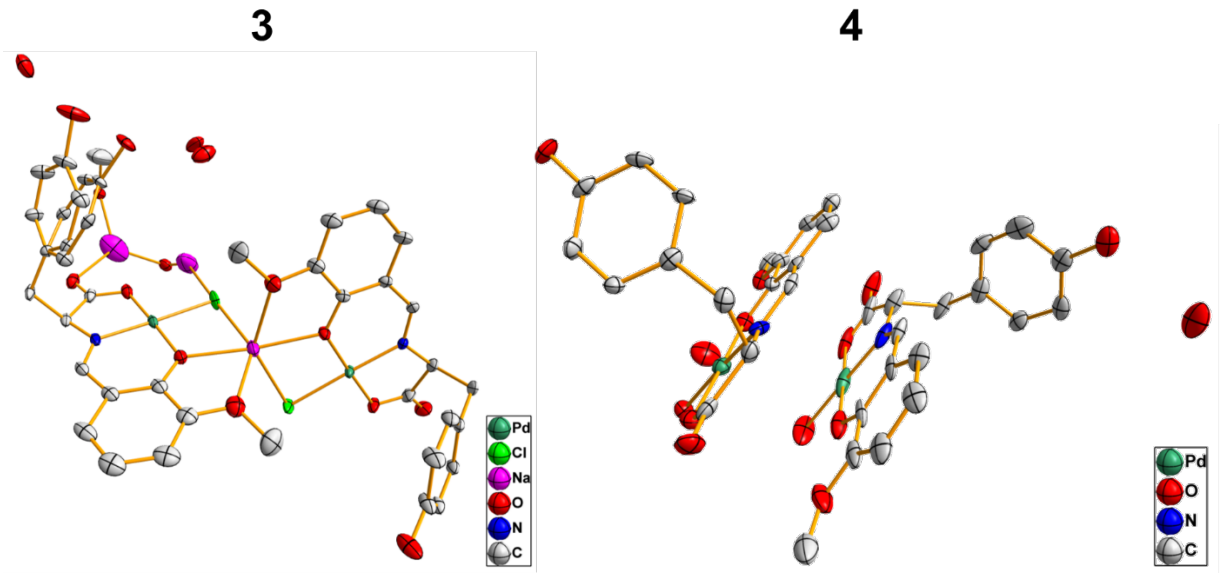

Fig. 3. Molecular structures of the asymmetric unit of complexes **3** and **4**. Thermal ellipsoids are plotted at 30% probability level. Hydrogen atoms are omitted for clarity. Solution of **3** is just preliminary due to disorder problems for the second sodium ion.

Tables

Table 1. The activity of the title compounds expressed as MIC (MBC or MFC) [µg/ml] and {MBC/MIC or MFC/MIC} against the reference strains of bacteria and fungi.
The standard antibiotics used as positive controls: ciprofloxacin (CIP) for bacteria and nystatin (NY*) for fungi.

	Species	**MIC (MBC or MFC) [µg/ml] and {MBC/MIC or MFC/MIC} of the tested compounds**				**CIP/NY***
		L2	**4**	**3**	**1**	
Gram-positive bacteria	*Staphylococcus aureus* ATCC 25923	1000 (1000) {1}	250 (1000) {4}	250 (1000) {4}	500 (2000) {4}	0.488
	Staphylococcus aureus ATCC 43300	2000 (2000) {1}	1000 (1000) {1}	1000 (1000) {1}	1000 (2000) {2}	0.244
	Staphylococcus aureus ATCC 6538	2000 (>2000) {>1}	1000 (1000) {1}	1000 (1000) {1}	1000 (2000) {2}	0.244
	Staphylococcus epidermidis ATCC 12228	500 (2000) {4}	250 (500) {2}	250 (1000) {4}	500 (1000) {2}	0.122

	Micrococcus luteus ATCC 10240	500 (1000) {2}	125 (500) {4}	125 (500) {4}	125 (1000) {8}	0.976
	Bacillus subtilis ATCC 6633	500 (1000) {2}	500 (1000) {2}	500 (1000) {2}	500 (1000) {2}	0.031
	Bacillus cereus ATCC 10876	1000 (>2000) {>2}	500 (>2000) {>4}	500 (>2000) {>4}	1000 (>2000) {>2}	0.061
Gram-negative bacteria	*Escherichia coli* ATCC 25922	500 (1000) {2}	500 (1000) {2}	1000 (1000) {1}	1000 (1000) {1}	0.004
	Klebsiella pneumoniae ATCC 13883	1000 (1000) {1}	1000 (1000) {1}	1000 (1000) {1}	500 (1000) {2}	0.122
	Salmonella typhimurium ATCC 14028	1000 (1000) {1}	1000 (2000) {2}	1000 (2000) {2}	1000 (1000) {21}	0.061
	Proteus mirabilis ATCC 12453	1000 (2000) {2}	1000 (2000) {2}	1000 (2000) {2}	1000 (1000) {1}	0.030
	Bordetella bronchiseptica ATCC 4617	500 (1000) {2}	500 (2000) {4}	500 (2000) {4}	500 (2000) {4}	0.976
	Pseudomonas aeruginosa ATCC 9027	2000 (2000) {1}	1000 (2000) {2}	1000 (2000) {2}	1000 (2000) {2}	0.488
Fungi	*Candida parapsilosis* ATCC 22019	62.5 (250) {4}	125 (250) {2}	125 (250) {2}	125 (250) {2}	0.244*
	Candida albicans ATCC 2091	62.5 (125) {2}	62.5 (125) {2}	62.5 (125) {2}	62.5 (125) {2}	0.488*
	Candida albicans ATCC 10231	62.5 (125) {2}	62.5 (125) {2}	62.5 (125) {2}	62.5 (125) {2}	0.244*
	Candida glabrata ATCC 90030	250 (500) {2}	250 (1000) {4}	250 (1000) {4}	250 (1000) {4}	0.244*
	Candida krusei ATCC 14243	250 (1000) {4}	250 (1000) {4}	250 (500) {2}	250 (500) {2}	0.244*

References

1. Nadeem, S.; Bolte, M.; Ahmad, S.; Fazeelat, T.; Tirmizi, S. A.; Rauf, M. K.; Sattar, S. A.; Siddiq, S.; Hameed, A.; Haider, S. Z. *Inorganica Chimica Acta* **2010,** *363* (13), 3261–3269.
2. Fanelli, M.; Formica, M.; Fusi, V.; Giorgi, L.; Micheloni, M.; Paoli, P. *Coordination Chemistry Reviews* **2016,** *310*, 41–79.
3. Graham, R. D.; Williams, D. R. *Journal of Inorganic and Nuclear Chemistry* **1979,** *41* (8), 1245–1249.
4. Ares, R.; López-Torres, M.; Fernández, A.; Pereira, M.T.; Suárez, A.; Mosteiro, R.; Fernández, J. J.; Vila, J. M. *Journal of Organometallic Chemistry* **2003,** *665* (1-2), 87–94.
5. Garoufis, A.; Hadjikakou, S. K.; Hadjiliadis, N. *Coordination Chemistry Reviews* **2009,** *253* (9-10), 1384–1397.
6. Balzarini, J.; Orzeszko, B.; Maurin, J. K.; Orzeszko, A. *Eur J Med Chem* **2007,** *42* (7), 993–1003.
7. Singh, R. V.; Fahmi, N.; Biyala, M. K. *Journal of the Iranian Chemical Society* **2005,** *2* (1), 40–46.
8. Amir, M. K.; Khan, S. Z.; Hayat, F.; Hassan, A.; Butler, I. S.; Zia-ur-Rehman. *Inorganica Chimica Acta* **2016,** *451*, 31–40.
9. Bandyopadhyay, N.; Zhu, M.; Lu, L.; Mitra, D.; Das, M.; Das, P.; Samanta, A.; Naskar, J. P. *Eur J Med Chem* **2015,** *89*, 59–66.
10. Fong, T. T.-H.; Lok, C.-N.; Chung, C. Y.-S.; Fung, Y.-M. E.; Chow, P.-K.; Wan, P.-K.; Che, C.-M. *Angew Chem Int Ed Engl* **2016,** *55* (39), 11935–11939.
11. Abu-Surrah, A. S.; Abu Safieh, K. A.; Ahmad, I. M.; Abdalla, M. Y.; Ayoub, M. T.; Qaroush, A. K.; Abu-Mahtheieh, A. M. *Eur J Med Chem* **2010,** *45* (2), 471–475.
12. Gligorijevic, N.; Todorovic, T.; Radulovic, S.; Sladic, D.; Filipovic, N.; Godevac, D.; Jeremic, D.; Andelkovic, K. *Eur J Med Chem* **2009,** *44* (4), 1623–1629.
13. Guney, E.; Yilmaz, V. T.; Sengul, A.; Buyukgungor, O. *Inorganica Chimica Acta* **2010,** *363* (2), 438–448.
14. Ulukaya, E.; Ari, F.; Dimas, K.; Ikitimur, E. I.; Guney, E.; YILMAZ, V. T. *Eur J Med Chem* **2011,** *46* (10), 4957–4963.
15. Coskun, M. D.; Ari, F.; Oral, A. Y.; Sarimahmut, M.; Kutlu, H. M.; YILMAZ, V. T.; ULUKAYA, E. *Bioorg Med Chem* **2013,** *21* (15), 4698–4705.
16. Ulukaya, E.; Frame, F. M.; Cevatemre, B.; Pellacani, D.; Walker, H.; Mann, V. M.; Simms, M. S.; Stower, M. J.; YILMAZ, V. T.; Maitland, N. J. *PLoS One* **2013,** *8* (5), e64278.
17. Ari, F.; Cevatemre, B.; Armutak, E. I. I.; Aztopal, N.; YILMAZ, V. T.; ULUKAYA, E. *Bioorg Med Chem* **2014,** *22* (17), 4948–4954.
18. Karakas, D.; Cevatemre, B.; Aztopal, N.; Ari, F.; Yilmaz, V. T.; ULUKAYA, E. *Bioorg Med Chem* **2015,** *23* (17), 5580–5586.
19. IKITIMUR-ARMUTAK, E. I.; ULUKAYA, E.; GUREL-GUREVIN, E.; YAYLIM, I.; ISBILEN-BASOK, B.; SENNAZLI, G.; YUZBASIOGLU-OZTURK, G.; SONMEZ, K.; CELIK, F.; KUCUKHUSEYIN, O.; KORKMAZ, G.; YILMAZ, V. T.; ZEYBEK, S. U. *In Vivo* **2016,** *30* (4), 457–464.
20. ULUKAYA, E.; Ari, F.; Dimas, K.; Sarimahmut, M.; Guney, E.; Sakellaridis, N.; YILMAZ, V. T. *J Cancer Res Clin Oncol* **2011,** *137* (10), 1425–1434.

21. Genova, P.; Varadinova, T.; Matesanz, A. I.; Marinova, D.; Souza, P. *Toxicol Appl Pharmacol* **2004,** *197* (2), 107–112.

22. Shaheen, F.; Badshah, A.; Gielen, M.; Gieck, C.; Jamil, M.; Vos, D. de. *Journal of Organometallic Chemistry* **2008,** *693* (6), 1117–1126.

23. Salas, P. F.; Herrmann, C.; Orvig, C. *Chem Rev* **2013,** *113* (5), 3450–3492.

24. Gaber, M.; El-Ghamry, H. A.; Fathalla, S. K. *Spectrochim Acta A Mol Biomol Spectrosc* **2015,** *139*, 396–404.

25. Liu, T. Z.; Chou, L. Y.; Humphreys, M. H. *Toxicology Letters* **1979,** *4* (6), 433–438.

26. Fernley, H. N. 18 Mammalian Alkaline Phosphatases. *Hydrolysis*: *Other C-N bonds, phosphate esters*; The Enzymes; Elsevier, 1971; pp 417–447.

27. Lazarević, T.; Rilak, A.; Bugarčić, Ž. D. *Eur J Med Chem* **2017**.

28. Gao, E.-j.; Wang, K.-H.; Zhu, M.-c.; Liu, L. *Eur J Med Chem* **2010,** *45* (7), 2784–2790.

29. Gao, E.; Liu, C.; Zhu, M.; Lin, H.; Wu, Q.; Liu, L. *ACAMC* **2009,** *9* (3), 356–368.

30. Pranczk, J.; Jacewicz, D.; Wyrzykowski, D.; Chmurzynski, L. *CPA* **2014,** *10* (1), 2–9.

31. Gildner, P. G.; Colacot, T. J. *Organometallics* **2015,** *34* (23), 5497–5508.

32. Mogorosi, M. M.; Mahamo, T.; Moss, J. R.; Mapolie, S. F.; Slootweg, J. C.; Lammertsma, K.; Smith, G. S. *Journal of Organometallic Chemistry* **2011,** *696* (23), 3585–3592.

33. Shabbir, M.; Akhter, Z.; Ahmad, I.; Ahmed, S.; Shafiq, M.; Mirza, B.; McKee, V.; Munawar, K. S.; Ashraf, A. R. *Journal of Molecular Structure* **2016,** *1118*, 250–258.

34. Muche, S.; Levacheva, I.; Samsonova, O.; Biernasiuk, A.; Malm, A.; Lonsdale, R.; Popiołek, Ł.; Bakowsky, U.; Hołyńska, M. *Journal of Molecular Structure* **2017,** *1127*, 231–236.

35. Muche, S.; Hołyńska, M. *Journal of Molecular Structure* **2017,** *1142*, 168–174.

36. Satheesh, C. E.; Raghavendra Kumar, P.; Sharma, P.; Lingaraju, K.; Palakshamurthy, B. S.; Raja Naika, H. *Inorganica Chimica Acta* **2016,** *442*, 1–9.

37. Elshaarawy, R. F. M.; Mostafa, T. B.; Refaee, A. A.; El-Sawi, E. A. *RSC Adv* **2015,** *5* (84), 68260–68269.

38. Budige, G.; Puchakayala, M. R.; Kongara, S. R.; Hu, A.; Vadde, R. *Chem. Pharm. Bull.* **2011,** *59* (2), 166–171.

39. Rîmbu, C.; Danac, R.; Pui, A. *Chem. Pharm. Bull.* **2014,** *62* (1), 12–15.

40. Muche, S.; Levacheva, I.; Samsonova, O.; Pham, L.; Christou, G.; Bakowsky, U.; Hołyńska, M. *Inorg. Chem.* **2014,** *53* (14), 7642–7649.

41. Puthraya, K. H.; Srivastava, T. S.; Amonkar, A. J.; Adwankar, M. K.; Chitnis, M. P. *J Inorg Biochem* **1986,** *26* (1), 45–54.

42. Mital, R.; Shah, G. M.; Srivastava, T. S.; Bhattacharya, R. K. *Life Sciences* **1992,** *50* (11), 781–790.

43. Offiong, O. E.; Nfor, E.; Ayi, A. A.; Martelli, S. *Transition Metal Chemistry* **2000,** *25* (4), 369–373.

44. Reddy, E. R.; Trivedi, R.; Sarma, A. V. S.; Sridhar, B.; Anantaraju, H. S.; Sriram, D.; Yogeeswari, P.; Nagesh, N. *Dalton Trans* **2015,** *44* (40), 17600–17616.

45. European Committee for Antimicrobial Susceptibility Testing (EUCAST) (2003): Determination of minimum inhibitory concentrations (MICs) of antibacterial agents by broth dilution. EUCAST discussion document E. Dis 5.1. *Clinical Microbiology and Infection* **2003,** *9* (8), ix–xv.

46. Clinical and Laboratory Standards Institute. *Clinical and Laboratory Standards Institute. Reference method for broth dilution antifungal susceptibility testing of yeasts. M27-S4.*: Wayne, PA, USA,, 2012.

47. Laczkowski, K.; Misiura, K.; Biernasiuk, A.; Malm, A.; Siwek, A.; Plech, T. *LDDD* **2013,** *10* (9), 798–807.

48. Wiegand, I.; Hilpert, K.; Hancock, R. E. W. *Nat Protoc* **2008,** *3* (2), 163–175.

49. O'Donnell, F.; Smyth, T. J. P.; Ramachandran, V. N.; Smyth, W. F. *Int J Antimicrob Agents* **2010,** *35* (1), 30–38.

Novel Pd(II) Schiff Base complexes derived from *ortho*-vanillin and *L*-tyrosine or *L*-glutamic acid: Synthesis, characterization, crystal structures and biological properties.

*Simon Muche[a], Anna Biernasiuk[b], Anna Malm[b], Łukasz Popiołek[c], Anna Hordyjewska[d], Anna Olszewska[e], Małgorzata Hołyńska[a]**

[a] Fachbereich Chemie und Wissenschaftliches Zentrum für Materialwissenschaften, Philipps-Universität Marburg, Hans-Meerwein-Strasse, D-35043, Marburg, Germany.

[b] Department of Pharmaceutical Microbiology, Medical University of Lublin, Chodźki 1, 20-093 Lublin, Poland.

[c] Department of Organic Chemistry, Medical University of Lublin, Chodźki 4A, 20-093, Lublin, Poland

[d] Department of Medicinal Chemistry, Medical University of Lublin, Chodźki 4A, 20-093, Lublin, Poland

[e] Department of Human Physiology, Medical University of Lublin, Chodźki 4A, 20-093, Lublin, Poland

---

SUPPORTING INFORMATION

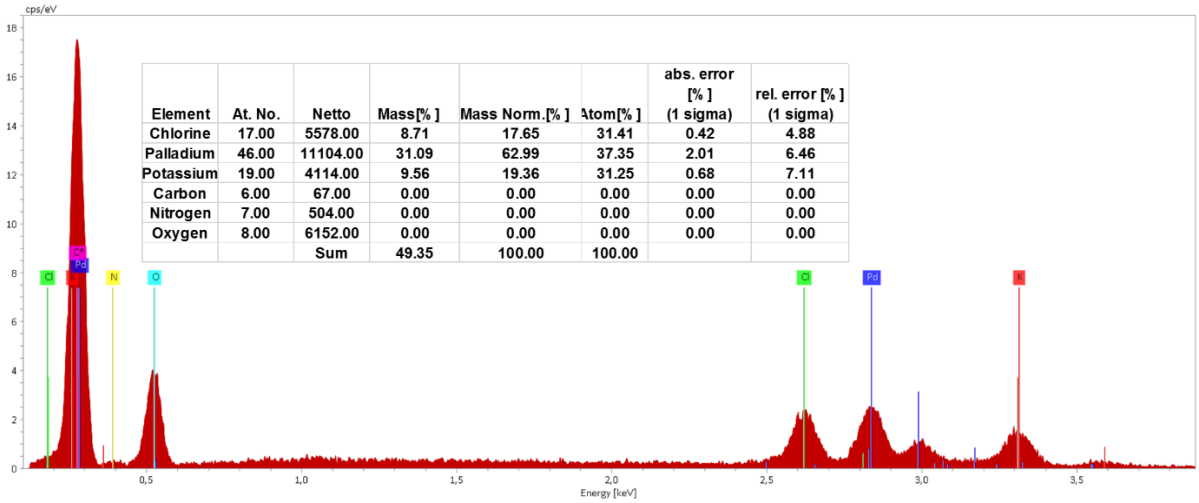

Element	At. No.	Netto	Mass[%]	Mass Norm.[%]	Atom[%]	abs. error [%] (1 sigma)	rel. error [%] (1 sigma)
Chlorine	17.00	5578.00	8.71	17.65	31.41	0.42	4.88
Palladium	46.00	11104.00	31.09	62.99	37.35	2.01	6.46
Potassium	19.00	4114.00	9.56	19.36	31.25	0.68	7.11
Carbon	6.00	67.00	0.00	0.00	0.00	0.00	0.00
Nitrogen	7.00	504.00	0.00	0.00	0.00	0.00	0.00
Oxygen	8.00	6152.00	0.00	0.00	0.00	0.00	0.00
		Sum	49.35	100.00	100.00		

Figure S1: EDX spectrum of **1** and Pd:Cl:K ratio.

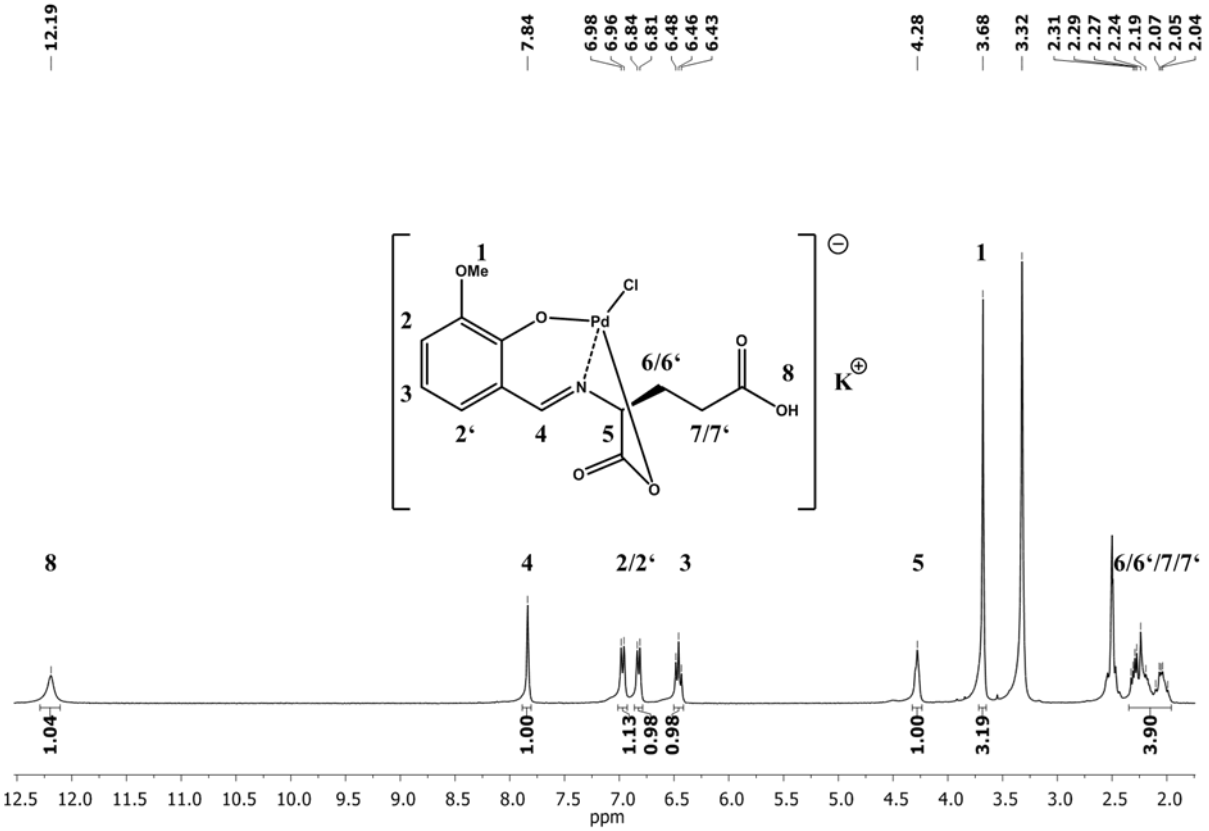

Figure S2: ^{1}H-NMR spectrum of **1** recorded in DMSO-d_6 and assignment of the signals.

160919_EM_742_De #93-106 RT: 1.03-1.14 AV: 7 NL: 4.84E4
F: FTMS + p ESI Full ms [100.00-1000.00]

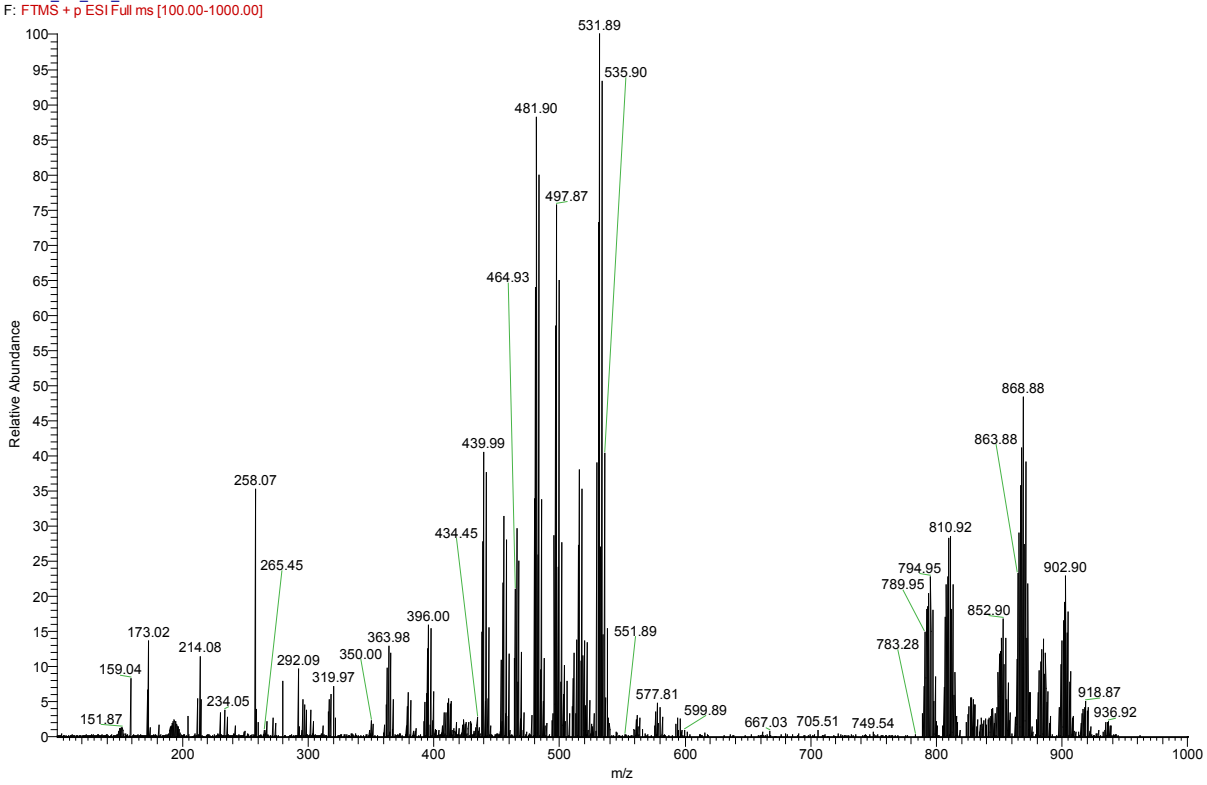

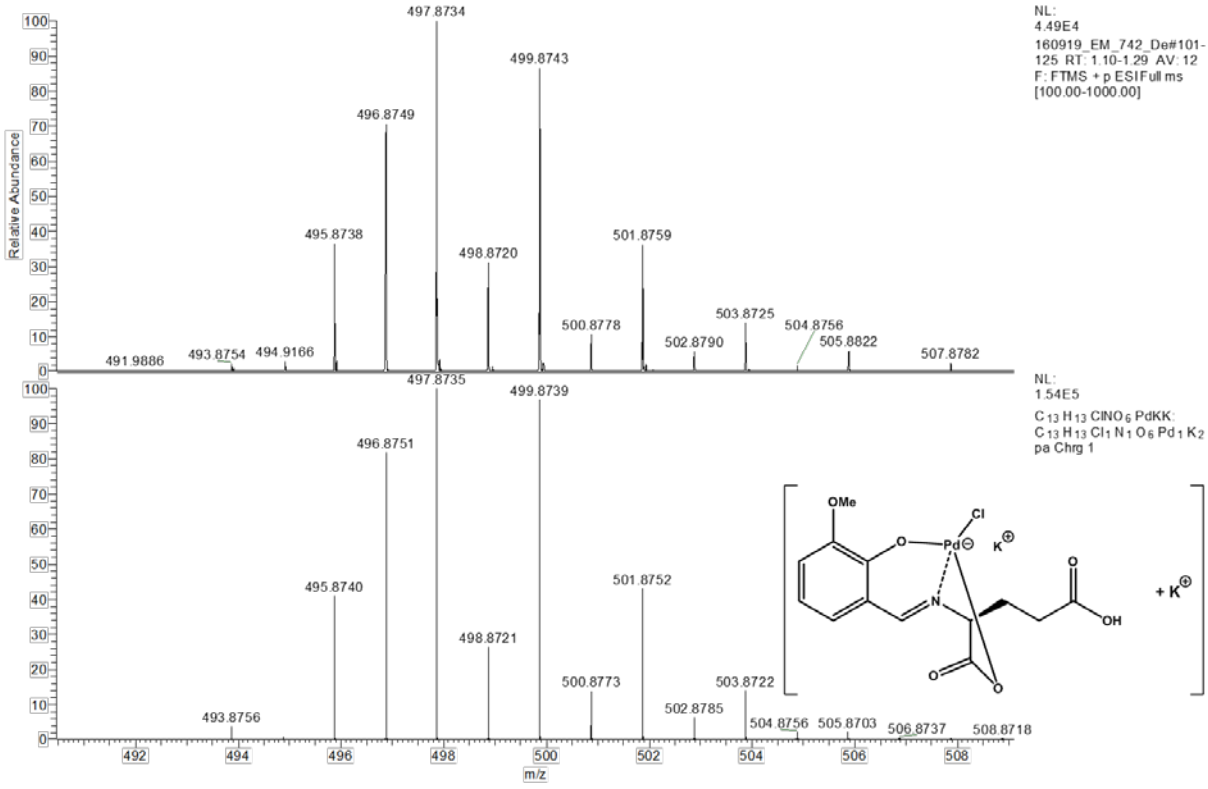

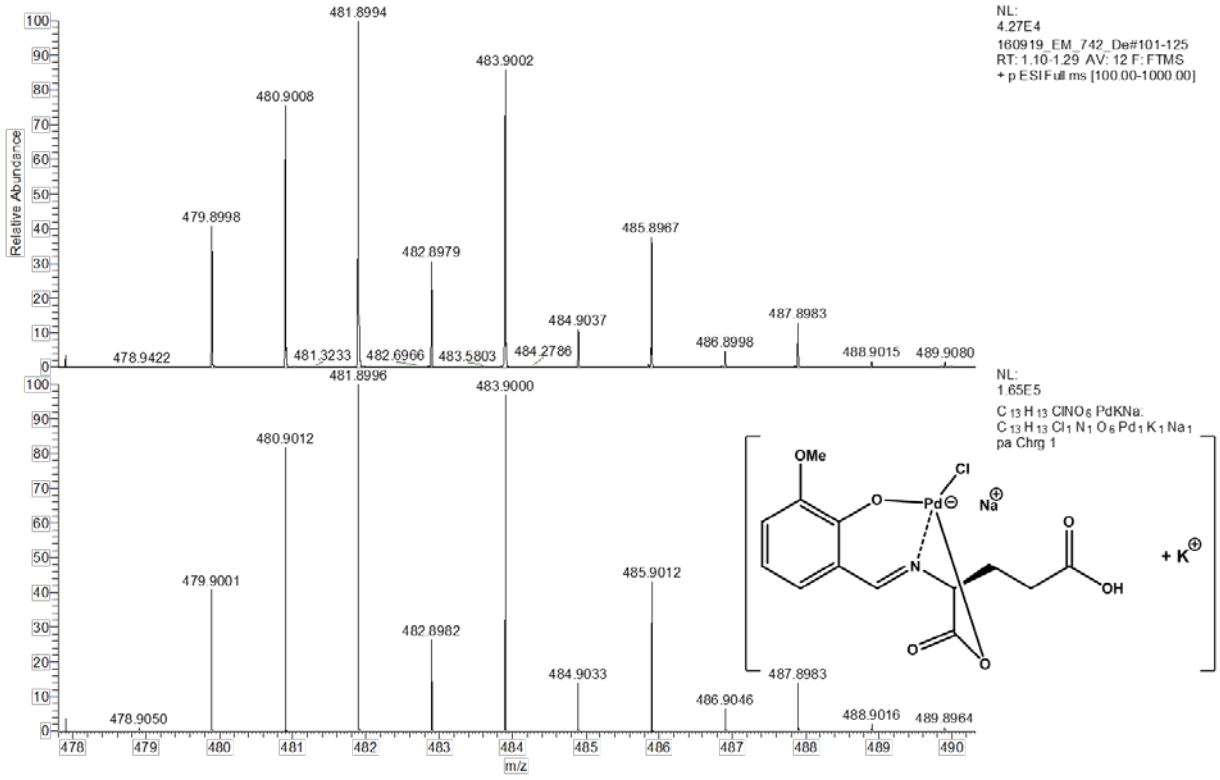
NL:
4.27E4
160919_EM_742_De#101-125
RT: 1.10-1.29 AV: 12 F: FTMS
+ p ESI Full ms [100.00-1000.00]
Relative Abundance
481.8994
483.9002
480.9008
479.8998
485.8967
482.8979
484.9037
487.8983
486.8998
478.9422
481.3233
482.6966
483.5803
484.2786
488.9015
489.9080
NL:
1.65E5
C13 H13 ClNO6 PdKNa:
C13 H13 Cl1 N1 O6 Pd1 K1 Na1
pa Chrg 1
481.8996
483.9000
480.9012
479.9001
485.9012
482.8982
484.9033
487.8983
486.9046
478.9050
488.9016
489.8964
OMe
Cl
Pd
Na
O
N
OH
+ K
m/z

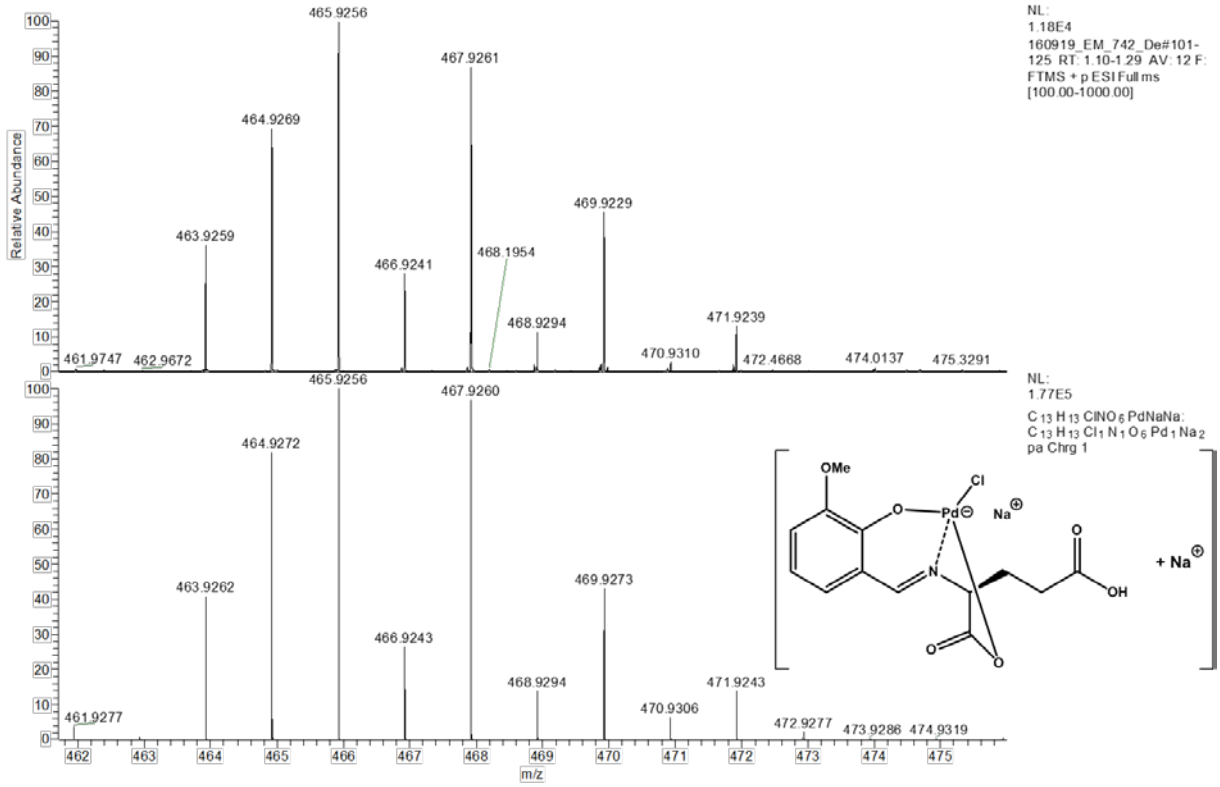
NL:
1.18E4
160919_EM_742_De#101-125 RT: 1.10-1.29 AV: 12 F: FTMS + p ESI Full ms [100.00-1000.00]
Relative Abundance
465.9256
467.9261
464.9269
469.9229
463.9259
468.1954
466.9241
471.9239
468.9294
461.9747
462.9672
470.9310
472.4668
474.0137
475.3291
NL:
1.77E5
C13 H13 ClNO6 PdNaNa:
C13 H13 Cl1 N1 O6 Pd1 Na2
pa Chrg 1
465.9256
467.9260
464.9272
463.9262
469.9273
466.9243
468.9294
471.9243
461.9277
470.9306
472.9277
473.9286
474.9319
OMe
Cl
Pd
Na
O
N
OH
+ Na
m/z

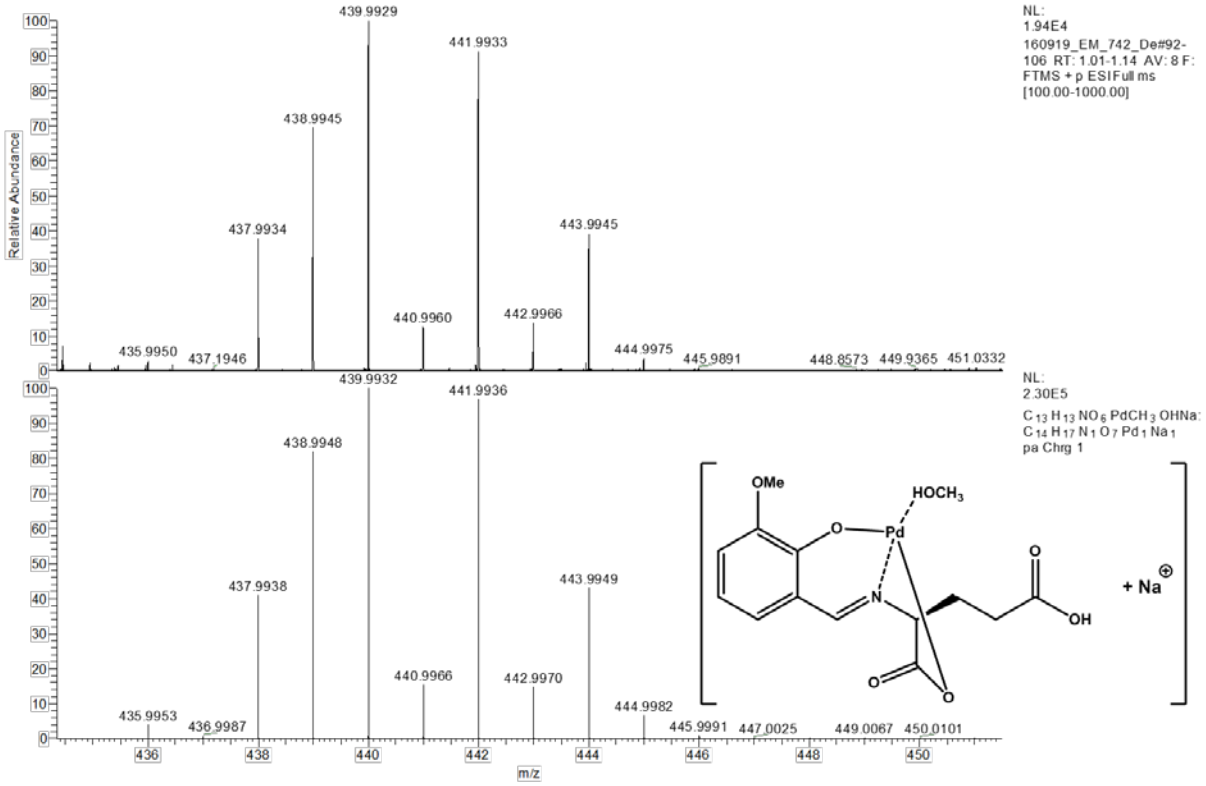

Figure S3: ESI(+)-MS of **1** recorded in methanol with simulation of the identified peaks and structural suggestions.

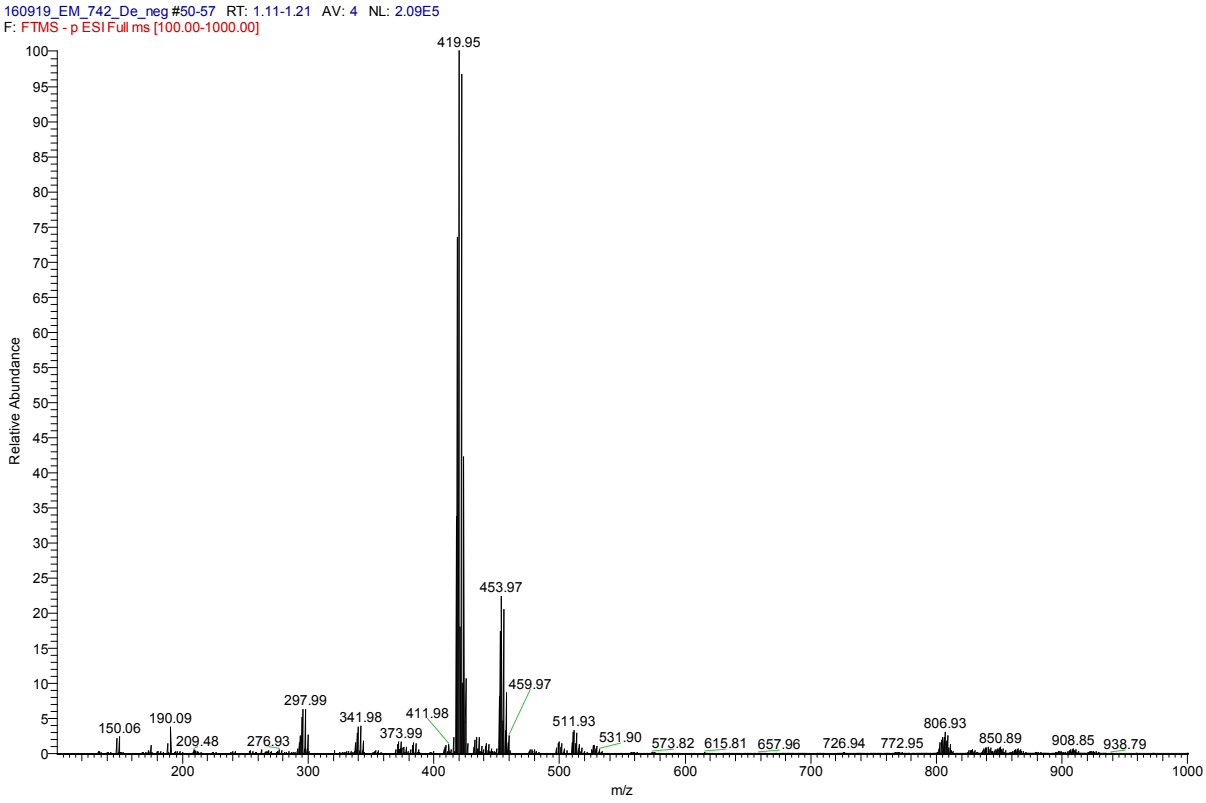

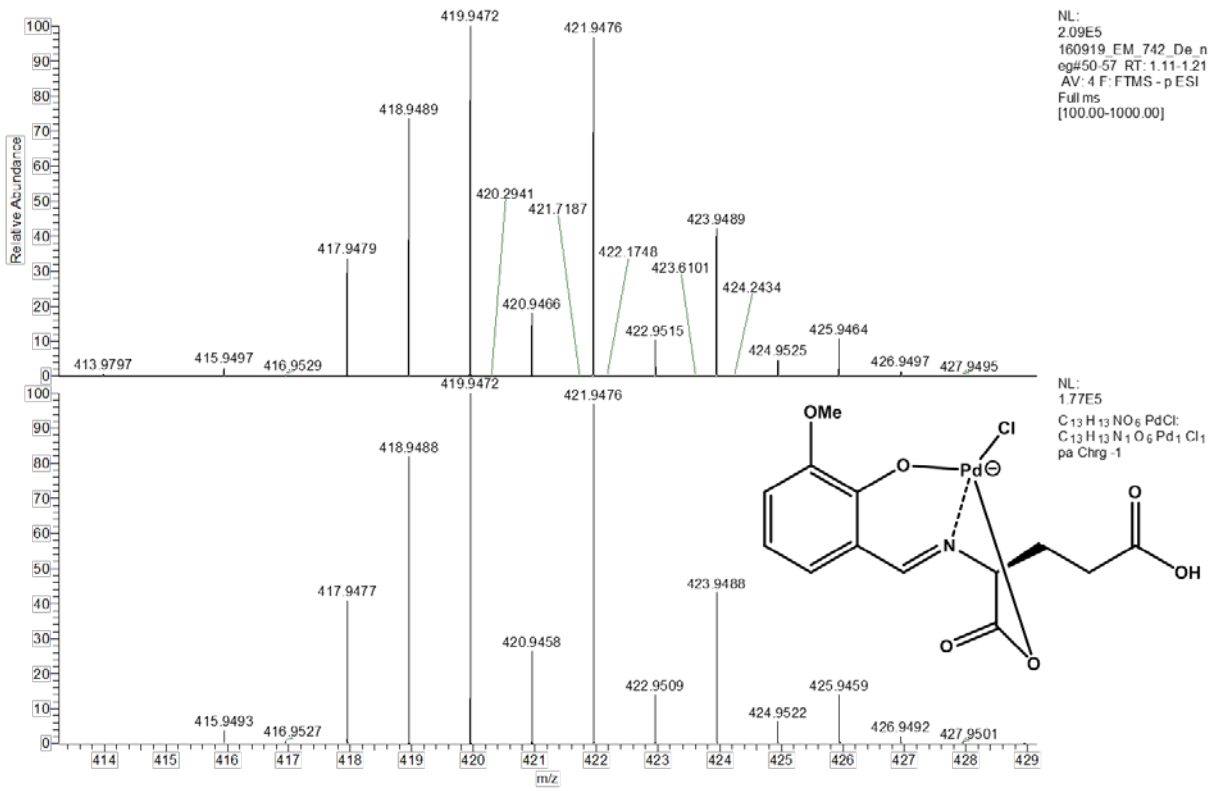

Figure S4: ESI(-)-MS of **1** recorded in methanol with simulation of the identified peaks and structural suggestions.

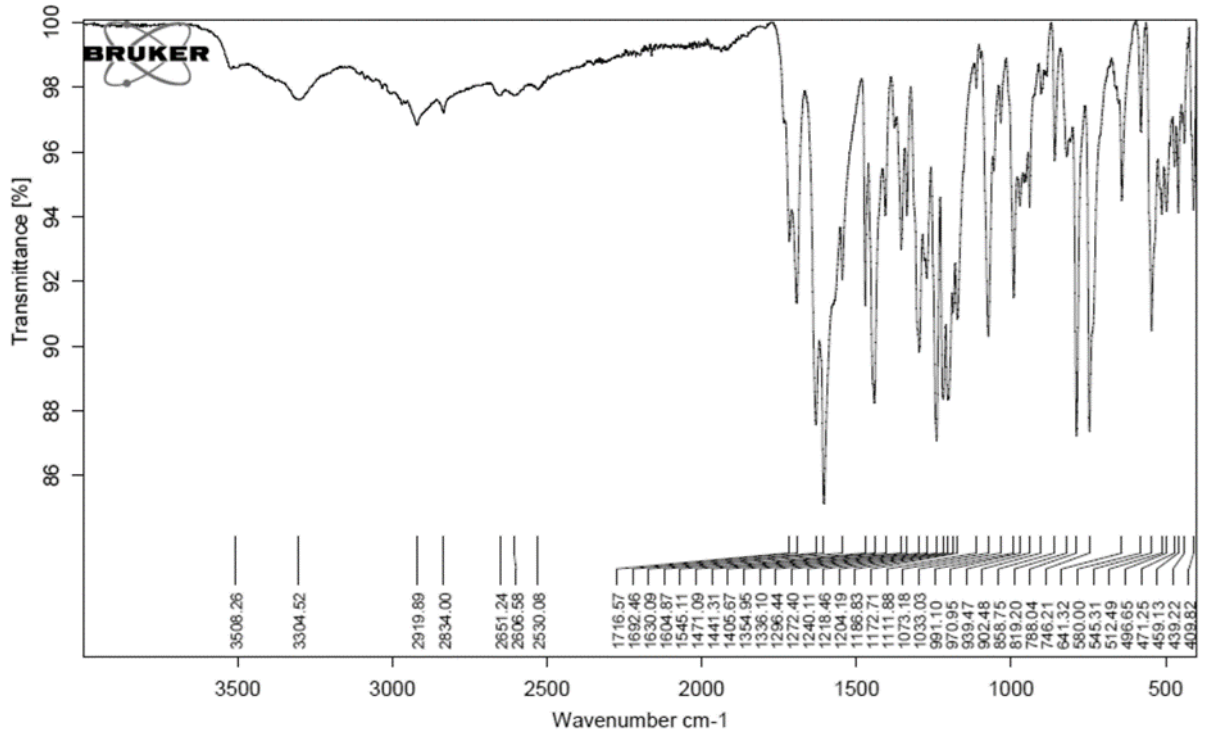

Figure S5: IR spectrum of **1** dried *in vacuo*.

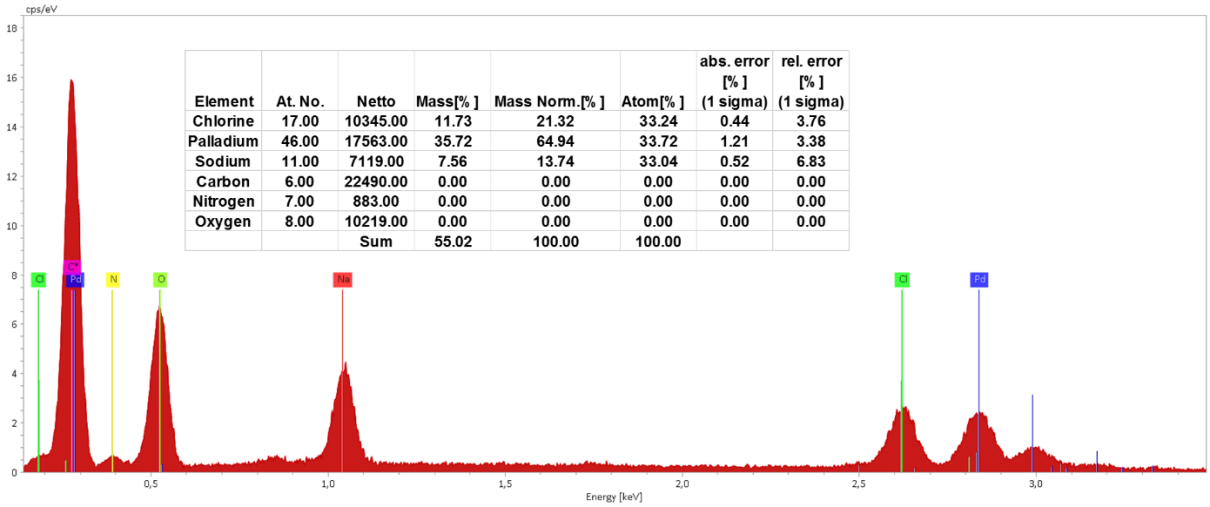

Element	At. No.	Netto	Mass[%]	Mass Norm.[%]	Atom[%]	abs. error [%] (1 sigma)	rel. error [%] (1 sigma)
Chlorine	17.00	10345.00	11.73	21.32	33.24	0.44	3.76
Palladium	46.00	17563.00	35.72	64.94	33.72	1.21	3.38
Sodium	11.00	7119.00	7.56	13.74	33.04	0.52	6.83
Carbon	6.00	22490.00	0.00	0.00	0.00	0.00	0.00
Nitrogen	7.00	883.00	0.00	0.00	0.00	0.00	0.00
Oxygen	8.00	10219.00	0.00	0.00	0.00	0.00	0.00
		Sum	55.02	100.00	100.00		

Figure S6: EDX spectrum of **2** and Pd:Cl:Na ratio.

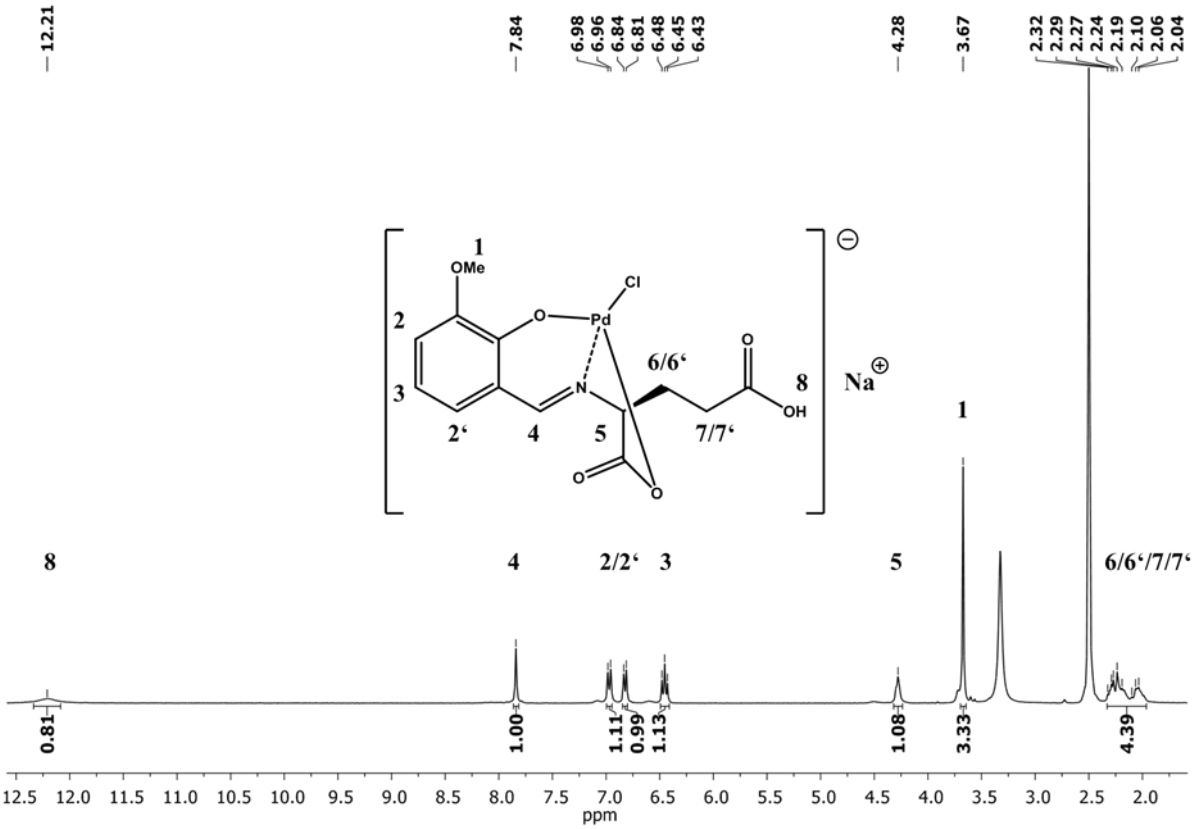

Figure S7: ^{1}H-NMR spectrum of **2** recorded in DMSO-d_6 and assignment of the signals.

160919_EM_741_De #114-131 RT: 1.22-1.35 AV: 9 NL: 8.64E4
F: FTMS + p ESI Full ms [100.00-1000.00]

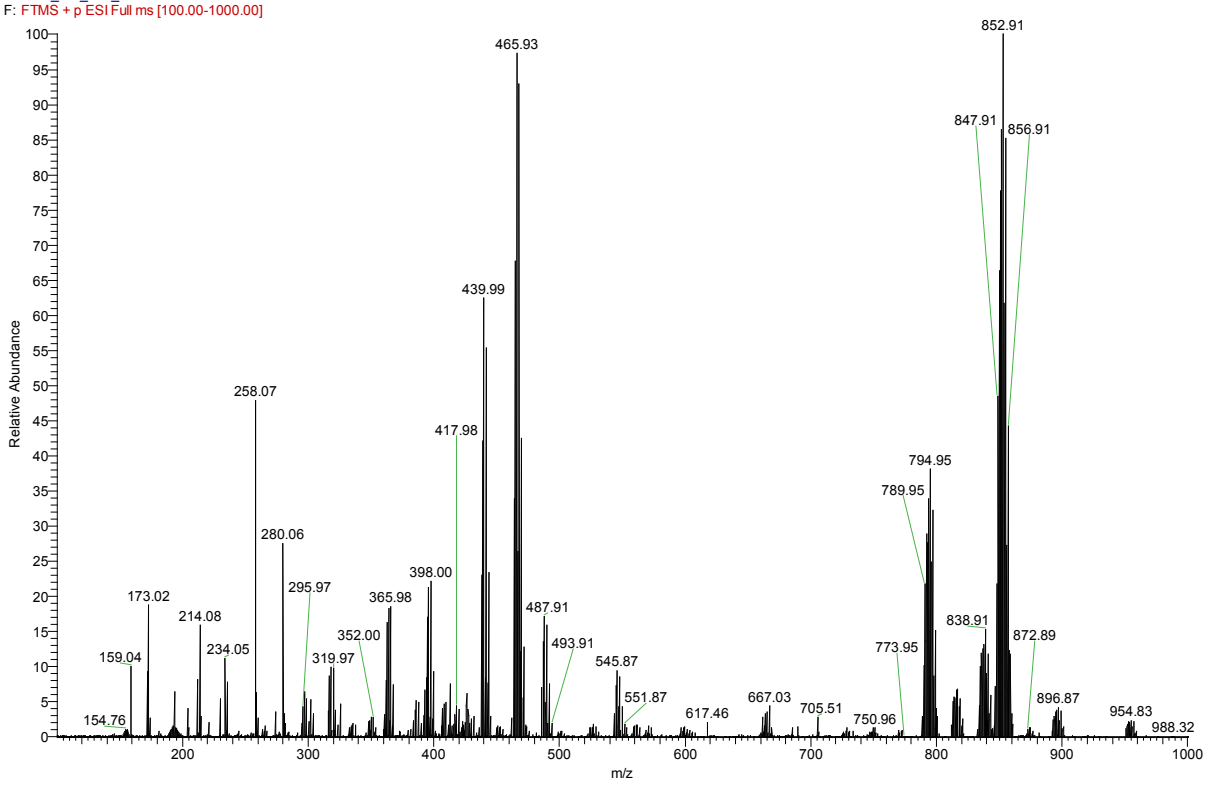

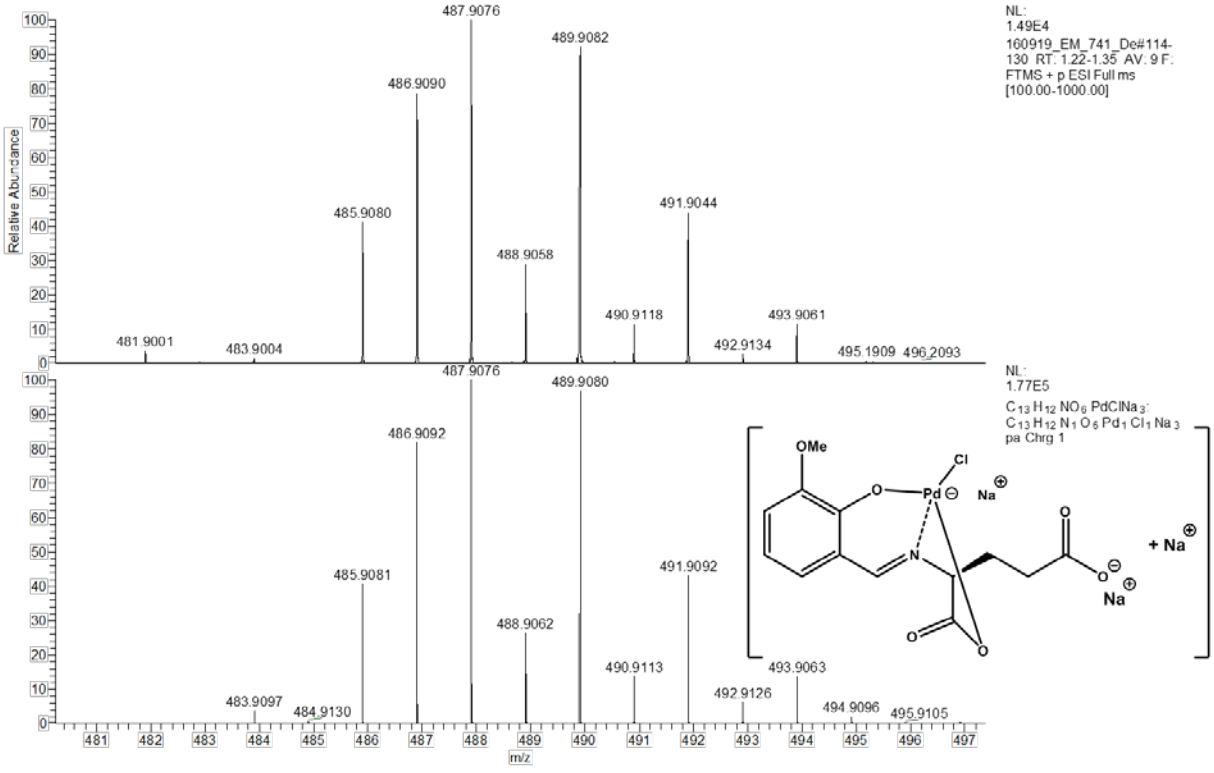

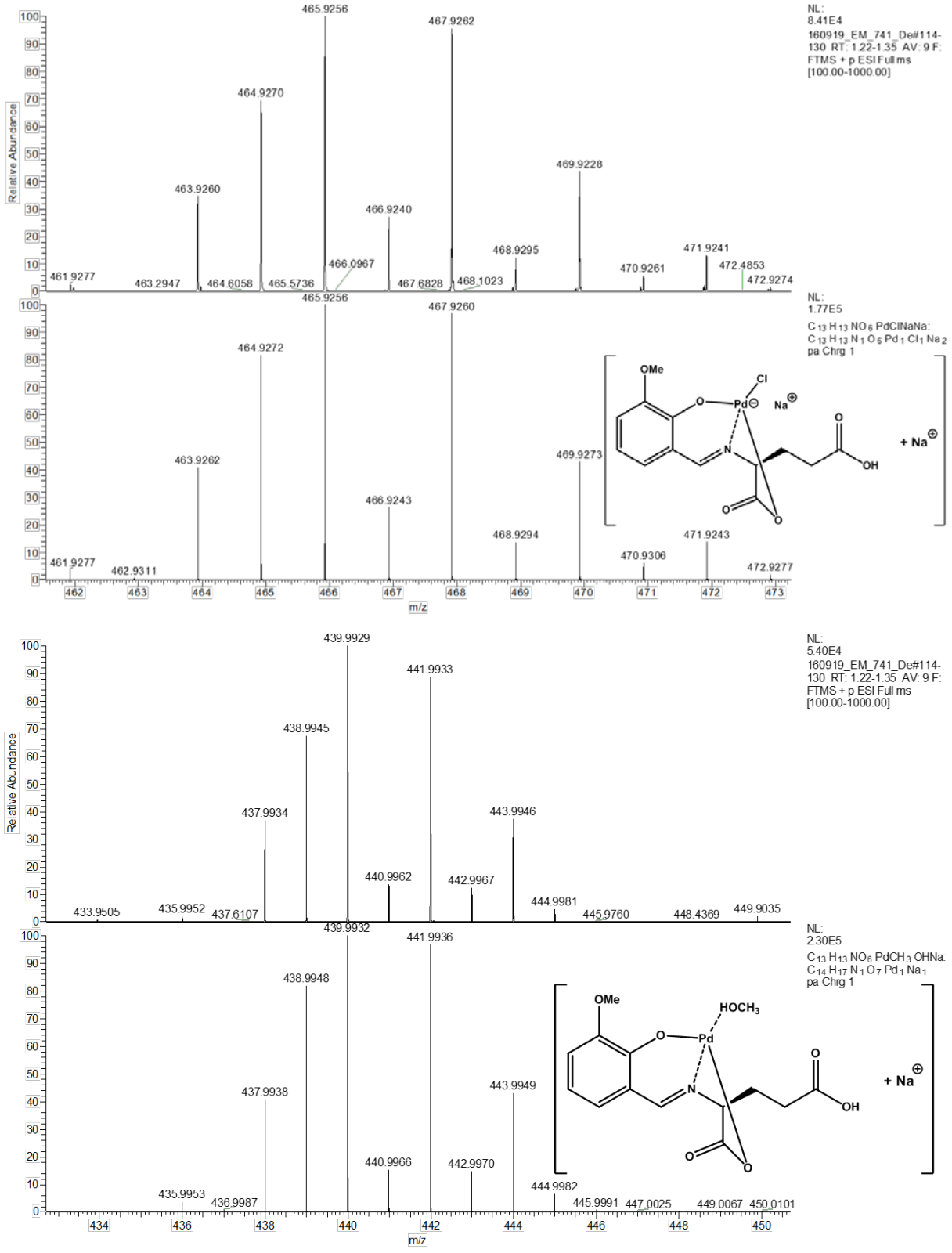

Figure S8: ESI(+)-MS of **2** recorded in methanol with simulation of the identified peaks and structural suggestions.

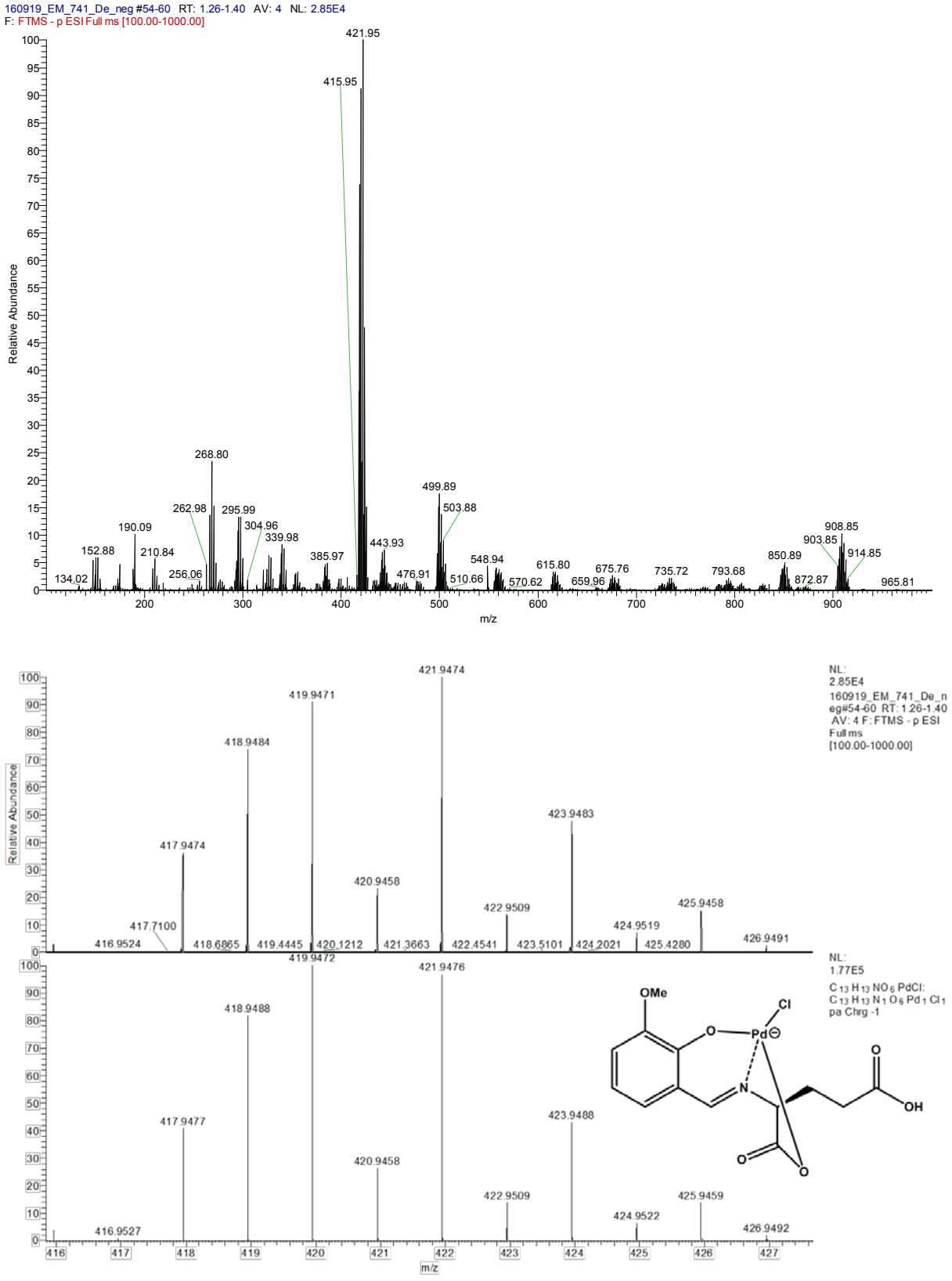

Figure S9: ESI(-)-MS of **2** recorded in methanol with simulation of the identified peaks and structural suggestions.

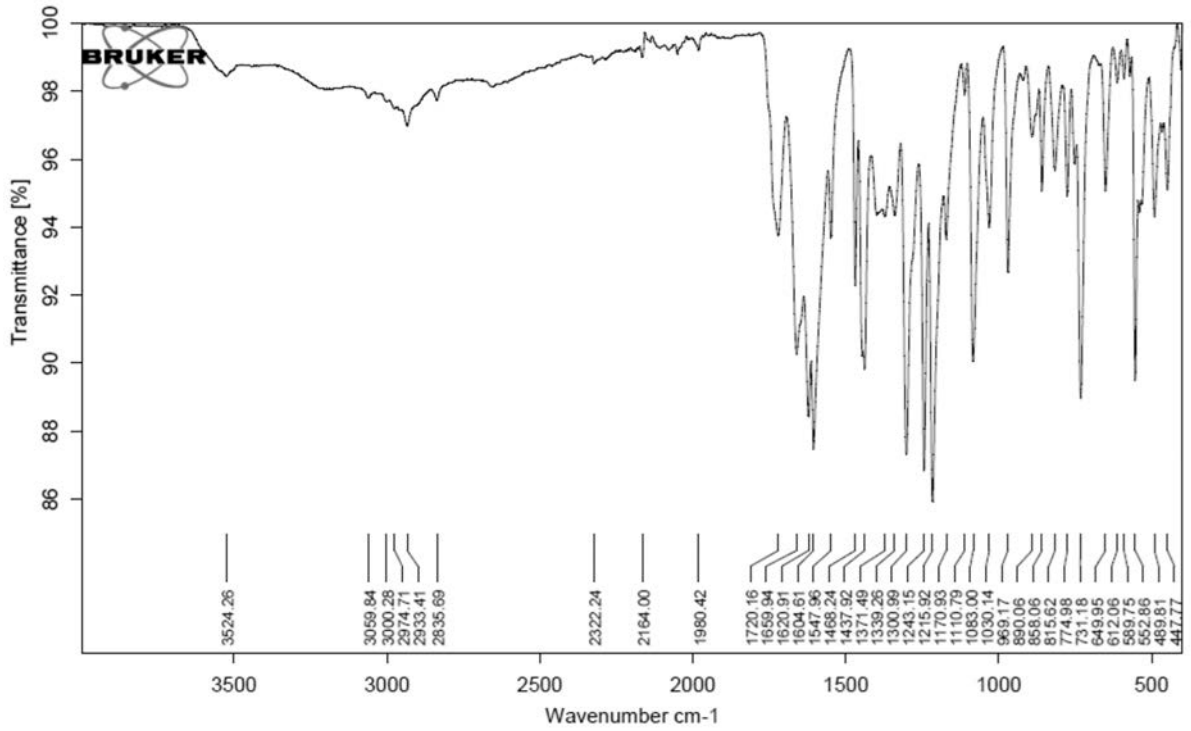

Figure S10: IR spectrum of **2** dried *in vacuo*.

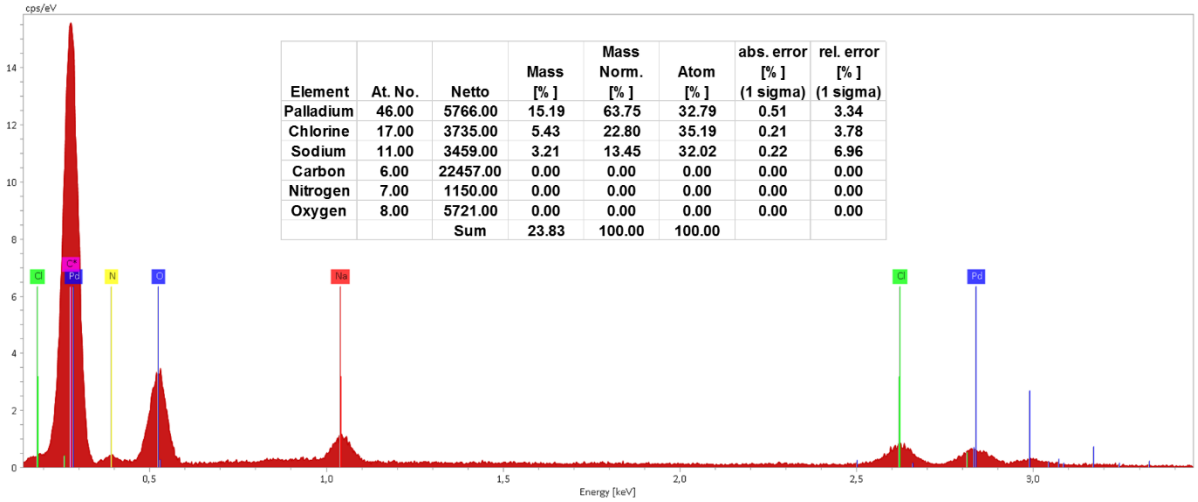

Element	At. No.	Netto	Mass [%]	Mass Norm. [%]	Atom [%]	abs. error [%] (1 sigma)	rel. error [%] (1 sigma)
Palladium	46.00	5766.00	15.19	63.75	32.79	0.51	3.34
Chlorine	17.00	3735.00	5.43	22.80	35.19	0.21	3.78
Sodium	11.00	3459.00	3.21	13.45	32.02	0.22	6.96
Carbon	6.00	22457.00	0.00	0.00	0.00	0.00	0.00
Nitrogen	7.00	1150.00	0.00	0.00	0.00	0.00	0.00
Oxygen	8.00	5721.00	0.00	0.00	0.00	0.00	0.00
		Sum	23.83	100.00	100.00		

Figure S11: EDX spectrum of **3** and Pd:Cl:Na ratio.

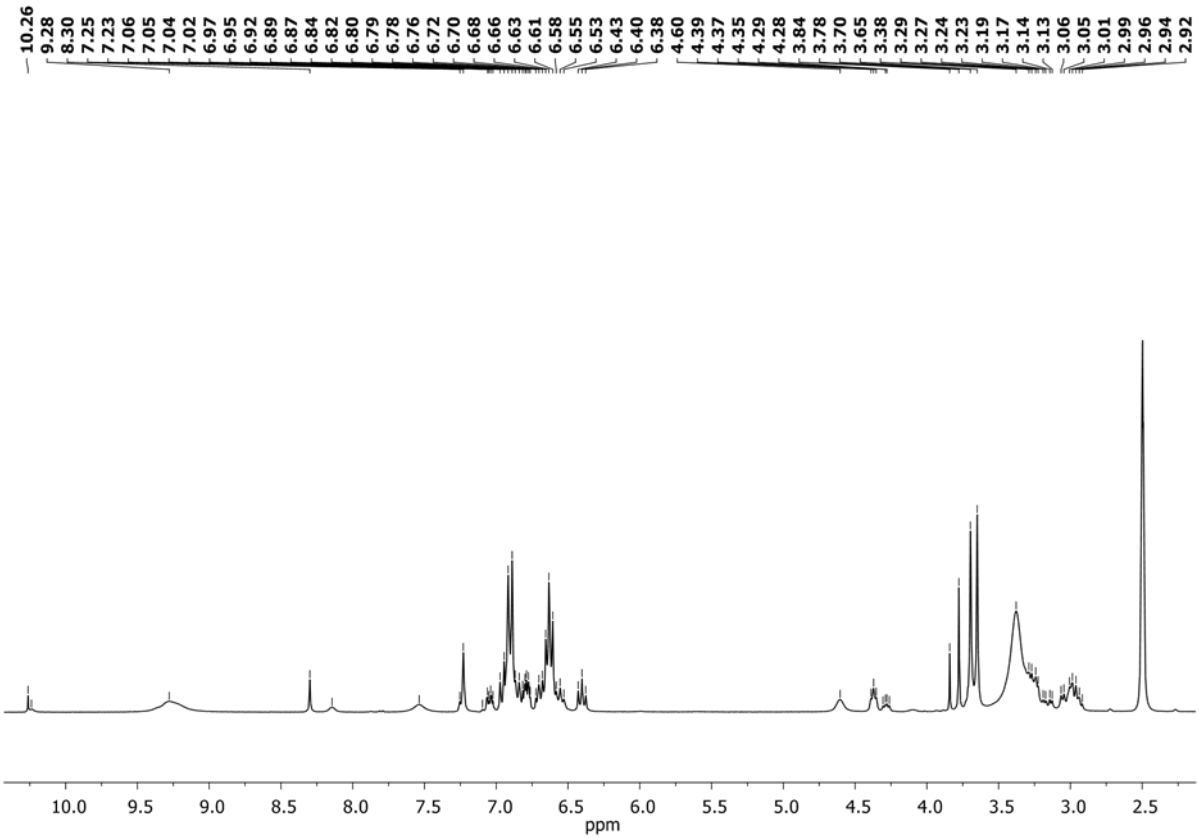

Figure S12: ^{1}H-NMR spectrum of **3** recorded in DMSO-d_6.

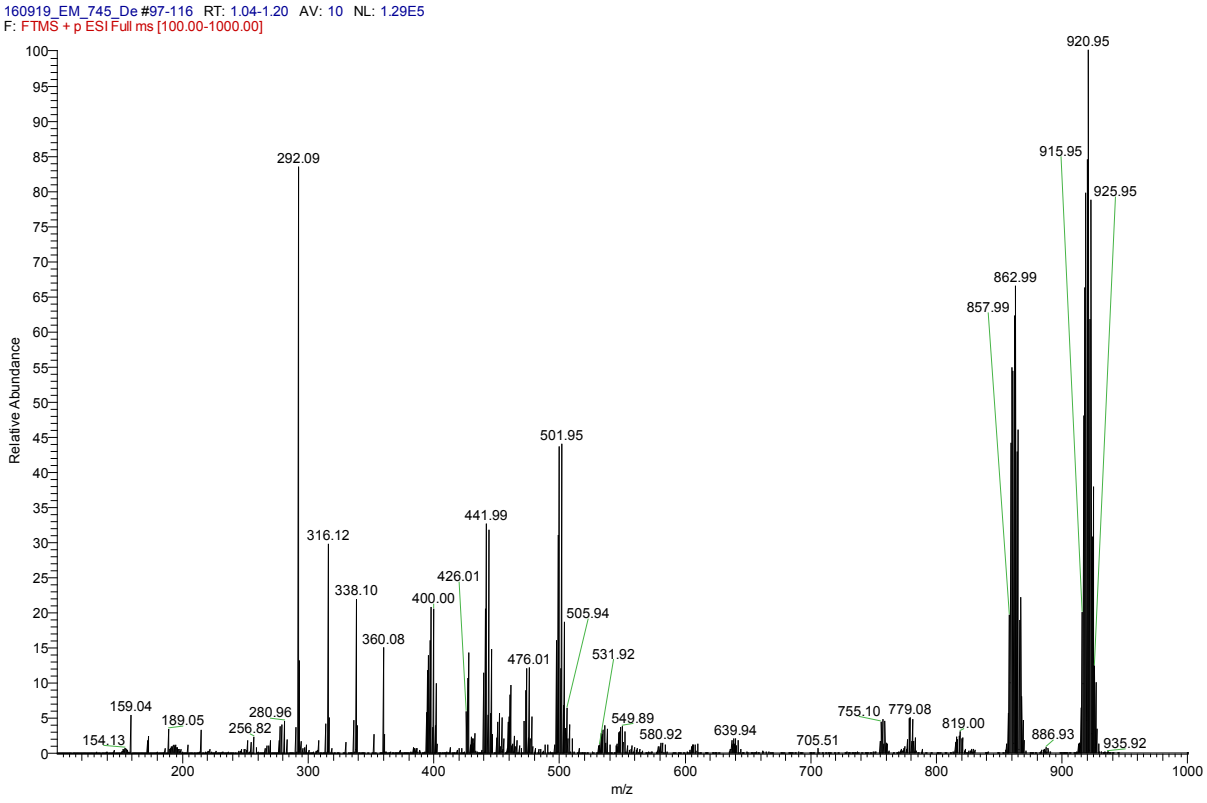

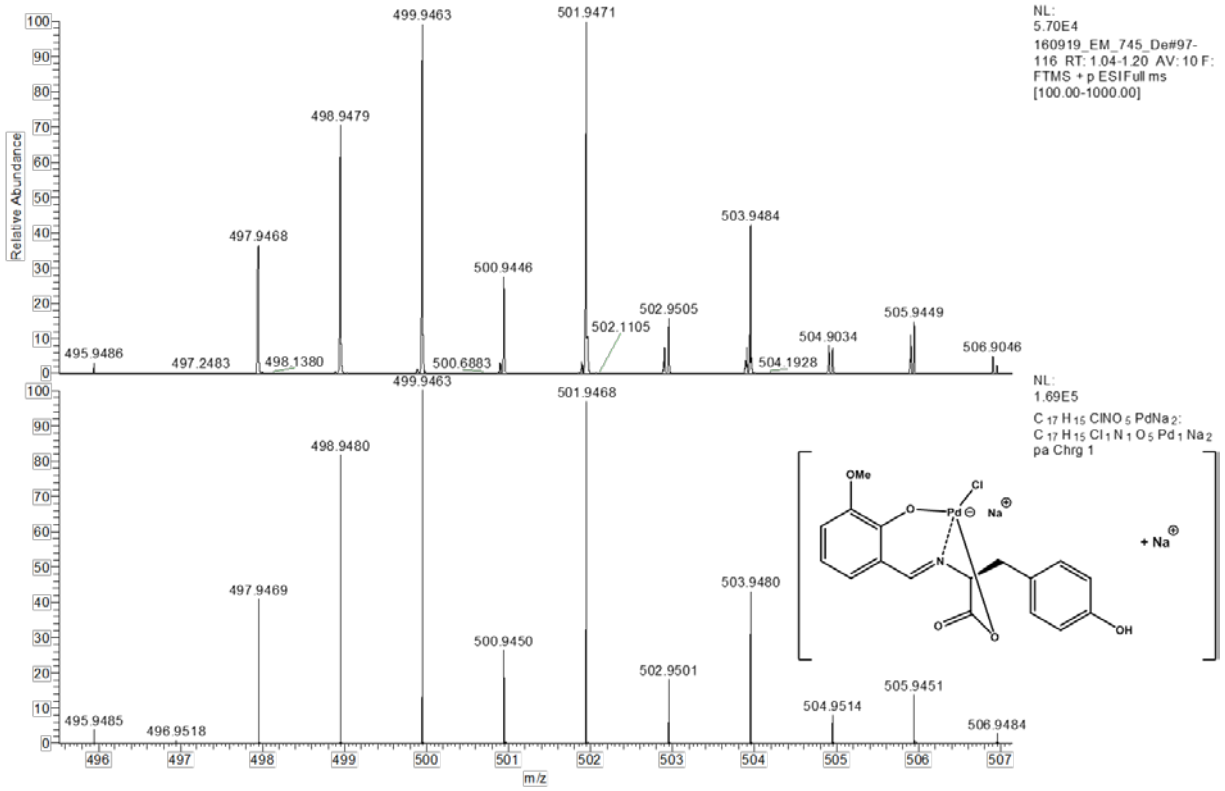
NL:
5.70E4
160919_EM_745_De#97-116 RT: 1.04-1.20 AV: 10 F: FTMS + p ESI Full ms [100.00-1000.00]
Relative Abundance
499.9463
501.9471
498.9479
497.9468
503.9484
500.9446
502.9505
502.1105
505.9449
504.9034
506.9046
495.9486
497.2483
498.1380
500.6883
504.1928
NL:
1.69E5
C 17 H 15 ClNO 5 PdNa 2:
C 17 H 15 Cl 1 N 1 O 5 Pd 1 Na 2
pa Chrg 1
499.9463
501.9468
498.9480
497.9469
503.9480
500.9450
502.9501
505.9451
504.9514
506.9484
495.9485
496.9518
OMe
Cl
O
Pd
Na
N
O
O
OH
+ Na
m/z

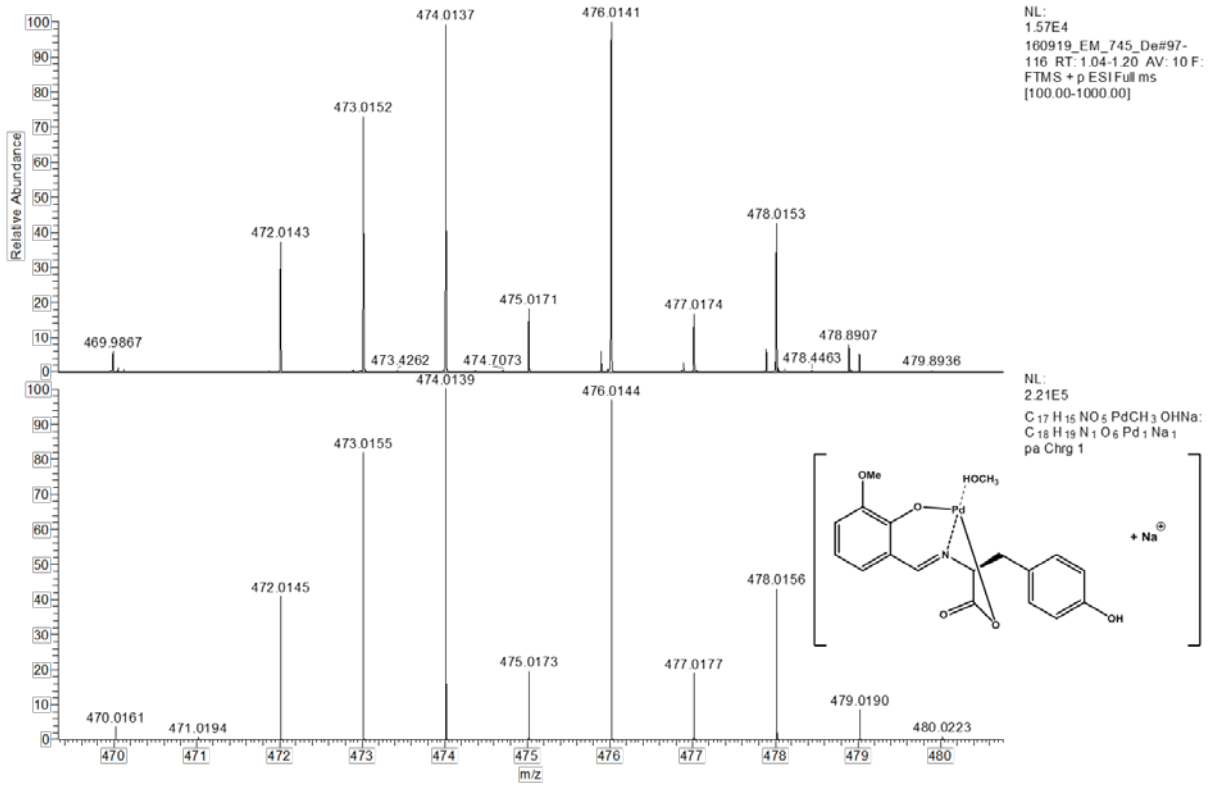
NL:
1.57E4
160919_EM_745_De#97-116 RT: 1.04-1.20 AV: 10 F: FTMS + p ESI Full ms [100.00-1000.00]
Relative Abundance
474.0137
476.0141
473.0152
472.0143
478.0153
475.0171
477.0174
478.8907
469.9867
473.4262
474.7073
478.4463
479.8936
NL:
2.21E5
C 17 H 15 NO 5 PdCH 3 OHNa:
C 18 H 19 N 1 O 6 Pd 1 Na 1
pa Chrg 1
474.0139
476.0144
473.0155
472.0145
478.0156
475.0173
477.0177
479.0190
470.0161
471.0194
480.0223
OMe
HOCH3
O
Pd
N
O
O
OH
+ Na
m/z

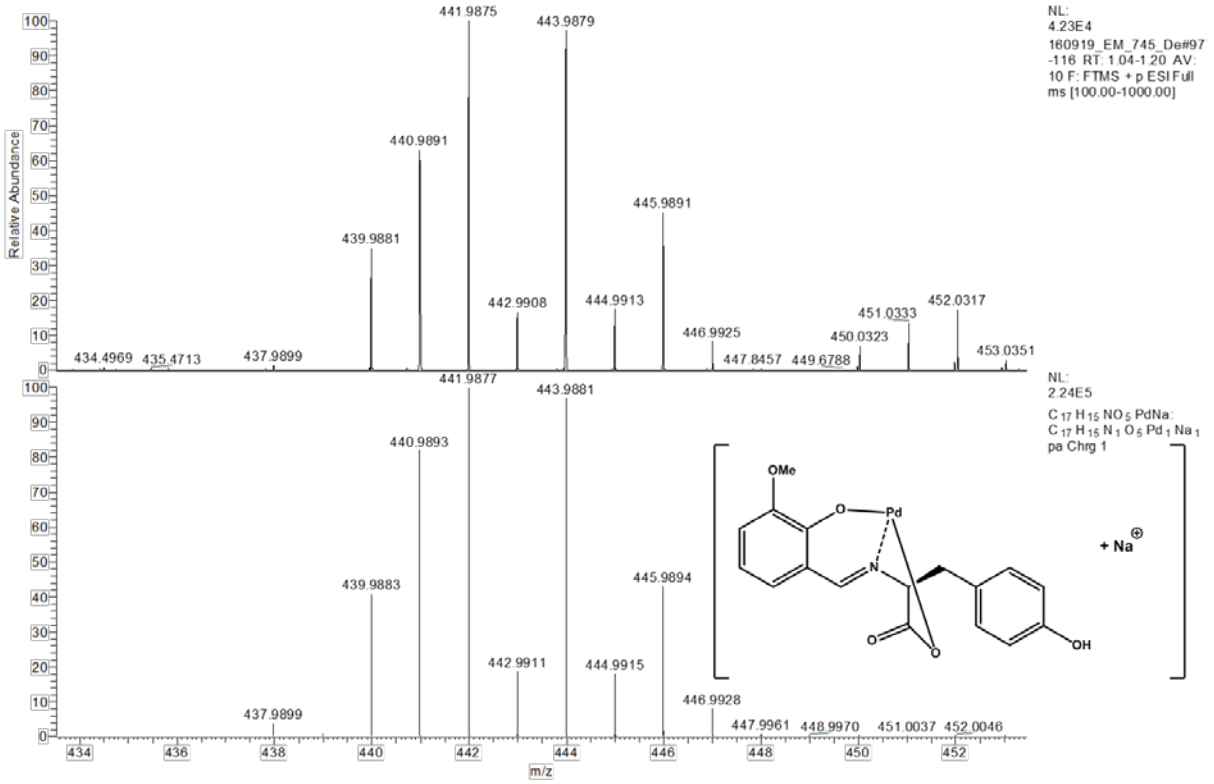
NL:
4.23E4
160919_EM_745_De#97
-116 RT: 1.04-1.20 AV:
10 F: FTMS + p ESI Full
ms [100.00-1000.00]
Relative Abundance
441.9875
443.9879
440.9891
445.9891
439.9881
442.9908
444.9913
452.0317
451.0333
446.9925
450.0323
453.0351
434.4969
435.4713
437.9899
447.8457
449.6788
NL:
2.24E5
C17 H15 NO5 PdNa:
C17 H15 N1 O5 Pd1 Na1
pa Chrg 1
441.9877
443.9881
440.9893
439.9883
445.9894
442.9911
444.9915
446.9928
437.9899
447.9961
448.9970
451.0037
452.0046
OMe
O
Pd
N
O
O
+ Na
OH
434
436
438
440
442
444
446
448
450
452
m/z

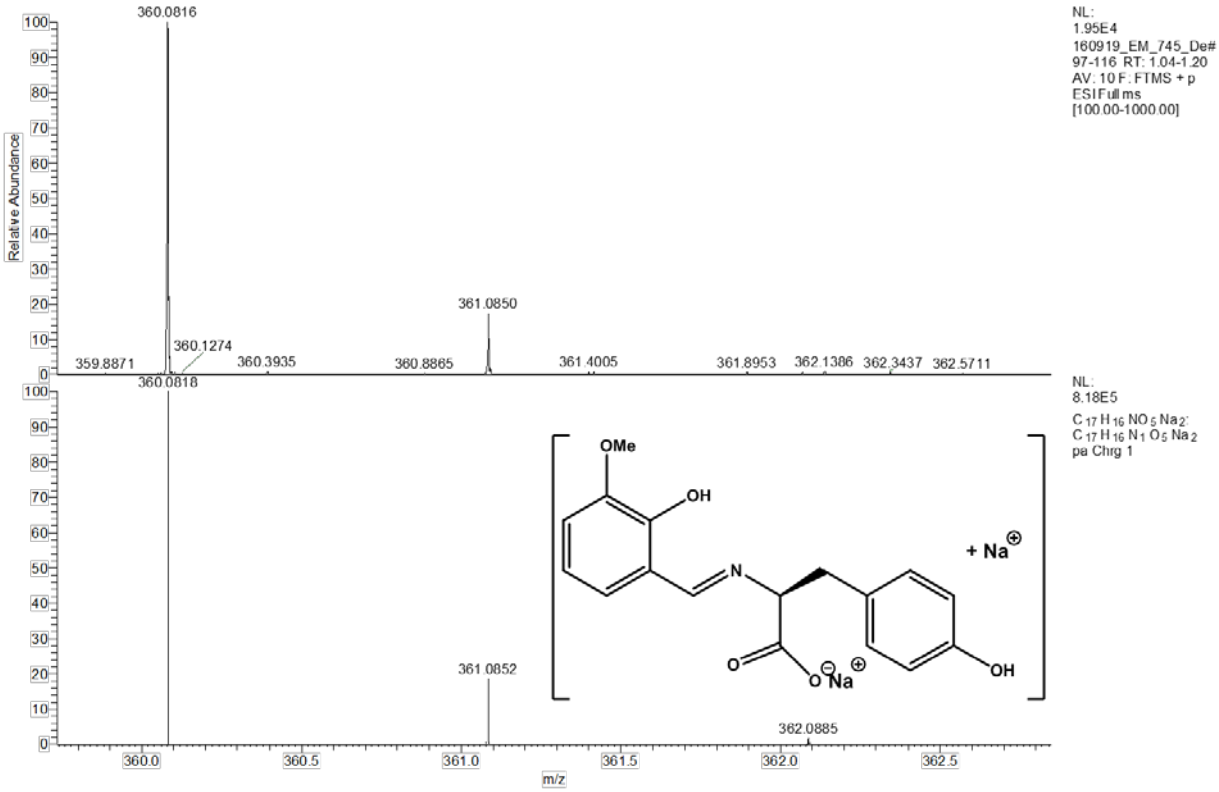
NL:
1.95E4
160919_EM_745_De#
97-116 RT: 1.04-1.20
AV: 10 F: FTMS + p
ESI Full ms
[100.00-1000.00]
Relative Abundance
360.0816
361.0850
360.1274
359.8871
360.3935
360.8865
361.4005
361.8953
362.1386
362.3437
362.5711
360.0818
NL:
8.18E5
C17 H16 NO5 Na2:
C17 H16 N1 O5 Na2
pa Chrg 1
OMe
OH
N
+ Na
O
O
Na
OH
361.0852
362.0885
360.0
360.5
361.0
361.5
362.0
362.5
m/z

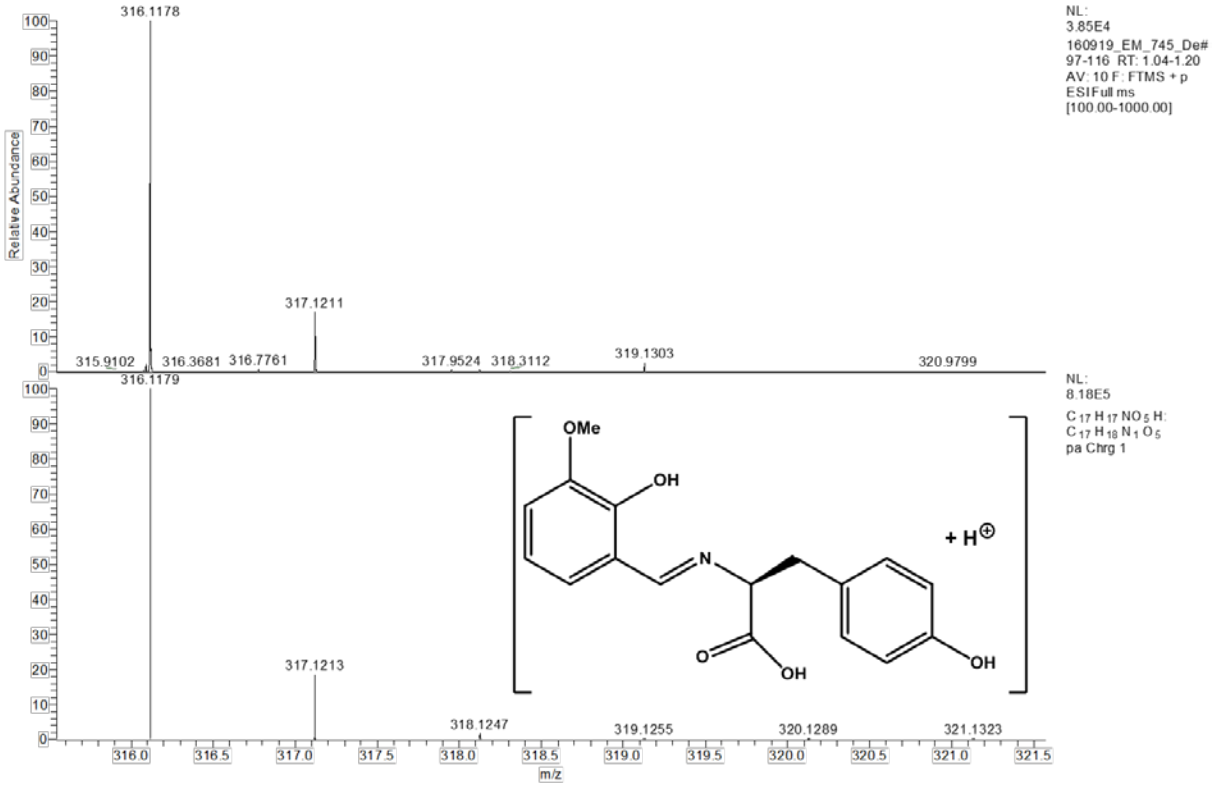
316.1178
317.1211
315.9102
316.3681
316.7761
317.9524
318.3112
319.1303
320.9799
NL:
3.85E4
160919_EM_745_De#
97-116 RT: 1.04-1.20
AV: 10 F: FTMS + p
ESI Full ms
[100.00-1000.00]
Relative Abundance
316.1179
317.1213
318.1247
319.1255
320.1289
321.1323
OMe
OH
N
O
OH
OH
+ H⊕
NL:
8.18E5
C17 H17 NO5 H:
C17 H18 N1 O5
pa Chrg 1
m/z

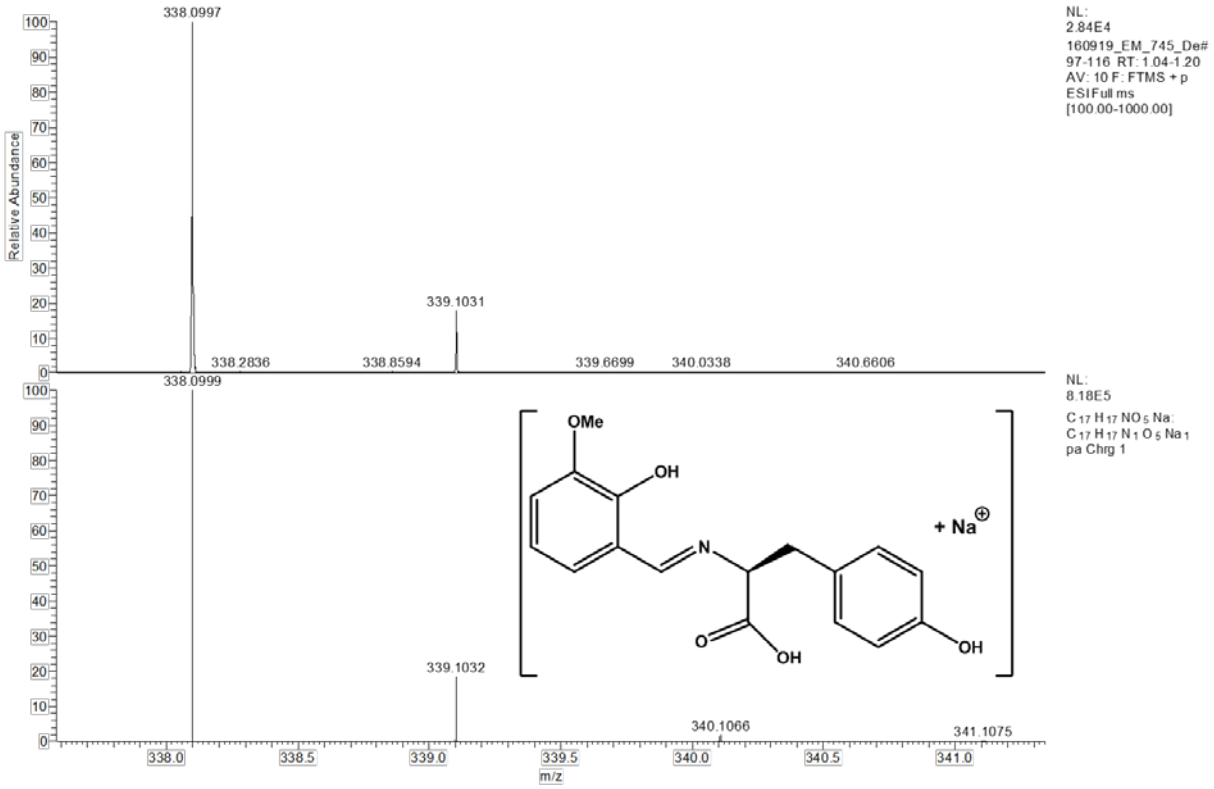
338.0997
339.1031
338.2836
338.8594
339.6699
340.0338
340.6606
NL:
2.84E4
160919_EM_745_De#
97-116 RT: 1.04-1.20
AV: 10 F: FTMS + p
ESI Full ms
[100.00-1000.00]
Relative Abundance
338.0999
339.1032
340.1066
341.1075
OMe
OH
N
O
OH
OH
+ Na⊕
NL:
8.18E5
C17 H17 NO5 Na:
C17 H17 N1 O5 Na1
pa Chrg 1
m/z

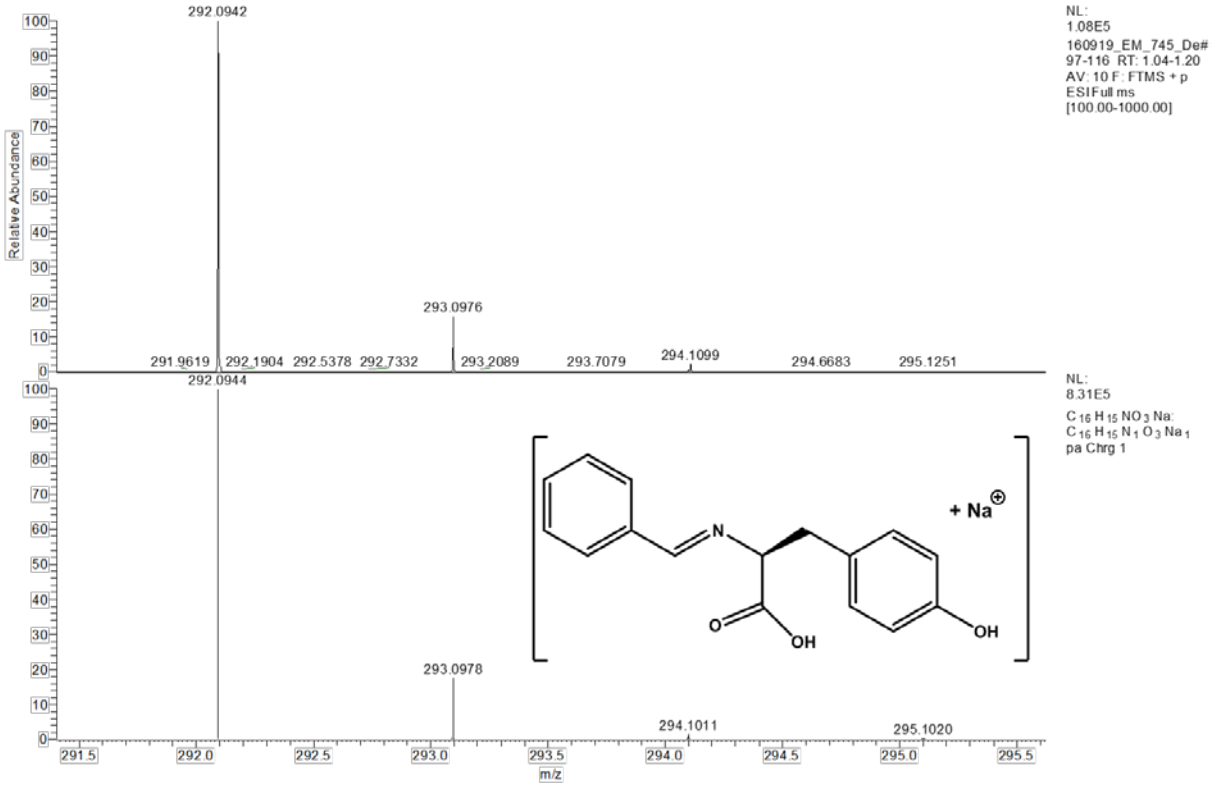

Figure S13: ESI(+)-MS of **3** recorded in methanol with simulation of the identified peaks and structural suggestions.

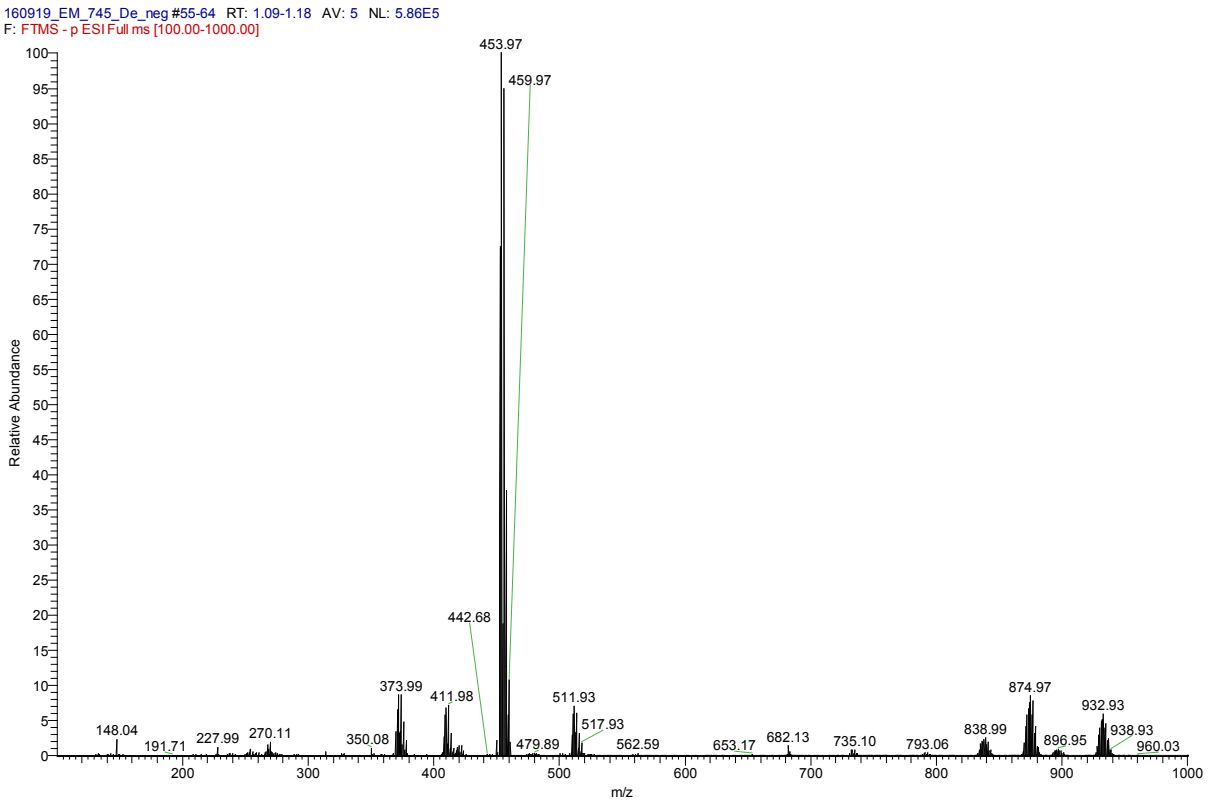

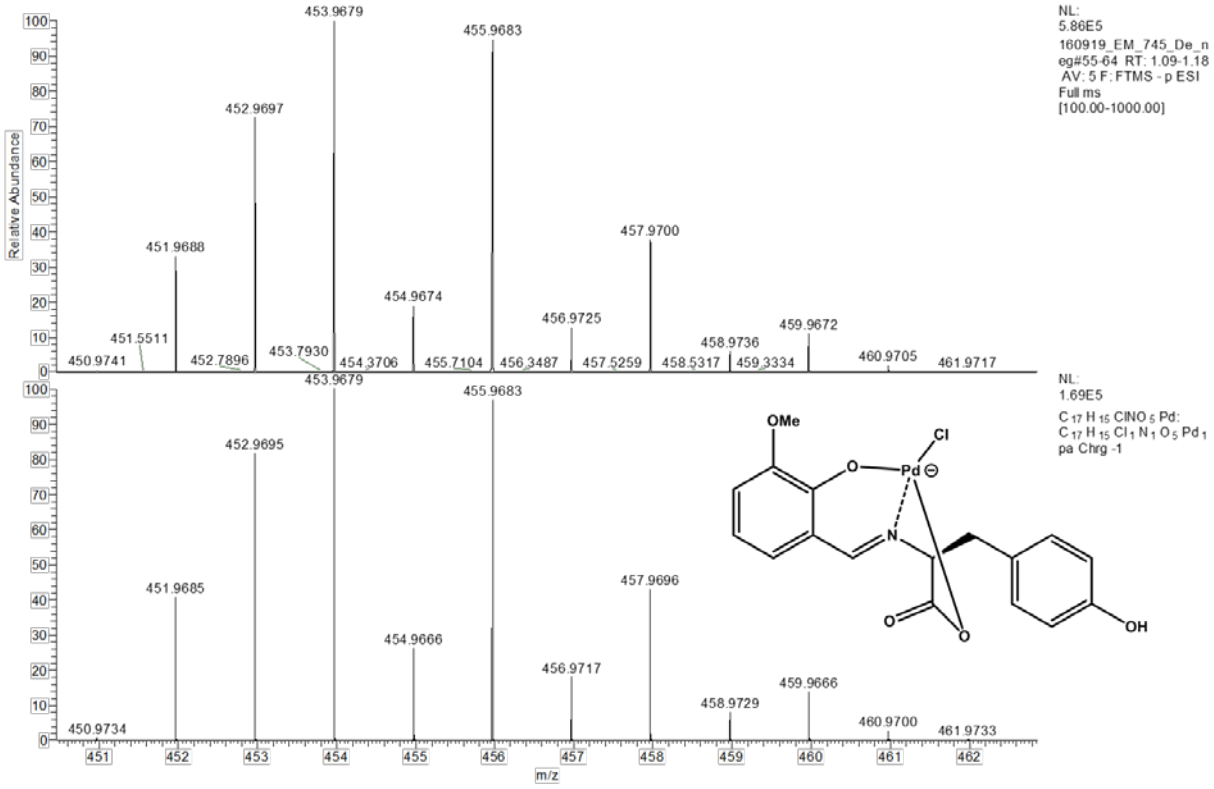

Figure S14: ESI(-)-MS of **3** recorded in methanol with simulation of the identified peaks and structural suggestions.

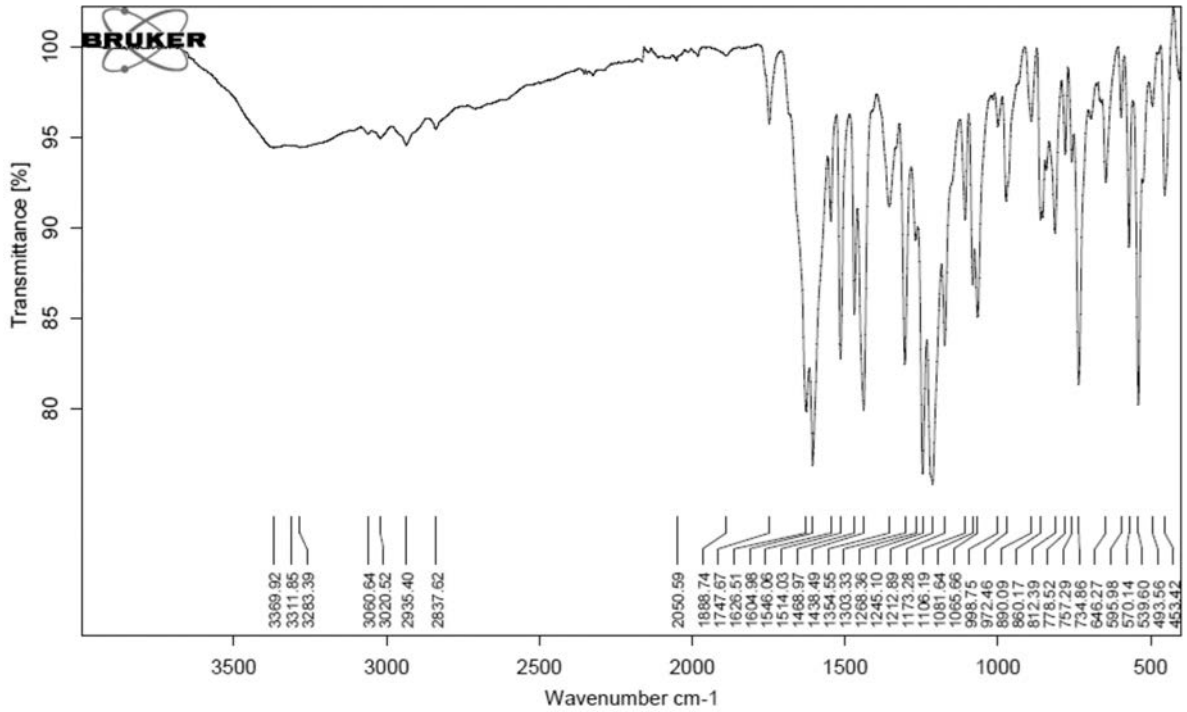

Figure S15: IR spectrum of **3** dried *in vacuo.*

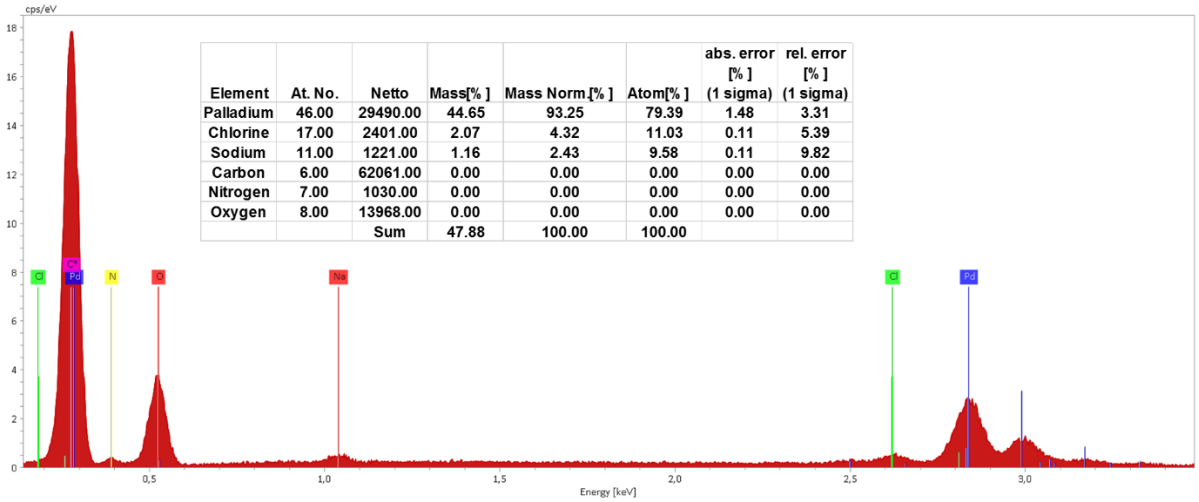

Element	At. No.	Netto	Mass[%]	Mass Norm.[%]	Atom[%]	abs. error [%] (1 sigma)	rel. error [%] (1 sigma)
Palladium	46.00	29490.00	44.65	93.25	79.39	1.48	3.31
Chlorine	17.00	2401.00	2.07	4.32	11.03	0.11	5.39
Sodium	11.00	1221.00	1.16	2.43	9.58	0.11	9.82
Carbon	6.00	62061.00	0.00	0.00	0.00	0.00	0.00
Nitrogen	7.00	1030.00	0.00	0.00	0.00	0.00	0.00
Oxygen	8.00	13968.00	0.00	0.00	0.00	0.00	0.00
		Sum	47.88	100.00	100.00		

Figure S16: EDX spectrum of **4** and Pd:Cl:Na ratio.

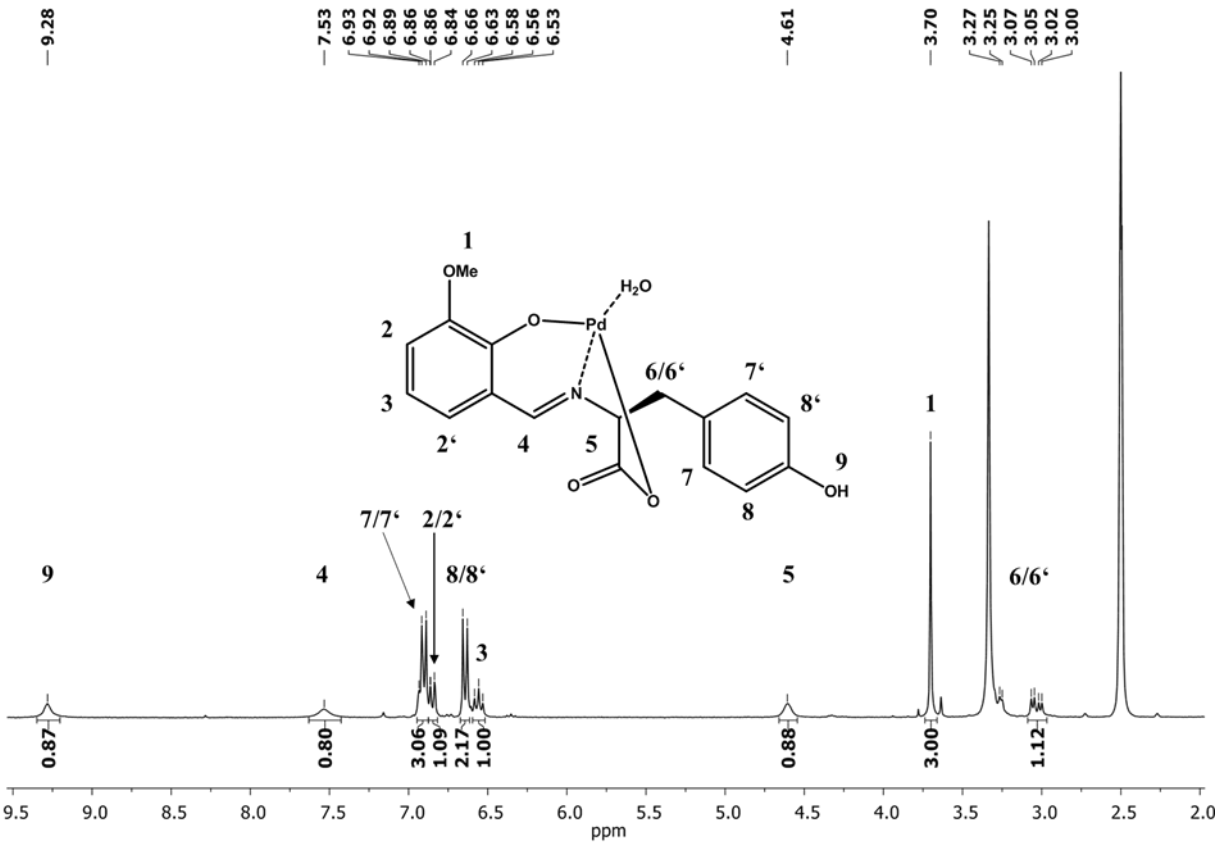

Figure S17: ^{1}H-NMR spectrum of **4** recorded in DMSO-d_6 and assignment of the signals.

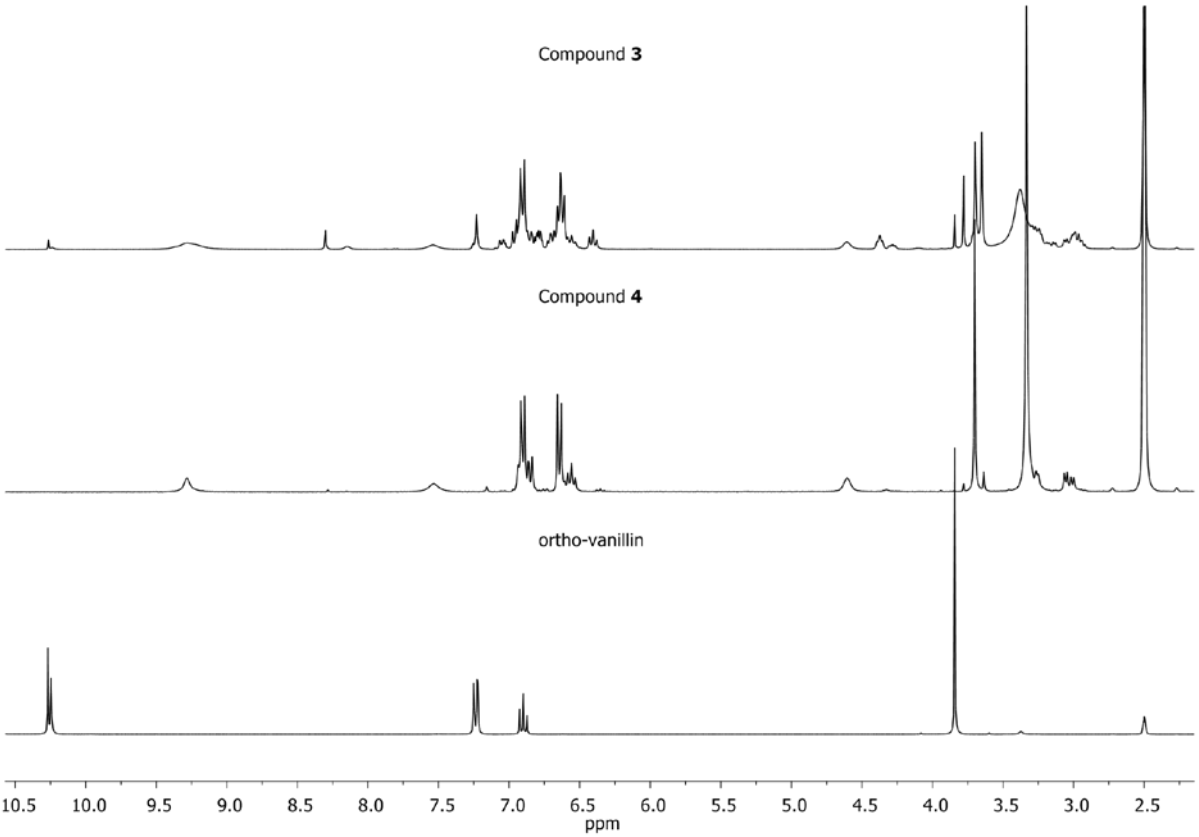

Figure S18: Stacked ^{1}H-NMR spectra of **3**, **4** and *ortho*-vanillin recorded in DMSO-d_6.

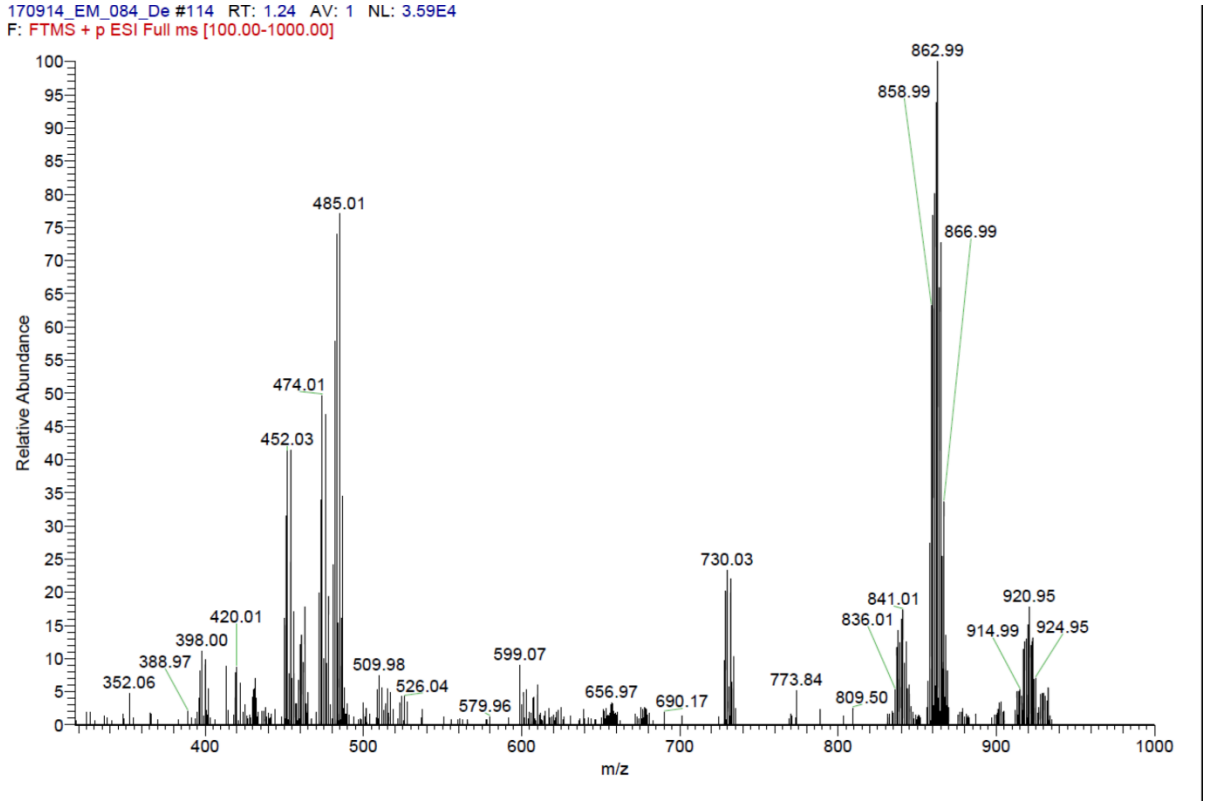

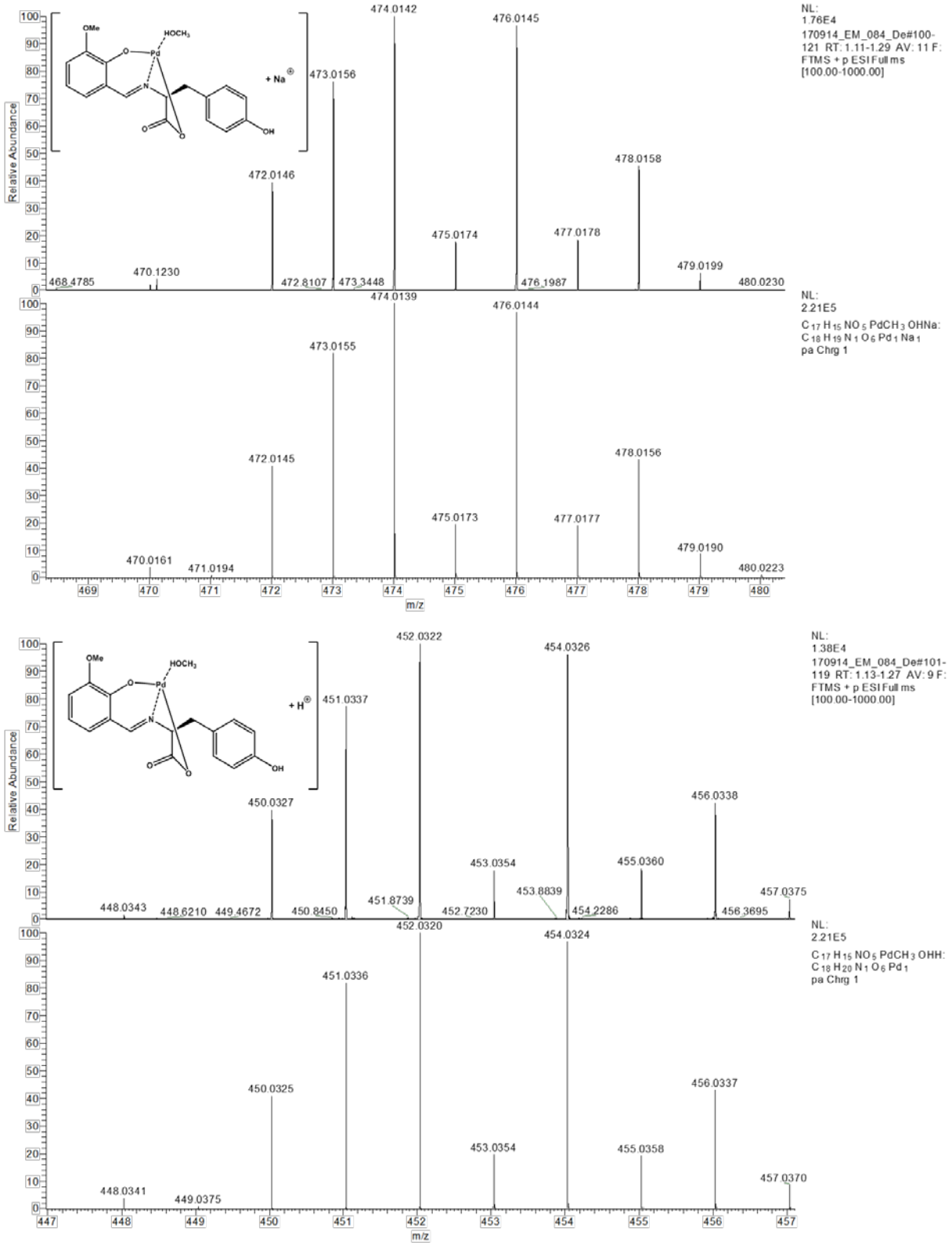

Figure S19: ESI(+)-MS of **4** recorded in methanol with simulation of the identified peaks and structural suggestions.

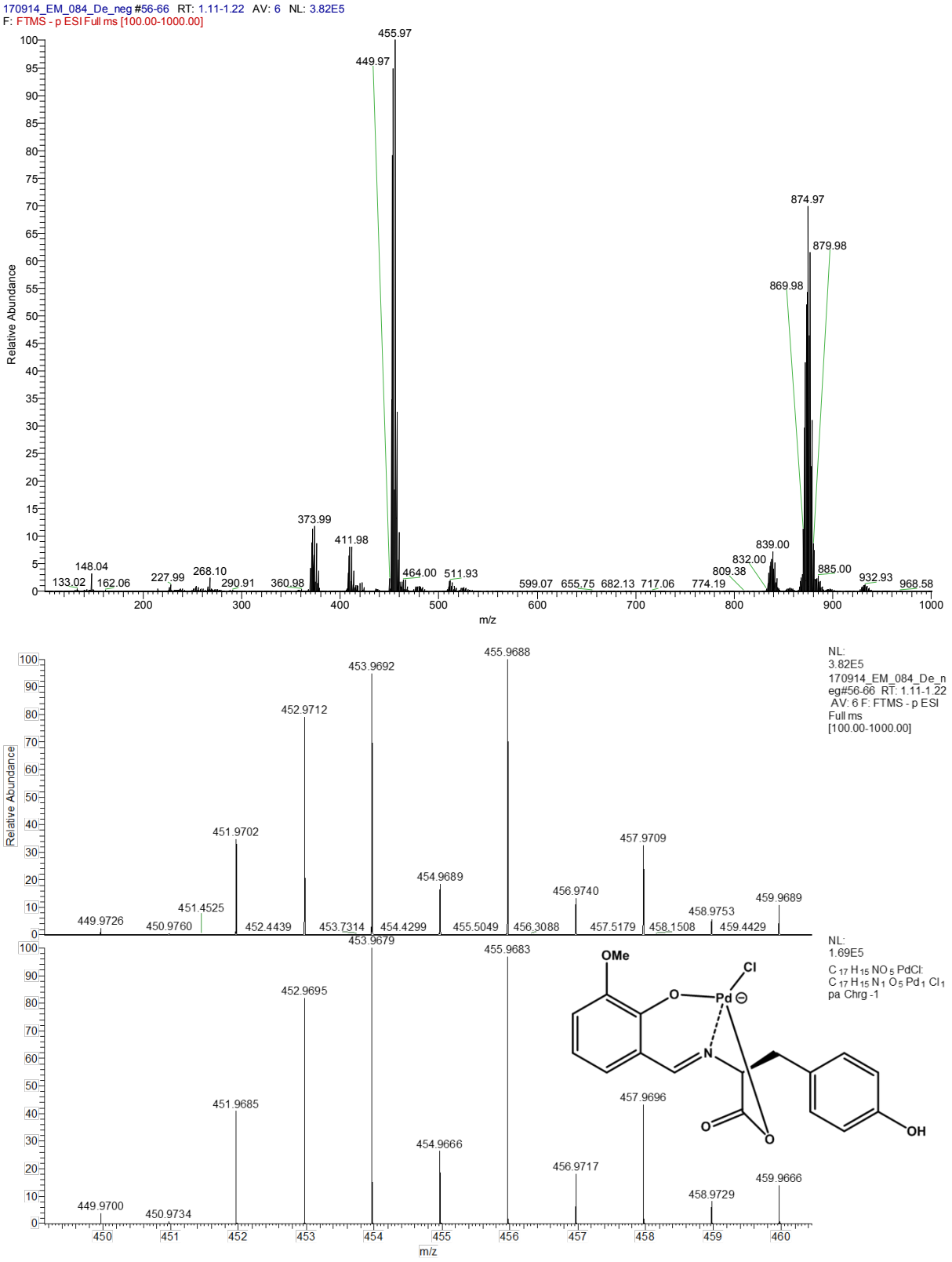

Figure S20: ESI(-)-MS of **4** recorded in methanol with simulation of the identified peaks and structural suggestions.

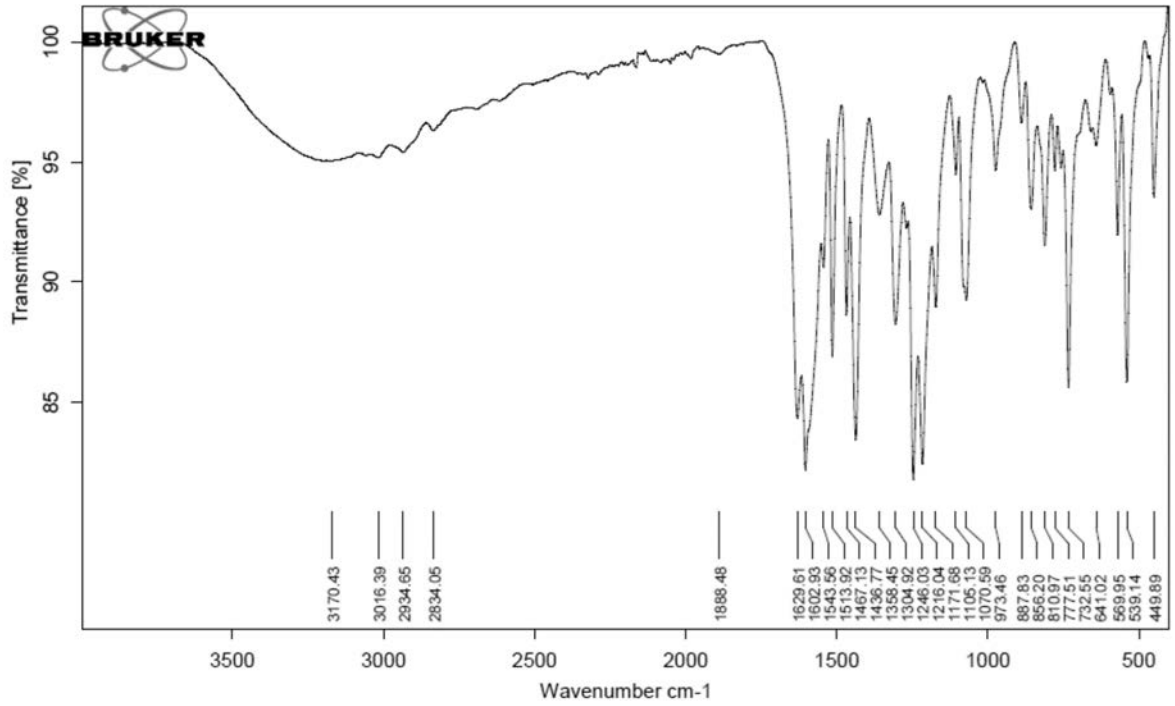

Figure S21: IR spectrum of **4** dried *in vacuo.*

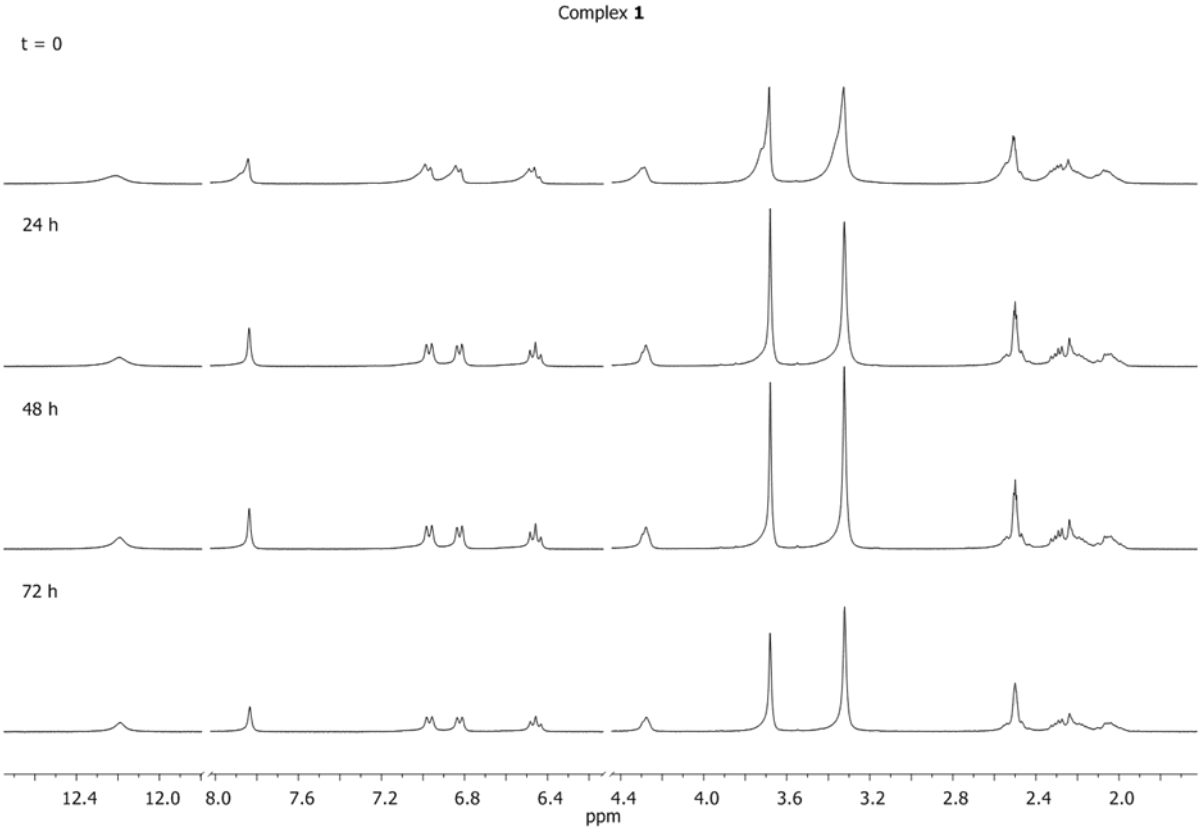

Figure S22: ^{1}H-NMR spectra of **1** recorded in DMSO-d_6 over 72 h in intervals of 24 h.

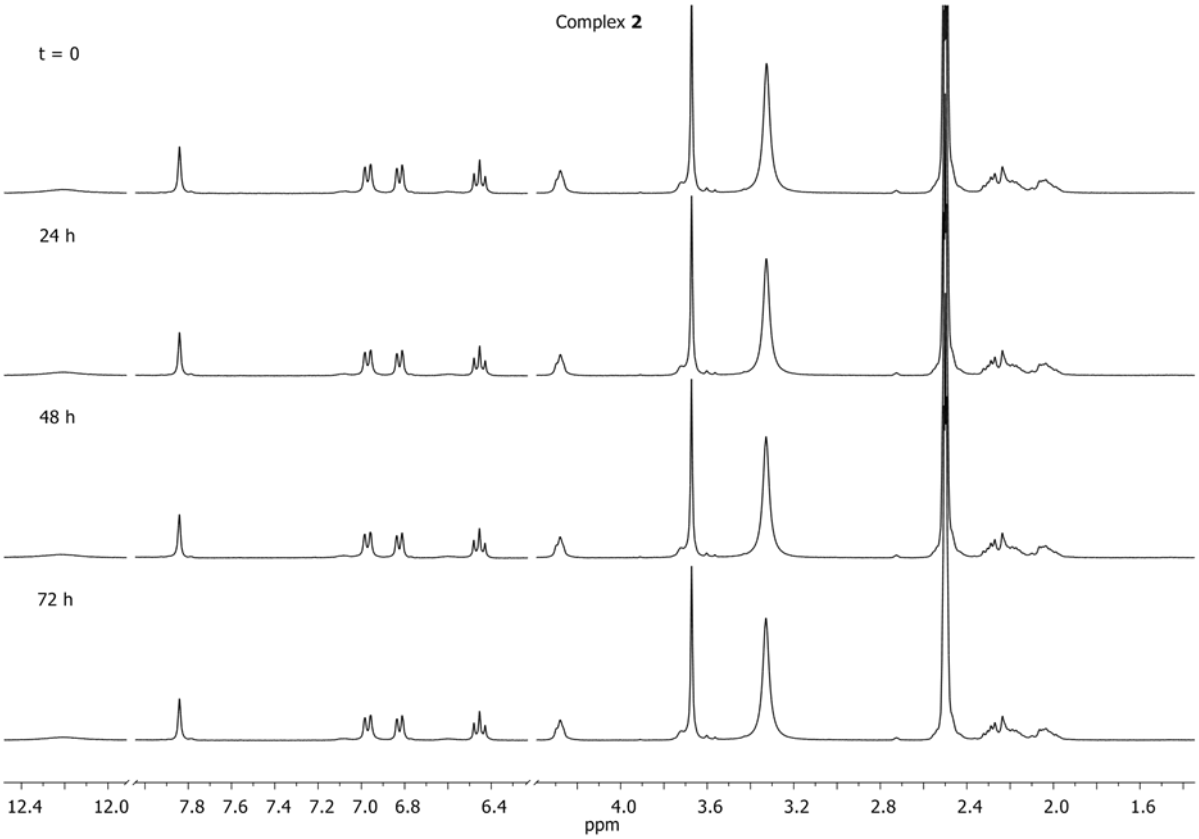

Figure S23: ^{1}H-NMR spectra of **2** recorded in DMSO-d_6 over 72 h in intervals of 24 h.

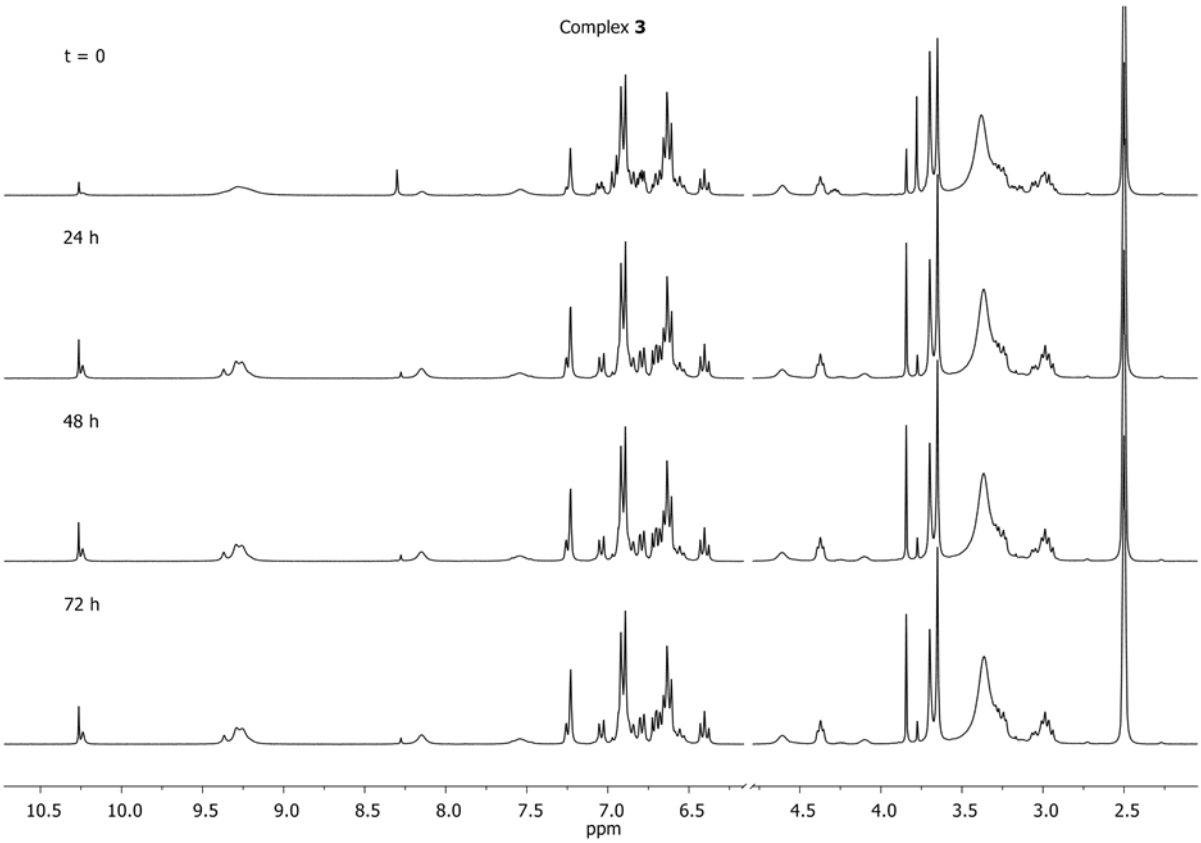

Figure S24: ^{1}H-NMR spectra of **3** recorded in DMSO-d_6 over 72 h in intervals of 24 h.

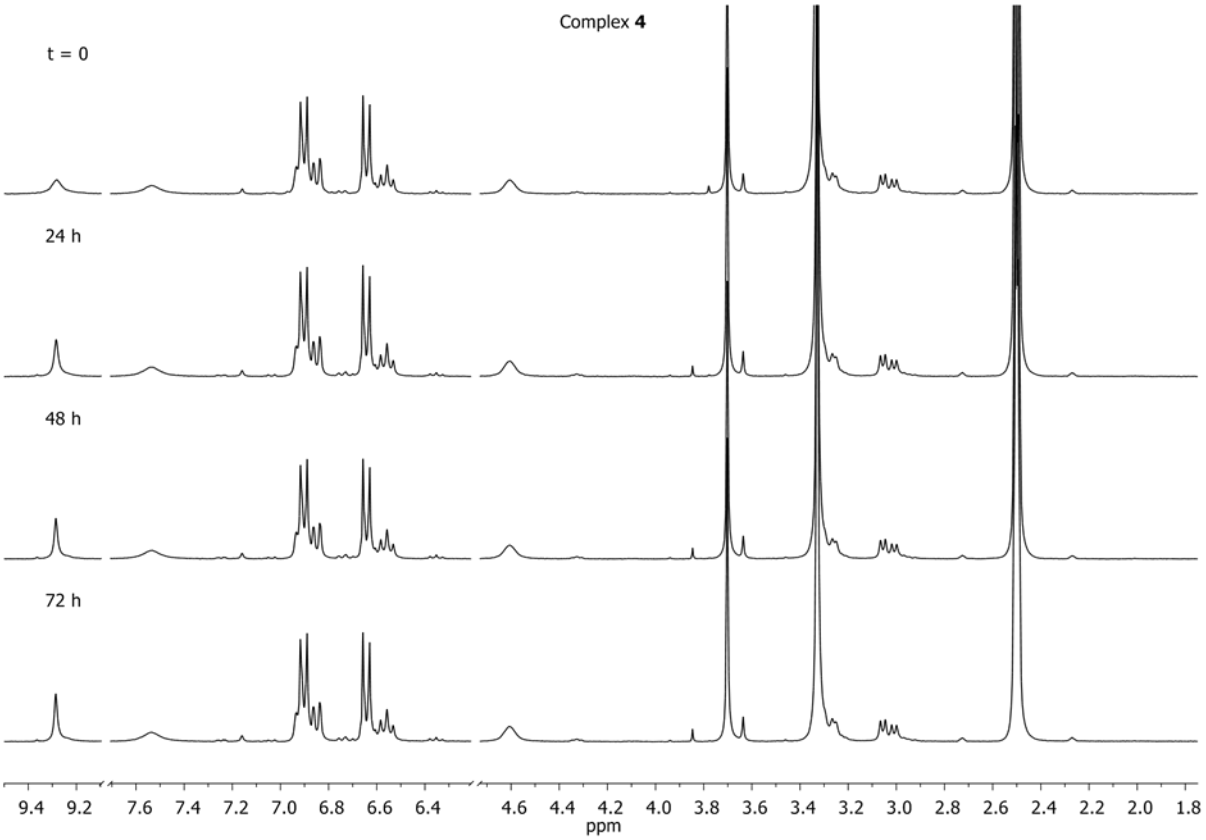

Figure S25: ^{1}H-NMR spectra of **4** recorded in DMSO-d_6 over 72 h in intervals of 24 h.

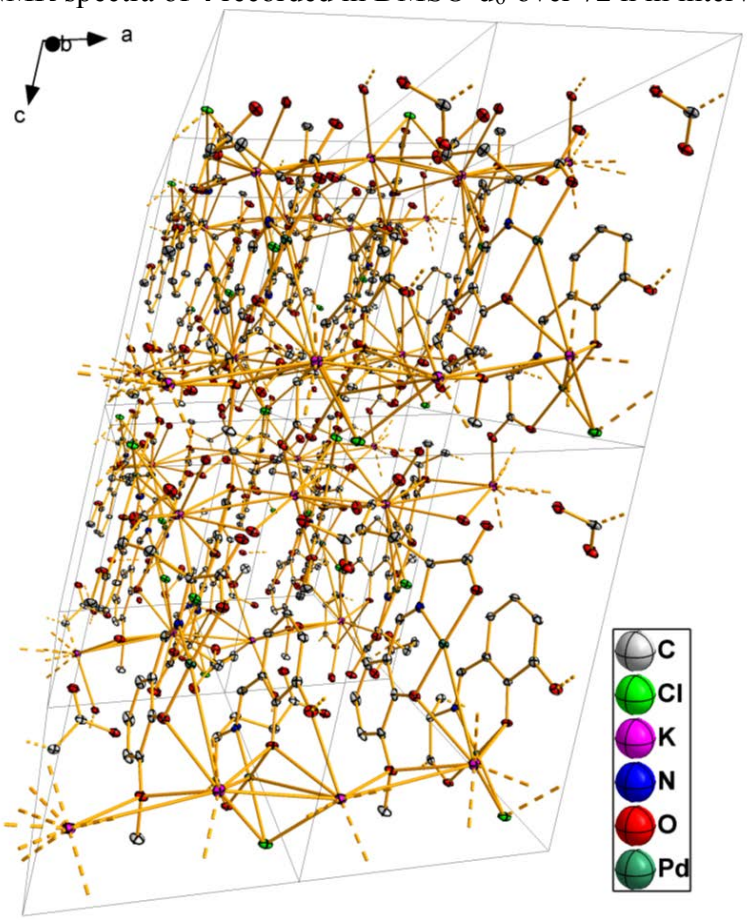

Figure S26: Packing diagram of **1**. View along the *b*-axis.

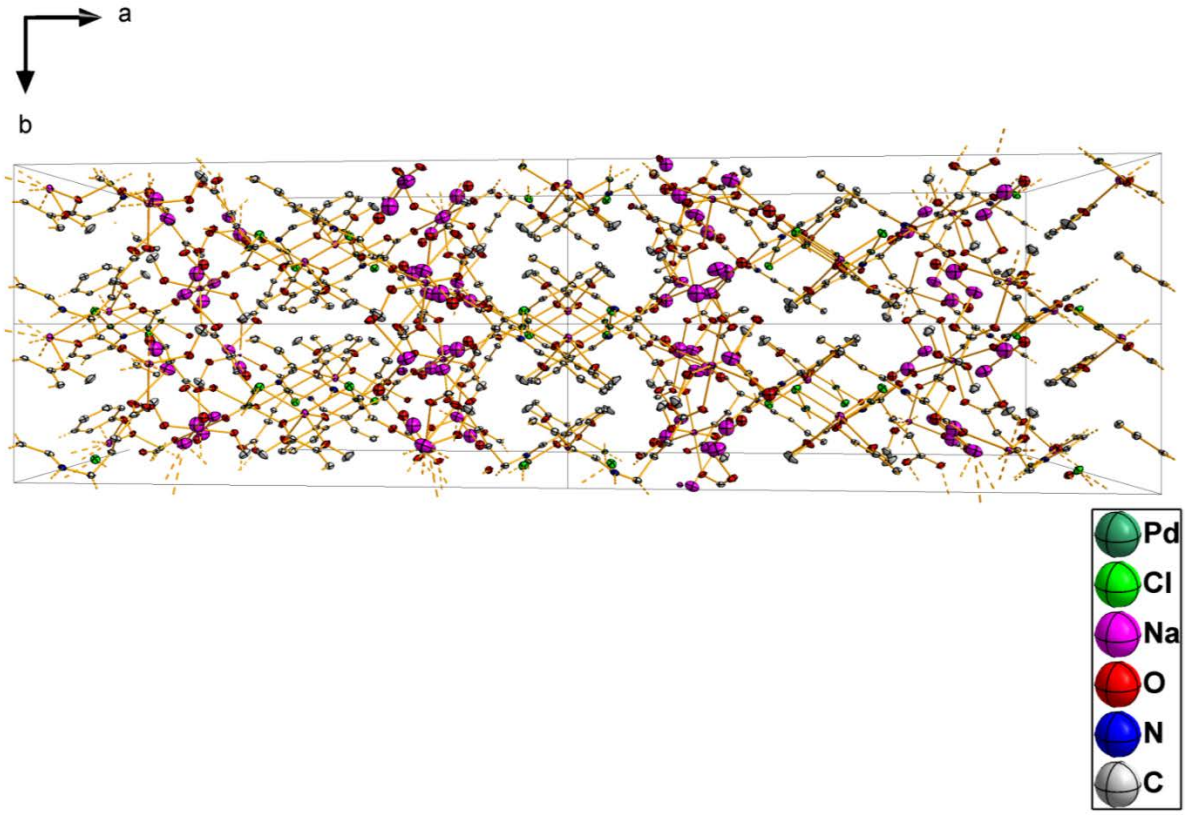

Figure S27: Packing diagram of **2**· View along the *c*-axis.

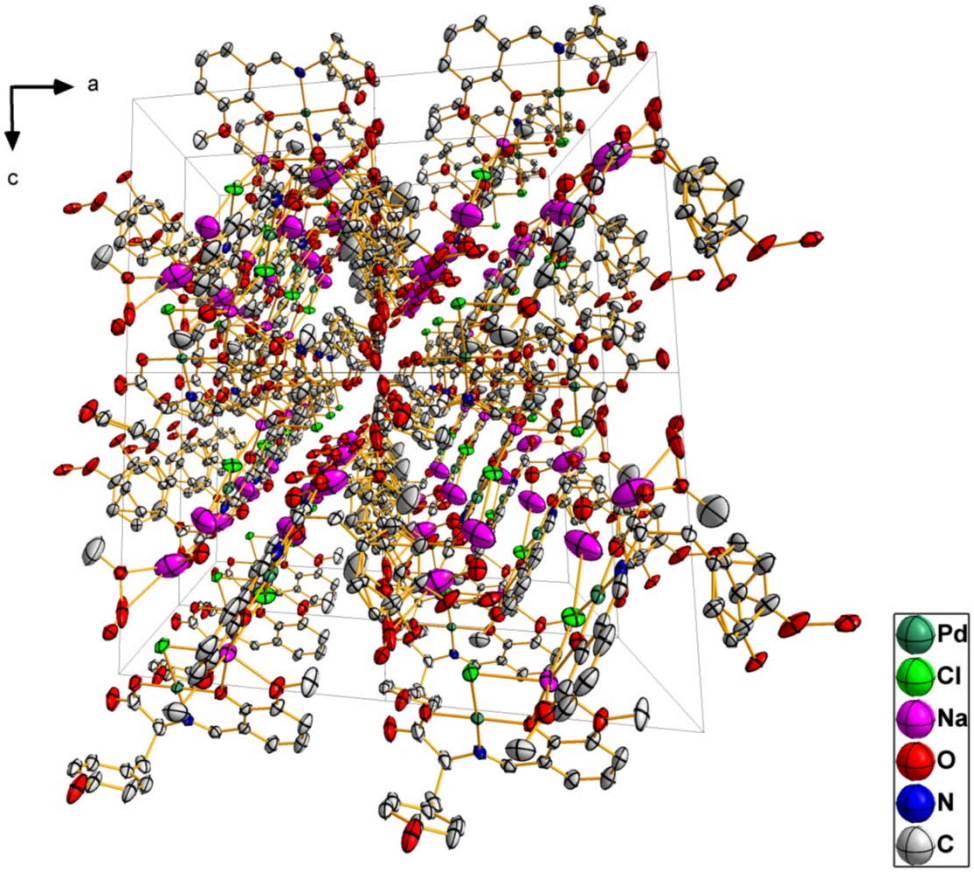

Figure S28: Packing diagram of **3**· View along the *b*-axis.

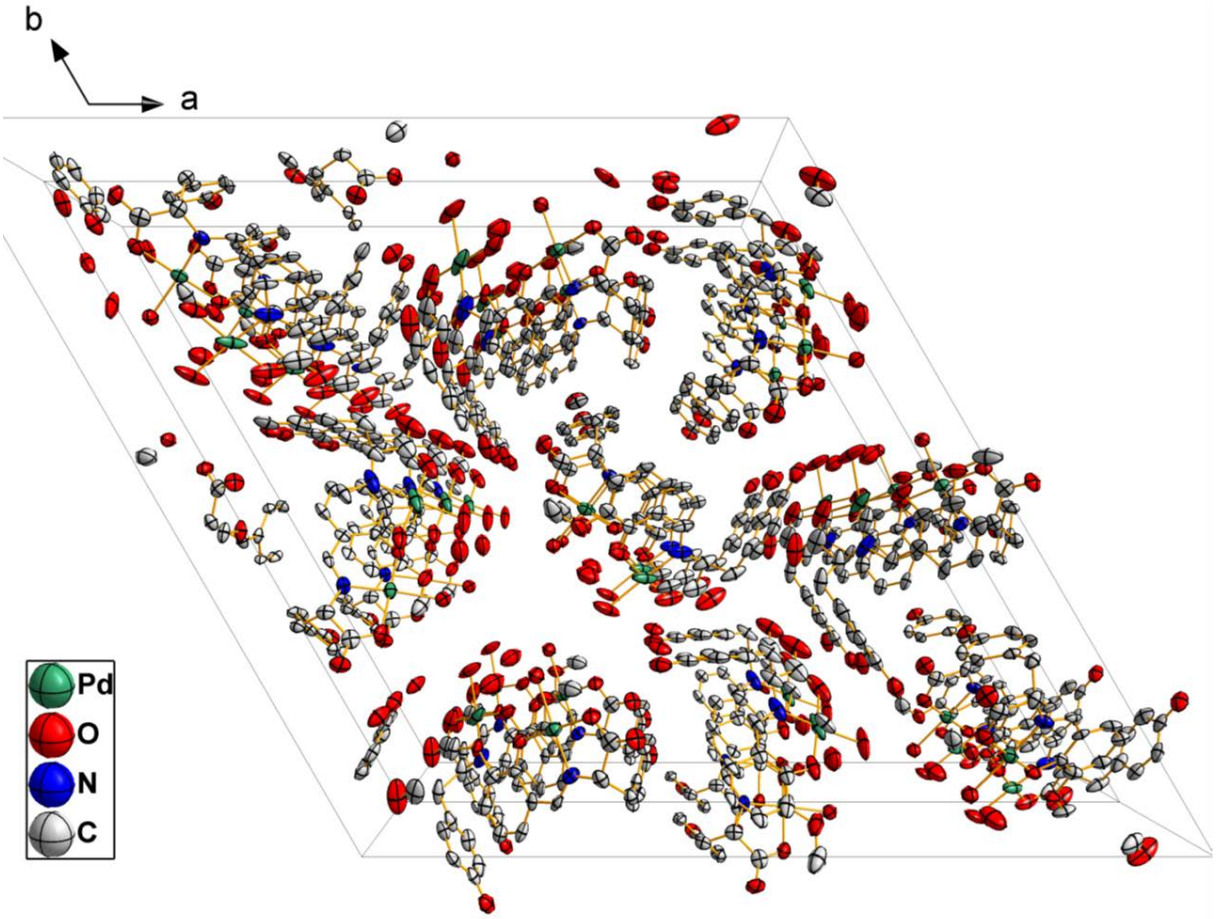

Figure S29: Packing diagram of **4**. View along the *c*-axis.

Tables

Tab. S1. The cell proliferation in % after 72h exposition on studied compounds with L929 cells.

Dose/Compound	**L2**	**1**	**3**	**4**
200 µM	77%	84%	73%	77%
100 µM	79%	90%	77%	79%
50 µM	73%	72%	78%	73%
25 µM	76%	75%	82%	76%

Tab. S2. The cell proliferation in % after 48h exposition on studied compounds with L929 cells.

Dose/Compound	**L2**	**1**	**3**	**4**
200 µM	72%	90%	73%	80%
100 µM	84%	87%	80%	85%
50 µM	83%	83%	84%	74%
25 µM	88%	87%	86%	85%

Tab. S3. The cell proliferation in % after 24h exposition on studied compounds with L929 cells.

Dose/Compound	**L2**	**1**	**3**	**4**
200 µM	84%	91%	86%	79%
100 µM	76%	88%	85%	87%
50 µM	90%	90%	77%	73%
25 µM	90%	86%	80%	91%

% means that cell are alive per 100 cells according to the control

5. Zusammenfassung

Ziel der vorliegenden Arbeit war die Synthese und vollständige Charakterisierung von Schiff'sche Base-Liganden mit *ortho*-Vanillin als Aldehydquelle und ausgewählten Aminosäuren als Aminquelle. Diese Liganden, entweder in Reinform oder *in situ* generiert, sollten anschließend mit verschiedenen Metallsalzen zu Metallkomplexen umgesetzt werden. Dabei sollten messbare Einkristalle der Komplexe erhalten werden, um eine sichere Strukturaufklärung zu ermöglichen. Die erhaltenen Liganden und Komplexe sollten, wenn angebracht, hinsichtlich ihres biologischen Potenzials untersucht werden.

Es konnten Liganden mit *L*-Glutaminsäure, *L*-Tyrosin und *L*-Glutamin als Natriumsalze in hohen Ausbeuten erhalten und vollständig charakterisiert werden. Untersuchungen zur Stabilität mittels ^{1}H-NMR-Spektroskopie zeigten, dass alle Liganden in wässriger Lösung teilweise in ihre Edukte zerfallen und sich ein Gleichgewicht einstellt. In Studien zum antimikrobiellen Potenzial der Liganden mit *L*-Glutaminsäure und *L*-Tyrosin konnte gezeigt werden, dass die Liganden antimikrobielle Aktivität gegenüber verschiedenen Mikroorganismen, insbesondere Hefepilzen der Gattung *Candida* besaßen. Allerdings war diese Aktivität auf *ortho*-Vanillin zurückzuführen, welches durch den Zerfall des Liganden in wässrigem Milieu freigesetzt wurde. Nennenswerte antiproliferative Eigenschaften gegenüber Zellen der Linien L929 und Hep G2 konnten in MTT-Tests nicht beobachtet werden.

Die Umsetzung des *L*-Glutaminsäure-haltigen Liganden mit Metallsalzen lieferte folgende Komplexe:

- Mit Nickel(II)-chlorid wurde ein pentadecanuklearer Ni(II)-Komplex in Form eines Rades erhalten, welcher ein seltenes Beispiel für ungeradzahlige radförmige Ni(II)-Komplexe darstellt. Dieser Komplex war stabil in Methanol bzw. einem Wasser/Methanol-Gemisch und nur schwach zytotoxisch gegenüber L929- und B16-Zellen. Die Untersuchung der magnetischen Eigenschaften zeigte ein dominantes antiferromagnetisches Verhalten, sowie intermolekulare Wechselwirkungen bei Temperaturen unterhalb von 24 K.
- Mit Kupfer(II)-sulfat und unter Zugabe von Salzsäure am Ende der Reaktion konnte ein tetratnuklearer Cu(II)-Komplexe mit stark verzerrter Heterokubanstruktur erhalten werden, welcher über den betrachteten Zeitraum von 48 h stabil blieb. Die Aminosäurereste waren nicht an der Koordination der Metallzentren beteiligt. Der Komplex zeigte milde bis moderate antibakterielle Aktivität, sowie gute antifungale Aktivität gegenüber Organsimen der Gattung *Candida*. Gegenüber L929- und Hep G2-Zellen konnte eine moderate Zytotoxizität beobachtet werden.

- Mit Eisen(III)-perchlorat wurden zwei mononukleare anionische Fe(III)-Komplexe, bei denen entweder Natrium oder Kalium das Gegenion darstellte, erhalten. Von dem Kalium-haltigen Komplex konnte keine eindeutige Kristallstruktur gewonnen werden. XRPD-Studien lassen aber eine Isostrukturalität vermuten. Das Eisenzentrum war verzerrt-oktaedrisch von zwei Ligandmolekülen umgeben. Mittels EPR wurde ein Spin von S = 5/2 nachgewiesen.
- Mit Palladium(II)-chlorid konnten zwei mononukleare Pd(II)-Komplexe erhalten werden, in denen das Palladiumzentrum quadratisch-planar von einem Ligandmolekül und einem Chloridion koordiniert wird und insgesamt einfach negativ geladen ist. Zur Kompensation der Ladung dienten entweder ein Natrium- oder ein Kaliumion. Abhängig vom Gegenion konnte eine unterschiedliche Packung in der Kristallstruktur beobachtet werden. Der hinsichtlich seines biologischen Potenzials untersuchte Kalium-haltige Komplex war stabil in DMSO über den untersuchten Zeitraum von 72 h und zeigte moderate bis gute antimikrobielle Aktivität. Gegenüber Zellen der Linie L929 war der Komplex inaktiv. Untersuchungen an weiteren humanen Krebszelllinien stehen noch aus.

Bei der Umsetzung des *L*-Glutamin-haltigen Liganden konnten nur mit Eisen(III)-perchlorat Komplexe erhalten werden. Dabei war der Zusatz von Natrium- bzw. Kaliumazid essentiell für das Wachstum von Kristallen. Die Komplexe waren von Struktur und Eigenschaften her analog zu den Komplexen mit dem *L*-Glutaminsäure-haltigen Ligand. Allerdings konnten hier die Kristallstrukturen der Komplexe mit beiden Gegenionen, Kalium und Natrium, erhalten werden Diese unterschieden sich durch die Packung im Festkörper.

Für den *L*-Tyrosin-haltigen Liganden konnten Komplexe mit Nickel und Palladium erhalten werden:

- Mit Nickel(II)-chlorid wurden zwei Metallkomplexe erhalten, welche isostrukturell sind und sich nur durch das koordinierte Lösungsmittel, Methanol oder DMF, unterschieden. Die Komplexe waren tetranuklear und zeigten als Strukturmotiv nicht den üblichen Ni-O-Heterokuban, sondern eine äußerst seltene schüsselartige Struktur. Dabei blieben die Tyrosin-Seitenketten ungebunden. Beide Solvate erwiesen sich sowohl in Lösung als auch im festen Zustand als stabil
- Mit Palladium(II)-chlorid konnten zwei mononukleare Pd(II)-Komplexe mit quadratisch-planarer Geometrie um das Palladiumzentrum erhalten werden. Die Koordinationssphäre wurde entweder durch ein Chloridion oder ein Wassermolekül vervollständigt. Im Falle

des chlorhaltigen Komplexes kompensierte ein Natriumion die negative Ladung. Der Komplex mit dem koordinierten Wassermolekül war insgesamt neutral. Während der neutrale Komplex in DMSO über 72 h stabil blieb, zeigte der anionische Komplex Zerfallsprodukte im ^{1}H-NMR-Spektrum. Beide Komplexe wiesen moderate bis gute antimikrobielle Aktivität auf. Gegenüber Zellen der Linie L929 waren beide Komplexe inaktiv. Untersuchungen an weiteren humanen Krebszelllinien stehen noch aus.

Die geplante Synthese einer Schiff'schen Base durch die Kondensationsreaktion von *ortho*-Vanillin und *L*-Cystein war, anders als in diversen Publikationen behauptet, nicht erfolgreich. Stattdessen wurde das entsprechende Thiazolidin als Racemat erhalten. Die Umsetzung mit verschiedenen Metallsalzen lieferte keine Metallkomplexe in kristalliner Form. Allerdings konnten durch Zugabe von Zinkchlorid messbare Kristalle des Thiazolidins erhalten werden. Obwohl das gesamte kristalline Präzipitat racemisch war, wurde in mehreren Messungen nur die Struktur des 2R,4R-Diastereomers bestimmt. Dieses lag im Kristall als Zwitterion vor.

Zusammenfassend konnten insgesamt drei Schiff'sche Basen als Natriumsalze synthetisiert und charakterisiert werden. Die Umsetzung der Liganden mit Metallsalzen führte zu einer Vielzahl von neuen Metallkomplexen, die eine hohe strukturelle Vielfalt und interessante Eigenschaften aufwiesen.

6. Summary

The presented work describes the synthesis and full characterization of Schiff base ligands derived from *ortho*-vanillin as an aldehyde source and selected amino acids as amine sources. The ligands, either in pure form or generated *in situ*, were used in reactions with various metal salts to afford metal complexes. Single crystals suitable for X-ray measurement were grown to allow a confident structure determination. When possible, the biological activity of the ligands as well as the metal were investigated.

Ligands derived from *L*-glutamic acid, *L*-tyrosine und *L*-glutamine were successfully synthesized as sodium salts in high yields and fully characterized. Investigations of stability by ^{1}H-NMR revealed partial reversion of the ligands to their respective starting materials in aqueous solution. Antimicrobial studies on the ligands derived from *L*-glutamic acid and *L*-tyrosine indicated activity against various microorganisms, in particular against fungi from the genus *Candida*. However, the activity was traced back to *ortho*-vanillin, which is released due to decomposition in aqueous solution. No significant antiproliferative activity against cells from the lines L929 and Hep G2 was observed in MTT-assays.

The reaction of the *L*-glutamic acid-containing ligand with various metal salts led to following complexes:

- With nickel(II) chloride, a pentadecanuclear wheel-shaped complex was obtained, which is a rare example of an odd-numbered wheel-shaped Ni(II) complexes. The complex was found to be stable in methanol and a water/methanol mixture, and showed only low cytotoxicity against L929 and B16 cells. The investigation of the magnetic properties revealed dominant antiferromagnetic behavior as well as intramolecular interactions below 24 K.
- The reaction with copper(II) sulfate and addition of hydrochloric acid at the end of the reaction led to the formation of a tetranuclear Cu(II) complex with a highly distorted heterocubane structure. The complex was found to be stable over the investigated period of 48 h. The amino acid side chains were not involved in complex formation. The complex showed mild to moderate activity against gram-positive bacteria and good antifungal activity against fungi of the genus *Candida*. Moderate cytotoxic activity was observed against L929 and Hep G2 cells.
- Two mononuclear anionic Fe(III) complexes with either sodium or potassium counter ions were produced from the reaction with iron(III) perchlorate. For the potassium-containing complex a reliable crystal structure was not obtained, but XRPD studies suggesting isostructurality. Two ligand molecules coordinate the iron center in a distorted octahedral manner. EPR studies revealed a spin of S = 5/2.

- Usage of palladium(II) chloride led to two square-planar Pd(II) complexes, where the Pd center is coordinated by one ligand molecule and one chloride ion. Either a sodium or a potassium ion compensated the negative charge of the complex molecule. Depending on the nature of the counter ion, a different packing within the crystals structure was observed. The potassium-containing complex, which was used for studies of the biologic potential, was found to be stable in DMSO over the investigated period of 72 h. The complex showed moderate to good antimicrobial activity, but was found to be inactive against L929 cells. Continuing studies with further human cancer cell lines are in progress.

Complexes with the *L*-glutamine-containing ligand were only obtained for the reaction with iron(III) perchlorate. These were analogous in structure and properties to the Fe(III) complexes described above. But in this case, crystal structures were obtained for both sodium and potassium salts. The complexes differed in their packing in the solid state.

With the *L*-tyrosine-containing ligand, complexes from nickel and palladium were obtained:

- The reaction with nickel(II) chloride led to two isostructural tetranuclear Ni(II) complexes, which differed in the coordinated solvent, methanol or DMF. The complexes did not showed the common Ni-O heterocubane structure, but rather a very rare bowl-shaped motif was observed. The *L*-tyrosine side chains remained pendant. Both solvates were found to be stable in the liquid and solid state.
- Usage of palladium(II) chloride led to two square-planar Pd(II) complexes. The Pd centers were coordinated by one ligand molecule and either one chloride ion, leading to an anionic complex, or a water molecule, leading to a neutral complex. A sodium ion compensated the negative charge. While the neutral complex was found to be stable in DMSO over the investigated period of 72 h, the ^{1}H-NMR spectrum of the anionic complex in d_6-DMSO indicated immediate decomposition. Both complexes showed moderate to good antimicrobial activity, but were found to be inactive against L929 cells. Continuing studies with further human cancer cell lines are in progress.

The synthesis of a Schiff base from *ortho*-vanillin and *L*-cysteine through a condensation reaction was not successful, despite various published claims to the contrary. Instead, the corresponding racemic thiazolidine was produced. The reaction with various metal salts did not lead to crystalline metal complexes, but addition of zinc chloride facilitated the growth of suitable crystals for X-ray measurement of the thiazolidine. Although the bulk material was

racemic, in multiple measurements only the crystal structure of the 2R,4R-diastereomer was determined, which exists in a zwitterionic form within the crystal.

In conclusion, three Schiff base ligands as sodium salts could be synthesized and fully characterized. The reaction of the ligands with metal salts led to a wide variety of novel metal complexes, possessing a high structural diversity and interesting properties.

7. Anhang

7.1 Vollständige Publikationsliste

8. "Novel Pd(II) Schiff Base complexes derived from *ortho*-vanillin and *L*-tyrosine or *L*-glutamic acid: Synthesis, characterization, crystal structures and biological properties."
Muche, S.; Biernasiuk, A.; Malm, A.; Popiołek, Ł.; Hordyjewska, A.; Olszewska, A.; Hołyńska, M. *Manuskript in Vorbereitung*

7**.** "A gap is filled: First structures of enantiopure iron(III) complexes with Schiff base ligands derived from *ortho*-vanillin and *L*-glutamine or *L*-glutamic acid."
Muche, S.; Harms, K.; Burghaus, O.; Hołyńska, M. *Polyhedron*; Manuskript akzeptiert

6**.** "Synthesis, characterization and crystal structure of (2RS,4R)-2-(2-hydroxy-3-methoxyphenyl)thiazolidine-4-carboxylic acid."
Muche, S.; Müller, M.; Hołyńska, M. *Journal of Molecular Structure*; Manuskript akzeptiert

5. "New insights into the coordination chemistry of Schiff bases derived from amino acids: Planar [Ni_4] complexes with tyrosine side-chains."
Muche, S.; Hołyńska, M. *Journal of Molecular Structure* **2017**, *1142*, 168–174.

4. "Synthesis, structure and stability of a chiral imine-based Schiff-base ligand derived from L-glutamic acid and its [Cu_4] complex."
Muche, S.; Levacheva, I.; Samsonova, O.; Biernasiuk, A., Malm, A. Lonsdale, R.; Popiołek, L., Bakowsky, U.; Hołyńska, M. *Journal of Molecular Structure* **2017**, *1127*, 231-236.

3. "A chiral, low-cytotoxic Ni_{15}-wheel complex."
Muche, S.; Levacheva, I.; Samsonova, O.; Pham, L.; Christou, G.; Bakowsky, U.; Hołyńska, M. *Inorganic chemistry* **2014**, *53* (14), 7642–7649.

2. "Unprecedented non-cytotoxic [$Co^{III}_4Ln^{III}$]-core complexes with a tripodal oxime ligand – synthesis, structure, properties and potential applications."
Premužić, D., Muche, S., Hołyńska, M., *New J. Chem*. **2014**, *38*, 2894-2901

1. "Tetranuclear Homo- and Heterometallic Manganese(III) and Nickel(II) Complexes: Synthesis, Structure, and Magnetic Studies."
Nayak, S.; Novitchi, G.; Muche, S.; Luneau, D.; Dehnen, S. *Z. anorg. allg. Chem.* **2012,** *638* (7-8), 1127–113

7.2 Liste der Präsentationen

Polynuclear metal complexes and their possible biological applications.

Muche, S., Hołyńska, M.

Posterbeitrag zum “12th International Symposium on Applied Bioinorganic Chemistry”

3-6.12.2013, Guangzhou, VR China.

7.3 Abkürzungsverzeichnis

A. flavus	*Aspergillus flavus*
A. niger	*Aspergillus niger*
AFM	Atomic Force Microscope
B. simplex	*Bacillus simplex*
B. subtilis	*Bacillus subtilis*
BSA	Bovine serum albumin (Rinderalbumin)
C. albicans	*Candida albicans*
C. krusei	*Candida krusei*
C. neoformans	*Cryptococcus neoformans*
DLS	Dynamic Light Scattering
DMF	Dimethylformamid
DMSO	Dimethylsulfoxid
DNA	Deoxyribonucleic acid (Desoxyribonukleinsäure)
E. acetylicum	*Exiguobacterium acetylicum*
E. coli	*Escherichia coli*
EC_{50}	mittlere effektive Konzentration
EDX	Energiedispersive Röntgenmikroanalyse
EPR	electron paramagnetic resonance
ESI	Elektrospray-Ionisation
EtOH	Ethanol
F. oxysporum	*Fusarium oxysporum*
FAB-MS	Fast Atom Bombardement-Massenspektrometrie
IC_{50}	Mittlere inhibitorische Konzentration
IR	Infrarot
K. pneumoniae	*Klebsiella pneumoniae*
L	Ligand
LM	Lösungsmittel
M	molar
µM	mikromolar, µmol/L
M. tuberculosis	*Myobacterium tuberculosis*
MeCN	Acetonitril
MeOH	Methanol
MIC	Minimale inhibitorische Konzentration
MS	Massenspektrometrie

NMR	Nuclear magnetic resonance, Kernresonanz
oVan	*ortho*-Vanillin
P. aeruginosa	*Pseudomonas aeruginosa*
P. aeruginosa	*Pseudomonas aeruginosa*
P. putida	*Pseudomonas putida*
P. vulgaris	*Proteus vulgaris*
S. aureues	*Staphylococcus aureus*
S. haemolytius	*Streptococcus haemolytius*
S. typhi	*Salmonella typhi*
SMM	Single molecule magnet, Einzelmolekülmagnet
TG-DTG	Thermogravimetrie-Differenzierte Thermogravimetrie
TGA	Thermogravimetrische Analyse
UV/Vis	Ultraviolettes und sichtbares Licht
XRPD	Röntgenpulverdiffraktometrie

7.4 Sonstige im Rahmen dieser Arbeit erhaltene Ergebnisse

In diesem Abschnitt sollen kurz weitere Ergebnisse vorgestellt werden, die im Rahmen der vorliegenden Arbeit erhalten wurden, aber aus unterschiedlichen Gründen nicht zur Publikationsreife gelangt sind.

7.4.1 Metall-verbrückte Ni_{15}-Räder

Ein Projekt von nicht geringem Umfang war die Arbeit an Metall-verbrückten Ni_{15}-Rädern. Die jeweils erhaltenen kristallographischen Datensätze der nachfolgend beschriebenen Verbindungen waren allesamt von zu schlechter Qualität, weshalb eine Veröffentlichung nicht in Betracht gezogen werden konnte. Des Weiteren sind die Methoden für die weitere Charakterisierung der Komplexe aufgrund deren Natur stark eingeschränkt, wodurch die mangelnde Qualität der Datensätze nicht kompensiert werden konnte. Zur Verfügung standen lediglich IR, Elementaranalyse und EDX.

Die Substitution von Nickelchlorid in der Synthese des Ni_{15}-Rades durch Nickelperchlorat eröffnete die Synthese neuer Verbindungen, bei denen der fünfzehnkernige Nickelkomplex nach wie vor das zentrale Strukturmotiv darstellt. Die reine Substitution der Metallsalze bei ansonsten gleichbleibender Einwaage und Reaktionsführung führte zu Kristallen, deren Struktur zwei Ni_{15}-Räder sowie ein weiteres Ni(II)-Ion zeigt. Dieses Nickelion wird koordiniert von einem carbonylischem Sauerstoffatom sowie fünf Wassermolekülen. Durch eine Reihe von

Wasserstoffbrückenbindungen zu Wassermolekülen, die sich zwischen den Ringen befinden, sind beide Ringe miteinander verbunden. Zum Ladungsausgleichen werden zwei Gegenionen benötigt, wovon bisher nur eines, ein Perchloration, gefunden werden konnte.

Wird die Base Natriumacetat gegen MOAc mit M = K, Cs, Rb ausgetauscht, werden Kristalle erhalten, deren Struktur Alkalimetall-verbrückte Ni_{15}-Räder zeigen. Im Falle von Kalium werden die Ringe durch ein Ion verbrückt, während in den Verbindungen, die Cäsium und Rubidium enthalten, die Ringe von zwei Ionen verbrückt werden. Die Verbrückung erfolgt dabei durch die Koordination von carbonylischen Sauerstoffatomen an die Alkalimetallionen. Wassermoleküle sättigen die Koordinationssphäre ab. Der Ladungsausgleich erfolgt durch Perchlorationen. In der Packung werden dadurch entlang der kristallographischen *b*-Achse Ketten von verbrückten Ringen gebildet, in denen die Ringe versetzt zueinander stehen, wie exemplarisch für die Kaliumverbindung in Abbildung 31 gezeigt ist Die Synthesen müssen mit einem Viertel der Stoffmenge, welche für das publizierte Ni_{15}-Rad verwendet wurde, durchgeführt werden, da sonst hauptsächlich ein grünlicher Niederschlag entsteht. Als Nebenprodukt fällt das jeweilige schwerlösliche Alkalimetallperchlorat an. Im Falle von Kalium stellt dies bei der genutzten Konzentration jedoch kein Problem dar, da das Löslichkeitsprodukt hoch genug ist und Kaliumperchlorat noch nicht ausfällt. Die Löslichkeitsprodukte von Cäsium- und Rubidiumperchlorat sind jedoch derart gering, dass diese als kristalline Nebenprodukte ausfallen und dadurch die Synthese von sauberen Produkten unmöglich wird. Aus diesem Grund wurde der Versuch unternommen, das Nickelperchlorat durch andere Salze mit großen Anionen zu substituieren. Die Wahl fiel dabei auf Nickelsulfat, -acetat und -acetylacetonat. Außerdem wurden die Synthesen jeweils in Wasser/Methanol oder Wasser/Ethanol-Gemischen durchgeführt, da das Lösungsmittel ebenfalls Einfluss auf die Kristallqualität hat. Im Falle von Nickelsulfat wurden türkisfarbene Kristalle erhalten, welche als $M_2[Ni(H_2O)_6](SO_4)_2$ mit M = Rb, Cs identifiziert werden konnten. Die Ansätze mit Nickelacetat bzw. –acetylacetonat lieferten Kristalle in der gewohnt grünen Farbe. Ein Nebenprodukt wurde nicht beobachtet. Die Strukturen zeigten jeweils die bekannten verbrückten Ni_{15}-Räder. Die Verfeinerung der Anionen erwies sich jedoch auf Grund der schlechten Kristallqualität als unmöglich. Erste Versuche lassen auch darauf schließen, dass eine Verbrückung mit Cobalt- und Manganion möglich ist.

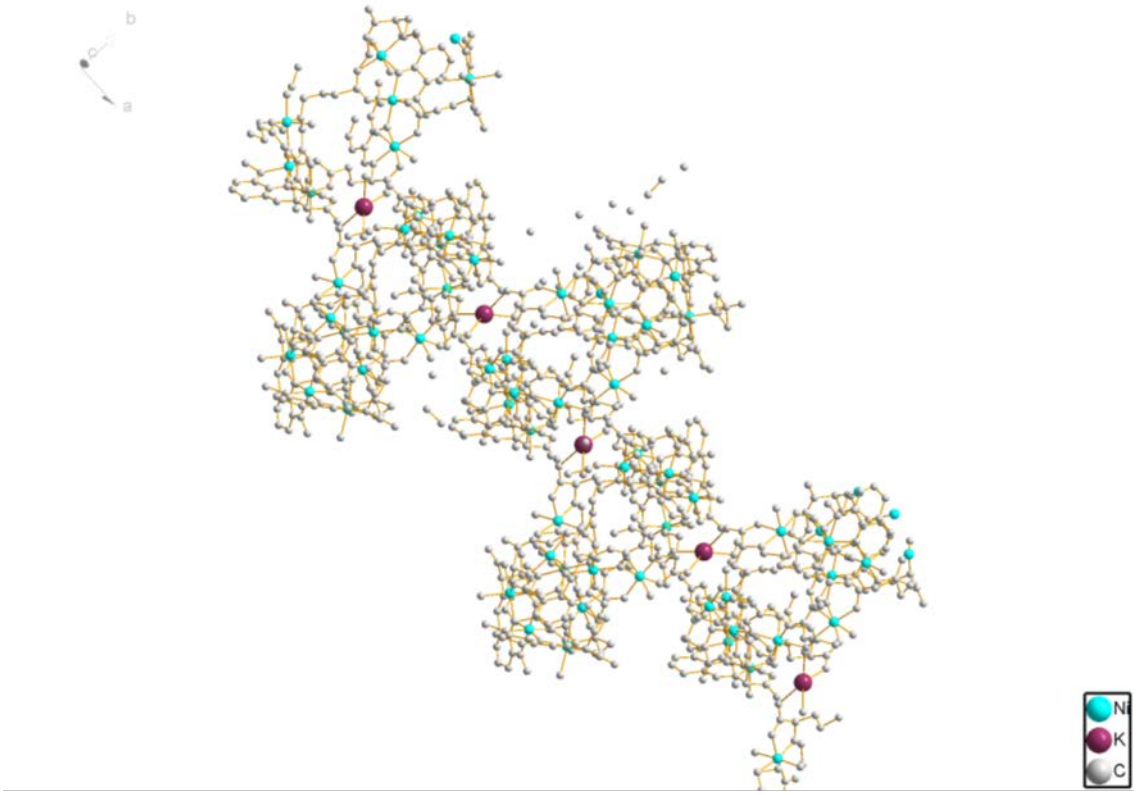

Abbildung 31: Kette aus Kalium-verbrückten Ni_{15}-Rädern entlang der *b*-Achse (Struktur nicht fertig gelöst).

7.4.2 Titan(IV)-Komplex mit einem Liganden aus *ortho*-Vanillin und *L*-Glutamin

Aus der Reaktion im Mikromaßstab nach dem Schema in Abbildung 32 konnten messbare rote, nadelförmige Kristalle erhalten und die Kristallstruktur bestimmt werden.

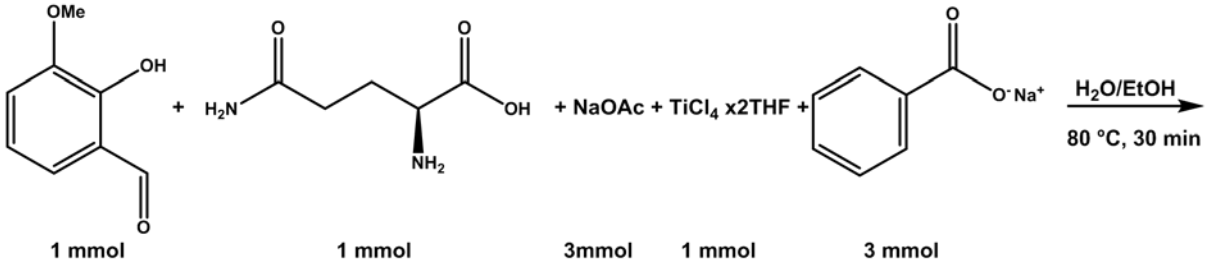

Abbildung 32: Reaktionsschema zur Synthese des Ti(IV)-Komplexes im Mikromaßstab.

Dabei handelte es sich um einen dinuklearen Ti(IV)-Komplex (Abb. 33), welcher im monoklinen Kristallsystem in der Raumgruppe *C* 1 2 1 kristallisiert. Jedes Titanzentrum wird koordiniert von einem Molekül *ortho*-Vanillin (oVan) über dessen deprotonierte Phenolgruppe und das Sauerstoffatom der Aldehydgruppe und einem Ligandmolekül, einer Schiff'schen Base bestehend aus *ortho*-Vanillin und *L*-Glutamin (L). Der Ligand koordiniert über das freie Elektronenpaar der Iminfunktion, der deprotonierten Phenolgruppe sowie der

Carboxylatgruppe an das Metallzentrum. Die erhaltenen C-O- und Ti-O-Bindungslängen der Carboxylatgruppe (C=O: 1.217 Å, 1.227 Å; C-O: 1.308 Å, 1.303 Å; Ti-O: 1.950 Å, 1.978 Å) stehen im Einklang mit Werten, welche für bereits publizierte Titan-Komplexe mit diesem Koordinationsmuster erhalten wurden. Daraus kann geschlussfolgert werden, dass die Säurefunktion deprotoniert vorliegt und die Koordination an das Titanzentrum über das deprotonierte Sauerstoffatom erfolgt. Die beiden Titanzentren sind durch ein weiteres Sauerstoffatom miteinander verbunden. Dadurch ergibt sich eine verzerrt oktaedrische Koordinationsgeometrie um die Titanzentren. Der Komplex kann auch als Sauerstoff-verbrücktes Dimer von monomeren $[Ti^{IV}(L)(oVan)]^{+}$-Einheiten betrachtet werden, welcher insgesamt von der Ladung her neutral ist. Weiterhin co-kristallisieren zwei Moleküle Benzoesäure, sowie Lösungsmittel. Der Zusatz von Natriumbenzoat ist essentiell, da sonst kein Kristallwachstum beobachtet werden kann. Leider war es nicht möglich, den Komplex sauber herzustellen. Sowohl im Mikromaßstab, als auch bei der Skalierung zu einem Arbeitsvolumen von 25 mL fiel während der Synthese und der anschließenden Kristallisation durch langsame Evaporation des Lösungsmittels eine größere Menge eines hell-orangenen Pulvers an. Dieses musste fortwährend durch Filtration entfernt werden. Dennoch war das erhaltene kristalline Material nicht völlig rein, wie aufgenommene ^{1}H-NMR-Spektren zeigten. Außerdem rekristallisiert nach einiger Zeit auch das Natriumbenzoat. Das erhaltene Pulver löst sich ausschließlich in DMSO, während der Komplex auch löslich in Wasser und Methanol ist. Das ^{1}H-NMR-Spektum des Pulvers zeigt lediglich Signale von Natriumbenzoat bzw. Benzoesöure und *ortho*-Vanillin. Das typische Signal des Protons an der Imingruppe ist abwesend.

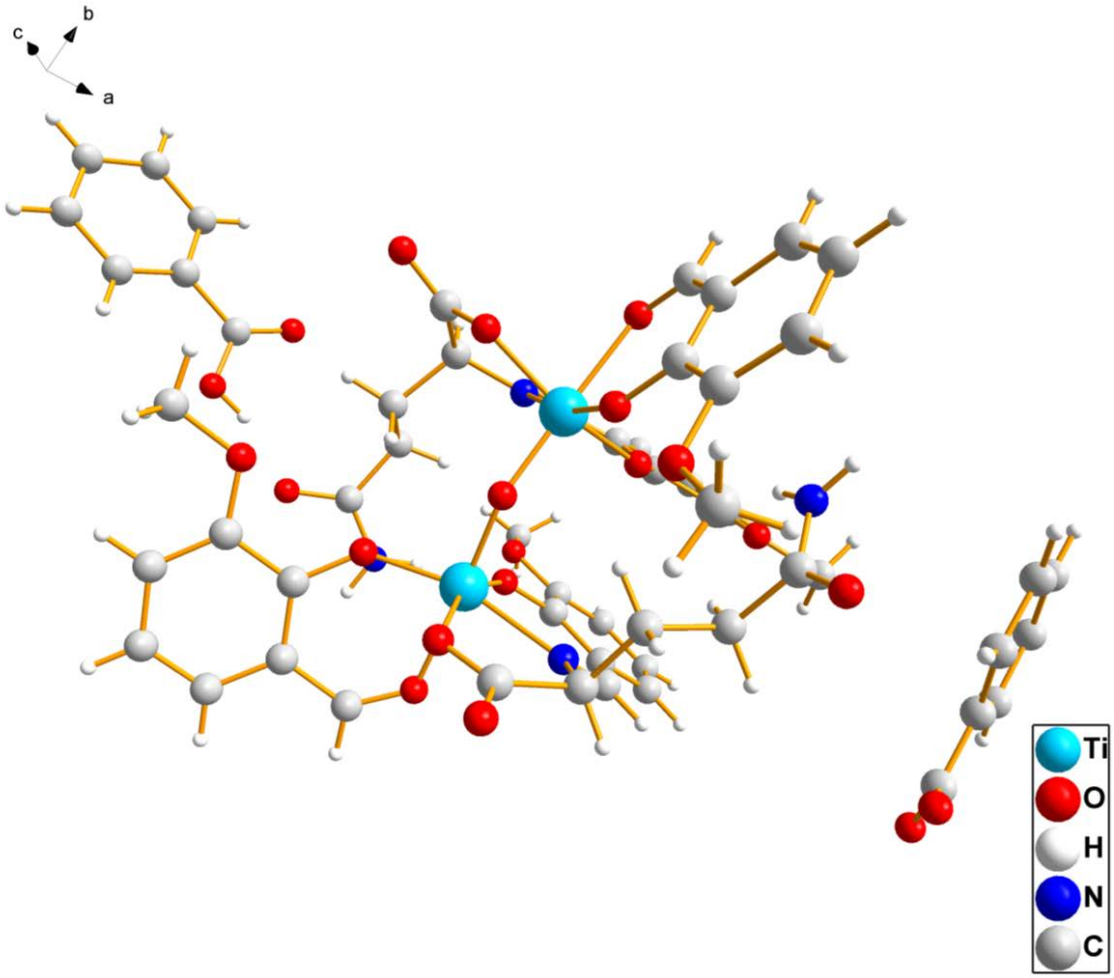

Abbildung 33: Kristallstruktur des dinuklearen Ti(IV)-Komplexes mit einem Liganden aus *ortho*-Vanillin und *L*-Glutamin. Zur besseren Übersicht wurden die Lösungsmittelmoleküle weggelassen.

Sämtliche Bemühungen, die Synthese dahingehend zu optimieren ein sauberes Produkt in hoher Ausbeute zu erhalten, waren erfolglos. Dabei wurden verschiedene Konzentrationen der Edukte, verschiedene Lösungsmittel und Lösungsmittelzusammensetzungen, unterschiedliche Basen, unterschiedliche Reaktionszeiten sowie eine Variation der Reihenfolge bei Zugabe der Edukte getestet. Ebenfalls kann der Niederschlag nicht verhindert werden, wenn die Zusammensetzung des Reaktionsansatzes dem Verhältnis der Reaktanden gemäß der Kristallstruktur entspricht. Aus genannten Gründe wurde die Arbeit an diesem Komplex eingestellt.

7.4.3 Mononuklearer Fe(III)-*ortho*-Vanillin-Komplex [Fe(oVan)$_2$(H$_2$O)(Cl)]

Im Rahmen eines Vertiefungsprojektes wurden Ansätze im Mikromaßstab mit *L*-Lysin•HCl als Aminquelle durchgeführt. Dabei wurden bei Zugabe von Eisen(III)-chlorid aus einem

Wasser/Methanol-Gemisch orangene Kristalle erhalten, von denen die Struktur bestimmt werden konnte. Es handelte sich dabei um einen mononuklearen Fe(III)-Komplex, welcher im monoklinen Kristallsystem in der Raumgruppe $P2_1/c$ kristallisiert. Das Metallzentrum wird von zwei Molekülen *ortho*-Vanillin über die deprotonierten Phenolgruppen und die Sauerstoffatome der Aldehydgruppen koordiniert wird. In den axialen Positionen befinden ein Chloridion und ein Wassermolekül. Die oktaedrische Koordinationsgeometrie ist leicht verzerrt (Abb.34). Obwohl der Komplex noch nicht literaturbekannt war, wurde die Arbeit daran eingestellt. Zum einen ist der erhaltene Komplex lediglich ein Produkt aus einer Reaktion, die eigentlich die Synthese von Eisenkomplexen mit einer Schiff'schen Base aus *ortho*-Vanillin und *L*-Lysin als Ligand zum Ziel hatte. Zum anderen sind zwei isostrukturelle Komplexe bereits bekannt: Ein entsprechender Fe(II)-Komplex mit *ortho*-Vanillin und zwei Wassermolekülen in axialer Position und Perchlorat als Gegenion[44] und ein Fe(III)-Komplex mit Ethylvanillin als Ligand und einem Wassermolekül sowie einem Chloridion in axialer Position[111]

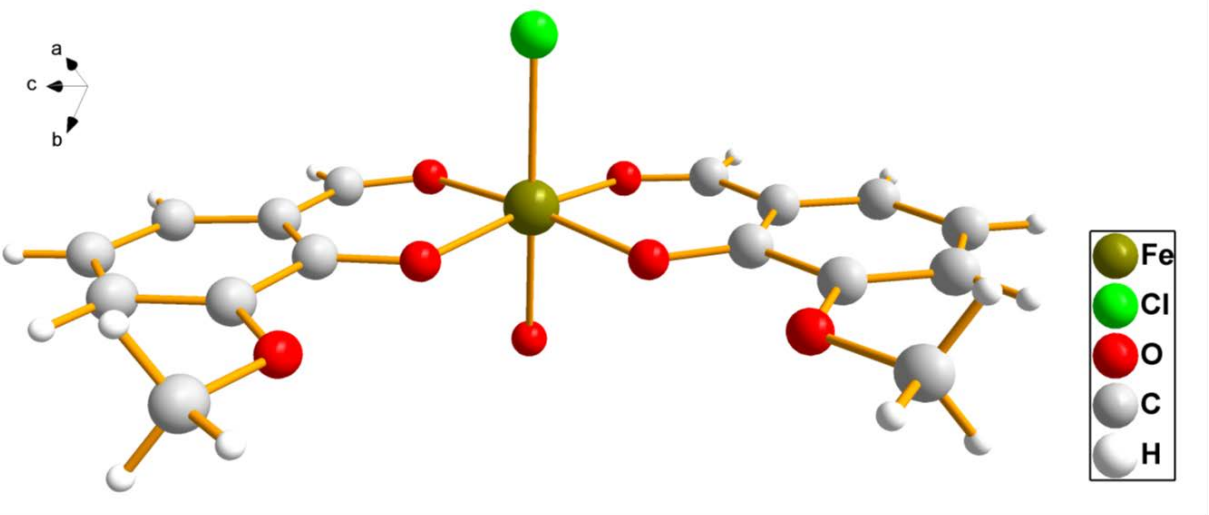

Abbildung 34: Kristallstruktur des Komplexes $[Fe(oVan)_2(H_2O)(Cl)]$.

7.5 Abbildungsverzeichnis

7.6 Zusammensetzung der Lösungen für die 96-*well*-Mikrotestplatten

Die folgende Tabelle gibt die Zusammensetzungen der Lösungen für die Reaktionen im Mikromaßstab in 96-*well*-Mikrotestplatten wider. Angegeben sind neben den Zusammensetzung für die Stock-Lösungen (12 mL) ebenfalls die Konzentration pro *well*. Die Lösungen wurden in 15 mL-Falcontubes angesetzt und bei 4 °C im Kühlschrank aufbewahrt. Bei der Vorbereitung der Platten ist darauf zu achten, möglichst schnell zu pipettieren bzw. vorgekühlte Platten zu verwenden, um ein Abbdampfen der flüchtigen Lösungsmittel zu verhindern.

Bedingung

Gemisch MeOH/EtOH mit anderem LM (LM = H_2O, DMF, MeCN)

Anteil MeOH/EtOH [%]	100	90	80	75	70	60	50	45	40	35	30	25
Zusammensetzung pro *well* [µL]:												
MeOH/EtOH	150	130	110	100	90	70	50	40	30	20	10	0
LM	0	20	40	50	60	80	100	110	120	130	140	150
Zusammensetzung der Stock-Lösung (12 mL) der jeweiligen Bedingung [mL]:												
MeOH/EtOH	12	10.4	8.8	8	7.2	5.6	4	3.2	2.4	1.6	0.8	0
LM	0	1.6	3.2	4	4.8	6.4	8	8.8	9.6	10.4	11.2	12

Additive

Zusatz Additiv [mmol] bezogen auf 25 mL Ansatzgröße:

5	4.5	4	3.5	3	2.5	2	1.5	1	0.5	0.25	0.1

Konzentration [mol/L] bezogen auf 25 mL Ansatzgröße:

0.2	0.18	0.16	0.14	0.12	0.1	0.08	0.06	0.04	0.02	0.01	0.004

Konzentration Additiv [mol/L] in 150 µL, um bei Zugabe der Reaktionslösung die gewünschte Konzentration bezogen auf 25 ml zu erreichen

0.2667	0.24	0.2133	0.1867	0.16	0.1333	0.1067	0.08	0.0533	0.0267	0.0133	0.0053

Einwaage [mg] für 12 mL Stock-Lösung (7.2 mL MeOH/EtOH + 4.8 mL H_2O) der jeweiligen Bedingung:

Natriumchlorid	187.01	168.31	149.61	130.91	112.20	93.50	74.80	56.10	37.40	18.70	9.35	3.74
Natriumbenzoat	461.15	415.04	368.92	322.81	276.69	230.58	184.46	138.35	92.23	46.12	23.06	9.22
Natriumazid	208.03	187.23	166.43	145.62	124.82	104.02	83.21	62.41	41.61	20.80	10.40	4.16

NaOH/HCl

Gesamtvolumen 150 µL mit MeOH bzw. EtOH/H_2O 1:2 (50 µL MeOH\EtOH + x µL H_2O + y µL NaOH/HCl)

Zugabe 2 *M* NaOH/HCl [µL]	100	90	80	75	70	60	50	40	30	20	10	5
benötigtes Volumen H_2O [µL]	0	10	20	25	30	40	50	60	70	80	90	95
Zusammensetzung der Stock-Lösung (12 mL) der jeweiligen Bedingung [mL]:												
NaOH/HCl (2 *M*)	8	7.2	6.4	6	5.6	4.8	4	3.2	2.4	1.6	0.8	0.4
H_2O	0	0.8	1.6	2	2.4	3.2	4	4.8	5.6	6.4	7.2	7.6
MeOH/EtOH	4	4	4	4	4	4	4	4	4	4	4	4

8. Literaturverzeichnis

1. Schiff, H. *Ann. Chem. Pharm.* **1864,** *131* (1), 118–119.
2. Clayden, J.; Greeves, N.; Warren, S.; Wothers, P. *Organic chemistry;* Oxford University Press: Oxford, 2001.
3. Bruice, P. Y. *Organic chemistry*, 4th ed.; Pearson/Prentice Hall: Upper Saddle River, NJ, 2004.
4. Berg, J. M.; Tymoczko, J. L.; Stryer, L.; Gatto, G. J. *Biochemie*, 7. Auflage; Springer Spektrum: Berlin, 2013.
5. Lehwess-Litzmann, A.; Neumann, P.; Parthier, C.; Ludtke, S.; Golbik, R.; Ficner, R.; Tittmann, K. *Nat Chem Biol* **2011,** *7* (10), 678–684.
6. Creaven, B. S.; Devereux, M.; Karcz, D.; Kellett, A.; McCann, M.; Noble, A.; Walsh, M. *J Inorg Biochem* **2009,** *103* (9), 1196–1203.
7. Creaven, B. S.; Czegledi, E.; Devereux, M.; Enyedy, E. A.; Foltyn-Arfa Kia, A.; Karcz, D.; Kellett, A.; McClean, S.; Nagy, N. V.; Noble, A.; Rockenbauer, A.; Szabo-Planka, T.; Walsh, M. *Dalton Trans* **2010,** *39* (45), 10854–10865.
8. Raman, N.; Joseph, J.; Velan, A. S. K.; Pothiraj, C. *Mycobiology* **2006,** *34* (4), 214–218.
9. Horrocks, P.; Pickard, M. R.; Parekh, H. H.; Patel, S. P.; Pathak, R. B. *Org Biomol Chem* **2013,** *11* (29), 4891–4898.
10. Budige, G.; Puchakayala, M. R.; Kongara, S. R.; Hu, A.; Vadde, R. *Chem. Pharm. Bull.* **2011,** *59* (2), 166–171.
11. Mohamed, G. G.; Omar, M. M.; Ibrahim, A. A. *Spectrochim Acta A Mol Biomol Spectrosc* **2010,** *75* (2), 678–685.
12. Nair, M. S.; Joseyphus, R. S. *Spectrochim Acta A Mol Biomol Spectrosc* **2008,** *70* (4), 749–753.
13. Winter, C. A.; Risley, E. A.; Nuss, G. W. *Experimental Biology and Medicine* **1962,** *111* (3), 544–547.
14. Zangrando, E.; Islam, M. T.; Islam, M. A.-A. A.A.; Sheikh, M. C.; Tarafder, M.T.H.; Miyatake, R.; Zahan, R.; Hossain, M. A. *Inorganica Chimica Acta* **2015,** *427*, 278–284.
15. González, A.; Gómez, E.; Cortés-Lozada, A.; Hernández, S.; Ramírez-Apan, T.; Nieto-Camacho, A. *Chem. Pharm. Bull.* **2009,** *57* (1), 5–15.
16. Lian, W.-J.; Wang, X.-T.; Xie, C.-Z.; Tian, H.; Song, X.-Q.; Pan, H.-T.; Qiao, X.; Xu, J.-Y. *Dalton Trans* **2016,** *45* (22), 9073–9087.
17. Ekengard, E.; Kumar, K.; Fogeron, T.; Kock, C. de; Smith, P. J.; Haukka, M.; Monari, M.; Nordlander, E. *Dalton Trans* **2016,** *45* (9), 3905–3917.
18. Nikhil Batra, Shikha Batra, Navneet Aggarwa, Badri Prakash Nagori. *American Journal of Pharmtech Research* **2013,** *3* (4), 1–19.
19. Adao, P.; Kuznetsov, M. L.; Barroso, S.; Martins, A. M.; Avecilla, F.; Costa Pessoa, J. *Inorg Chem* **2012,** *51* (21), 11430–11449.
20. Hsieh, S.-H.; Kuo, Y.-P.; Gau, H.-M. *Dalton Trans* **2007,** No. 1, 97–106.
21. Yang, W.; Liu, H.; Du, D.-M. *Org Biomol Chem* **2010,** *8* (13), 2956–2960.
22. Che, C.-M.; Chan, S.-C.; Xiang, H.-F.; Chan, M. C. W.; Liu, Y.; Wang, Y. *Chem Commun (Camb)* **2004,** No. 13, 1484–1485.

23. Zhou, L.; Kwok, C.-C.; Cheng, G.; Zhang, H.; Che, C.-M. *Opt Lett* **2013,** *38* (14), 2373–2375.

24. Sano, T.; Nishio, Y.; Hamada, Y.; Takahashi, H.; Usuki, T.; Shibata, K. *J. Mater. Chem.* **2000,** *10* (1), 157–161.

25. Li, S.-H.; Chen, F.-R.; Zhou, Y.-F.; Wang, J.-N.; Zhang, H.; Xu, J.-G. *Chem. Commun.* **2009,** No. 28, 4179–4181.

26. Lee, S. A.; You, G. R.; Choi, Y. W.; Jo, H. Y.; Kim, A. R.; Noh, I.; Kim, S.-J.; Kim, Y.; Kim, C. *Dalton Trans* **2014,** *43* (18), 6650–6659.

27. Ganguly, A.; Paul, B. K.; Ghosh, S.; Kar, S.; Guchhait, N. *Analyst* **2013,** *138* (21), 6532–6541.

28. Gavey, E. L.; Beldjoudi, Y.; Rawson, J. M.; Stamatatos, T. C.; Pilkington, M. *Chem Commun (Camb)* **2014,** *50* (28), 3741–3743.

29. Zhang, Y.-Z.; Wang, B.-W.; Sato, O.; Gao, S. *Chem Commun (Camb)* **2010,** *46* (37), 6959–6961.

30. Wang, Q.-L.; Zhang, Y.-Z.; Southerland, H.; Prosvirin, A. V.; Zhao, H.; Dunbar, K. R. *Dalton Trans* **2014,** *43* (18), 6802–6810.

31. Wang, X.-Y.; Prosvirin, A. V.; Dunbar, K. R. *Angew Chem Int Ed Engl* **2010,** *49* (30), 5081–5084.

32. Ababei, R.; Pichon, C.; Roubeau, O.; Li, Y.-G.; Brefuel, N.; Buisson, L.; Guionneau, P.; Mathoniere, C.; Clerac, R. *J Am Chem Soc* **2013,** *135* (39), 14840–14853.

33. Kubo, I.; Kinst-Hori, I. *J. Agric. Food Chem.* **1999,** *47* (11), 4574–4578.

34. Watanabe, K.; Ohta, T.; Shirasu, Y. *Mutat Res* **1989,** *218* (2), 105–109.

35. Takahashi, K.; Sekiguchi, M.; Kawazoe, Y. *Biochem Biophys Res Commun* **1989,** *162* (3), 1376–1381.

36. Kim, J. H.; Lee, H.-O.; Cho, Y.-J.; Kim, J.; Chun, J.; Choi, J.; Lee, Y.; Jung, W. H. *PLoS One* **2014,** *9* (2), e89122.

37. Hannemann, A.; Cytlak, U. M. C.; Gbotosho, O. T.; Rees, D. C.; Tewari, S.; Gibson, J. S. *Blood Cells Mol Dis* **2014,** *53* (1-2), 21–26.

38. Lin, Z.-D.; Zeng, W. *Acta Crystallogr E Struct Rep Online* **2006,** *62* (5), m1074-m1076.

39. Odabaşoğlu, M.; Arslan, F.; Ölmez, H.; Büyükgüngör, O. *Dyes and Pigments* **2007,** *75* (3), 507–515.

40. Zianna, A.; Chrissafis, K.; Hatzidimitriou, A.; Lalia-Kantouri, M. *J Therm Anal Calorim* **2015,** *120* (1), 59–66.

41. Mistri, S.; Bertolasi, V.; Manna, S. C. *Polyhedron* **2015,** *88*, 101–109.

42. Wang, Q.; Wang, D.-Q. *Acta Crystallogr Sect E Struct Rep Online* **2008,** *64* (Pt 2), m298.

43. Costa Pessoa, J.; Cavaco, I.; Correia, I.; Tomaz, I.; Duarte, T.; Matias, P.M. *J Inorg Biochem* **2000,** *80* (1–2), 35–39.

44. Wang, Y.-Z.; Wang, P.; Li, C.; Su, Y.-Q. *Synthesis and Reactivity in Inorganic, Metal-Organic, and Nano-Metal Chemistry* **2015,** *46* (6), 868–871.

45. Sun, H.; She, L.; Fang, S.; Li, X. *Polyhedron* **2008,** *27* (2), 854–860.

46. Zhou, J.; Fang, S.; Sun, H.; Li, X. *Acta Crystallogr E Struct Rep Online* **2006,** *62* (12), m3451-m3452.

47. Lalia-Kantouri, M.; Gdaniec, M.; Czapik, A.; Chrissafis, K.; Ferenc, W.; Sarzynski, J.; Papadopoulos, C. D. *J Therm Anal Calorim* **2012,** *109* (1), 131–139.

48. Papadopoulos, C. D.; Hatzidimitriou, A. G.; Voutsas, G. P.; Lalia-Kantouri, M. *Polyhedron* **2007,** *26* (5), 1077–1086.

49. Anastasiadou, D.; Zianna, A.; Gdaniec, M.; Sigalas, M. P.; Coutouli-Argyropoulou, E.; Czapik, A.; Lalia-Kantouri, M. *Polyhedron* **2015,** *87*, 275–285.

50. Wu, J.; Jung, J.; Zhang, P.; Zhang, H.; Tang, J.; Le Guennic, B. *Chem. Sci.* **2016,** *7* (6), 3632–3639.

51. H. Lin, H. Su, Y.-L. Feng. *Z. Kristallogr. NCS* **2006,** No. 221, 173–175.

52. Gao, T.; Gao, P.; Li, H.-F.; Zhang, J.-W.; Xu, L.-L. *Acta Crystallogr Sect E Struct Rep Online* **2012,** *68* (Pt 2), m152.

53. Jia, R.; Gao, T.; Chen, R.; Yang, Y.; Gao, P.; Wang, Y.; Yan, P. *Aust. J. Chem.* **2015**.

54. Gao, P.; Hou, H.-G.; Gao, T.; Yang, J.-L.; Yang, Y. *Acta Crystallogr Sect E Struct Rep Online* **2011,** *67* (Pt 11), m1522.

55. Costes, J.-P.; Dahan, F.; Duhayon, C.; Mota, A. J. *Polyhedron* **2015,** *96*, 51–56.

56. Costes, J.-P.; Vendier, L. *Eur. J. Inorg. Chem.* **2010,** *2010* (18), 2768–2773.

57. Zou, X.; Yan, P.; Zhang, J.; Zhang, F.; Hou, G.; Li, G. *Dalton Trans* **2013,** *42* (36), 13190–13199.

58. Tang, J.; Hewitt, I.; Madhu, N. T.; Chastanet, G.; Wernsdorfer, W.; Anson, C. E.; Benelli, C.; Sessoli, R.; Powell, A. K. *Angew Chem Int Ed Engl* **2006,** *45* (11), 1729–1733.

59. Costes, J.-P.; Dahan, F.; Nicodème, F. *Inorg. Chem.* **2001,** *40* (20), 5285–5287.

60. Yu, G.-M.; Zhao, L.; Zou, L.-F.; Guo, Y.-N.; Xu, G.-F.; Li, Y.-H.; Tang, J. *J Chem Crystallogr* **2011,** *41* (5), 606–609.

61. Ayikoe, K.; Butcher, R. J.; Gultneh, Y. *Acta Crystallogr Sect E Struct Rep Online* **2010,** *66* (Pt 11), m1487-8.

62. Zhang, S.-H.; Zhang, Y. D.; Zou, H. H.; Guo, J. J.; Li, H. P.; Song, Y.; Liang, H. *Inorganica Chimica Acta* **2013,** *396*, 119–125.

63. Costes, J.-P.; Novitchi, G.; Vendier, L.; Pilet, G.; Luneau, D. *Comptes Rendus Chimie* **2012,** *15* (10), 849–855.

64. Qin, X.; Ding, S.; Xu, X.; Wang, R.; Song, Y.; Wang, Y.; Du, C.-f.; Liu, Z.-l. *Polyhedron* **2014,** *83*, 36–43.

65. Zhang, K.; Dai, J.; Wang, Y.-H.; Zeng, M.-H.; Kurmoo, M. *Dalton Trans* **2013,** *42* (15), 5439–5446.

66. Langley, S. K.; Chilton, N. F.; Gass, I. A.; Moubaraki, B.; Murray, K. S. *Dalton Trans* **2011,** *40* (47), 12656–12659.

67. Zhang, S.-H.; Li, N.; Ge, C.-M.; Feng, C.; Ma, L.-F. *Dalton Trans* **2011,** *40* (12), 3000–3007.

68. Zhang, S.-H.; Zhao, R.-X.; Li, H.-P.; Ge, C.-M.; Li, G.; Huang, Q.-P.; Zou, H.-H. *Journal of Solid State Chemistry* **2014,** *216*, 30–35.

69. Costes, J.-P.; Vendier, L.; Wernsdorfer, W. *Dalton Trans* **2011,** *40* (8), 1700–1706.

70. Hussain, B.; Savard, D.; Burchell, T. J.; Wernsdorfer, W.; Murugesu, M. *Chem Commun (Camb)* **2009,** No. 9, 1100–1102.

71. Hewitt, I. J.; Tang, J.; Madhu, N. T.; Anson, C. E.; Lan, Y.; Luzon, J.; Etienne, M.; Sessoli, R.; Powell, A. K. *Angew Chem Int Ed Engl* **2010,** *49* (36), 6352–6356.

72. Gao, T.; Li, G.-M.; Gao, P.; Sun, W.-B.; Xu, H.; Wang, C.; Hou, G.-F.; Yan, P.-F. *Z. anorg. allg. Chem.* **2011,** *637* (14-15), 2223–2227.

73. Lalia-Kantouri, M.; Papadopoulos, C. D.; Hatzidimitriou, A. G.; Skoulika, S. *Struct Chem* **2009,** *20* (2), 177–184.

74. Andruh, M. *Dalton Trans* **2015,** *44* (38), 16633–16653.

75. Thevenon, A.; Garden, J. A.; White, A. J. P.; Williams, C. K. *Inorg Chem* **2015,** *54* (24), 11906–11915.

76. Griffiths, K.; Gallop, C. W. D.; Abdul-Sada, A.; Vargas, A.; Navarro, O.; Kostakis, G. E. *Chemistry* **2015,** *21* (17), 6358–6361.

77. Griffiths, K.; Kumar, P.; Mattock, J. D.; Abdul-Sada, A.; Pitak, M. B.; Coles, S. J.; Navarro, O.; Vargas, A.; Kostakis, G. E. *Inorg Chem* **2016,** *55* (14), 6988–6994.

78. Mohd Tajuddin, A.; Bahron, H.; Kassim, K.; Ibrahim, W. N. W.; Fun, H. K. Synthesis and Characterization of Palladium(II) Schiff Base and their Catalytic Activities for Heck Reaction. In *Advances in chemistry research II*, Selected, peer reviewed papers from the 2nd International Conference on Chemical Engineering and Advanced Materials (CEAM 2012), July 13 - 15, 2012, Guangzhou, China; Chen, S., Ed.; ttp Trans Tech Publ: Durnten-Zurich, 2012; pp 736–740.

79. Bahron, H.; Mohd Tajuddin, A.; Ibrahim, W. N. W.; Hemamalini, M.; Fun, H.-K. *Acta Crystallogr Sect E Struct Rep Online* **2011,** *67* (Pt 6), m759-60.

80. Lange, T. S.; Kim, K. K.; Singh, R. K.; Strongin, R. M.; McCourt, C. K.; Brard, L. *PLoS One* **2008,** *3* (5), e2303.

81. Kim, K. K.; Singh, R. K.; Strongin, R. M.; Moore, R. G.; Brard, L.; Lange, T. S. *PLoS One* **2011,** *6* (4), e19049.

82. Ansari, K. I.; Kasiri, S.; Grant, J. D.; Mandal, S. S. *J Biomol Screen* **2011,** *16* (1), 26–35.

83. Prakash, G.; Manikandan, R.; Viswanathamurthi, P.; Velmurugan, K.; Nandhakumar, R. *Journal of Photochemistry and Photobiology B: Biology* **2014,** *138*, 63–74.

84. Lin, R.-K.; Hsu, C.-H.; Chiu, C.-I.; Lai, Y.-J.; Lai, a. F.-J.; Chien, C.-M.; Lin, C.-C. *Jnl Chinese Chemical Soc* **2014,** *61* (12), 1333–1340.

85. Hong, M.; Geng, H.; Niu, M.; Wang, F.; Li, D.; Liu, J.; Yin, H. *Eur J Med Chem* **2014,** *86*, 550–561.

86. Jakkali Chandregowda Dharshan, Karagadi Anantha Adiga Vishnumurthy, Yadav Dhasharatha Bodke, Hosadu Manjappaiah Vagdevi, Nayakarahatty Devanna Jayanna, Ramappa Raghavendra. *Der Pharma Chemica* **2012,** *4* (1), 272–281.

87. Abdel-Rahman, L. H.; Abu-Dief, A. M.; El-Khatib, R. M.; Abdel-Fatah, S. M. *Bioorg Chem* **2016,** *69*, 140–152.

88. Yousef Ebrahimipour, S.; Mohamadi, M.; Sheikhshoaie, I.; Suárez, S.; Baggio, R.; Khaleghi, M. *Res Chem Intermed* **2016,** *42* (2), 611–623.

89. Rogolino, D.; Carcelli, M.; Bacchi, A.; Compari, C.; Contardi, L.; Fisicaro, E.; Gatti, A.; Sechi, M.; Stevaert, A.; Naesens, L. *J Inorg Biochem* **2015,** *150*, 9–17.

90. AlAjmi, M. F.; Hussain, A.; Alsalme, A.; Khan, R. A. *RSC Adv* **2016,** *6* (23), 19475–19481.

91. Malik, W. U.; Bembi, R.; Sushila, M. *Journal of the Indian Chemical Society* **1977,** *54* (8), 762–764.

92. Heinert, D.; Martell, A. E. *J. Am. Chem. Soc.* **1962,** *84* (17), 3257–3263.

93. Malik, W. U.; Bembi, R.; Sushila, M. *Journal of the Indian Chemical Society* **1979,** *56* (776-778).

94. Malik, W. U.; Bembi, R.; Bhargava, P. P.; Sushila; Tandon, O. P. *Journal of the Indian Chemical Society* **1980,** *57* (5), 455–458.

95. Bembi, R.; Tandon, O. P. *Journal of Inorganic and Nuclear Chemistry* **1981,** *43* (3), 565–569.

96. Jiang, Y.; Chen, D.; Chen, W. *Huaxue Yanjiu Yu Yingyong* **1999,** *11* (4), 402–405.

97. Dang, Y.-l.; Xie, H.-q.; Zhuo, L.-h. *Xinyang Shifan Xueyuan Xuebao, Ziran Kexueban* **2004,** *17* (4), 422–424.

98. Nair, M. S.; Raj, C. R. S.; Arish, D.; Kumari, S. S. *Journal of the Indian Chemical Society* **2010,** *87* (6), 729–734.

99. Sivasankaran Nair, M.; Suda Kumari, S.; Neelakantan, M. A. *Journal of Coordination Chemistry* **2007,** *60* (12), 1291–1302.

100. Yan Xiao, Caifeng Bi, Yuhua Fan, Cindy Cui, Xia Zhang, Q. Ping Dou. *int J Oncol* **2008,** *33*, 1073–1079.

101. Xiao, Y.; Bi, C.; Fan, Y.; Liu, S.; Zhang, X.; Zhang, D.; Wang, Y.; Zhu, R. *Journal of Coordination Chemistry* **2009,** *62* (18), 3029–3039.

102. Wei, Q.; Dong, J.; Zhao, P.; Li, M.; Cheng, F.; Kong, J.; Li, L. *J Photochem Photobiol B* **2016,** *161*, 355–367.

103. Gao, J.; Guo, Y.; Wang, J.; Wang, Z.; Jin, X.; Cheng, C.; Li, Y.; Li, K. *Spectrochim Acta A Mol Biomol Spectrosc* **2011,** *78* (4), 1278–1286.

104. Roy, R.; Saha, M. C.; Roy, P. S. *Transition Met Chem* **1990,** *15* (1), 51–57.

105. Ebel, M.; Rehder, D. *Inorg Chem* **2006,** *45* (18), 7083–7090.

106. Ebel, M.; Rehder, D. *Inorganica Chimica Acta* **2003,** *356*, 210–214.

107. Grüning, C.; Rehder, D. *J Inorg Biochem* **2000,** *80* (1-2), 185–189.

108. Jing, B.-Q.; Li, L.-Z.; Wang, D.-Q.; Xu, T. *Acta Crystallogr E Struct Rep Online* **2005,** *61* (10), m2106-m2108.

109. Pu, X.; Li, L.; Dong, J.; Jing, B. *Acta Crystallogr Sect E Struct Rep Online* **2011,** *67* (Pt 4), m465-6.

110. Nayak, S.; Novitchi, G.; Muche, S.; Luneau, D.; Dehnen, S. *Z. anorg. allg. Chem.* **2012,** *638* (7-8), 1127–1133.

111. Jiang, X.-F.; Zhao, R.-X.; Zhang, S.-H. *Acta Crystallogr E Struct Rep Online* **2014,** *70* (Pt 11), 269–271.